INSTITUTE OF ORGANIC CHEMISTRY POLISH ACADEMY OF SCIENCES

DISSERTATION

in the form of a coherent thematic series of articles published in scientific journals

Synthesis and photophysical properties of novel merocyanine dyes

Kateryna Vygranenko, M.Sc.

Supervisor: prof. dr hab. Daniel Tomasz Gryko

Warsaw 2023

Praca doktorska wykonana w ramach projektu:

"New generation of fluorescent probes for stimulated emission depletion microscopy"

Realizowanego w ramach programu TEAM

Fundacji na rzecz Nauki Polskiej

Numer grantu: POIR.04.04.00-00-3CF4/16-00-TEAM/2016-3/22

Acknowledgements:

To start with, I would like to express my gratitude to my supervisor Prof. Daniel T. Gryko, who gave me an opportunity to be a PhD student in his group. Prof. Gryko possesses the most important skills of team leader – excellent time-management and effective organisation of team cooperation. His contribution to my success is hard to overestimate. Again, I thank him for his guidance, encouragement, support and patience throughout the years.

Secondly, I am very grateful to all current and past group members for their support during hard times, encouragement in moments of complete disappointment, sharing their knowledge and experience, cosy working environment and feeling that you are not alone among your problems. Special thanks to Dr. Yevgen Poronik for teaching me to pay a lot of attention to details, Dr. Olena Vakuliuk, who took care of me like mother, Dr. Mariusz Tasior and Dr. Beata Koszarna for their optimism and support regardless the situation, Jaqueline Stella Araujo Badaro, Dr. David Young, and Dr. Dinesh Kumar for their contribution to my English practice and support. In particular, I would like to thank Olena Vakuliuk and Yevgen Poronik once more for their friendship, guidance and company in the lab for over the years.

Again, I would like to give special thanks to Dr. David Young for the proofreadings.

I also thank all my collaborators, especially Dr. Antoni Wrzosek and Prof. Adam Szewczyk for great support and guidance in bio-imaging studies, Prof. Denis Jacquemin and Manon H. E. Bousquet for theoretical calculations, Dr. Łukasz Dobrzycki for X-Ray diffraction measurements, Brunella Bardi, Prof. Francesca Terenziani and Prof. Anna Painelli for spectroscopic characterization and theoretical calculations.

Additionally, I would like to thank the FNP-TEAM for funding my PhD.

Finally, I want to thank the whole Poland for being the first country to help in the darkest times, for compassion and empathy, for being always ready to help and share their home and resources with refugees.

I dedicate this thesis to my parents and my husband, whose encouragement, support and love made it possible to finish my research.

TABLE OF CONTENTS

1. LIST OF PUBLICATIONS INCLUDED IN THE DOCTORAL THESIS

1. Yevgen M. Poronik, **Kateryna V. Vygranenko**, Dorota Gryko and Daniel T. Gryko, *Chem. Soc. Rev.*, 2019, *48*, 5242-5265. 'Rhodols – synthesis, photophysical properties and applications as fluorescent probes'. IF_{2023} = 60.615.

2. **Kateryna V. Vygranenko**, Yevgen M. Poronik, Antoni Wrzosek, Adam Szewczyk and Daniel T. Gryko, *Chem. Comm.*, 2021, *57*, 7782-7785. 'Red emissive sulfone-rhodols as mitochondrial imaging agents'. IF_{2023} = 6.065.

3. **Kateryna V. Vygranenko**, Yevgen M. Poronik, Manon H. E. Bousquet, Olena Vakuliuk, Denis Jacquemin and Daniel T. Gryko, *Chem. Comm.*, 2022, *58,* 1542-1545. 'Direct transformation of coumarins into orange-red emitting rhodols'. IF_{2023} = 6.065.

4. Brunella Bardi, **Kateryna V. Vygranenko**, Beata Koszarna, Olena Vakuliuk, Łukasz Dobrzycki, Daniel T. Gryko, Francesca Terenziani and Anna Painelli, *Chem. - A Eur. J.*, 2023 - doi.org/10.1002/chem.202300979. 'A novel method for the synthesis of merocyanines: new photophysical possibilities for a well-known class of fluorophores'. IF_{2023} = 5.02.

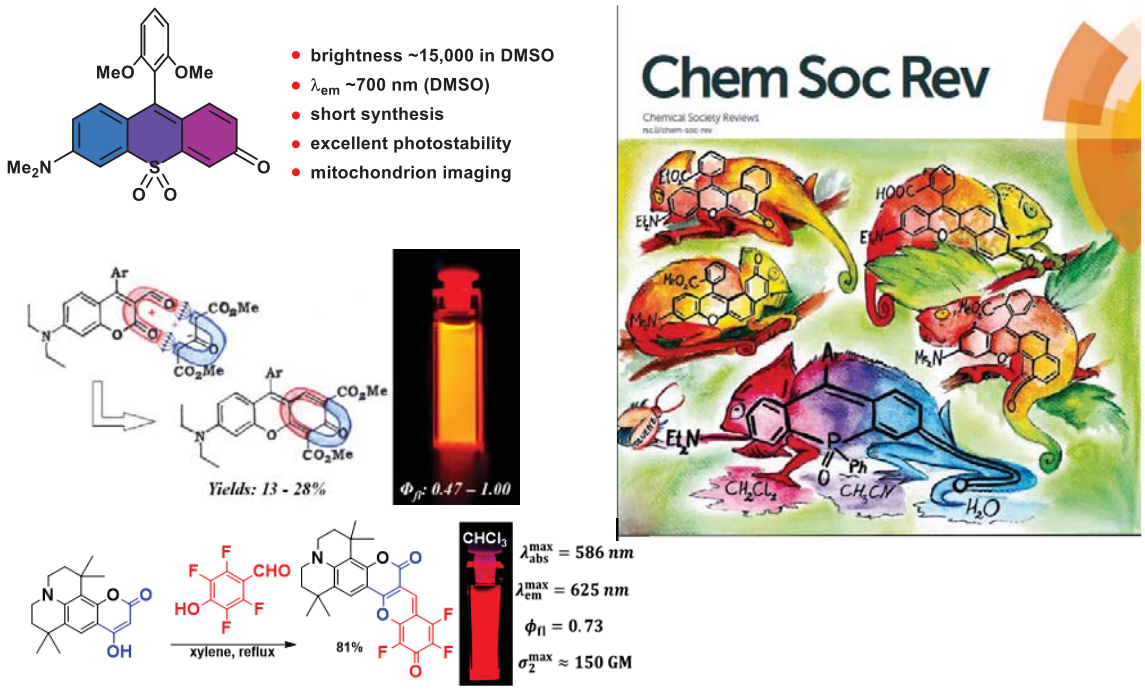

2. LIST OF PUBLICATIONS NOT INCLUDED IN THE DOCTORAL THESIS

1. Olena Vakuliuk, Yong Woong Jun, **Kateryna Vygranenko**, Guillaume Clermont, Ye Jin Reo, Mireille Blanchard-Desce, Kyo Han Ahn, Daniel T. Gryko, *Chem. Eur. J*., 2019, *25*, 13354–13362. 'Modified isoindolediones as bright fluorescent probes for cell and tissue imaging' $IF_{2023} = 5.02$.

2. Łukasz Kielesiński, Irena Deperasińska, Olaf Morawski, **Kateryna V. Vygranenko**, Erik T. Ouellette and Daniel T. Gryko, *J. Org. Chem*., 2022, *87*, 5961−5975. 'Polarized, V-shaped, and conjoined biscoumarins: from lack of dipole moment alignment to high brightness'. $IF_{2022} = 4.198$.

3. PARTICIPATION IN CONFERENCES AND SEMINARS.

1. 2nd CHAOS Training School C-H Activation in Organic Synthesis, Athens, Greece, 10-13.09.2019.

2. The training workshop, Newark, NJ, USA, 30.04.2022. “How to approach computer simulations for molecules and materials: from theory to practice”.

3. The 19th international symposium on novel aromatic compounds (ISNA 2019), Warsaw, Poland, 3-8.07.2022. ‘Direct transformation of coumarins into orange-red emitting rhodols’.

4. ABSTRACT IN ENGLISH

The main objective of my PhD course was to gain deep insight the synthesis and optical properties of rhodols, which might be applied in cell imaging and STED microscopy. I have started with development of the synthesis rhodols possessing endocyclic sulfone fragment. This was achieved via the 3-step synthesis of corresponding rhodamines, followed by the substitution of dimethylamino moiety with the oxygen atom. Having new sulfone-rhodols in hand, I decided to modify one of them by incorporation of hexyl chain with the quaternary phosphonium center at the terminal position to make the dye suitable for cell imaging. These compounds possess intriguing optical properties i.e. high fluorescent quantum yields and high Stokes shifts as well as excellent photostabilities.

The next goal was to develop the synthetic approach towards rhodols from coumarins via Knoevenagel condensation. For this purpose, I have synthesized 4-hydroxycoumarins possessing diethylamino moiety and the coumarin analogue with the annulated nitrogen atom at the position 7 and after additional 3 steps I have obtained 3-formyl-coumarins as the rhodol precursors. This double Knoevenagel condensation of 3-formyl coumarins with dimethyl 1,3-acetonedicarboxylate is absolutely unprecedent, because at the second step the source of carbonyl group is lactone ester, which is typically considered to be inert in this type of reactions. I have performed a huge part of work trying to find the best conditions for this condensation. In this case I tried various Lewis acids, bases, solvents, different temperature and the reaction time. Besides, on the basis of the electronic spectroscopy I have developed a convenient method for screening multiple experiments in the tiny scale to evaluate conversion and yields of reactions without workup and purification. As a matter of fact, the best catalyst revealed to be piperidine. This reaction allowed me to obtain new rhodols possessing two ester groups in 13-28% yield. The obtained rhodols demonstrate excellent quantum yields: 0.47 – 1.00 in DCM and DMSO.

The final of my research was a discovery of an extraordinary straightforward one-step synthesis of rhodols from *m*-aminophenols and tetrafluorohydroxybenzaldehyde. This method is similar to classic Friedel-Crafts condensation with a difference that a molecule of HF forms during the reaction instead of water as in the original method. The reaction successfully proceeds in toluene or xylene at elevated temperatures and does not require any bases or other additives. The product precipitates from the reaction mixture and can be purified via simple recrystallization. This approach is applicable to *m*-aminophenols, 4-hydroxy-7-aminocoumarins and hydroxyaminonaphthalenes, that allowed me to obtain an uncommon π-expanded linear rhodol and π-expanded rhodol analogues. This is the first representative of π-expanded rhodols with the additional benzene ring from amino side possessing the linear chromophore.

5. ABSTRACT IN POLISH / STRESZCZENIE W JĘZYKU POLSKIM

Głównym celem mojej pracy doktorskiej było pogłębienie wiedzy na temat syntezy i właściwości optycznych rodoli, które mogą znaleźć zastosowanie w obrazowaniu komórkowym i mikroskopii STED. W pierwszej fazie opracowałam syntezę rodoli posiadających endocykliczny fragment sulfonowy. Osiągnęłam to poprzez 3-etapową syntezę odpowiednich rodamin, a następnie podstawienie ugrupowania dimetyloaminowego atomem tlenu. Mając w ręku nowe rodole sulfonowe, zdecydowałam się zmodyfikować jeden z nich poprzez włączenie łańcucha heksylowego z czwartorzędowym centrum fosfoniowym w pozycji końcowej, aby barwnik nadawał się do obrazowania mitochondriów w komórkach eukariotycznych. Związki te posiadają intrygujące właściwości optyczne, tj. wysokie wydajności kwantowe fluorescencji i wysokie przesunięcia Stokesa, a także doskonałą fotostabilność.

Kolejnym celem było opracowanie syntetycznego podejścia do rodoli z kumaryn poprzez kondensację Knoevenagela. W tym celu zsyntetyzowałam 4-hydroksykumaryny posiadające ugrupowanie dietyloaminowe i analog kumaryny z pierścieniowym atomem azotu w pozycji 7 i po dodatkowych 3 etapach otrzymałam 3-formylo-kumaryny jako prekursory rodolu. Zastosowana w ostatnim etapie podwójna kondensacja Knoevenagela 3-formylokumaryn z 1,3-acetonodikarboksylanem dimetylu jest absolutnie bezprecedensowa, ponieważ w drugim etapie źródłem grupy karbonylowej jest ester laktonowy, który zwykle uważa się za niereaktywny w tego typu reakcjach. W czasie optymalizacji tej kondensacji, próbowałam różnych kwasów Lewisa, zasad, rozpuszczalników, różnej temperatury i czasu reakcji. Poza tym na podstawie spektroskopii elektronowej opracowałam wygodną metodę „skriningu" wielu eksperymentów w małej skali w celu oceny konwersji i wydajności reakcji bez obróbki i oczyszczania. W rzeczywistości najlepszym katalizatorem okazała się być piperydyna. Ta reakcja pozwoliła mi otrzymać nowe rodole posiadające dwie grupy estrowe z wydajnością 13-28%. Otrzymane rodole wykazują doskonałe wydajności kwantowe fluorescencji: 0,47 – 1,00 w DCM i DMSO.

Zwieńczeniem moich badań było odkrycie niezwykle prostej, jednoetapowej syntezy rodoli z *m*-aminofenoli i tetrafluorohydroksybenzaldehydu. Metoda ta opiera się na klasycznej reakcji Friedela-Craftsa po której następuje wewnątrzcząsteczkowe aromatyczne podstawienie nukleofilowe. Reakcja z powodzeniem przebiega w toluenie lub ksylenie w podwyższonej temperaturze i nie wymaga żadnych katalizatorów. Produkt wytrąca się z mieszaniny reakcyjnej i można go oczyścić przez prostą rekrystalizację. Podejście to ma zastosowanie do *m*-aminofenoli, 4-hydroksy-7-aminokumaryn i hydroksyaminonaftalenów, co pozwoliło mi uzyskać rzadki liniowy π-rozszerzony rodol i analogi rodolu o π-rozszerzonym łańcuchu. Jest to pierwszy przedstawiciel π-rozprężonych rodoli z dodatkowym pierścieniem benzenowym od strony aminowej, posiadający liniowy chromofor.

6. GUIDE TO THE DOCTORAL THESIS

6.1 Purpose of the work

The study of biological systems at the cellular and subcellular levels is greatly aided by small molecule fluorophores of which members of the xanthene family, including fluorescein and rhodamine, have proven to be invaluable.[1] Recently, there has been an increased focus on the manipulation of the photophysical properties of these ubiquitous dyes through structural modifications. In particular π-expansion, and replacement of the xanthene oxygen atom bridge with silicon,[2–4] phosphorus,[5] sulfur,[6] or carbon[7–9] in rhodamine,[10–13] fluorescein,[14,15] and rhodol[16] scaffolds have proven to be effective. The dyes from this extended family, despite their structural and functional diversity, share the quintessential characteristics: (a) planar aromatic structures; (b) excellent spectroscopic properties including intense absorption and fluorescence; (c) relatively small Stokes shifts; (d) biocompatibility. These features made them particularly attractive in fluorescence microscopy.

Since the design of commercially available confocal microscopes in 1960s, fluorescence microscopy has been one of the most important cell research methods, indispensable for life sciences. Moreover, as biological material by itself shows weak fluorescence response, the usage of fluorescent markers in microscopy techniques allows selective visualization of the diverse intracellular structures and monitoring different cellular processes.

The main drawback of this technique however was its spatial resolution which does not exceed 200 nm in the object plane (x, y) and 600 nm along the optical axis. The development of optical methods in microscopy has led to the emergence of a large number of modern techniques. In 1994 Stimulated Emission Depletion Microscopy (STED microscopy) was proposed as a new super resolution scanning fluorescence microscopy method.[17] This approach is based on reducing the diameter of dots with an additional STED laser, which suppresses spontaneous emission in the outer region of the fluorescent spot due to the effect of stimulated emission. The beams of the exciting and STED lasers are carefully aligned, and the intensity distribution of the STED laser in focus has the form of a “donut”, with zero intensity in the centre. As a result, at high intensities of the STED laser, only those molecules exhibit fluorescence, which are located close to the region with zero intensity, while in the high-intensity zone is mainly stimulated emission of fluorophores that are rejected in the optical path due to coincidence with the wavelength of the STED laser.[18] Sequential scanning of the entire sample gives a complete picture with super-resolution. In other words, a STED microscope is a laser scanning confocal microscope that reaches resolution beyond the diffraction limit by selective quenching of fluorescence.[19] Therefore, fluorescence microscopy has

proven to be the best method for studying the mechanisms of functioning of organisms at the cellular, subcellular and molecular levels. The first dye used for theoretical description of STED-microscopy was rhodamine B. Nevertheless, the majority of existing fluorescent dyes turned out to be ineligible for super resolution imaging due to low photostability or non-suitable optical properties. Over the last decade, STED microscopy has become a general fluorescent technique, rather than highly specific method. The desire to answer more advanced cell-biological questions has led to the increased need for more advanced dyes, which can fulfil principal requirements: large fluorescence quantum yield in the near-infrared region, large Stokes shift good cell-permeability and most importantly high photostability.

My PhD-Thesis has two goals, which I plan to realize in parallel. Predominantly I challenged myself with developing entirely new synthetic methodologies leading to rhodols, rhodols modified at central bridging atom and ‘rhodol-like’ merocyanines. The methodologies available in the spring 2018 when I started my research work, although useful had many limitations. Predominantly they did not enable an access to broader range of rhodols possessing additional functionalities and/or an altered chromophore. The parallel goal was to obtain rhodols with the combination of more suitable photophysical properties i.e. bathochromically shifted emission, large fluorescence quantum yield and enhanced photostability.

6.2 The current state of knowledge in a given field of chemistry

The first mention about rhodol appeared in 1889, when it was prepared in a roundabout way starting from the decomposition of fluorescein, and was named by Bayer as 'neuer Farbstoff'.[20] Being a structural hybrid of two dyes already known at that time – rhodamine and fluorescein – the new chromophore was named 'rhodafluor' (lately 'rhodol') – the one similar to rhodamine and at the same time possessing a 'phenol component' of fluorescein.[21] Rhodols inherited photophysical properties of the parent dyes in terms of large extinction coefficient, large fluorescence quantum yield and solubility in majority of solvents (Fig.1). On the other hand, rhodols are more photostable compared to fluoresceins.[16]

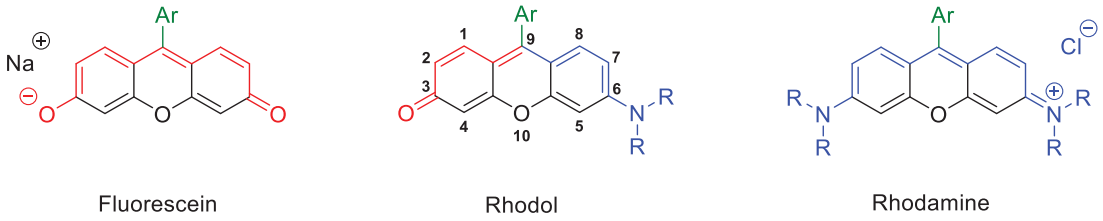

Figure 1. Structures of fluorescein, rhodol and rhodamine scaffolds.

All of the abovementioned dyes refer to polymethine dyes, since they possess a chromophore system, which consists of conjugated double bonds located between two terminal polar moieties. Rhodamine as one of the most distinguished representatives of cyanine dyes possesses a delocalized positive charge along the conjugated system, while fluorescein belongs to the oxonole group of dyes having a delocalized negative charge. In opposition to both parent dyes, rhodol corresponds to the merocyanine family and has an electronically neutral structure, which is illustrated in two limiting forms – neutral and dipolar (Figure 2).[22]

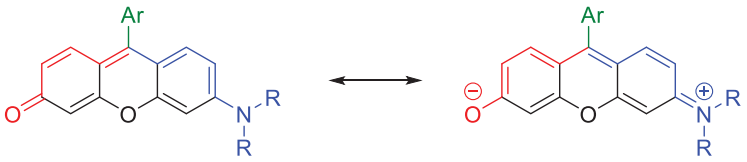

Neutral and dipolar limiting forms
of rhodol chromophore

Figure 2. Balance between neutral and dipolar limiting forms of rhodol chromophore.

Comparable to fluoresceins, rhodols illustrate positive solvatochromism possessing red-shifted absorption and emission maxima in polar solvents. In the same way as parent dyes, rhodols can be

modified to influence the conjugation chain and, as a matter of fact, the photophysical properties, which allows to obtain the desired compound suitable for various applications (Figure 3).

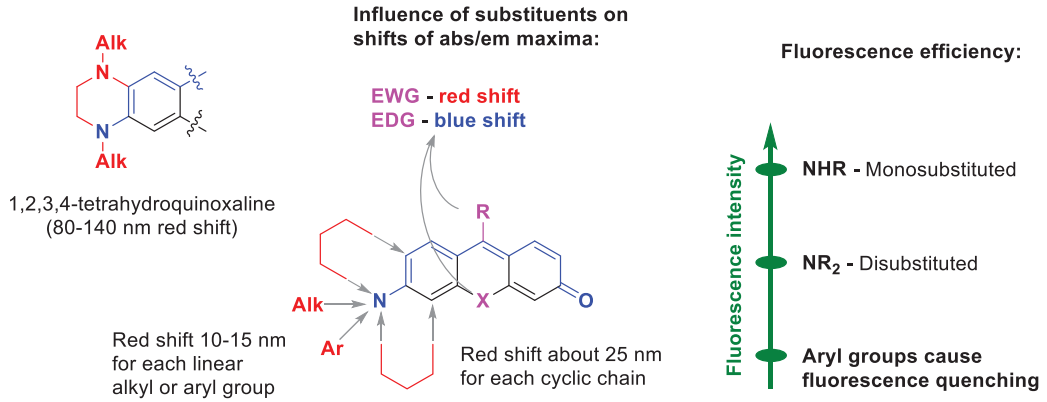

Figure 3. The influence of substituents on optical properties of rhodafluors.

The study of the substituent's nature influence on the absorption and emission spectra is rationalized by the Dewar-Knott rule.[23,24] It states that incorporation of electron-donating groups into *meso*-position 9 and bridging position 10 results in blue-shift of the absorption maxima, meanwhile the electron-withdrawing groups provoke the opposite effect.

Furthermore, the spectral characteristics of rhodol fluorophores, such as emission maximum and fluorescence quantum yield, are quite dependent on the substitution patterns of the nitrogen atom in a similar manner to rhodamine.[25,26] Rhodols with unsubstituted amino group exhibit very strong fluorescence at 516 nm. The addition of one alkyl substituent leads to the bathochromic shift of both absorption and emission maxima.[27] Meanwhile, rhodols comprising fully annulated terminal C-N bonds (julolidine moiety) exhibit even more red-shifted maxima, due to the restricted rotation of the amino group, though with reduced fluorescence quantum yields. In addition, the introduction of 1,2,3,4-tetrahydroquinoxaline moiety leads to the Stokes shift increase (80-140 nm) due to the presence of second electron-donating amino group in the neighboring position (Figure 3).[28,29]

The aryl moiety plays a substantial role in rhodamines, fluoresceins and rhodols, governing some of their chemical and photophysical properties. Although, it is located orthogonally to the xanthene scaffold and is not a part of the chromophore, it decreases the sensitivity of fluorophore's π-conjugated system to the nucleophiles.[30] The presence of the bulky substituent at *ortho*-position of benzene moiety increases the fluorescence efficiency, since it inhibits rotation of the aryl part and in this way minimizes the radiationless deactivation of the excited state.[31–34]

Consequently, the analysis of the abovementioned led me to the conclusion that synthesis of new derivatized rhodols may be the perfect starting point to develop a new generation of stable functional dyes possessing range of key properties such as: high photostability, cell permeability, intense fluorescence and susceptibility to external stimuli.

6.2.1 Synthesis of classic rhodols

The first rhodol was synthesized in 1889 by Bayer. Previously he had developed synthesis of fluorescein and rhodamine, which acquired later an industrial value. The further investigations led to the formation of first rhodol and, thus, a new class of the merocyanine dyes. For this purpose Bayer had utilized base-induced hydrolysis of fluorescein followed by the formation of dihydroxybenzoylbenzoic acid and its condensation with *m*-aminophenol (Scheme 1). Unfortunately, the authors did not provide any information about yields of both reactions.

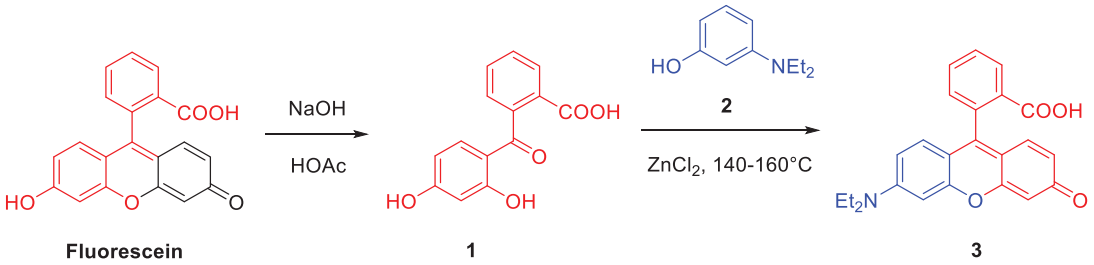

Scheme 1. Original method of rhodol formation based on a reversed substrate model.

Since 19th century this method still remains favored and is employed in many modern publications.[28,29,43–49,35–42] However, the way of synthesis of benzophenones nowadays is different, since hydrolysis of fluorescein is not very convenient. Another option is condensation of phthalic anhydride with resorcinol derivatives in the presence of Lewis acids. This method of rhodol synthesis is more convenient than 'classic' one (Scheme 2) particularly in the case of complex *m*-aminophenols.

The most common method of preparation of symmetrical rhodamines and fluoresceins is a Friedel-Crafts acylation which involves phthalic anhydride and resorcinol or 3-dialkylaminophenol.[50,51] However, this one-pot method is not applicable for rhodol attainment due to its asymmetrical structure. For this reason the most straightforward access to the rhodol structure is a two-step condensation of phthalic anhydride **3** with 3-dialkylaminophenol **2** followed by the reaction of the obtained benzophenone **4** with resorcinol **5** (Scheme 1).[52,53] Even though this is the original and short method leading to the formation of the rhodol, the first step suffers from a significant

disadvantage. The concurring formation of rhodamine B via the addition of second molecule of 3-dialkylaminophenol **2** is preferrable and proceeds almost immediately. For this reason it is crucial to use a considerable excess of phthalic anhydride to inhibit the side reaction.

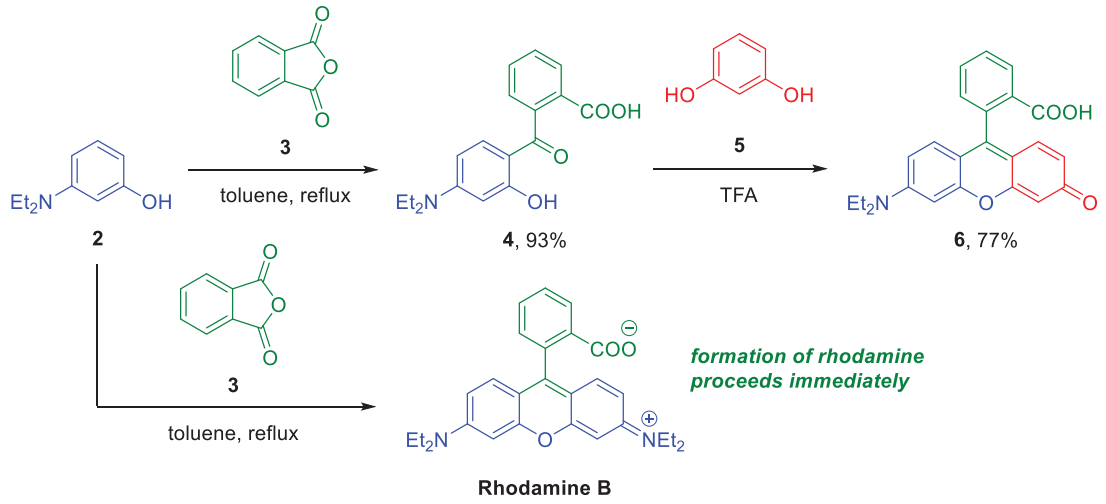

Scheme 2. 'Classic' method of rhodol synthesis from phthalic anhydride, 3-aminophenol and resorcinol.

Nevertheless, this simple procedure results in formation a rhodol skeleton possessing COOH group in the aryl moiety making product better soluble in water and more attractive for further modifications. Moreover, the carboxylic group equilibrates between spiro and open dye forms (Scheme 2). Acidic conditions stimulate the formation of the protonated or the spiroform, while in basic media rhodols are in the open dye form, since ring closure is impossible due to the salt formation. Despite all disadvantages, this method still remains one of the most inexpensive, fastest and the most straightforward approaches towards rhodols.[30,35,61–70,52,71,54–60]

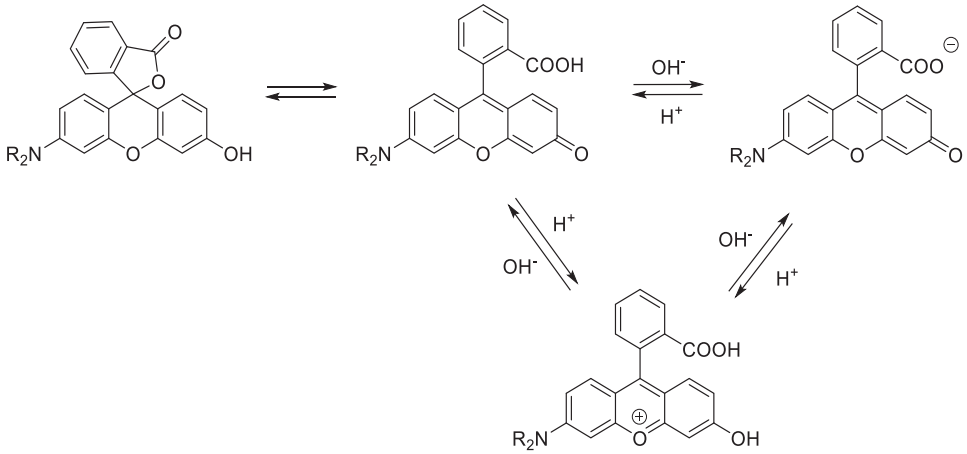

Scheme 3. The equilibrium between the dye open form and spiroform.

The use of acetophenone in the abovementioned method allows to incorporate a methyl group instead of aryl one at the meso-position of rhodol skeleton (Scheme 4).[50,72,73] The original procedure includes Fries rearrangement of 3-acetoxy-*N,N*-dimethylaniline into acetophenone, which occurs however, in only 16% yield.[50] On the other hand, the transformation of 7-diethylamino-4-hydroxycoumarin into acetophenone results in 90% yield via ring-opening followed by decarboxylation.[73] The condensation of acetophenone **7** with resorcinol **6** occurs in phosphoric acid and leads to the rhodol formation in 75 % yield. Even though this method allows to incorporate different substituents in position 9, the synthetic access to the starting aromatic ketones is quite limited.

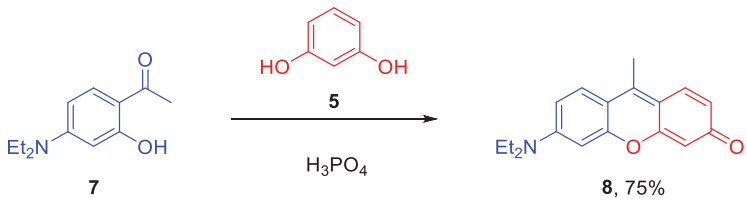

Scheme 4. The synthesis of rhodol **8** from acetophenone **7**.

A modification of the original method, employing monothioresorcinol **10** and benzophenone **9**, gives rhodol analogue **11** possessing the endocyclic sulphur instead of the oxygen atom.[50] On the other hand, the substitution of polyphosphoric acid with 50% sulfuric acid causes the conversion of monothioresorcinol into resorcinol, thus, resulting in the formation of O-rhodol instead of S-rhodol. By the time I started my investigation this was the only known example of rhodol with endocyclic sulphur atom.

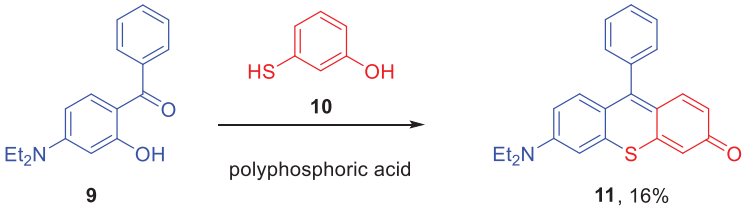

Scheme 5. The synthesis of rhodol with the endocyclic sulphur atom.

One of the most uncommon method is the condensation of phthalimide with *m*-aminophenols in the presence of sulfuric acid.[74] The authors apply double excess of aminophenol **13**, that surprisingly do not result in the formation of **Rhodamine 110**, but leads to the cleavage of C-N bond to form rhodol **14**.

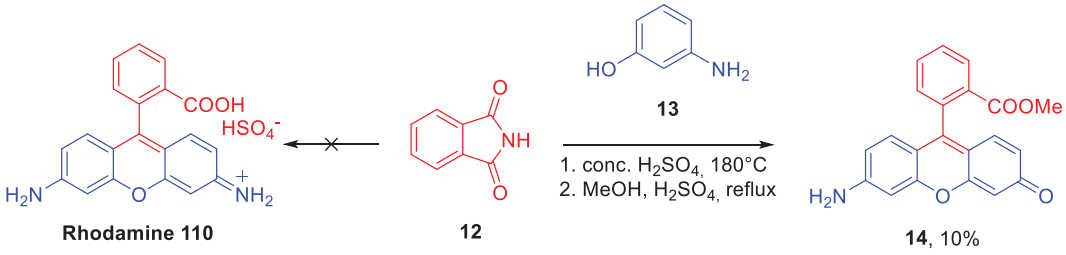

Scheme 6. Rhodol formation from phthalimide.

The use of substituted unsymmetrical phthalic anhydrides for rhodol synthesis via 'classic' method results in the formation of the mixture of 5- and 6-substituted derivatives. The separation of these isomers is challenging and in some cases is even impossible. However, Chevalier has offered the solution to this issue.[75–77] His group has discovered that it is more convenient to use functionalized aldehydes, instead of phthalic anhydride derivatives, together with 8-hydroxyjulolidine. The intermediate **17** formed after the reaction of julolidine **16** with aldehyde **15** next undergoes the reaction with resorcinol affording rhodol **18** (Scheme 7). This type of Friedel-Crafts reaction is more common for synthesis of fluoresceins or rhodamines than for rhodols. Condensation of aldehyde with resorcinol or *m*-aminophenols affords methine intermediate which is more reactive than starting aldehyde, hence, the further reaction with second molecule of the substrate proceeds immediately and results in the formation of symmetric dye (rhodamine or fluorescein). That means that these conditions without any adjustment are not suitable for synthesis of unsymmetrical rhodols. Chevalier's group has solved this problem utilizing modern techniques, like RP-HPLC for analysis and purification. Furthermore, chromatography fractions need to be lyophilized. This method was applied to various aminophenols affording new rhodols.

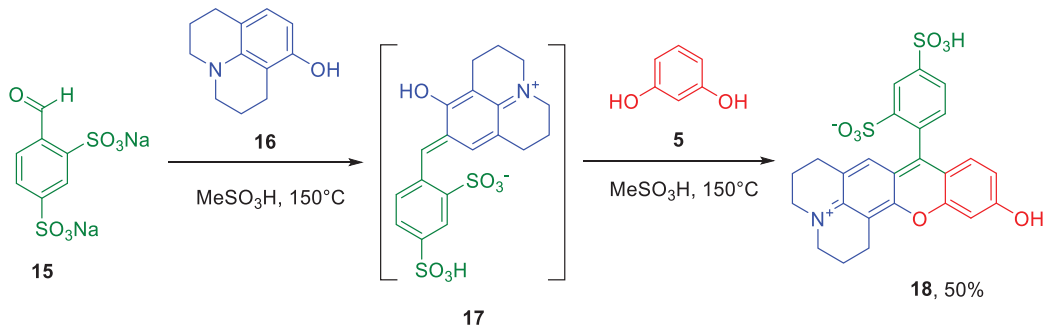

Scheme 7. Rhodol synthesis starting from benzaldehyde and 8-hydroxyjulolidine.

A more advanced synthetic route towards the rhodol chromophore is based on the preparation of the corresponding xanthone followed by the arylation with organo-metallic reagents (Scheme 8). This general strategy was utilized for the synthesis of both rhodamines and rhodols. The most challenging part is the preparation of the suitable xanthone scaffold, which allows for the modification of the main rhodol skeleton that is impossible to perform applying the conventional methods. This approach was used to prepare Singapore Green.[78] It starts from the condensation of 2-chloro-4-nitrobenzoic acid **19** and 3-acetamidophenol **20**, followed by the substitution of the amino with the alkoxy group. Consecutive reduction and protection afford compounds **24** and **25**. The following arylation and deprotection results in formation of Singapore Green dyes **26** and **27**.

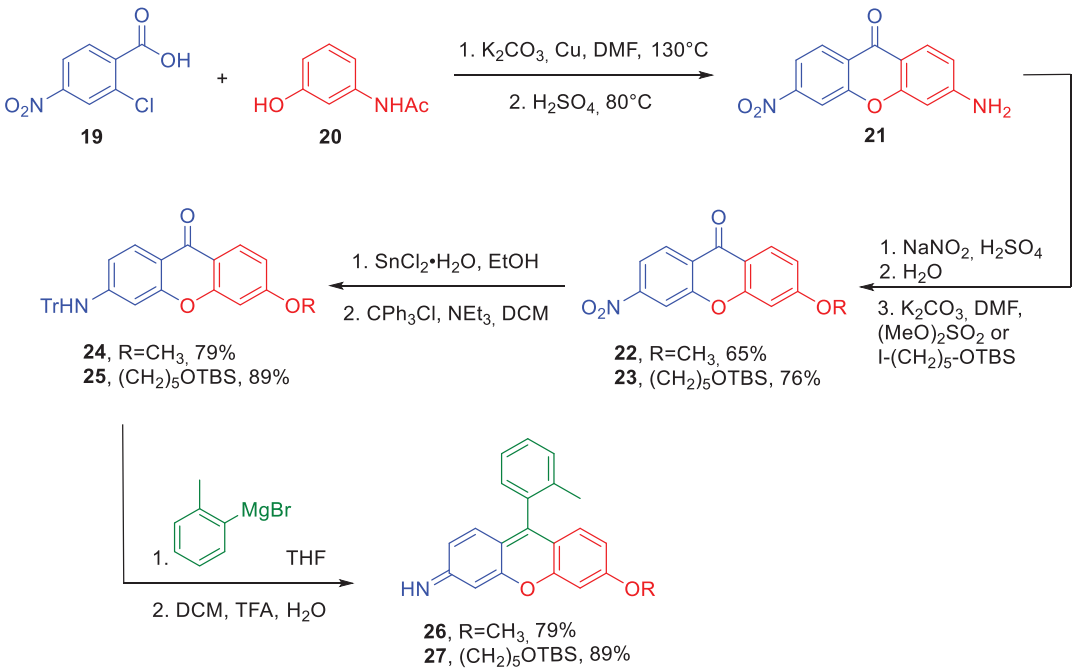

Scheme 8. The synthesis of Singapore Green **26** and **27**.

Alternatively, substitution of *meso*-position of xanthone can be beneficial in combination with a triflation of both hydroxy groups, followed by the amination of one of them (Scheme 9).[79,80] The subsequent quenching of the remaining triflate group, its further protection with *tert*-butyldimethylsilyloxy group and arylation lead to the formation of the variety of rhodols **36-39**. The method has a great potential to increase the scope of new rhodols by the preparation of the rhodol heteroanalogues on the one hand, and introducing a plethora of secondary and tertiary amines on the other hand.

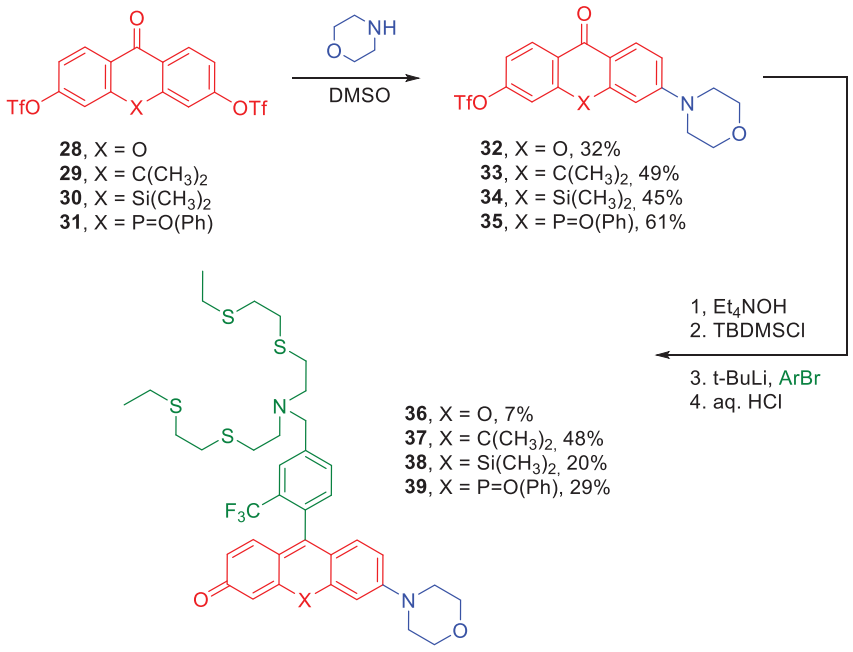

Scheme 9. General synthesis of rhodols from xanthone derivatives.

Another alteration of this procedure starts from fluorescein possessing carboxylic group in lactone form. In the original procedure one hydroxy group undergoes protection with MOMCl, while another one is transformed into triflate yielding compound **40** (Scheme 10).[81,82] The subsequent amination in the presence of Pd catalyst, followed by deprotection of another OH group results in formation of a range of rhodols **41a-p** possessing different amino groups. This approach with a few slight modifications was successfully applied in the investigations by some other scientific groups.[82–87] The reactivity of the carboxylic groups in the benzene ring at the *meso*-position is quite different so these can be converted independently.[88]

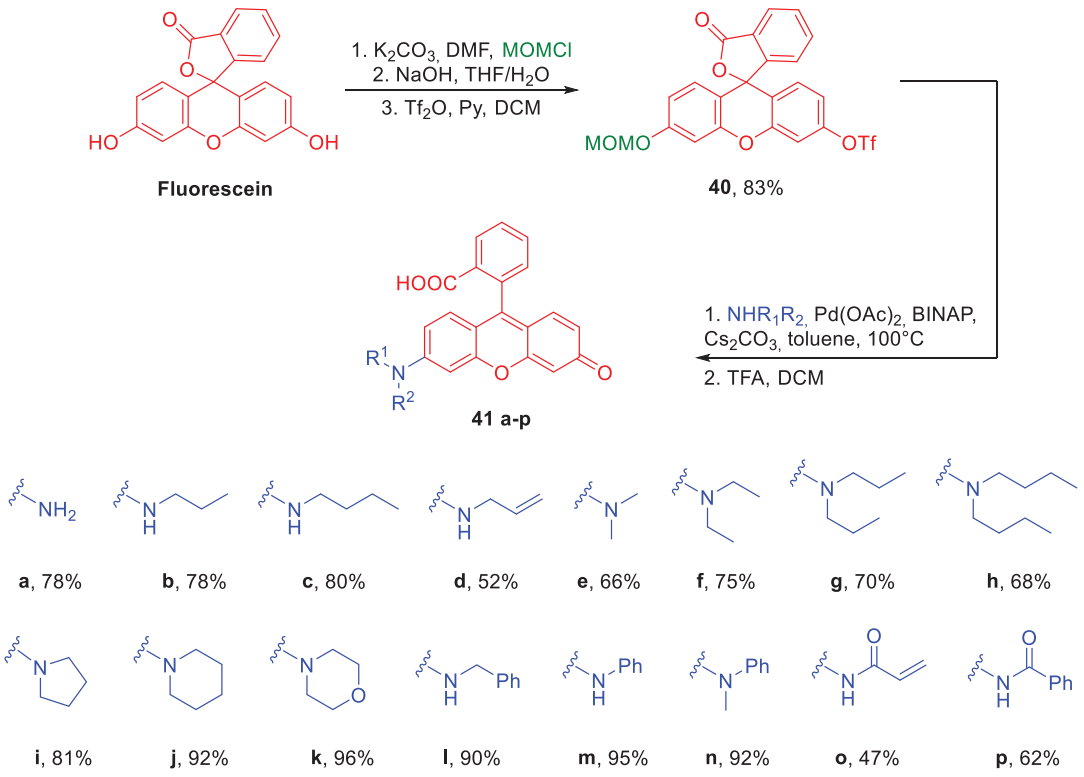

Scheme 10. Synthesis of rhodols possessing various amino substituents via the catalyzed amination of fluorescein.

The following method shows a partial analogy with the amination of triflated fluoresceins. Fluorescein derivatives like Pennsylvania Green (**42**) can undergo the substitution of hydroxy group with the iodine atom, followed by the Buchwald-Hartwig amination reaction with microwave irradiation resulting in the formation of rhodol **44** (Scheme 11).[89]

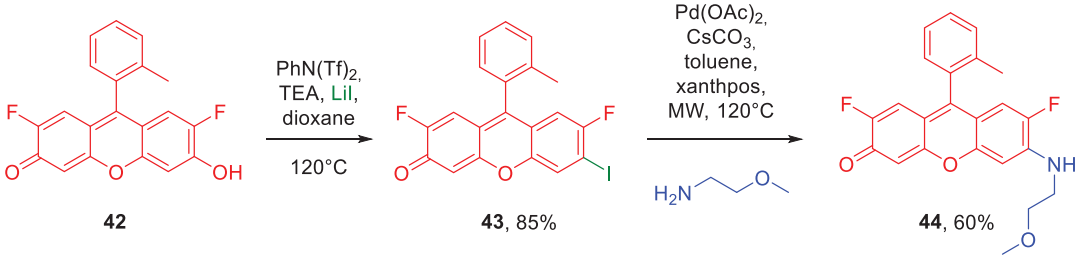

Scheme 11. Rhodol preparation method via iodine derivative of fluorescein.

6.2.2 Synthesis of π-expanded rhodols and 'rhodol-type merocyanines'

Seminaphthorhodafluors or 'SNARFs' are also members of rhodol family. These molecules possess a substituted naphthalene moiety instead of benzene from the side of hydroxy group. Initially, the authors have utilized 1,6-naphthalenediol **47** and 4-diethylamino-2-hydroxybenzophenone derivative **4** in the presence of methanesulfonic acid (Scheme 12).[56] This is an another alteration of the routine rhodol synthesis in which resorcinol is substituted with various naphthalenediols. In some cases carboxylic group at the upper ring undergoes esterification to facilitate the purification process of products.

Originally abbreviation 'SNARF' corresponded only to the rhodols obtained in the reaction with 1,6-naphthalenediol by Haugland's group in 1991.[56] However, in following publications authors have applied this name to fluorophores obtained from another naphthalenediols, including benzocoumarin **51**.[55,90–96]

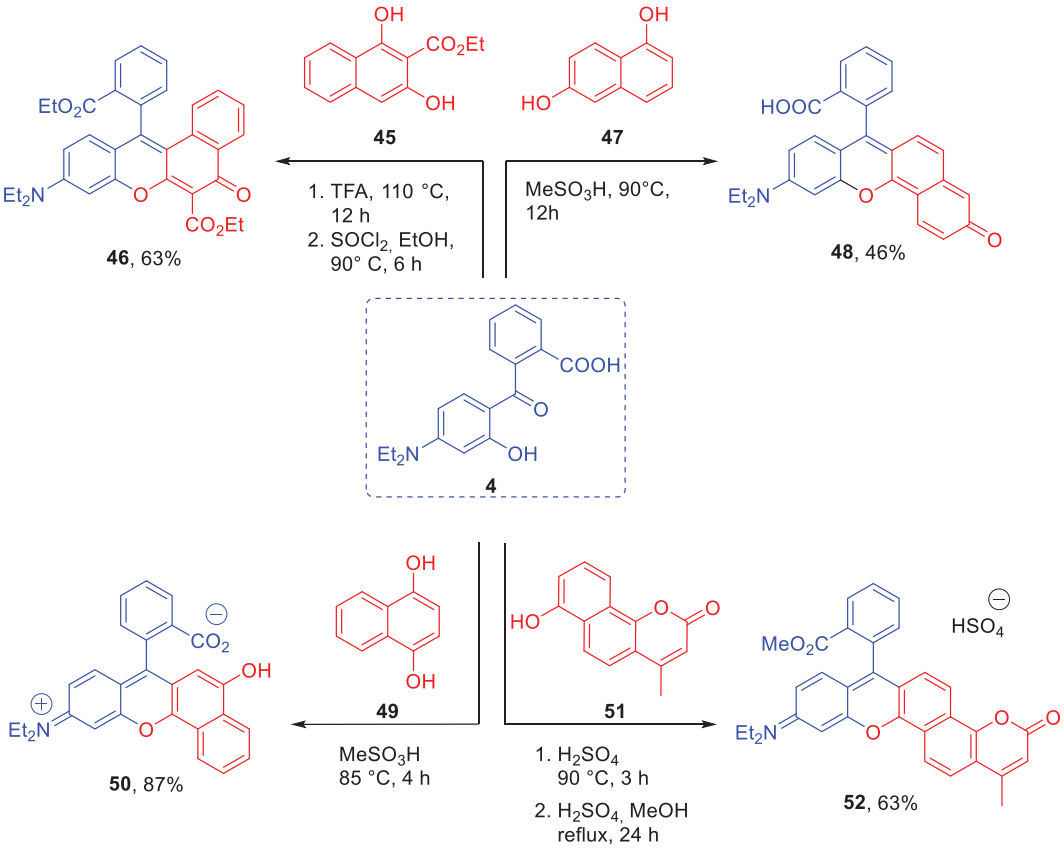

Scheme 12. Preparation of seminaphthorhodafluors.

The use of aldehyde **15** and *m*-aminophenol instead of ready benzophenone is the adjustment of the abovementioned method. The one pot reaction of compounds **15** and **16** together with 1,6-

naphthalenediol **47** in the presence of phosphoric acid using microwave irradiation leads to the formation of rhodol **53** (Scheme 13).[97] This approach suffers from several significant drawbacks: low yield of rhodol (due to the formation of corresponding fluorescein in large amounts) as well as the difficulties with products' separation and purification. Meanwhile, Chevalier's group has managed to receive the same product in 43% yield applying two-step method, which was already mentioned (Scheme 7).[75]

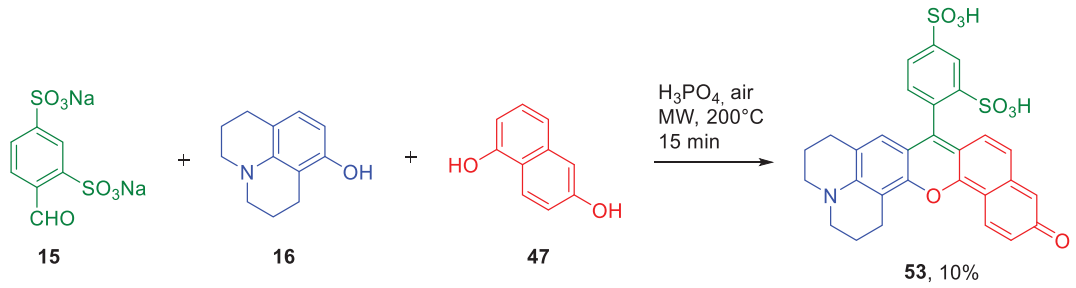

Scheme 13. One-pot three component method for SNARF preparation.

Exceptional representatives of π-expanded rhodols are fluorophores possessing naphthalene fragment from amino side. This can be probably explained by difficulty of synthesis of the corresponding substrates for such reversed ring configuration in comparison to the original pattern. Rhodol **56** was obtained as a result of condensation between 1-hydroxy-6-piperazine-naphthalene (**55**) and benzophenone **54** in the presence of trifluoroacetic acid (Scheme 14).[44]

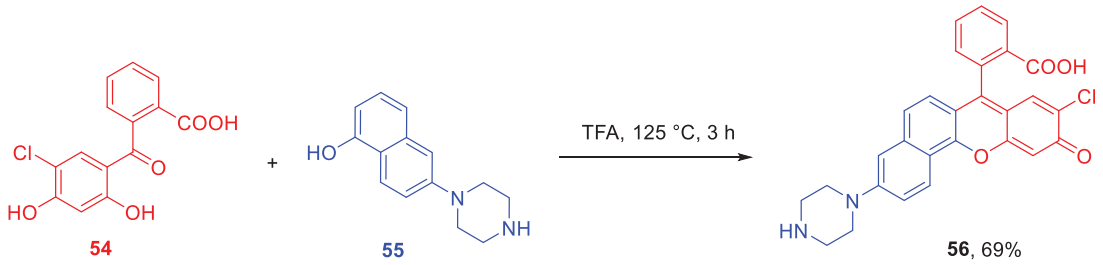

Scheme 14. Reversed substrate pattern method for synthesis of naphthorhodol.

The aryl moiety at position 9 typically does not influence the photophysical properties since it is located orthogonally to the main chromophore scaffold. Linking of the aryl fragment to the xanthene core gives rise to so-called V-shaped dyes.[98,99] Even though the expansion is not caused by addition of another benzene ring, additional bond between aryl and xanthene moieties introduces π-expansion, so compounds **60-62** can be still formally classified as π-expanded rhodols (Scheme 15).

Firstly, the authors have synthesized a V-shaped fluorescein **57**, which revealed to have a significant bathochromic shift of both absorption and emission maxima in comparison to original fluorescein. However, poor solubility and low quantum yield diminished the advantages. To improve the spectroscopic properties authors modified the core incorporating piperidine moieties. Thus, fluorescein **57** was subjected to the triflation procedure, followed by the amination of the obtained intermediates **58** and **59** with piperidine. As a result 3 rhodol derivatives **60-62** formed as well as a V-shaped rhodamine **63** as a minor product. In comparison to fluorescein **57**, these products exhibit higher fluorescence quantum yields and the red-shifted both absorption and emission maxima.

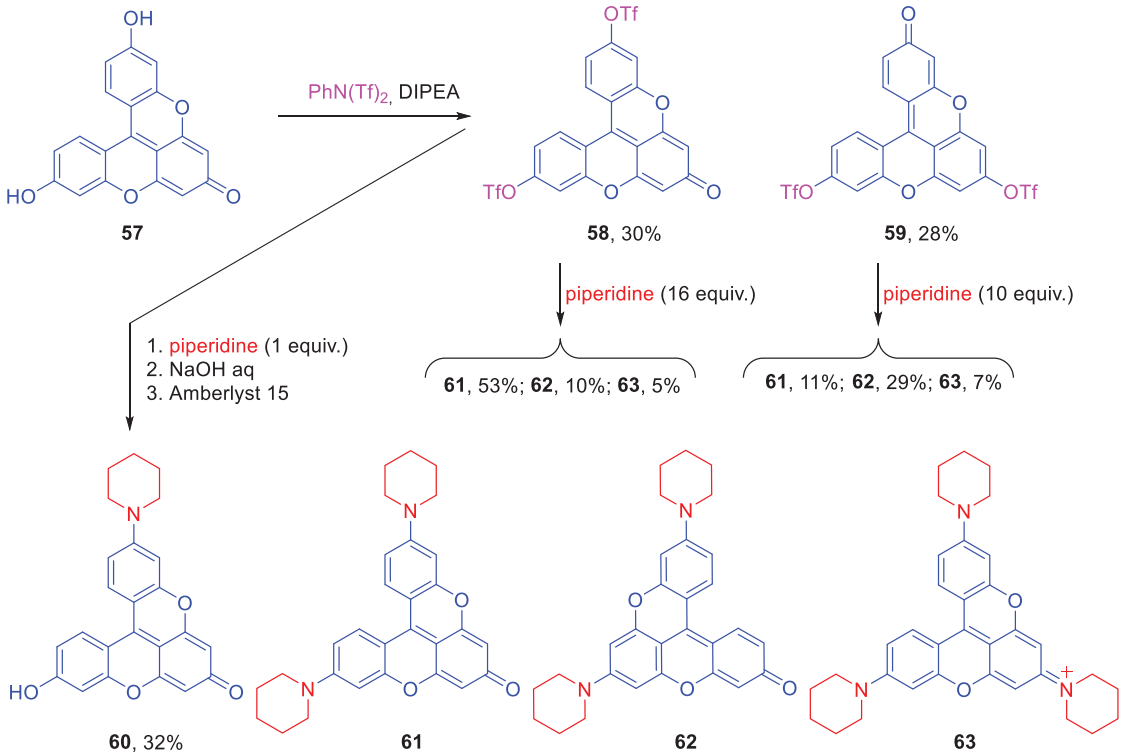

Scheme 15. Preparation of V-shaped rhodol derivatives.

6.2.3 Synthesis of rhodols with an endocyclic heteroatom

Another strategy to change the photophysical properties of merocyanine dyes is substitution of bridging oxygen atom with carbon, silicon, selenium or phosphorus containing fragments (Figure 3). The modifications of the rhodol core in this regard can be achieved in various manners.

Similarly to previously reported fluorescein and rhodamines,[30,31,102,51,53,55,61,64,65,100,101] the substitution of the endocyclic electron-donor oxygen atom in rhodol scaffold with more electron-deficient silica, selenium or phosphorus containing moieties as well as carbon fragment leads to the bathochromic shift of both absorption and emission maxima. Furthermore, rhodols with phosphine oxide moiety exhibit an extraordinary photostability,[5] compared to that of C-substituted rhodols.[9] The orbital interaction between the newly incorporated bridging moiety and xanthene scaffold leads to the red-shifted absorption and emission properties. This effect can be enhanced by introduction of more electron-withdrawing moiety.

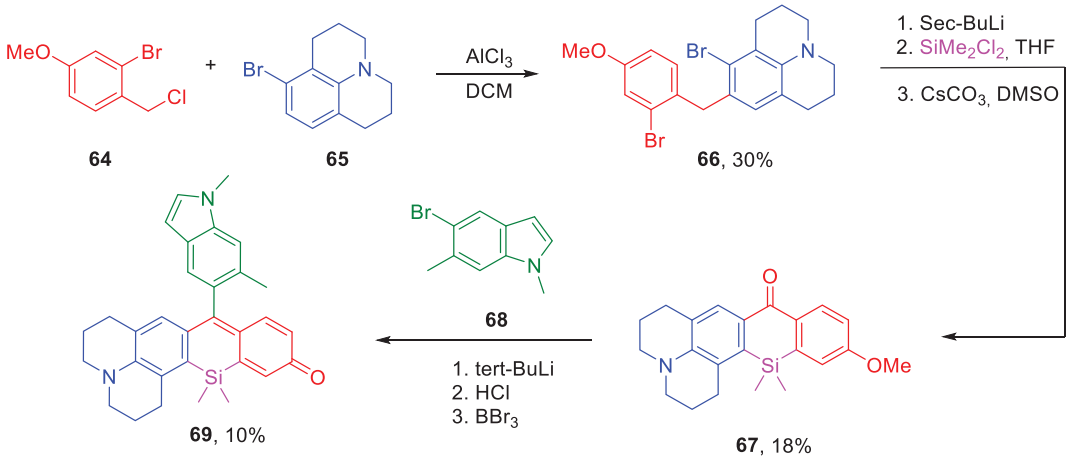

Scheme 16. Preparation of Si-rhodols.

A few approaches towards Si-rhodols were reported. One of them is based on synthesis of the silicon-containing xanthone **67** starting from 8-bromojulolidine **65** and 2-bromo-4-methoxybenzyl chloride **64**, followed by ring closure via silylation and oxidation of methylene fragment (Scheme 16).[103] The subsequent arylation of xanthone **67** and deprotection of hydroxy group results in formation of Si-rhodol **69**.

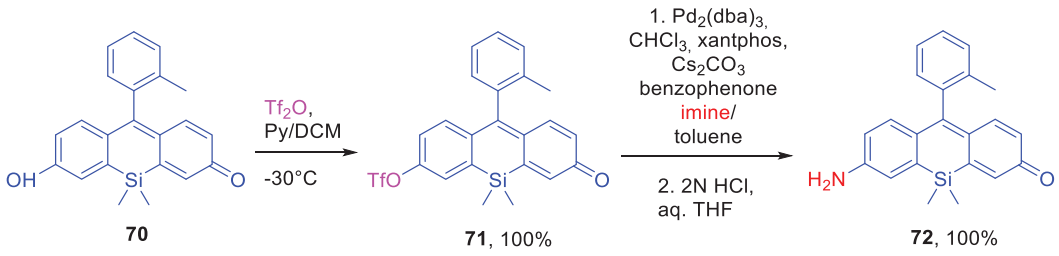

Scheme 17. Preparation of Si-rhodols via Pd-catalyzed amination of the corresponding fluorescein.

Another approach towards Si-rhodols starts from the corresponding fluorescein analogue **70**,[104] which is subjected to the triflation of hydroxy group and its following substitution with amino group in the Pd-catalyzed conditions (Scheme 17).[105]

The preparation method for the carborhodols is the most complex among other rhodol analogues. The synthetic approach consists of 11 steps and proceeds through the formation of unsymmetric xanthone derivative **77** possessing carbon bridge, followed by the arylation and deprotection od hydroxy group (Scheme 18).[106]

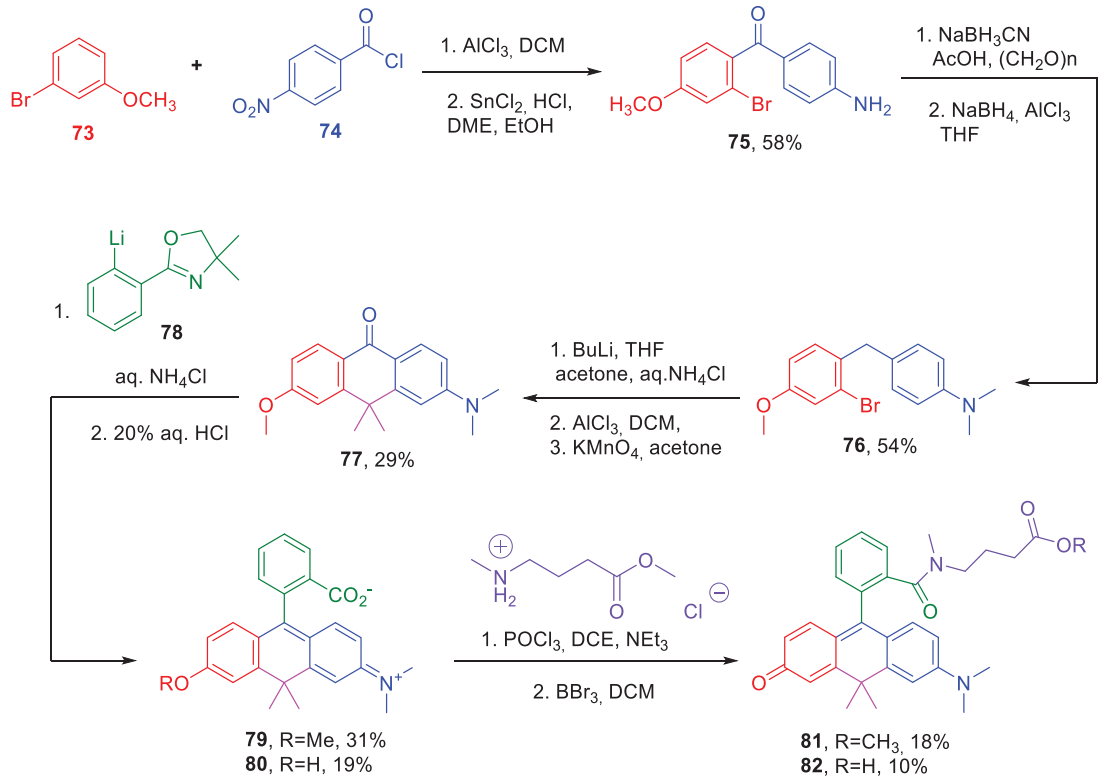

Scheme 18. Preparation of C-rhodols.

The transformation of rhodamines into rhodols via hydrolysis was first reported in the end of 20th century.[27] This method seemed to be inefficient with classic oxygen-bridged rhodamines, thus, it was forgotten for many years. However, rhodamines possessing electron-withdrawing endocyclic heteroatom appeared to be more reactive in terms of the hydrolysis to form rhodols. Thus, P=O-bridged rhodamines **84-87** easily undergo substitution of diethylamino moiety with the oxygen atom under basic conditions resulting in formation of P=O-rhodols **88-91** in high yields.[107] The use of highly concentrated solutions of sodium hydroxide leads to the formation of the corresponding fluoresceins. The authors also emphasize that the presence of a bulky substituent at *ortho*-position

of aryl moiety is crucial to avoid nucleophilic attack of the hydroxyl ion at position 9, that leads to the breaking of chromophore conjugation and, thus, to discoloration.

The same approach was utilized for the synthesis of fluorene analogue of rhodol. Grzybowski et.al. has performed an unprecedented synthesis of rhodamine analogues, which possess central five-membered ring instead of 6-membered heterocycle.[108] Such rhodamine **91** was subjected to the hydrolysis reaction in the presence of NaOH resulting in the formation of rhodol analogue **92** (Scheme 19).

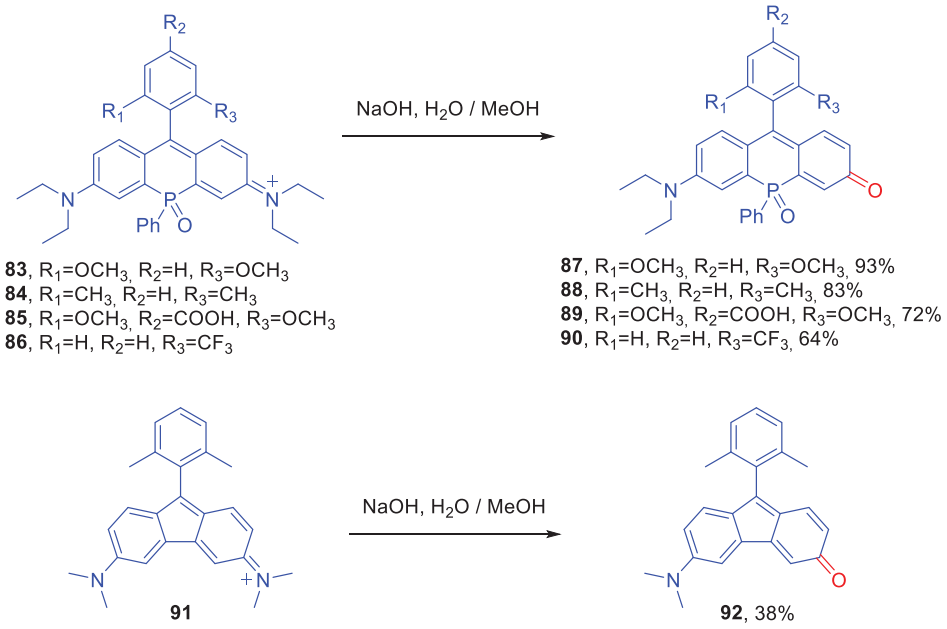

Scheme 19. Formation of the rhodol-type chromophore via the hydrolysis of corresponding rhodamines.

Rhodols bearing endocyclic selenium atom are known as well and can be obtained starting from transformation of 3-bromo-N,N-diethylaniline **94** into diselenide **95**.[109] This method was originally used for synthesis of rhodamines containing endocyclic selenium atom.[110,111] I this case, to obtain rhodol **98** the authors had to couple diselenide **95** with allyloxybenzamide **96** affording xanthone **97** and then to perform arylation and deprotection of hydroxy group.

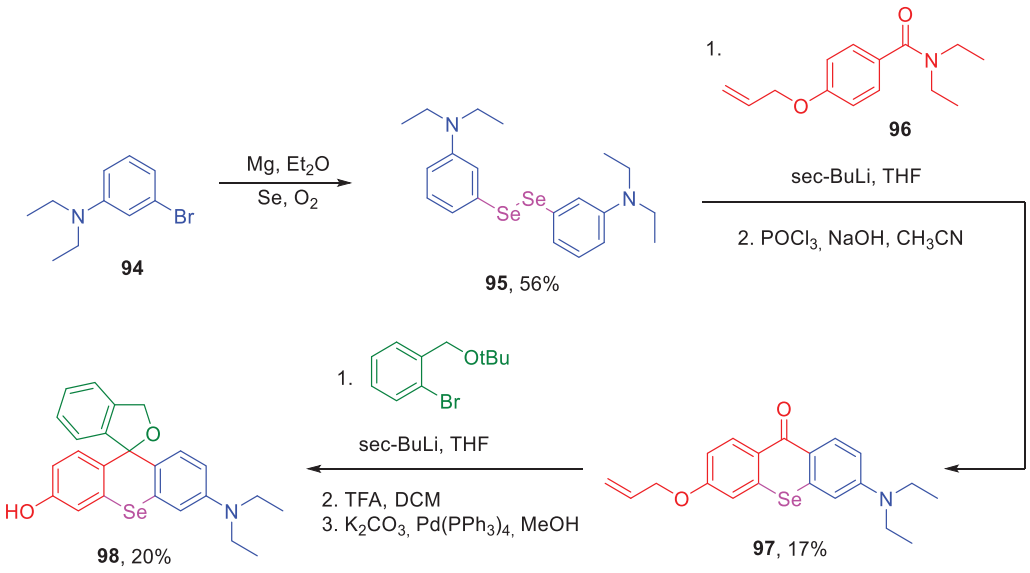

Scheme 20. Preparation of Se-rhodols.

To sum up, all synthetic approaches towards rhodols can be differentiated into 3 general techniques: (a) condensation of aromatic 4-amino-2-hydroxyketones with resorcinols or vice versa – 2,4-dihydroxybenzophenons with *m*-aminophenols, (b) formation of the correspondent xanthones and their further arylation and (c) catalytic amination of the appropriate fluorescein derivative. Besides, there are some methods for the preparation of individual compounds without the possibility of employing them as a general synthetic approach (e.g. Schemes 5 and 6). Besides, the syntheses of rhodol analogues possessing endocyclic heteroatoms different from oxygen still are not developed enough. Formation of C-rhodols is the most challenging and rhodols possessing sulfur groups were unknown. Another issue is synthesis of π-expanded rhodols. Even though there were several reports about these compounds, still their formation and the usage are challenging due to the unavailability of the substrates, difficulty in their synthesis, low yields due to side reactions or poor solubility of products making them inappropriate for further studies.

6.3 Results and discussions

6.3.1 Red emissive sulfone-rhodols as mitochondrial imaging agents

By the time I started my first project, I had performed literature search and found out that there was only one example of rhodol with endocyclic sulfur atom.[58] Besides, there was no single report on rhodols containing sulfone or sulfoxide fragment either.[16] Taking into consideration that C-, Si-, Se- and P-rhodols possess red-shifted absorption and emission maxima, higher quantum yields and better photostability in comparison to O-rhodols, I have concluded that considering electron-withdrawing properties of the SO_2 moiety, SO_2-rhodols may exhibit even better photophysical properties than other representatives of this family. Since P=O rhodamines successfully undergo transformation into rhodols due to the presence of electron-withdrawing P=O moiety,[107] I expected that the presence of stronger SO_2 group should accelerate such reaction as well. I have started my work from synthesis of the scope of sulfone-rhodamines using the earlier reported synthetic approach, which starts from crosslinking of 4,4′-methylenebis(N,N-dimethylaniline) **98** with oleum.[31] At this point I decided to substitute oleum with chlorosulfonic acid, since it is more commercially available and more convenient to work with (Scheme 21). As a matter of fact I have received a product **99** with yield slightly higher than in the original method. The conditions of the subsequent oxidation were altered as well. I have utilized sodium hydroxide in the presence of TBAB instead of iron (III) chloride in hydrochloric acid and obtained xanthone **100** in 83% yield (35.7% in the original approach).

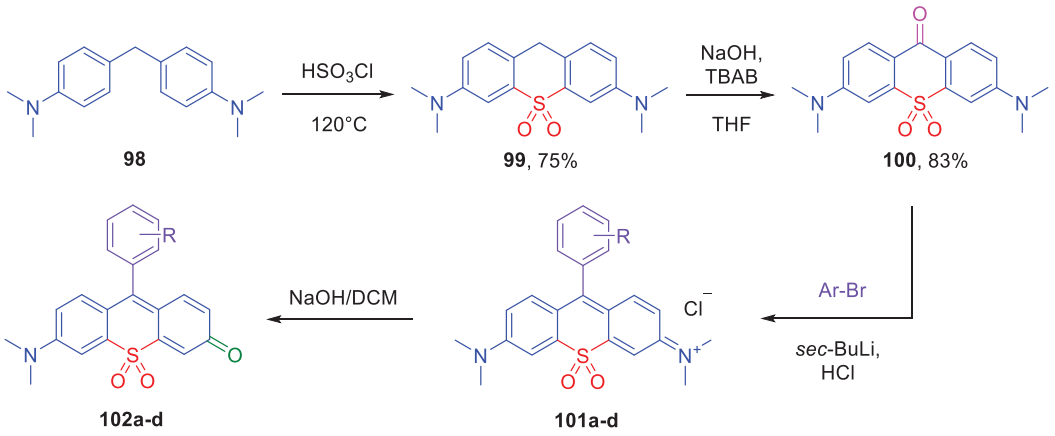

Scheme 21. Synthetic procedure for SO_2-rhodols

Another controversy was the choice of aryl bromides for future rhodamines. It was very important to choose the most fitting substituents in SO_2-rhodols, because even small structural changes can influence the photophysical properties. The attack of nucleophile at C9-position of unhindered rhodols leads to the interruption of the π-conjugation and, thus, to the decoloration.[101] Besides, this substituent had to be bulky enough to prevent the addition of nucleophile. For example, P=O-rhodols possessing methyl group in *ortho*-position undergo nucleophilic attack under basic conditions, because CH_3 group is not big enough to shield carbon in *meso*-position, while CF_3 or OMe, manage to prevent disruption of chromophore's π-conjugation system.[107]

For this reason, I have chosen anthracene and aryls possessing trifluoromethyl and methoxy group in *o*-position. Despite my expectations, I was not able to obtain pure SO_2-rhodamines **101a-d**. Mass analysis showed that there was always a second rhodamine possessing a monomethylamino moiety due to the cleavage of one methyl group. It was impossible to purify products using column chromatography with any liquid or solid phases. Recrystallization did not help either. I decided to use these rhodamines in next step without any purification. The subsequent hydrolysis cleanly afforded SO_2-rhodols **102a-d** (Figure 4).

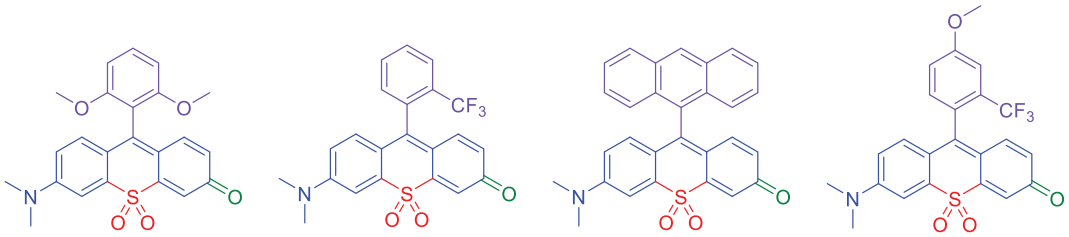

Figure 4. Obtained sulfone-rhodols **102a-d**

The subsequent idea was to modify one of the obtained rhodols by introduction of triphenylphosphonium salt to make it suitable for cell imaging. For this reason, I have performed cleavage of methyl group of rhodol **103d** followed by monoalkylation with 1,6-dibromohexane (Scheme 22).

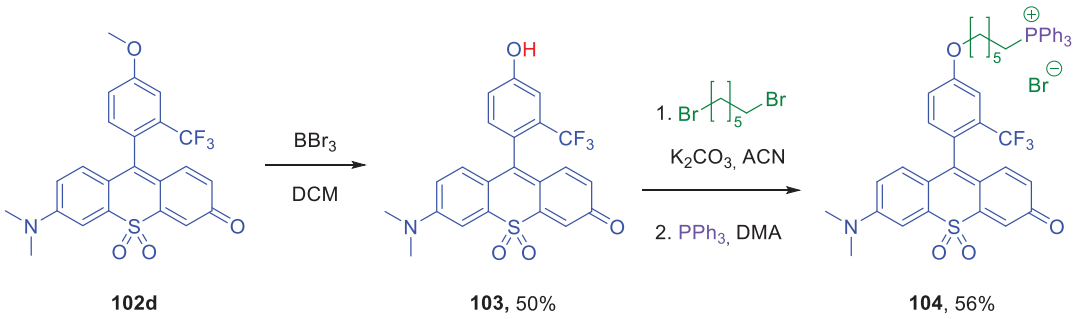

Scheme 22. Synthesis of rhodol for mitochondria imaging

The further reaction with triphenylphosphine leads to SO_2-rhodol **104**. The last step is very unreliable, since even small changes can influence the conversion, purity and yield. It should be conducted under inert atmosphere, at high temperature with 10 eq. of PPh_3 and short reaction time. Unfortunately, both substrate and product decompose if the reaction time is prolonged. Compound **104** was successfully used for staining mitochondria in cardiac H9C2 cell line.

As I expected, fluorophores **102a-d**, **103** and **104** exhibited red-shifted absorption and emission maxima in comparison to the classic rhodol. Besides, they demonstrated a significant positive solvatochromism: from λ_{abs} = 543 − 553 nm in toluene to λ_{abs} = 667− 669 nm in H_2O/DMSO mixture (Figure 5).

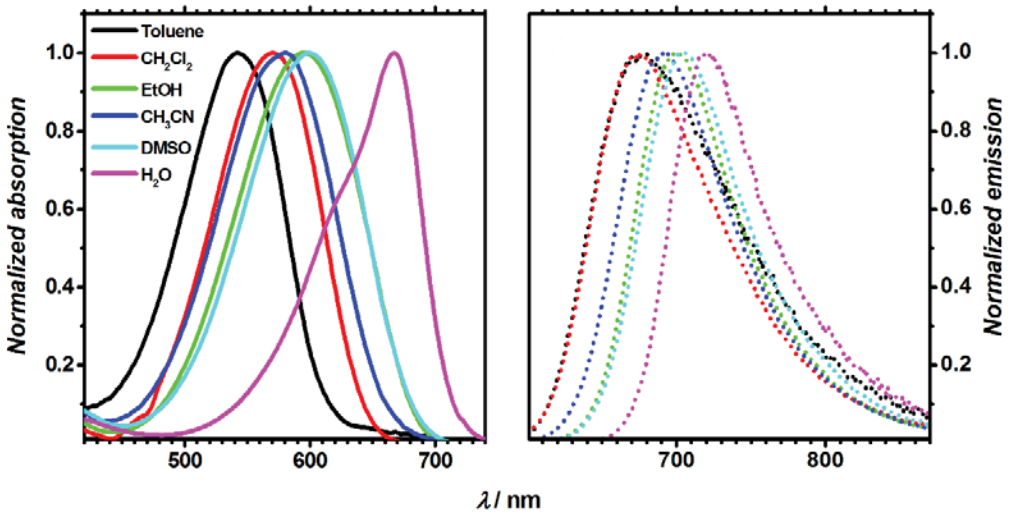

Figure 5. Absorption (solid) and emission (dotted) spectra of rhodol **102a** in different solvents.

These compounds possess high quantum yields in polar solvents − around 0.5 in ethanol, acetonitrile and DMSO with brightness up to 35,000×M^{-1}×cm^{-1}. The only exception is rhodol **102c** – the quantum yield of this compound is low in any solvent (from 0.01 in DMSO to 0.13 in DCM).

Another advantage of these new core-modified rhodols is their photostability. Dyes **102a** and **103** displayed excellent photostability comparable to that of Rhodamine 6G and Cresyl Violet.

6.3.2 Direct transformation of coumarins into orange-red emitting rhodols

Next project was focused on the idea of transformation of coumarins into rhodols. The root of this concept goes back to the work reported by Gandioso et.al, which based on the transformation of coumarin's lactone group into thiolactone (C=S) to make it reactive enough for the condensation with activated CH_2 group.[112,113] First, I tried to apply this approach to a few bis-coumarins,[114] to which I had access, to obtain new V-shaped rhodols. I have managed to obtain bis-thio derivatives, but these compounds revealed to be too capricious and unstable in the reaction mixture. The final second step was very challenging and the product I obtained displayed poor solubility. Then I decided to change the reaction platform to start from compounds which would express similar reactivity. First, I synthesized a scope of 3-formyl coumarins **108a-h** (Scheme 23).

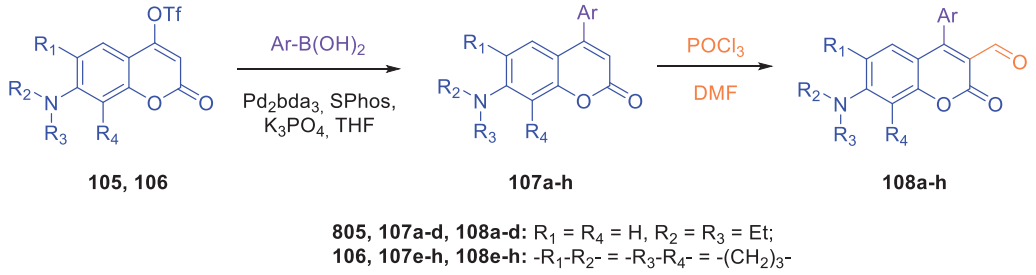

Scheme 23. Synthesis of 3-formyl-4-arylcoumarins.

This approach proceeded through the already known formation of 4-hydroxy coumarins from *m*-aminophenols and 'magic malonate' followed by triflation of the hydroxy group.[115–117] Next I performed Suzuki reaction with various aryl moieties to afford coumarins **107a-h**. The following formylation allowed me obtaining 3-formyl coumarins **108a-h** in reasonable yields (Table 1).

Table 1. Yields of compounds **107a-h** and **108a-h**

Nr	R_1	R_2	R_3	R_4	*Ar*	*Yield, %*
107a	H	Et	Et	H	*o*-tolyl	97
107b	H	Et	Et	H	2,6-dimethoxyphenyl	76
107c	H	Et	Et	H	2,3-dimethoxyphenyl	92
107d	H	Et	Et	H	pyrenyl	86
107e	$-(CH_2)_3-$		$-(CH_2)_3-$		*o*-tolyl	90

107f	-$(CH_2)_3$-		-$(CH_2)_3$-	2,6-dimethoxyphenyl	94
107g	-$(CH_2)_3$-		-$(CH_2)_3$-	2,3-dimethoxyphenyl	89
107h	-$(CH_2)_3$-		-$(CH_2)_3$-	2,4-dimethoxyphenyl	84
108a	H	Et	Et H	*o*-tolyl	60
108b	H	Et	Et H	2,6-dimethoxyphenyl	50
108c	H	Et	Et H	2,3-dimethoxyphenyl	28
108d	H	Et	Et H	pyrenyl	80
108e	-$(CH_2)_3$-		-$(CH_2)_3$-	*o*-tolyl	84
108f	-$(CH_2)_3$-		-$(CH_2)_3$-	2,6-dimethoxyphenyl	87
108g	-$(CH_2)_3$-		-$(CH_2)_3$-	2,3-dimethoxyphenyl	86
108h	-$(CH_2)_3$-		-$(CH_2)_3$-	2,4-dimethoxyphenyl	32

The following step was to perform the reaction between 3-formylcoumarin **108a** and Lawesson's reagent. Unfortunately, I did not manage to obtain the desired product and the use of P_2S_5 did not help either. Meanwhile, I decided to try the direct transformation of 3-formylcoumarins into rhodols without the conversion into the intermediate thione.

My first attempt was performed with 4-tolyl-3-formylcoumarin **108a** and dimethyl 1,3-acetonedicarboxylate in the presence of $InCl_3$ and acetic acid anhydride. As a matter of fact, I have obtained a mixture of lots of products, in which I have managed to identify and purify the desired rhodol **109**. However, the yield was extremely low and the purification required several chromatographic steps. Thus, I have embarked on the long optimization choosing coumarin **108a** and dimethyl 1,3-acetonedicarboxylate as model substrates. In numerous attempts I have altered acidic and basic catalysts, solvents as well as temperature and the reaction time. Finally, I have found that the best results I observed when 2,6-lutidine was used. The yield of the product **X** was 26%. However, when I tried to perform this reaction with coumarin **108b** I faced another issue: there was no substrate in the mixture, but there was a lot of unreacted intermediate (e.g. **109a**) even after 24h of heating.

At this point I had to start another optimization to find better conditions. Together with Dr. Poronik I have found, that substrate, intermediate and final product have yellow, orange and pink colours respectively that prompted us to the idea, that reactions for optimisation can be performed in very small scales and the conversion can be monitored using spectrophotometer. On the basis of the Lambert-Beer law, I was able to calculate concentrations of the substrate, intermediate and the product to find the reaction conversion and the product yield. Characteristic band of rhodol was 537 nm, while for substrate **108b** and intermediate it was 437 nm and 448 nm respectively. This optimization technique enabled screening multiple reaction conditions in short time. Eventually, I

found that the best catalytic system is a piperidine in methanol. The final step in the optimization was to analyse how the excess of dimethyl 1,3-acetonedicarboxylate influences the reaction kinetics. I have checked the rate of condensation with 2, 5 and 10 eq. of dimethyl 1,3-acetonedicarboxylate and the best results were achieved with 10 eq. of the diester. The main drawback of this method is that acetonedicarboxylate is a highly reactive compound capable to undergo self-condensation along with numerous other undesired processes in the presence of piperidine. These by-products possess characteristic bands in the electronic spectrum which can overlap with the diagnostic peaks, thus making the visualization method less precise.

The double Knoevenagel condensation allows to obtain a range of new rhodols **109 – 116** (Scheme 24).

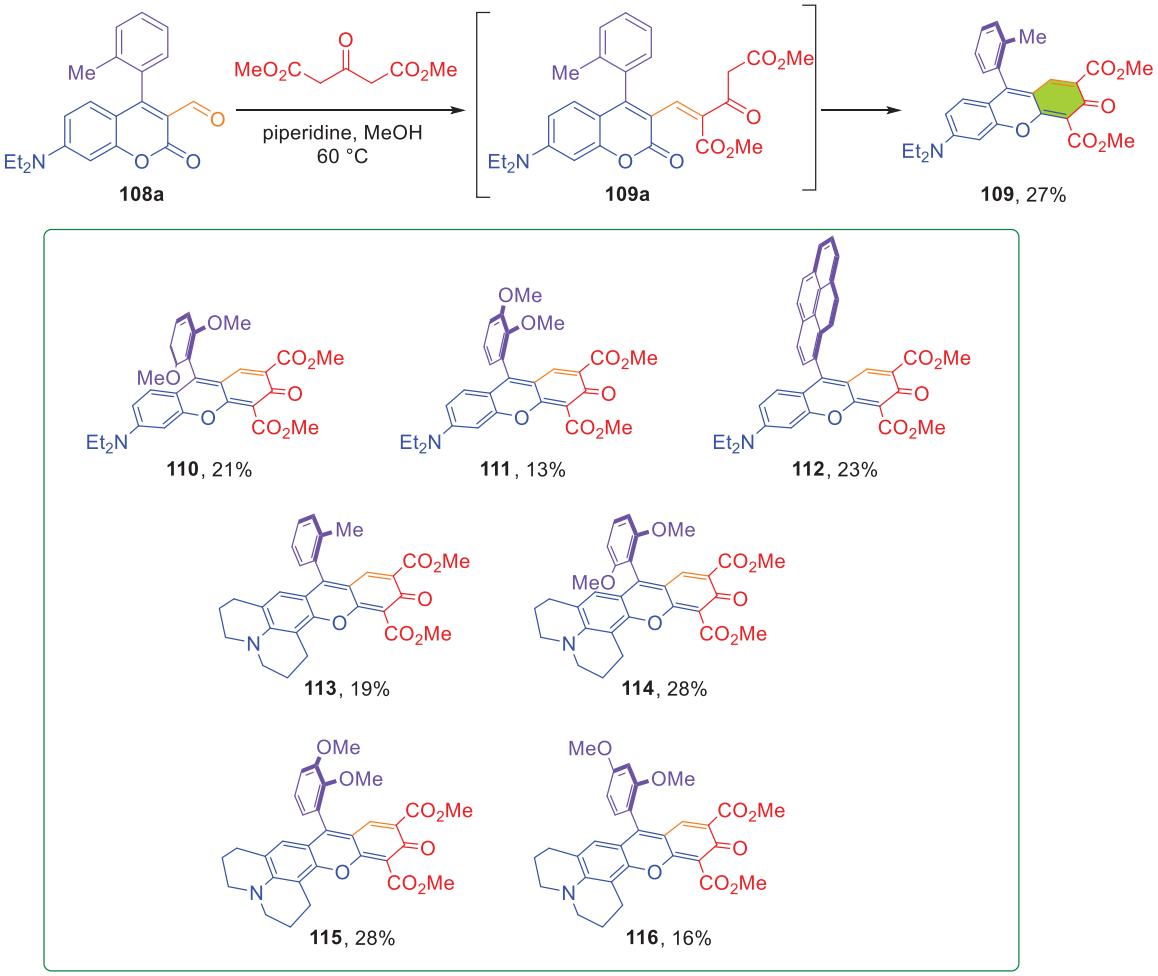

Scheme 24. Knoevenagel condensation of 3-formylcoumarin with dimethyl 1,3-acetonedicarboxylate and scope of the obtained rhodols

These new dyes absorb light around 535-560 nm and emit at 560-590 nm (Figure 6). They do not possess a significant positive solvatochromism, like the majority of other merocyanine dyes, however, they display large fluorescence quantum yields: 0.47 – 0.68 for rhodols **109-112** and 0.86 – 1.00 for dyes **113-116**.

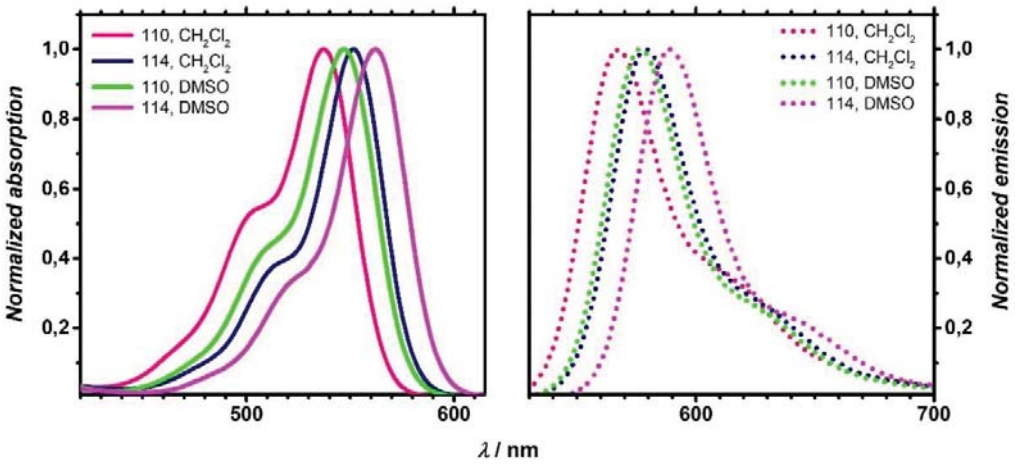

Figure 6. Absorption (solid) and emission (dotted) spectra of rhodols **110** and **114**.

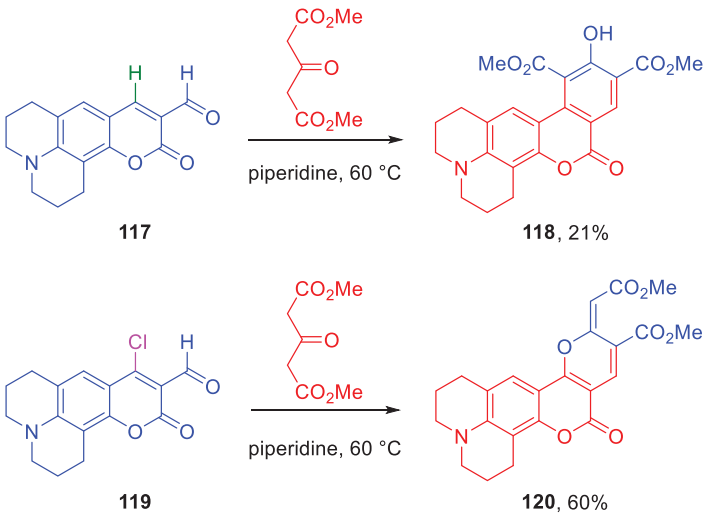

117 **118**, 21%

119 **120**, 60%

Scheme 25. Condensation of other 3-formylcoumarins with dimethyl 1,3-acetonedicarboxylate

I was curious whether applying this method I would be able to obtain rhodols with unsubstituted position 9 or with chlorine atom at C9, which could be suitable for further modifications. For this

reason, I have utilized the corresponding coumarins **117** and **119**. To my surprise, I did not observe even a trace of expected rhodols (Scheme 25). Instead, I had got yellow and red solids with the identical signals in the MS spectrum. The structures were identified by means of X-ray diffraction analysis.

6.3.3 One-step transformation of aminophenols and coumarins into rhodols and 'rhodol-like' merocyanines

My final project was focused on the one-step preparation of rhodols and 'rhodol-like' merocyanines starting from easily available substrates. This idea appeared in reference to the reported earlier procedure of nucleophilic substitution of activated fluoroarenes with phenols.[118] Taking into consideration, that *m*-aminophenols easily undergo the condensation with aldehydes, I concluded, that an appropriate arenes possessing a formyl along with the adjacent position prone to the aromatic nucleophilic substitution can be utilized in synthesis of rhodols. At this point I decided that the best compound for this aim should be 4-hydroxy-2,3,5,6-tetrafluorobenzaldehyde **122**. Since it was not easily available in large amounts, I had to introduce a formyl group into 2,3,5,6-tetrafluorophenol using Duff reaction.[119–121] Next I have employed this compound in the reaction with 1,1,7,7-tetramethyl-8-hydroxyjulolidine **121** in toluene at 60 °C without any additives (Scheme 26). To my satisfaction, I have observed the colour change from white to deep pink and glittering crystals precipitated from the reaction mixture upon cooling. As the yield of rhodols **X** was not acceptable I modified the conditions and found that temperature rise positively affects the reaction outcome resulting in the increase of the reaction yield from 37% to 83%. At the same time other changes i.e. the addition of Lewis acids, bases or the solvent change did not influence the reaction positively (Table 2). I have concluded, that nonpolar solvents and high temperature allow to achieve the highest possible yields without any catalysts or additives.

Table 2. Optimization parameters for reaction of phenol **121** with aldehyde **122**

Entry	**solvent**	**Temp. / °C**	**catalyst**	**time / h**	**yield**
1	toluene	60	none	12	37%
2	toluene	90	none	1	83%
3	toluene	90	$AlCl_3$	1	68%
4	toluene	90	$Sc(OTf)_3$	1	70%
5	toluene	90	2,4,6-tri-*tert*-butylpyridine	1	78%
6	toluene	90	phosphazene base P_1-t-Bu	1	trace amount

7	HFIP	80	none	1	0%
8	mesitylene	165	none	1	75%
9	xylenes	135	none	1	75%

Having the optimised procedure in hands, I decided to apply it to other already available *m*-aminophenols and obtained several new rhodols **124-127**. My next idea was to expand the reaction scope by the synthesis of π-expanded 'rhodol-type' merocyanines.

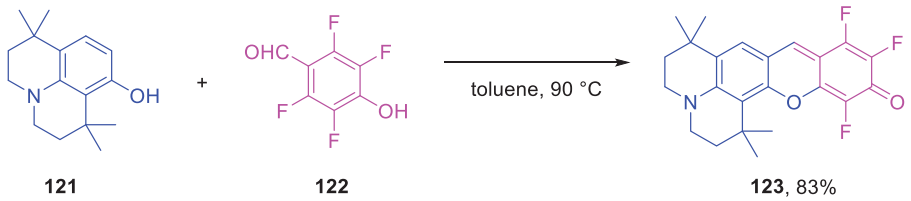

121 **122** **123**, 83%

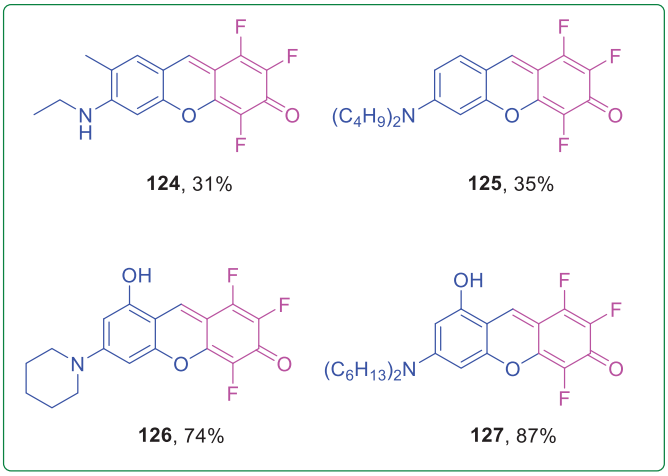

124, 31% **125**, 35%

126, 74% **127**, 87%

Scheme 26. One-step synthesis of rhodols **123-127** from aminophenols and tetrafluorohydroxybenzaldehyde (**122**)

The 7-(dihexylamino)naphthalen-2-ol (**129**) was obtained from 2,7-dihydroxynaphthalene **128** via Bucherer reaction. Since I expected that merocyanine **130** would be hardly soluble, I had chosen di-hexylamino moiety to improve this physicochemical property. Even though, the yield of this reaction was very poor, the product was subjected to the condensation conditions with aldehyde **123** affording 'rhodol-like' merocyanine **130** in 20% yield.

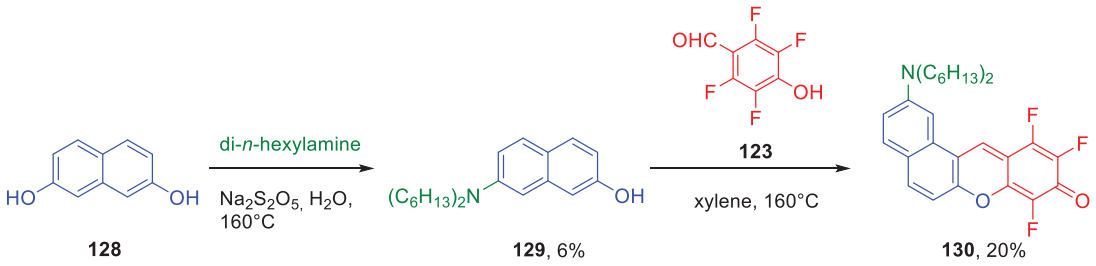

Scheme 27. Preparation of 'rhodol-like' merocyanine **130**

At the time when I started my research, I had performed literature search, which indicated clearly that linear π-expanded 'rhodol-like' merocyanines were something really uncommon and their synthesis might be challenging. The reason for this is that the position 1 in compound **129** is much more electron-rich than position 3 causing all electrophilic aromatic substitutions to proceed towards dye **130**, and not to its linear isomer. I decided to synthesize the π-expanded rhodol precursor with the occupied position 1 thus to suppress the condensation into the position 3. This time I have performed Bucherer reaction of 2,7-dihydroxynaphthalene (**128**) and di-*i*-propylamine. To my surprise, I have obtained a naphthalene derivative **131** with a mono-substituted amino fragment. The following allylation, rearrangement and reduction of double bond resulted in formation of product **133**. The condensation with benzaldehyde **122** in toluene at 90 °C failed, so I have finally managed to obtain merocyanine **134** after 72 h reaction in xylene at 160 °C.

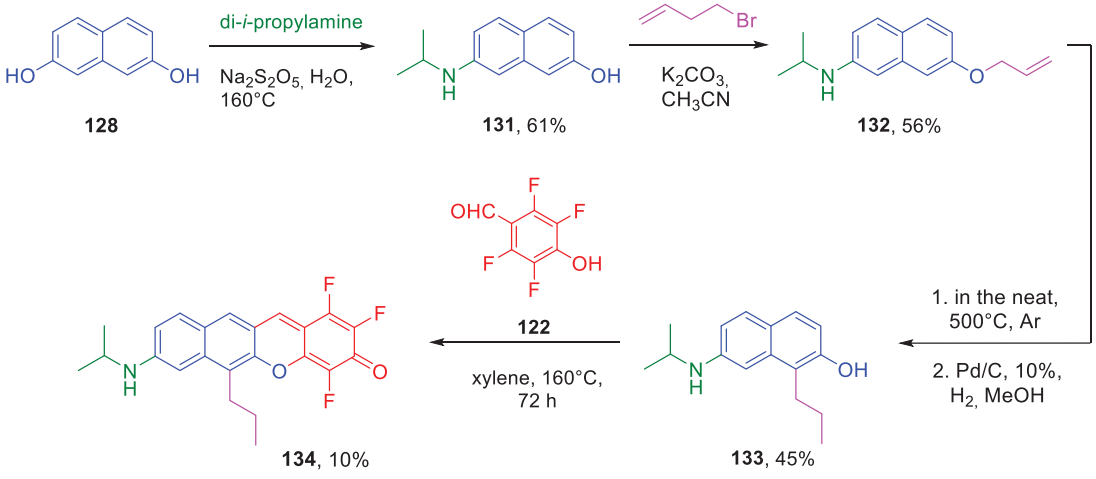

Scheme 28. Synthetic procedure for linear π-expanded 'rhodol-like' merocyanine **134**

The last idea was to investigate if I could apply this procedure for 4-hydroxycoumarins to obtain 'coumarino-rhodols'. For this aim, I obtained coumarins **136** and **137** from 3-dibutylaminophenol **135** and 1,1,7,7-tetramethyl-8-hydroxyjulolidine **121**. As in previous case, I had to apply solvent with the high boiling point. Finally, I managed to obtain merocyanine dyes **138** and **139** in 81% and 51% yields respectively.

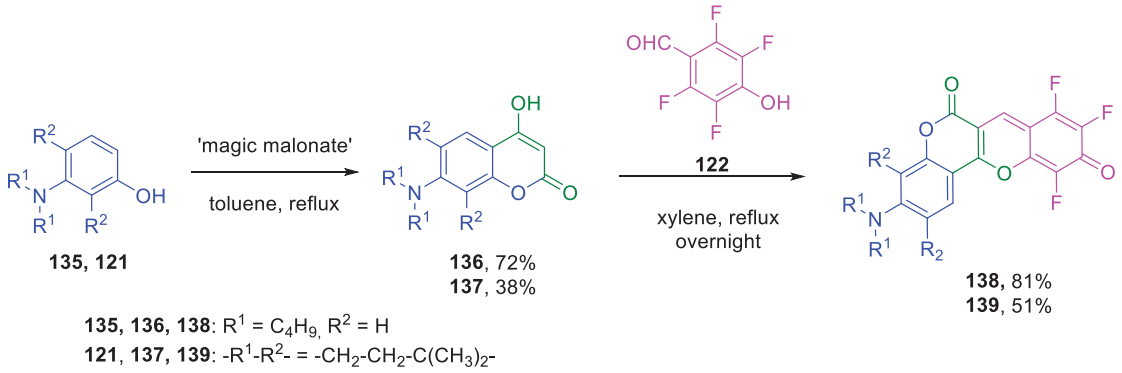

Scheme 27. One-pot synthesis of 'rhodol-like' merocyanines **138-139** from 4-hydroxycoumarins **136-137**

The new dyes display gentle positive solvatochromism of both absorption and emission. As it was expected, the substitution of nitrogen with one ethyl moiety (**124**) results in a blue-shift of absorption (491 – 536 nm) and emission (550 – 555 nm). Meanwhile the full substitution with alkyl chains results in bathochromic shift and higher Φ_{fl} (533/547 nm with Φ_{fl} 89% in case of compound **125** versus 527/547 nm with 77% yield for **124** in acetone) (Table 3). The red-shift is even higher in case of fully annulated terminal C-N bond (λ_{abs} = 498 – 554 nm, λ_{em} = 546 – 576 nm with quantum yield up to 85 % in acetone). The presence of hydroxy group at position 8 in some rhodols (**126**, **127**) does not have a significant influence on the photophysical properties. The distinction of rhodols **138** and **139** is that they show increased Stokes shifts in comparison to classic rhodols **123** – **127** and their emissions are red-shifted by 50-70 nm.

Table 3. Spectroscopic properties of the obtained merocyanine dyes in chosen solvents - toluene as nonpolar and acetone as a polar one. Full spectroscopic data can be found in the publication.

	Solvent	λ_{abs}^{max} ***[nm]***	λ_{em}^{max} ***[nm]***	Φ_{fl} ***[%]***
123	Toluene	542	558	0.68
	Acetone	546	567	0.85
124	Toluene	491	550	0.43
	Acetone	527	547	0.77

125	Toluene	528	550	0.68
	Acetone	533	557	0.89
126	Acetone	533	555	0.91
127	Toluene	527	550	0.68
	Acetone	534	552	0.90
130	Toluene	519	578	0.10
	Acetone	575	798	0.01
134	Toluene	527	594	0.52
	Acetone	545	685	0.34
138	Toluene	528	586	0.21
	Acetone	566	619	0.71
139	Toluene	575	598	0.51
	Acetone	581	655	0.38

The incorporation of benzene ring into the rhodol scaffold results in the formation of π-expanded rhodols **130** and **134**. These compounds possess large Stokes shifts (up to 4900 cm^{-1} in acetone for **130** and 4400 cm^{-1} in acetonitrile for **134**). Rhodol **130** display a significant positive solvatochromism possessing emission maxima from 578 nm in hexane to 798 nm in acetone yet with low Φ_{fl}, which almost disappear in polar solvents. In contrast, rhodol **134** shows blue-shifted absorption and emission compared to **130** (λ_{abs} = 527 – 547 nm and λ_{em} =594 – 721 nm with somewhat higher quantum yields). Both dyes **130** and **134** possess broad and quite featureless absorption curves (Figure 7).

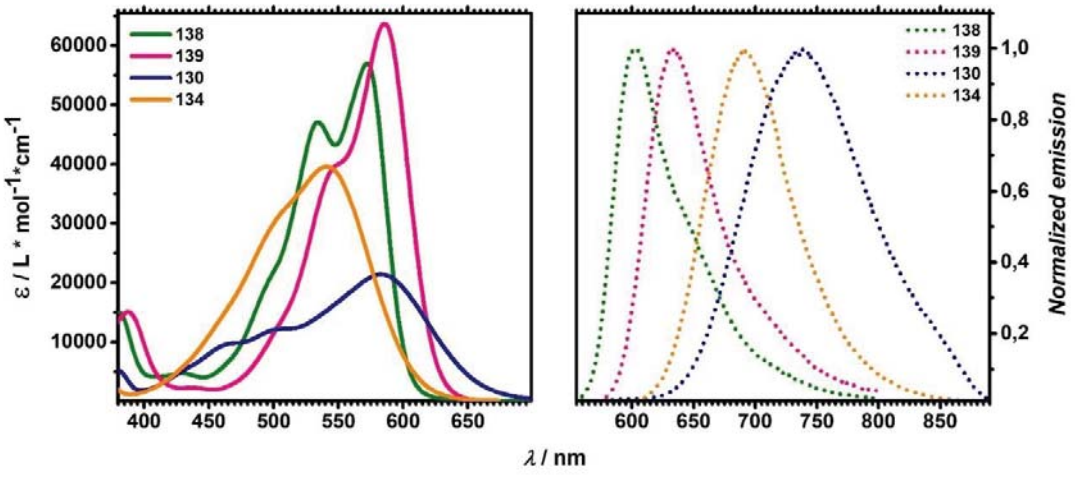

Figure 7. Absorption (solid) and emission (dotted) of 'rhodol-like' merocyanines **130**, **134**, **138** and **139** measured in methylene chloride.

6.4 Summary and conclusions

I have developed an unprecedented chromophore which possesses an SO_2 group in the middle of a rhodol skeleton. Moreover it has been achieved in a straightforward manner and the procedure consists of only four steps. Electronic spectra of all these modified rhodols display strong absorption in the range of 500-600 nm, which is almost independent of the nature of the solvent. Red fluorescence is markedly stronger in polar solvents reaching 50% in DMSO. I have found that rhodol analogs with the bridging oxygen atom replaced by an SO_2 group, and equipped with a triphenylphosphonium functionality, selectively accumulates in mitochondria and allows for selective penetration and well-resolved fluorescent imaging at nanomolar concentrations.

I have also developed an unprecedented synthesis of rhodols from coumarins. Moreover it has been achieved in a straightforward manner and the procedure consists of only four steps from easily available, commercial substrates. This approach involves the double Knoevenagel condensation of 3-formylcoumarins via activation of a lactone's C=O. This is the first example of this type reactivity for the ubiquitous lactone group described in the literature. To test the influence of different aryl groups on both the synthesis and the photophysical properties of the resulting dyes, I have prepared an extensive family of rhodols. Their electronic spectra display strong absorption in the range of 500-600 nm, which is almost independent of the nature of the solvent. Orange-red fluorescence is very strong in both non-polar and polar solvents reaching 100% in some cases.

Finally I developed a strikingly simple synthetic strategy to rhodols and 'rhodols-type' merocyanines bearing unprecedented sets of substituents. This approach relies on the tandem reaction of dialkylaminophenols, dialkylaminonaphthols and 4-hydroxycoumarins with tetrafluorohydroxybenzaldehyde, with two-steps occurring one after another, namely a Friedel-Crafts reaction followed by intramolecular nucleophilic aromatic substitution. This constitutes the shortest pathway towards rhodols ever developed. Three heretofore unknown merocyanine-based architectures were prepared using this strategy from dialkylaminonaphthols and 4-hydroxycoumarins. The ability to change the structure of original rhodol chromophore into π-expanded merocyanines translates to a comprehensive method for the modulation of photophysical properties such as shifting the absorption and emission bands across almost the entire visible spectrum, reaching the highest recorded Stokes shift i.e. 4800 cm^{-1}, ca. 80,000 M^{-1} cm^{-1} brightness, two-photon absorption cross-section above 150 GM and switching-on/off solvatofluorochromism. Together with collaborating group from Parma found that replacing linear with non-linear

conjugation in rhodols-type architectures leads to profound changes in the photophysics originating from differences in permanent dipole moment changes between ground and the excited states.

Summing up, I realized most of the goals initially stated. In particular I developed three new synthetic methodologies affording rhodols-type fluorophores. Photostability of these rhodols and 'rhodol-like' merocyanines is not better compared to classical rhodols and other photostable dyes. They are not however markedly less stable either. I demonstrated new synthetic routes which allow the fine-tuning of the properties for xanthene dyes. Thanks to the widespread use of this class of fluorophores in multifarious applications, I believe that my results are of paramount importance for a very broad pool of scientists in different fields.

7. BIBLIOGRAPHY

1 A. Yamagami, H. Ishimura, A. Katori, K. Kuramochi and K. Tsubaki, *Org. Biomol. Chem.*, 2016, **14**, 10963–10972.

2 P. Shieh, V. T. Dien, B. J. Beahm, J. M. Castellano, T. Wyss-Coray and C. R. Bertozzi, *J. Am. Chem. Soc.*, 2015, **137**, 7145–7151.

3 G. Lukinavičius, L. Reymond, K. Umezawa, O. Sallin, E. D'Este, F. Göttfert, H. Ta, S. W. Hell, Y. Urano and K. Johnsson, *J. Am. Chem. Soc.*, 2016, **138**, 9365–9368.

4 T. Ikeno, T. Nagano and K. Hanaoka, *Chem. - An Asian J.*, 2017, **12**, 1435–1446.

5 M. Grzybowski, M. Taki and S. Yamaguchi, *Chem. - A Eur. J.*, 2017, **23**, 13028–13032.

6 J. Liu, Y.-Q. Sun, H. Zhang, H. Shi, Y. Shi and W. Guo, *ACS Appl. Mater. Interfaces*, 2016, **8**, 22953–22962.

7 A. N. Butkevich, G. Y. Mitronova, S. C. Sidenstein, J. L. Klocke, D. Kamin, D. N. H. Meineke, E. D'Este, P.-T. Kraemer, J. G. Danzl, V. N. Belov and S. W. Hell, *Angew. Chemie Int. Ed.*, 2016, **55**, 3290–3294.

8 J. B. Grimm, A. J. Sung, W. R. Legant, P. Hulamm, S. M. Matlosz, E. Betzig and L. D. Lavis, *ACS Chem. Biol.*, 2013, **8**, 1303–1310.

9 M. V. Sednev, C. A. Wurm, V. N. Belov and S. W. Hell, *Bioconjug. Chem.*, 2013, **24**, 690–700.

10 S. Takahashi, Y. Kagami, K. Hanaoka, T. Terai, T. Komatsu, T. Ueno, M. Uchiyama, I. Koyama-Honda, N. Mizushima, T. Taguchi, H. Arai, T. Nagano and Y. Urano, *J. Am. Chem. Soc.*, 2018, **140**, 5925–5933.

11 L. D. Lavis, *Biochemistry*, 2017, **56**, 5165–5170.

12 Y. J. Gong, X. B. Zhang, G. J. Mao, L. Su, H. M. Meng, W. Tan, S. Feng and G. Zhang, *Chem. Sci.*, 2016, **7**, 2275–2285.

13 J. Chan, S. C. Dodani and C. J. Chang, *Nat. Chem.*, 2012, 4, 973–984.

14 C. Deo, S.-H. Sheu, J. Seo, D. E. Clapham and L. D. Lavis, *J. Am. Chem. Soc.*, 2019, **141**, 13734–13738.

15 P. Shieh, M. J. Hangauer and C. R. Bertozzi, *J. Am. Chem. Soc.*, 2012, **134**, 17428–17431.

16 Y. M. Poronik, K. V. Vygranenko, D. Gryko and D. T. Gryko, *Chem. Soc. Rev.*, 2019, **48**, 5242–5265.

17 S. W. Hell and J. Wichmann, *Opt. Lett.*, 1994, **19**, 782.

18 H. Blom and J. Widengren, *Curr. Opin. Chem. Biol.*, 2014, 20, 127–133.

19 K. I. Willig, J. Keller, M. Bossi and S. W. Hell, *New J. Phys.*, 2006, **8**, 1–8.

20 Farbenfabriken vorm. Frieds. Bayer & Co. in Elberfeld, *DE54085*, 1889.

21 Badische Anilin- und Soda-Fabrik, *DE54684*, 1890.

22 V. Z. Shirinian and A. A. Shimkin, in *Heterocyclic Polymethine Dyes*, Springer Berlin Heidelberg, Berlin, Heidelberg, 2008, pp. 75–105.

23 M. J. S. Dewar, *J. Chem. Soc.*, 1950, 2329–2334.

24 J. Fabian and H. Hartmann, in *Reactivity and Structure Concepts in Organic Chemistry; V. 12*, eds. K. Hafner, C. W. Rees, B. M. Trost, L.-M. Lehn, P. von Rague Schleyer and R. Zahnradnik, Springer-Verlag, Berlin Heidelberg New York, 1980, pp. 162–197.

25 Y. M. Poronik, K. V. Vygranenko, D. Gryko and D. T. Gryko, *Chem. Soc. Rev.*, 2019, 48, 5242–5265.

26 J. B. Grimm, A. K. Muthusamy, Y. Liang, T. A. Brown, W. C. Lemon, R. Patel, R. Lu, J. J. Macklin, P. J. Keller, N. Ji and L. D. Lavis, *Nat. Methods*, 2017, **14**, 987–994.

27 J. E. Whitaker, R. P. Haugland, D. Ryan, P. C. Hewitt, R. P. Haugland and F. G. Prendergast, *Anal. Biochem.*, 1992, **207**, 267–279.

28 W. Chen, S. Xu, J. J. Day, D. Wang and M. Xian, *Angew. Chemie - Int. Ed.*, 2017, **56**, 16611–16615.

29 T.-B. Ren, W. Xu, W. Zhang, X.-X. Zhang, Z.-Y. Wang, Z. Xiang, L. Yuan and X.-B. Zhang, *J. Am. Chem. Soc.*, 2018, **140**, 7716–7722.

30 S. S. Patil, K. G. Thorat, R. Mallah and N. Sekar, *J. Fluoresc.*, 2016, **26**, 2187–2197.

31 J. Liu, Y. Q. Sun, H. Zhang, H. Shi, Y. Shi and W. Guo, *ACS Appl. Mater. Interfaces*, 2016, **8**, 22953–22962.

32 Y. Koide, Y. Urano, K. Hanaoka, T. Terai and T. Nagano, *ACS Chem. Biol.*, 2011, **6**, 600–608.

33 J. Arden-Jacob, J. Frantzeskos, N. U. Kemnitzer, A. Zilles and K. H. Drexhage, in *Spectrochimica Acta - Part A Molecular and Biomolecular Spectroscopy*, 2001, vol. 57, pp. 2271–2283.

34 Z. Lei, X. Li, Y. Li, X. Luo, M. Zhou and Y. Yang, *J. Org. Chem.*, 2015, **80**, 11538–11543.

35 G. A. Smith, J. C. Metcalfe and S. D. Clarke, *J. Chem. Soc. Perkin Trans. 2*, 1993, 1195.

36 W. Xuan, Y. Cao, J. Zhou and W. Wang, *Chem. Commun.*, 2013, **49**, 10474–10476.

37 B. C. Dickinson, Y. Tang, Z. Chang and C. J. Chang, *Chem. Biol.*, 2011, **18**, 943–948.

38 S. J. Lippard and S. Burdette, *US2003008405A1*, 2003.

39 S. J. Lippard and S. Hilderbrand, *US2003068275(A1)*, 2003.

40 K. Huang, M. Liu, X. Wang, D. Cao, F. Gao, K. Zhou, W. Wang and W. Zeng, *Tetrahedron Lett.*, 2015, **56**, 3769–3773.

41 K. Huang, L. Yu, P. Xu, X. Zhang and W. Zeng, *RSC Adv.*, 2015, **5**, 17797–17801.

42 K. Huang, M. Liu, Z. Liu, D. Cao, J. Hou and W. Zeng, *Dyes. Pigments.*, 2015, **118**, 88–94.

43 M. A. Clark, K. Duffy, J. Tibrewala and S. J. Lippard, *Org. Lett.*, 2003, **5**, 2051–2054.

44 M. A. Clark, S. A. Hilderbrand and S. J. Lippard, *Tetrahedron Lett.*, 2004, **45**, 7129–7131.

45 S. C. Burdette and S. J. Lippard, *Inorg. Chem.*, 2002, **41**, 6816–6823.

46 S. J. Lippard and C. C. Woodroofe, *US2004224420A1*, 2004.

47 X. Zhu, M. Xiong, H. Liu, G. Mao, L. Zhou, J. Zhang, X. Hu, X.-B. Zhang and W. Tan, *Chem. Commun.*, 2016, **52**, 733–736.

48 E. Tomat and S. J. Lippard, *Inorg. Chem.*, 2010, **49**, 9113–9115.

49 M. Ren, B. Deng, K. Zhou, J. Y. Wang, X. Kong and W. Lin, *J. Mater. Chem. B*, 2017, **5**, 1954–1961.

50 R. R. Sauers, S. N. Husain, A. P. Piechowski and G. R. Bird, *Dyes. Pigments.*, 1987, **8**, 35–53.

51 B. C. Dickinson, C. Huynh and C. J. Chang, *J. Am. Chem. Soc.*, 2010, **132**, 5906–5915.

52 M. Kondo, M. Tanaka, N. Sakamoto and H. Ooyoshi, *EP0511019(A2)*, 1992.

53 S. V Patel, M. P. Patel and R. G. Patel, *J. Serb. Chem. Soc*, 2005, **70**, 931–936.

54 H. Zheng, X. Q. Zhan, Q. N. Bian and X. J. Zhang, *Chem. Commun.*, 2013, **49**, 429–447.

55 Y. Zhao, Y. Ren, H. Li, T. Han, H. Chen and W. Guo, *Dyes. Pigments.*, 2016, **132**, 255–261.

56 J. E. Whitaker, R. P. Haugland and F. G. Prendergast, *Anal. Biochem.*, 1991, **194**, 330–344.

57 K. Tiensomjitr, R. Noorat, S. Chomngam, K. Wechakorn, S. Prabpai, P. Kanjanasirirat, Y. Pewkliang, S. Borwornpinyo and P. Kongsaeree, *Spectrochim. Acta. A*, 2018, **195**, 136–141.

58 M. Taki, K. Akaoka, K. Mitsui and Y. Yamamoto, *Org. Biomol. Chem.*, 2014, **12**, 4999–5005.

59 F. Mao, W.-Y. Leung and R. P. Haugland, *US6130101(A)*, 1997.

60 J. Han and K. Burgess, *Chem. Rev.*, 2010, **110**, 2709–2728.

61 E. A. Halabi, Z. Thiel, N. Trapp, D. Pinotsi and P. Rivera-Fuentes, *J. Am. Chem. Soc.*, 2017, **139**, 13200–13207.

62 G. S. Ghotekar, A. C. Shaikh and M. Muthukrishnan, *J. Org. Chem.*, 2019, **84**, 2269–2276.

63 K. R. Gee, M. Poot, D. H. Klaubert, W.-C. Sun, R. P. Haugland and F. Mao, *US6162931(A)*, 1996.

64 Z. Diwu, J. Liu and K. Gee, *US2004147747(A1)*, 2004.

65 Z. Diwu, J. Liu, R. P. Haugland and K. R. Gee, *US2002059684(A1)*, 2002.

66 T. Chin, Frederick, J. Klockow, K. Hettie and T. Glass, *WO2016210054(A1)*, 2016.

67 R. Alford, H. M. Simpson, J. Duberman, G. C. Hill, M. Ogawa, C. Regino, H. Kobayashi and P. L. Choyke, *Mol. Imaging*, 2009, **8**, 341–354.

68 S. Kamino, H. Ichikawa, S. ichi Wada, Y. Horio, Y. Usami, T. Yamaguchi, T. Koda, A. Harada, K. Shimanuki, M. Arimoto, M. Doi and Y. Fujita, *Bioorganic Med. Chem. Lett.*, 2008, **18**, 4380–4384.

69 M. Kamiya, D. Asanuma, E. Kuranaga, A. Takeishi and M. Sakabe, *J. Am. Chem. Soc.*, 2011, **133**, 12960–12963.

70 X. Jiao, C. Liu, K. Huang, S. Zhang, S. He, L. Zhao and X. Zeng, *Org. Biomol. Chem.*, 2015, **13**, 6647–6653.

71 W. Dong, H. Wen, X. F. Yang and H. Li, *Dyes. Pigments.*, 2013, **96**, 653–658.

72 E. M. Poronik, M. P. Shandura and Y. P. Kovtun, *Chem. Heterocycl. Compd.*, 2005, **41**, 546–547.

73 Y. M. Poronik, M. P. Shandura and Y. P. Kovtun, *Dyes. Pigments.*, 2007, **72**, 199–207.

74 X. Lv, J. Liu, Y. Liu, Y. Zhao, M. Chen, P. Wang and W. Guo, *Sensors Actuators, B Chem.*, 2011, **158**, 405–410.

75 A. Chevalier, P. Y. Renard and A. Romieu, *Chem. - A Eur. J.*, 2014, **20**, 8330–8337.

76 A. Chevalier, K. Renault, F. Boschetti, P. Y. Renard and A. Romieu, *Eur. J. Org. Chem.*, 2015, **2015**, 152–165.

77 S. Orenga, V. Chalansonnet, A. Chevalier, P.-Y. Renard, A. Romieu and B. Roubinet, *US2016146814A1*, 2016.

78 J. Li and S. Q. Yao, *Org. Lett.*, 2009, **11**, 405–408.

79 S. C. Dodani, A. Firl, J. Chan, C. I. Nam, A. T. Aron, C. S. Onak, K. M. Ramos-Torres, J. Paek, C. M. Webster, M. B. Feller and C. J. Chang, *Proc. Natl. Acad. Sci.*, 2014, **111**, 16280–16285.

80 D. K. Sharma, S. T. Adams, K. L. Liebmann, A. Choi and S. C. Miller, *Org. Lett.*, 2019, **21**, 1641–1644.

81 D. Yang and T. Peng, *WO2009121244 (A1)*, 2009.

82 R. U. Kulkarni, D. J. Kramer, N. Pourmandi, K. Karbasi, H. S. Bateup and E. W. Miller, *Proc. Natl. Acad. Sci.*, 2017, **114**, 2813–2818.

83 T. Peng and D. Yang, *Org. Lett.*, 2010, **12**, 4932–4935.

84 A. A. Contractor and E. W. Miller, *Biochemistry*, 2018, **57**, 237–240.

85 T. Peng, N. K. Wong, X. Chen, Y. K. Chan, D. H. H. Ho, Z. Sun, J. J. Hu, J. Shen, H. El-Nezami and D. Yang, *J. Am. Chem. Soc.*, 2014, **136**, 11728–11734.

86 K. Kawai, N. Ieda, K. Aizawa, T. Suzuki, N. Miyata and H. Nakagawa, *J. Am. Chem. Soc.*, 2013, **135**, 12690–12696.

87 T. Fiala, E. V. Mosharov, J. Wang, A. M. Mendieta, S. J. Choi, E. Fialova, C. Hwu, D. Sulzer and D. Sames, *ACS Chem. Neurosci.*, 2022, **13**, 1251–1262.

88 B. F. Dutter, A. Ender, G. A. Sulikowski, C. David Weaver and C. D. Weaver, *Org. Biomol. Chem.*, 2018, **16**, 5575–5579.

89 J. M. Meinig, L. Fu and B. R. Peterson, *Angew. Chemie - Int. Ed.*, 2015, **54**, 9696–9699.

90 C. Richter, N. P. Ernsting and R. Mahrwald, *Synth.*, 2016, **48**, 1217–1225.

91 E. Nakata, Y. Yukimachi, Y. Nazumi, Y. Uto, H. Maezawa, T. Hashimoto, Y. Okamoto and H. Hori, *Chem. Commun.*, 2010, **46**, 3526.

92 Y. Liu, K. Xiang, B. Tian and J. Zhang, *Luminescence*, 2017, **32**, 78–85.

93 J. Liu, Z. Diwu and W.-Y. Leung, *Bioorg. Med. Chem. Lett.*, 2001, **11**, 2903–2905.

94 Y. Fu, M. M. Collinson and D. A. Higgins, *J. Am. Chem. Soc.*, 2004, **126**, 13838–13844.

95 L. G. Wang, I. Munhenzva, M. Sibrian-Vazquez, J. O. Escobedo, C. H. Kitts, F. R. Fronczek and R. M. Strongin, *J. Org. Chem.*, 2019, **84**, 2585–2595.

96 L. Wang, C. W. Barth, M. Sibrian-Vazquez, J. O. Escobedo, M. Lowry, J. Muschler, H. Li, S. L. Gibbs and R. M. Strongin, *ACS omega*, 2017, **2**, 154–163.

97 S. A. Hilderbrand and R. Weissleder, *Tetrahedron Lett.*, 2007, **48**, 4383–4385.

98 A. Yamagami, H. Ishimura, A. Katori, K. Kuramochi and K. Tsubaki, *Org. Biomol. Chem.*, 2016, **14**, 10963–10972.

99 A. Yamagami, K. Kawano, S. Futaki, K. Kuramochi and K. Tsubaki, *Tetrahedron*, 2017, **73**, 7061–7066.

100 J. B. Grimm, A. J. Sung, W. R. Legant, P. Hulamm, S. M. Matlosz, E. Betzig and L. D. Lavis, *ACS Chem. Biol.*, 2013, **8**, 1303–1310.

101 L. Geng, X. F. Yang, Y. Zhong, Z. Li and H. Li, *Dyes. Pigments.*, 2015, **120**, 213–219.

102 H. J. Rivera-Jacquez and A. E. Masunov, *Spectrochim. Acta. A*, 2018, **198**, 123–135.

103 A. Roth, H. Li, C. Anorma and J. Chan, *J. Am. Chem. Soc.*, 2015, **137**, 10890–10893.

104 T. Egawa, Y. Koide, K. Hanaoka, T. Komatsu, T. CooTeraiper and T. Nagano, *Chem. Commun.*, 2011, **47**, 4162–4164.

105 T. Nagano, K. Hanaoka, T. Egawa, Y. Kushida, K. Numasawa, T. Myochin and W. Piao, *EP2942352(A1)*, 2015.

106 M. V. Sednev, C. A. Wurm, V. N. Belov and S. W. Hell, *Bioconjug. Chem.*, 2013, **24**, 690–700.

107 M. Grzybowski, M. Taki and S. Yamaguchi, *Chem. - A Eur. J.*, 2017, **23**, 13028–13032.

108 M. Grzybowski, O. Morawski, K. Nowak and P. Garbacz, *Chem. Commun.*, 2022, **58**, 5455–5458.

109 Y. Ichikawa, M. Kamiya, F. Obata, M. Miura, T. Terai, T. Komatsu, T. Ueno, K. Hanaoka, T. Nagano and Y. Urano, *Angew. Chemie - Int. Ed.*, 2014, **53**, 6772–6775.

110 D. J. Del Valle, D. J. Donnelly, J. J. Holt and M. R. Detty, *Organometallics*, 2005, **24**, 3807–3810.

111 M. R. Detty, P. N. Prasad, D. J. Donnelly, T. Ohulchanskyy, S. L. Gibson and R. Hilf, *Bioorg. Med. Chem.*, 2004, **12**, 2537–2544.

112 A. Gandioso, R. Bresolí-Obach, A. Nin-Hill, M. Bosch, M. Palau, A. Galindo, S. Contreras, A. Rovira, C. Rovira, S. Nonell and V. Marchán, *J. Org. Chem.*, 2018, **83**, 1185–1195.

113 A. Gandioso, M. Palau, R. Bresolí-Obach, A. Galindo, A. Rovira, M. Bosch, S. Nonell and V. Marchán, *J. Org. Chem.*, 2018, **83**, 11519–11531.

114 Ł. Kielesiński, I. Deperasińska, O. Morawski, K. V. Vygranenko, E. T. Ouellette and D. T. Gryko, *J. Org. Chem.*, 2022, **87**, 5961–5975.

115 R. S. Coleman and M. L. Madaras, *J. Org. Chem.*, 1998, **63**, 5700–5703.

116 T. Kappe, *Encycl. Reagents Org. Synth.*, , DOI:10.1002/047084289X.RB202.

117 L. Schmidt, T. Doroshenko, P. Barbie, A. Grüter, G. Jung and U. Kazmaier, *Synth.*, 2016, **48**, 3077–3086.

118 D. T. Gryko, D. Wyrostek, A. Nowak-Król, K. Abramczyk and M. K. Rogacki, *Synth.*, 2008, 4028–4032.

119 J. C. Duff and E. H. Bills, *J. Chem. Soc.*, 1932, 1987–1988.

120 K. Skonieczny, G. Charalambidis, M. Tasior, M. Krzeszewski, A. Kalkan-Burat, A. G. Coutsolelos and D. T. Gryko, *Synth.*, 2012, **44**, 3683–3687.

121 W. E. Smith, *J. Org. Chem.*, 1972, **37**, 3972–3973.

8. ORIGINAL PUBLICATIONS

Volume 48 | Number 20 | 21 October 2019 | Pages 5179–5304

Chem Soc Rev

Chemical Society Reviews

rsc.li/chem-soc-rev

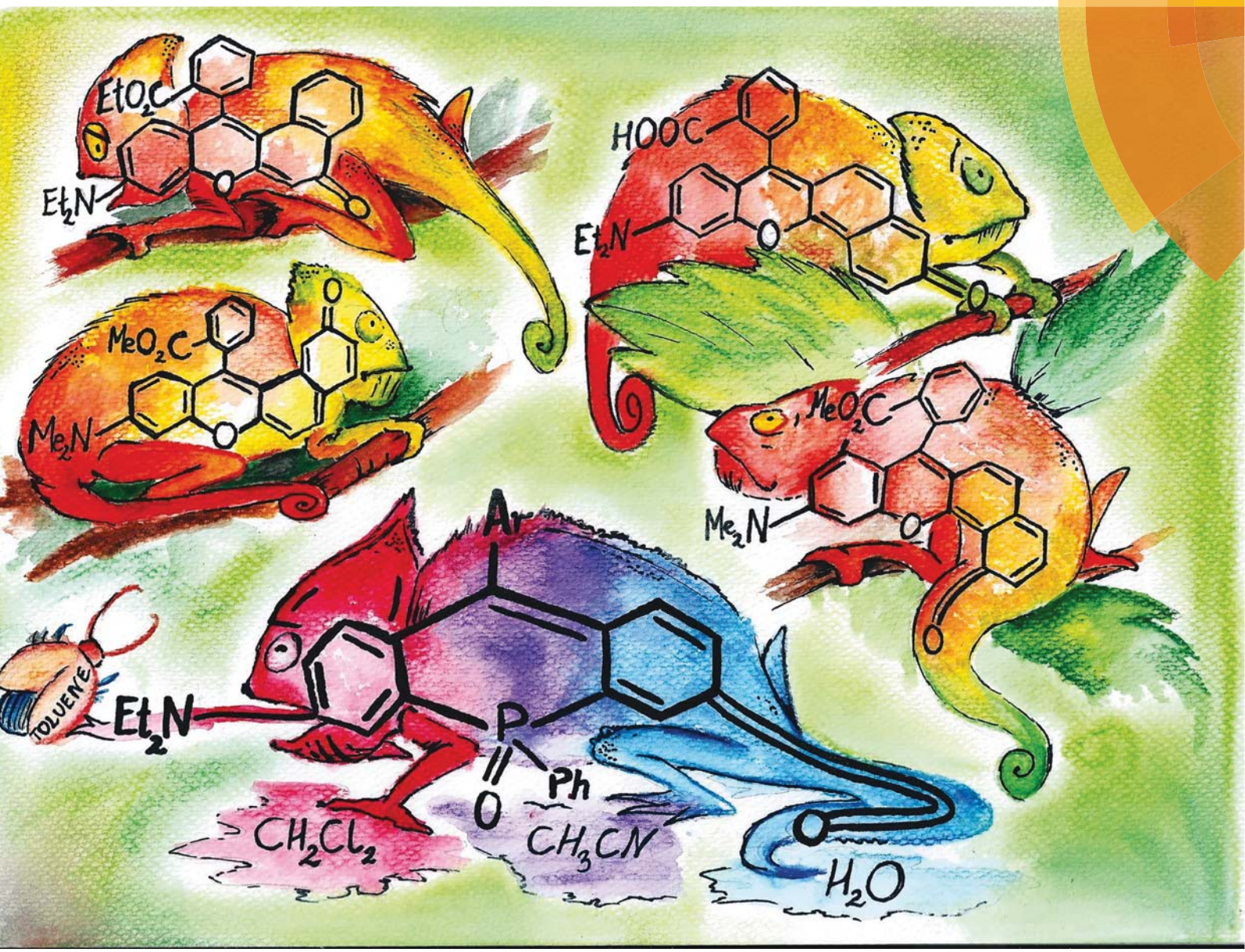

ISSN 0306-0012

ROYAL SOCIETY OF CHEMISTRY | Celebrating IYPT 2019

REVIEW ARTICLE

Yevgen M. Poronik, Daniel T. Gryko *et al.*

Rhodols – synthesis, photophysical properties and applications as fluorescent probes

Chem Soc Rev

REVIEW ARTICLE

View Article Online
View Journal | View Issue

Cite this: *Chem. Soc. Rev.*, 2019, **48**, 5242

Rhodols – synthesis, photophysical properties and applications as fluorescent probes†

Yevgen M. Poronik, Kateryna V. Vygranenko, Dorota Gryko* and Daniel T. Gryko*

The formal replacement of one dialkylamino group in rhodamines with a hydroxyl group transforms them into rhodols. This apparently minor difference is not as small as one may think; rhodamines belong to the cyanine family whereas rhodols belong to merocyanines. Discovered in the late 19th century, rhodols have only very recently begun to gain momentum in the field of advanced fluorescence imaging. This is in part due to the increased understanding of their photophysical properties, and new methods of synthesis. Rationalization of how the nature and arrangement of polar substituents around the core affect the photophysical properties of rhodols is now possible. The emergence of so-called π-expanded and heteroatom-modified rhodols has also allowed their fluorescence to be bathochromically shifted into regions applicable for biological imaging. This review serves to outline applicable synthetic strategies for the synthesis of rhodols, and to highlight important structure–property relationships. In the first part of this Review, various synthetic methods leading to rhodols are presented, followed by structural considerations and an overview of photophysical properties. The second part of this review is entirely devoted to the applications of rhodols as fluorescent reporters in biological imaging.

Received 28th February 2019

DOI: 10.1039/c9cs00166b

rsc.li/chem-soc-rev

1. Introduction

Rhodols belong to the xanthene dye family and have recently become popular fluorescent scaffolds with many applications connected to fluorescence microscopy. Though these dyes have been known since the 19th century their appearance in the literature has remained limited, being largely overshadowed by the more popular xanthene chromophores – rhodamine and fluorescein. Since the title chromophore was first indirectly synthesized from fluorescein in 1889,[1] it was named rhodol[2] highlighting its similarity to rhodamine yet emphasizing the inclusion of a 'phenol functionality' (Fig. 1). Until 1990 rhodols remained largely forgotten and only a few reports appeared in the literature,[3–17] presumably due to the fact that more

Institute of Organic Chemistry, Polish Academy of Sciences, Kasprzaka 44/52, 01-224 Warsaw, Poland. E-mail: dorota.gryko@icho.edu.pl, dtgryko@icho.edu.pl

† Electronic supplementary information (ESI) available. See DOI: 10.1039/c9cs00166b

Yevgen M. Poronik

Dr Yevgen Poronik received his MSc (2001) from Department of Chemical Technology of Kyiv Technical University and PhD (2006) from Institute of Organic Chemistry, Ukrainian Academy of Sciences, under the supervision of Prof. Yuriy Kovtun. He worked as a post-doctoral researcher at Institute of Organic Chemistry of Polish Academy of Sciences in the group of Prof. Daniel Gryko. He is currently a research assistant in the same group, working on new donor–acceptor chromophoric systems, synthesis and application of functional organic dyes.

Kateryna V. Vygranenko

Kateryna Vygranenko was born in Ukraine in 1992. She obtained her MSc from Taras Shevchenko National University of Kyiv in 2015. She is a PhD student at the Institute of Organic Chemistry Polish Academy of Sciences under the supervision of Prof. Daniel Gryko. Her research interest currently focuses on developing new organic dyes for STED-microscopy.

ChemComm

COMMUNICATION

View Article Online
View Journal | View Issue

Cite this: *Chem. Commun.*, 2021, **57**, 7782

Received 21st May 2021,
Accepted 6th July 2021

DOI: 10.1039/d1cc02687a

rsc.li/chemcomm

Red emissive sulfone-rhodols as mitochondrial imaging agents†

Kateryna V. Vygranenko,[a] Yevgen M. Poronik,[a] Antoni Wrzosek,[b] Adam Szewczyk*[b] and Daniel T. Gryko *[a]

The controlled hydrolysis of sulfone-rhodamines affords a series of core-modified red-emitting rhodols, the fluorescence of which is sensitive to solvent polarity with pronounced bathochromic shifts recorded in both DMSO and CH_3CN combined with an up to 8-fold increase in the fluorescence quantum yield.

The iconic fluorescent dyes fluorescein and rhodamine, were first reported by Baeyer and Ceresole in 1871 and 1888, respectively.[1,2] These discoveries were the harbingers of modern fluorophore chemistry, which rapidly spread in the following years.[3–10] One of the lesser known cousins of these two dyes is rhodol.[11] This dye, a structural hybrid of rhodamine and fluorescein, inherited their photophysical properties in terms of large extinction coefficient, high fluorescence quantum yield and solubility in a majority of solvents. Unlike rhodamines and fluoresceins, however, rhodols belong to merocyanines that contain a polymethine chain and two terminal heteroatoms in their chromophore. Numerous analogues of rhodol have been reported during last decade.[12–17] More importantly they have been selected for several key applications such as fluorescent reporters in biological imaging, membrane potential sensors in cells and organelles, and photosensitizers in antitumor therapy.[18–21] Over the years the motivation to shift both absorption and emission bathochromically to the red and NIR regions has increased in parallel with the importance of fluorescence imaging in cell biology.[22–26] Along these lines, very recently the synthesis of a plethora of new fluorophores including sulfone-rhodamines, which exhibit both absorption and emission maxima in the near-infrared region, have been reported.[27] We reasoned that if the rhodamine scaffold is replaced by a rhodol, the resulting and heretofore unknown sulfone-rhodols could possess attractive photophysical properties. Here we focus on realization of this vision.

The stepwise synthesis of sulfone-rhodols from benzene-based building blocks would be a long adventure. In an attempt to overcome this, we hypothesized that rhodamines possessing an endocyclic strong electron-withdrawing group may undergo basic hydrolysis to produce the corresponding sulfone-rhodols, in a similar manner to that observed for P-rhodamines.[28] Taking this into consideration, we have designed the following strategy: synthesis of 9-aryl substituted sulfone-rhodamines followed by conversion into the corresponding rhodols upon basic hydrolysis.

The design of a specific pattern of substituents on SO_2-rhodols is a very important issue, as relatively small structural changes can have a pivotal effect on photophysical properties. The aryl moiety plays a substantial role in rhodamines, fluoresceins and rhodols, governing some of their chemical and photophysical properties.[29,30] Although, it is located orthogonally to the xanthene scaffold and is not a part of the chromophore, it still decreases the sensitivity of the fluorophore's π-conjugation system to nucleophiles. Nucleophilic addition to the C9-position of unsubstituted rhodols results in discoloration of the dye due to interruption of the conjugation chain. Moreover, the size of the *ortho*-substituent also plays a crucial role in the stability of the chromophore towards nucleophilic attack. Consequently, P=O-rhodols possessing an *ortho*-tolyl group at the *meso*-position undergo slow discoloration under basic conditions because of the nucleophilic attack of the hydroxyl anion at the C9-position, while bulkier *ortho*-substituents, like CF_3 or OMe, prevent disruption of the chromophore's π-conjugation system.[26] For both rhodamines and fluoresceins, substituents at the *ortho*-position prevent the rotation of aryl groups, thus minimizing radiationless deactivation of the excited stated and increasing the fluorescence efficiency. For the outlined reasons we decided to exclusively use sterically hindered substituents at the C9-position in this study.

[a] *Institute of Organic Chemistry, Polish Academy of Sciences, Kasprzaka 44/52, 01-224 Warsaw, Poland. E-mail: dtgryko@icho.edu.pl*
[b] *Nencki Institute of Experimental Biology, Polish Academy of Sciences, Pasteura 3, 02-093 Warsaw, Poland. E-mail: a.szewczyk@nencki.edu.pl*

† Electronic supplementary information (ESI) available: Experimental description, copies of ^1H and ^{13}C NMR spectra as well as crystallographic details. CCDC 2084645. For ESI and crystallographic data in CIF or other electronic format see DOI: 10.1039/d1cc02687a

Supporting information

Red emissive sulfone-rhodols as mitochondrial imaging agents

Kateryna V. Vygranenko,[a] Yevgen M. Poronik,[a] Antoni Wrzosek,[b] Adam Szewczyk,[b*] and Daniel T. Gryko[a*]

a. Institute of Organic Chemistry, Polish Academy of Sciences, Kasprzaka 44/52, 01-224 Warsaw, Poland. E-mail: dtgryko@icho.edu.pl.

b. Nencki Institute of Experimental Biology of Polish Academy of Sciences, Pasteura 3, 02-093 Warsaw, Poland. E-mail: a.szewczyk@nencki.gov.pl

Table of Contents

Instrumentation and Materials

All chemicals were used as received unless otherwise noted. All reported ^{1}H NMR spectra were collected using 500 MHz and 600 MHz spectrometers. Chemical shifts (δ ppm) were determined with TMS as the internal reference; *J* values are given in Hz. Chromatography was performed on silicagel (230-400 mesh). Preparative thin layer chromatography (TLC) was carried out using Merck PLC Silica gel 60 F_{254} 1 mm plates. The mass spectra were obtained via electron ionization (EI-MS) or electrospray ionization (ESI-MS). All photophysical studies have been performed with freshly-prepared air-equilibrated solutions at room temperature (298 K).

A Shimadzu UV-3600i Plus spectrophotometer and an Edinburgh Instruments Spectrofluorometer FS5 equipped with Hamamatsu R13456 PMT were used to acquire the absorption and emission spectra. Fluorescence lifetimes were measured on Fluorolog TCSPC Horiba. Spectrophotometric grade solvents were used without further purification. Fluorescence quantum yields were determined in toluene, CH_2Cl_2, CH_3CN, EtOH, DMSO and H_2O (with 2% DMSO) using cresyl violet in EtOH (for measurements in CH_2Cl_2, CH_3CN, EtOH, DMSO and H_2O) and sulforhodamine SR101 (for measurements in toluene) as standards. Photostability was determined using an Asahi Spectra Max-350 as a light source and Shimadzu UV-3600i Plus spectrophotometer. FluoroBrite™ DMEM, Foetal Bowine Serum (FBS), 0.25% Trypsin-EDTA, antibiotics (Penicillin/Streptomycin), L-Glutamine were parched from Gibco, and DMEM High Glucose, Dulbeco's Phosphate Buffered Saline from Biowest. The MitoTracker™ Green FM was purchased from Molecular Probes.

Experimental part

General procedure for the preparation of compounds **4-7**.

To a solution of bromoarene (2.4 mmol) in 9 mL of anhydrous THF was slowly added sec-BuLi (1.4 M in cyclohexane, 1.7 mL, 2.4 mmol) at −78 °C and the resulting mixture was stirred for 2 h at the same temperature. A suspension of ketone **3** (200 mg, 0.6 mmol) in THF (25 mL) was added dropwise over 20 min. The reaction mixture was allowed to warm up to room temperature overnight. To the solution, 30 mL of 2 M HCl was added and the stirring was continued for 18 h. During this time, the color of the mixture changed from brown to deep green. The mixture was diluted with water and washed five times with Et_2O to remove unreacted xanthone and byproducts. The aqueous layer was then extracted three times with CH_2Cl_2. The combined CH_2Cl_2 layers were dried over Na_2SO_4. The drying agent was filtered off and the filtrate was evaporated. The product was recrystallized from the mixture of Et_2O/DCM/MeOH. However, the pure product was not obtained due to the fast cleavage of methyl group from diethylamino fragment.

Compound **4**. Yield 70%.

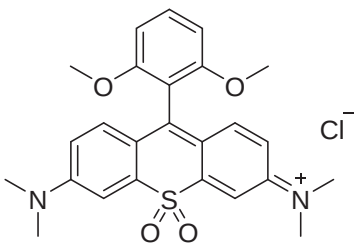

4

It was not possible to get clean NMR spectra, though MS spectrum suggests product **4**. HRMS (ESI) calcd. for $C_{25}H_{27}N_2O_4S$ 451.1692 $[M]^{+\bullet}$, found 451.1696.

Compound **5**. Yield 57%.

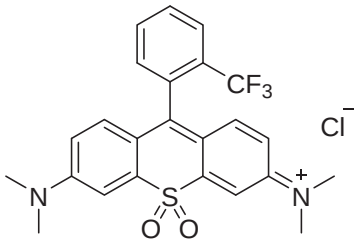

5

It was not possible to get clean NMR spectra, though MS spectrum suggests product **5**. HRMS (ESI) calcd. for $C_{24}H_{22}N_2O_2F_3S$ 459.1354 $[M]^{+\bullet}$, found 459.1318.

Compound **6**. Yield 42%.

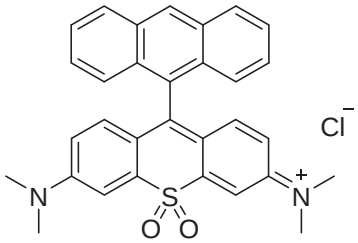

6

It was not possible to get clean NMR spectra, though MS spectrum suggests product **6**. HRMS (ESI) calcd. for $C_{31}H_{27}N_2O_2S$ 491.1793 $[M]^{+\bullet}$, found 491.1793.

Compound **7**. Yield 78%.

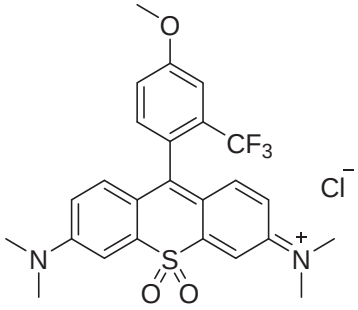

7

It was not possible to get clean NMR spectra, though MS spectrum suggests product 4d. HRMS (ESI) calcd. for $C_{25}H_{24}N_2O_3F_3S$ 489.1460 $[M]^{+\bullet}$, found 489.1460.

General procedure for the preparation of compounds **8-11**. To a solution of SO_2-Rhodamine (0.040 mmol) in 50.0 mL of CH_2Cl_2 and 20.0 mL of 0.5 M NaOH aq. was added. The mixture was stirred for 1 h at room temperature, diluted with DCM, and washed four times with water. The organic layer was dried over Na_2SO_4. The drying agent was filtered off and solvents were evaporated under reduced pressure. The product was purified using column chromatography (silica, CH_2Cl_2 : acetone 95:5). After evaporation of the solvent and drying under vacuum rhodols were obtained as violet-blue solids.

Compound **8**. Yield 25%. M.p. 224-225°C

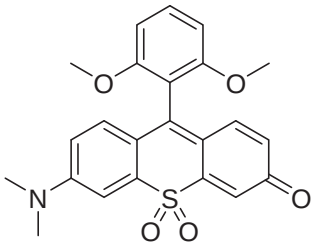

8

^{1}H NMR (500 MHz, $CDCl_3$) δ: 7.45 (t, 1H, J = 8.4 Hz), 7.39 (d, 1H, J = 2.7 Hz), 7.28 (d, 1H, J = 1.9 Hz), 6.94 (d, 1H, J = 9.9 Hz), 6.92 (d, 1H, J = 9.2 Hz), 6.68 (d, 2H, J = 8.4 Hz), 6.60 (dd, 1H, J_1 = 8.4 Hz, J_2 = 2.7 Hz), 6.28 (dd, 1H, J_1 = 9.9 Hz, J_2 = 1.9 Hz), 3.69 (s, 6H), 3.14 (s, 6H); ^{13}C NMR (126 MHz, $CDCl_3$) δ: 186.9, 160.8, 154.7, 148.1 (2), 143.1, 141.3, 136.6, 134.1, 130.2, 128.5, 124.1, 122.0, 117.2, 115.0, 110.0, 106.7, 58.9, 43.1; HRMS (ESI) calc. for $C_{23}H_{21}NO_5SNa$ 446.1038 $[M + Na]^+$, found 446.1034.

Compound **9**. Yield 25%. M.p. 210-212°C

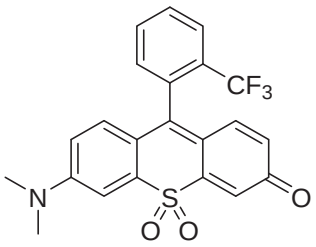

9

Yield 39%. ^{1}H NMR (500 MHz, $CDCl_3$) δ: 7.89 (d, 1H, J = 7.6 Hz), 7.73 (t, 1H, J = 7.3 Hz), 7.69 (t, 1H, J = 7.5 Hz), 7.43 (d, 1H, J = 2.4 Hz), 7.33 (d, 2H, J = 9.1 Hz), 6.68 (t, 1H, J = 10.1 Hz), 6.65 (s, 1H), 6.58 (dd, 1H, J_1 = 9.1 Hz, J_2 = 2.4 Hz), 6.27 (dm, 1H), 3.17 (s, 6H); ^{13}C NMR (126 MHz, $CDCl_3$) δ: 183.6, 151.9, 145.6, 144.9, 140.0, 137.7, 134.6, 133.7, 132.1, 131.2, 129.6, 127.5, 126.9, 126.9, 126.5, 120.8, 118.9, 114.0, 107.5, 40.3; HRMS (ESI) calcd. for $C_{22}H_{17}NO_3SF_3$ 432.0881 $[M + H]^+$, found 432.0874.

Compound **10**. Yield 11%. M.p. 250°C(dec.)

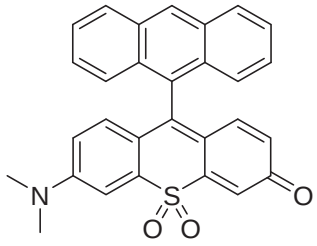

10

^{1}H NMR (600 MHz, $CDCl_3$) δ: 8.65 (s, 1H), 8.11 (d, 2H, J = 8.52 Hz), 7.69 (d, 2H, J = 8.7 Hz), 7.51 (m, 3H), 7.44 (m, 3H), 6.50 (d, 1H, J = 10 Hz), 6.42 (d, 1H, J = 9.3 Hz), 6.36 (dd, 1H, J_1 = 9.2 Hz, J_2 = 2.8 Hz), 6.10 (dd, 1H, J_1 = 9.9 Hz, J_2 = 1.7 Hz), 3.13 (s, 6H); ^{13}C NMR (151 MHz, $CDCl_3$) δ: 183.4, 152.0, 148.1, 144.7, 140.2, 138.1, 135.1, 130.9, 130.2, 128.8, 128.7, 128.3, 127.8, 127.4, 126.0, 125.9, 125.5, 122.3, 119.5, 114.5, 107.5, 40.3; HRMS (ESI) calcd. for $C_{29}H_{22}NO_3S$ 464.1320 $[M + H]^+$, found 464.1337.

Compound **11**. Yield 25%. M.p. 238-240°C

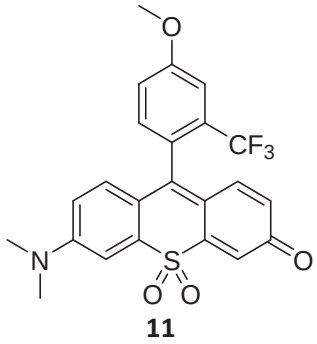

11

^{1}H NMR (500 MHz, $CDCl_3$) δ: 7.42 (d, 1H, J = 2.8 Hz), 7.36 (d, 1H, J = 1.9 Hz), 7.31 (d, 1H, J = 2.0 Hz), 7.21 (d, 2H, J = 1.6 Hz), 6.74 (dd, 2H, J_1 = 19.4 Hz, J_2 = 9.6 Hz), 6.59 (dd, 1H, J_1 = 9.2 Hz, J_2 = 2.8 Hz), 6.28 (dd, 1H, J_1 = 10.0 Hz, J_2 = 2.0 Hz), 3.95 (s, 3H), 3.17 (s, 6H); ^{13}C NMR (126 MHz, $CDCl_3$) δ: 182.6, 160.2, 151.9, 146.0, 145.0, 140.0, 137.9, 134.7, 132.5, 130.8, 127.5, 126.4, 125.2, 121.3, 119.3, 117.4, 114.0, 107.4, 55.8, 40.3; HRMS (ESI) calcd. for $C_{23}H_{19}NO_4SF_3$ 462.0987 $[M + H]^+$, found 462.0983.

Compound **12**.

A solution of **11** (400 mg, 0.87 mmol) in dry DCM (50 ml) under Ar was cooled to at 0˚C and boron tribromide (225 mg, 0.9 mmol, 0.085 ml) was added dropwise upon stirring. The reaction was allowed to warm to rt and left stirring overnight. The mixture was diluted with 25 ml of saturated sodium bicarbonate and organic layer was separated, dried over sodium sulfate, filtrated and concentrated under the low pressure. The product was purified utilizing column chromatography (CH_2Cl_2 : acetone 95:5).

Yield 50%. M.p. 186-188°C

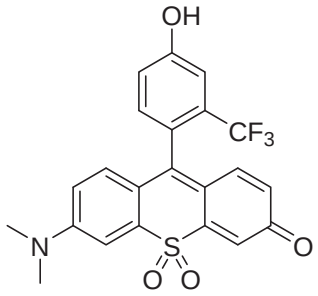

12

^{1}H NMR (500 MHz, DMSO-d_6) δ: 10.59 (s, 1H), 7.35 (1H, d, J = 3 Hz), 7.28 (2H, m), 7.20 (1H, dd, J_1 = 8.5 Hz, J_2 = 2.5 Hz), 7.01 (1H, d, J = 2 Hz), 6.86 (1H, dd, J_1 = 9 Hz, J_2 = 2.5 Hz), 6.79 (1H, d, J = 10 Hz), 6.72 (1H, d, J = 9.5 Hz), 6.27 (1H, dd, J_1 = 10 Hz, J_2 = 3 Hz), 3.15 (6H, s); ^{13}C NMR (126 MHz, DMSO- d_6) δ: 182.26, 158.40, 151.95, 147.30, 144.88, 139.42, 138.05, 134.86, 133.02, 128.88, 128.64, 128.40, 126.72, 124.52, 124.24, 122.70, 122.34, 119.53, 119.41, 117.91, 114.82, 113.17, 113.13, 107.06; ^{19}F NMR (500 MHz, $CDCl_3$) δ: -58.42; HRMS (ESI) calcd. for $C_{22}H_{17}NO_4SF_3$ 448.0830 $[M + H]^+$, found 448.0820.

Compound **13**.

Compound **12** (194 mg, 0.43 mmol) was dissolved in dry CH_3CN (10 ml) followed by the addition of K_2CO_3 (240 mg, 1.74 mmol). 1,6-dibromohexane (159 mg, 0.65 mmol, 0.1 ml) was added under Ar and the reaction mixture was left refluxing for 18h. After the reaction complete, the solvent was evaporated under reduced pressure and the residue was dissolved in 50 ml of DCM. The organic layer was washes 3 times with water (50 ml), dried over Na_2SO_4 and concentrated in vacuo. The obtained solid was next boiled in 20 ml of hexane, filtered and washed again with hexane. The product was next purified via column chromatography (CH_2Cl_2 : acetone 95:5).

Yield 50%. M.p. 125-127°C(dec.)

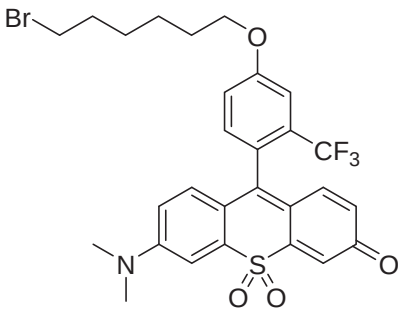

13

^{1}H NMR (500 MHz, $CDCl_3$) δ: 7.41 (d, 1H, J = 2 Hz), 7.35 (d, H, J = 2 Hz), 7.31 (d, 1H, J = 2 Hz), 7.19 (m, 2H), 6.77 (d, 1H, J = 10 Hz), 6.73 (d, 1H, J = 9 Hz), 6.58 (dd, 1H, J_1 = 9.5 Hz, J_2 = 3 Hz), 6.28 (dd, 1H, J_1 = 10 Hz, J_2 = 3 Hz), 4.09 (t, 2H, J = 6 Hz), 3.46 (t, 2H, J = 6 Hz), 3.17 (s, 6H), 1.92 (dq, 4H, J_1 = 22 Hz, J_2 = 7 Hz), 1.57 (m, 4H); ^{19}F NMR (500 MHz, $CDCl_3$) δ: -59.53; ^{13}C NMR (126 MHz, $CDCl_3$) δ: 183.63, 159.64, 151.80, 146.11, 144.92, 139.97, 137.94, 134.78, 132.46, 130.67, 127.41, 126.32, 124.94, 121.20, 119.29, 117.64, 113.97, 113.01, 107.38, 77.25, 77.00, 76.75, 68.42, 40.27, 33.70, 32.59, 28.90, 27.83, 25.25. HRMS (ESI) calcd. for $C_{28}H_{27}NO_4SBrF_3Na$ 632.0694 $[M + Na]^+$, found 632.0658.

Compound **14**.

73 mg (0,12 mmol) of **13** with 0,31g (1,2 mmol) of triphenylphosphine in 0,3 ml of DMA was heated at 120° for 35 min under Argon. After cooling the reaction was diluted with a mixture hexane/Et_2O, the crude product was filtered and washed again and next purified via column chromatography on a reversed phase (RP-18) in CH_3CN. After evaporation if the solvent the product was washed with EtOAc for 1h to give 12 mg of the product.

Yield 11%. M.p. 137-139^{o}C(dec.)

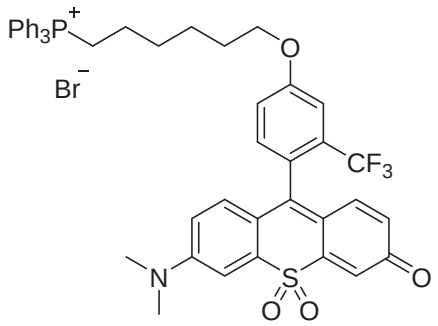

14

^{1}H NMR (500 MHz, CD_3CN) δ: 7.74 (bm, 15H), 7.42 (bd, 2H, J_1 = 6.5 Hz,), 7.3 (bs, 2H), 7.13 (bs, 1H), 6.83 (d, 1H, J = 10 Hz), 6.79 (d, 1H, J = 9.5 Hz), 6.73 (dd, 1H, J_1 = 9. Hz, J_2 = 3 Hz), 6.22 (dd, 1H, J_1 = 9 Hz, J_2 = 2 Hz), 4.11 (t, 2H, J = 6.5 Hz), 3.27 (bm, 2H), 3.17 (s, 6H), 1.78 (q, 2H, J = 7.5 Hz), 1.7 (q, 2H, J = 7.5 Hz), 1.63 (q, 2H, J = 7.5 Hz), 1.54 (q, 2H, J = 7.5 Hz); ^{19}F NMR (500 MHz, CD_3CN) δ: -59.95; HRMS (ESI) calcd. for $C_{46}H_{42}NO_4SF_3P$ 792.2524 $[M]^+$, found 792.2505.

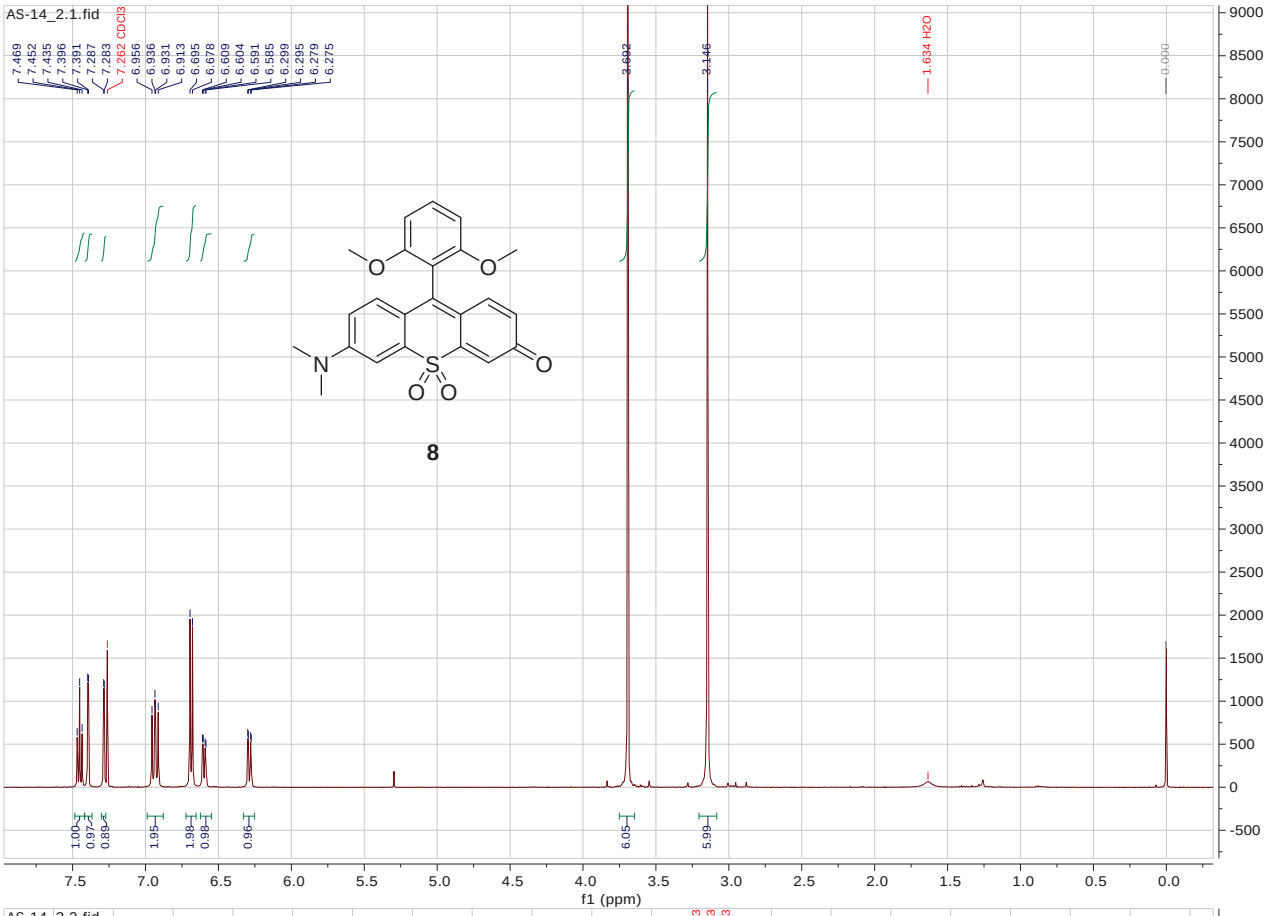

8

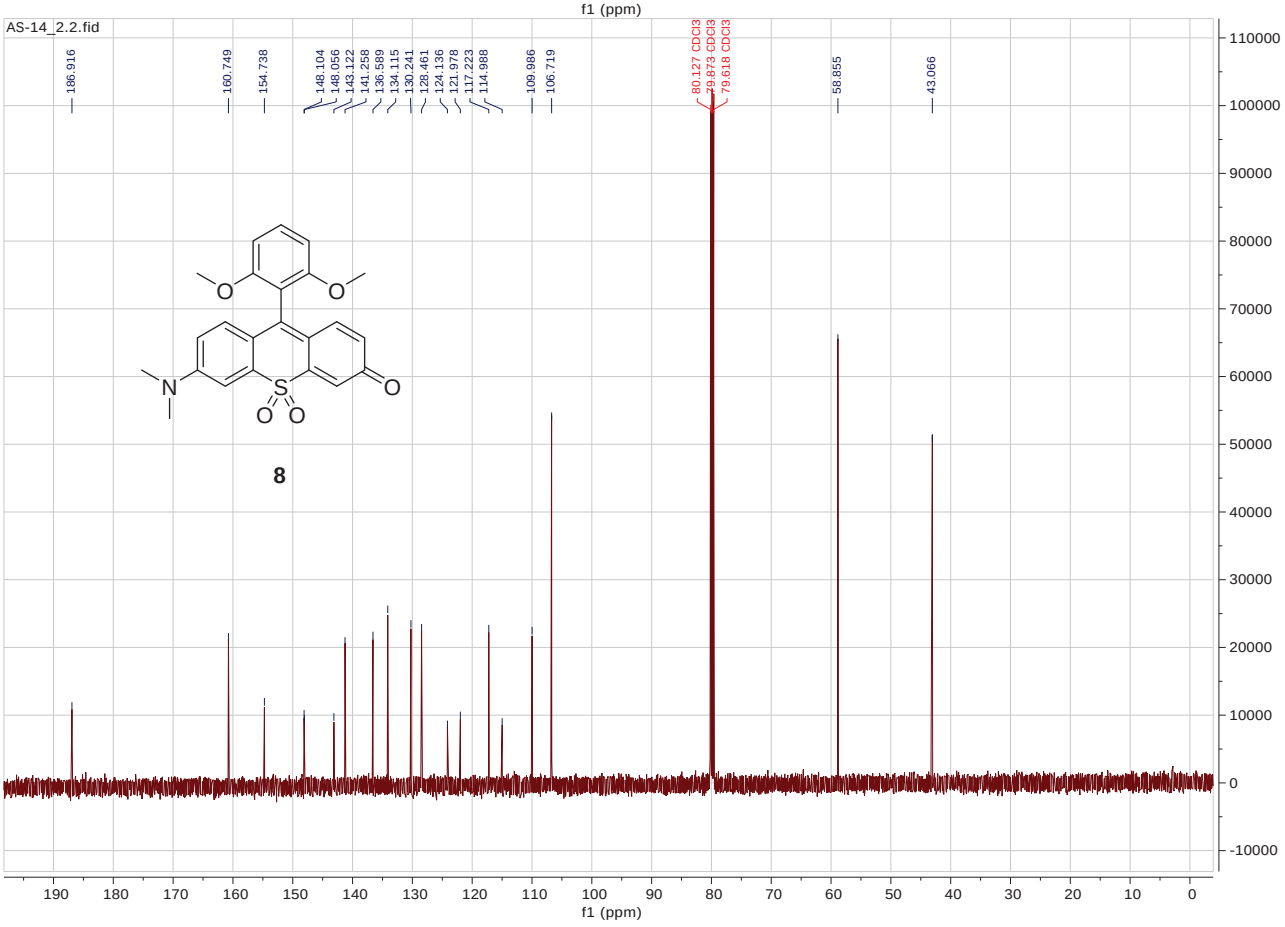

8

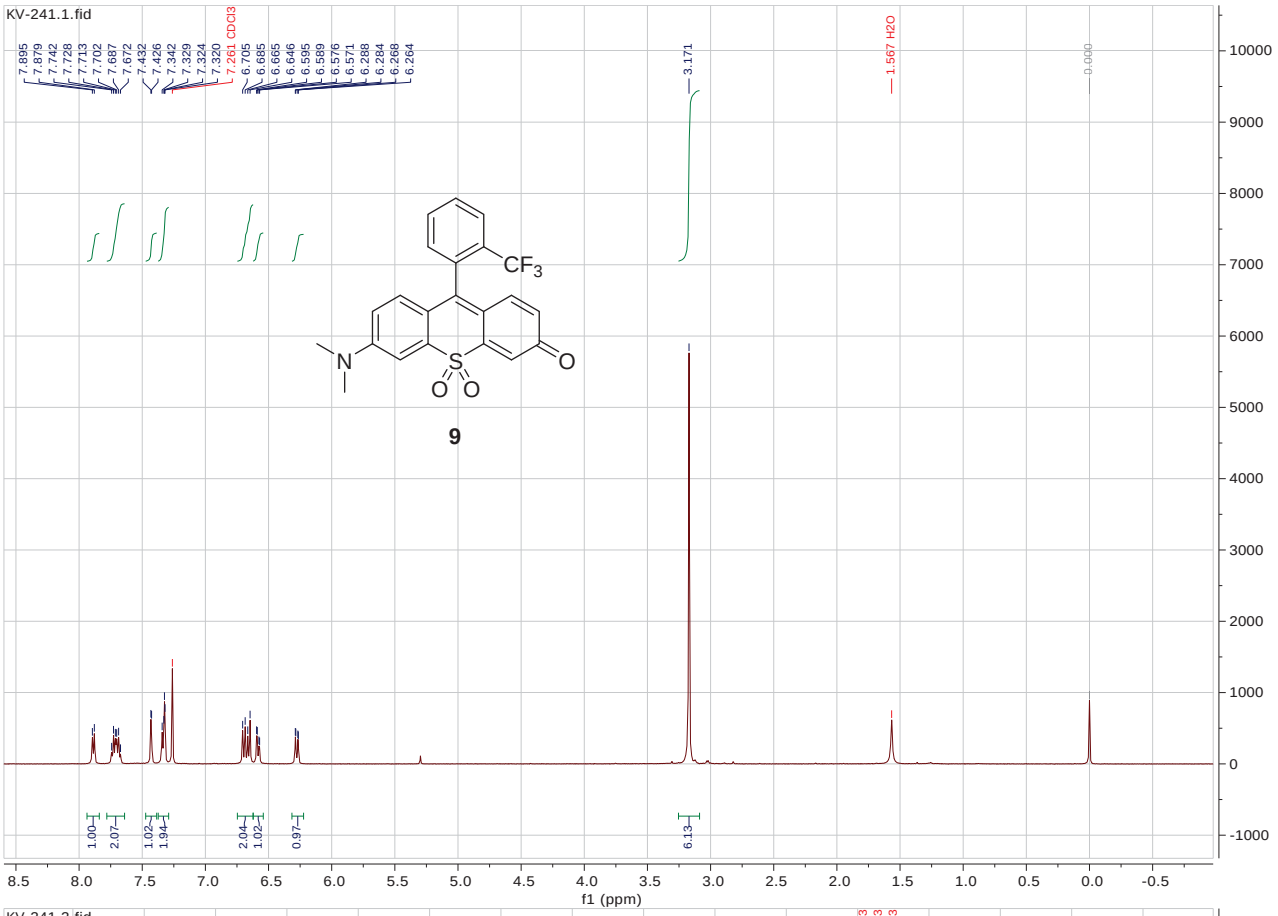
KV-241.1.fid
7.895
7.879
7.742
7.728
7.713
7.702
7.687
7.672
7.432
7.426
7.342
7.329
7.324
7.320
7.261 CDCl3
6.705
6.685
6.665
6.646
6.595
6.589
6.576
6.571
6.288
6.284
6.268
6.264
3.171
1.567 H2O
0.000
CF3
N
S
O
O
O
9
1.00
2.07
1.02
1.94
2.04
1.02
0.97
6.13
f1 (ppm)

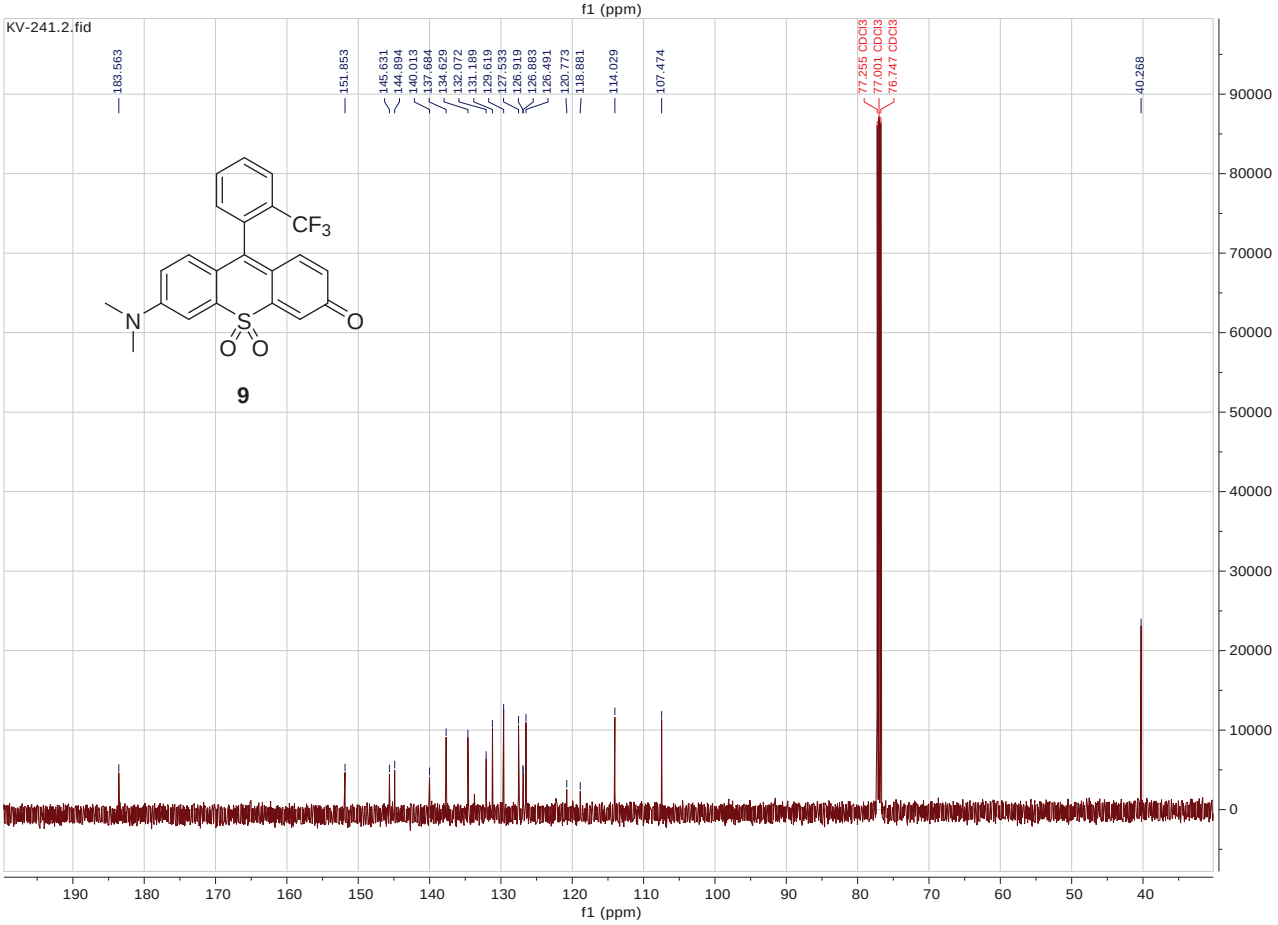
KV-241.2.fid
183.563
151.853
145.631
144.894
140.013
137.684
134.629
132.072
131.199
129.619
127.533
126.919
126.883
126.491
120.773
118.881
114.029
107.474
77.255 CDCl3
77.001 CDCl3
76.747 CDCl3
40.268
CF3
N
S
O
O
O
O
9
f1 (ppm)

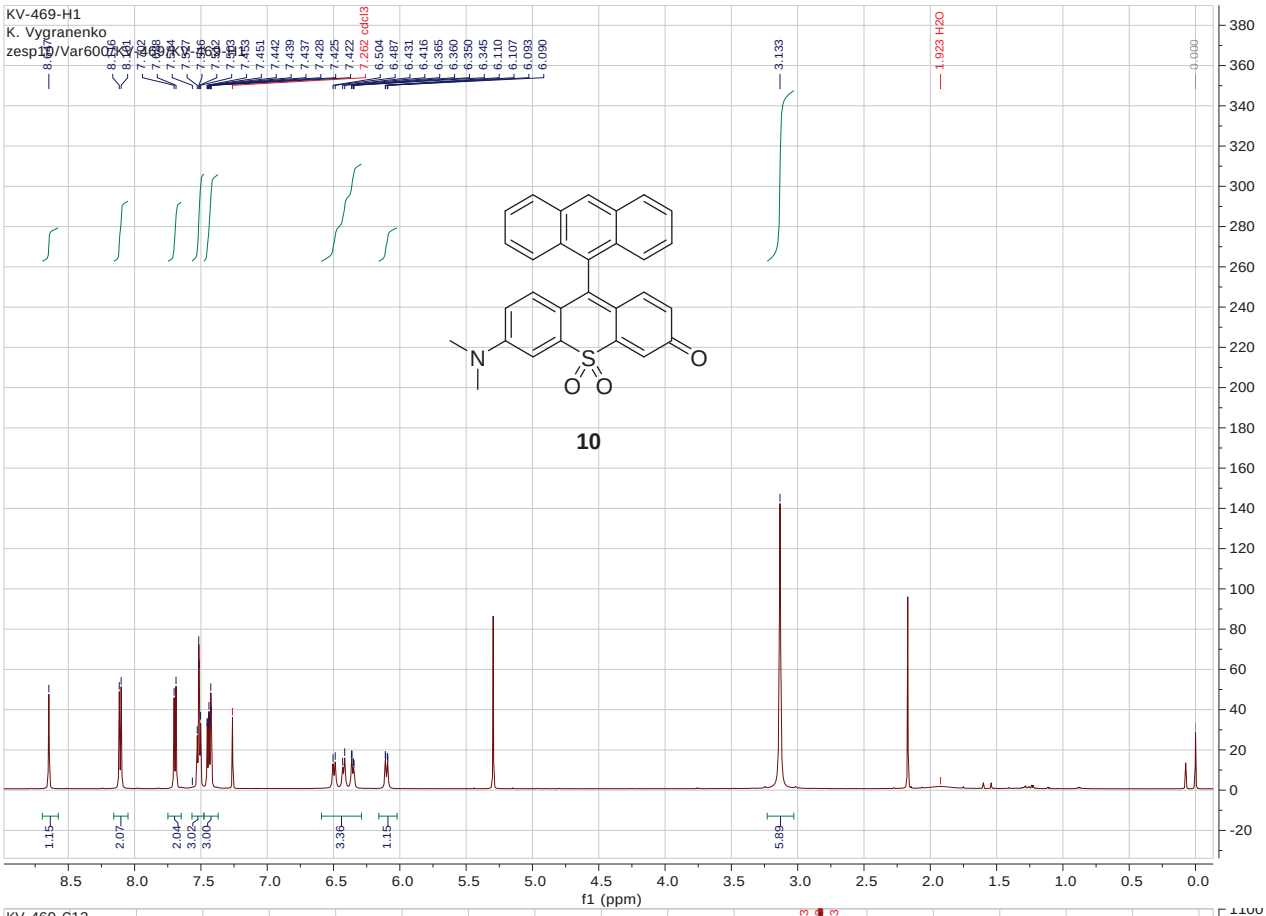

10

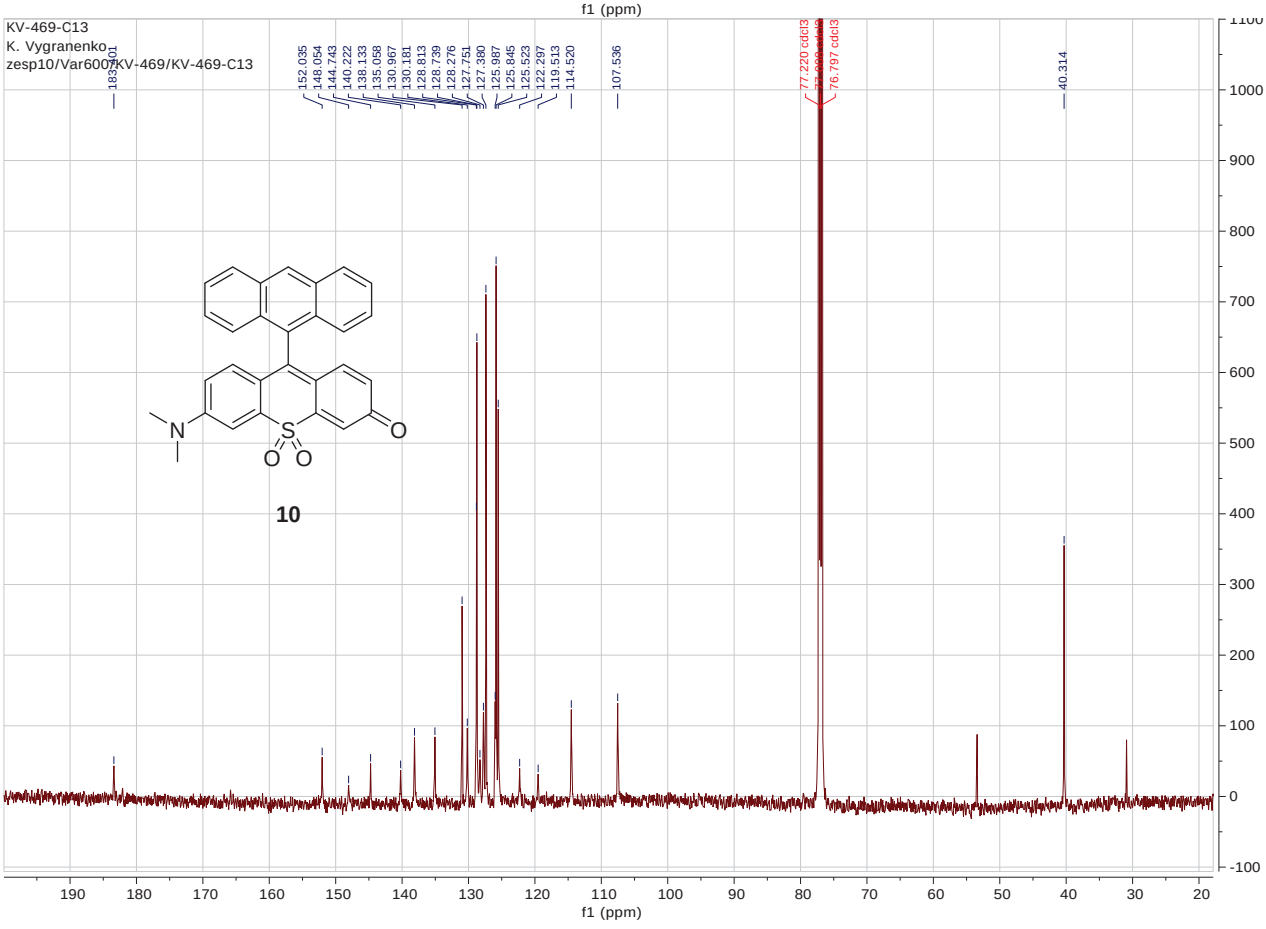

10

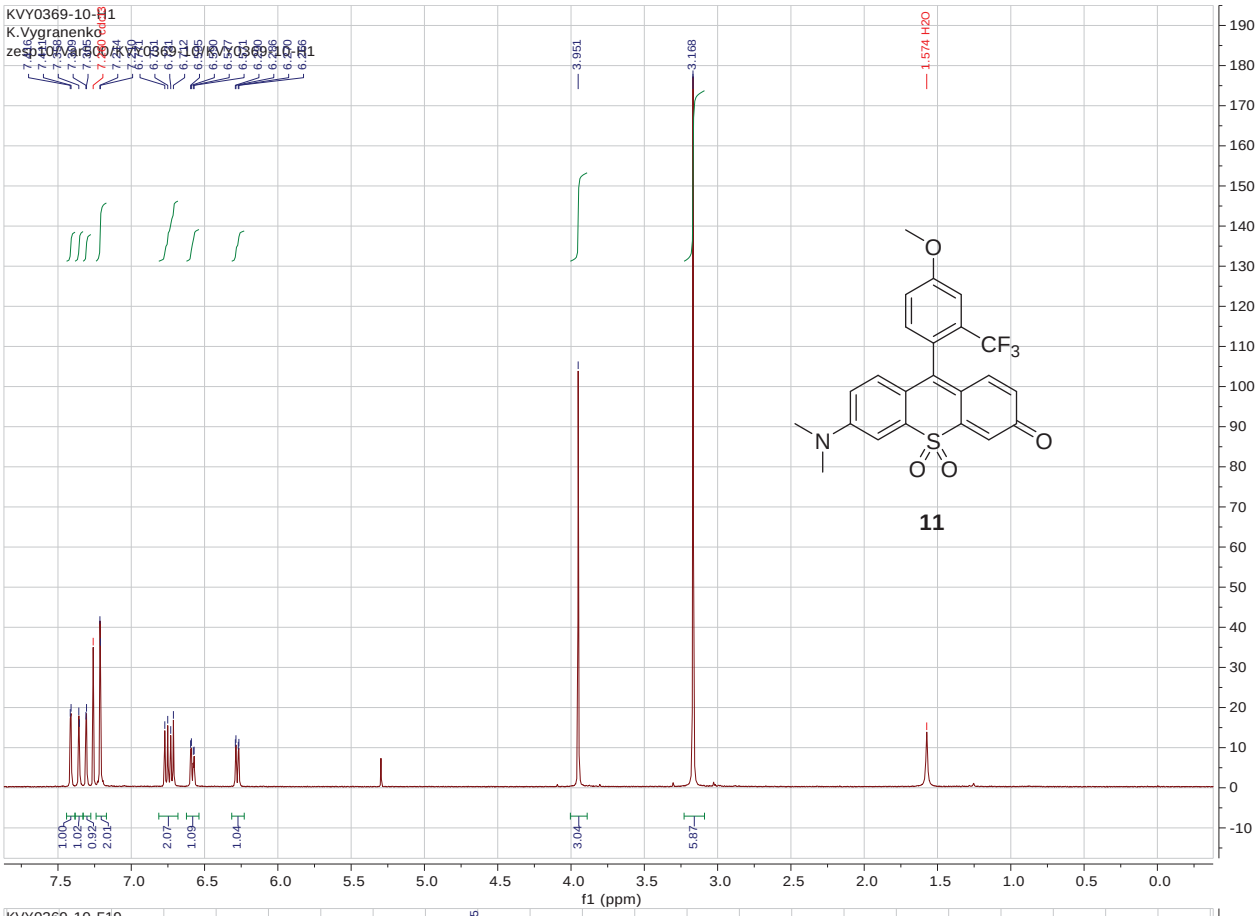
KVY0369-10-F1
K.Vygranenko
zesp10/Var500/KVY0369-10/KVY0369-10-F1
3.951
3.168
1.574 H2O
CF3
O
N
S
O
O
O
11
1.00
1.02
0.92
2.01
2.07
1.09
1.04
3.04
5.87
f1 (ppm)

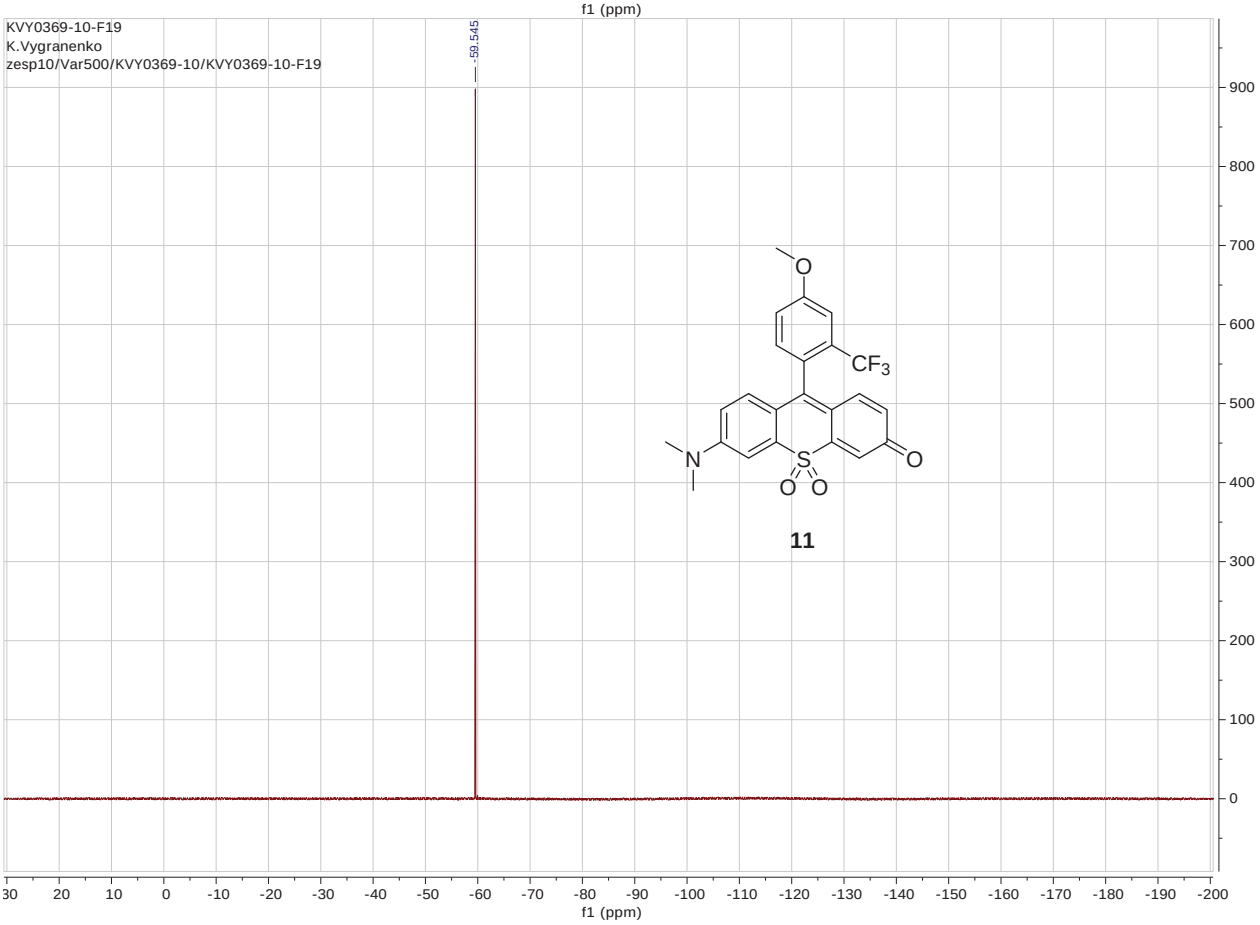
KVY0369-10-F19
K.Vygranenko
zesp10/Var500/KVY0369-10/KVY0369-10-F19
-59.545
CF3
O
N
S
O
O
O
11
f1 (ppm)

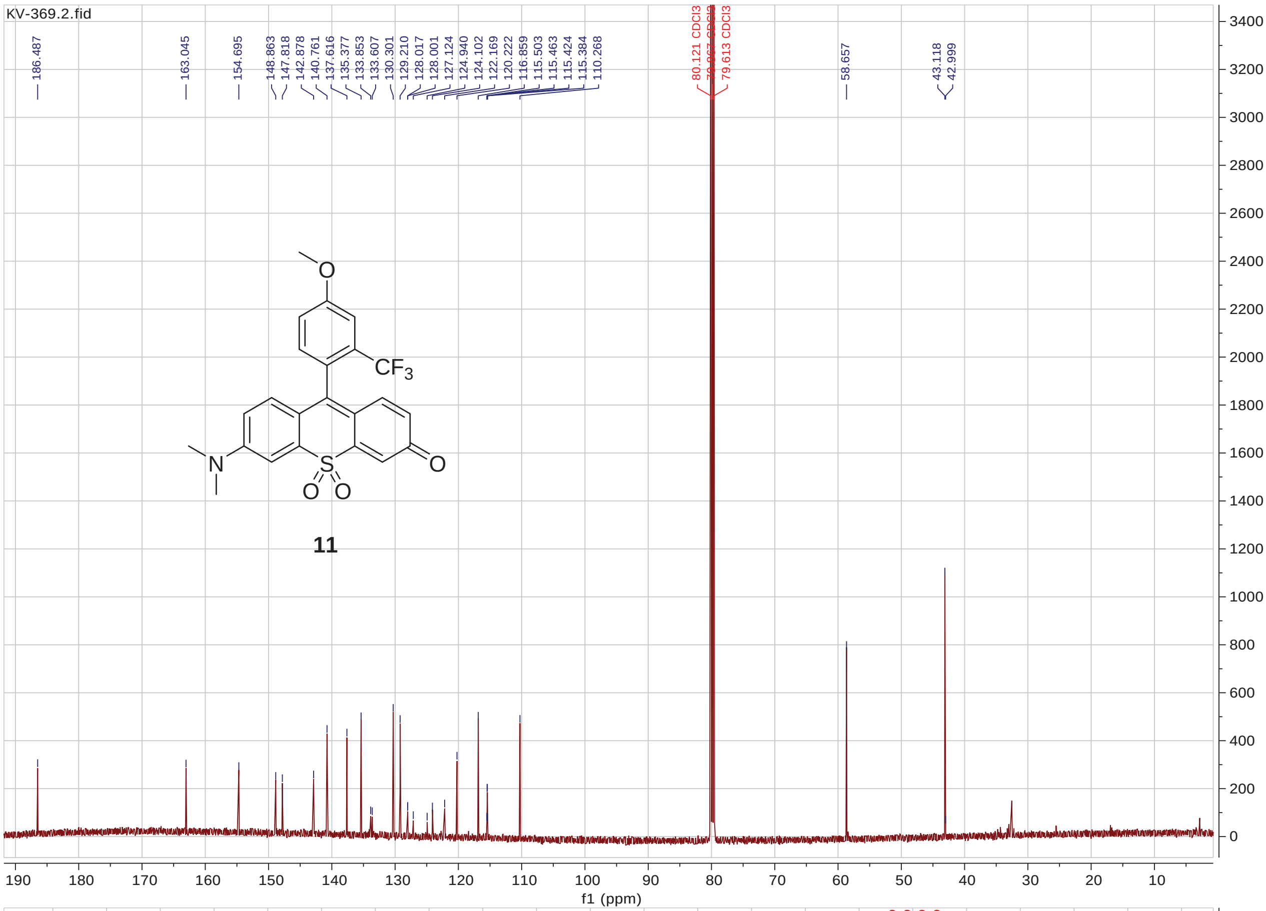

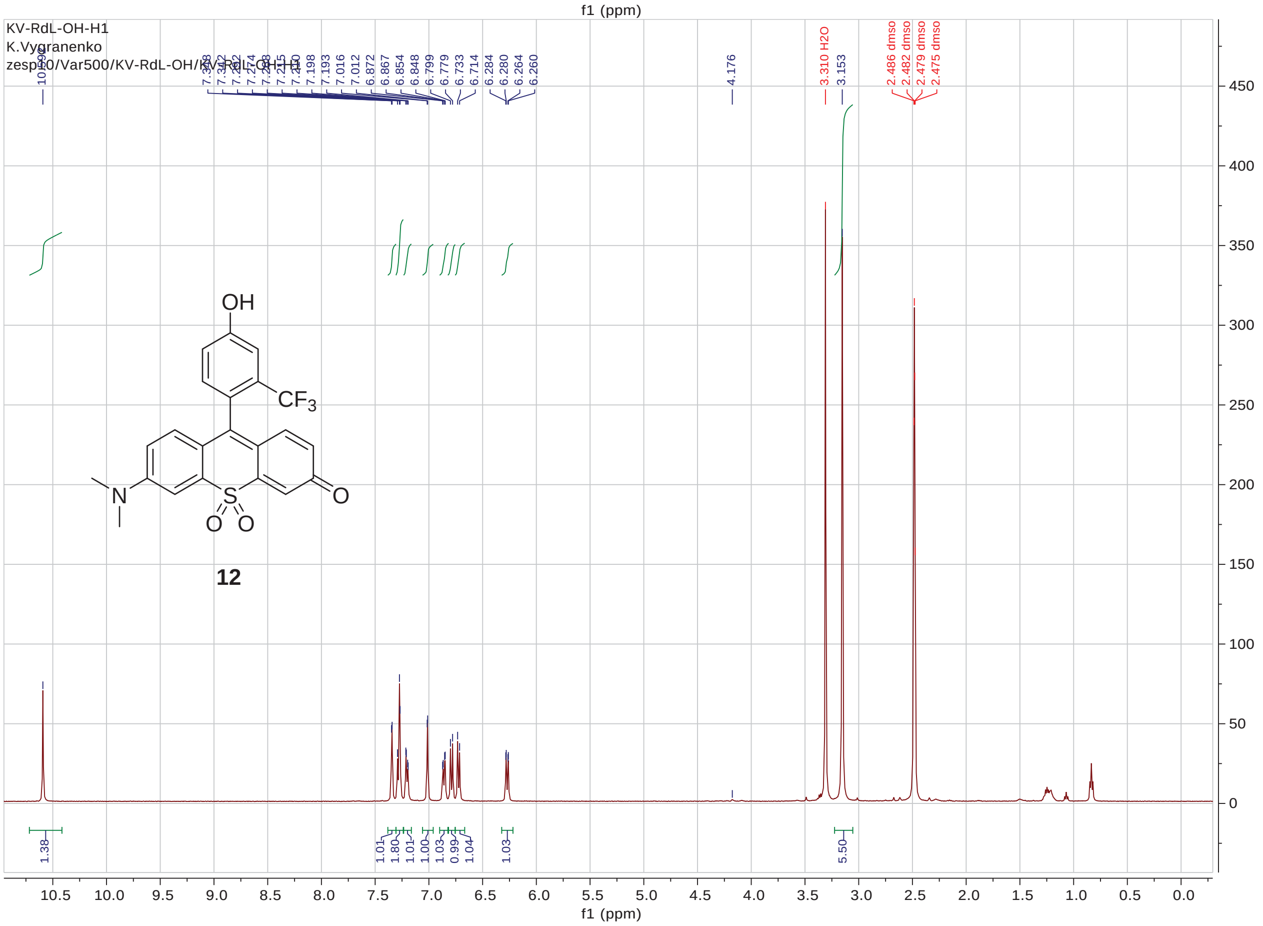

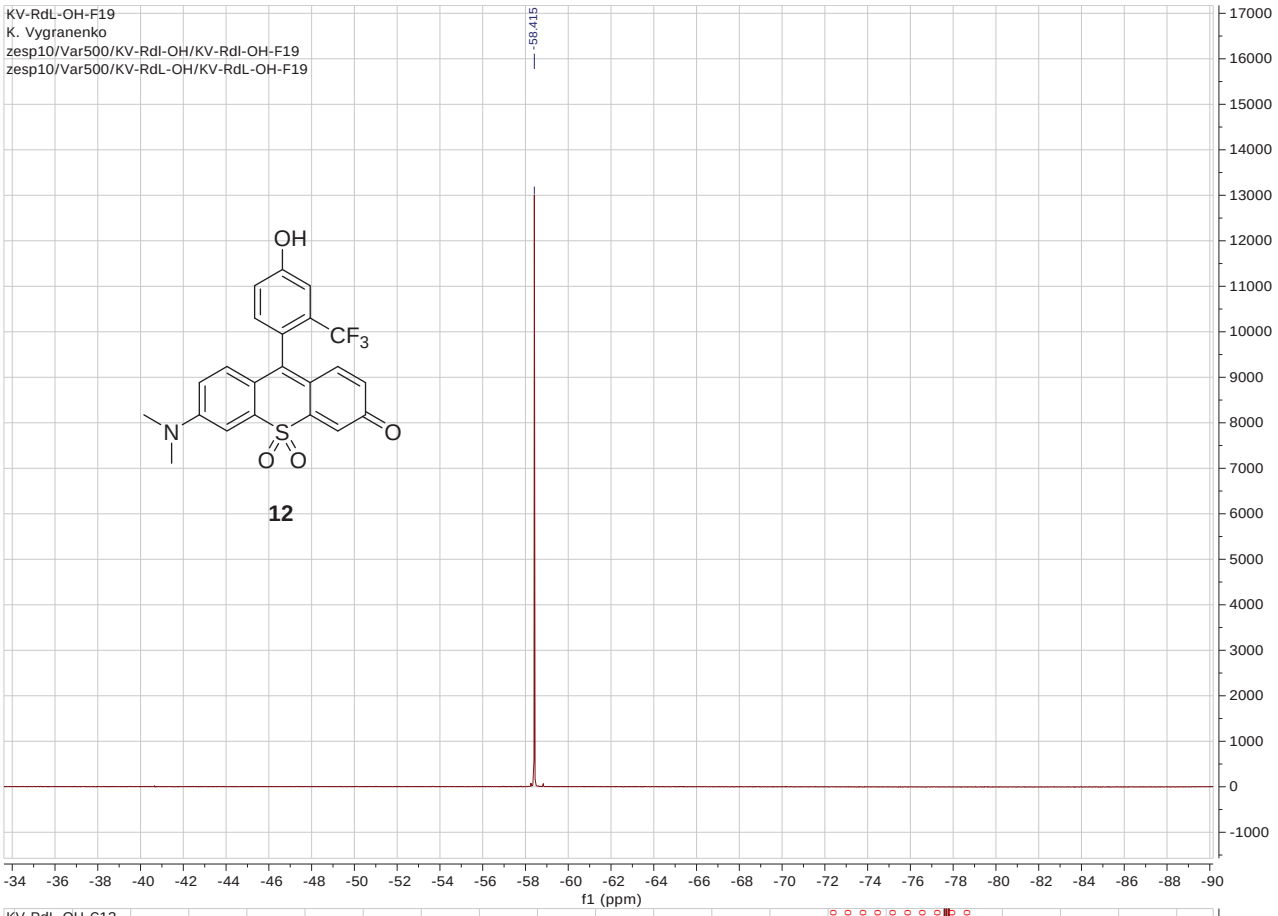
KV-RdL-OH-F19
K. Vygranenko
zesp10/Var500/KV-RdI-OH/KV-RdI-OH-F19
zesp10/Var500/KV-RdL-OH/KV-RdL-OH-F19
-58.415
OH
CF3
N
S
O
O
O
12
f1 (ppm)

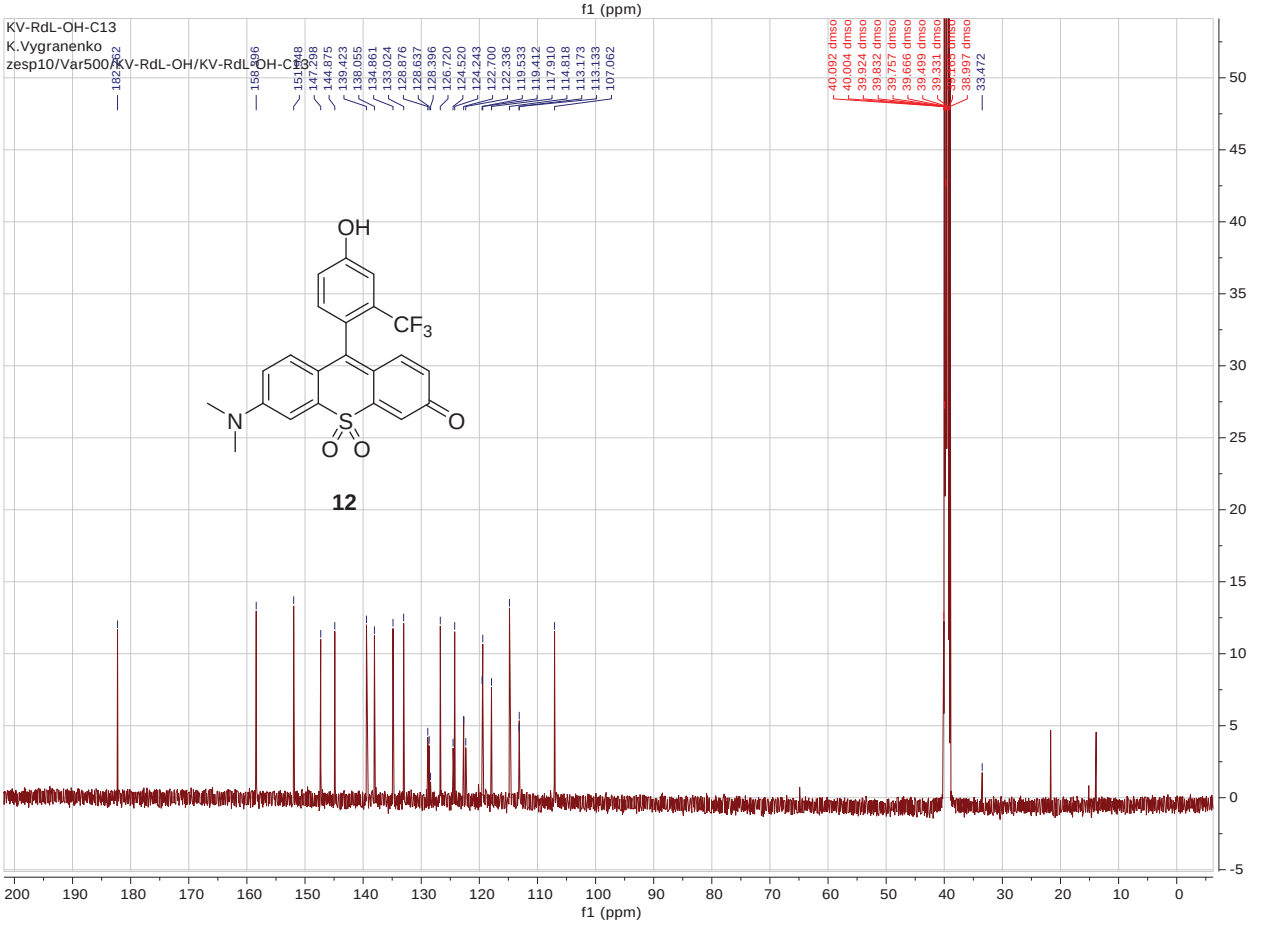
KV-RdL-OH-C13
K.Vygranenko
zesp10/Var500/KV-RdL-OH/KV-RdL-OH-C13
182.362
158.496
151.948
147.298
144.875
139.423
138.055
134.861
133.024
128.876
128.637
128.396
126.720
124.520
124.243
122.700
122.336
119.533
119.412
117.910
114.818
113.173
113.133
107.062
40.092 dmso
40.004 dmso
39.924 dmso
39.832 dmso
39.757 dmso
39.666 dmso
39.499 dmso
39.331 dmso
38.997 dmso
33.472
OH
CF3
N
S
O
O
O
12
f1 (ppm)

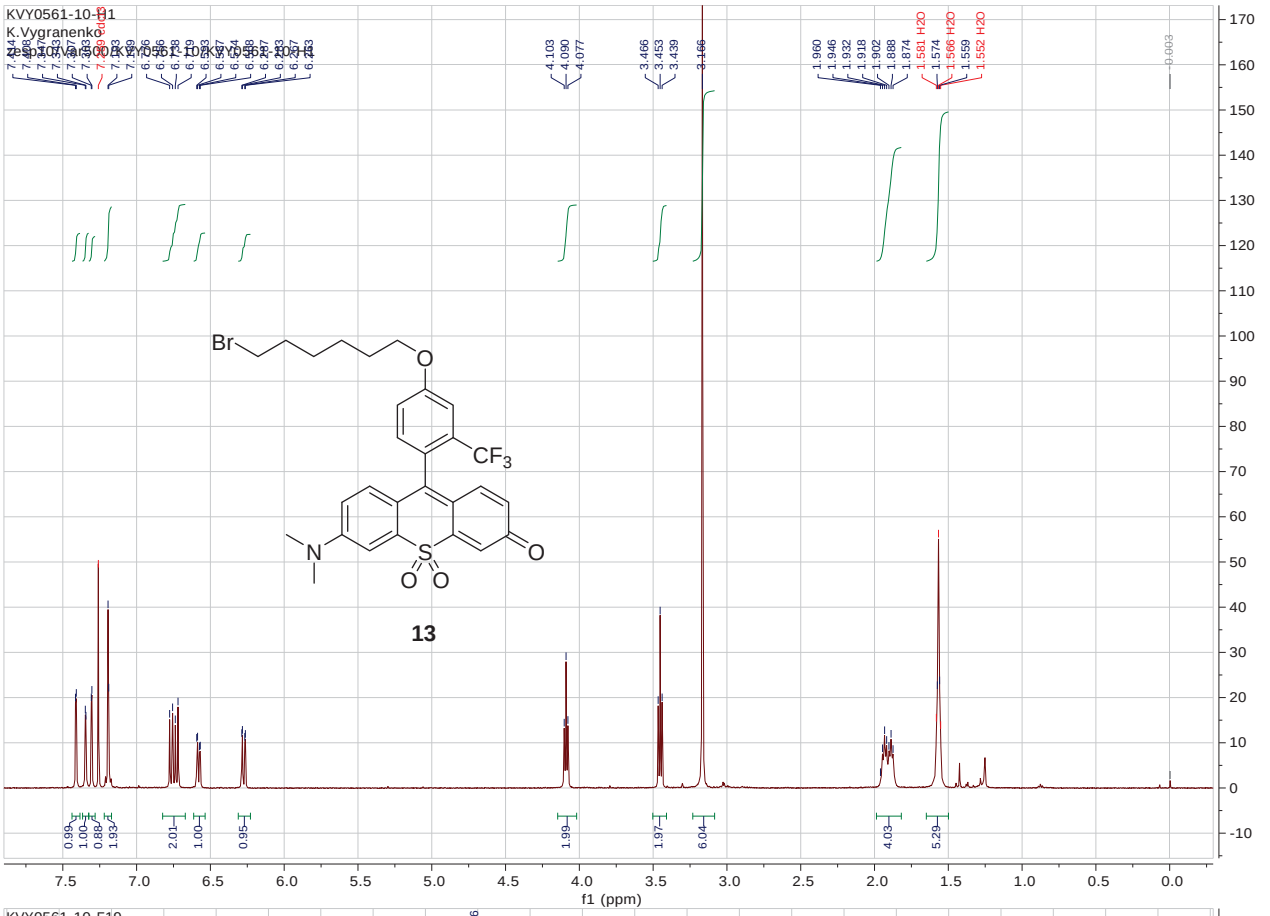
KVY0561-10-H1
K.Vygranenko
Br
O
CF3
N
S
O
O
O
13
f1 (ppm)

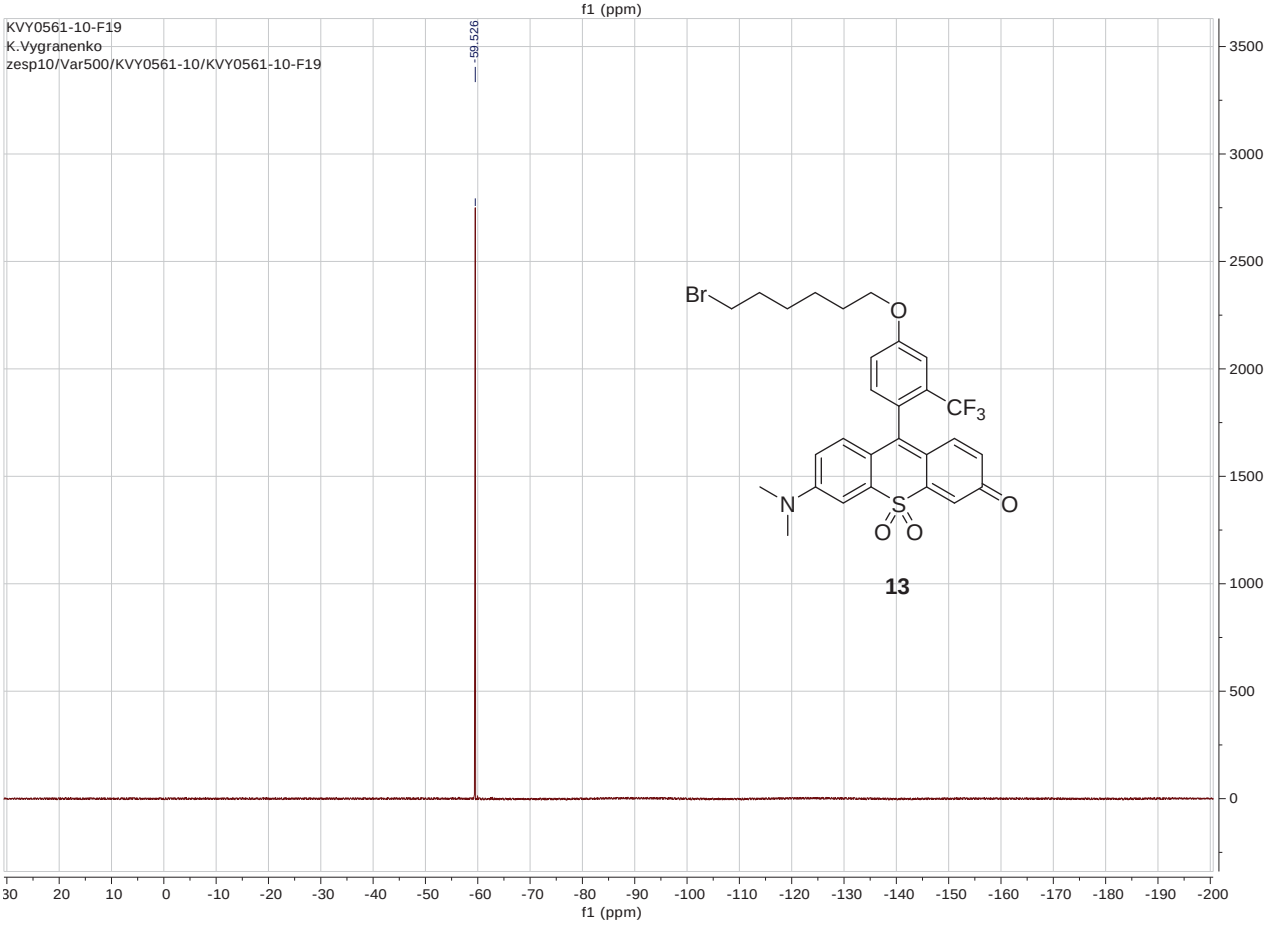
KVY0561-10-F19
K.Vygranenko
zesp10/Var500/KVY0561-10/KVY0561-10-F19
Br
O
CF3
N
S
O
O
O
13
f1 (ppm)

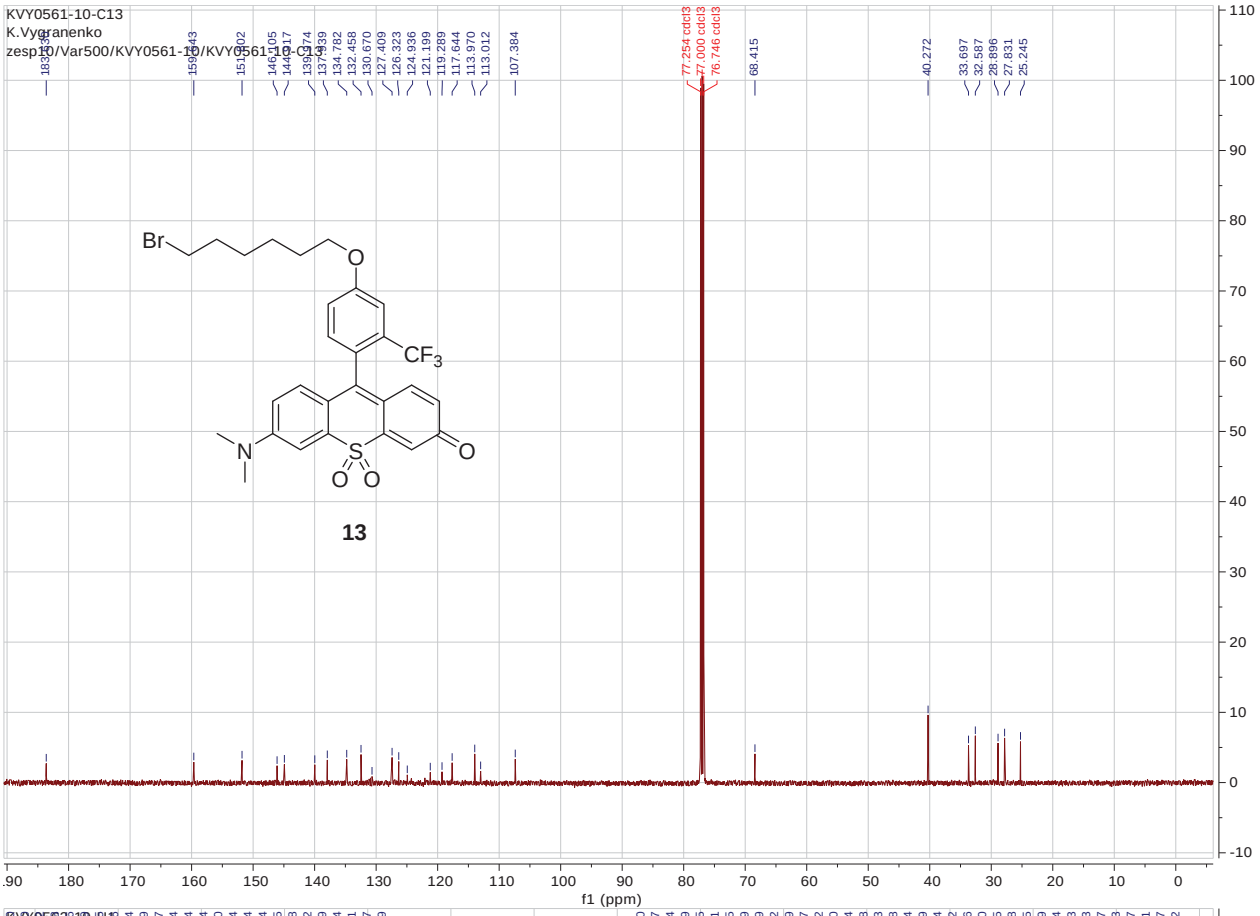
KVY0561-10-C13
K.Vygranenko
zesp10/Var500/KVY0561-10/KVY0561-10-C13
183.345
159.043
151.502
146.105
144.617
139.174
137.939
134.782
132.458
130.670
127.409
126.323
124.936
121.199
119.289
117.644
113.970
113.012
107.384
77.254 cdcl3
77.000 cdcl3
76.746 cdcl3
68.415
40.272
33.697
32.587
28.896
27.831
25.245
Br
O
CF3
N
S
O
O
O
13
f1 (ppm)

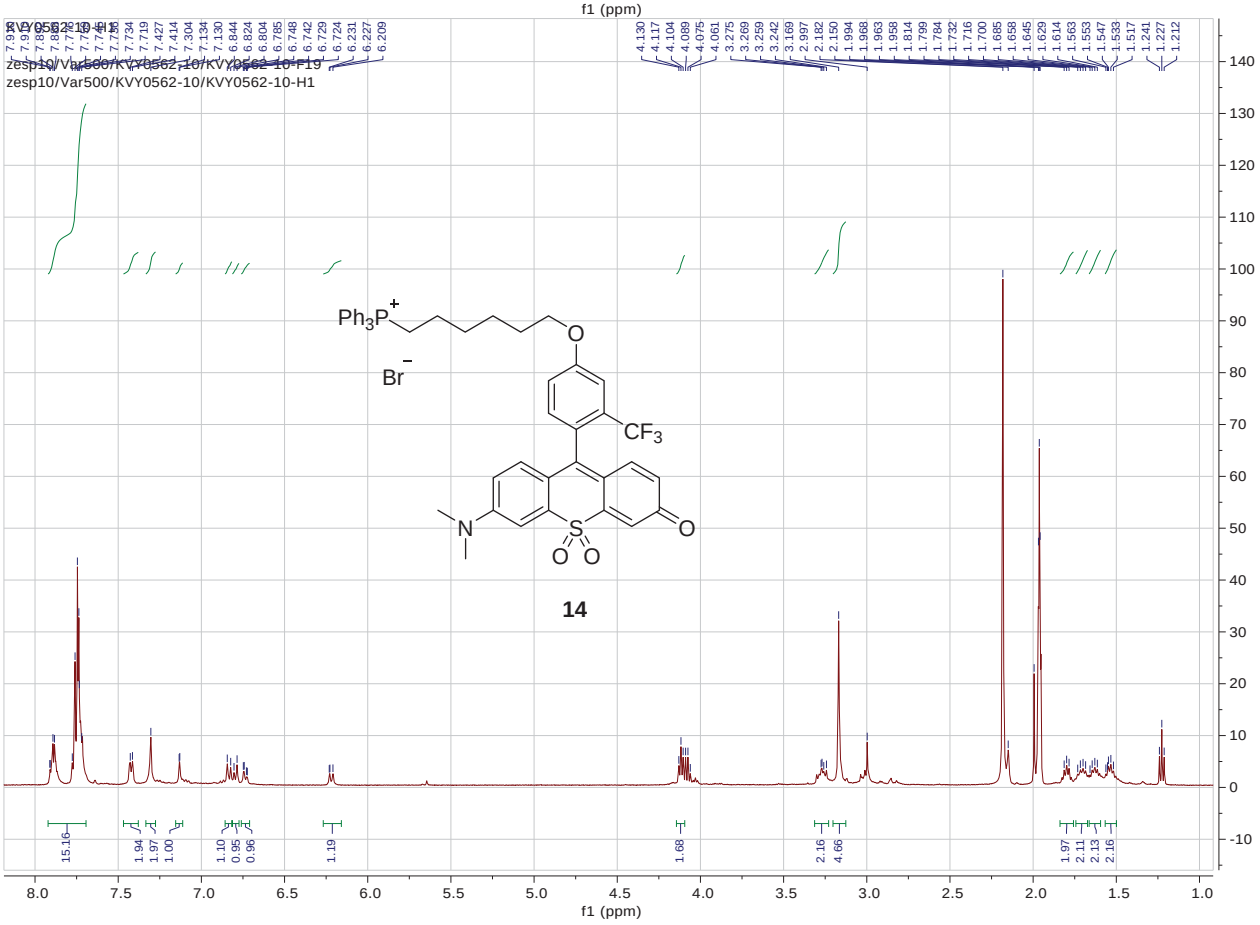
zesp10/Var500/KVY0562-10/KVY0562-10-H1
7.914
7.895
7.881
7.774
7.758
7.734
7.719
7.427
7.414
7.304
7.134
7.130
6.844
6.824
6.804
6.785
6.748
6.742
6.729
6.724
6.231
6.227
6.209
4.130
4.117
4.104
4.089
4.075
4.061
3.275
3.269
3.259
3.242
3.169
2.997
2.182
2.150
1.994
1.968
1.963
1.958
1.814
1.799
1.784
1.732
1.716
1.700
1.685
1.658
1.645
1.629
1.614
1.563
1.553
1.547
1.533
1.517
1.241
1.227
1.212
Ph3P
Br
O
CF3
N
S
O
O
O
14
15.16
1.94
1.97
1.00
1.10
0.95
0.96
1.19
1.68
2.16
4.66
1.97
2.11
2.13
2.16
f1 (ppm)

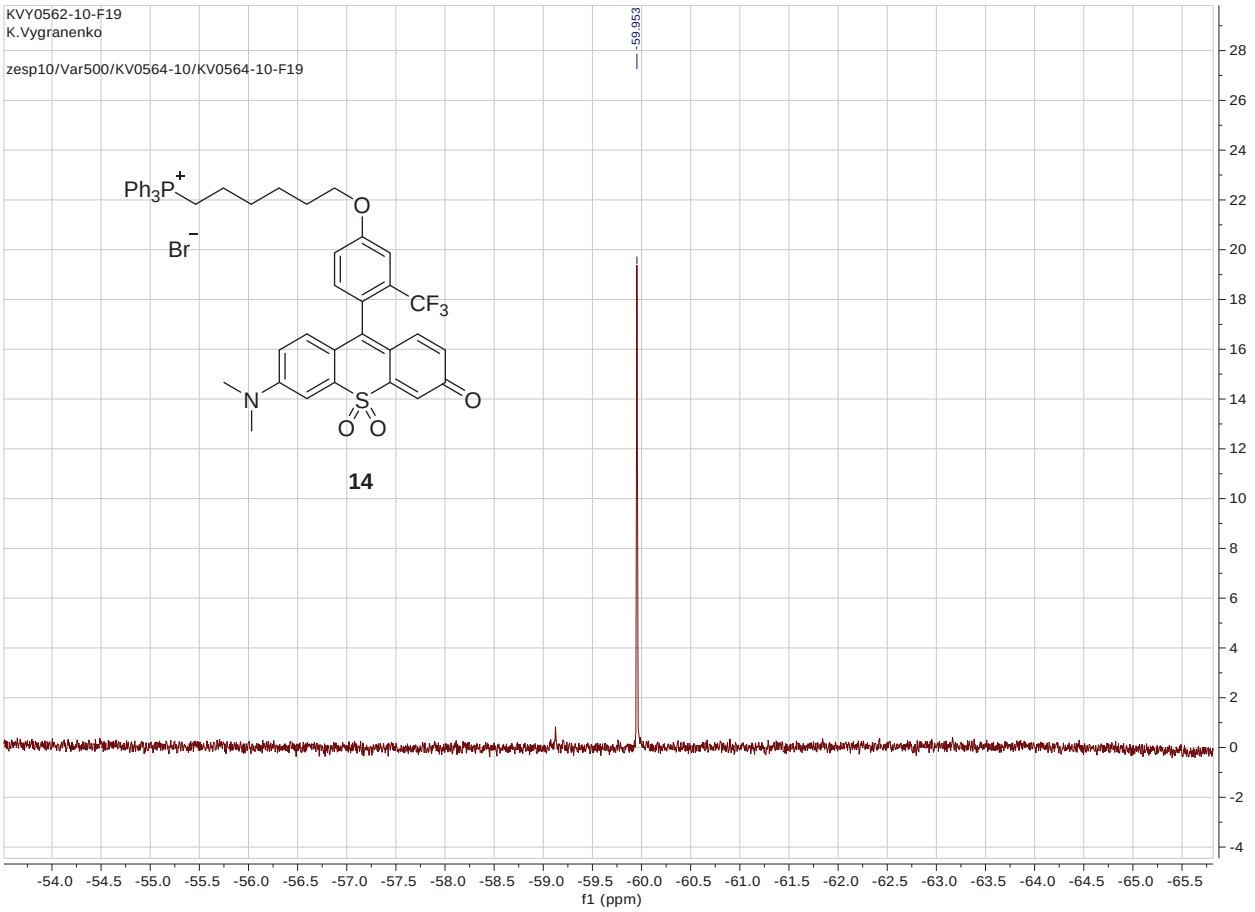

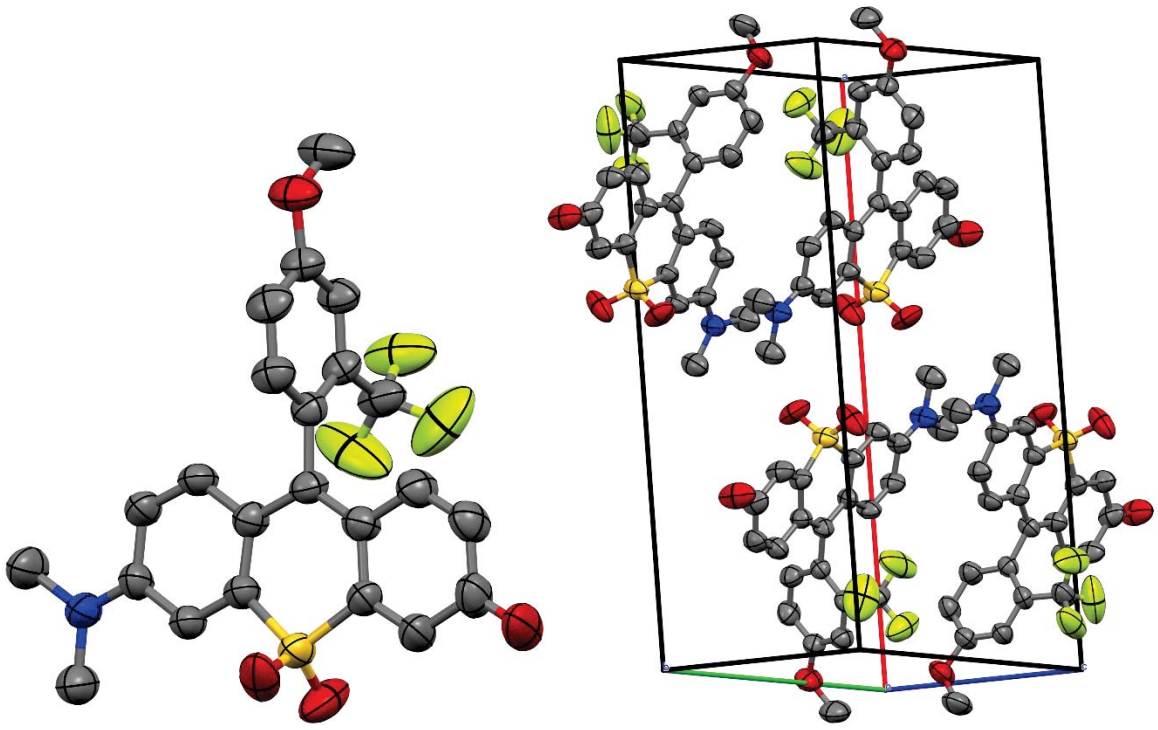

(a) X-ray structure (b) Crystal packing

Figure S1. X-Ray structure of compound **11** (a) and crystal packing (b).

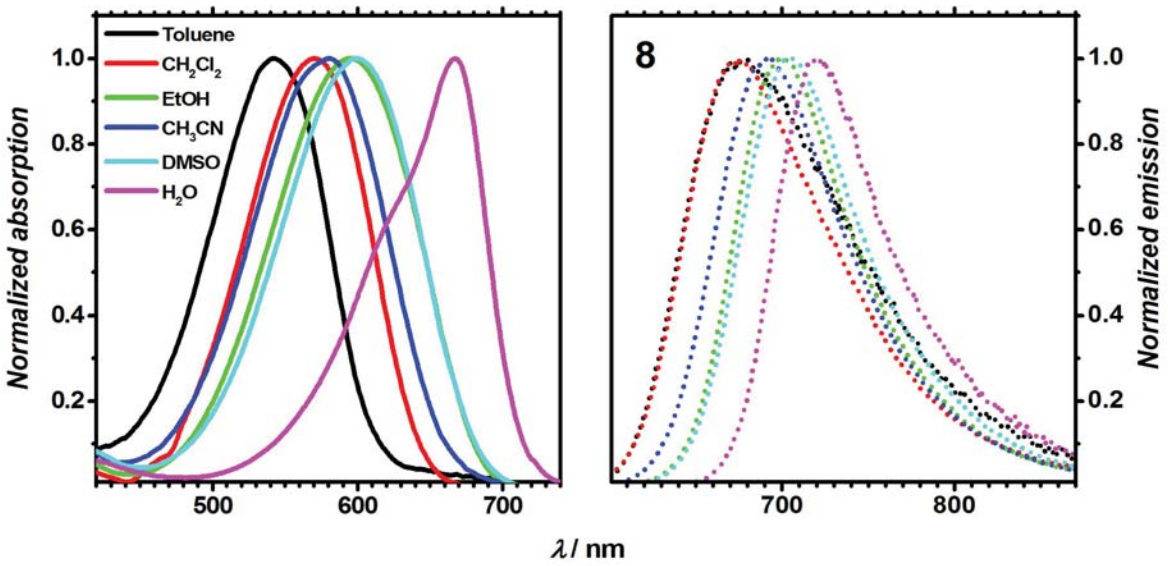

Figure S2. Absorption (solid) and emission (dotted) of compound **8** in toluene, CH_2Cl_2, EtOH, CH_3CN, DMSO, H_2O (containing 2% DMSO).

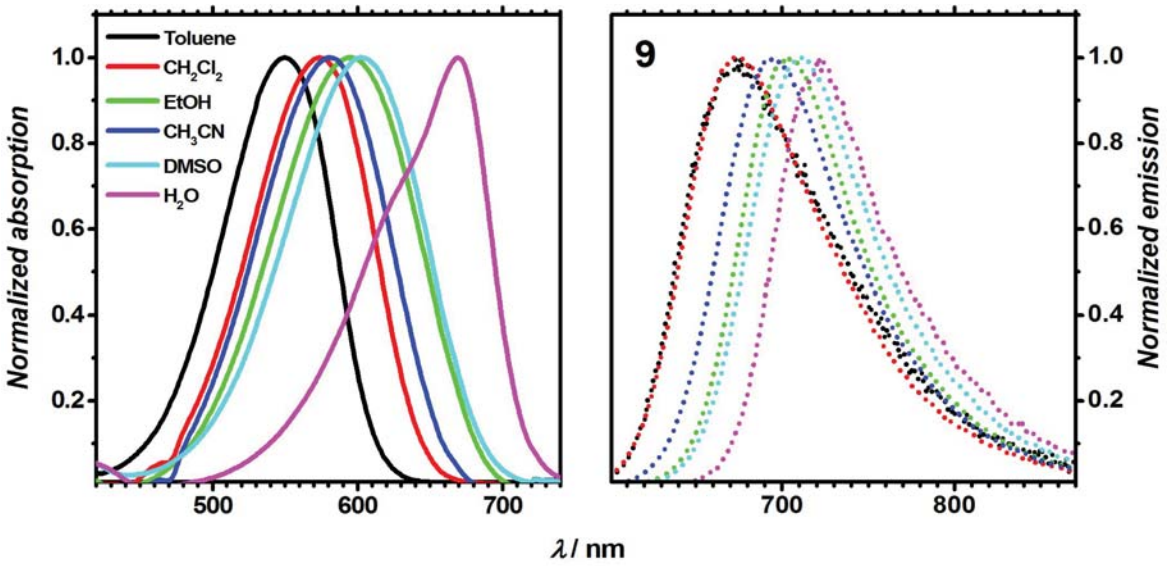

Figure S3. Absorption (solid) and emission (dotted) of compound **9** in toluene, CH_2Cl_2, EtOH, CH_3CN, DMSO, H_2O (containing 2% DMSO).

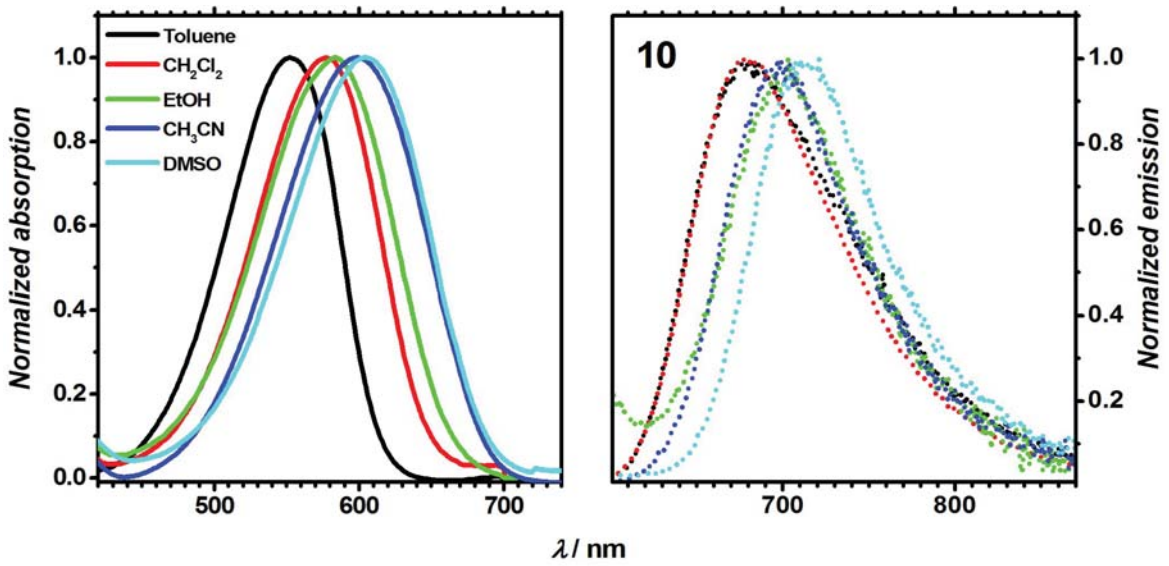

Figure S4. Absorption (solid) and emission (dotted) of compound **10** in toluene, CH_2Cl_2, EtOH, CH_3CN, DMSO, H_2O (containing 2% DMSO).

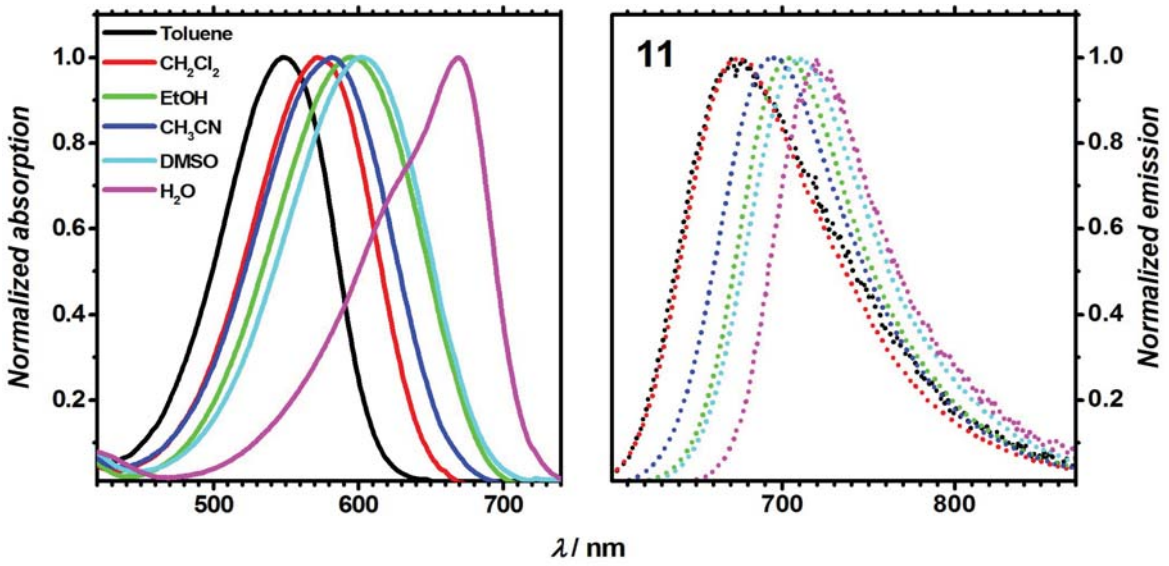

Figure S5. Absorption (solid) and emission (dotted) of compound **11** in toluene, CH_2Cl_2, EtOH, CH_3CN, DMSO, H_2O (containing 2% DMSO).

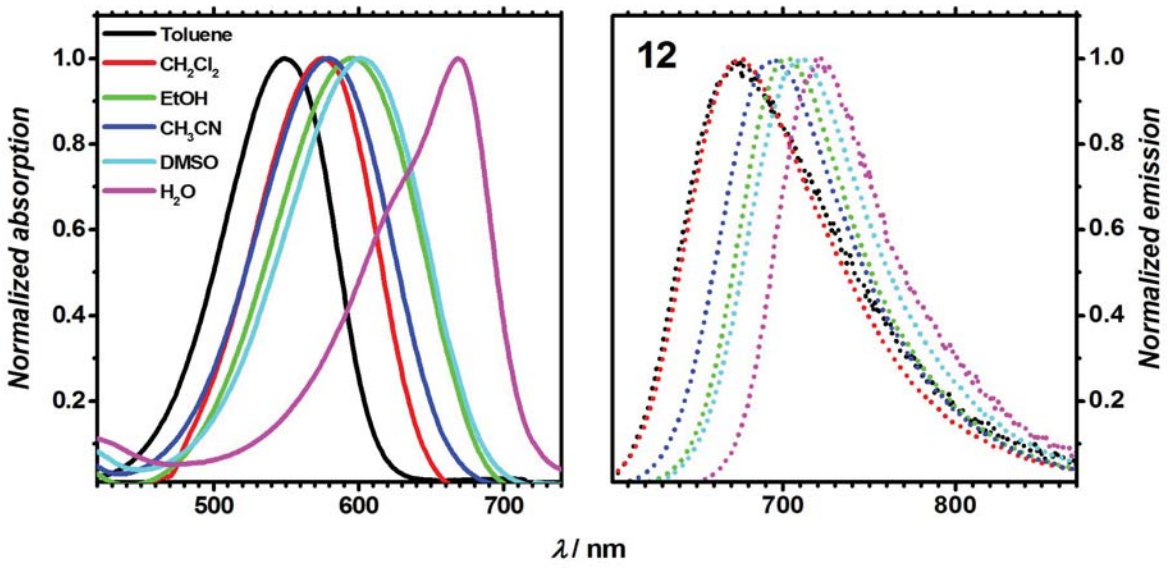

Figure S6. Absorption (solid) and emission (dotted) of compound **12** in toluene, CH_2Cl_2, EtOH, CH_3CN, DMSO, H_2O (containing 2% DMSO).

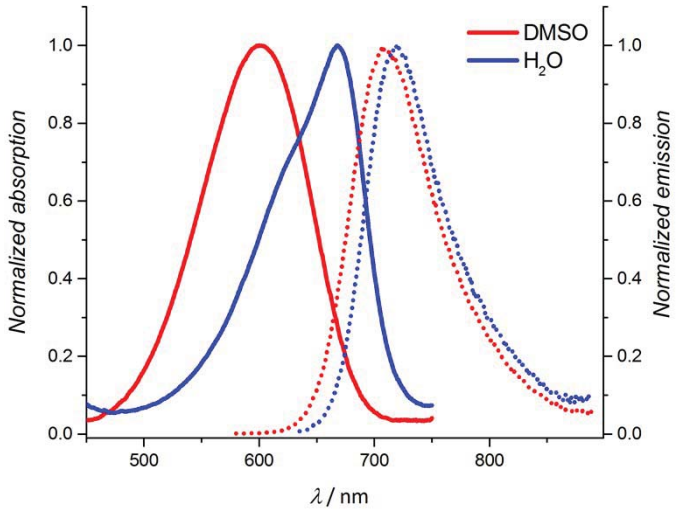

Figure S7. Absorption (solid) and emission (dotted) of compound **14** in DMSO and H_2O (2% of DMSO).

Time-resolved fluorescence data

Table S1. Fluorescence decay data for compounds **8** and **10**.[a]

Comp.	Solvent	λ_{exc} / nm	λ_{obs} / nm	A_1	A_2	τ_1 / ns	τ_2 [ns]	$k_r \cdot 10^{-8}$ / s^{-1}	$k_{nr} \cdot 10^{-8}$ / s^{-1}
8	CH_2Cl_2	336	670			4.20		1.02	1.36
	CH_3CN	336	700			5.24		0.99	0.92
	DMSO	336	700			4.33		1.15	1.16
10	CH_2Cl_2	336	670	38	62	0.46	2.06	2.83	18.9
	CH_3CN	336	700	100		0.32		0.25	31.0
	DMSO	336	700	94	6	0.32	6.13	0.31	31.1

[a]: The values of the radiative k_r and non-radiative k_{nr} rates are approximated on the basis of equations: $k_r = \Phi_f/\tau_1$ and $k_{nr} = 1/\tau_1 - k_r$

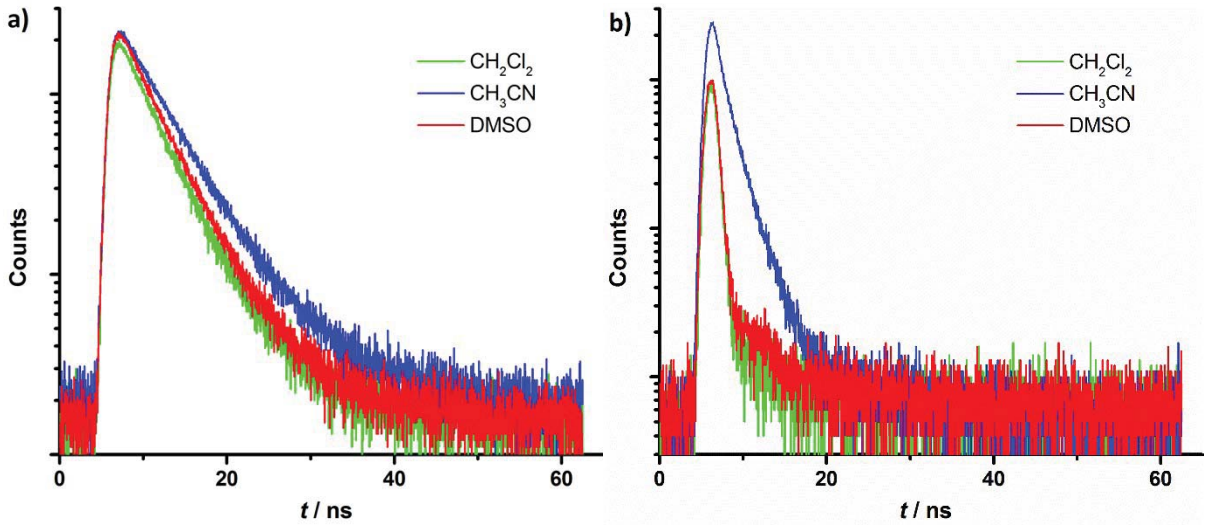

Figure S8. Fluorescence decay for **8** (a) and **10** (b) in CH_2Cl_2, CH_3CN and DMSO.

Absorption dependence on pH

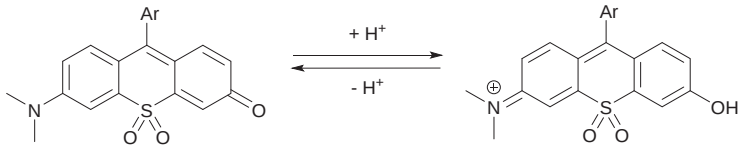

Scheme S1. SO_2-rhodol protonation

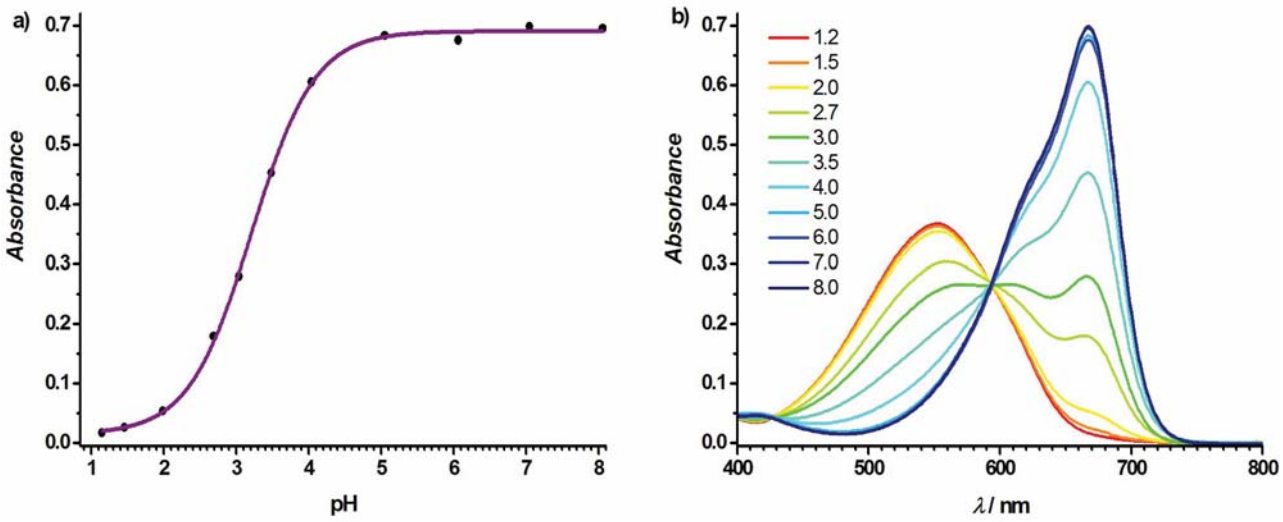

Figure S9. a) Absorption spectra of compound **8** at various pH values. b) The plots of absorbance of compound **8** at 667 nm as function of pH value and their fitting curve (pK_a = 3.21, r = 0.9994).

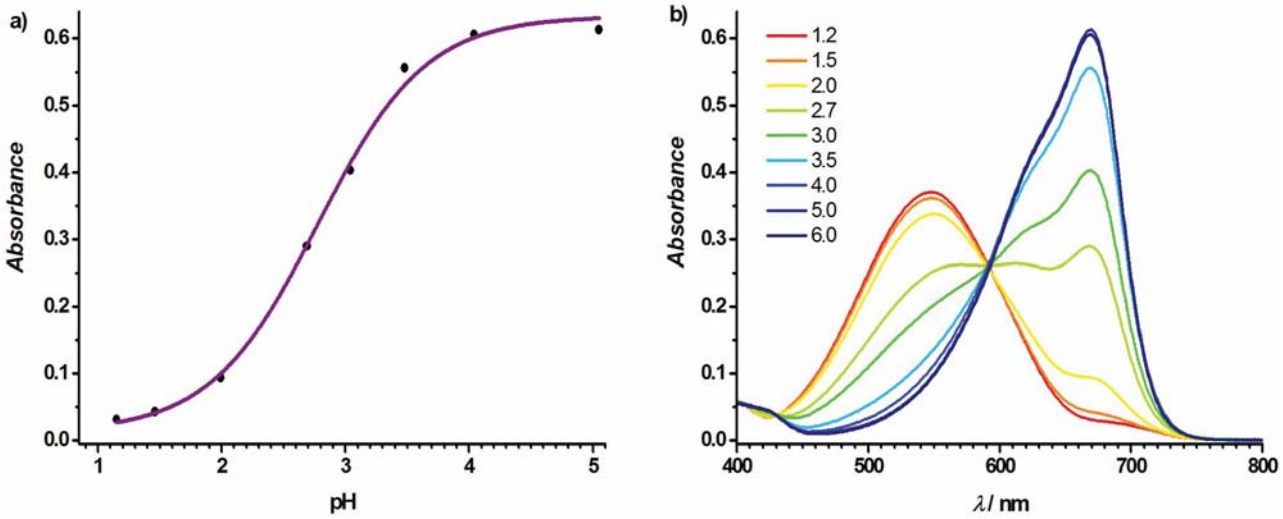

Figure S10. a) Absorption spectra of compound **9** at various pH values. b) The plots of absorbance of compound **9** at 669 nm as function of pH value and their fitting curve (pK_a = 2.78, r = 0.9964).

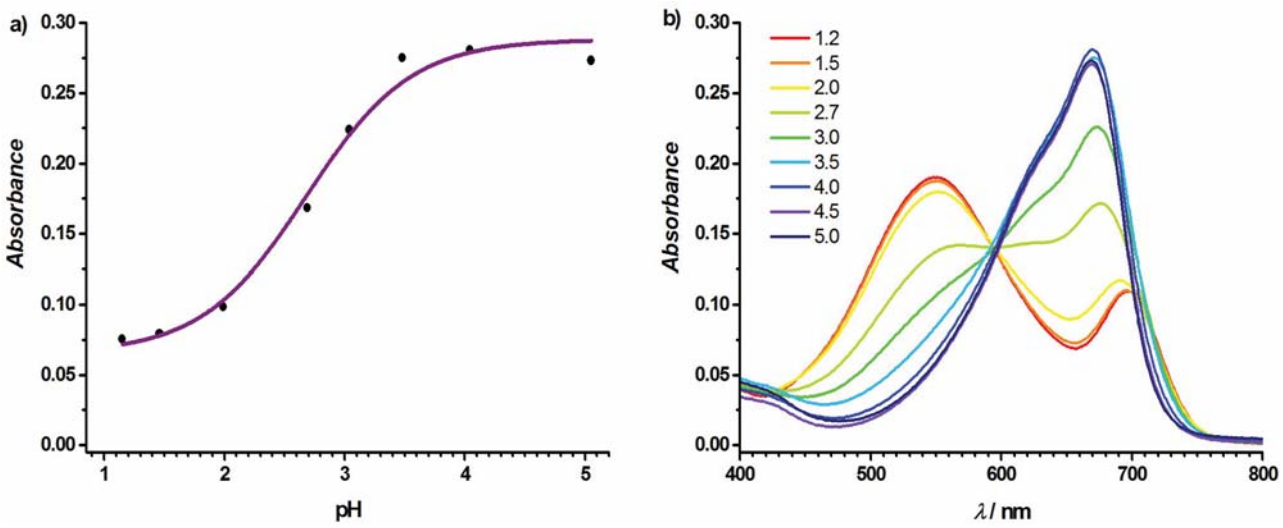

Figure S11. a) Absorption spectra of compound **11** at various pH values. b) The plots of absorbance of compound **11** at 669 nm as function of pH value and their fitting curve (pK_a = 2.68, r = 0.9841).

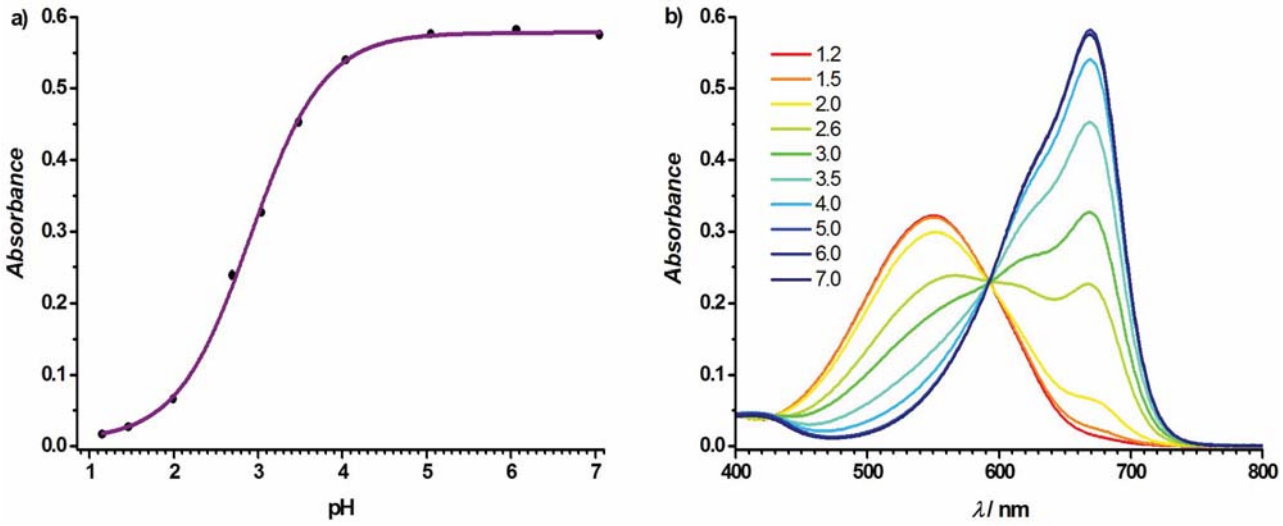

Figure S12. a) Absorption spectra of compound **12** at various pH values. b) The plots of absorbance of compound **12** at 669 nm as function of pH value and their fitting curve (pK_a = 2.91, r = 0.99894).

Compound **10** undergoes the formation of aggregates in DMSO-water media. The latter is not sensitive to a pH change.

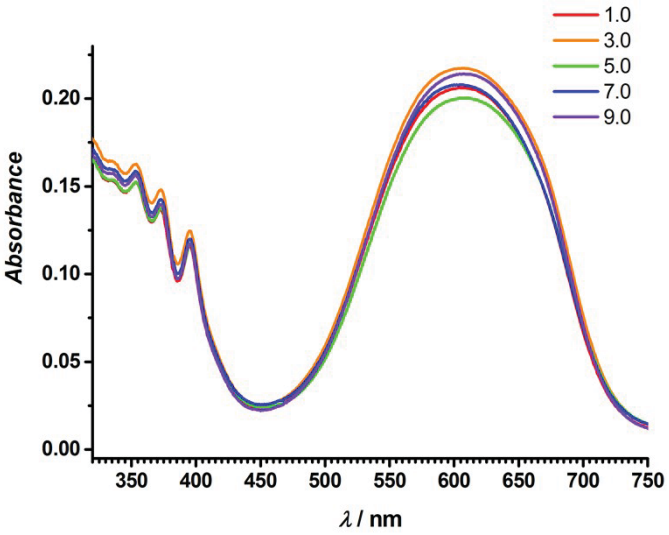

Figure S13. Absorption spectra of compound **10** at various pH values.

Photostability measurements

Photostability was determined through the variation in absorption of each sample at the appropriate absorption maximum wavelength (λ_{abs}) with respect to irradiation time. Ethanol was selected as the solvent. Concentrations giving similar optical densities (A ≈ 1) were used. Quartz cells of samples were irradiated with a 300 W Xe lamp (Asahi spectra MAX-350, light power: 0.16 W/cm2) for 150 min at 25 °C equipped with a UV/vis mirror module through a glass fiber. The absorption spectra were measured at appropriate times during the irradiation. Cresyl violet, Rhodamine 6G and DPP (2,5-dimethyl-3,6-bis(3,4-dimethoxyphenyl)pyrrolo[3,4-c]pyrrole1,4(2H,5H)-dione) were used as references.

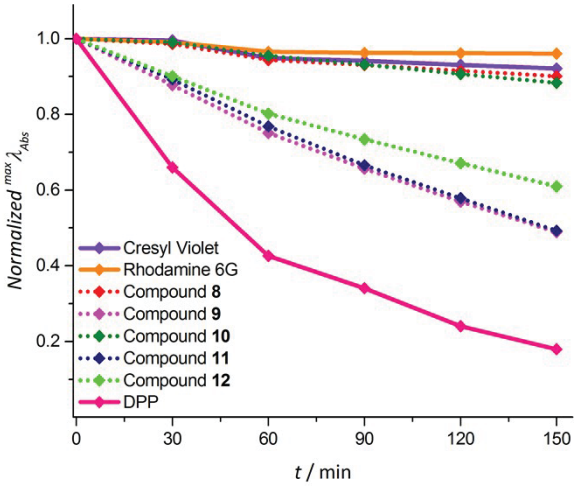

Figure S14. Photostability of sulfone-rhodols compared to the Rhodamine 6G, Cresyl Violet and DPP (2,5-dibutyl-3,6-bis(3,4-dimethoxyphenyl)pyrrolo[3,4-c]pyrrole-1,4(2H,5H)-dione) measured in EtOH using a collimated light source from a 300W Xe lamp.

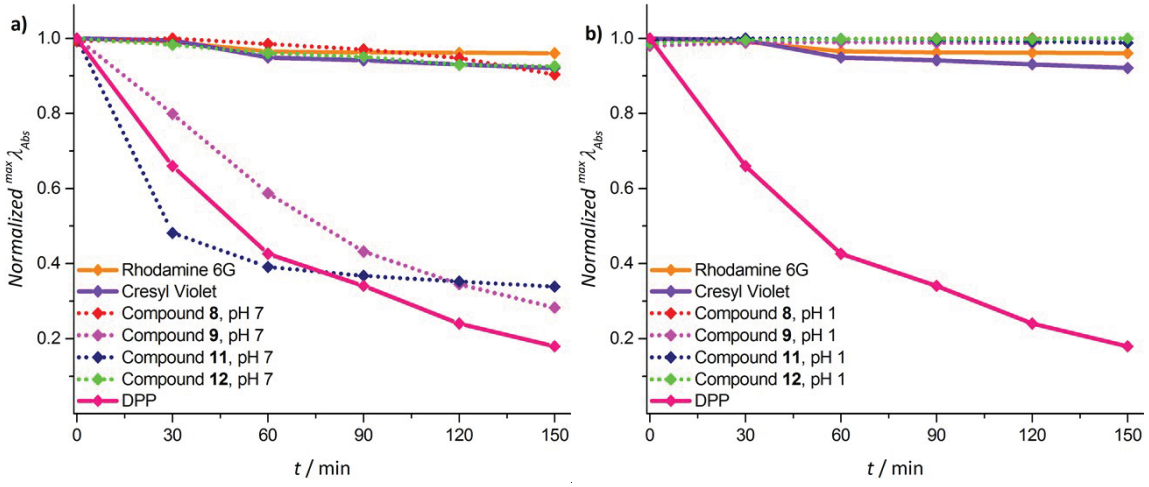

Figure S15. Photostability of sulfone-rhodols at pH 7 (a) and at pH1 (b) (in H_2O containing 2% DMSO) compared to the Rhodamine 6G, Cresyl Violet and DPP (2,5-dibutyl-3,6-bis(3,4-dimethoxyphenyl)pyrrolo[3,4-c]pyrrole-1,4(2H,5H)-dione) in EtOH measured using a collimated light source from a 300W Xe lamp.

Stability experiments were not performed for compound **10** as it precipitated in course of the stability test.

Cell culture conditions

The rat embryonic cardiomyoblast-derived cell line H9C2 were cultured at 37˚C in a humidified atmosphere containing 5% CO_2 in DMEM supplemented with 10% foetal bovine serum, 2 mM glutamine, 100 U/ml penicillin, and 100 g/ml streptomycin.

Fluorescence localization of 14 within the cells

The H9C2 cells were loaded with fluorophores in DMEM medium supplemented with 10% foetal bovine serum, 2 mM glutamine, 100 U/ml penicillin, and 100 g/ml streptomycin at 37˚C in a humidified atmosphere containing 5% CO_2 for 15-30 minutes with the **14** compound at the final concentration ranging from 200 to 500 nM. The final concentration of the MitoTracker™ Green FM was 150 nM. Both fluorophores were dissolved in DMSO and for the loading were supplemented with 20% Prluronic-127. The final concentration of the Pluronic-127 was kept below 0.05% in the loading buffer. Before measurements, the incubation medium was repleaced with FluoroBriteTM DMEM. The measurements were performed on Olympus IX83 confocal microscope with the water objective 60x UPLSAPO 60XW. The data were transferred to the ImageJ and prepared for presentation.

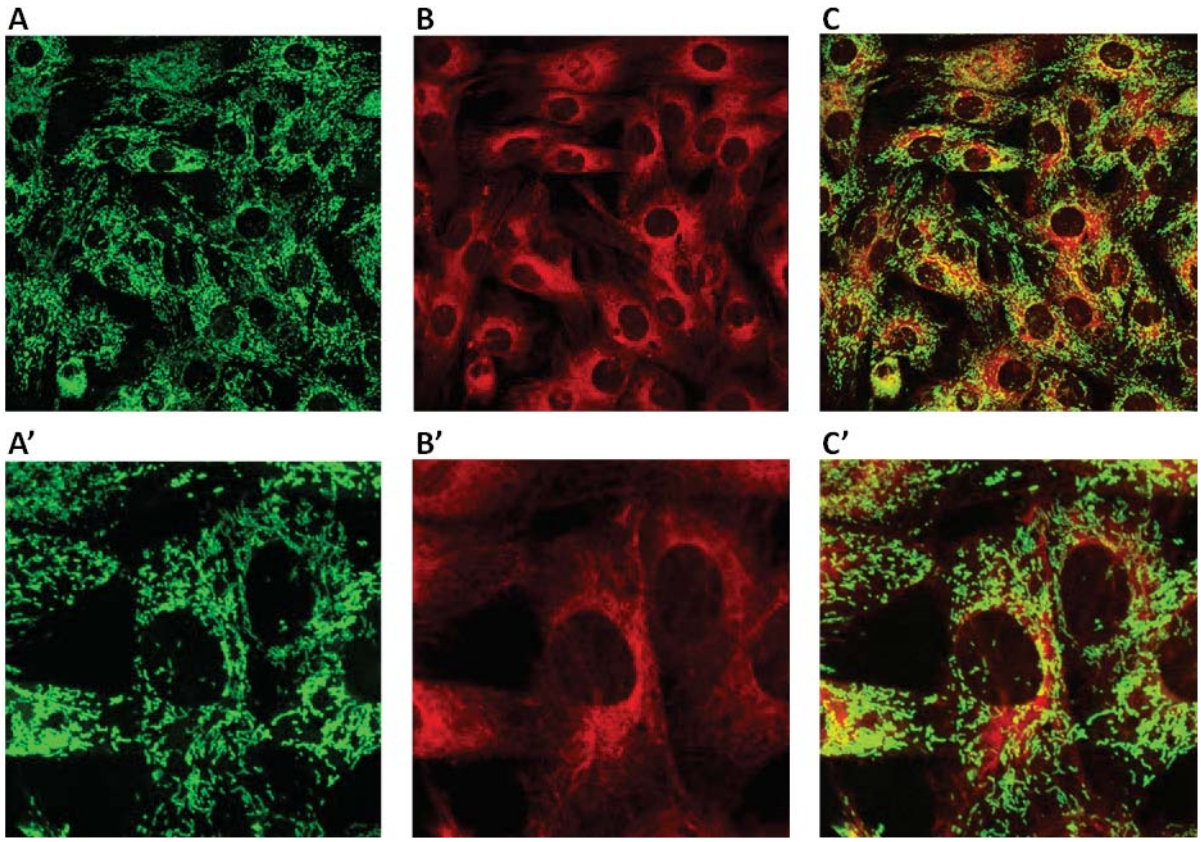

Figure S16. Intracellular localization of **13** compound as detected using confocal fluorescence microscopy. (A; A') The fluorescence of MitoTracker™ Green (green) as a well-established marker for

mitochondria, (B; B') the fluorescence of the **13** (red) recorded with 559 nm excitation wavelength and emission range 610–750 nm, (C; C') overlay picture recorded simultaneously for two fluorophore in living H9C2 cells line. A', B', C' pictures recorded for with higher magnification 3x.

Results

The dye **13** has a unlocalized distribution inside the H9C2 cells.

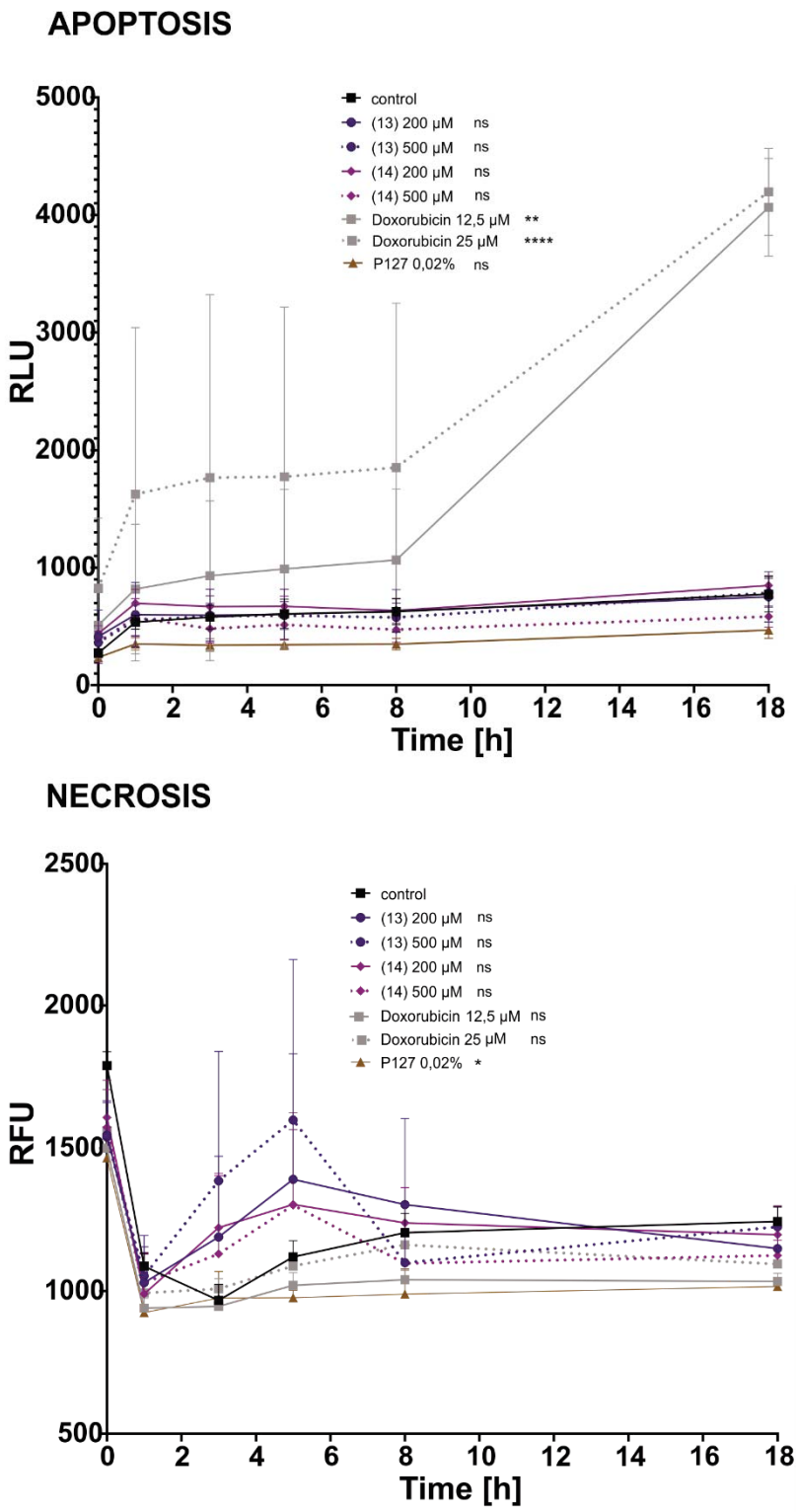

Figure S17. Effect of red emissive sulfonorhodols on apoptosis and necrosis of the H9C2 cells. Change in luminescence (RLU) as a measure of apoptosis and fluorescence (RFU) over the time. Statistical significance relative to the control was determined by two-way ANOVA with Tukey post-hoc test; $p>0.05$ (ns), $p<0.05$(*), $p<0.01$(**), $p<0.0001$(****); n=9

Methods

In order to determine the viability of cells under the influence of the tested red emissive sulfonorhodols **13** and **14**, an annexin V-based apoptosis and necrosis test (RealTime-Glo ™ Annexin V Apoptosis and Necrosis Assay, Promega) was performed, allowing the simultaneous examination of the effect of the substances on the induction of apoptotic and necrotic cell death.

Materials

RealTime-Glo ™ Annexin V Apoptosis and Necrosis Assay, Promega JA1011.

ChemComm

ROYAL SOCIETY OF CHEMISTRY

COMMUNICATION

View Article Online
View Journal | View Issue

Cite this: *Chem. Commun.*, 2022, **58**, 1542

Received 8th December 2021,
Accepted 31st December 2021

DOI: 10.1039/d1cc06924a

rsc.li/chemcomm

Direct transformation of coumarins into orange-red emitting rhodols†

Kateryna V. Vygranenko,[a] Yevgen M. Poronik,[a] Manon H. E. Bousquet,[b] Olena Vakuliuk,[a] Denis Jacquemin *[b] and Daniel T. Gryko *[a]

The lactone carbonyl group of coumarin derivatives has been shown to participate in intramolecular Knoevenagel condensations, enabling the unprecedented direct transformation of coumarins into rhodols. The resulting rhodols, possessing two ester groups, have very intense orange-red fluorescence.

Rhodols are merocyanine dyes occupying an intermediate position between rhodamines and fluoresceins.[1] Recently they have been successfully utilized to build various sensors for intracellular fluorescence imaging, examination of neuronal excitability and visualization of metastases.[2–6] Although various methods for the synthesis of rhodols and their analogues have been developed over the last decades they lack versatility and efficiency.[7–12] In particular they are not compatible with certain functional groups being present on substrates.

To overcome these limits we envisioned an entirely new retrosynthetic disconnection relying on 3-formylcoumarins and dimethyl 1,3-acetonedicarboxylate, that may in principle lead to rhodols *via* double Knoevenagel condensation (Scheme 1). The direct inspiration for this endeavour was Prelog's work on the synthesis of benzene derivatives from aliphatic precurors.[13,14] If successful this strategy would lead to heretofore unknown rhodols possessing two ester groups at positions 2 and 4.

Given the poor electrophilic properties of the carbon atom of the pyran-2-one heterocycle, Marchán and co-workers transformed coumarin into thionocoumarin in order to enable its further reaction with various nucleophiles.[15,16] Our application of this approach for V-shaped bis-coumarin gave the corresponding rhodol in 30% yield (see the ESI,† Scheme S4).

This prompted us to attempt the direct one-pot transformation of 3-formylcoumarins into rhodols. Our initial experiments have proven that for the reaction of 7-diethylamino-3-formylcoumarin with dimethyl 1,3-acetonedicarboxylate, the double Knoevenagel condensation proceeds only in the presence of indium chloride[17] and acetic anhydride. The yield of the expected product, however, was very low and its stability was poor due to the absence of any substituent at position 9 of the final rhodol. This position is subjected to nucleophilic attack by many nucleophiles, including water and methanol. Facing this obstacle we resolved to block the methine carbon atom with an *ortho*-substituted aryl group.[12] The additional advantage of this strategy is that the presence of a sterically hindered aryl group is known to be beneficial for increasing the fluorescence quantum yield of the resulting rhodol.[12,18,19]

To implement this approach we developed a synthetic route towards 4-aryl-3-formylcoumarins. Triflated hydroxycoumarins **S1** and **S9** were subjected to Suzuki coupling to form coumarins **S2–S5** and **S10–S13** which were converted into two series of aldehydes **1**, **S6–S8** and **S14–S17** respectively (see the ESI,† Schemes S2 and S3).[20,21]

The first attempts at performing the Knoevenagel condensation of formyl-coumarin **1** as a model substrate with dimethyl 1,3-acetonedicarboxylate (**2**) in the presence of $InCl_3$ and acetic acid anhydride resulted in the formation of the rhodol **4** in a very low yield accompanied by sizable quantity of intermediate **3** (Table 1 and Scheme 2). Various bases and Lewis acids in different solvents were trialled to improve this reaction (Table 1). Optimization resulted in finding that 2,6-lutidine is an optimal catalysts system

Scheme 1 Retrosynthetic concept of the coumarin into rhodol transformation.

[a] *Institute of Organic Chemistry, Polish Academy of Sciences, Kasprzaka 44/52, 01-224 Warsaw, Poland. E-mail: dtgryko@icho.edu.pl*
[b] *CEISAM Lab—UMR 6230, CNRS, University of Nantes, Nantes, France. E-mail: Denis.Jacquemin@univ-nantes.fr*

† Electronic supplementary information (ESI) available: Quantum chemical calculation and experimental data, synthetic procedures as well as, ^{1}H and $^{13}C\{^{1}H\}$ NMR spectra. CCDC 2125095 and 2125096. For ESI and crystallographic data in CIF or other electronic format see DOI: 10.1039/d1cc06924a

Supporting information

Direct transformation of coumarins into orange-red emitting rhodols

Kateryna V. Vygranenko,[a] Yevgen M. Poronik,[a] Manon H. E. Bousquet,[b] Olena Vakuliuk,[a] Denis Jacquemin*[b] and Daniel T. Gryko*[a]

a. Institute of Organic Chemistry, Polish Academy of Sciences, Kasprzaka 44/52, 01-224 Warsaw, Poland. E-mail: dtgryko@icho.edu.pl.

b. CEISAM Lab—UMR 6230, CNRS, University of Nantes, Nantes, France. E-mail : Denis.Jacquemin@univ-nantes.fr

Table of Contents

Instrumentation and Materials

All chemicals were used as received unless otherwise noted. All reported ^{1}H and ^{13}C NMR spectra were collected using 500 MHz and 600 MHz spectrometers. Chemical shifts (δ ppm) were determined with TMS as the internal reference; *J* values are given in Hz. Chromatography was performed on silicagel (230-400 mesh). Preparative thin layer chromatography (TLC) was carried out using Merck PLC Silica gel 60 F_{254} 1 mm plates. The mass spectra were obtained via electron ionization (EI-MS) or electrospray ionization (ESI-MS). All photophysical studies have been performed with freshly-prepared air-equilibrated solutions at room temperature (298 K).

A Shimadzu UV-3600i Plus spectrophotometer and an Edinburgh Instruments Spectrofluorometer FS5 equipped with Hamamatsu R13456 PMT were used to acquire the absorption and emission spectra. Spectrophotometric grade solvents were used without further purification. Fluorescence quantum yields were determined in CH_2Cl_2 and DMSO using Rhodamine 6G in EtOH and sulforhodamine SR101 (for measurements of compounds **8-11** in DMSO) as standards. Photostability was determined using an Asahi Spectra Max-350 as a light source and Shimadzu UV-3600i Plus spectrophotometer.

Optimization of reaction conditions for the rhodol synthesis

As a model reaction we chose the formation of rhodol **5** from coumarin aldehyde **S6** through intermediate **S20** (**Scheme S2**)

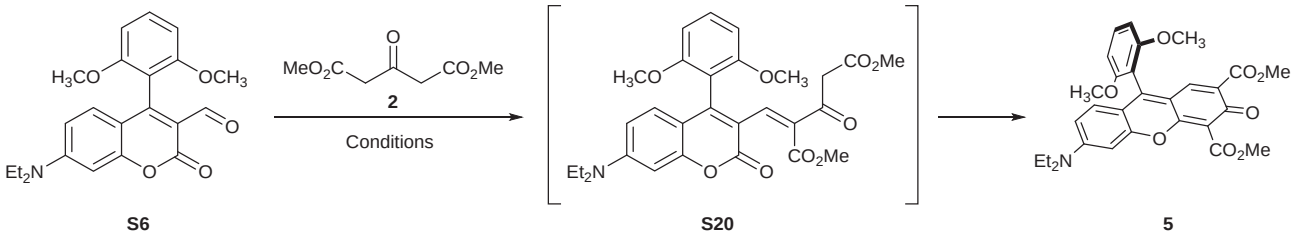

Scheme S1. The formation rhodol **5** from coumarin aldehyde **S6**.

Optical absorption measurement was chosen as a convenient instrumental method for the rhodol formation. The samples of coumarin aldehyde substrate were weighed with a 10^{-2} mg precision, that allows keeping the concentration of the substrate within the same range for all optimization experiments. First we determined molar absorptivity (ε) of coumarin aldehyde substrate, the intermediate and the rhodol product (Fig. S1). The concentration (c) of the substrate and the reaction product was calculated based on the Beer–Lambert law (Eq. 1), where A is absorbance and l is optical path length in cm:

$$A = \varepsilon l c \qquad (1)$$

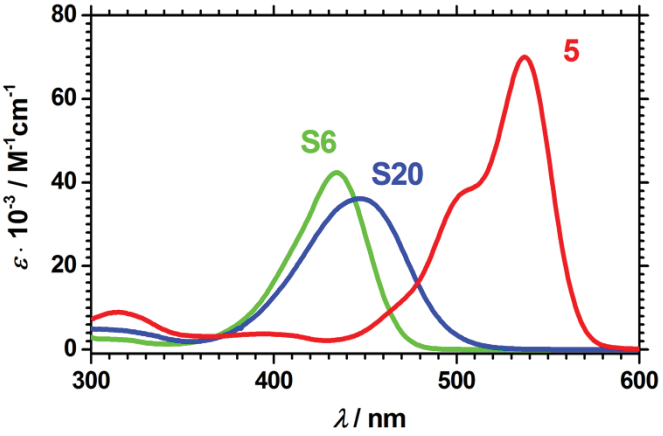

Figure S1. The absorption spectrum for **S6**, **S20** and **5** in CH_2Cl_2.

The standard procedure for all optimization experiments was chosen as follows:

Coumarin aldehyde (1mg) was dissolved in 1 mL of an appropriate solvent with a certain excess of **2** in the presence of basic catalyst at certain conditions**.** To check the concentration an 20 µL aliquot was taken from the reaction mixture and diluted to 5 mL with CH_2Cl_2. The absorption at the maxima was taken into account to calculate the concentration and the reaction yield of rhodol. Before the experiment started the exact amount of coumarin substrate was determined. In course of the reaction the concentrations of coumarin substrate and rhodol were monitored at equal time periods specified for each experiments. A dependence of the reaction yield on time allowed us finding optimal conditions for this type of transformation (Fig. S2).

To eliminate misinterpretations in the analysis of experiments we consider both spectroscopic data and TLC as in a number of experiments side reaction occurred that distorted the absorption data. For instance, all experiments in acetic anhydride as a solvent led to a formation of side products that has absorption in the same range as rhodol **5**, though rhodol formed very fast. We observed the similar situation for tests performed in pyridine or quinoline. The reactions were not efficient, besides that side products formed.

Studying model reaction in methanol in the presence of 1 eq. of piperidine we found that the use of 10eq. of dimethylacetondicarboxylate **2** leads to efficient conversion towards rhodol **5** with a minimum of side reactions, though due to the presence of little amount of side products having absorption at the spectral range of rhodol the reaction yield was overestimated (Fig. S2).

Using this method we have studied other rhodol formation to find the standard synthetic procedure. The chosen examples of the dependencies are shown in Fig. S2.

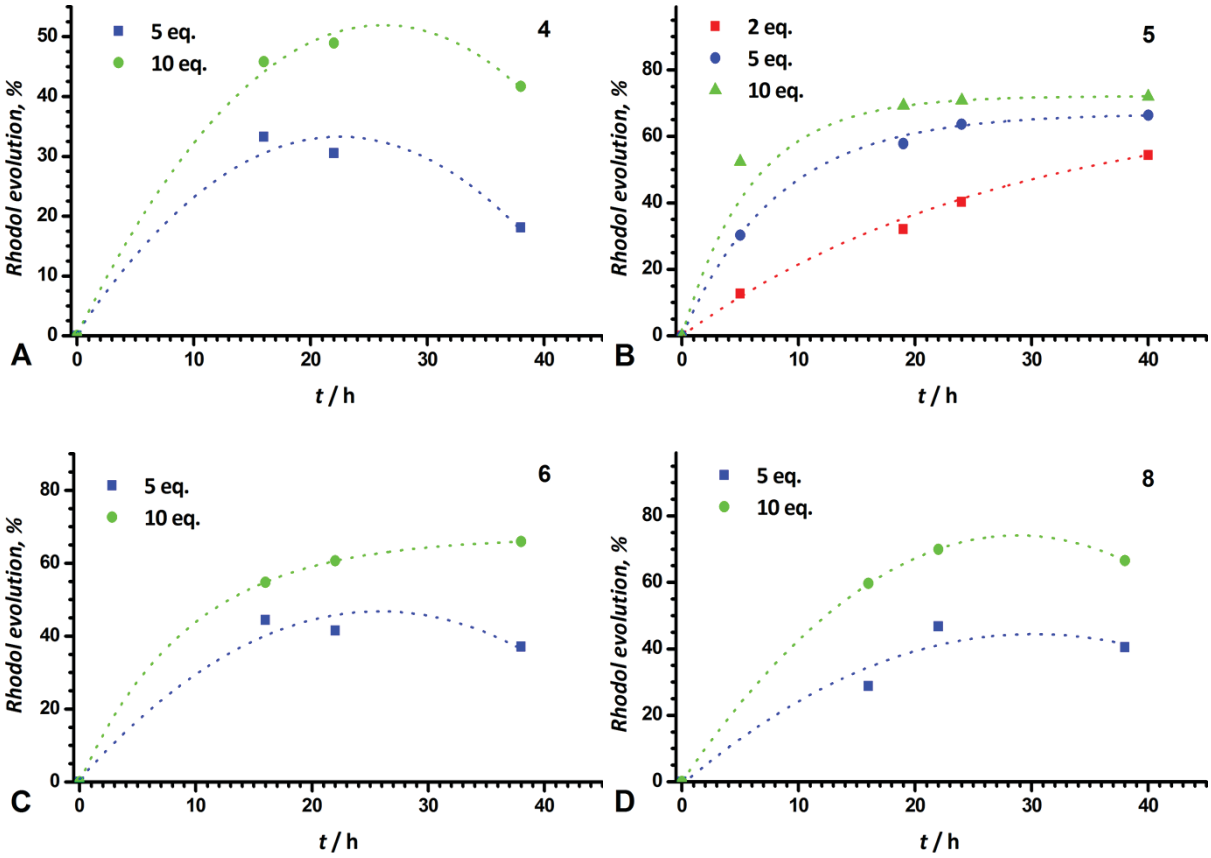

Figure S2. The optimization for the rhodols synthesis (A: Rhodol **4**; B: Rhodol **5**; C: Rhodol **6**; B: Rhodol **8**.). The rhodol evolution at using different excess of **2** based on the absorption at the correspondent absorption maxima. The intensity of rhodol signal is overestimated due to residual absorption of contaminants in this region.

Experimental part

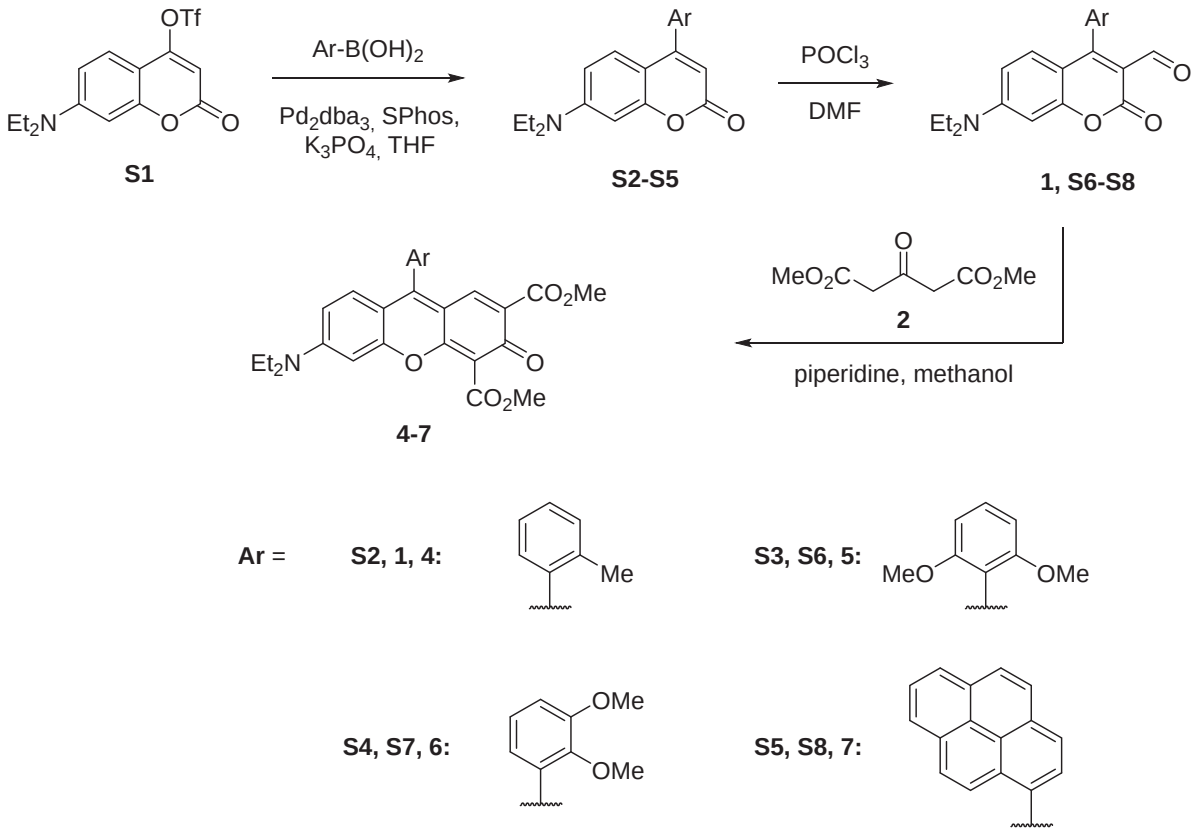

Scheme S2. Synthetic route from coumarin **S1** to rhodols **4-7**.

General procedure for the preparation of compounds **S2-S5**.

Compound **S1** (10 mmol), arylboronic acid (15 mmol), bis(dibenzylideneacetone)-palladium(0) (0,25 mmol), 2-dicyclohexylphosphino-2',6'-dimethoxybiphenyl (SPhos) (0,75 mmol) and tribasic potassium phosphate (40 mmol) were placed under Ar in a flame-dried Schlenk flask. Dry and degassed THF (50 ml) was added and the reaction mixture was stirred at 70°C for 4h under inert atmosphere. After the reaction was complete the mixture was diluted with DCM, filtered through celite and washed with $NaHCO_3$ solution (3 × 150 ml). The organic layer was dried over Na_2SO_4 and concentrated under vacuo. The residue was purified using column chromatography (hexane : EtOAc 1:1 + 1% AcOH).

Compound **S2**. Yield 97%. M.p. 95-96°C

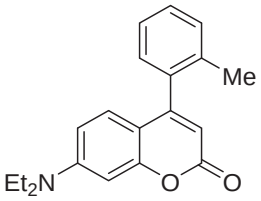

^{1}H NMR (500 MHz, $CDCl_3$) δ 7.35 (m, 1H, H-Ar), 7.32 – 7.27 (m, 2H, H-Ar), 7.16 (dd, *J* = 7.5, 1.5 Hz, 1H, H-Ar), 6.82 (d, *J* = 9.0 Hz, 1H, H-Ar), 6.56 (d, *J* = 2.6 Hz, 1H, H-Ar), 6.45 (dd, *J* = 9.0, 2.6 Hz, 1H, H-Ar), 5.94 (s, 1H, C-H), 3.40 (q, *J* = 7.1 Hz, 4H, CH_2), 2.18 (s, 3H, CH_3 - Ar), 1.20 (t, *J* = 7.1 Hz, 6H, CH_3); ^{13}C NMR (126 MHz, $CDCl_3$) δ 162.2, 156.4 (2), 150.7, 135.8, 135.3, 130.3, 128.7, 128.3, 127.8, 125.8, 108.8, 108.6, 108.5, 97.6, 44.7, 19.7, 12.4; HRMS (ESI) calc. for $C_{20}H_{21}NO_2Na$ 330.1470 $[M + Na]^+$, found 330.1465.

Compound **S3**. Yield 76%. M.p. 136-138°C

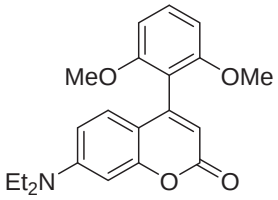

^{1}H NMR (500 MHz, $CDCl_3$) δ 7.36 (t, *J* = 8.4 Hz, 1H, H-Ar), 6.85 (d, *J* = 8.9 Hz, 1H, H-Ar), 6.66 (d, *J* = 8.4 Hz, 2H, H-Ar), 6.55 (d, *J* = 2.5 Hz, 1H, H-Ar), 6.45 (d, *J* = 8.9 Hz, 1H, H-Ar), 5.98 (s, 1H, C-H), 3.71 (s, 6H, OCH_3), 3.39 (q, *J* = 7.1 Hz, 4H, CH_2), 1.19 (t, *J* = 7.1 Hz, 6H, CH_3); ^{13}C NMR (126 MHz, $CDCl_3$) δ 162.6, 157.6, 156.3, 150.4, 130.3, 127.4, 113.5, 111.0, 109.2, 108.3, 104.0, 99.7, 55.9, 44.8, 12.5; HRMS (ESI) calc. for $C_{21}H_{23}NO_4Na$ 376.1525 $[M + Na]^+$, found 376.1535.

Compound **S4**. Yield 92%. M.p. 123-124°C

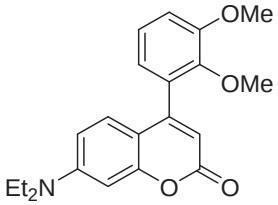

^{1}H NMR (500 MHz, $CDCl_3$) δ 7.14 (t, *J* = 7.9 Hz, 1H, Ar), 7.05 – 6.98 (m, 2H, Ar), 6.81 (dd, *J* = 7.6, 1.6 Hz, 1H, Ar), 6.58 (d, *J* = 2.5 Hz, 1H, Ar), 6.53 – 6.47 (m, 1H, Ar), 6.04 (s, 1H, C-H), 3.93 (s, 3H, OCH_3), 3.67 (s, 3H, OCH_3), 3.40 (q, *J* = 7.1 Hz, 4H, CH_2), 1.20 (t, *J* = 7.1 Hz, 6H, CH_3); ^{13}C NMR (126 MHz, $CDCl_3$) δ 162.2, 156.3, 153.7, 152.9, 150.6, 146.3, 130.6, 128.9, 124.2, 121.6, 113.1, 109.1, 108.5, 108.4, 97.4, 61.3, 55.9, 44.7, 12.4; HRMS (ESI) calc. for $C_{21}H_{23}NO_4Na$ 376.1525 $[M + Na]^+$, found 376.1532.

Compound **S5**. Yield 86%. M.p. 130-131°C

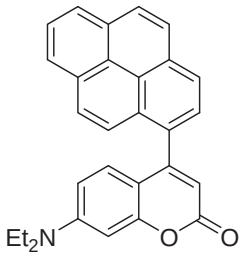

^{1}H NMR (500 MHz, $CDCl_3$) δ 8.28 – 8.22 (m, 2H, Ar), 8.19 (dd, *J* = 7.6, 1.2 Hz, 1H, Ar), 8.18 – 8.10 (m, 2H, Ar), 8.07 – 7.99 (m, 2H, Ar), 7.95 – 7.89 (m, 2H, Ar), 6.75 (d, *J* = 9.1 Hz, 1H, Ar), 6.64 (d, *J* = 2.6 Hz, 1H, Ar), 6.33 (dd, *J* = 9.1, 2.6 Hz, 1H, Ar), 6.24 (s, 1H, C-H), 3.39 (q, *J* = 7.1 Hz, 4H, CH_2), 1.19 (t, *J* = 7.1 Hz, 6H, CH_3); ^{13}C NMR (126 MHz, $CDCl_3$) δ 162.1, 156.5, 155.9, 150.8, 131.7, 131.3, 130.8, 128.6, 128.5, 128.2, 127.2, 126.3 (2), 125.7, 125.5, 124.7, 124.6 (2), 110.4, 109.5, 108.6, 97.6, 44.8, 12.4; HRMS (ESI) calc. for $C_{29}H_{23}NO_2Na$ 440.1626 $[M + Na]^+$, found 440.1613.

General procedure for the preparation of compounds **1**, **S6-S8**.

Phosphorus oxychloride (7,7 mmol) was added dropwise to a solution of 7-diethylamino-4-aryl-coumarin (**S2-S5**) (5 mmol) in DMF (15 ml) upon cooling on ice. The reaction mixture was allowed to stir at 50°C for 24h. The solution then was cooled to room temperature, poured into $NaHCO_3$ aqueous solution (20 g in 100 ml H_2O) with 300 ml of crashed ice. The precipitate which formed was filtered, washed with distilled water, dried under vacuum and purified via recrystallization from hexane + 2-propanol.

Compound **1**. Yield 60%. M.p. 160-161°C

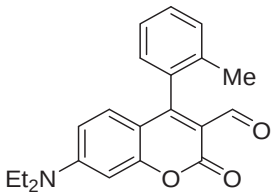

^{1}H NMR (500 MHz, $CDCl_3$) δ 9.83 (s, 1H, CHO), 7.39 (td, *J* = 7.5, 1.4 Hz, 1H, H-Ar), 7.35 – 7.26 (m, 2H, H-Ar), 7.06 (dd, *J* = 7.5, 1.4 Hz, 1H, H-Ar), 6.80 (d, *J* = 9.2 Hz, 1H, H-Ar), 6.52 (d, *J* = 2.6 Hz, 1H, H-Ar), 6.48 (dd, *J* = 9.2, 2.6 Hz, 1H, H-Ar), 3.45 (q, *J* = 7.1 Hz, 4H, CH_2), 2.10 (s, *J* = 2.4 Hz, 3H, CH_3-Ar), 1.23 (t, *J* = 7.1 Hz, 6H, CH_3); ^{13}C NMR (126 MHz, $CDCl_3$) δ 188.2, 162.0, 160.0, 157.8, 153.2, 135.1, 133.0, 130.5, 130.1, 128.9, 127.6, 125.8, 112.2, 109.8, 108.7, 97.0, 45.1, 19.4, 12.4; HRMS (ESI) calc. for $C_{21}H_{21}NO_3Na$ 358.1419 $[M + Na]^+$, found 358.1415.

Compound **S6**. Yield 50%. M.p. 213-215°C

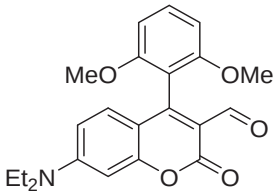

^{1}H NMR (500 MHz, $CDCl_3$) δ 9.81 (s, 1H, CHO), 7.41 (t, J = 8.4 Hz, 1H, H-Ar), 6.92 (d, J = 9.1 Hz, 1H, H-Ar), 6.67 (d, J = 8.4 Hz, 2H, H-Ar), 6.52 – 6.44 (m, 2H, H-Ar), 3.69 (s, 6H, OCH_3), 3.43 (q, J = 7.1 Hz, 4H, CH_2), 1.22 (t, J = 7.1 Hz, 6H, CH_3); ^{13}C NMR (126 MHz, $CDCl_3$) δ 188.7, 160.2, 157.7, 157.4, 157.1, 152.9, 130.9, 129.9, 113.4, 110.3, 109.4, 109.0, 103.9, 96.9, 55.9, 45.0, 12.5; HRMS (ESI) calc. for $C_{22}H_{23}NO_5Na$ 404.1474 $[M + Na]^+$, found 404.1486.

Compound **S7**. Yield 28%. M.p. 163-164°C

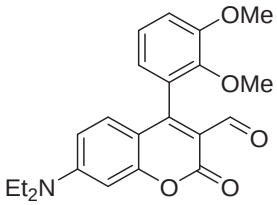

^{1}H NMR (500 MHz, $CDCl_3$) δ 9.98 (s, 1H, CHO), 7.16 (t, J = 7.9 Hz, 1H, H-Ar), 7.05 (d, J = 8.2 Hz, 1H, H-Ar), 6.93 (d, J = 9.1 Hz, 1H, H-Ar), 6.66 (d, J = 7.6 Hz, 1H, H-Ar), 6.53 – 6.45 (m, 2H, H-Ar), 3.94 (s, 3H, OCH_3), 3.67 (s, 3H, OCH_3), 3.43 (q, J = 7.1 Hz, 4H, CH_2), 1.22 (t, J = 7.1 Hz, 6H, CH_3); ^{13}C NMR (126 MHz, $CDCl_3$) δ 188.4, 160.5, 158.8, 157.6, 153.0, 152.7, 145.7, 130.9, 128.0, 124.2, 120.7, 113.1, 112.5, 109.7, 109.2, 97.0, 60.9, 55.8, 45.1, 12.4; HRMS (ESI) calc. for $C_{22}H_{23}NO_5Na$ 404.1474 $[M + Na]^+$, found 404.1479.

Compound **S8**. Yield 80%. M.p. 169-171°C

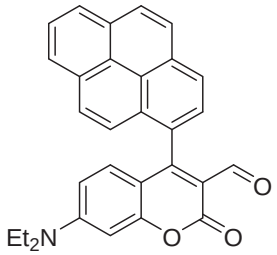

^{1}H NMR (500 MHz, $CDCl_3$) δ 9.79 (s, 1H, CHO), 8.30 - 8.22 (m, 2H, H-Ar), 8.21 – 8.12 (m, 3H, H-Ar), 8.04 (t, J = 7.6 Hz, 1H, H-Ar), 8.01 (d, J = 9.1 Hz, 1H, H-Ar), 7.83 (d, J = 7.8 Hz, 1H, H-Ar), 7.72 (d, J = 9.1 Hz, 1H, H-Ar), 6.63 – 6.55 (m, 2H, H-Ar), 6.30 (dd, J = 9.3, 2.6 Hz, 1H, H-Ar), 3.41 (q, J = 7.1 Hz, 4H, CH_2), 1.19 (t, J = 7.1 Hz, 6H, CH_3); ^{13}C NMR (126 MHz, $CDCl_3$) δ 188.0, 161.4, 160.0, 157.8, 153.2, 131.8, 131.3, 131.2, 130.8, 128.8, 128.7, 128.3, 128.0, 127.3, 126.4, 125.9 (2), 125.7, 124.5 (3), 124.1, 113.6, 109.9, 109.8, 97.0, 45.2, 12.4; HRMS (ESI) calc. for $C_{30}H_{24}NO_3$ 446.1756 $[M + H]^+$, found 446.1761.

General procedure for the preparation of compounds **4-7**.

Aldehyde (**1**, **S6-S8**) (1 mmol), dimethyl-1,3-acetonedicarboxylate (**2**) (10 mmol) and piperidine (1 mmol) were dissolved in methanol (3 ml) and allowed to stir at 60°C for 20h. The solvent was evaporated and the residue was washed with diethyl ether. The crude product was purified via column chromatography (CH_2Cl_2 : MeOH 93:7).

Compound **4**. Yield 28%. M.p. 258-260°C

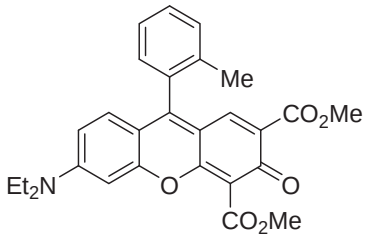

^{1}H NMR (500 MHz, $CDCl_3$) δ 7.52 (s, 1H, H-Ar), 7.45 (td, *J* = 7.6, 1.4 Hz, 1H, H-Ar), 7.4 – 7.33 (m, 2H, H-Ar), 7.12 (d, *J* = 7.5 Hz, 1H, H-Ar), 6.90 (d, *J* = 9.1 Hz, 1H, H-Ar), 6.62 – 6.55 (m, 2H, H-Ar), 4.01 (s, 3H, OCH_3), 3.81 (s, 3H, OCH_3), 3.50 (q, *J* = 7.3 Hz, 4H, CH_2), 2.06 (s, 3H, CH_3 - Ar), 1.26 (t, *J* = 7.1 Hz, 6H, CH_3); ^{13}C NMR (126 MHz, $CDCl_3$) δ 176.7, 167.1, 166.4, 156.2, 155.6, 155.3, 153.6, 136.0, 135.1, 132.1, 130.7 (2), 129.7, 129.0, 128.2, 126.1, 113.0, 112.1, 111.1, 110.9, 96.9, 52.3, 52.2, 45.3, 19.6, 12.6; HRMS (ESI) calc. for $C_{28}H_{28}NO_6$ 474.1917 $[M + H]^+$, found 474.1903.

Compound **5**. Yield 21%. M.p. 217-218°C

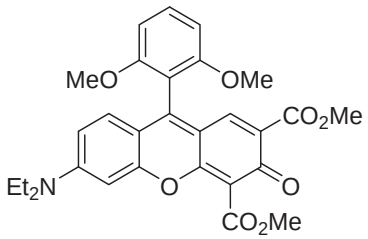

^{1}H NMR (500 MHz, $CDCl_3$) δ 7.61 (s, 1H, H-Ar), 7.51 – 7.41 (t, *J* = 8.4 Hz, 1H, H-Ar), 7.02 – 6.96 (m, 1H, H-Ar), 6.73 – 6.67 (m, 2H, H-Ar), 6.59 – 6.53 (m, 2H, H-Ar), 4.00 (s, 3H, OCH_3), 3.82 (s, 3H, OCH_3), 3.66 (s, 6H, OCH_3), 3.48 (q, *J* = 7.1 Hz, 4H, CH_2), 1.25 (t, *J* = 7.1 Hz, 6H, CH_3); ^{13}C NMR (126 MHz, $CDCl_3$) δ 176.8, 167.5, 166.7, 157.7, 156.3, 156.0, 153.4, 151.3, 135.8, 131.6, 130.4, 127.5, 113.3, 112.5, 111.5, 110.8, 109.5, 104.1, 96.7, 55.9, 52.2, 52.0, 45.1, 12.6; HRMS (ESI) calc. for $C_{29}H_{30}NO_8$ 520.1971 $[M + H]^+$, found 520.1978.

Compound **6**. Yield 13%. M.p. 210-211°C

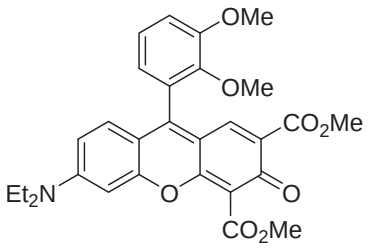

^{1}H NMR (500 MHz, $CDCl_3$) δ 7.70 (s, 1H, H-Ar), 7.21 (t, J = 7.9 Hz, 1H, H-Ar), 7.11 (dd, J = 8.3, 1.5 Hz, 1H, H-Ar), 7.06 – 7.01 (m, 1H, H-Ar), 6.73 (dd, J = 7.7, 1.5 Hz, 1H, H-Ar), 6.61 – 6.55 (m, 2H, H-Ar), 4.01 (s, 3H, OCH_3), 3.96 (s, 3H, OCH_3), 3.82 (s, 3H, OCH_3), 3.61 (s, 3H, OCH_3), 3.49 (q, J = 7.2 Hz, 4H, CH_2), 1.25 (t, J = 7.1 Hz, 6H, CH_3); ^{13}C NMR (126 MHz, $CDCl_3$) δ 176.6, 167.1, 166.4, 156.1, 155.6, 153.6, 152.9, 152.8, 146.5, 135.4, 131.0, 127.7, 126.7, 124.4, 121.8, 113.8, 112.8, 112.4, 111.2, 110.9, 96.7, 61.2, 55.8, 52.2, 52.0, 45.2, 12.5; HRMS (ESI) calc. for $C_{29}H_{30}NO_8$ 520.1977 $[M + H]^+$, found 520.1978.

Compound **7**. Yield 23%. M.p. 211-213°C

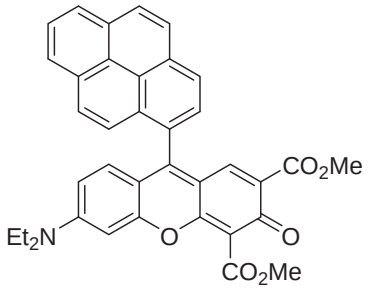

^{1}H NMR (500 MHz, $CDCl_3$) δ 8.33 (d, J = 7.8 Hz, 1H, H-Ar), 8.29 (d, J = 7.7 Hz, 1H, H-Ar), 8.25 – 8.15 (m, 3H, H-Ar), 8.07 (t, J = 7.6 Hz, 1H, H-Ar), 8.01 (d, J = 9.1 Hz, 1H, H-Ar), 7.86 (d, J = 7.8 Hz, 1H, H-Ar), 7.61 (d, J = 9.1 Hz, 1H, H-Ar), 7.43 (s, 1H, H-Ar), 6.73 (d, J = 9.4 Hz, 1H, H-Ar), 6.67 (d, J = 2.5 Hz, 1H, H-Ar), 6.41 (dd, J = 9.4, 2.5 Hz, 1H, H-Ar), 4.05 (s, 3H, OCH_3), 3.64 (s, 3H, OCH_3), 3.47 (q, J = 7.2 Hz, 4H, CH_2), 1.24 (t, J = 7.1 Hz, 6H, CH_3); ^{13}C NMR (126 MHz, $CDCl_3$) δ 176.7, 166.8, 166.4, 156.1, 155.6, 154.7, 153.6, 135.3, 132.3, 131.3, 130.8, 129.5, 129.1, 128.8, 128.3, 127.2, 126.9, 126.8, 126.6, 126.2, 126.0, 124.6 (2), 124.4, 124.1, 113.6, 113.0, 112.1, 111.1, 96.9, 52.4, 52.0, 45.3, 12.6; HRMS (ESI) calc. for $C_{37}H_{30}NO_6$ 584.2073 $[M + H]^+$, found 584.2075.

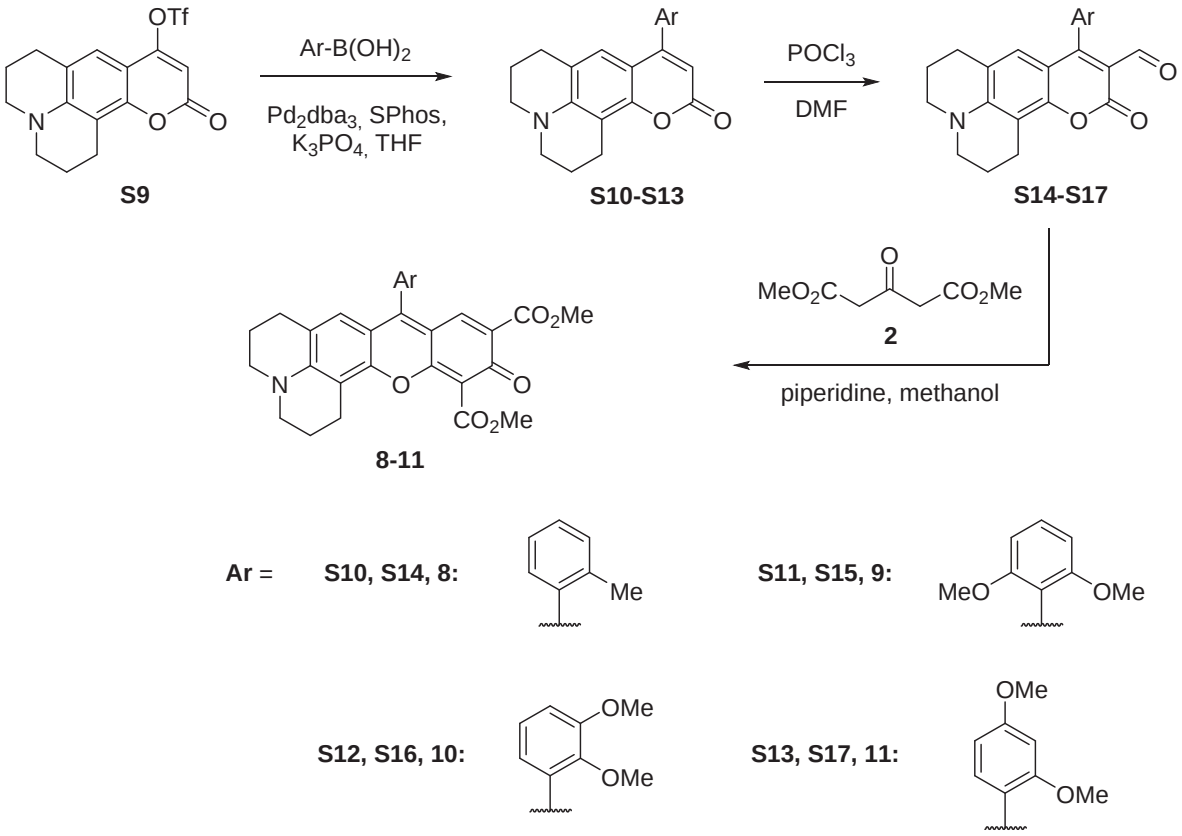

Scheme S3. Synthetic route from coumarin **S9** to rhodols **8-11**.

General procedure for the preparation of compounds **S10-S13**.

Compound **S9** (10 mmol), arylboronic acid (15 mmol), bis(dibenzylideneacetone)-palladium(0) (0.25 mmol), 2-dicyclohexylphosphino-2',6'-dimethoxybiphenyl (SPhos) (0.75 mmol) and tribasic potassium phosphate (40 mmol) were placed under Ar in a flame-dried Schlenk flask. Dry and degassed THF (75 ml) was added and the reaction mixture was stirred at 70°C for 7h under inert atmosphere. After the reaction was complete the mixture was diluted with DCM, filtered through celite and washed with $NaHCO_3$ solution (3 × 150 ml). The organic layer was dried over Na_2SO_4 and concentrated under vacuo. The residue was recrystallized from methanol.

Compound **S10**. Yield 90%. M.p. 166-167°C

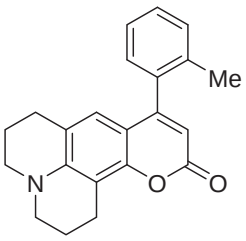

^{1}H NMR (600 MHz, $CDCl_3$) δ 7.37 – 7.34 (m, 1H, H-Ar), 7.32 – 7.26 (m, 2H, H-Ar), 7.14 (dd, *J* = 7.6, 1.4 Hz, 1H, H-Ar), 6.39 (s, 1H, H-Ar), 5.89 (s, 1H, C-H), 3.29 – 3.21 (m, 4H, CH_2), 2.95 (t, *J* = 6.5 Hz, 2H, CH_2), 2.60 (t, *J* = 6.5 Hz, 2H, CH_2), 2.17 (s, 3H, CH_3-Ar), 2.02 – 1.97 (m, 2H, CH_2), 1.93 – 1.88 (m, *J* = 7.9, 5.5 Hz, 2H, CH_2); ^{13}C NMR (151 MHz, $CDCl_3$) δ 162.5, 156.6, 151.4, 145.9, 136.2, 135.3, 130.2, 128.5, 128.4, 125.7, 123.8, 118.2, 108.3, 108.2, 106.8, 49.9, 49.5, 27.5, 21.5, 20.6, 20.5, 19.7; HRMS (ESI) calc. for $C_{22}H_{21}NO_2Na$ 354.1470 $[M + Na]^+$, found 354.1469.

Compound **S11**. Yield 94%.

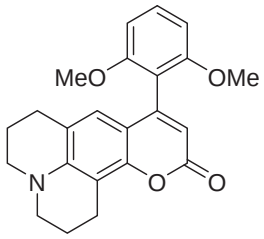

^{1}H NMR (500 MHz, $CDCl_3$) δ 7.36 (t, *J* = 8.4 Hz, 1H, H-Ar), 6.66 (d, *J* = 8.4 Hz, 2H, H-Ar), 6.43 (s, 1H, H-Ar), 5.92 (s, 1H, C-H), 3.70 (s, 6H, OCH_3), 3.23 – 3.19 (m, 4H, CH_2), 2.94 (t, *J* = 6.6 Hz, 2H, CH_2), 2.62 (t, *J* = 6.4 Hz, 2H, CH_2), 2.02 – 1.99 (m, 2H, CH_2), 1.97 – 1.93 (m, 2H, CH_2); ^{13}C NMR (126 MHz, $CDCl_3$) δ 162.9, 157.6, 151.4, 150.7, 145.6, 130.1, 123.4, 117.9, 114.0, 110.3, 109.0, 106.7, 104.1, 56.0, 50.0, 49.6, 27.5, 21.6, 20.8, 20.6; HRMS (ESI) calc. for $C_{23}H_{23}NO_4Na$ 400.1525 $[M + Na]^+$, found 400.1529.

Compound **S12**. Yield 89%. M.p. 208-210°C

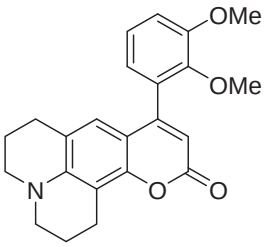

^{1}H NMR (500 MHz, $CDCl_3$) δ 7.13 (t, *J* = 7.9 Hz, 1H, H-Ar), 7.02 (dd, *J* = 8.3, 1.5 Hz, 1H, H-Ar), 6.78 (dd, *J* = 7.7, 1.5 Hz, 1H, H-Ar), 6.56 (s, 1H, H-Ar), 5.97 (s, 1H, C-H), 3.93 (s, 3H, OCH_3), 3.67 (s, 3H, OCH_3), 3.27 – 3.20 (m, 4H, CH_2), 2.94 (t, *J* = 6.5 Hz, 2H, CH_2), 2.69 – 2.55 (m, 2H, CH_2), 2.02 – 1.96 (m, 2H, CH_2), 1.92 – 1.87 (m, 2H, CH_2); ^{13}C NMR (126 MHz, $CDCl_3$) δ 162.5, 153.9, 152.8, 151.3, 146.2, 145.9, 131.0, 124.2, 124.1, 121.6, 118.1, 112.8, 108.4, 108.4, 106.6, 61.3, 55.8, 50.0, 49.5, 27.5, 21.5, 20.7, 20.5; HRMS (ESI) calc. for $C_{23}H_{23}NO_4Na$ 400.1525 $[M + Na]^+$, found 400.1522.

Compound **S13**. Yield 84%. M.p. 201-203°C

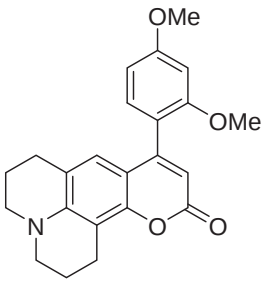

^{1}H NMR (500 MHz, $CDCl_3$) δ 7.13 – 7.08 (m, 1H, H-Ar), 6.59 – 6.57 (m, 3H, H-Ar), 5.95 (s, 1H, C-H), 3.87 (s, 3H, OCH_3), 3.73 (s, 3H, OCH_3), 3.23 (t, *J* = 5.8 Hz, 4H, CH_2), 2.93 (t, *J* = 6.5 Hz, 2H, CH_2), 2.64 (t, *J* = 6.4 Hz, 2H, CH_2), 2.01 - 1.96 (m, *J* = 6.2 Hz, 2H, CH_2), 1.94 – 1.89 (d, *J* = 6.0 Hz, 2H, CH_2); ^{13}C NMR (126 MHz, $CDCl_3$) δ 162.8, 161.5, 157.6, 153.9, 151.3, 145.6, 130.8, 124.2, 118.3, 117.8, 109.2, 108.8, 106.7, 104.5, 99.0, 55.6, 55.5, 49.9, 49.6, 27.6, 21.6, 20.8, 20.5; HRMS (ESI) calc. for $C_{23}H_{23}NO_4Na$ 400.1525 $[M + Na]^+$, found 400.1530.

General procedure for the preparation of compounds **S14-S17**.

Phosphorus oxychloride (7.7 mmol) was added dropwise to a solution of 7-diethylamino-4-aryl-coumarin (**S10-S13**) (5 mmol) in DMF (15 ml) upon cooling on ice. The reaction mixture was allowed to stir at 50°C for 24h. The solution then was cooled to room temperature, poured into $NaHCO_3$ aqueous solution (20 g in 100 ml H_2O) with 300 ml of crashed ice. The precipitate which formed was filtered, washed with distilled water and methanol, dried under vacuo and purified via recrystallization from $MeOH/CH_2Cl_2$.

Compound **S14**. Yield 84%. M.p. 201-203°C

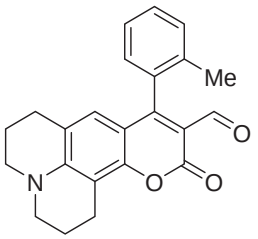

^{1}H NMR (500 MHz, $CDCl_3$) δ 9.80 (s, 1H, CHO), 7.38 (t, *J* = 7.5 Hz, 1H, H-Ar), 7.33 – 7.24 (m, 2H, H-Ar), 7.03 (d, *J* = 7.5 Hz, 1H, H-Ar), 6.35 (s, 1H, H-Ar), 3.36 – 3.32 (m, 4H, CH_2), 2.94 (t, *J* = 6.4 Hz, 2H, CH_2), 2.57 (t, *J* = 6.2 Hz, 2H, CH_2), 2.08 (s, 3H, CH_3-Ar), 2.00 (quint, *J* = 6.2 Hz, 2H, CH_2), 1.90 (quint, *J* = 6.3 Hz, 2H, CH_2); ^{13}C NMR (126 MHz, CDCl3) δ 188.4, 161.6, 160.3, 152.9, 149.0, 135.2, 133.5, 130.0, 128.7, 127.8, 126.1, 125.7, 119.5, 111.3, 108.4, 106.0, 50.3, 49.9, 27.5, 21.1, 20.2, 20.2, 19.5; HRMS (ESI) calc. for $C_{23}H_{22}NO_3$ 360.1600 $[M + H]^+$, found 360.1588.

Compound **S15**. Yield 87%. M.p. 263-265°C

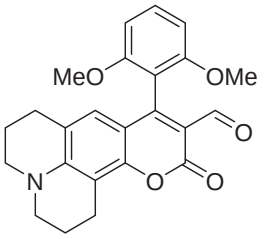

^{1}H NMR (500 MHz, $CDCl_3$) δ 9.77 (s, 1H, CHO), 7.41 (t, J = 8.4 Hz, 1H, H-Ar), 6.66 (d, J = 8.4 Hz, 2H, H-Ar), 6.49 (s, 1H, H-Ar), 3.68 (s, 6H, OCH_3), 3.34 – 3.28 (m, 4H, CH_2), 2.92 (t, J = 6.4 Hz, 2H, CH_2), 2.60 (t, J = 6.3 Hz, 2H, CH_2), 1.97 (quint, J = 6.1 Hz, 2H, CH_2), 1.91 (quint, J = 6.1 Hz, 2H, CH_2); ^{13}C NMR (126 MHz, $CDCl_3$) δ 188.8, 160.4, 157.3, 157.1, 152.8, 148.7, 130.7, 125.5, 119.1, 112.3, 110.8, 108.7, 105.8, 103.9, 56.0, 50.2, 49.9, 49.6, 27.5, 21.1, 20.3 (2); HRMS (ESI) calc. for $C_{24}H_{23}NO_5Na$ 428.1474 $[M + Na]^+$, found 428.1472.

Compound **S16**. Yield 86%. M.p. 242-244°C

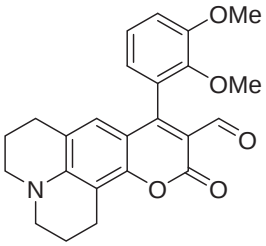

^{1}H NMR (500 MHz, $CDCl_3$) δ 9.89 (s, 1H, CHO), 7.15 (t, J = 7.9 Hz, 1H, H-Ar), 7.06 (d, J = 8.2 Hz, 1H, H-Ar), 6.64 (d, J = 7.6 Hz, 1H, H-Ar), 6.50 (s, 1H, H-Ar), 3.94 (s, 3H, OCH_3), 3.66 (s, 3H, OCH_3), 3.36 – 3.32 (m, 4H, CH_2), 2.91 (t, J = 6.4 Hz, 2H, CH_2), 2.59 (t, J = 6.4 Hz, 2H, CH_2), 1.97 (quint, J = 6.2 Hz, 2H, CH_2), 1.89 (quint, J = 6.0 Hz, 2H, CH_2); ^{13}C NMR (126 MHz, $CDCl_3$) δ 188.0, 160.1, 158.4, 152.3, 152.2, 148.7, 145.2, 127.8, 126.0, 123.7, 120.3, 119.2, 112.6, 110.6, 108.3, 105.3, 60.4, 55.4, 49.9, 49.4, 27.0, 20.5, 19.7 (2); HRMS (ESI) calc. for $C_{24}H_{23}NO_5Na$ 428.1474 $[M + Na]^+$, found 428.1481.

Compound **S17**. Yield 32%. M.p. 210-211°C

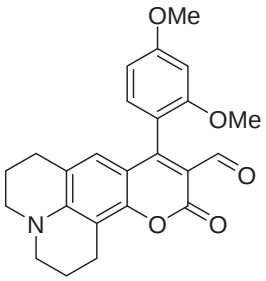

^{1}H NMR (500 MHz, $CDCl_3$) δ 9.80 (s, 1H, CHO), 6.97 (d, J = 8.3 Hz, 1H, H-Ar), 6.60 (dd, J = 8.3, 2.3 Hz, 1H, H-Ar), 6.57-6.56 (m, 2H, H-Ar), 3.88 (s, 3H, OCH_3), 3.70 (s, 3H, OCH_3), 3.35 – 3.29 (m, 4H, CH_2), 2.92 (t,

J = 6.4 Hz, 2H, CH_2), 2.64 – 2.58 (m, 2H, CH_2), 2.02 – 1.95 (m, 2H, CH_2), 1.93 – 1.88 (m, 2H, CH_2); ^{13}C NMR (126 MHz, $CDCl_3$) δ 188.9, 161.7, 160.3, 159.1, 157.7, 152.9, 148.6, 130.3, 126.3, 119.1, 114.8, 112.1, 109.1, 106.0, 104.5, 98.7, 55.7, 55.5, 50.2, 49.9, 27.5, 21.1, 20.3 (2); HRMS (ESI) calc. for $C_{24}H_{23}NO_5Na$ 428.1474 $[M + Na]^+$, found 428.1472.

General procedure for the preparation of compounds **8-11**.

3-formyl coumarin (**S14-S17**) (1 mmol), dimethyl-1,3-acetonedicarboxylate (**2**) (10 mmol) and piperidine (1 mmol) were dissolved in methanol (5 ml) and allowed to stir at 60°C for 20h. The solvent was evaporated and the residue was washed with diethyl ether. The crude product was purified via column chromatography (CH_2Cl_2 : MeOH 9:1).

Compound **8**. Yield 19%. M.p. 265-266°C

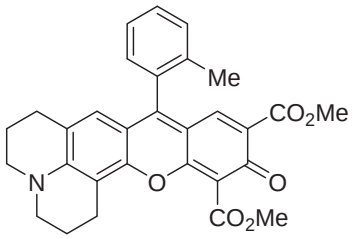

^{1}H NMR (500 MHz, $CDCl_3$) δ 7.49 – 7.41 (m, 2H, H-Ar), 7.38 – 7.33 (m, 2H, H-Ar), 7.10 – 7.08 (m, 1H, H-Ar), 6.47 (s, 1H, H-Ar), 3.98 (s, 3H, OCH_3), 3.80 (s, 3H, OCH_3), 3.41 -3.37 (m, 4H, CH_2), 2.95 – 2.91 (m, 2H, CH_2), 2.63 (t, *J* = 6.2 Hz, 2H, CH_2), 2.08 – 1.99 (m, 5H, CH_3-Ar, CH_2), 1.98 – 1.89 (m, 2H, CH_2); ^{13}C NMR (126 MHz, $CDCl_3$) δ 176.2, 167.4, 166.6, 155.8, 155.0, 151.1, 149.7, 136.0, 134.8, 132.5, 130.6, 129.5, 129.0, 127.8, 126.1, 126.0, 121.2, 112.2, 111.1, 110.8, 105.8, 52.2, 52.1, 50.5, 50.2, 27.5, 20.9, 20.0, 19.8, 19.6; HRMS (ESI) calc. for $C_{30}H_{28}NO_6$ 498.1917 $[M + H]^+$, found 498.1921.

Compound **9**. Yield 28%. M.p. 260-262°C

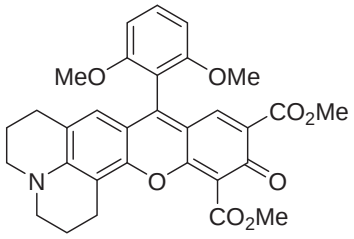

^{1}H NMR (500 MHz, $CDCl_3$) δ 7.57 (s, 1H, H-Ar), 7.46 (t, *J* = 8.4 Hz, 1H, H-Ar), 6.70 (d, *J* = 8.4 Hz, 2H, H-Ar), 6.57 (s, 1H, H-Ar), 3.98 (s, 3H, OCH_3), 3.82 (s, 3H, OCH_3), 3.65 (s, 6H, OCH_3), 3.41 – 3.34 (m, 4H, CH_2), 2.93 (t, *J* = 6.4 Hz, 2H, CH_2), 2.65 (t, *J* = 6.2 Hz, 2H, CH_2), 2.03 - 1.98 (m, 2H, CH_2), 1.97 – 1.92 (m, 2H, CH_2); ^{13}C NMR (126 MHz, $CDCl_3$) δ 176.4, 167.9, 166.9, 157.7, 156.3, 151.3, 151.0, 149.6, 135.5,

131.5, 127.0, 126.1, 120.9, 112.1, 111.8, 111.5, 109.9, 105.5, 104.1, 56.0, 52.1, 52.0, 50.5, 50.2, 27.6, 21.1, 20.2, 19.8; HRMS (ESI) calc. for $C_{31}H_{30}NO_8$ 544.1971 $[M + H]^+$, found 544.1970.

Compound **10**. Yield 28%. M.p. 200°C (dec.)

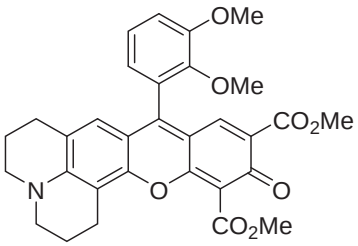

^{1}H NMR (500 MHz, $CDCl_3$) δ 7.66 (s, 1H, H-Ar), 7.21 (t, J = 7.9 Hz, 1H, H-Ar), 7.10 (d, J = 8.2 Hz, 1H, H-Ar), 6.74 – 6.68 (m, 1H, H-Ar), 6.60 (s, 1H, H-Ar), 3.98 (s, 3H, OCH_3), 3.97 (s, 3H, OCH_3), 3.81 (s, 3H, OCH_3), 3.59 (s, 3H, OCH_3), 3.41 – 3.37 (m, 4H, CH_2), 2.92 (t, J = 6.4 Hz, 2H, CH_2), 2.65 – 2.62 (m, 2H, CH_2), 2.03 – 2.00 (m, 2H, CH_2), 1.95 – 1.90 (m, 2H, CH_2); ^{13}C NMR (126 MHz, $CDCl_3$) δ 176.2, 167.6, 166.6, 152.9, 146.5, 135.3, 127.1 (2), 126.6, 124.3, 121.9, 113.6, 111.4, 105.6, 61.2, 55.8, 52.1, 52.0, 50.5, 50.2, 27.5, 20.9, 20.1, 19.8; HRMS (ESI) calc. for $C_{31}H_{30}NO_8$ 544.1971 $[M + H]^+$, found 544.1974.

Compound **11**. Yield 16%. M.p. 181°C(dec.)

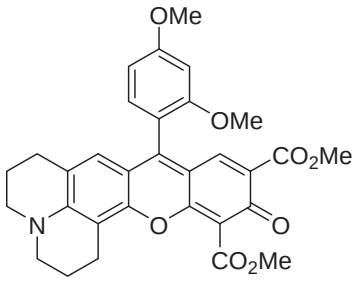

^{1}H NMR (500 MHz, $CDCl_3$) δ 7.64 (s, 1H, H-Ar), 7.02 (d, J = 8.3 Hz, 1H, H-Ar), 6.68 – 6.60 (m, 3H, H-Ar), 3.97 (s, 3H, OCH_3), 3.91 (s, 3H, OCH_3), 3.82 (s, 3H, OCH_3), 3.68 (s, 3H, OCH_3), 3.40 – 3.36 (m, 4H, CH_2), 2.92 (t, J = 6.3 Hz, 2H, CH_2), 2.66 (t, J = 6.3 Hz, 2H, CH_2), 2.01 (quint, J = 6.2 Hz, 2H, CH_2), 1.99 – 1.90 (m, 2H, CH_2); ^{13}C NMR (126 MHz, $CDCl_3$) δ 176.2, 167.7, 166.7, 162.2, 158.0, 156.1, 153.1, 151.3, 149.5, 135.8, 131.4, 127.1, 126.6, 120.8, 114.0, 112.0, 111.9, 111.5, 105.6, 104.9, 99.1, 55.7, 55.5, 52.1, 52.0, 50.5, 50.2, 27.6, 21.0, 20.1, 19.8; HRMS (ESI) calc. for $C_{31}H_{30}NO_8$ 544.1971 $[M + H]^+$, found 544.1975.

General procedure for the preparation of compounds **12, 13**.

3-formyl coumarin (**S18**, **S19**) (1 mmol), dimethyl-1,3-acetonedicarboxylate (**2**) (10 mmol) and piperidine (1 mmol) were dissolved in methanol (5 ml) and allowed to stir at 60°C for 20h. The precipitate which formed was filtered and recrystallized from MeOH/CH_2Cl_2.

Compound **12**. Yield 21%. M.p. M.p. 250°C(dec.)

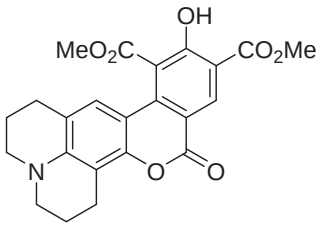

Starting compound **S18** was synthesized following a procedure described in the literature.[1]

^{1}H NMR (500 MHz, $CDCl_3$) δ 11.66 (s, 1H, OH), 8.92 (s, 1H, H-Ar), 7.09 (s, 1H, H-Ar), 4.01 (s, 3H, OCH_3), 3.99 (s, 3H, OCH_3), 3.28 – 3.24 (m, 4H, CH_2), 2.89 (t, J = 6.5 Hz, 2H, CH_2), 2.74 (t, J = 6.3 Hz, 2H, CH_2), 1.98 (quint, J = 6.1 Hz, 4H, CH_2); ^{13}C NMR (126 MHz, $CDCl_3$) δ 169.5, 168.4, 162.6, 160.8, 149.4, 146.1, 139.0, 135.6, 122.9, 117.9, 115.6, 111.7, 110.5, 107.4, 103.4, 52.9, 52.7, 49.9, 49.3, 27.9, 21.5, 20.7, 20.6; HRMS (EI) calc. for $C_{23}H_{21}NO_7$ 423.1318 $M^{+\cdot}$, found 423.1302.

Compound **30**. Yield 60%. M.p. 288-289°C

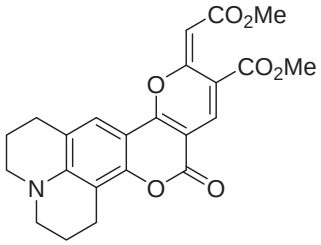

Starting compound **S19** was synthesized following a procedure described in the literature.[2]

^{1}H NMR (500 MHz, 1,1,2,2-CD_2Cl_4) δ 8.04 (s, 1H), 7.58 (s, 1H), 6.38 (s, 1H), 3.82 (s, 3H, OCH_3), 3.76 (s, 3H, OCH_3), 3.37 – 3.32 (m, 4H, CH_2), 2.85 – 2.82 (m, 4H, CH_2), 1.99 – 1.94 (m, 4H, CH_2); ^{13}C NMR (500 MHz, 1,1,2,2- CD_2Cl_4) δ 165.6, 163.4, 161.6, 159.6, 154.6, 151.9, 149.0, 136.9, 121.6, 119.9, 113.3, 106.0, 99.8, 95.8, 94.6, 52.2, 51.0, 50.2, 49.7, 27.7, 20.9, 20.1, 19.9; HRMS (ESI) calc. for $C_{23}H_{21}NO_7Na$ 446.1216 $[M + Na]^+$, found 446.1218.

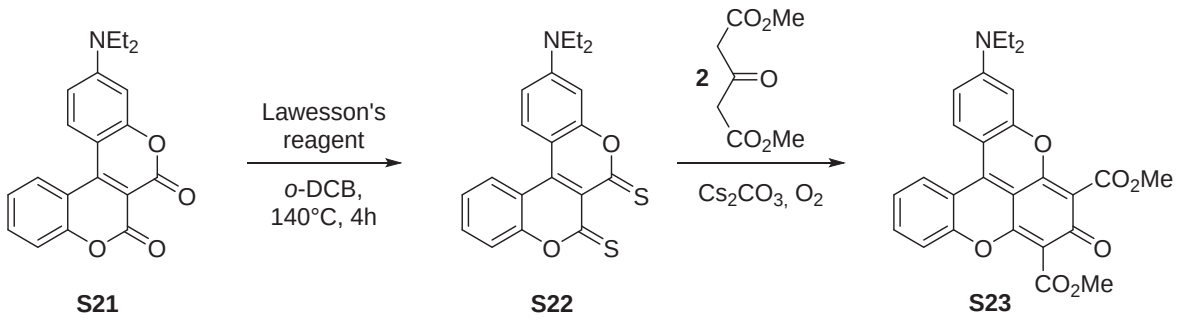

Scheme S4. Transformation of bis-coumarins into V-shaped rhodols.

Compound **S22**. Yield 18%. M.p. 170-171°C

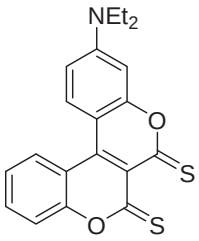

The starting compound **S21** was synthesized according to the literature procedure.[3] The bis-coumarin **S21** (1 mmol) together with Lawesson's reagent (1,25 mmol) were dissolved in 25 ml of dry *o*-DCB and the reaction was heated at 140°C for 4 hours. After the solvent was evaporated under the vacuo, the residue was filtered through a silica pad, washed with mixture of hexane and CH_2Cl_2 (1:1) and concentrated under vacuo. The product was next purified via DCVC (CH_2Cl_2 : hexane 1:2) followed by the recrystallization from the mixture of hexane and CH_2Cl_2.

^{1}H NMR (500 MHz, $CDCl_3$) δ 8.07 (dd, J = 8.1, 1.5 Hz, 1H, H-Ar), 7.96 (d, J = 9.3 Hz, 1H, H-Ar), 7.66 (ddd, J = 8.5, 7.2, 1.5 Hz, 1H, H-Ar), 7.42 (dd, J = 8.4, 1.2 Hz, 1H, H-Ar), 7.35 (ddd, J = 8.3, 7.3, 1.3 Hz, 1H, H-Ar), 6.75 (dd, J = 9.4, 2.7 Hz, 1H, H-Ar), 6.60 (d, J = 2.6 Hz, 1H, H-Ar), 3.50 (q, J = 7.2 Hz, 4H, CH_2), 1.28 (t, J = 7.2 Hz, 6H, CH_3); ^{13}C NMR (126 MHz, $CDCl_3$) δ 190.6, 190.5, 158.6, 155.2, 153.3, 139.8, 134.1, 131.0, 129.2, 124.8, 121.1, 117.3, 117.0, 111.3, 105.6, 97.0, 45.4, 12.5; HRMS (EI) calc. for $C_{20}H_{17}NO_2S_2$ 367.0701 $M^{+\cdot}$, found 367.0706.

Compound **S23**. Yield 30%. M.p. 294-295°C

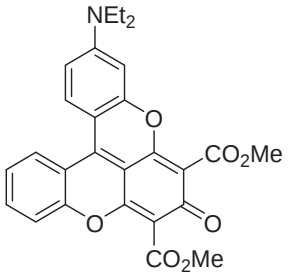

0,03 mmol of compound **S22**, 0,072 mmol of Cs_2CO_3 and 0,3 mmol od dimethyl 1,3-acetonedicarboxylate were mixed together in 2 ml of CH_3CN and were allowed to stir at r.t. overnight. The solvent was evaporated and the residue was purified using DCVC (0,1-2% MeOH in CH_2Cl_2).

^{1}H NMR (500 MHz, $CDCl_3$) δ 8.27 (d, *J* = 8.1 Hz, 1H, H-Ar), 8.14 (d, *J* = 9.4 Hz, 1H, H-Ar), 7.65 (t, *J* = 7.8 Hz, 1H, H-Ar), 7.46 (d, *J* = 8.3 Hz, 1H, H-Ar), 7.37 (t, *J* = 7.7 Hz, 1H, H-Ar), 6.74 (dd, *J* = 9.4, 2.7 Hz, 1H, H-Ar), 6.55 (d, *J* = 2.6 Hz, 1H, H-Ar), 3.98 (d, *J* = 7.1 Hz, 6H, OCH_3), 3.51 (q, *J* = 7.1 Hz, 4H, CH_2), 1.29 (t, *J* = 7.1 Hz, 6H, CH_3); ^{13}C NMR (126 MHz, $CDCl_3$) δ 175.4, 165.6, 165.4, 157.3, 154.2, 152.8, 151.3, 150.7, 140.1, 134.0, 129.7, 128.2, 124.5, 118.8, 116.3, 110.5, 105.4, 105.1, 98.1, 52.3, 52.3, 45.1, 12.6; HRMS (EI) calc. for $C_{27}H_{23}NO_7$ 473.1457 $M^{+\cdot}$, found 473.1470.

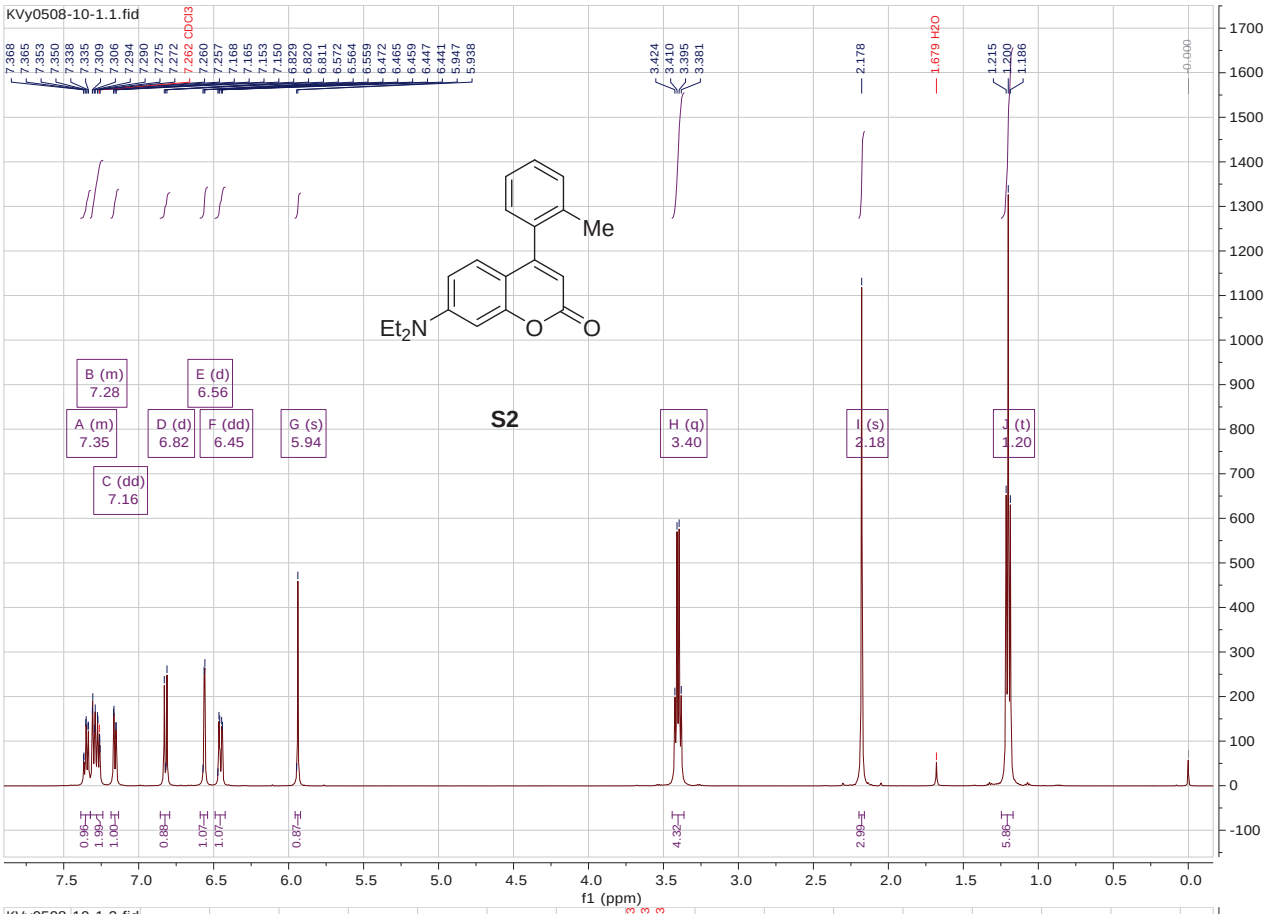
KVy0508-10-1.1.fid
Me
Et2N
O
O
S2
B (m) 7.28
A (m) 7.35
C (dd) 7.16
D (d) 6.82
E (d) 6.56
F (dd) 6.45
G (s) 5.94
H (q) 3.40
I (s) 2.18
J (t) 1.20
f1 (ppm)

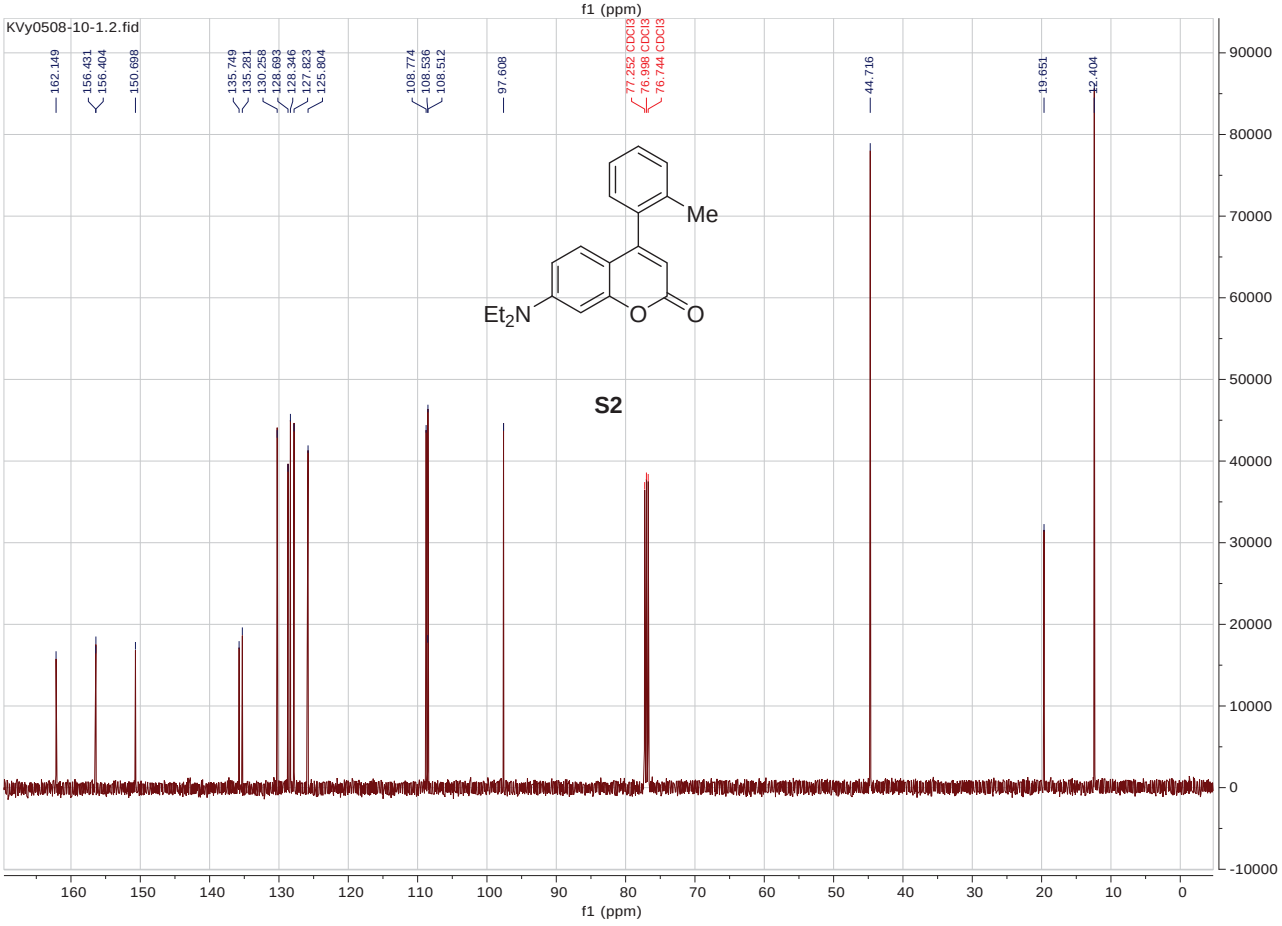
KVy0508-10-1.2.fid
Me
Et2N
O
O
S2
f1 (ppm)

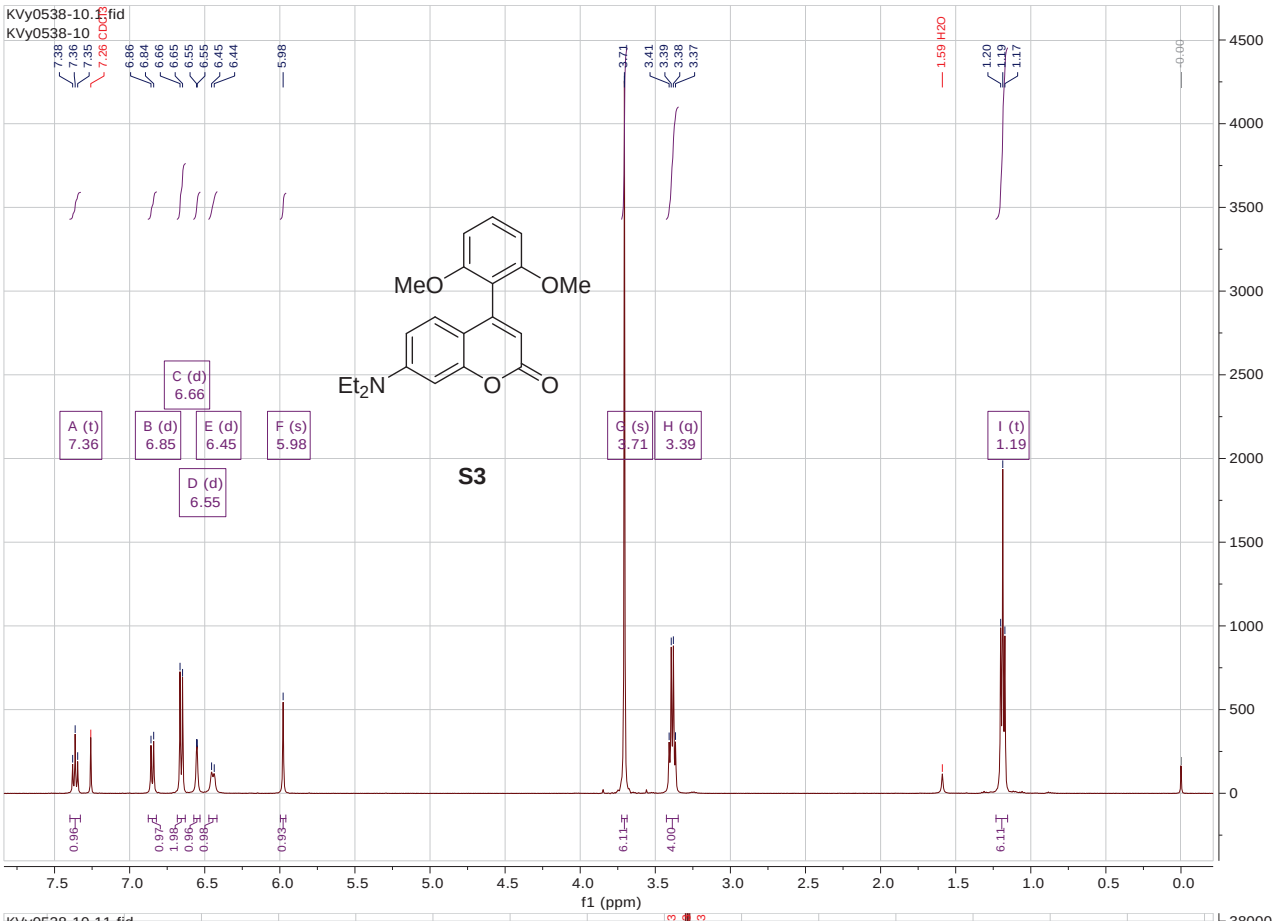
KVy0538-10.11.fid
KVy0538-10
MeO
OMe
Et2N
O
O
S3
A (t) 7.36
B (d) 6.85
C (d) 6.66
D (d) 6.55
E (d) 6.45
F (s) 5.98
G (s) 3.71
H (q) 3.39
I (t) 1.19
f1 (ppm)

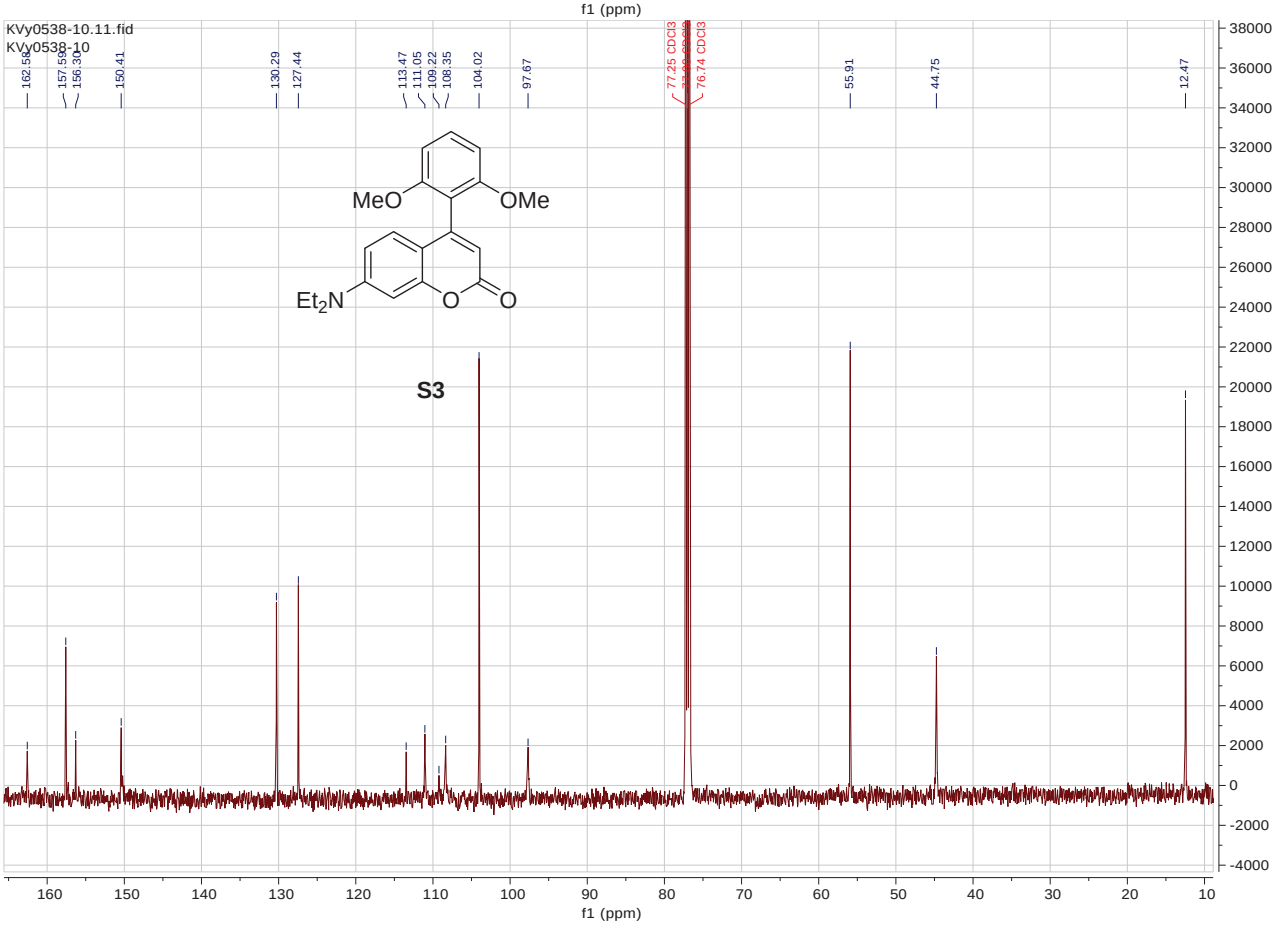
KVy0538-10.11.fid
KVy0538-10
MeO
OMe
Et2N
O
O
S3
f1 (ppm)

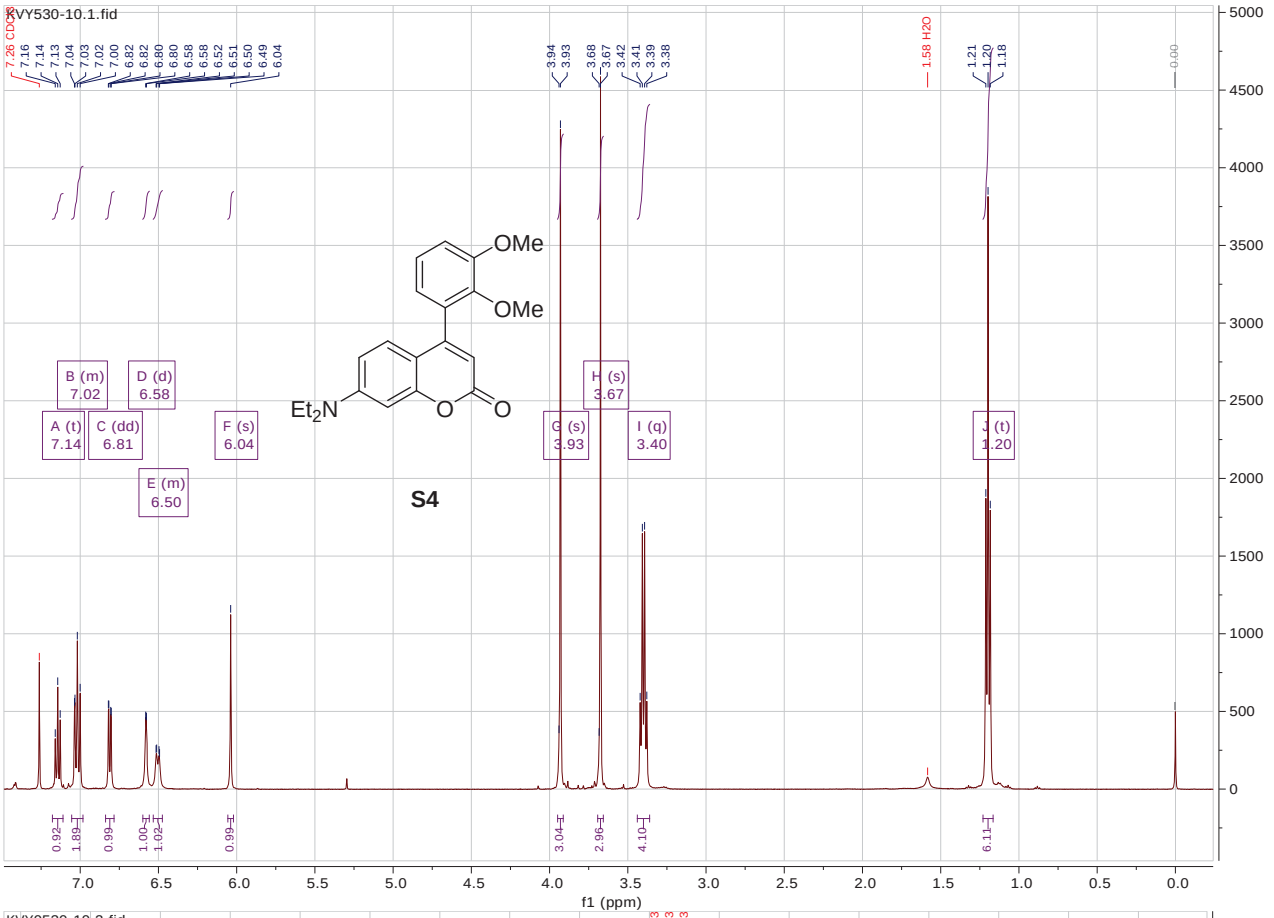
KVY530-10.1.fid
OMe
OMe
Et2N
O
O
S4
B (m) 7.02
D (d) 6.58
A (t) 7.14
C (dd) 6.81
F (s) 6.04
E (m) 6.50
H (s) 3.67
G (s) 3.93
I (q) 3.40
J (t) 1.20
f1 (ppm)

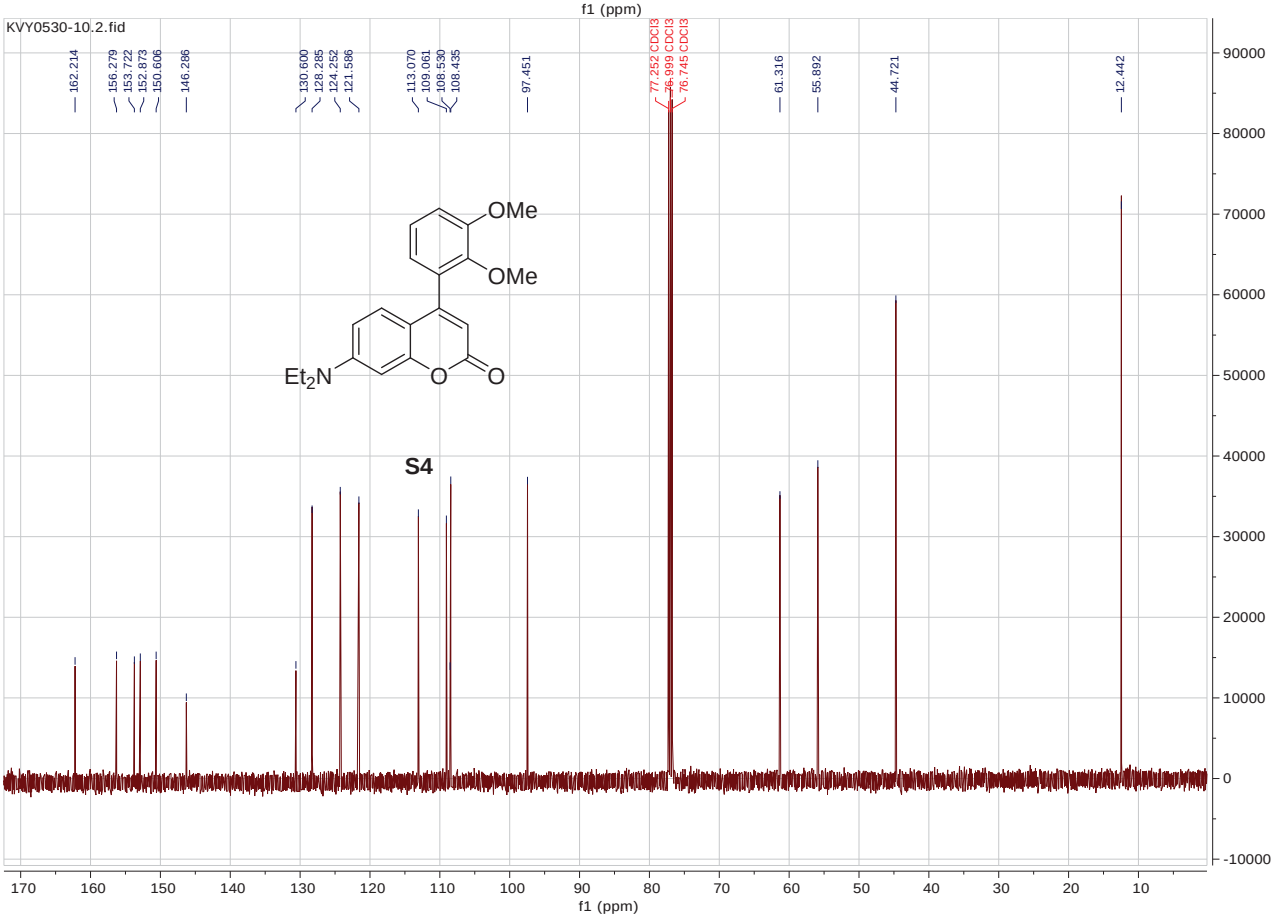
KVY0530-10.2.fid
OMe
OMe
Et2N
O
O
S4
f1 (ppm)

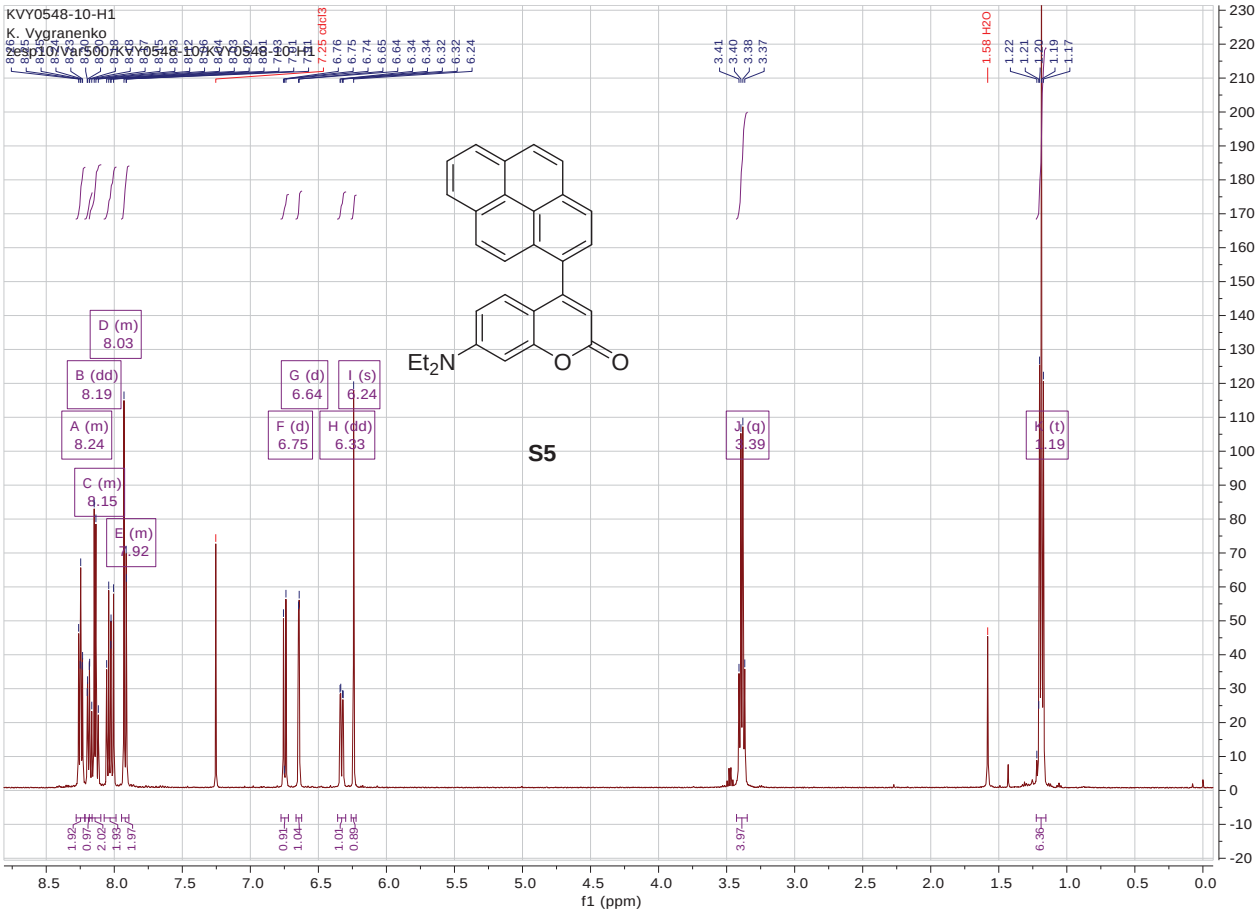
KVY0548-10-H1
K. Vygranenko
zesp10/Var500/KVY0548-10/KVY0548-10-1H1
D (m) 8.03
B (dd) 8.19
A (m) 8.24
C (m) 8.15
E (m) 7.92
G (d) 6.64
I (s) 6.24
F (d) 6.75
H (dd) 6.33
J (q) 3.39
K (t) 1.19
S5
f1 (ppm)

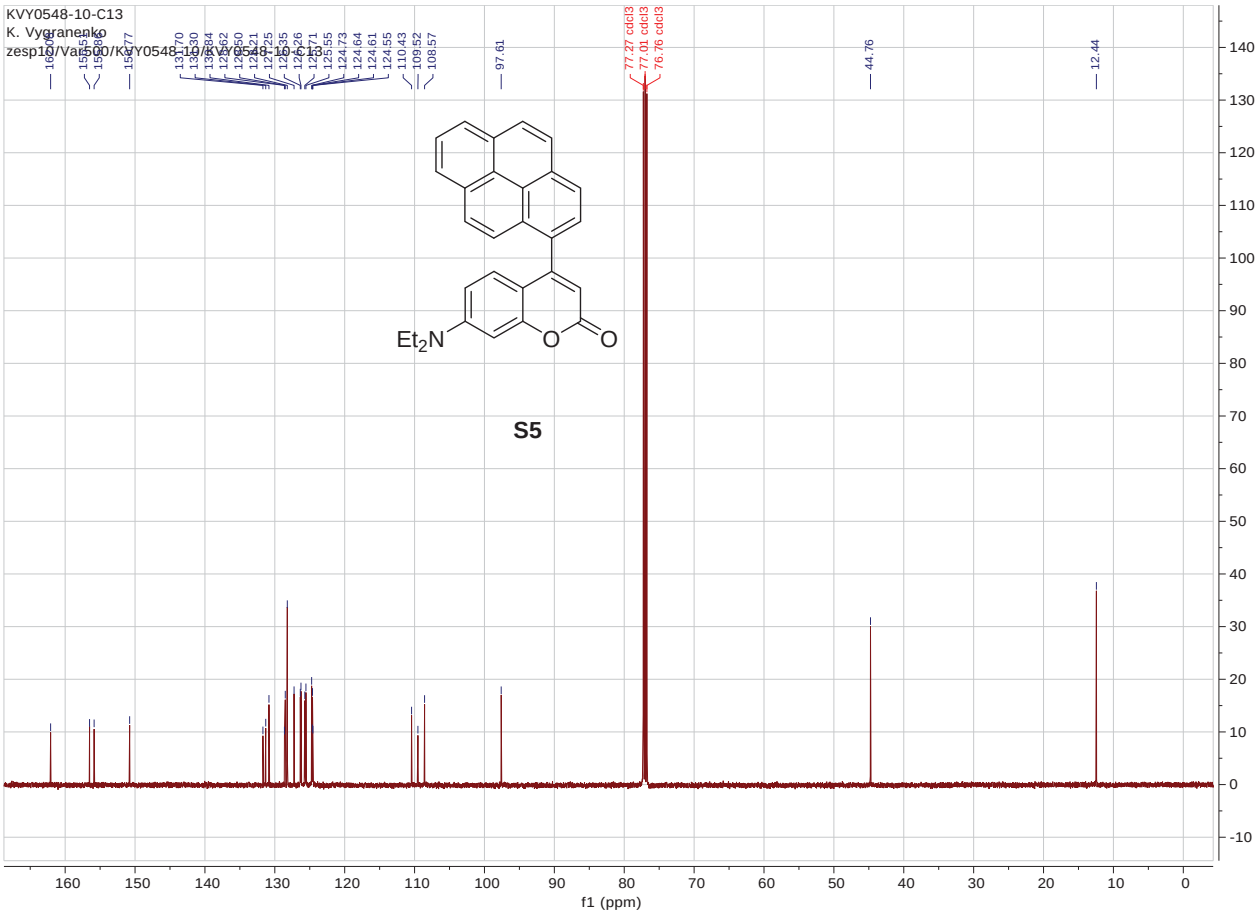
KVY0548-10-C13
K. Vygranenko
zesp10/Var500/KVY0548-10/KVY0548-10-C13
S5
f1 (ppm)

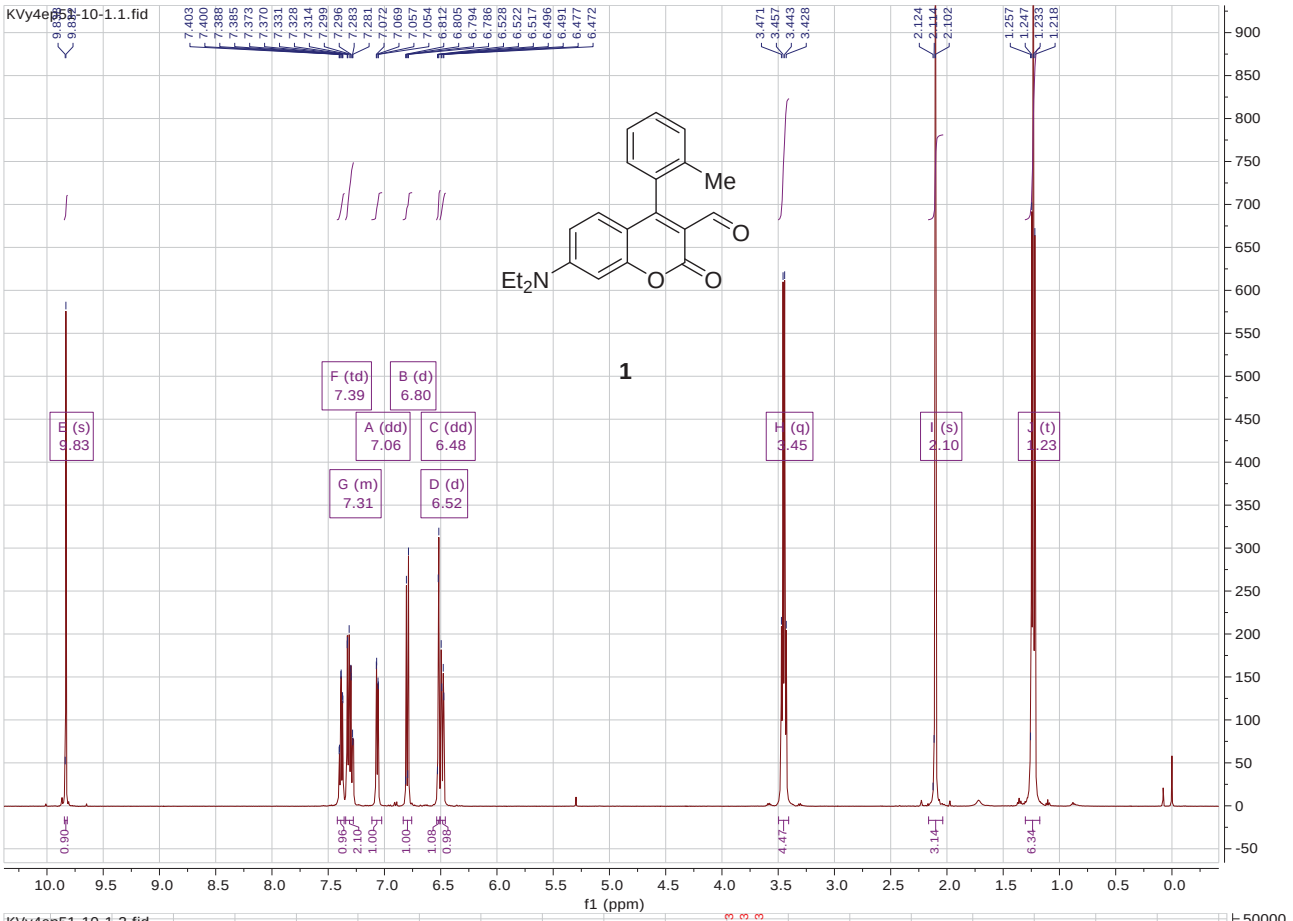
KVy4ep51-10-1.1.fid
Me
O
Et2N
O
O
1
F (td) 7.39
B (d) 6.80
A (dd) 7.06
C (dd) 6.48
G (m) 7.31
D (d) 6.52
E (s) 9.83
H (q) 3.45
I (s) 2.10
J (t) 1.23
f1 (ppm)

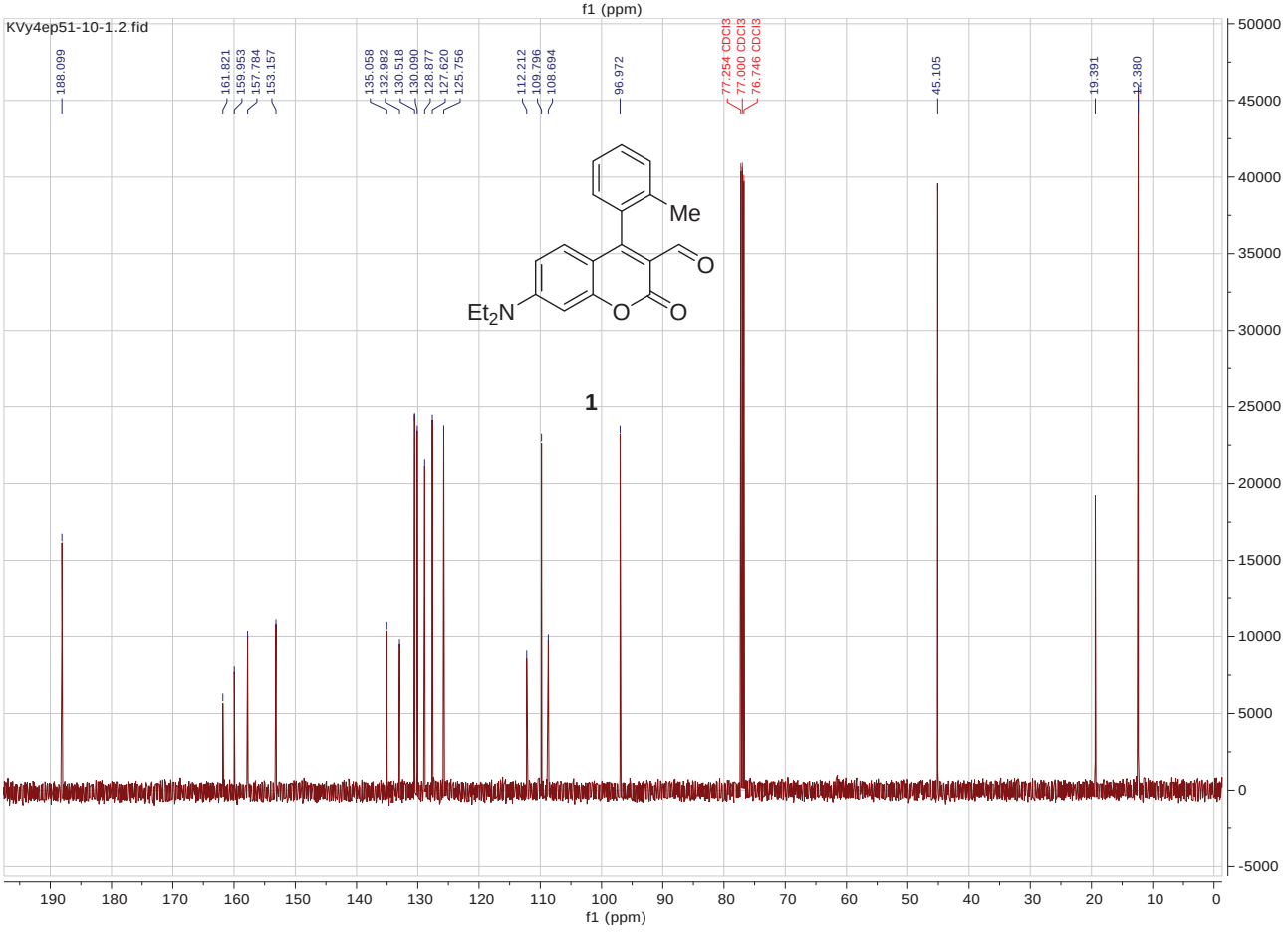
KVy4ep51-10-1.2.fid
188.099
161.821
159.953
157.784
153.157
135.058
132.982
130.518
130.090
128.877
127.620
125.756
112.212
109.796
108.694
96.972
77.254 CDCl3
77.000 CDCl3
76.746 CDCl3
45.105
19.391
12.380
Me
O
Et2N
O
O
1
f1 (ppm)

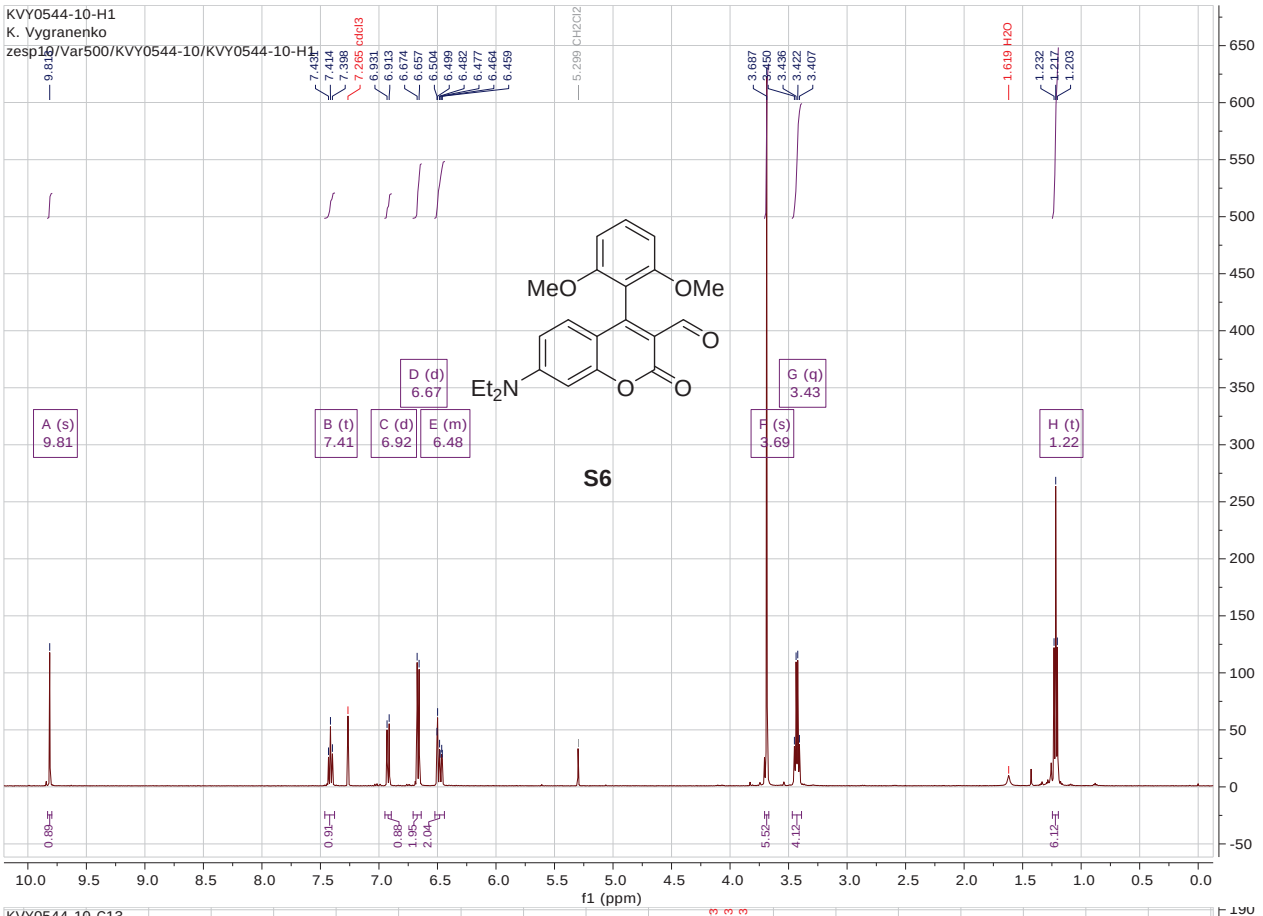
KVY0544-10-H1
K. Vygranenko
zesp10/Var500/KVY0544-10/KVY0544-10-H1
MeO
OMe
O
Et2N
O
O
A (s) 9.81
B (t) 7.41
C (d) 6.92
D (d) 6.67
E (m) 6.48
F (s) 3.69
G (q) 3.43
H (t) 1.22
S6
f1 (ppm)

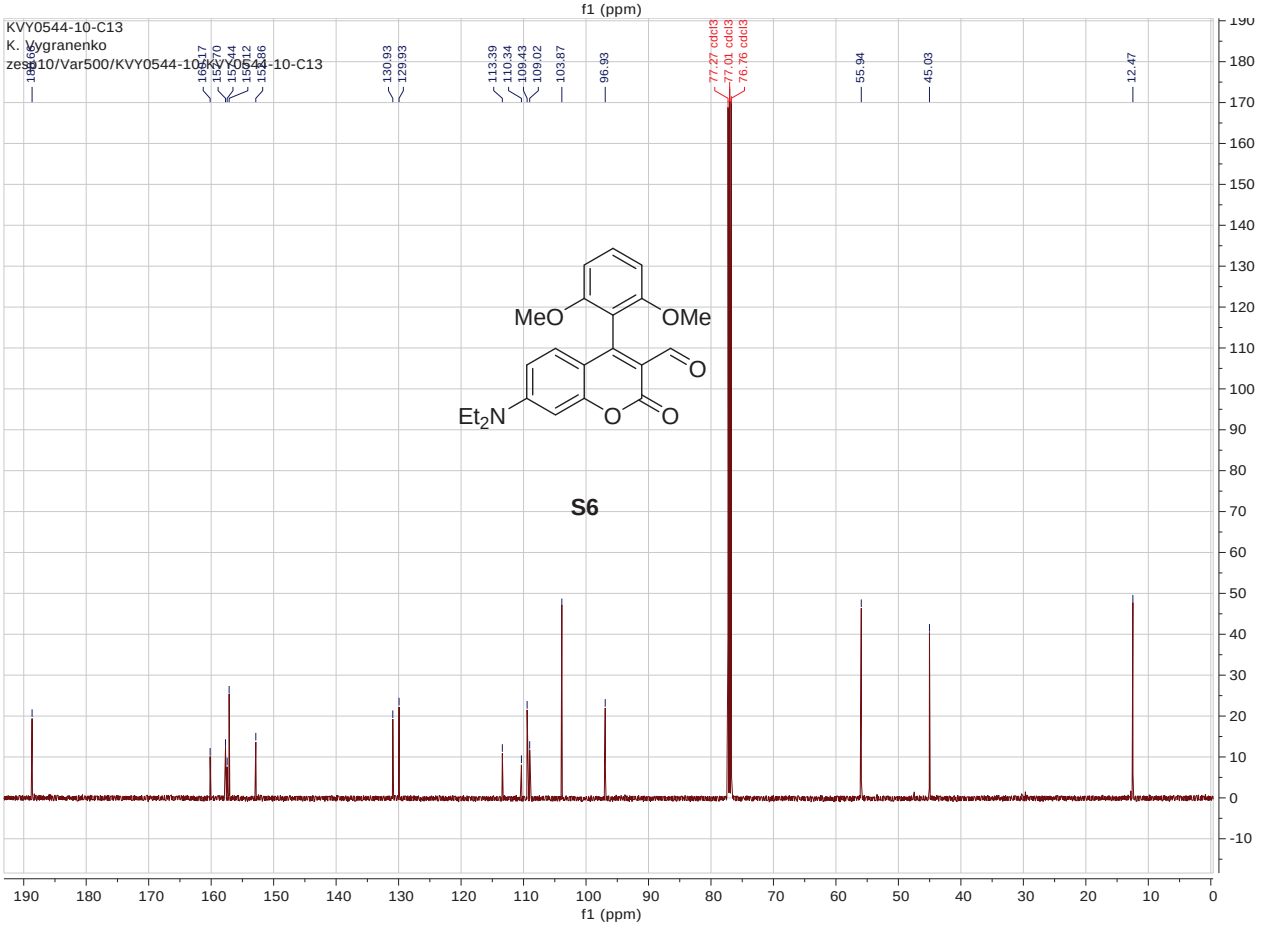
KVY0544-10-C13
K. Vygranenko
zesp10/Var500/KVY0544-10/KVY0544-10-C13
MeO
OMe
O
Et2N
O
O
S6
f1 (ppm)

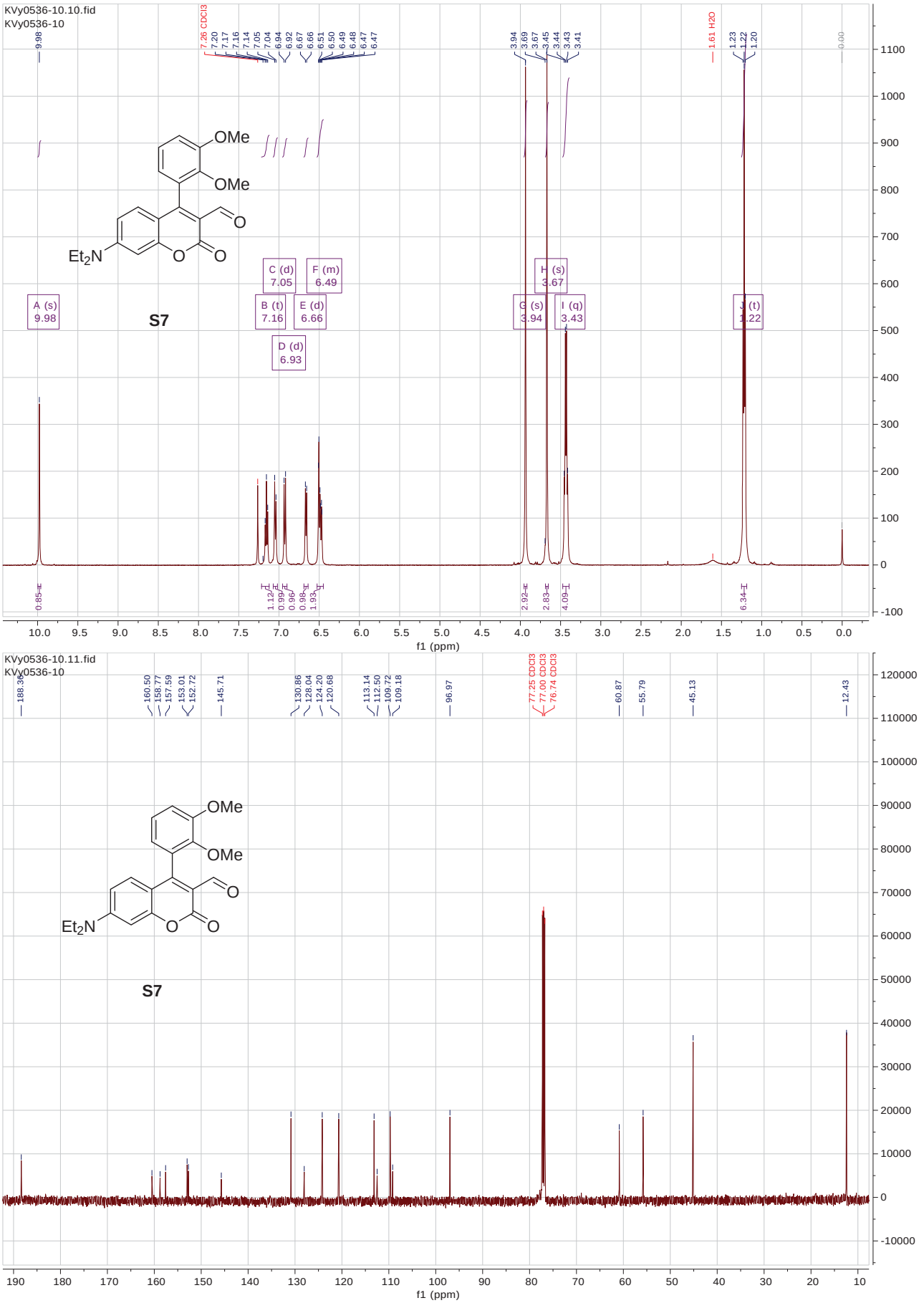
KVy0536-10.10.fid
KVy0536-10
OMe
OMe
O
Et2N
O
O
S7
A (s) 9.98
B (t) 7.16
C (d) 7.05
D (d) 6.93
E (d) 6.66
F (m) 6.49
G (s) 3.94
H (s) 3.67
I (q) 3.43
J (t) 1.22
f1 (ppm)
KVy0536-10.11.fid
KVy0536-10
OMe
OMe
O
Et2N
O
O
S7
f1 (ppm)

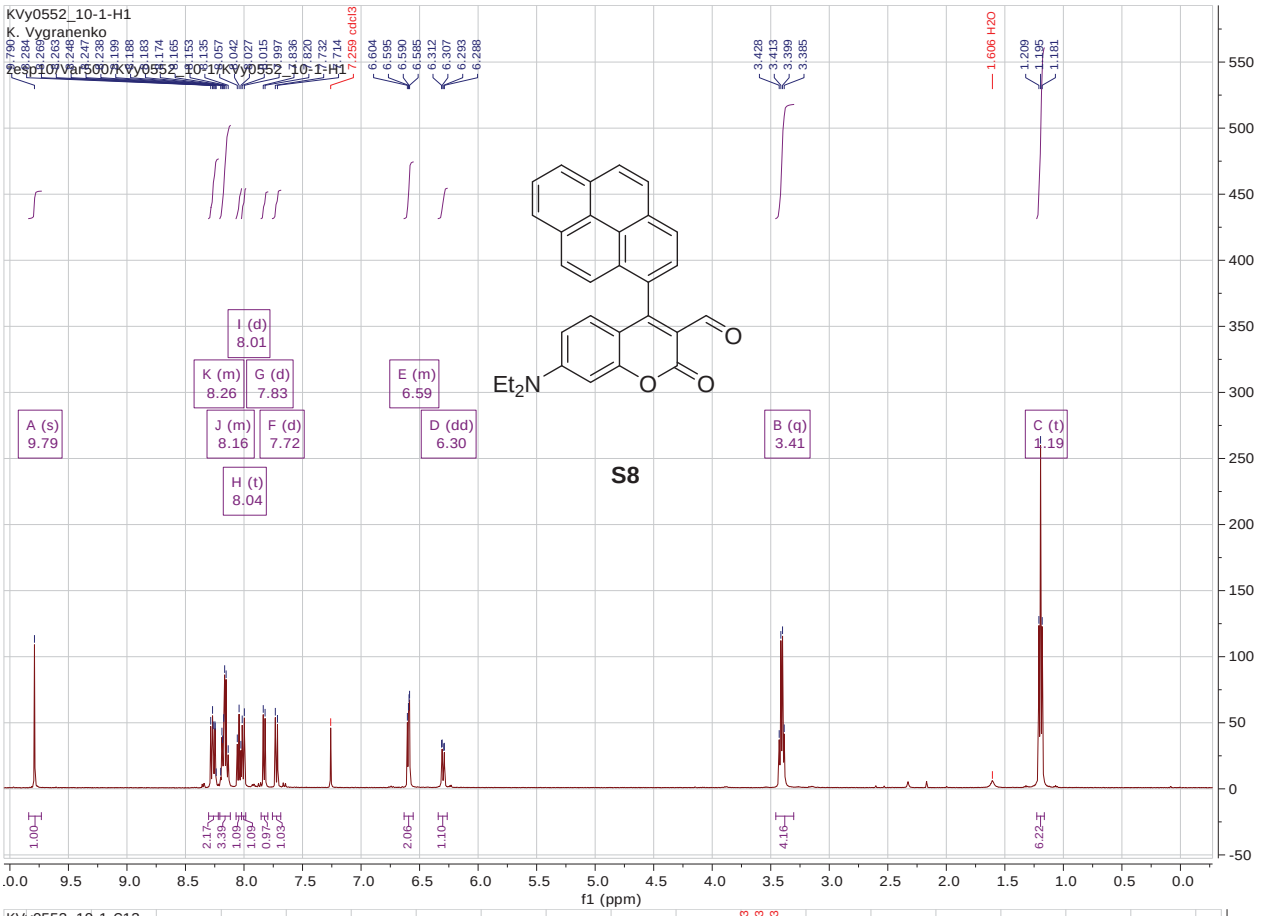
KVy0552_10-1-H1
K. Vygranenko
zesp10/Var500/KVy0552_10-1/KVy0552_10-1-H1
A (s) 9.79
I (d) 8.01
K (m) 8.26
G (d) 7.83
J (m) 8.16
F (d) 7.72
H (t) 8.04
E (m) 6.59
D (dd) 6.30
B (q) 3.41
C (t) 1.19
Et2N
O
O
O
S8
f1 (ppm)

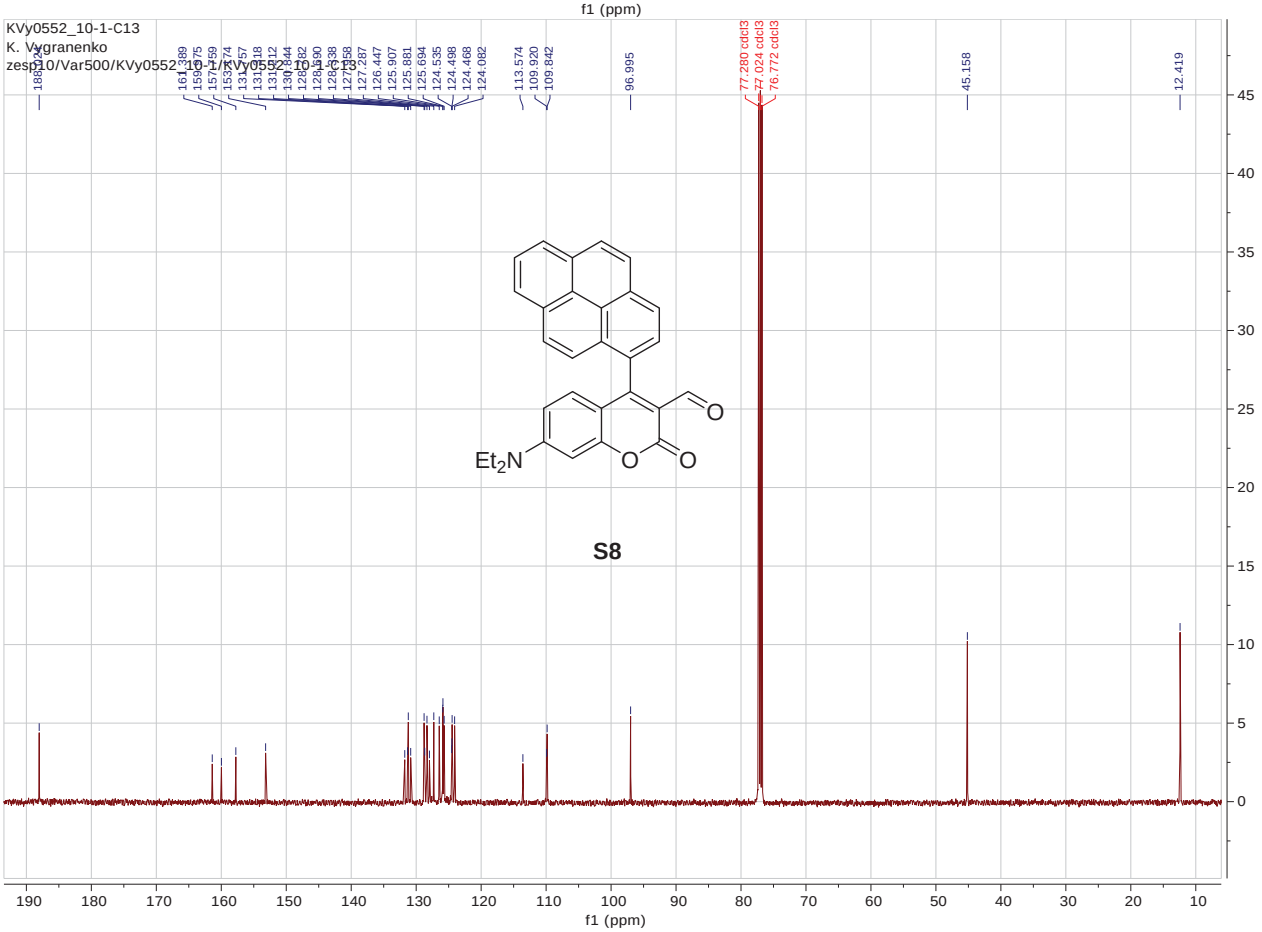
KVy0552_10-1-C13
K. Vygranenko
zesp10/Var500/KVy0552_10-1/KVy0552_10-1-C13
Et2N
O
O
O
S8
f1 (ppm)

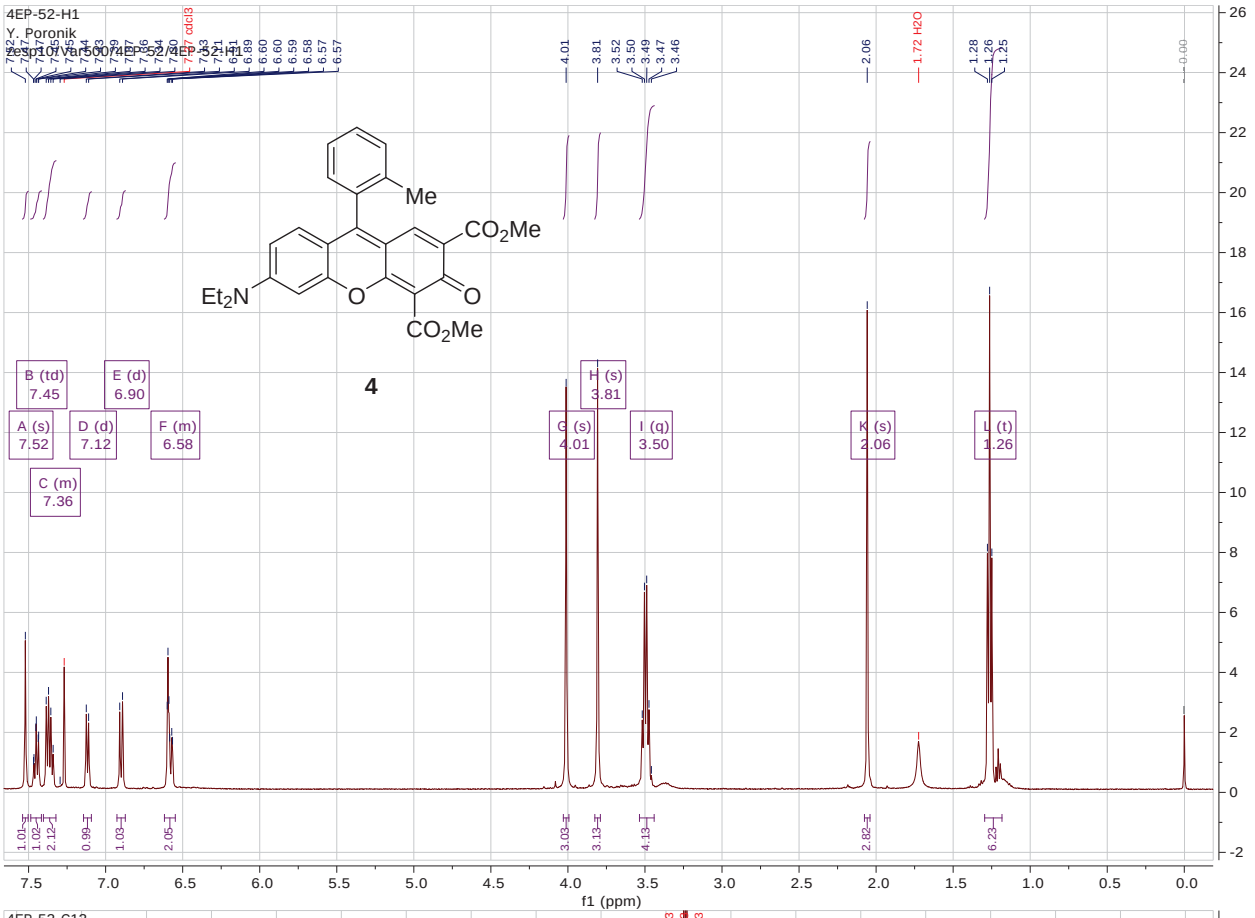
4EP-52-H1
Y. Poronik
zesp10/Var500/4EP-52/4EP-52-H1
Me
CO2Me
Et2N
O
O
CO2Me
4
B (td) 7.45
E (d) 6.90
H (s) 3.81
A (s) 7.52
D (d) 7.12
F (m) 6.58
G (s) 4.01
I (q) 3.50
K (s) 2.06
L (t) 1.26
C (m) 7.36
f1 (ppm)

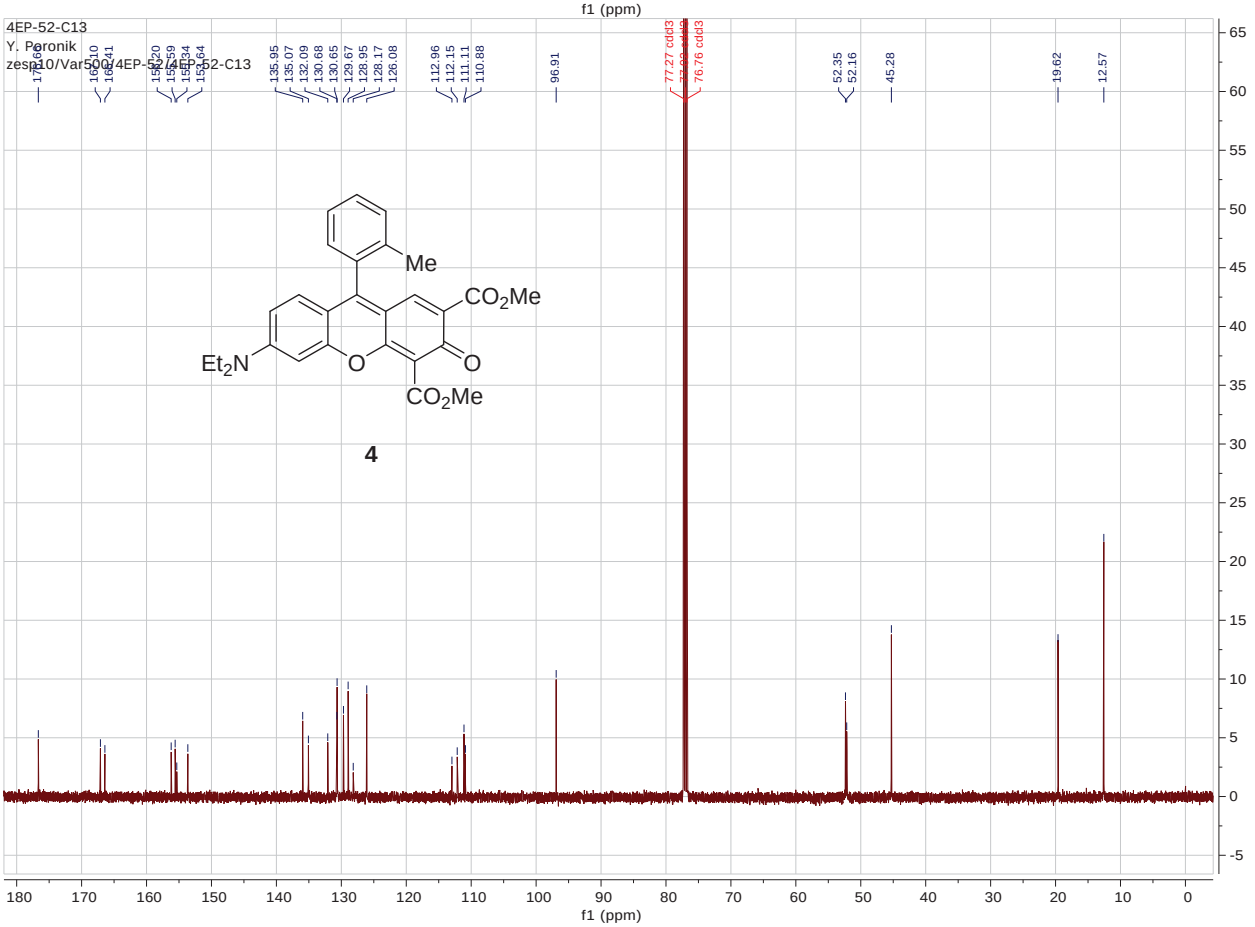
4EP-52-C13
Y. Poronik
zesp10/Var500/4EP-52/4EP-52-C13
Me
CO2Me
Et2N
O
O
CO2Me
4
f1 (ppm)

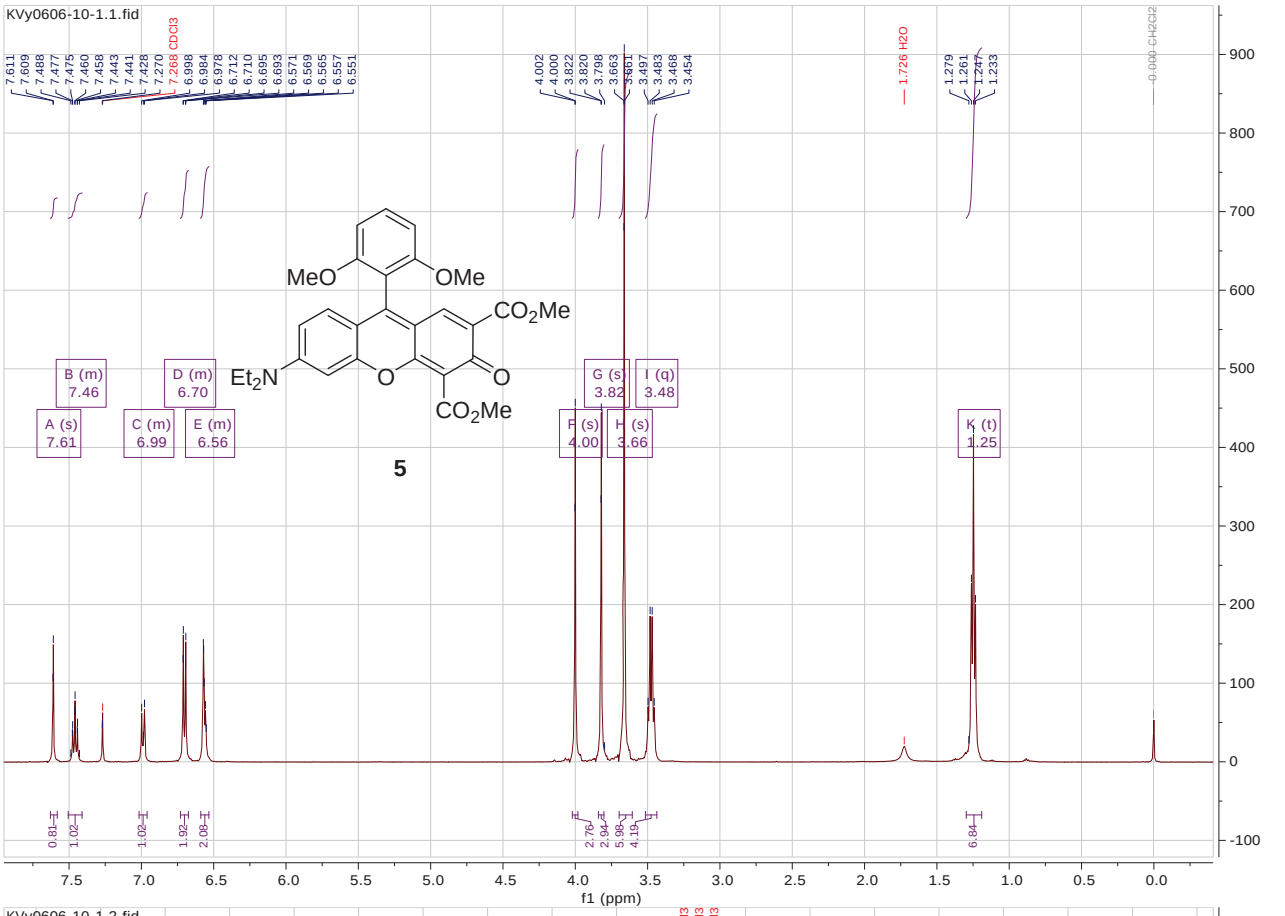
KVy0606-10-1.1.fid
MeO
OMe
CO2Me
Et2N
O
O
CO2Me
5
A (s) 7.61
B (m) 7.46
C (m) 6.99
D (m) 6.70
E (m) 6.56
F (s) 4.00
G (s) 3.82
H (s) 3.66
I (q) 3.48
K (t) 1.25
f1 (ppm)

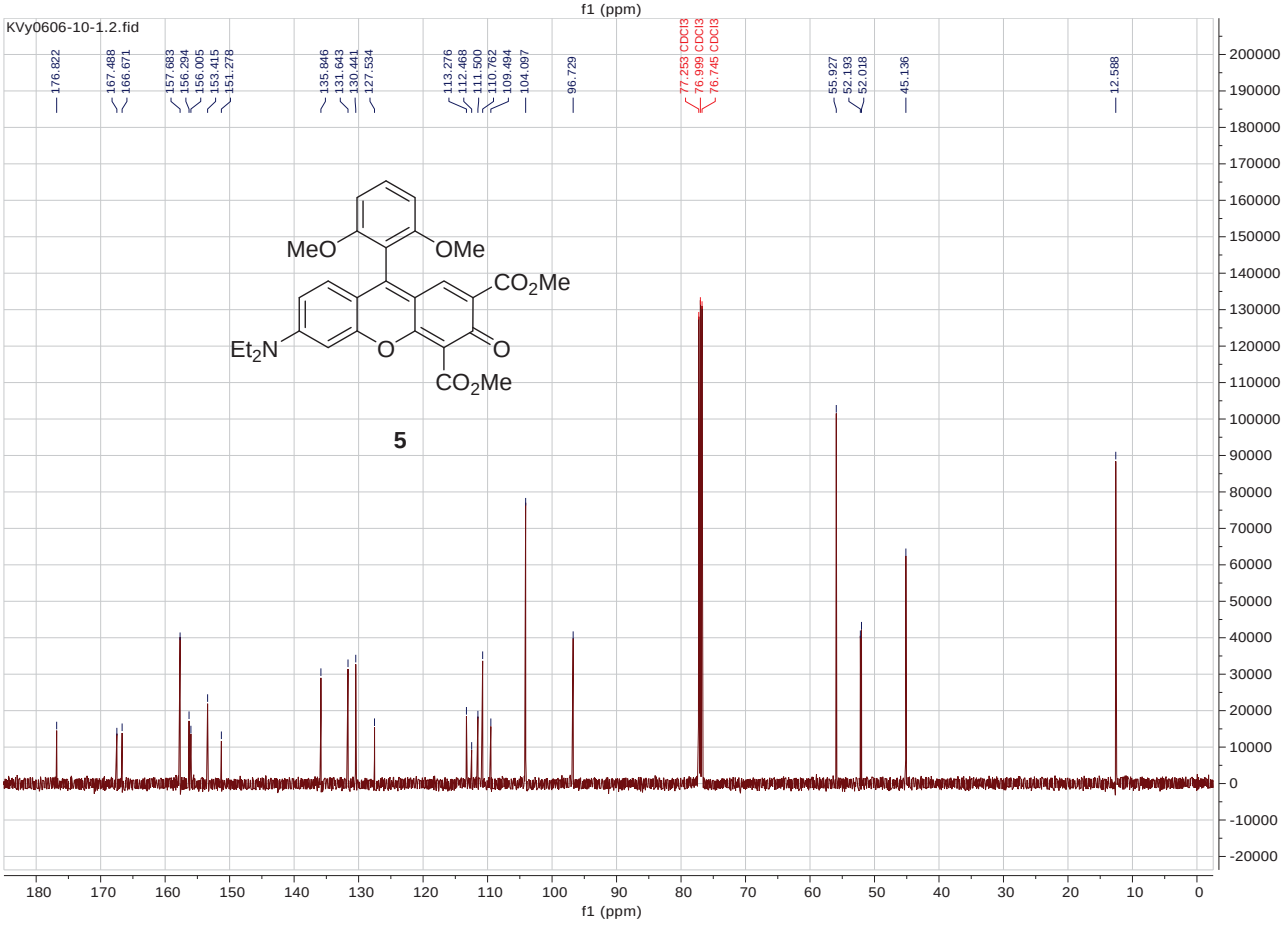
KVy0606-10-1.2.fid
MeO
OMe
CO2Me
Et2N
O
O
CO2Me
5
f1 (ppm)

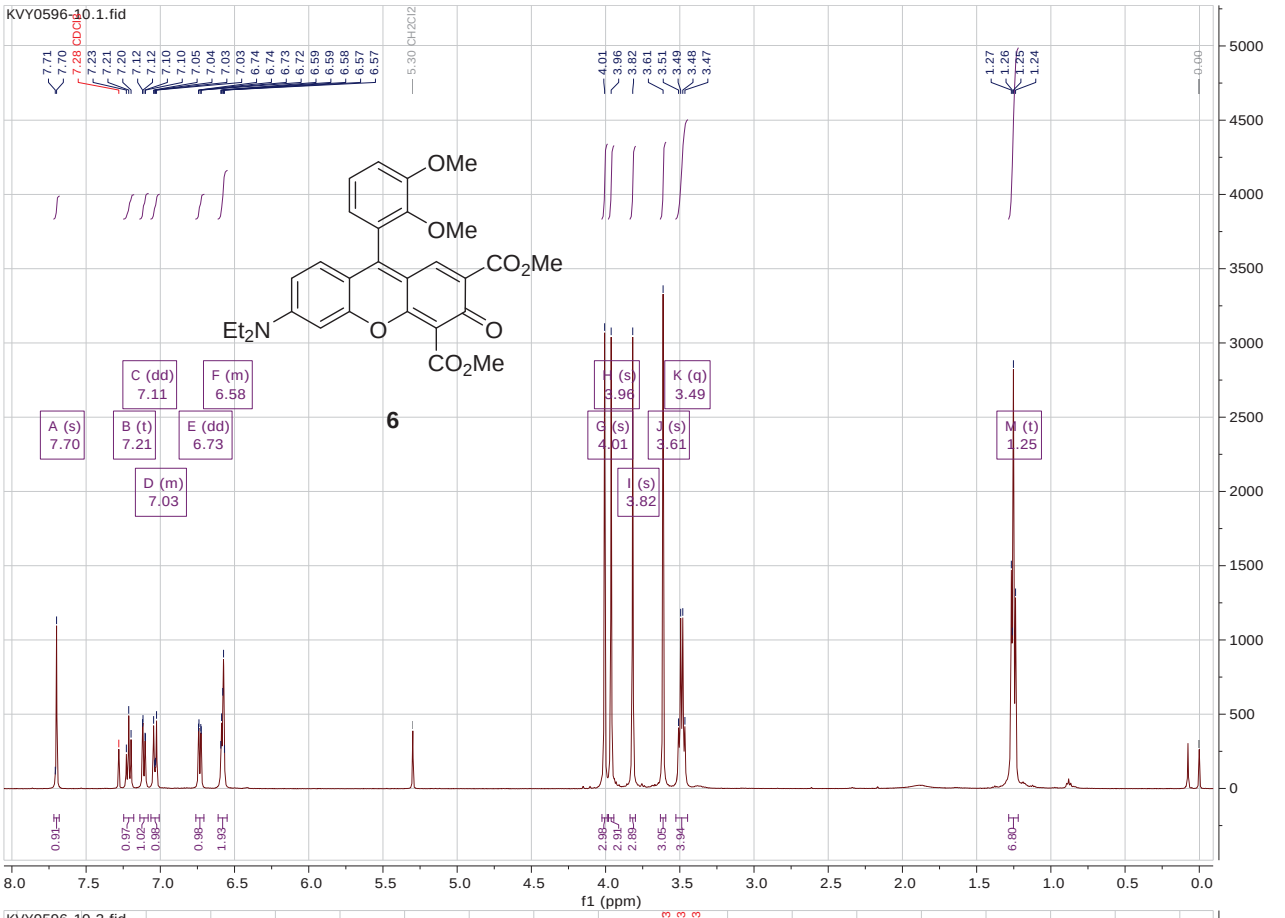
KVY0596-10.1.fid
OMe
OMe
CO2Me
Et2N
O
O
CO2Me
6
A (s) 7.70
B (t) 7.21
C (dd) 7.11
D (m) 7.03
E (dd) 6.73
F (m) 6.58
G (s) 4.01
H (s) 3.96
I (s) 3.82
J (s) 3.61
K (q) 3.49
M (t) 1.25
f1 (ppm)

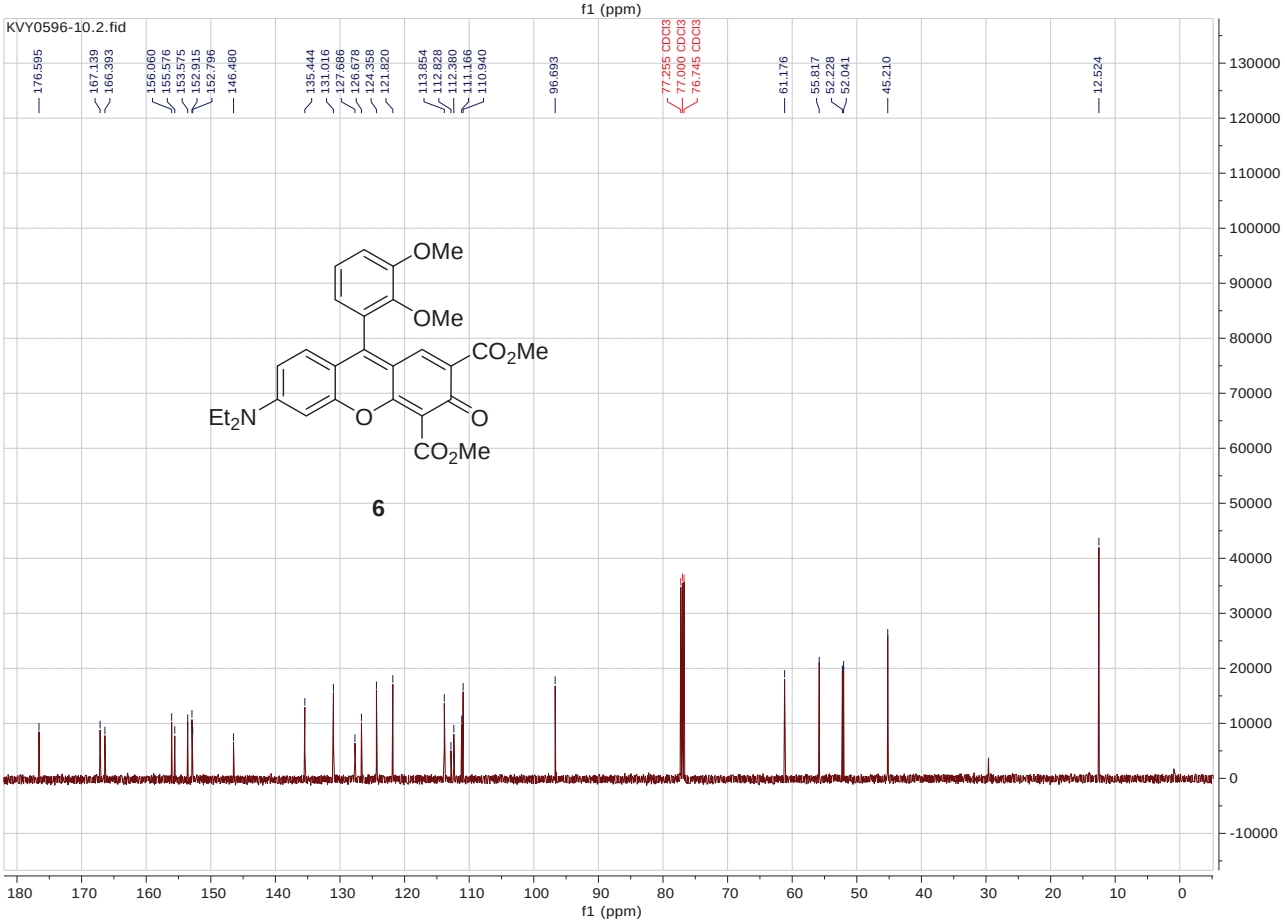
KVY0596-10.2.fid
OMe
OMe
CO2Me
Et2N
O
O
CO2Me
6
f1 (ppm)

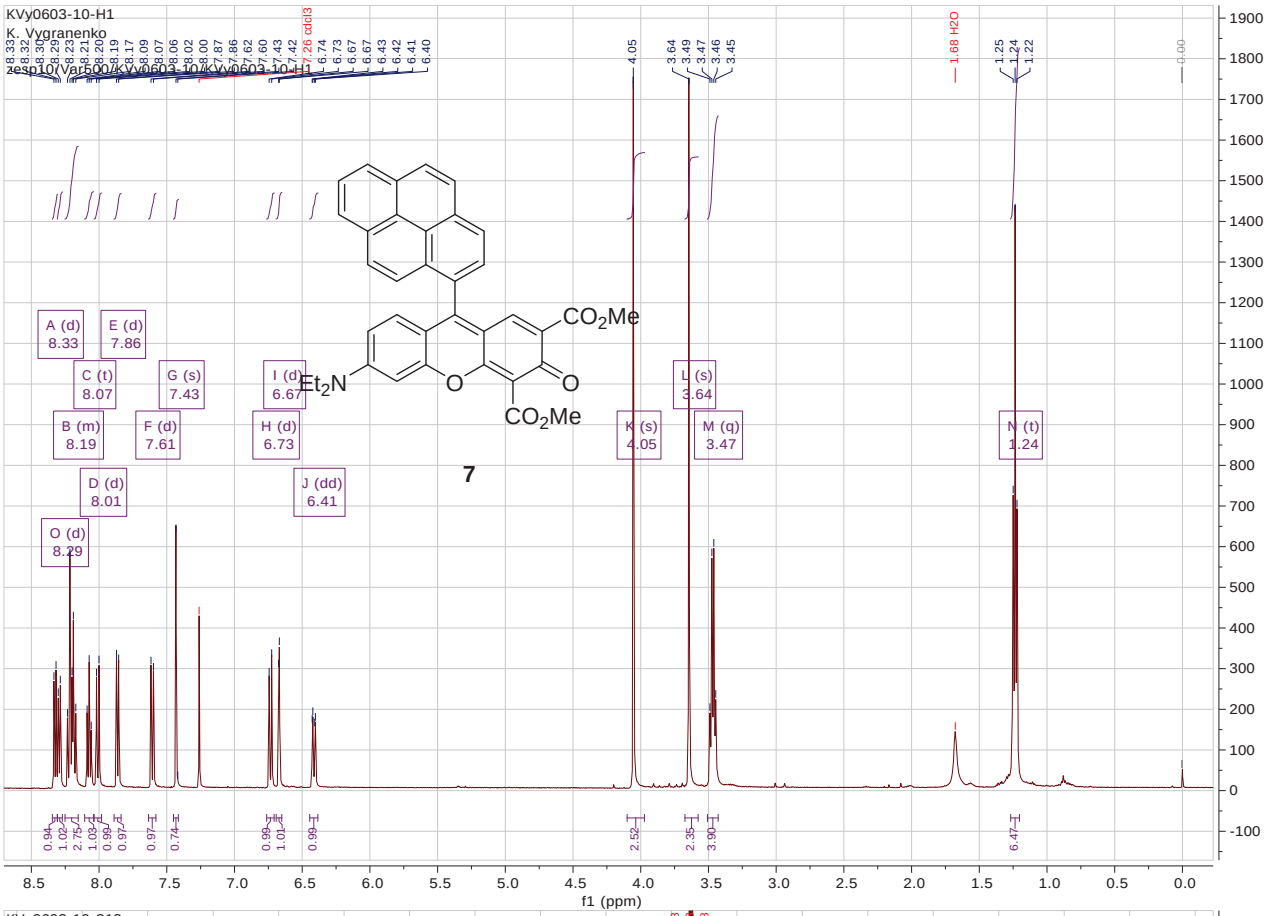
KVy0603-10-H1
K. Vygranenko
zesp10/Var500/KVy0603-10/KVy0603-10-H1
A (d) 8.33
E (d) 7.86
C (t) 8.07
G (s) 7.43
B (m) 8.19
F (d) 7.61
I (d) 6.67
H (d) 6.73
D (d) 8.01
J (dd) 6.41
O (d) 8.29
K (s) 4.05
L (s) 3.64
M (q) 3.47
N (t) 1.24
7
f1 (ppm)

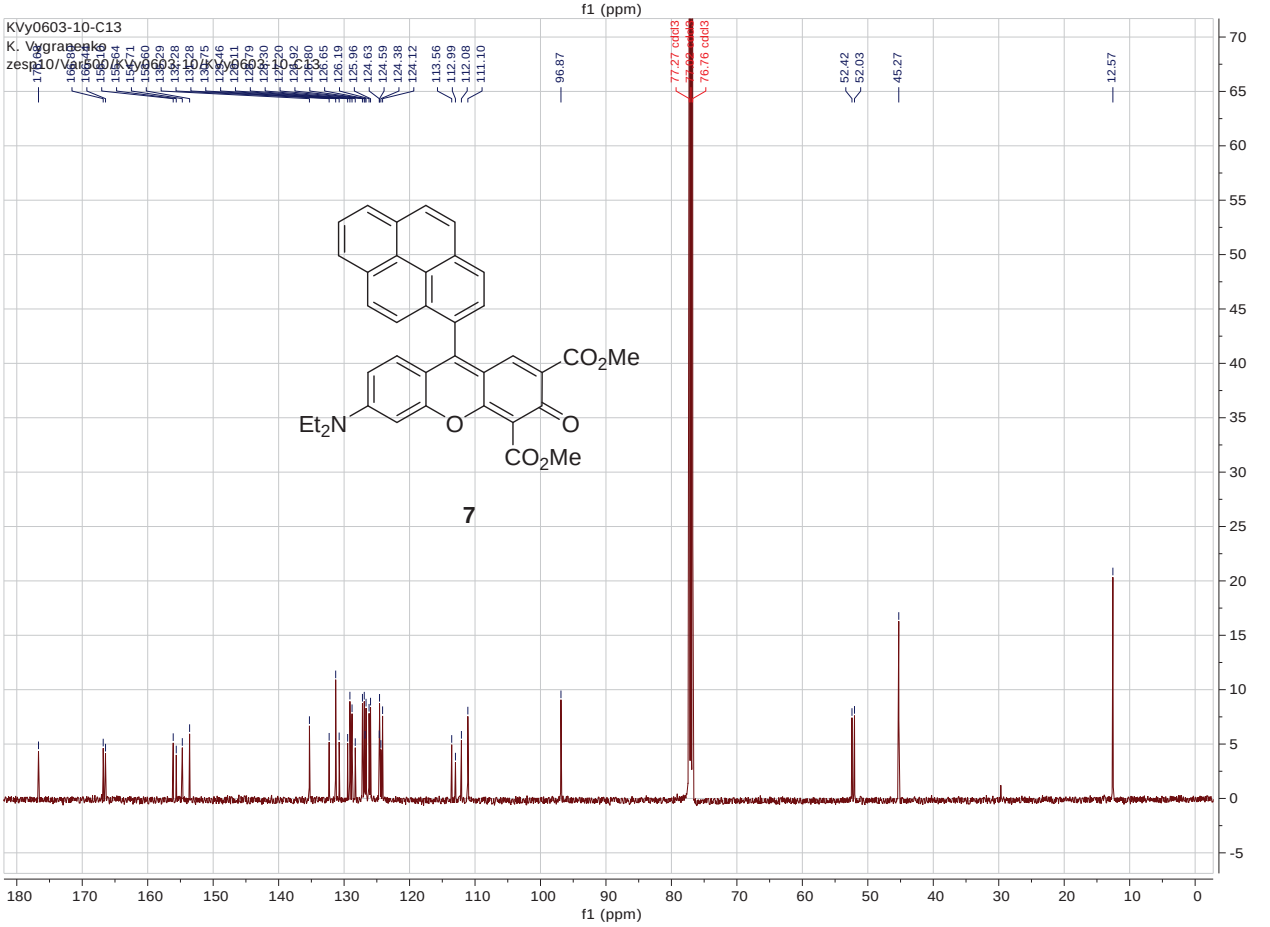
KVy0603-10-C13
K. Vygranenko
zesp10/Var500/KVy0603-10/KVy0603-10-C13
7
f1 (ppm)

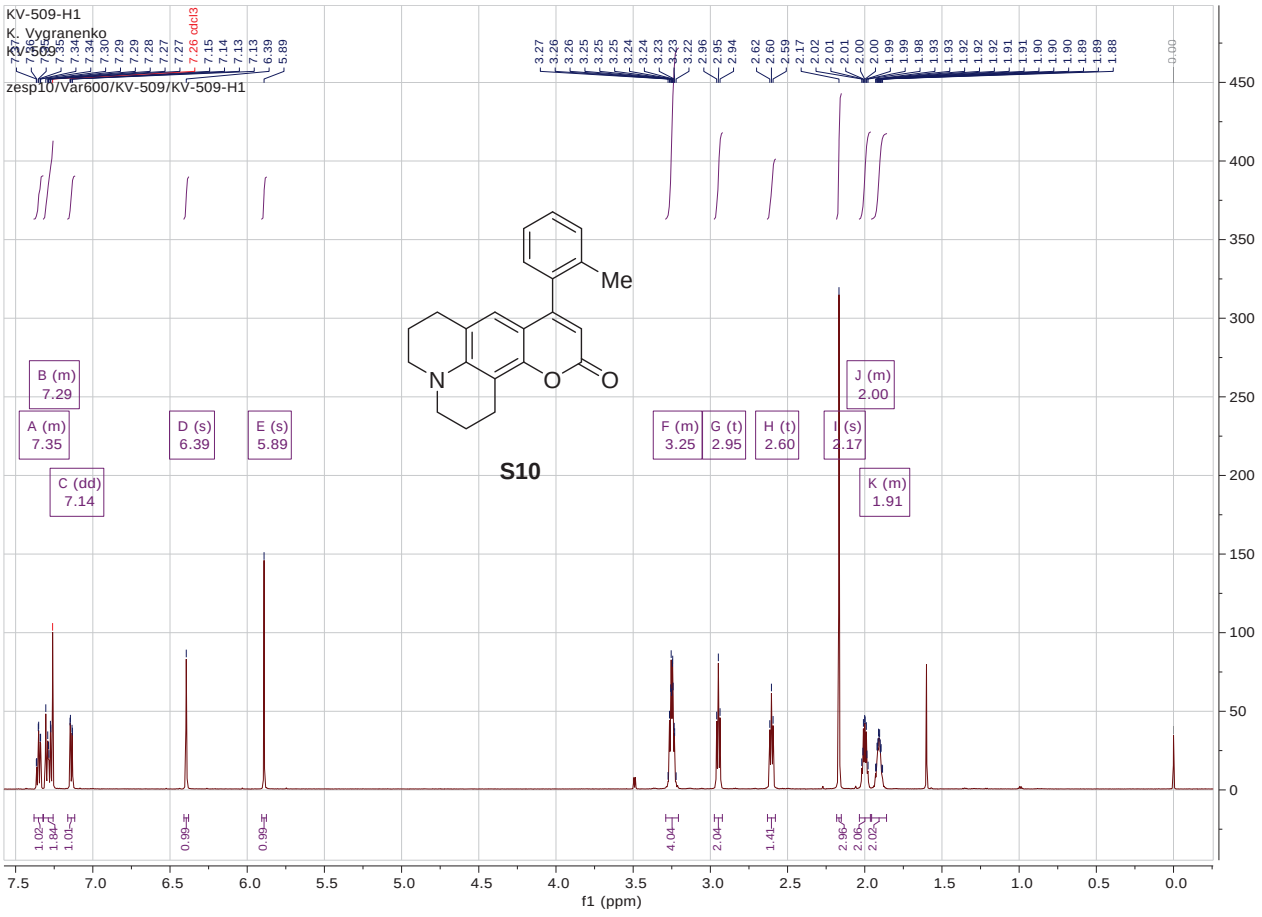
KV-509-H1
K. Vygranenko
KV-509
zesp10/Var600/KV-509/KV-509-H1
Me
N
O
O
S10
B (m) 7.29
A (m) 7.35
C (dd) 7.14
D (s) 6.39
E (s) 5.89
F (m) 3.25
G (t) 2.95
H (t) 2.60
I (s) 2.17
J (m) 2.00
K (m) 1.91
f1 (ppm)

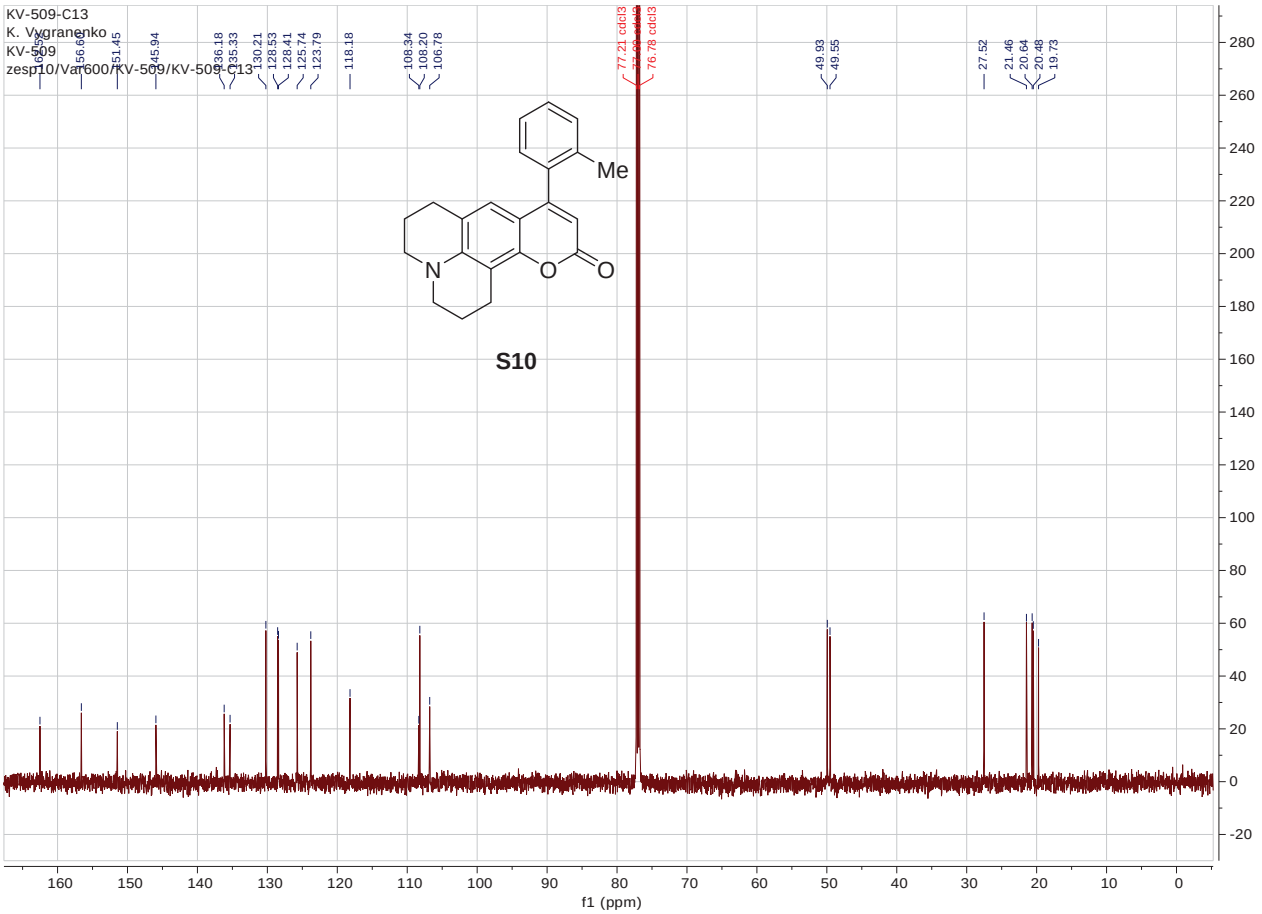
KV-509-C13
K. Vygranenko
KV-509
zesp10/Var600/KV-509/KV-509-C13
Me
N
O
O
S10
f1 (ppm)

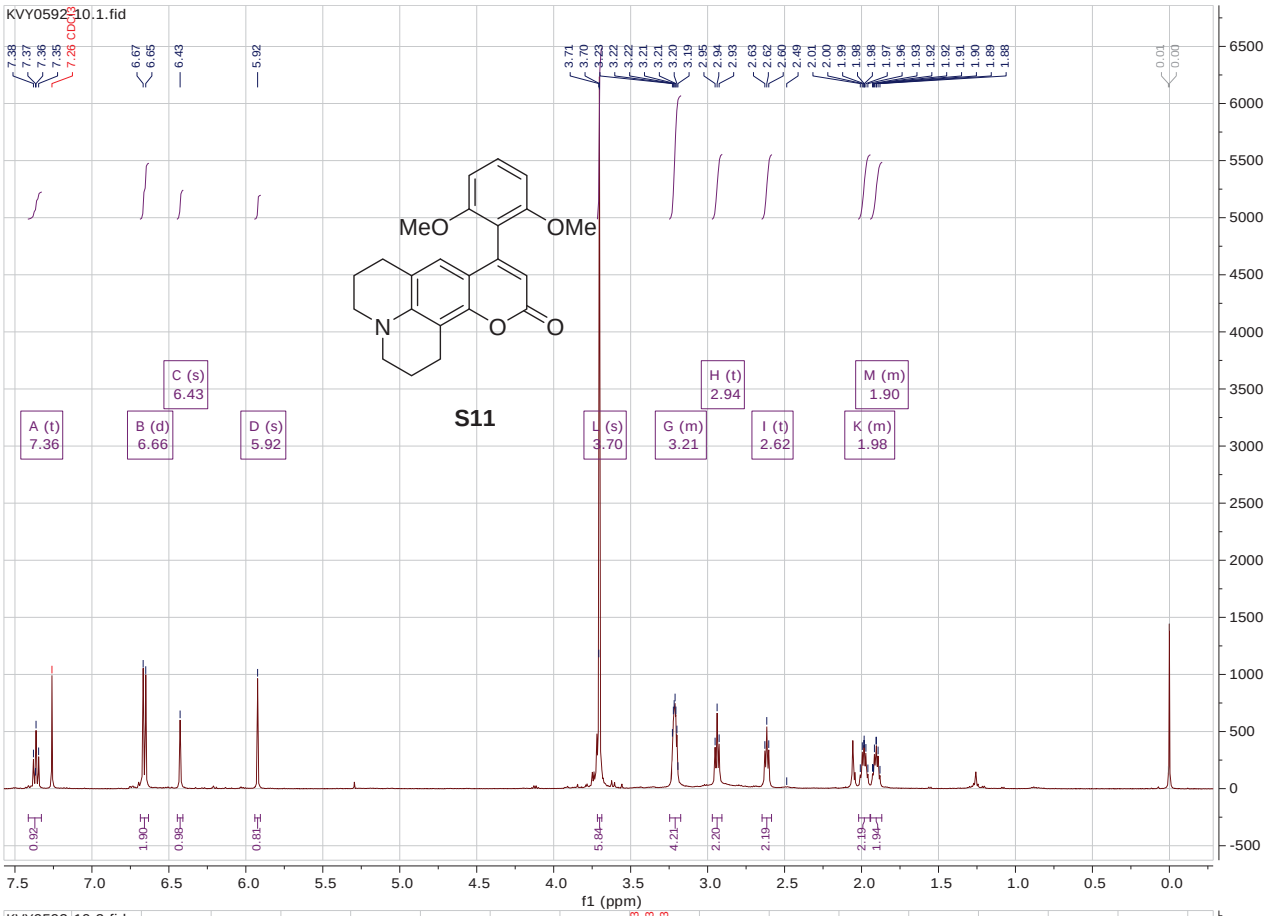
KVY0592-10.1.fid
MeO
OMe
N
O
O
S11
A (t) 7.36
B (d) 6.66
C (s) 6.43
D (s) 5.92
L (s) 3.70
G (m) 3.21
H (t) 2.94
I (t) 2.62
K (m) 1.98
M (m) 1.90
f1 (ppm)

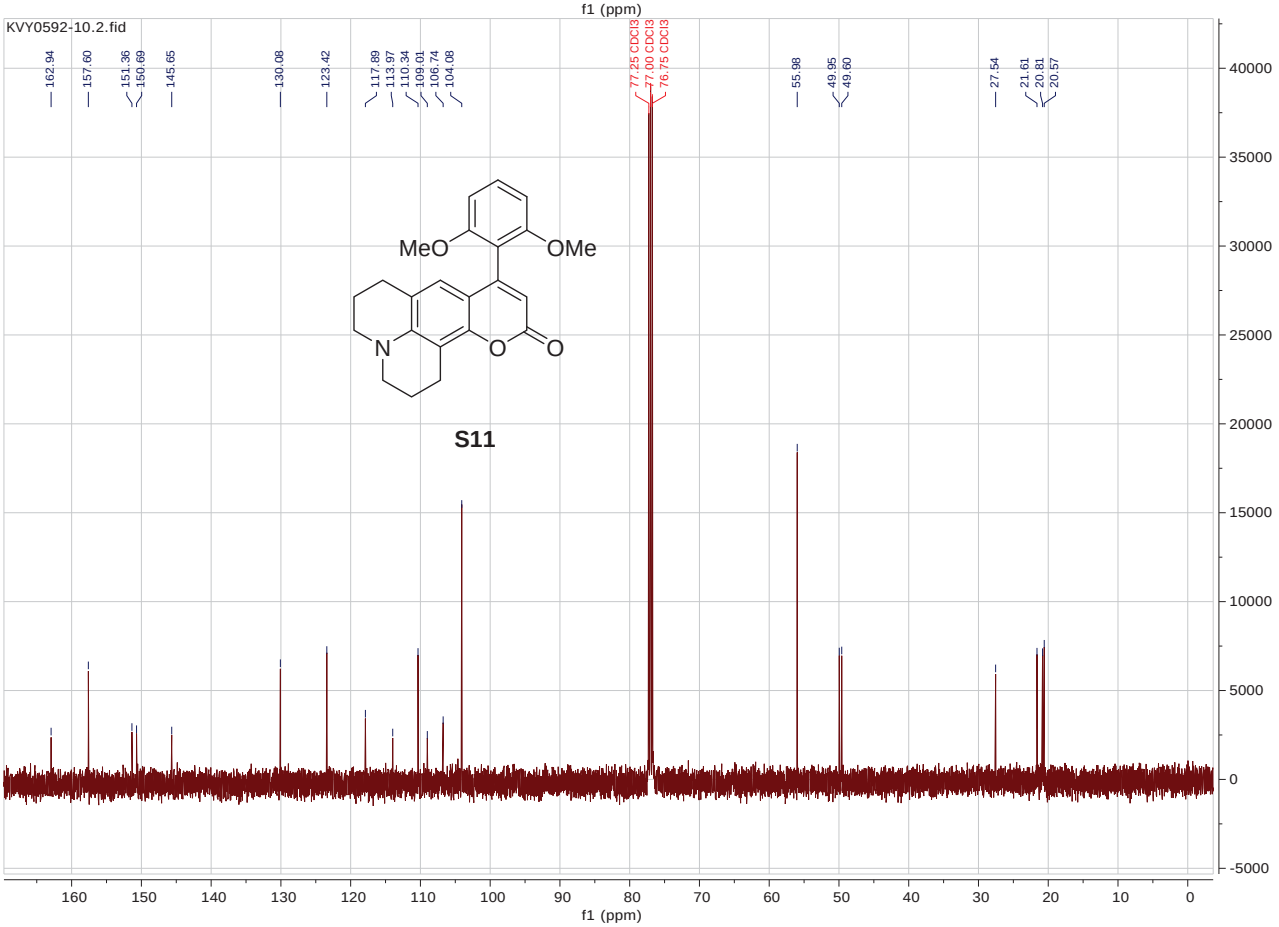
KVY0592-10.2.fid
MeO
OMe
N
O
O
S11
f1 (ppm)

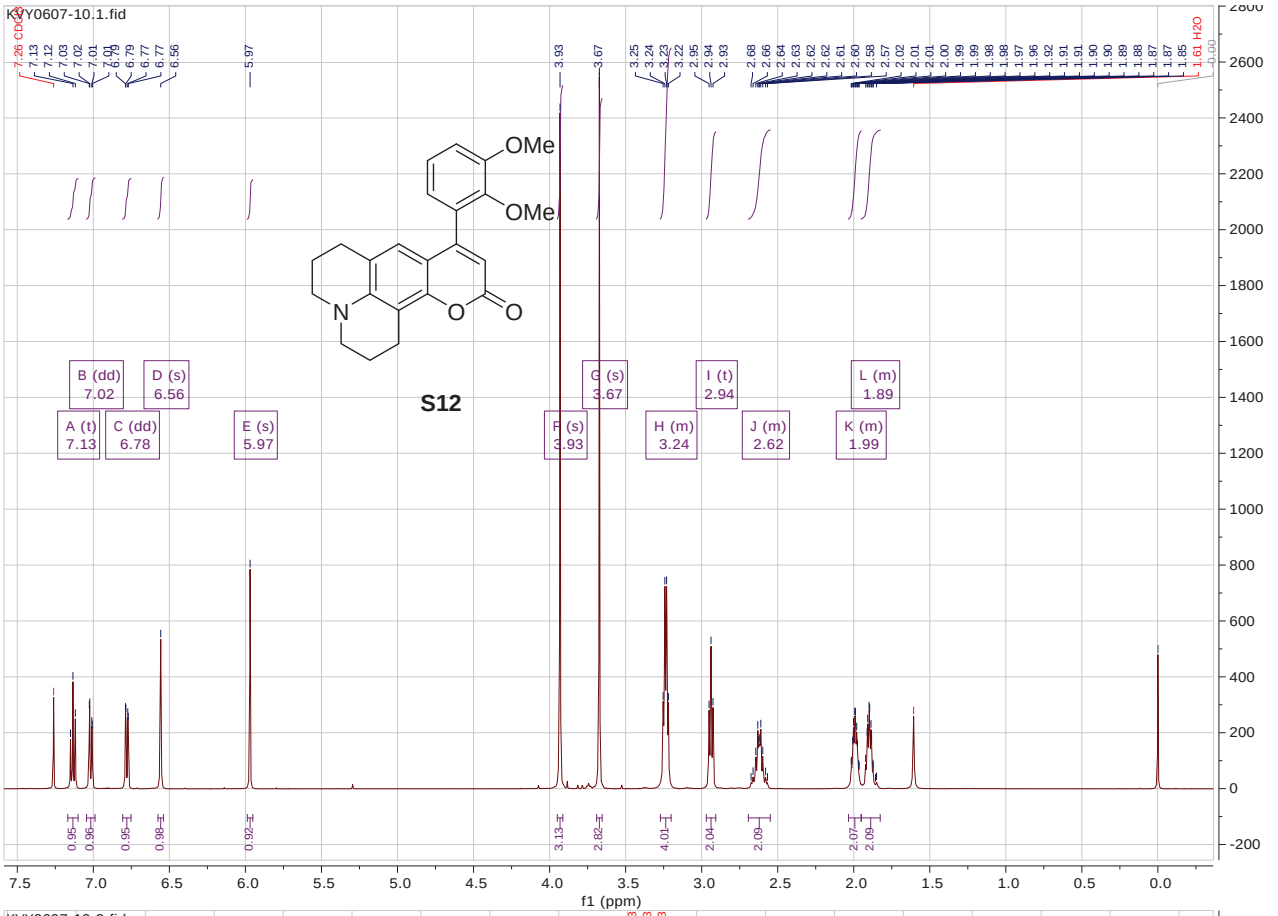
KVY0607-10.1.fid
OMe
OMe
N
O
O
S12
B (dd) 7.02
D (s) 6.56
A (t) 7.13
C (dd) 6.78
E (s) 5.97
G (s) 3.67
I (t) 2.94
L (m) 1.89
H (m) 3.24
J (m) 2.62
K (m) 1.99
f1 (ppm)

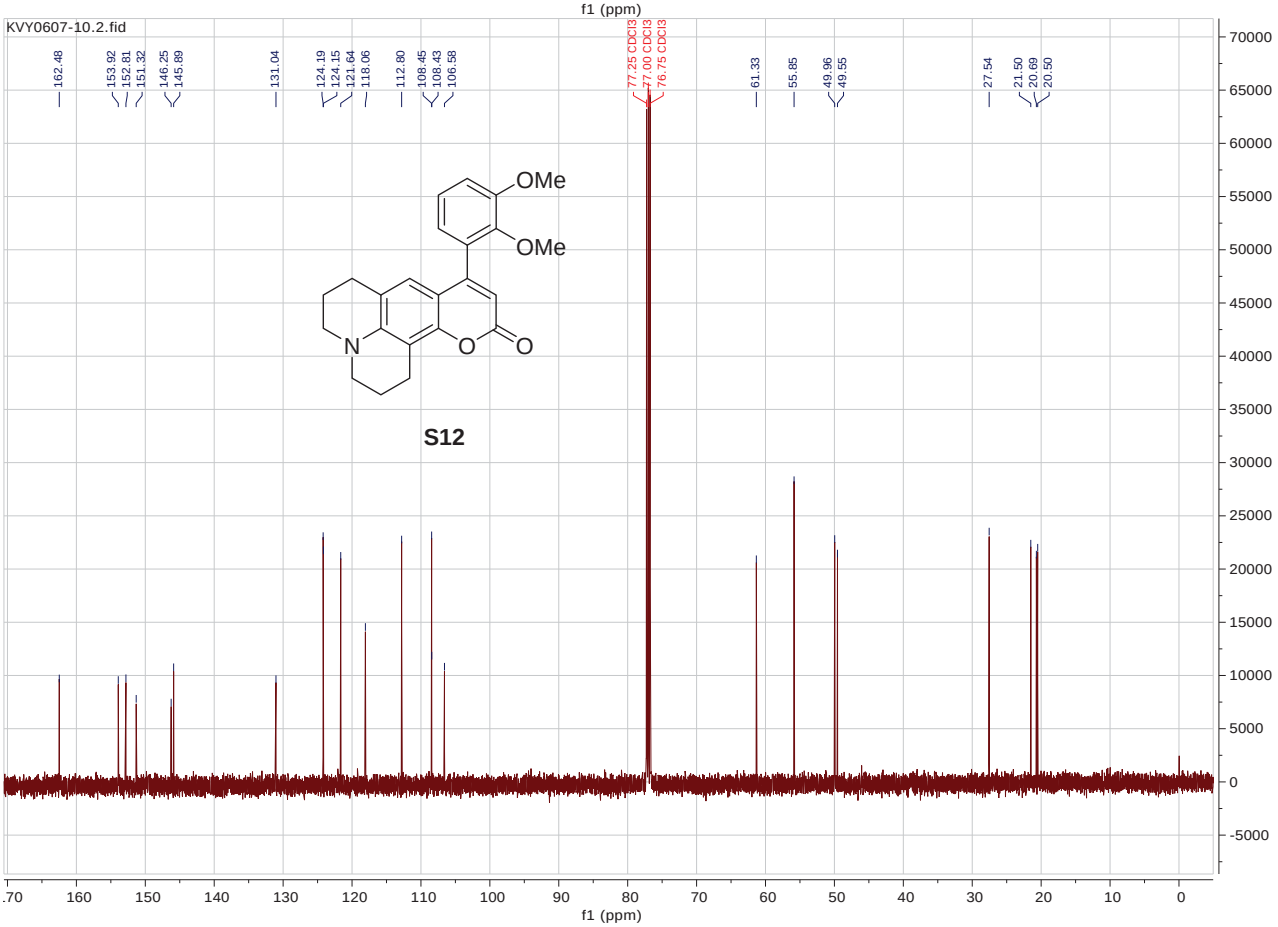
KVY0607-10.2.fid
OMe
OMe
N
O
O
S12
f1 (ppm)

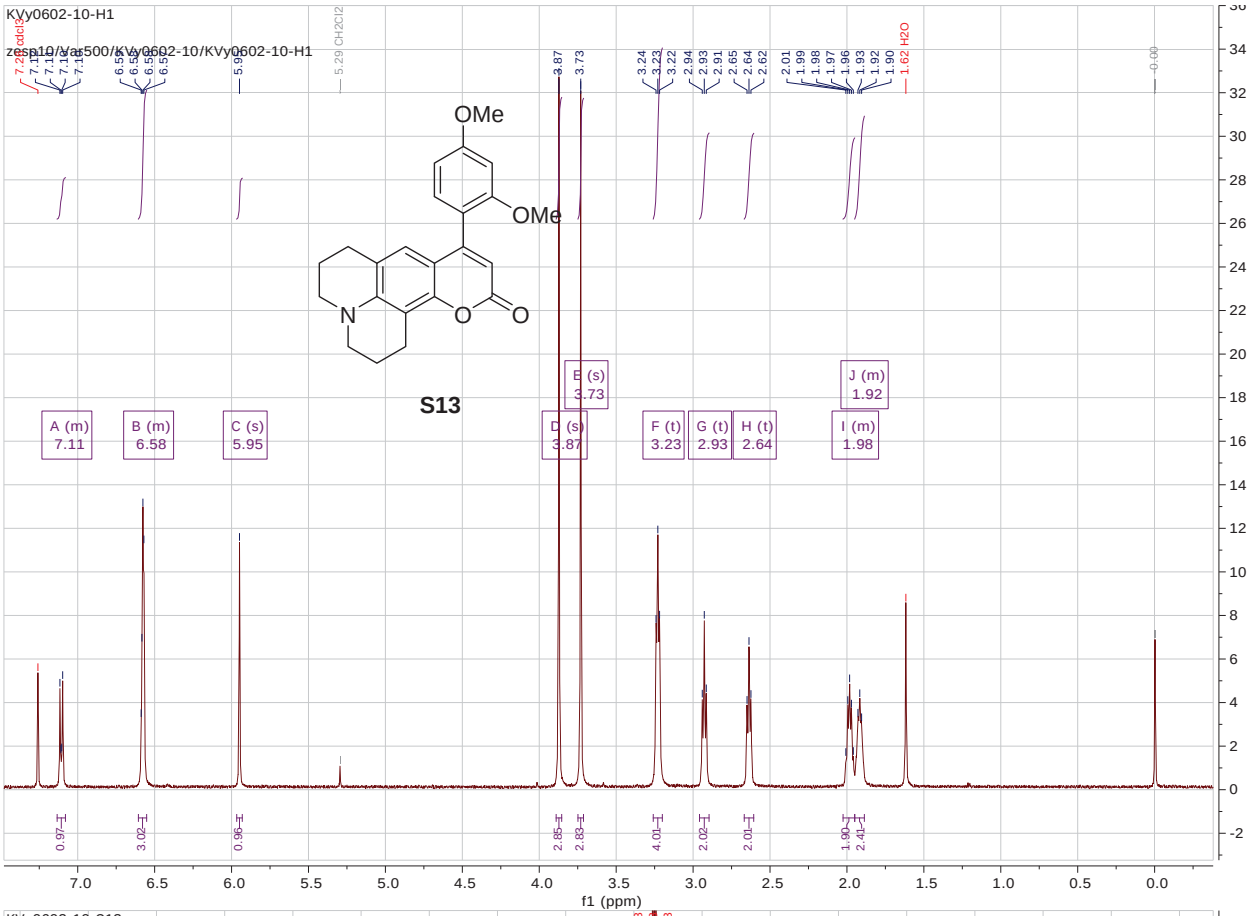
KVy0602-10-H1
zesp10/Var500/KVy0602-10/KVy0602-10-H1
OMe
OMe
N
O
O
S13
A (m) 7.11
B (m) 6.58
C (s) 5.95
D (s) 3.87
E (s) 3.73
F (t) 3.23
G (t) 2.93
H (t) 2.64
I (m) 1.98
J (m) 1.92
f1 (ppm)

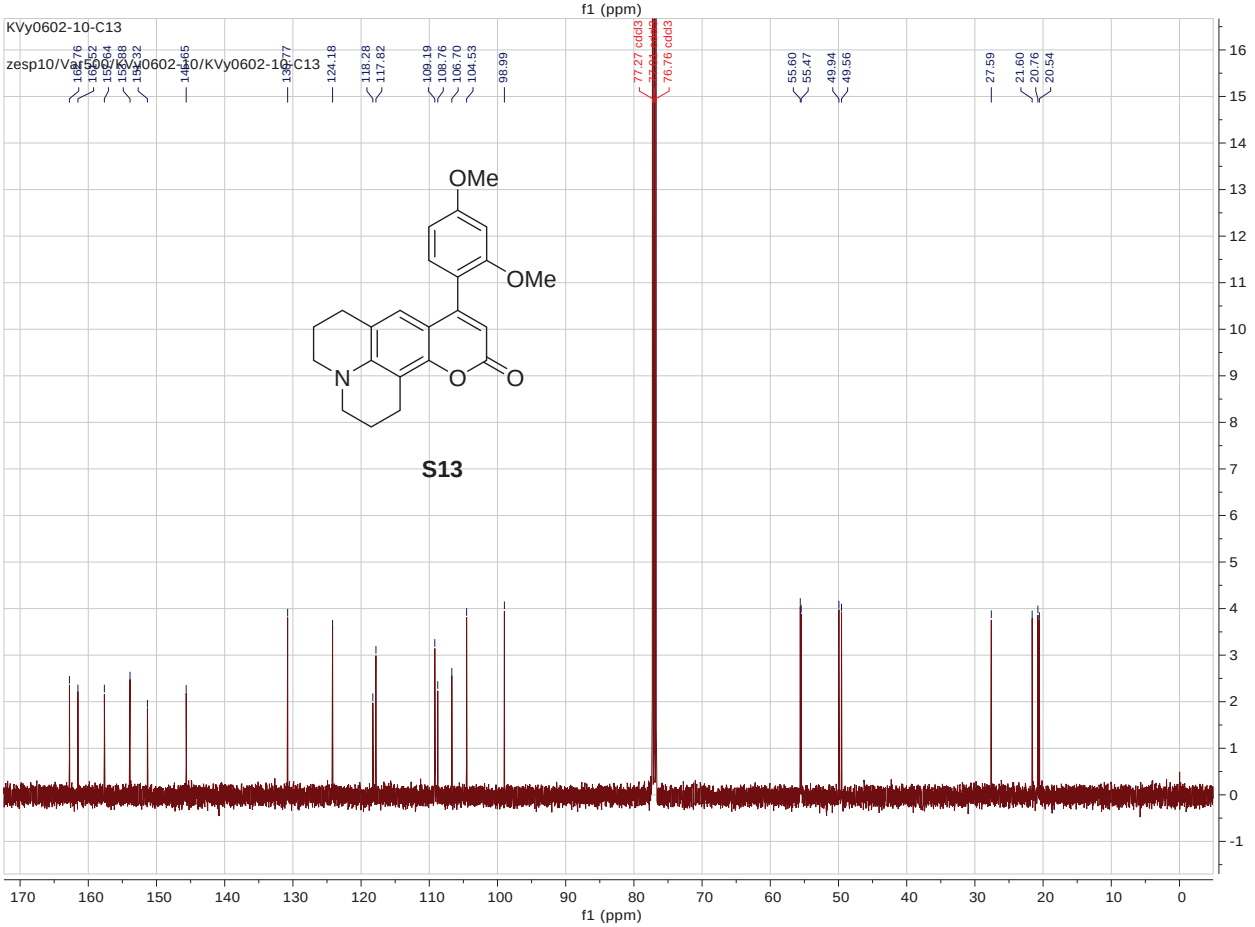
KVy0602-10-C13
zesp10/Var500/KVy0602-10/KVy0602-10-C13
OMe
OMe
N
O
O
S13
f1 (ppm)

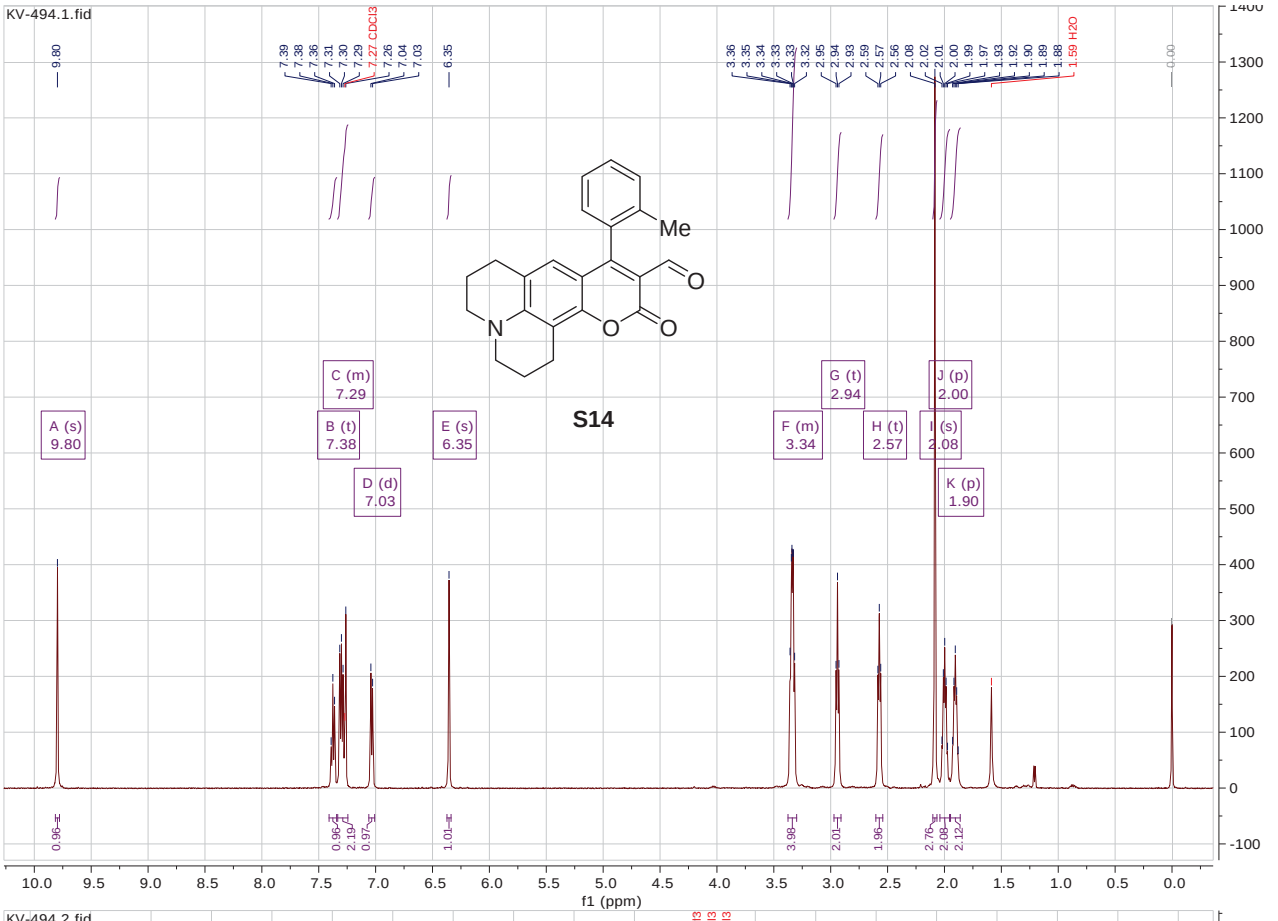
KV-494.1.fid
Me
O
N
O
O
S14
A (s) 9.80
B (t) 7.38
C (m) 7.29
D (d) 7.03
E (s) 6.35
F (m) 3.34
G (t) 2.94
H (t) 2.57
I (s) 2.08
J (p) 2.00
K (p) 1.90
f1 (ppm)

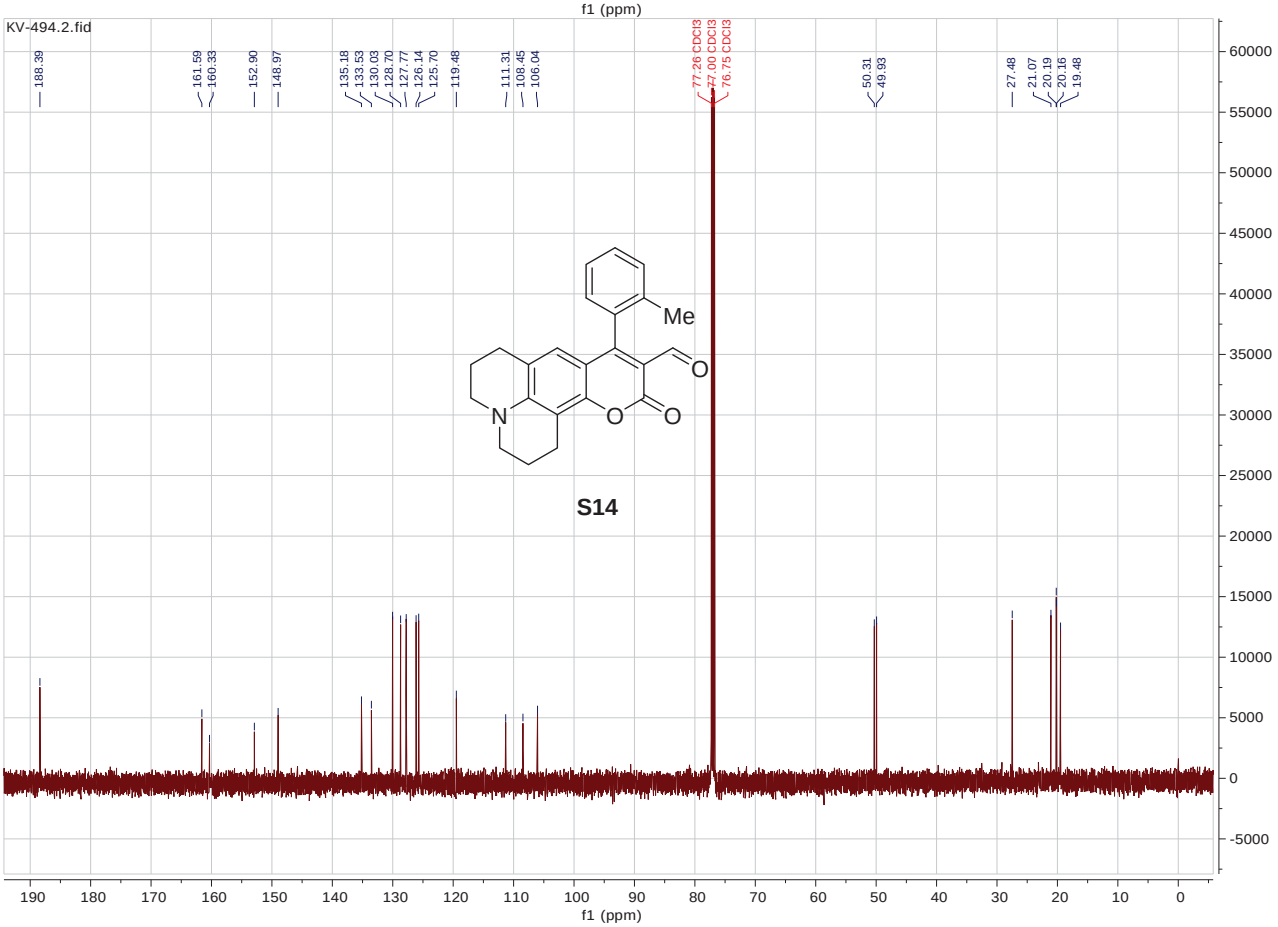
KV-494.2.fid
Me
O
N
O
O
S14
f1 (ppm)

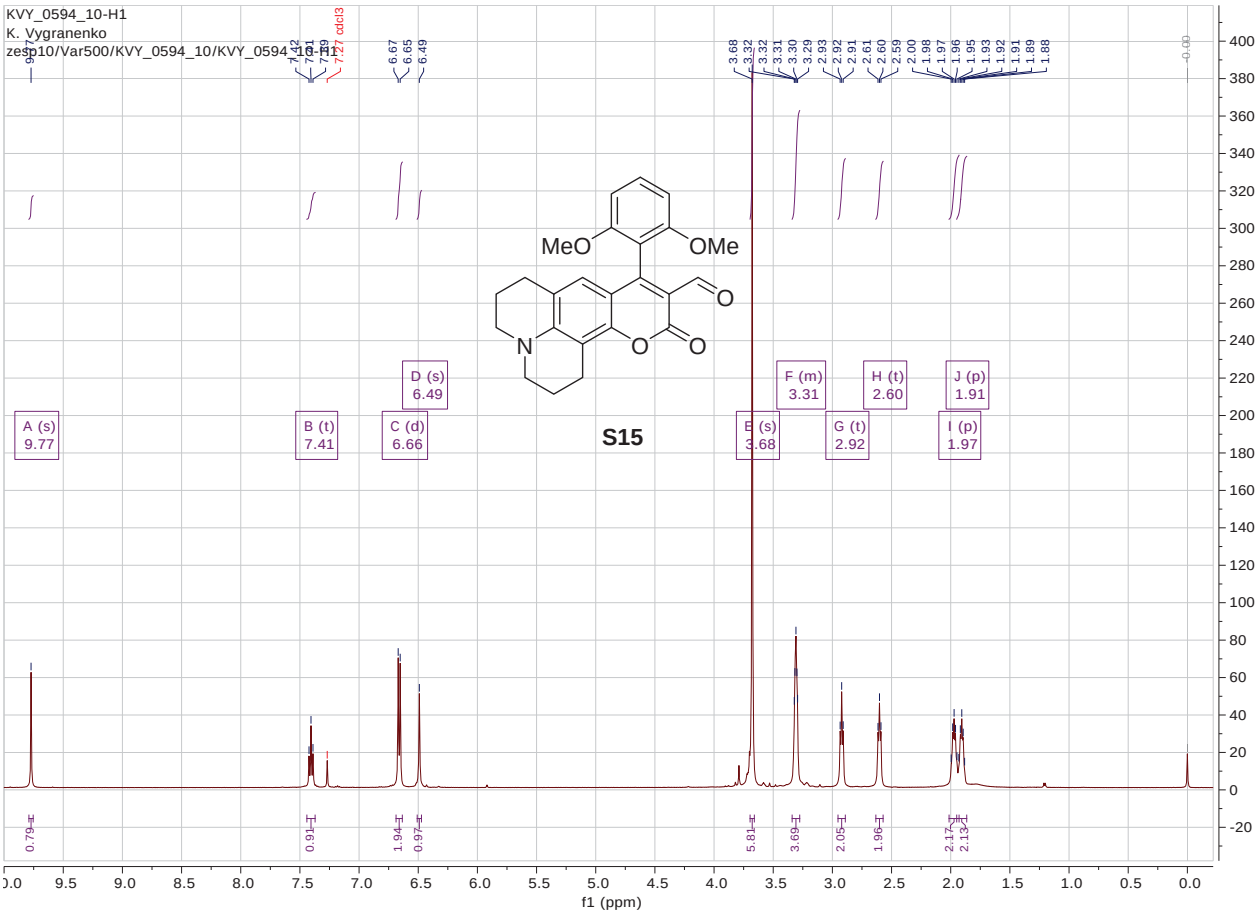
KVY_0594_10-H1
K. Vygranenko
zesp10/Var500/KVY_0594_10/KVY_0594_10-H1
MeO
OMe
O
N
O
O
S15
A (s) 9.77
B (t) 7.41
C (d) 6.66
D (s) 6.49
E (s) 3.68
F (m) 3.31
G (t) 2.92
H (t) 2.60
I (p) 1.97
J (p) 1.91
f1 (ppm)

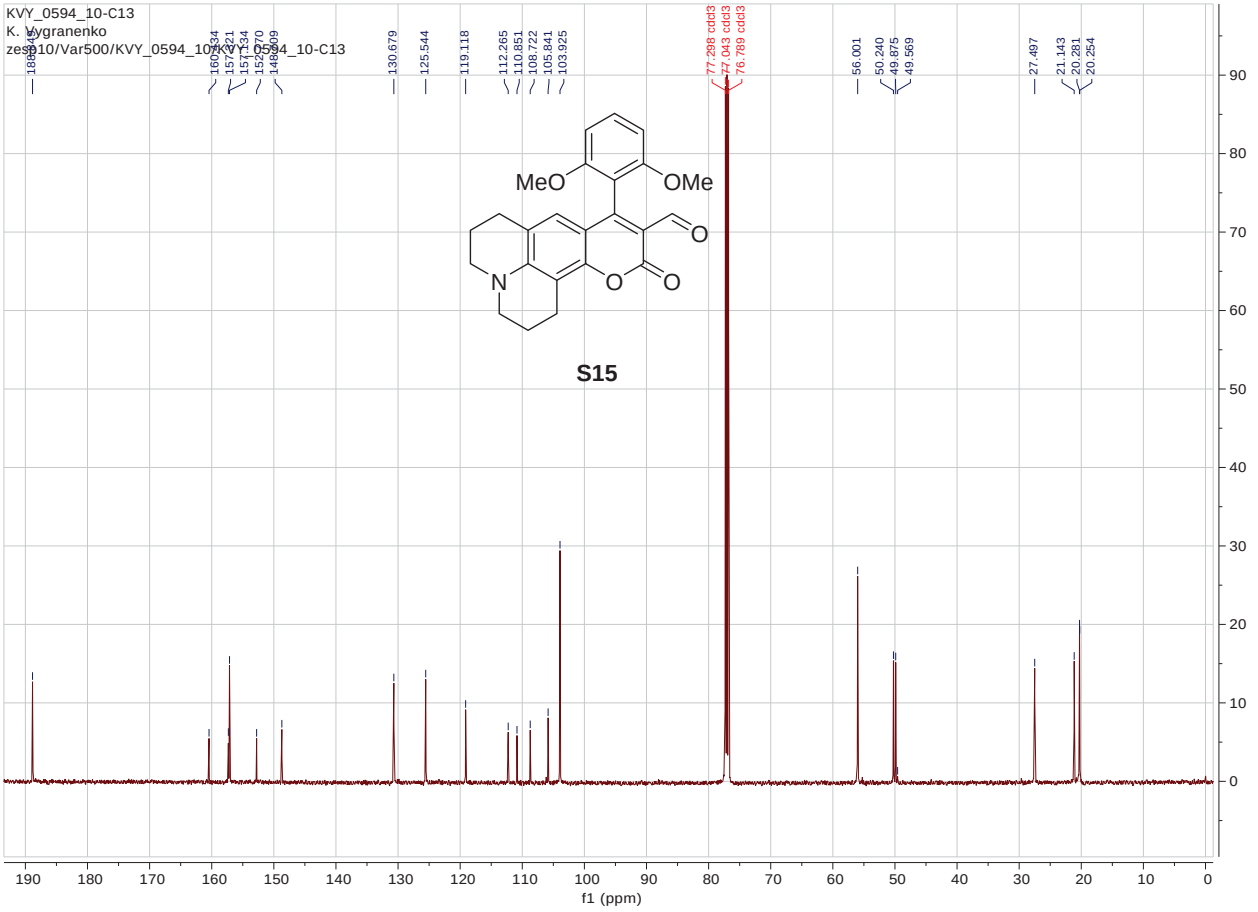
KVY_0594_10-C13
K. Vygranenko
zesp10/Var500/KVY_0594_10/KVY_0594_10-C13
MeO
OMe
O
N
O
O
S15
f1 (ppm)

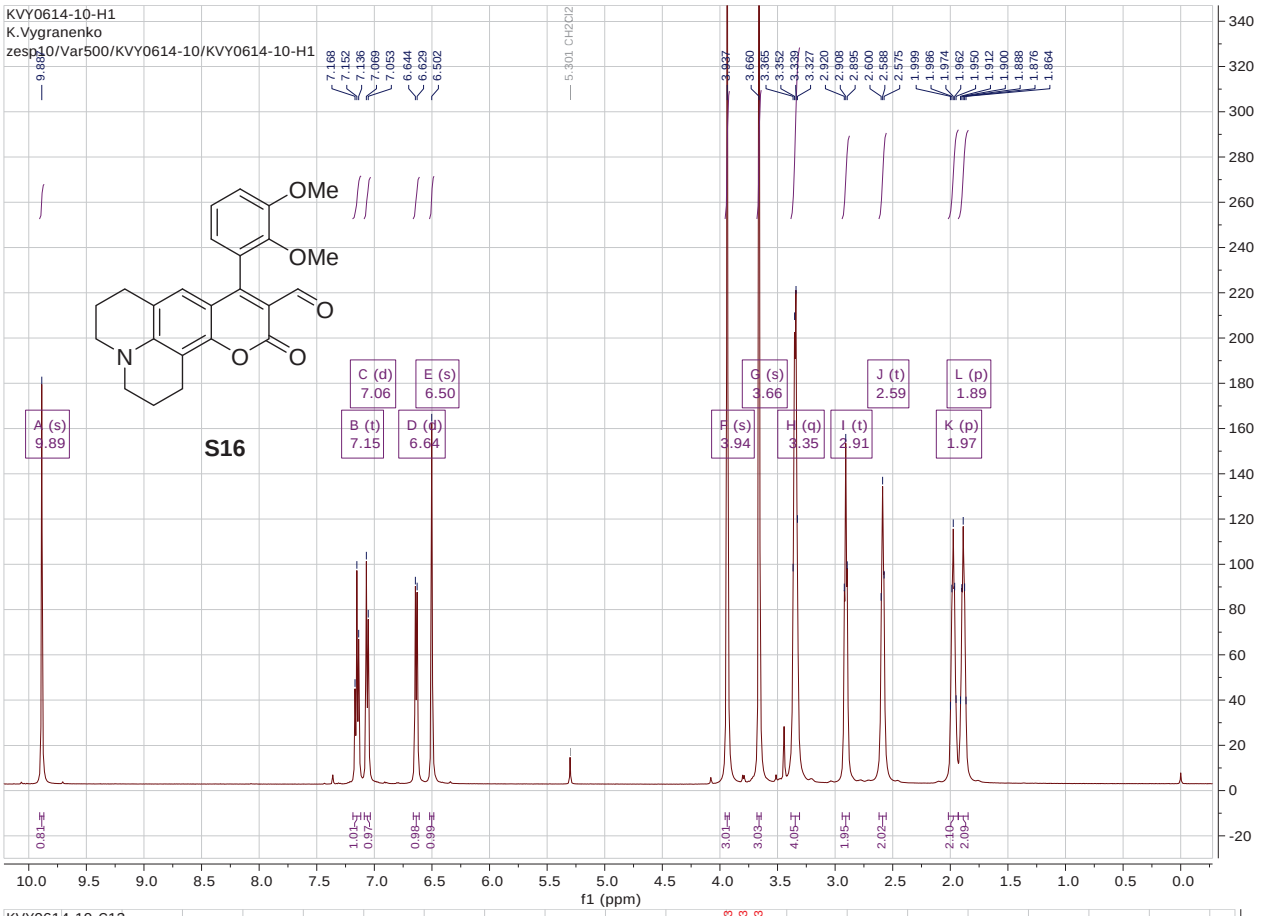
KVY0614-10-H1
K.Vygranenko
zesp10/Var500/KVY0614-10/KVY0614-10-H1
OMe
OMe
O
N
O
O
S16
A (s) 9.89
B (t) 7.15
C (d) 7.06
D (d) 6.64
E (s) 6.50
F (s) 3.94
G (s) 3.66
H (q) 3.35
I (t) 2.91
J (t) 2.59
K (p) 1.97
L (p) 1.89
f1 (ppm)

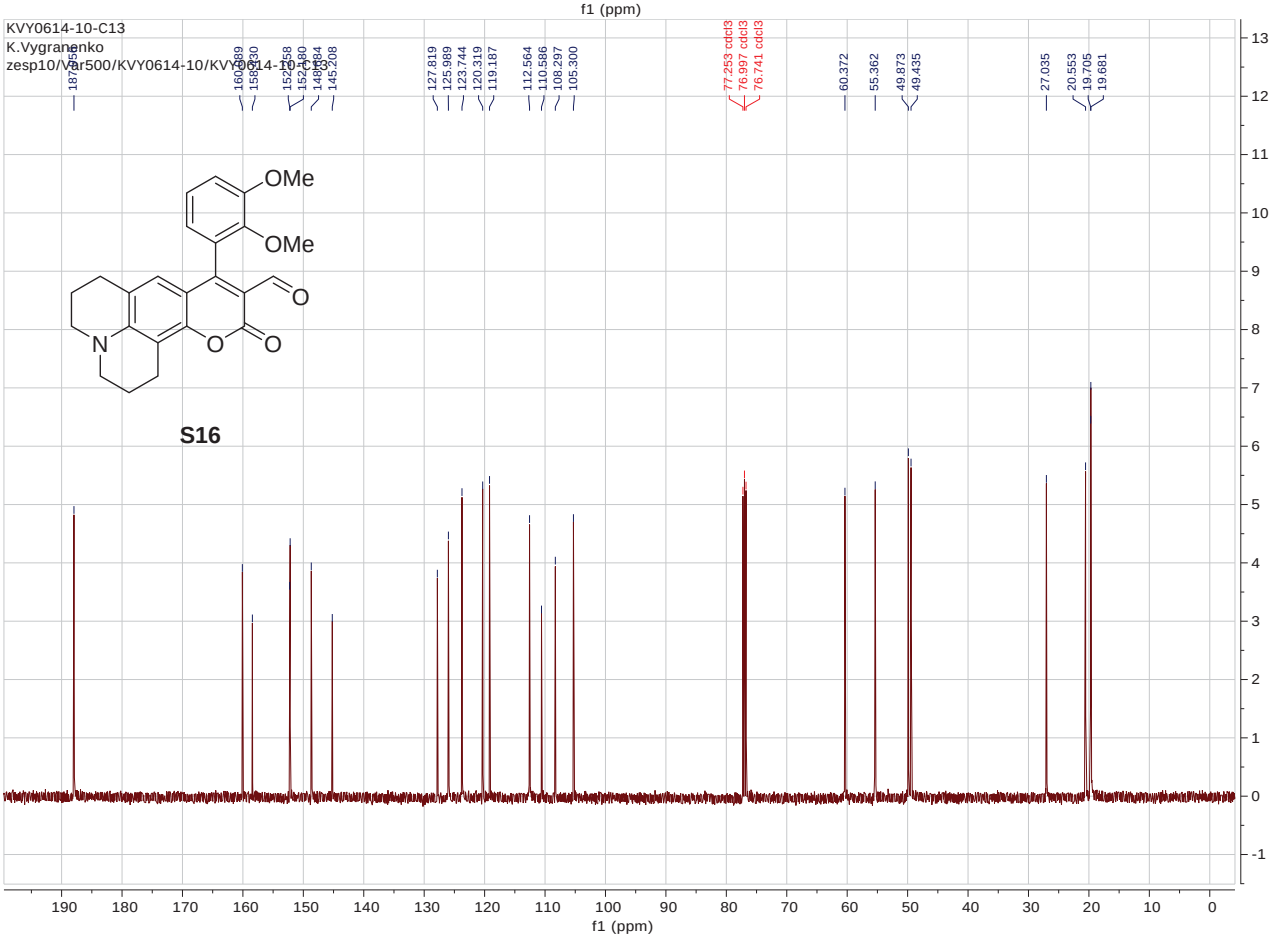
KVY0614-10-C13
K.Vygranenko
zesp10/Var500/KVY0614-10/KVY0614-10-C13
OMe
OMe
O
N
O
O
S16
f1 (ppm)

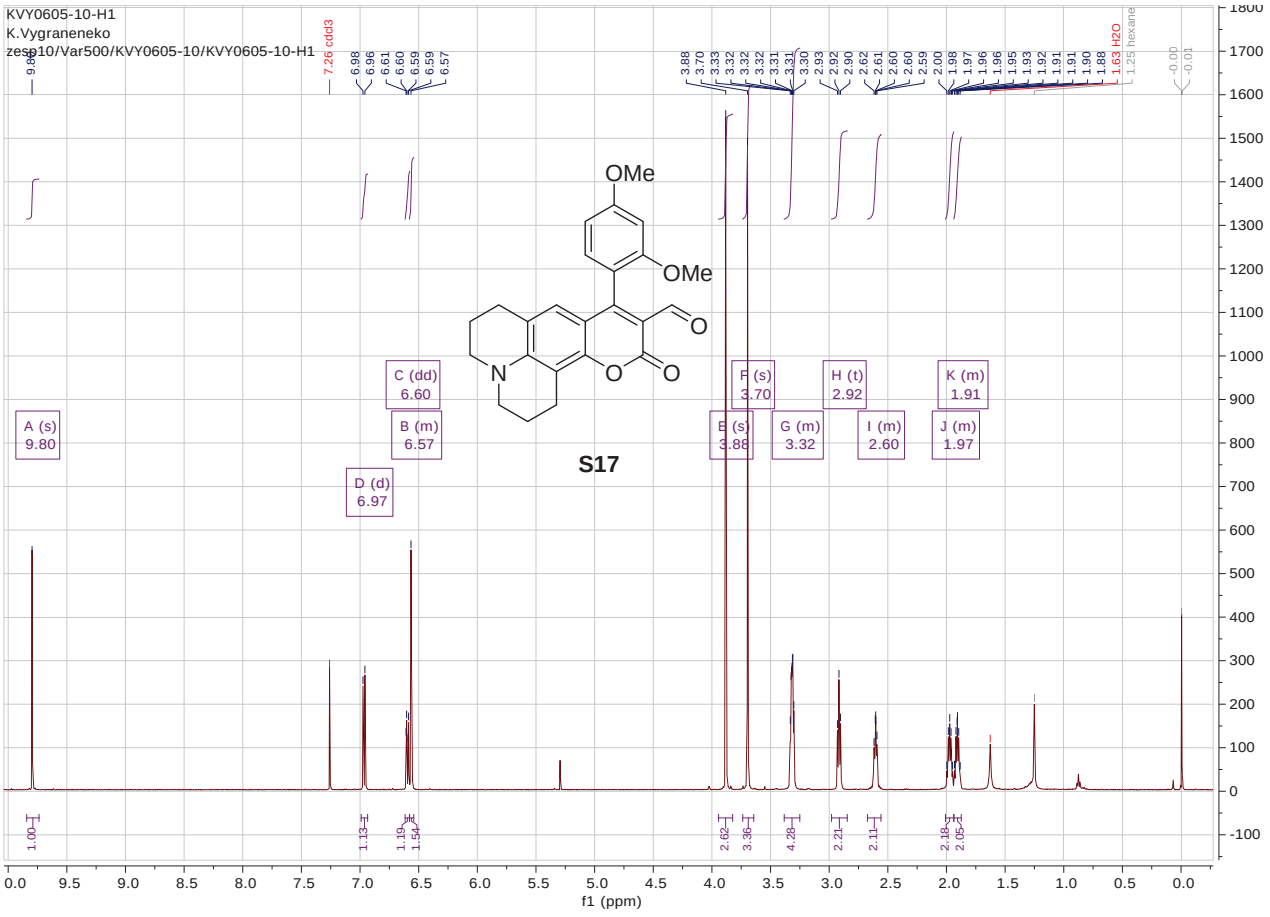
KVY0605-10-H1
K.Vygraneneko
zesp10/Var500/KVY0605-10/KVY0605-10-H1
OMe
OMe
O
N
O
O
A (s) 9.80
B (m) 6.57
C (dd) 6.60
D (d) 6.97
E (s) 3.88
F (s) 3.70
G (m) 3.32
H (t) 2.92
I (m) 2.60
J (m) 1.97
K (m) 1.91
S17
f1 (ppm)

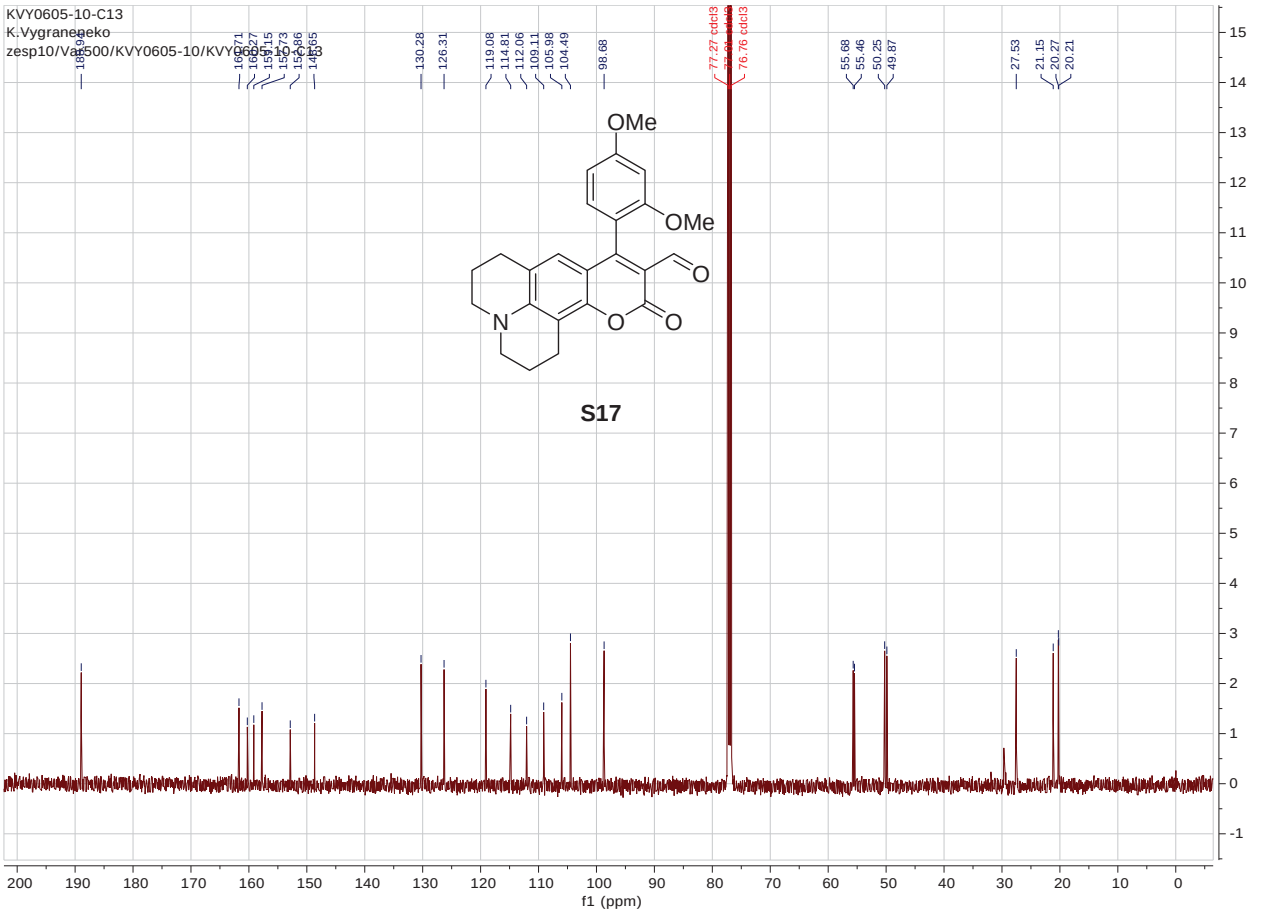
KVY0605-10-C13
K.Vygraneneko
zesp10/Var500/KVY0605-10/KVY0605-10-C13
OMe
OMe
O
N
O
O
S17
f1 (ppm)

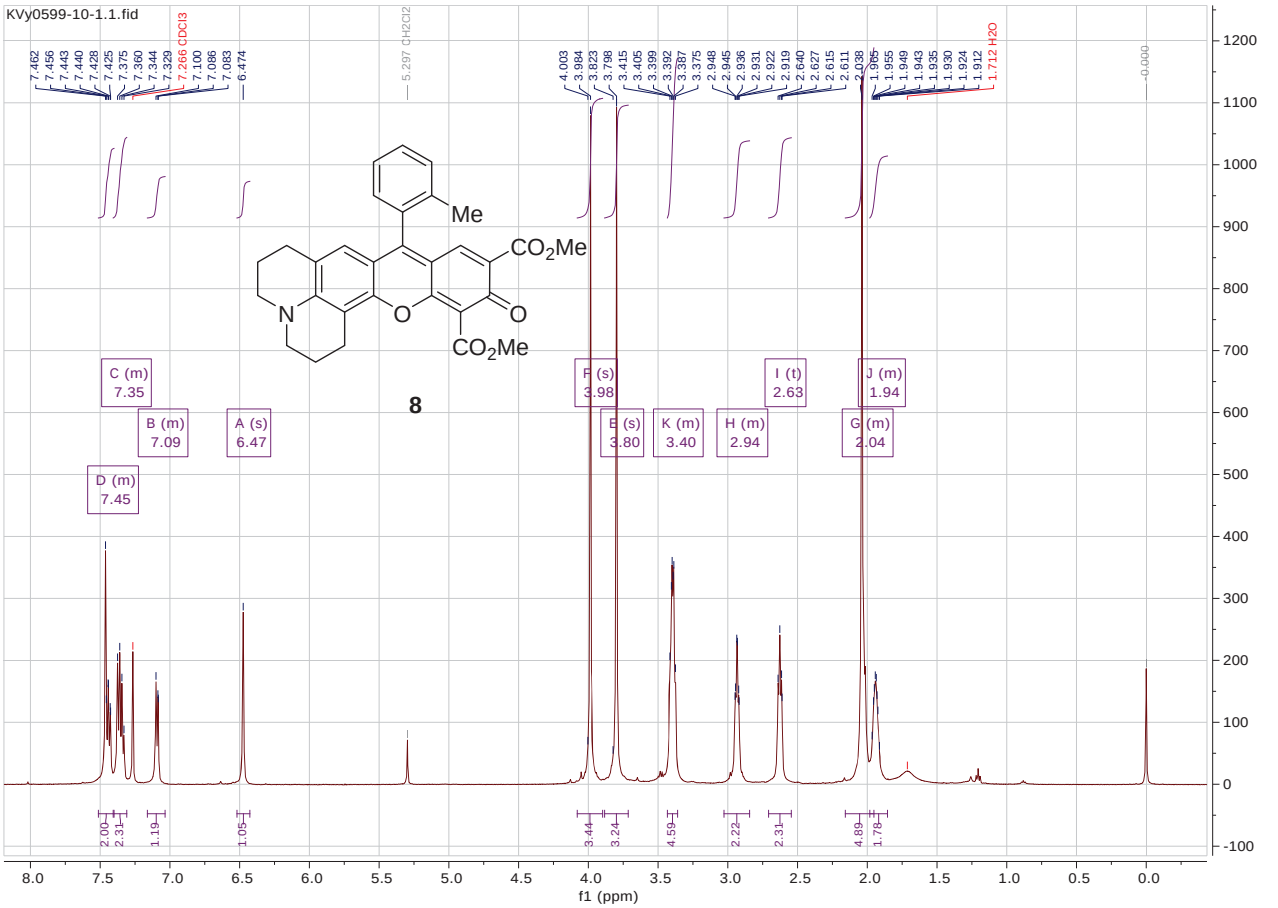
KVy0599-10-1.1.fid
Me
CO2Me
CO2Me
N
O
O
8
C (m) 7.35
B (m) 7.09
A (s) 6.47
D (m) 7.45
F (s) 3.98
E (s) 3.80
K (m) 3.40
H (m) 2.94
I (t) 2.63
J (m) 1.94
G (m) 2.04
f1 (ppm)

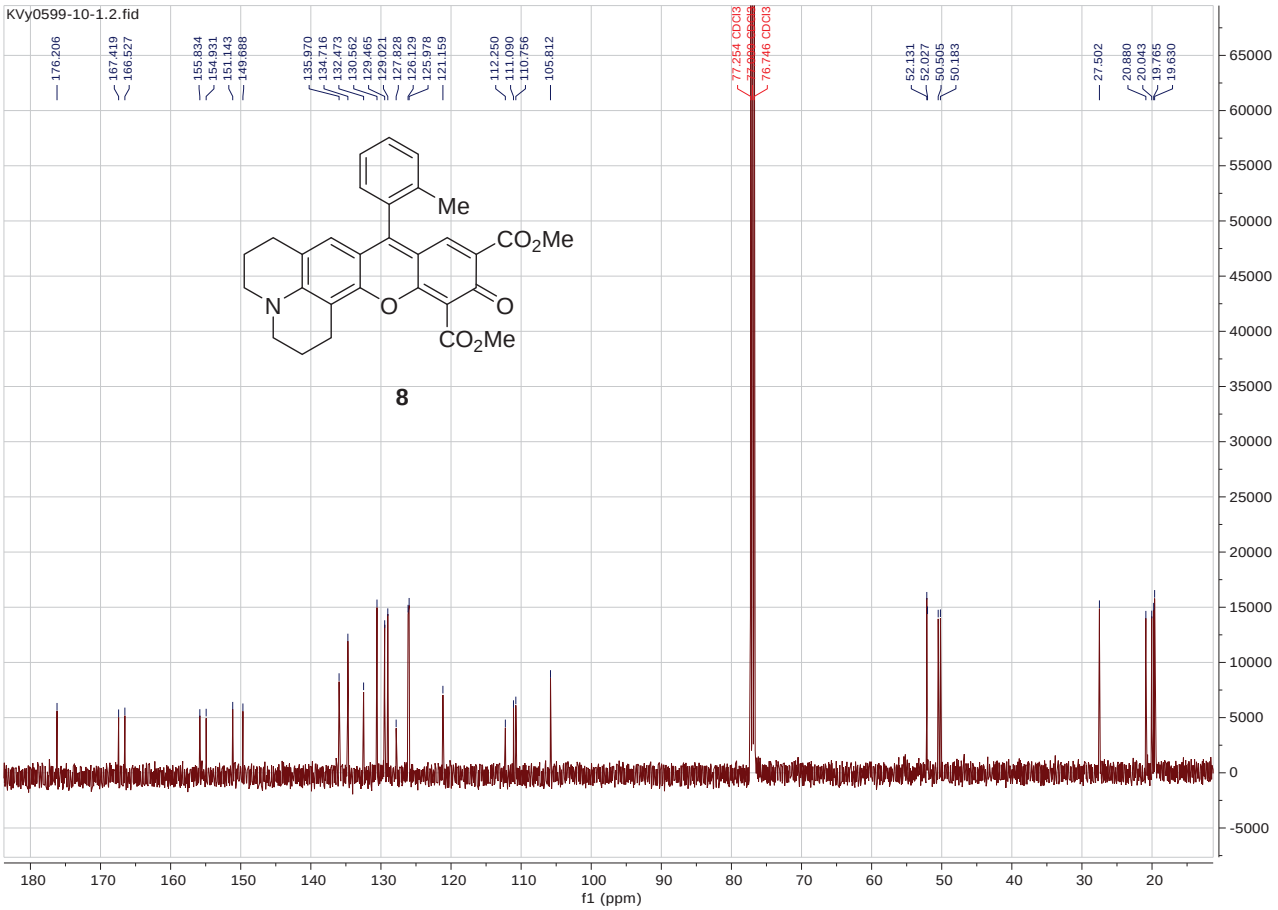
KVy0599-10-1.2.fid
Me
CO2Me
CO2Me
N
O
O
8
f1 (ppm)

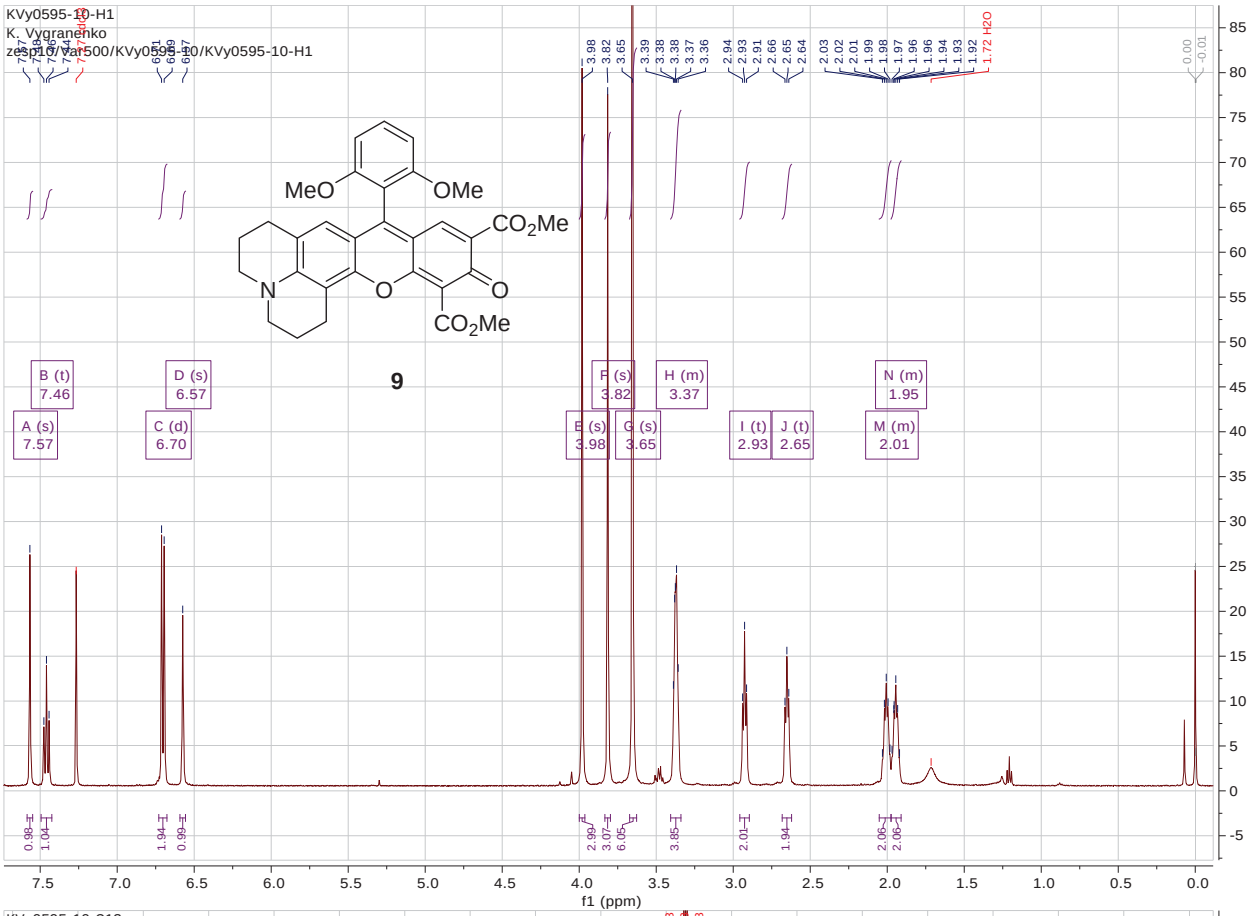
KVy0595-10-H1
K. Vygranenko
zesp10/var500/KVy0595-10/KVy0595-10-H1
MeO
OMe
CO2Me
N
O
O
CO2Me
9
B (t) 7.46
D (s) 6.57
F (s) 3.82
H (m) 3.37
N (m) 1.95
A (s) 7.57
C (d) 6.70
E (s) 3.98
G (s) 3.65
I (t) 2.93
J (t) 2.65
M (m) 2.01
f1 (ppm)

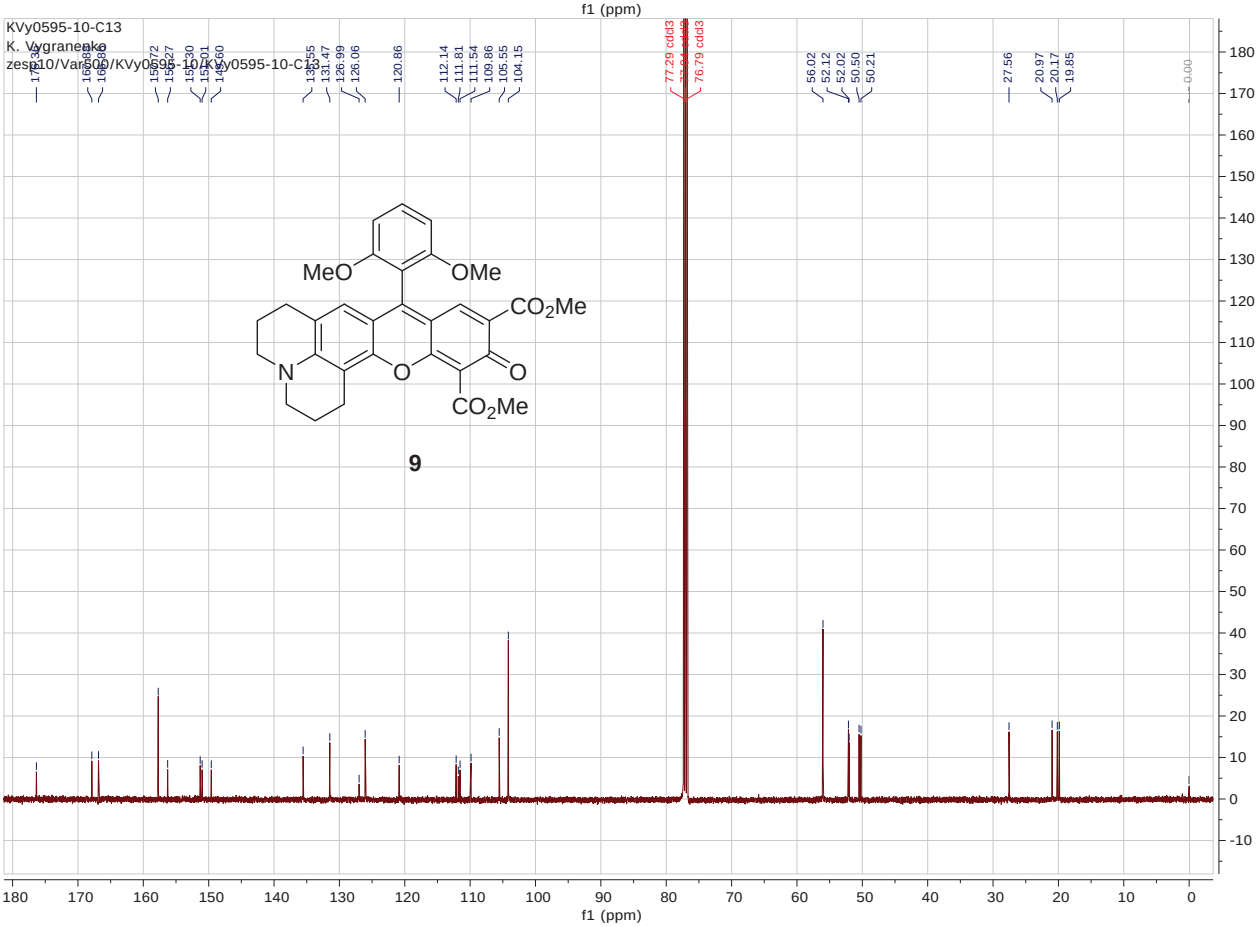
KVy0595-10-C13
K. Vygranenko
zesp10/var500/KVy0595-10/KVy0595-10-C13
MeO
OMe
CO2Me
N
O
O
CO2Me
9
f1 (ppm)

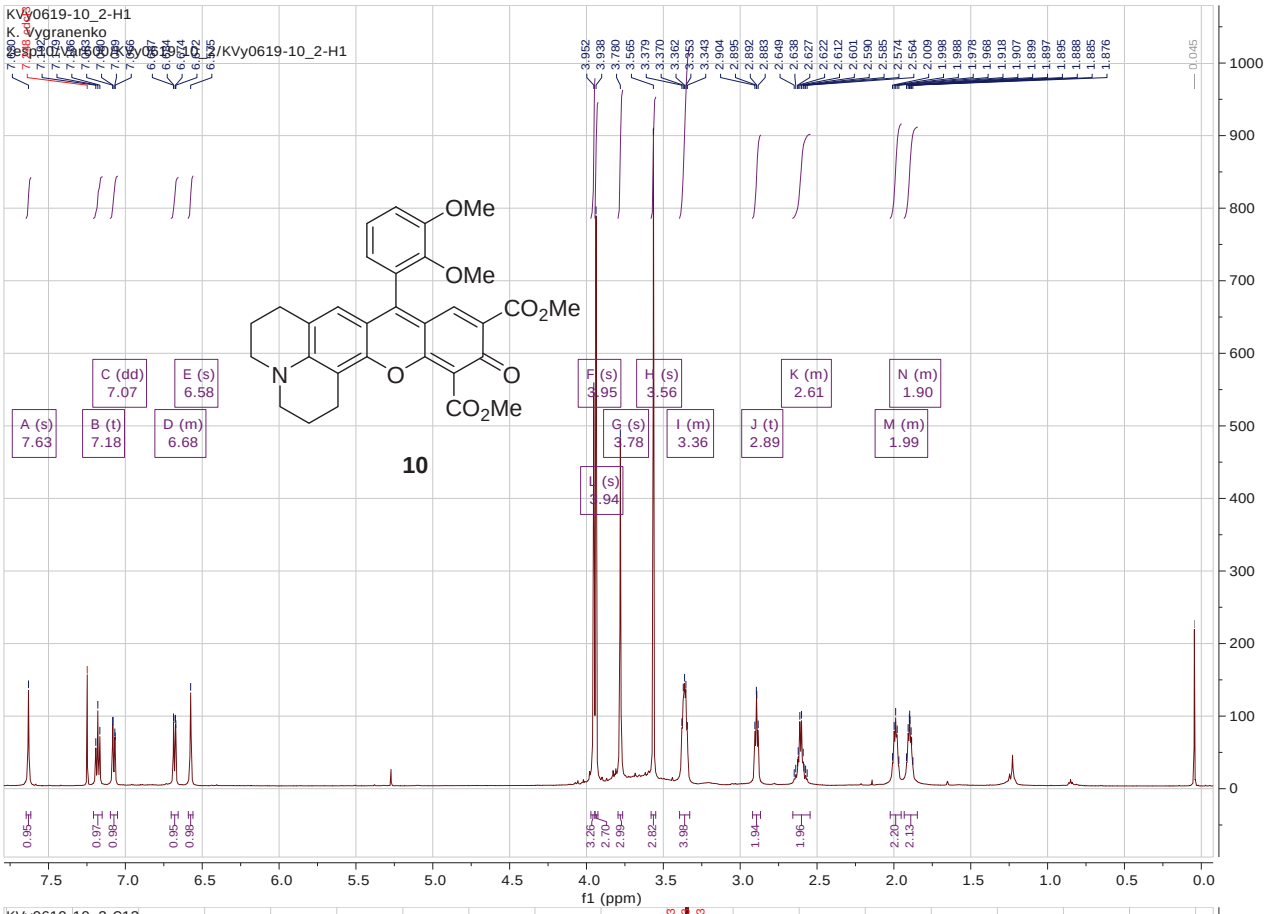
KVy0619-10_2-H1
K. Vygranenko
OMe
OMe
CO2Me
CO2Me
10
A (s) 7.63
B (t) 7.18
C (dd) 7.07
D (m) 6.68
E (s) 6.58
F (s) 3.95
G (s) 3.78
H (s) 3.56
I (m) 3.36
J (t) 2.89
K (m) 2.61
L (s) 2.94
M (m) 1.99
N (m) 1.90
f1 (ppm)

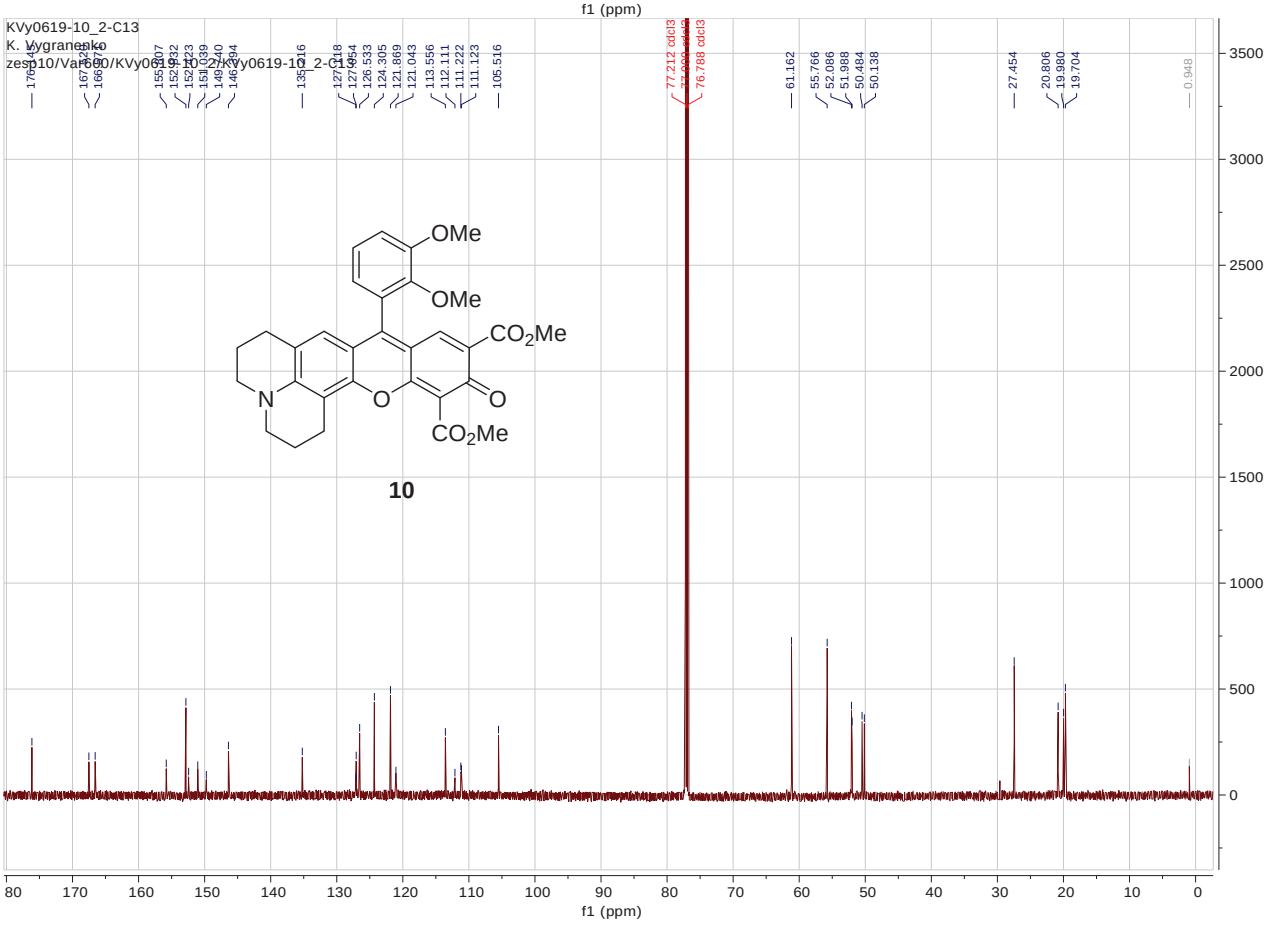
KVy0619-10_2-C13
K. Vygranenko
OMe
OMe
CO2Me
CO2Me
10
f1 (ppm)

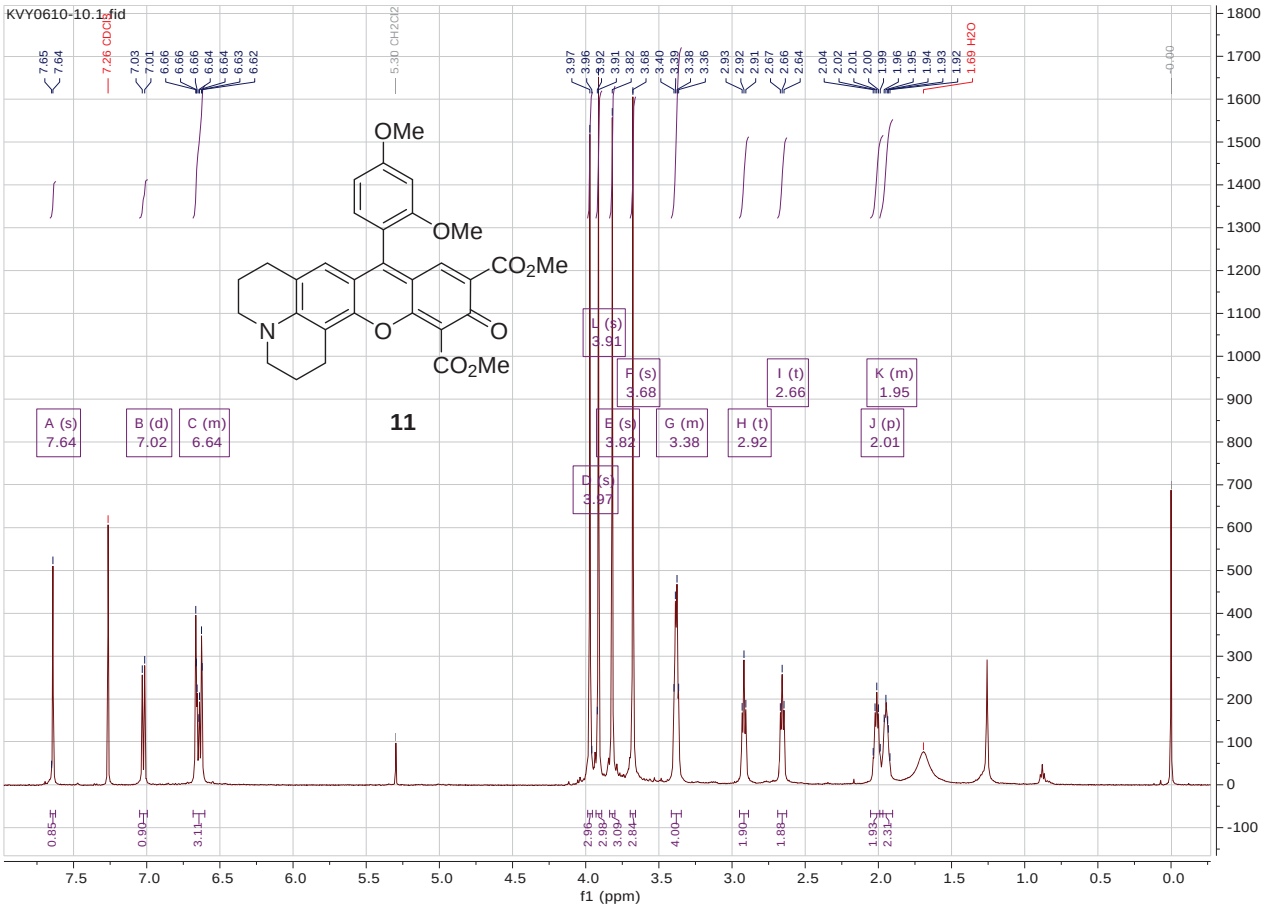
KVY0610-10.1.fid
OMe
OMe
CO2Me
CO2Me
N
O
O
11
A (s) 7.64
B (d) 7.02
C (m) 6.64
D (s) 3.97
E (s) 3.82
F (s) 3.68
G (m) 3.38
H (t) 2.92
I (t) 2.66
J (p) 2.01
K (m) 1.95
L (s) 3.91
f1 (ppm)

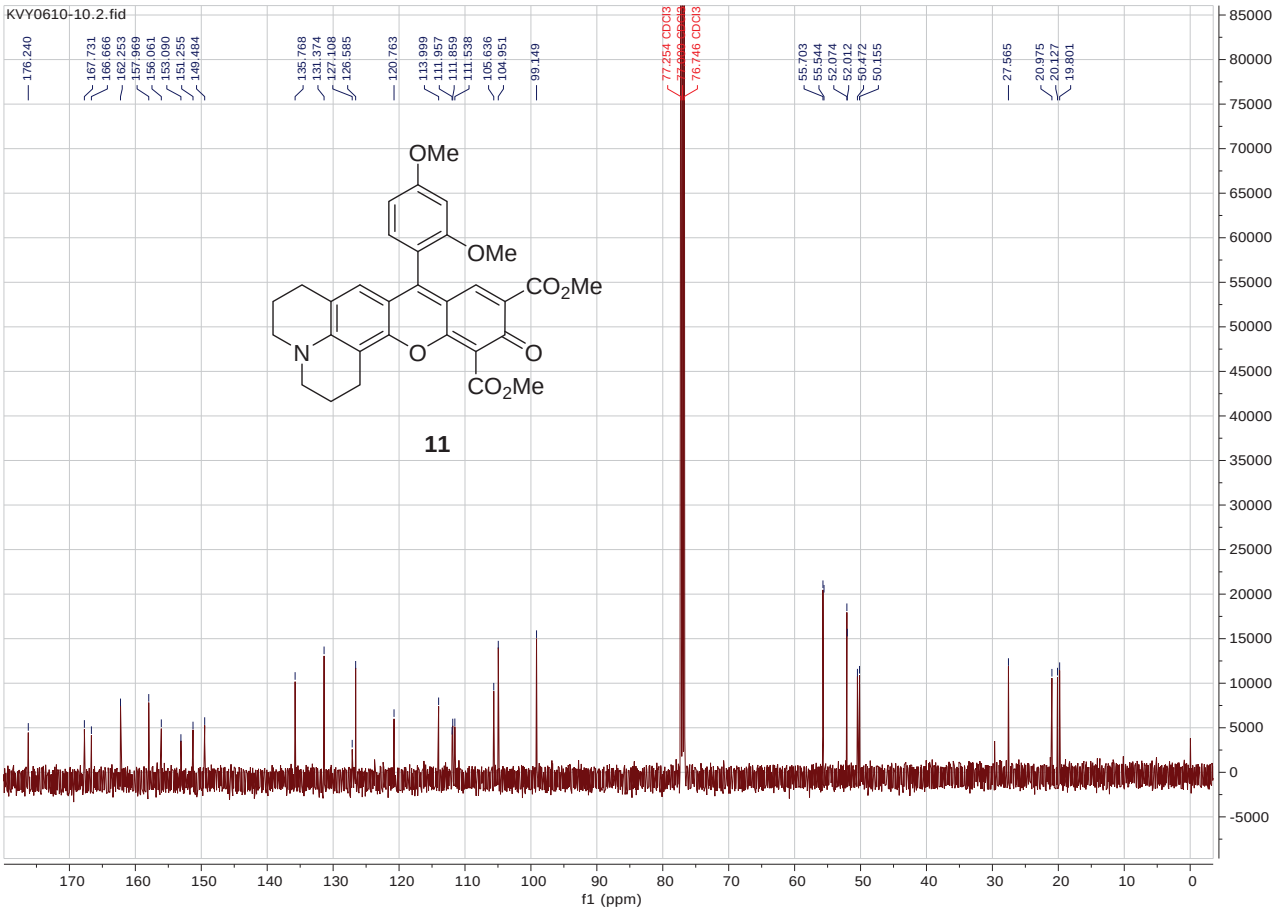
KVY0610-10.2.fid
OMe
OMe
CO2Me
CO2Me
N
O
O
11
f1 (ppm)

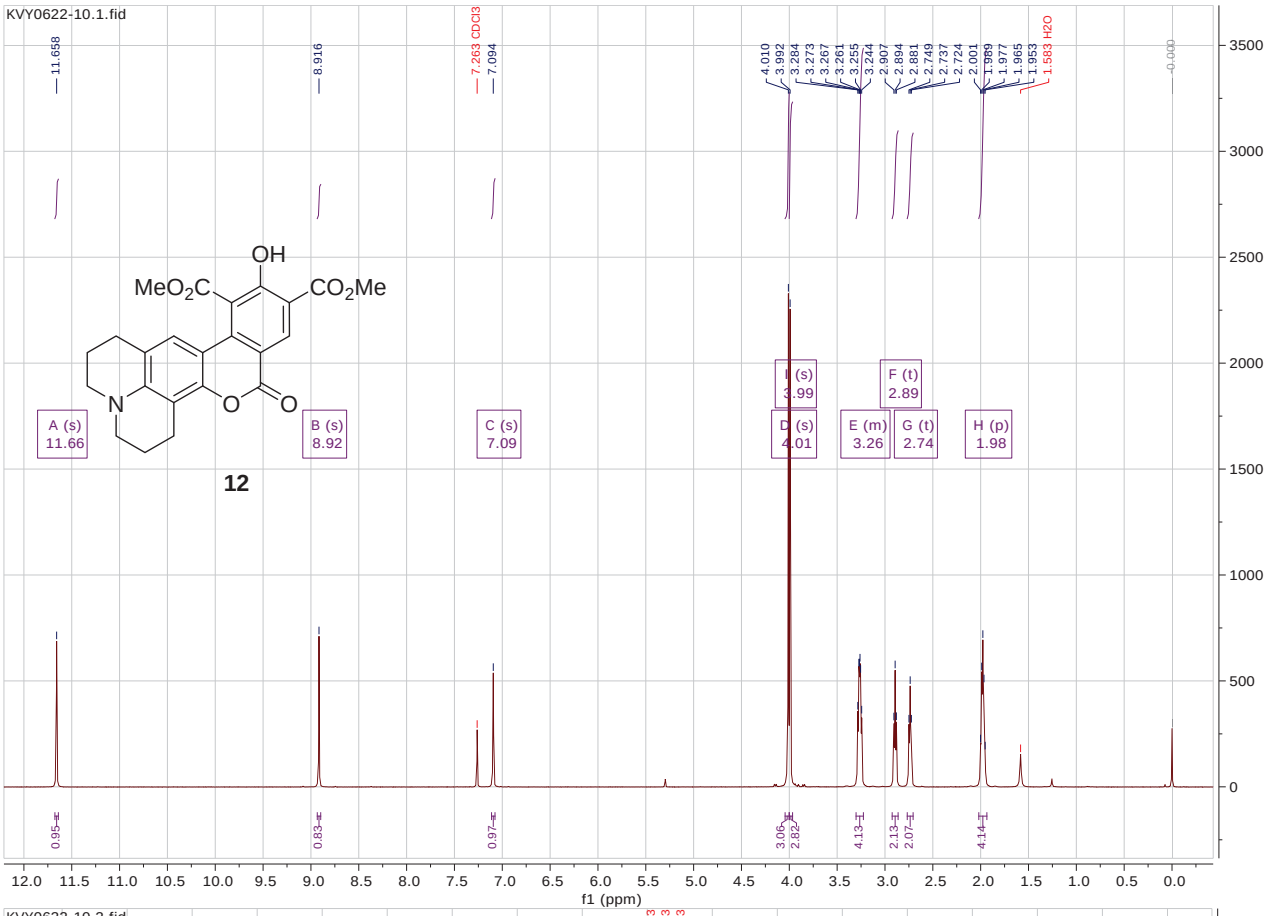
KVY0622-10.1.fid
OH
MeO2C
CO2Me
N
O
O
12
A (s) 11.66
B (s) 8.92
C (s) 7.09
D (s) 4.01
E (m) 3.26
F (t) 2.89
G (t) 2.74
H (p) 1.98
f1 (ppm)

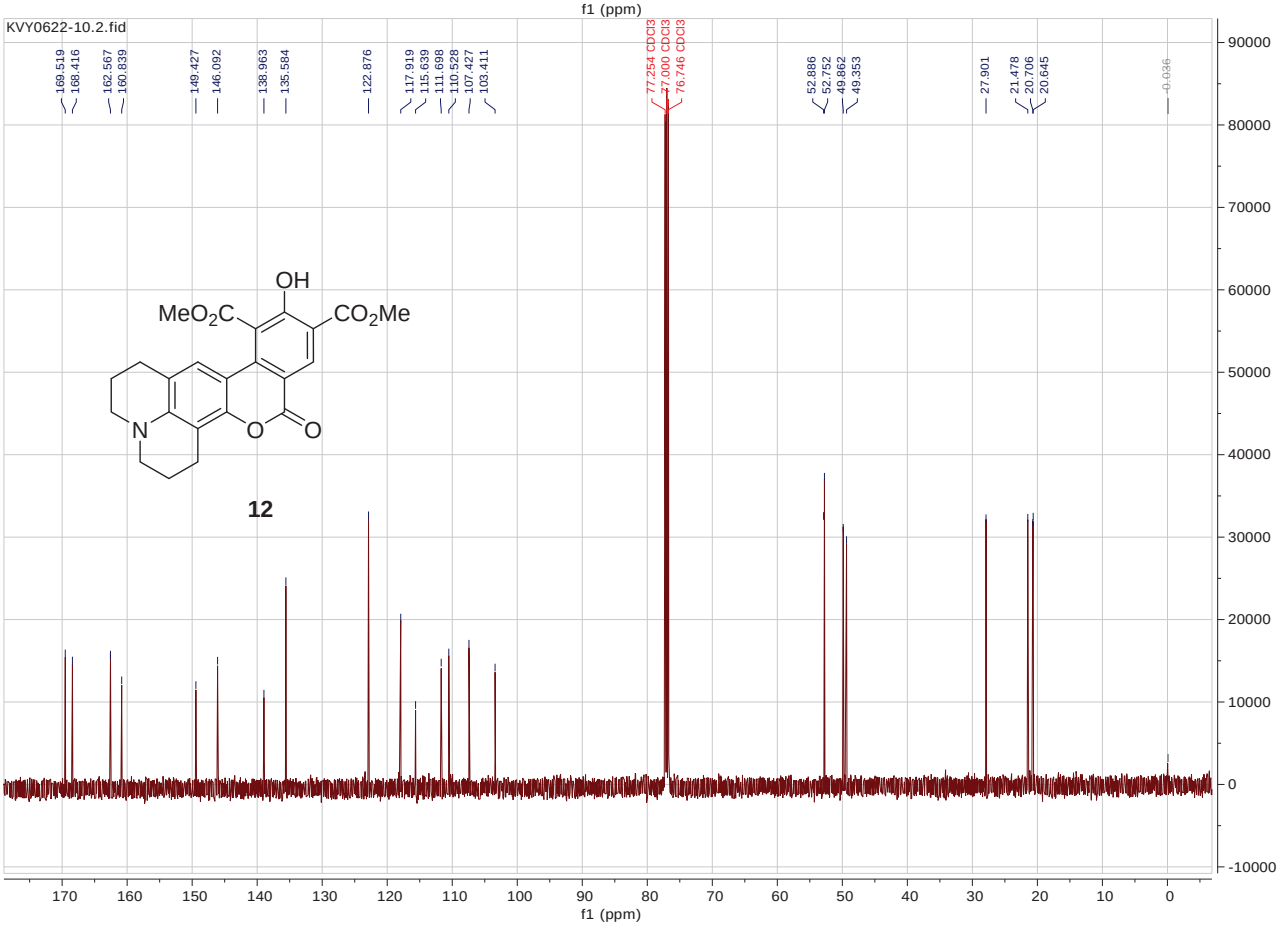
KVY0622-10.2.fid
OH
MeO2C
CO2Me
N
O
O
12
f1 (ppm)

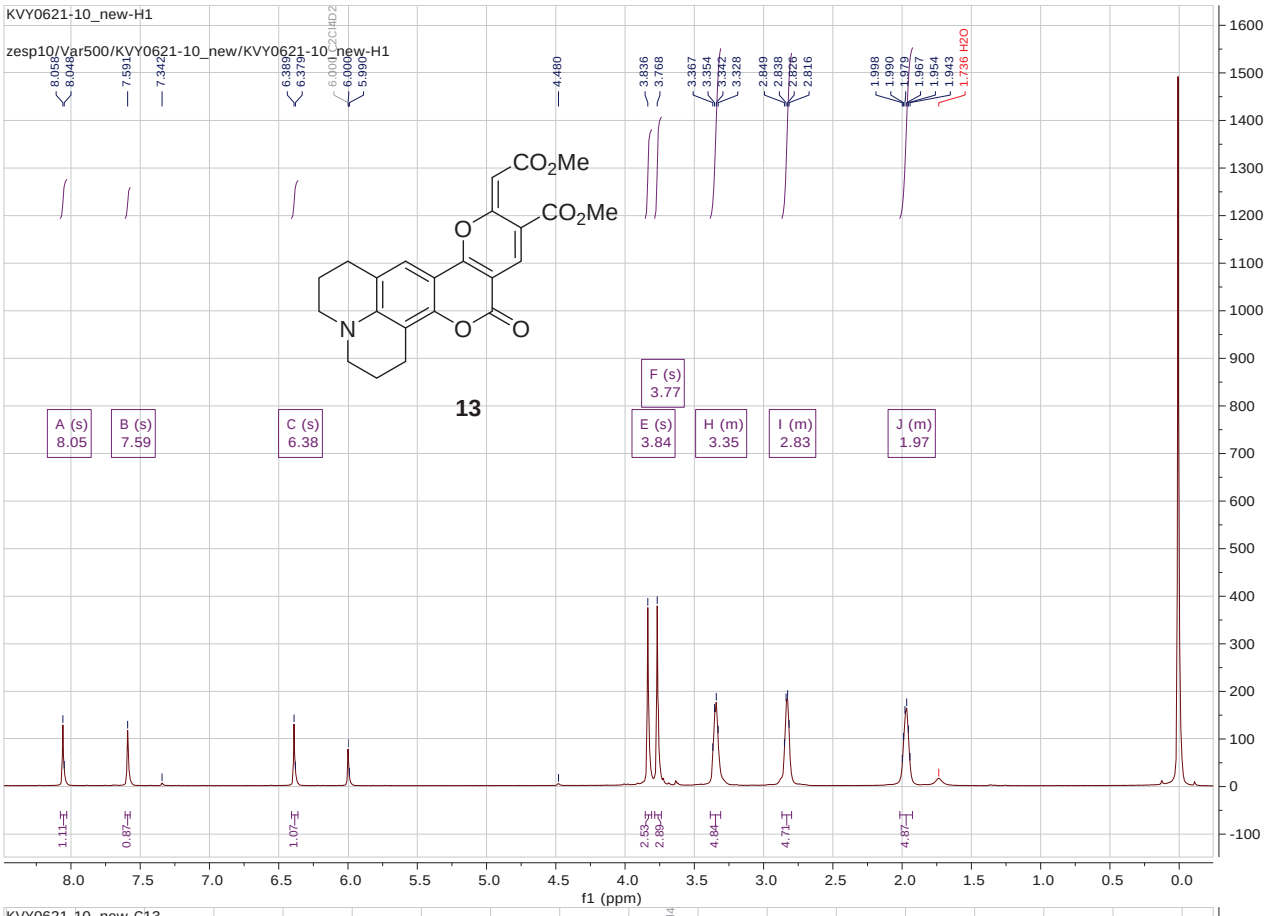
KVY0621-10_new-H1
zesp10/Var500/KVY0621-10_new/KVY0621-10_new-H1
CO2Me
CO2Me
O
N
O
O
13
A (s) 8.05
B (s) 7.59
C (s) 6.38
F (s) 3.77
E (s) 3.84
H (m) 3.35
I (m) 2.83
J (m) 1.97
f1 (ppm)

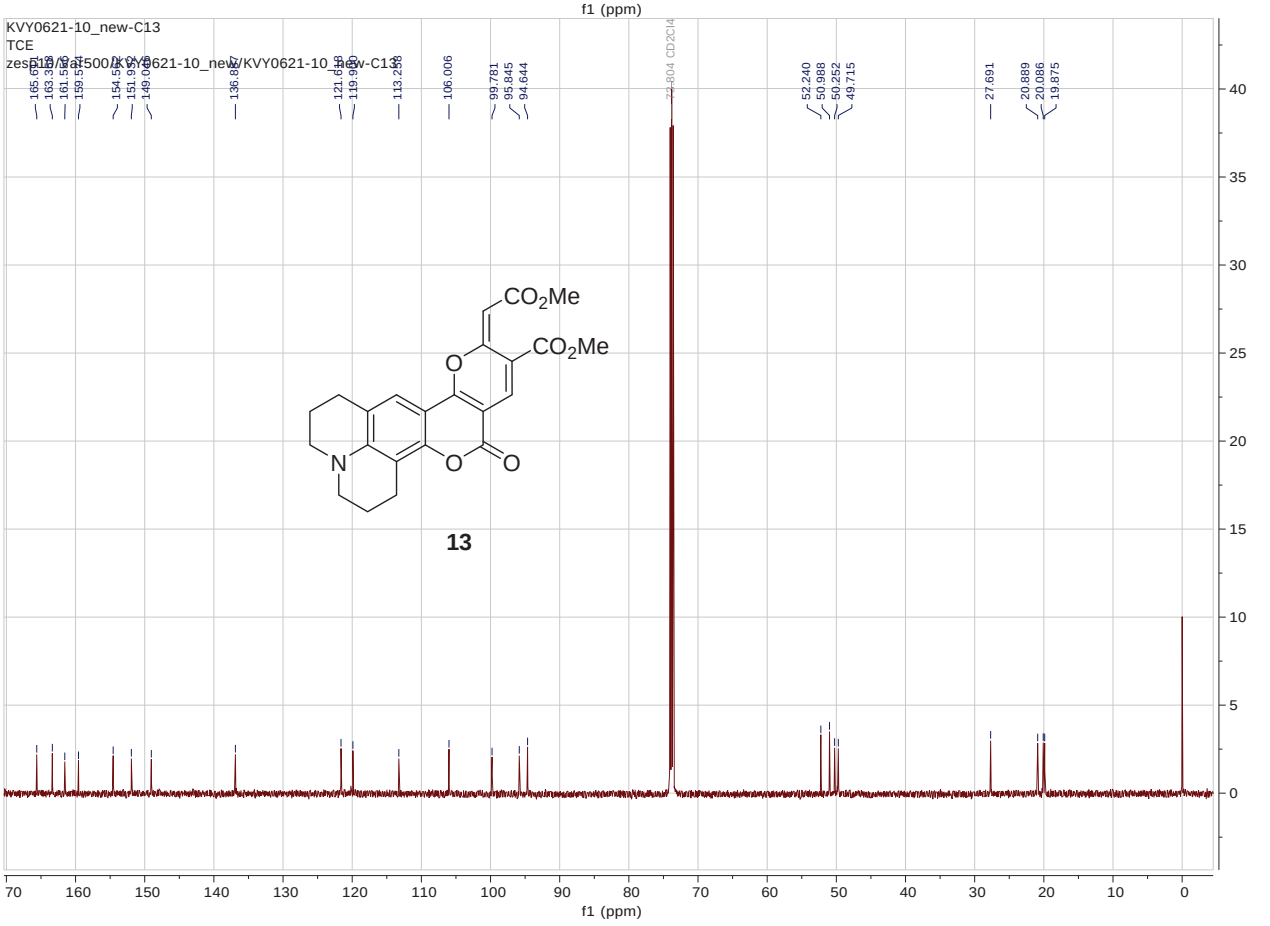
KVY0621-10_new-C13
TCE
CO2Me
CO2Me
O
N
O
O
13
f1 (ppm)

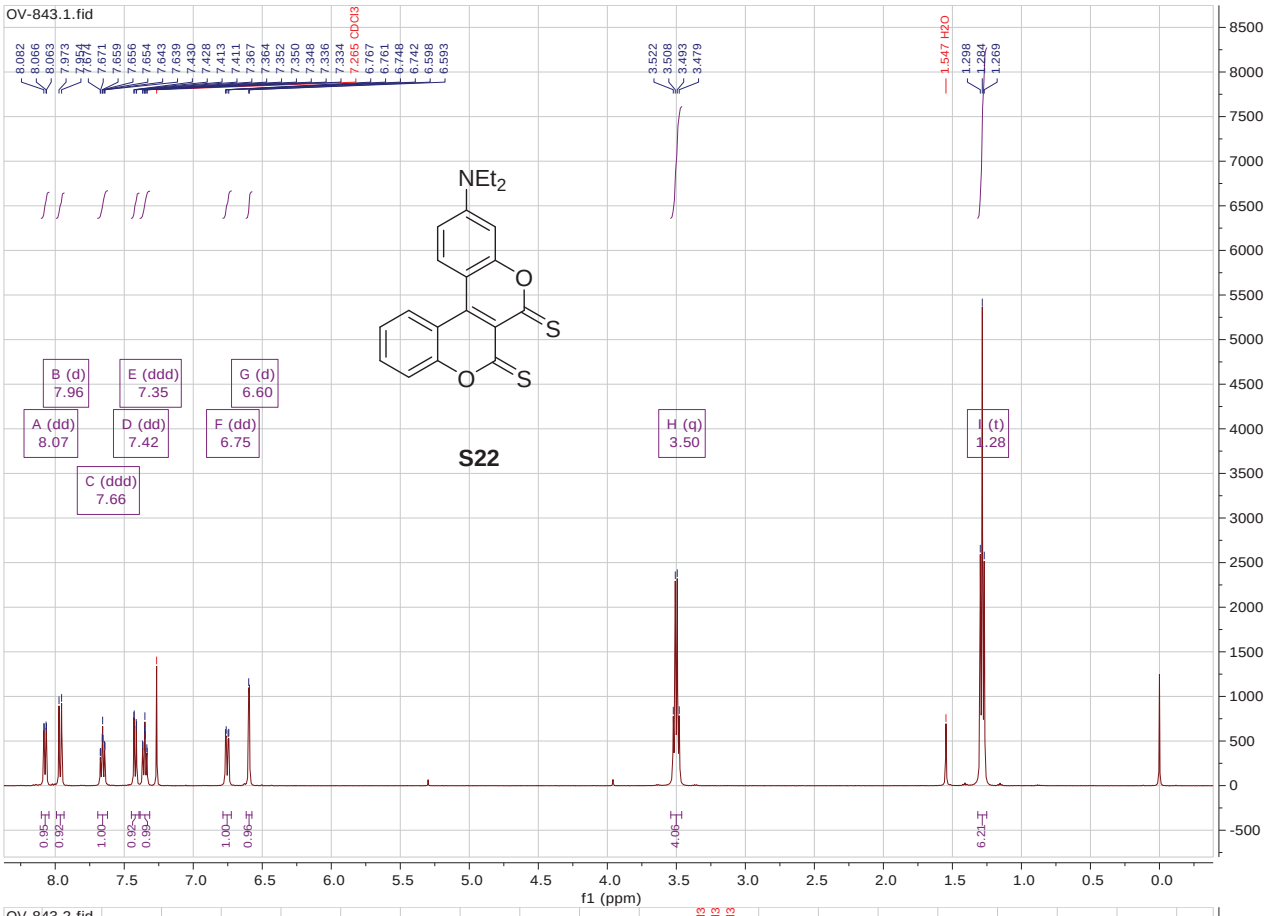
OV-843.1.fid
8.082
8.066
8.063
7.973
7.954
7.674
7.671
7.659
7.656
7.654
7.643
7.639
7.430
7.428
7.413
7.411
7.367
7.364
7.352
7.350
7.348
7.336
7.334
7.265 CDCl3
6.767
6.761
6.748
6.742
6.598
6.593
3.522
3.508
3.493
3.479
1.547 H2O
1.298
1.284
1.269
NEt2
O
S
O
S
B (d) 7.96
E (ddd) 7.35
G (d) 6.60
A (dd) 8.07
D (dd) 7.42
F (dd) 6.75
C (ddd) 7.66
H (q) 3.50
I (t) 1.28
S22
0.95
0.92
1.00
0.92
0.99
1.00
0.96
4.06
6.21
f1 (ppm)

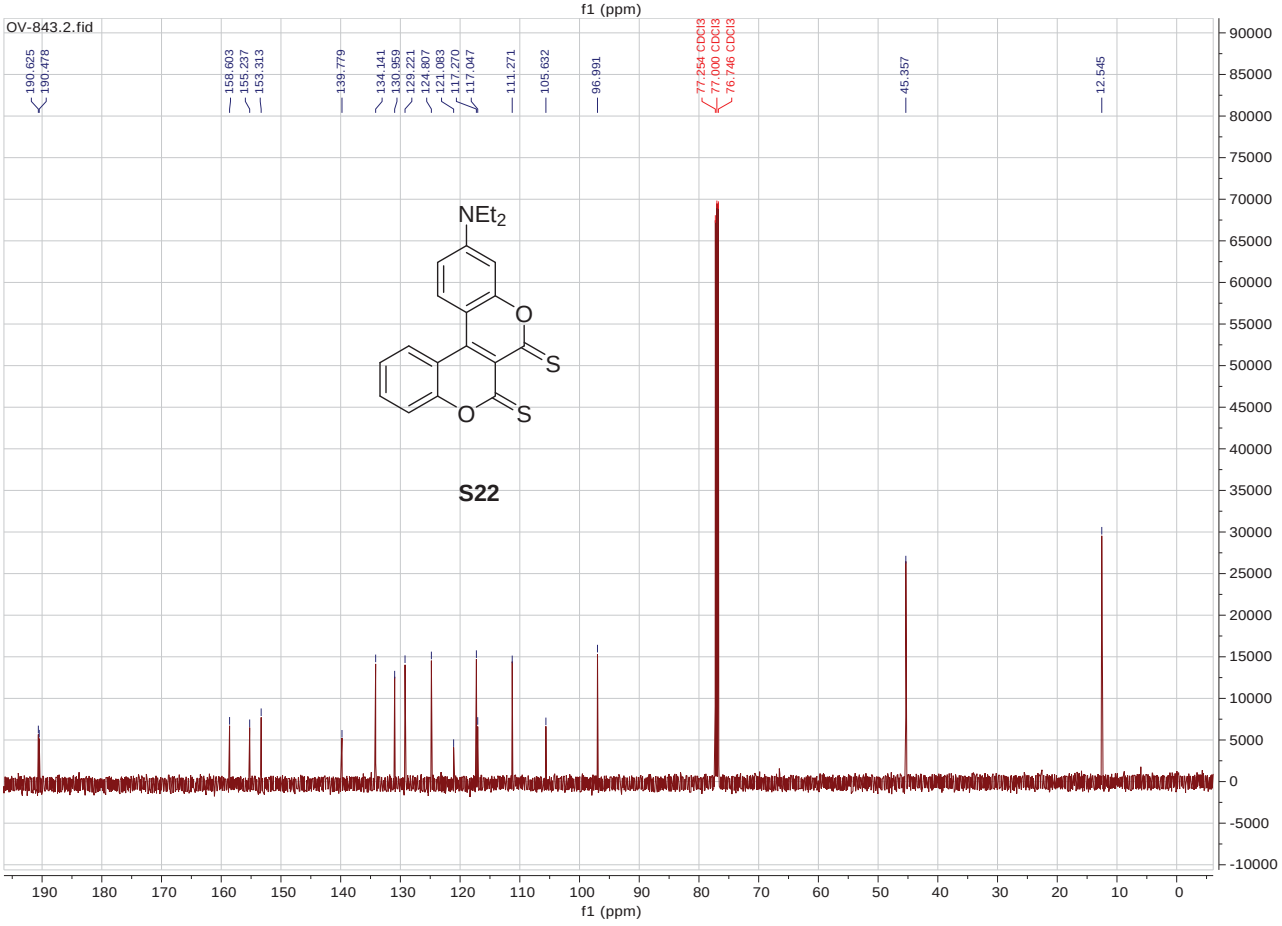
OV-843.2.fid
190.625
190.478
158.603
155.237
153.313
139.779
134.141
130.959
129.221
124.807
121.083
117.270
117.047
111.271
105.632
96.991
77.254 CDCl3
77.000 CDCl3
76.746 CDCl3
45.357
12.545
NEt2
O
S
O
S
S22
f1 (ppm)

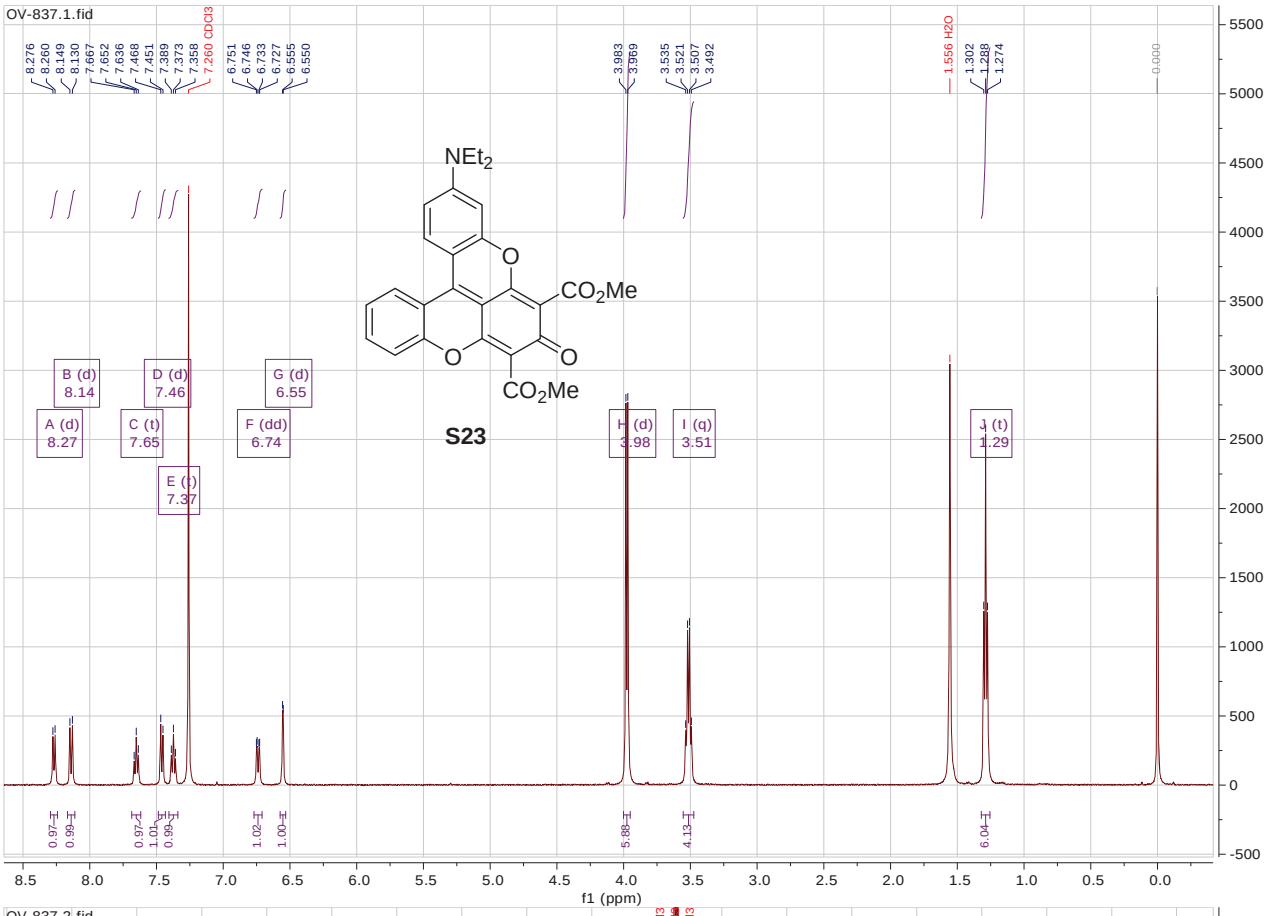
OV-837.1.fid
NEt2
CO2Me
CO2Me
S23
A (d) 8.27
B (d) 8.14
C (t) 7.65
D (d) 7.46
E (t) 7.37
F (dd) 6.74
G (d) 6.55
H (d) 3.98
I (q) 3.51
J (t) 1.29
f1 (ppm)

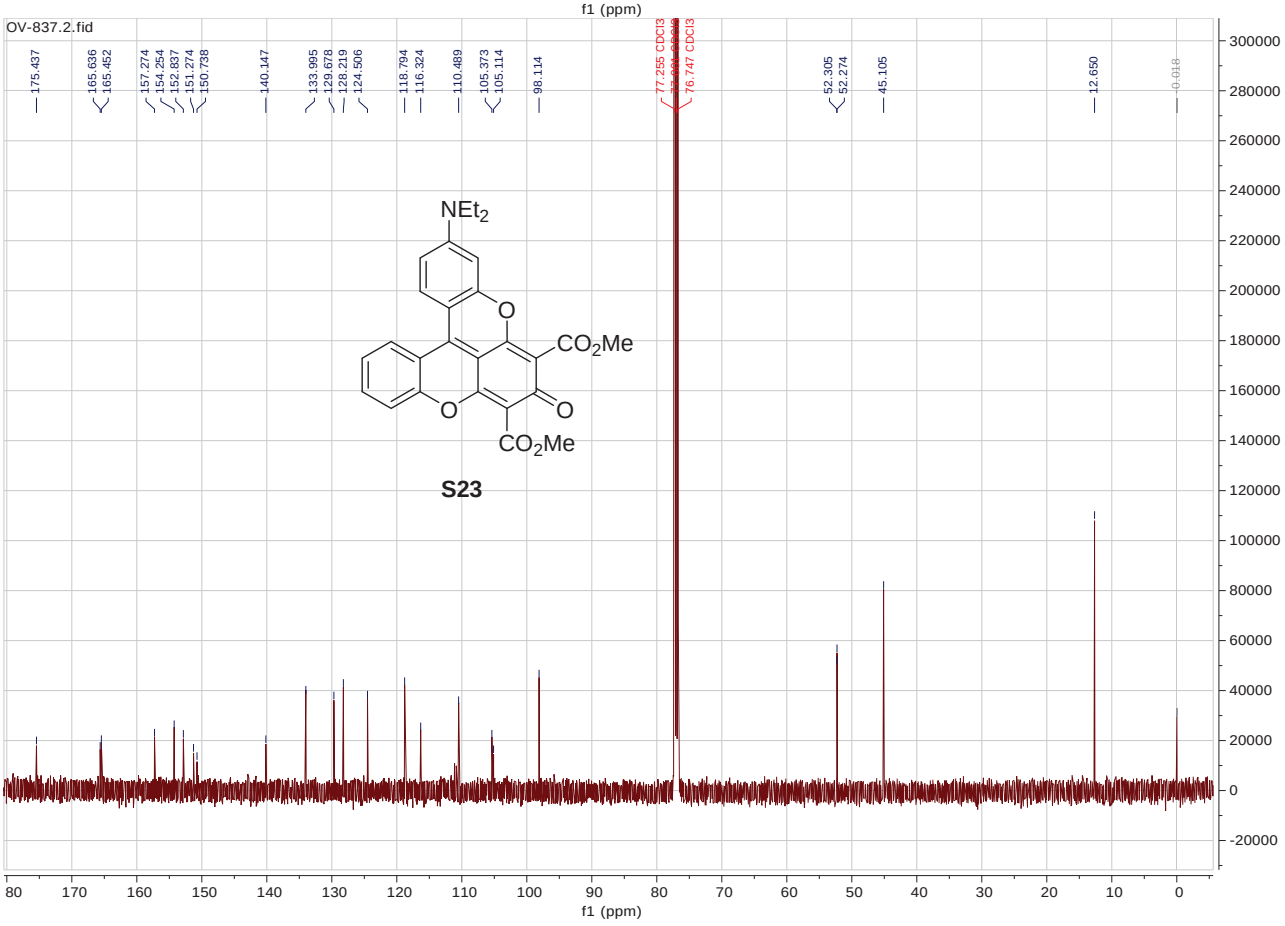
OV-837.2.fid
NEt2
CO2Me
CO2Me
S23
f1 (ppm)

Crystal Structure Report for 12

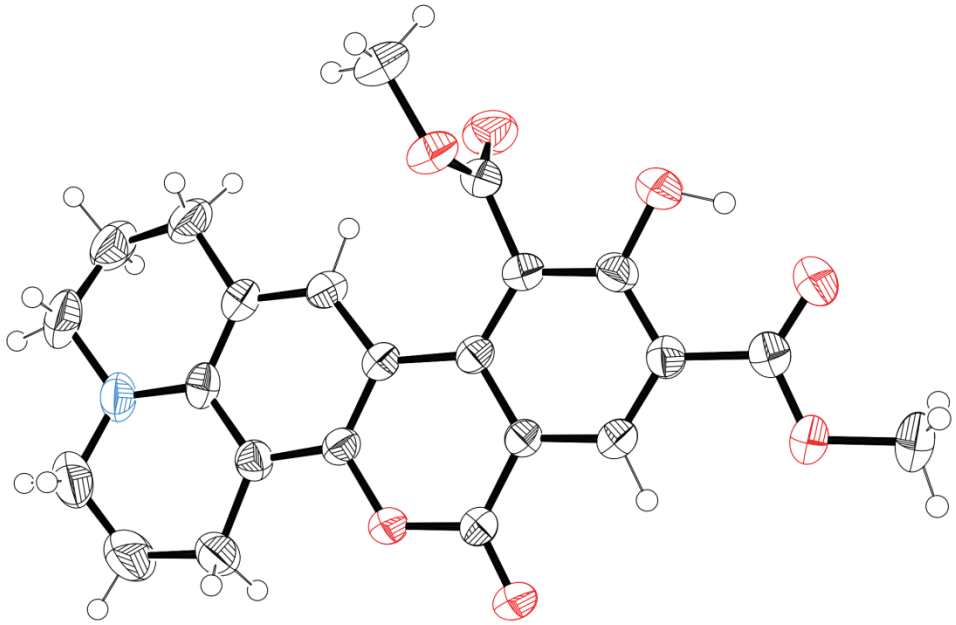

Figure S3. The ORTEP drawing[4] of X-ray diffraction analysis for compound **12**. CCDC 2125095.

A yellow prisms-like specimen of $C_{23}H_{21}NO_7$, approximate dimensions 0.194 mm x 0.244 mm x 0.368 mm, was used for the X-ray crystallographic analysis. The X-ray intensity data were measured.

Table S1. Data collection details for **12**.

Axis	dx/mm	2θ/°	ω/°	ϕ/°	χ/°	Width/°	Frames	Time/s	Wavelength/Å	Voltage/kV	Current/mA	Temperature/K
Omega	39.835	-97.72	-192.85	-178.62	24.03	2.00	54	88.00	1.54184	45	30.0	n/a
Omega	39.835	-101.63	-206.31	-24.27	43.23	2.00	56	88.00	1.54184	45	30.0	n/a
Omega	39.835	-101.30	-209.35	-83.58	50.32	2.00	57	88.00	1.54184	45	30.0	n/a
Phi	39.835	-18.13	-3.92	-116.00	23.00	2.00	92	88.00	1.54184	45	30.0	n/a
Omega	39.835	-100.90	-111.03	-90.42	-30.05	2.00	54	88.00	1.54184	45	30.0	n/a
Omega	39.835	-100.79	-203.51	-119.88	40.40	2.00	55	88.00	1.54184	45	30.0	n/a
Omega	39.835	36.11	-52.45	-114.35	52.48	2.00	47	88.00	1.54184	45	30.0	n/a
Phi	39.835	85.61	-280.32	0.00	-58.06	2.00	180	88.00	1.54184	45	30.0	n/a
Omega	39.835	27.38	-337.08	0.00	-54.74	2.00	57	88.00	1.54184	45	30.0	n/a
Omega	39.835	-101.22	-108.86	19.45	-42.31	2.00	56	88.00	1.54184	45	30.0	n/a
Omega	39.835	-100.90	-205.62	22.16	43.34	2.00	56	88.00	1.54184	45	30.0	n/a
Omega	39.835	-100.87	-206.52	-166.47	46.12	2.00	56	88.00	1.54184	45	30.0	n/a
Omega	39.835	-101.30	-204.15	-50.83	40.80	2.00	55	88.00	1.54184	45	30.0	n/a
Omega	39.835	-99.71	-200.88	-223.75	36.03	2.00	55	88.00	1.54184	45	30.0	n/a
Omega	39.835	84.67	-280.79	90.00	-54.74	2.00	58	88.00	1.54184	45	30.0	n/a
Omega	39.835	-101.22	-209.09	-148.00	49.76	2.00	57	88.00	1.54184	45	30.0	n/a
Omega	39.835	84.67	-280.79	180.00	-54.74	2.00	58	88.00	1.54184	45	30.0	n/a
Omega	39.835	84.67	-280.79	0.00	-54.74	2.00	58	88.00	1.54184	45	30.0	n/a
Omega	39.835	-100.35	-109.65	72.81	-32.08	2.00	54	88.00	1.54184	45	30.0	n/a
Omega	39.835	27.38	-337.08	153.00	-54.74	2.00	57	88.00	1.54184	45	30.0	n/a
Phi	39.835	-100.61	-174.76	-44.00	23.00	2.00	28	88.00	1.54184	45	30.0	n/a
Omega	39.835	84.67	-280.79	270.00	-54.74	2.00	58	88.00	1.54184	45	30.0	n/a
Omega	39.835	-101.52	-206.51	57.38	44.15	2.00	56	88.00	1.54184	45	30.0	n/a
Omega	39.835	-100.23	-106.60	-144.54	-49.09	2.00	57	88.00	1.54184	45	30.0	n/a
Omega	39.835	-100.91	-106.03	-34.93	-55.74	2.00	58	88.00	1.54184	45	30.0	n/a
Omega	39.835	-101.15	-205.37	80.53	41.85	2.00	56	88.00	1.54184	45	30.0	n/a
Omega	39.835	12.38	-353.08	270.00	-54.74	2.00	58	88.00	1.54184	45	30.0	n/a

Axis	dx/mm	2θ/°	ω/°	ϕ/°	χ/°	Width/°	Frames	Time/s	Wavelength/Å	Voltage/kV	Current/mA	Temperature/K
Omega	39.835	-97.67	-64.94	-136.03	-74.84	2.00	46	88.00	1.54184	45	30.0	n/a
Phi	39.835	70.61	-295.32	0.00	-58.06	2.00	180	88.00	1.54184	45	30.0	n/a

A total of 1869 frames were collected. The total exposure time was 45.69 hours. The frames were integrated with the Bruker SAINT software package using a narrow-frame algorithm. The integration of the data using a monoclinic unit cell yielded a total of 20848 reflections to a maximum θ angle of 68.75° (0.83 Å resolution), of which 3496 were independent (average redundancy 5.963, completeness = 97.3%, R_{int} = 6.44%, R_{sig} = 4.22%) and 2521 (72.11%) were greater than 2σ(F^2). The final cell constants of a = 11.7140(13) Å, b = 9.9926(12) Å, c = 16.775(2) Å, β = 98.713(7)°, volume = 1940.9(4) $Å^3$, are based upon the refinement of the XYZ-centroids of 7169 reflections above 20 σ(I) with 5.329° < 2θ < 136.6°. Data were corrected for absorption effects using the numerical method (SADABS). The ratio of minimum to maximum apparent transmission was 0.825. The calculated minimum and maximum transmission coefficients (based on crystal size) are 0.7320 and 0.8440.

The structure was solved and refined using the Bruker SHELXTL Software Package, using the space group P 1 21/n 1, with Z = 4 for the formula unit, $C_{23}H_{21}NO_7$. The final anisotropic full-matrix least-squares refinement on F^2 with 326 variables converged at R1 = 4.93%, for the observed data and wR2 = 13.29% for all data. The goodness-of-fit was 1.015. The largest peak in the final difference electron density synthesis was 0.650 $e^-/Å^3$ and the largest hole was -0.324 $e^-/Å^3$ with an RMS deviation of 0.044 $e^-/Å^3$. On the basis of the final model, the calculated density was 1.449 g/cm^3 and F(000), 888 e^-.

Table S2. Sample and crystal data for **12**.

Identification code	KVy0620A	
Chemical formula	$C_{23}H_{21}NO_7$	
Formula weight	423.41 g/mol	
Temperature	296(2) K	
Wavelength	1.54178 Å	
Crystal size	0.194 x 0.244 x 0.368 mm	
Crystal habit	yellow prisms	
Crystal system	monoclinic	
Space group	P 1 21/n 1	
Unit cell dimensions	a = 11.7140(13) Å	α = 90°
	b = 9.9926(12) Å	β = 98.713(7)°
	c = 16.775(2) Å	γ = 90°
Volume	1940.9(4) $Å^3$	
Z	4	
Density (calculated)	1.449 g/cm^3	
Absorption coefficient	0.903 mm^{-1}	
F(000)	888	

Table S3. Data collection and structure refinement for **12**.

Theta range for data collection	4.31 to 68.75°
Index ranges	-14<=h<=14, -11<=k<=10, -20<=l<=20
Reflections collected	20848
Independent reflections	3496 [R(int) = 0.0644]
Coverage of independent reflections	97.3%
Absorption correction	numerical
Max. and min. transmission	0.8440 and 0.7320
Structure solution technique	direct methods

Structure solution program	SHELXL-2014 (Sheldrick, 2014)	
Refinement method	Full-matrix least-squares on F^2	
Refinement program	SHELXL-2014 (Sheldrick, 2014)	
Function minimized	$\Sigma w(F_o^2 - F_c^2)^2$	
Data / restraints / parameters	3496 / 0 / 326	
Goodness-of-fit on F^2	1.015	
Final R indices	2521 data; I>2σ(I)	R1 = 0.0493, wR2 = 0.1180
	all data	R1 = 0.0726, wR2 = 0.1329
Weighting scheme	$w=1/[\sigma^2(F_o^2)+(0.0563P)^2+0.9257P]$ where $P=(F_o^2+2F_c^2)/3$	
Largest diff. peak and hole	0.650 and -0.324 eÅ^{-3}	
R.M.S. deviation from mean	0.044 eÅ^{-3}	

Table S4. Atomic coordinates and equivalent isotropic atomic displacement parameters (Å^2) for **12**. U(eq) is defined as one third of the trace of the orthogonalized U_{ij} tensor.

	x/a	y/b	z/c	U(eq)
N1	0.79545(16)	0.8429(2)	0.96972(13)	0.0496(5)
O1	0.40679(11)	0.73599(15)	0.98848(9)	0.0430(4)
O2	0.22301(12)	0.69230(18)	0.98329(10)	0.0534(5)
O3	0.42098(15)	0.32825(19)	0.27994(10)	0.0564(5)
O4	0.65852(14)	0.33896(17)	0.22349(11)	0.0592(5)
O5	0.63780(12)	0.53689(17)	0.28201(9)	0.0484(4)
O6	0.20390(14)	0.27387(19)	0.26422(11)	0.0596(5)
O7	0.08283(13)	0.38296(18)	0.17120(11)	0.0560(5)
C1	0.9165(2)	0.8403(3)	0.0081(2)	0.0665(8)
C2	0.9551(2)	0.7029(3)	0.0347(2)	0.0626(8)
C3	0.88157(19)	0.6484(3)	0.09211(18)	0.0543(7)
C4	0.75485(17)	0.6737(2)	0.06535(13)	0.0387(5)
C5	0.71712(17)	0.7696(2)	0.00534(14)	0.0383(5)
C6	0.59773(17)	0.7873(2)	0.98031(13)	0.0369(5)
C7	0.5524(2)	0.8849(3)	0.91468(18)	0.0501(6)
C8	0.6456(3)	0.9451(4)	0.8743(2)	0.0893(11

	x/a	y/b	z/c	U(eq)
				)
C9	0.7564(2)	0.9621(3)	0.9255(2)	0.0719(9)
C10	0.67491(17)	0.6033(2)	0.10043(14)	0.0377(5)
C11	0.55527(16)	0.6212(2)	0.08003(13)	0.0335(5)
C12	0.52187(16)	0.7126(2)	0.01808(13)	0.0343(5)
C13	0.31944(16)	0.6681(2)	0.01591(13)	0.0365(5)
C14	0.35030(16)	0.5755(2)	0.08252(12)	0.0316(5)
C15	0.46661(16)	0.5535(2)	0.11724(12)	0.0314(5)
C16	0.48664(17)	0.4678(2)	0.18456(13)	0.0351(5)
C17	0.39510(18)	0.4064(2)	0.21439(13)	0.0381(5)
C18	0.28036(17)	0.4263(2)	0.17743(13)	0.0370(5)
C19	0.26035(17)	0.5115(2)	0.11245(13)	0.0356(5)
C20	0.60377(18)	0.4383(2)	0.23082(14)	0.0394(5)
C21	0.7529(2)	0.5265(3)	0.32706(17)	0.0644(8)
C22	0.18693(19)	0.3537(2)	0.20899(14)	0.0430(6)
C23	0.9883(2)	0.3055(4)	0.1955(2)	0.0831(10)

Table S5. Bond lengths (Å) for **12**.

N1-C5	1.379(3)	N1-C9	1.441(3)
N1-C1	1.466(3)	O1-C13	1.364(2)
O1-C12	1.384(2)	O2-C13	1.203(2)
O3-C17	1.345(3)	O3-H3	0.95(3)
O4-C20	1.198(3)	O5-C20	1.328(3)
O5-C21	1.446(3)	O6-C22	1.216(3)
O7-C22	1.319(3)	O7-C23	1.458(3)
C1-C2	1.492(4)	C1-H1A	0.99(3)
C1-H1B	1.08(4)	C2-C3	1.489(4)
C2-H2A	0.98(3)	C2-H2B	1.06(3)
C3-C4	1.506(3)	C3-H3A	0.99(3)
C3-H3B	1.00(3)	C4-C10	1.373(3)
C4-C5	1.411(3)	C5-C6	1.409(3)
C6-C12	1.385(3)	C6-C7	1.506(3)

C7-C8	1.496(4)	C7-H7A	0.95(3)
C7-H7B	0.95(3)	C8-C9	1.454(4)
C8-H8A	0.97	C8-H8B	0.97
C9-H9A	0.97	C9-H9B	0.97
C10-C11	1.403(3)	C10-H10	0.97(3)
C11-C12	1.395(3)	C11-C15	1.457(3)
C13-C14	1.454(3)	C14-C19	1.390(3)
C14-C15	1.415(3)	C15-C16	1.408(3)
C16-C17	1.393(3)	C16-C20	1.500(3)
C17-C18	1.406(3)	C18-C19	1.375(3)
C18-C22	1.476(3)	C19-H19	0.98(2)
C21-H21A	0.96	C21-H21B	0.96
C21-H21C	0.96	C23-H23A	0.96
C23-H23B	0.96	C23-H23C	0.96

Table S6. Bond angles (°) for **12**.

C5-N1-C9	118.8(2)	C5-N1-C1	117.6(2)
C9-N1-C1	116.8(2)	C13-O1-C12	122.32(17)
C17-O3-H3	104.4(17)	C20-O5-C21	116.72(19)
C22-O7-C23	115.7(2)	N1-C1-C2	112.1(2)
N1-C1-H1A	102.2(18)	C2-C1-H1A	113.6(18)
N1-C1-H1B	110.9(19)	C2-C1-H1B	108.8(19)
H1A-C1-H1B	109.(3)	C1-C2-C3	110.6(3)
C1-C2-H2A	107.3(16)	C3-C2-H2A	111.0(16)
C1-C2-H2B	108.8(15)	C3-C2-H2B	110.8(15)
H2A-C2-H2B	108.(2)	C2-C3-C4	112.7(2)
C2-C3-H3A	113.8(18)	C4-C3-H3A	107.4(18)
C2-C3-H3B	113.8(19)	C4-C3-H3B	107.4(18)
H3A-C3-H3B	101.(3)	C10-C4-C5	119.56(19)
C10-C4-C3	119.5(2)	C5-C4-C3	121.0(2)
N1-C5-C4	120.84(19)	N1-C5-C6	120.0(2)
C4-C5-C6	119.16(19)	C12-C6-C5	118.2(2)
C12-C6-C7	120.25(19)	C5-C6-C7	121.5(2)
C8-C7-C6	113.0(2)	C8-C7-H7A	108.1(19)
C6-C7-H7A	111.(2)	C8-C7-H7B	109.0(19)
C6-C7-H7B	112.0(19)	H7A-C7-H7B	103.(3)
C9-C8-C7	115.2(3)	C9-C8-H8A	108.5
C7-C8-H8A	108.5	C9-C8-H8B	108.5
C7-C8-H8B	108.5	H8A-C8-H8B	107.5
N1-C9-C8	113.1(2)	N1-C9-H9A	109.0
C8-C9-H9A	109.0	N1-C9-H9B	109.0
C8-C9-H9B	109.0	H9A-C9-H9B	107.8
C4-C10-C11	123.4(2)	C4-C10-H10	115.0(14)
C11-C10-H10	121.5(14)	C12-C11-C10	114.99(19)
C12-C11-C15	119.07(17)	C10-C11-C15	125.9(2)

C6-C12-O1	113.74(18)	C6-C12-C11	124.53(18)
O1-C12-C11	121.73(18)	O2-C13-O1	116.56(19)
O2-C13-C14	125.79(19)	O1-C13-C14	117.63(17)
C19-C14-C15	121.01(19)	C19-C14-C13	117.17(18)
C15-C14-C13	121.80(17)	C16-C15-C14	117.22(18)
C16-C15-C11	125.66(18)	C14-C15-C11	117.12(18)
C17-C16-C15	120.82(18)	C17-C16-C20	114.90(19)
C15-C16-C20	124.26(18)	O3-C17-C16	117.33(19)
O3-C17-C18	121.62(19)	C16-C17-C18	121.0(2)
C19-C18-C17	118.28(19)	C19-C18-C22	122.8(2)
C17-C18-C22	118.9(2)	C18-C19-C14	121.59(19)
C18-C19-H19	122.0(12)	C14-C19-H19	116.4(12)
O4-C20-O5	124.6(2)	O4-C20-C16	124.9(2)
O5-C20-C16	110.47(18)	O5-C21-H21A	109.5
O5-C21-H21B	109.5	H21A-C21-H21B	109.5
O5-C21-H21C	109.5	H21A-C21-H21C	109.5
H21B-C21-H21C	109.5	O6-C22-O7	123.0(2)
O6-C22-C18	123.4(2)	O7-C22-C18	113.6(2)
O7-C23-H23A	109.5	O7-C23-H23B	109.5
H23A-C23-H23B	109.5	O7-C23-H23C	109.5
H23A-C23-H23C	109.5	H23B-C23-H23C	109.5

Table S7. Torsion angles (°) for **12**.

C5-N1-C1-C2	42.9(4)	C9-N1-C1-C2	-166.2(3)
N1-C1-C2-C3	-58.2(4)	C1-C2-C3-C4	44.2(4)
C2-C3-C4-C10	164.4(3)	C2-C3-C4-C5	-16.2(4)
C9-N1-C5-C4	-163.7(2)	C1-N1-C5-C4	-13.4(3)
C9-N1-C5-C6	18.1(3)	C1-N1-C5-C6	168.3(2)
C10-C4-C5-N1	179.2(2)	C3-C4-C5-N1	-0.1(3)
C10-C4-C5-C6	-2.5(3)	C3-C4-C5-C6	178.1(2)
N1-C5-C6-C12	-179.4(2)	C4-C5-C6-C12	2.3(3)
N1-C5-C6-C7	0.2(3)	C4-C5-C6-C7	-178.0(2)
C12-C6-C7-C8	-173.4(3)	C5-C6-C7-C8	6.9(4)
C6-C7-C8-C9	-31.8(4)	C5-N1-C9-C8	-43.1(4)
C1-N1-C9-C8	166.4(3)	C7-C8-C9-N1	49.8(4)
C5-C4-C10-C11	-0.1(3)	C3-C4-C10-C11	179.3(2)
C4-C10-C11-C12	2.8(3)	C4-C10-C11-C15	-177.4(2)
C5-C6-C12-O1	-179.19(18)	C7-C6-C12-O1	1.1(3)
C5-C6-C12-C11	0.5(3)	C7-C6-C12-C11	-179.1(2)
C13-O1-C12-C6	177.40(19)	C13-O1-C12-C11	-2.3(3)
C10-C11-C12-C6	-3.0(3)	C15-C11-C12-C6	177.2(2)
C10-C11-C12-O1	176.71(19)	C15-C11-C12-O1	-3.1(3)
C12-O1-C13-O2	-176.7(2)	C12-O1-C13-C14	4.5(3)
O2-C13-C14-C19	-1.6(3)	O1-C13-C14-C19	177.10(19)

O2-C13-C14-C15	-179.9(2)	O1-C13-C14-C15	-1.2(3)
C19-C14-C15-C16	-2.0(3)	C13-C14-C15-C16	176.32(19)
C19-C14-C15-C11	177.85(19)	C13-C14-C15-C11	-3.9(3)
C12-C11-C15-C16	-174.23(19)	C10-C11-C15-C16	6.0(3)
C12-C11-C15-C14	6.0(3)	C10-C11-C15-C14	-173.8(2)
C14-C15-C16-C17	0.9(3)	C11-C15-C16-C17	-178.9(2)
C14-C15-C16-C20	-177.24(19)	C11-C15-C16-C20	3.0(3)
C15-C16-C17-O3	-178.59(19)	C20-C16-C17-O3	-0.3(3)
C15-C16-C17-C18	1.1(3)	C20-C16-C17-C18	179.4(2)
O3-C17-C18-C19	177.6(2)	C16-C17-C18-C19	-2.0(3)
O3-C17-C18-C22	-3.3(3)	C16-C17-C18-C22	177.1(2)
C17-C18-C19-C14	1.0(3)	C22-C18-C19-C14	-178.1(2)
C15-C14-C19-C18	1.0(3)	C13-C14-C19-C18	-177.3(2)
C21-O5-C20-O4	4.9(3)	C21-O5-C20-C16	-175.93(19)
C17-C16-C20-O4	81.0(3)	C15-C16-C20-O4	-100.7(3)
C17-C16-C20-O5	-98.1(2)	C15-C16-C20-O5	80.2(3)
C23-O7-C22-O6	-4.6(4)	C23-O7-C22-C18	174.9(2)
C19-C18-C22-O6	176.8(2)	C17-C18-C22-O6	-2.3(4)
C19-C18-C22-O7	-2.7(3)	C17-C18-C22-O7	178.2(2)

Table S8. Anisotropic atomic displacement parameters (Å^2) for **12**. The anisotropic atomic displacement factor exponent takes the form: $-2\pi^2[h^2 a^{*2} U_{11} + ... + 2 h k a^* b^* U_{12}]$

	U_{11}	U_{22}	U_{33}	U_{23}	U_{13}	U_{12}
N1	0.0406(10)	0.0441(12)	0.0659(14)	0.0033(11)	0.0139(9)	-0.0097(8)
O1	0.0297(7)	0.0482(9)	0.0505(10)	0.0159(8)	0.0039(7)	0.0018(6)
O2	0.0299(8)	0.0651(11)	0.0631(11)	0.0227(9)	0.0001(7)	0.0034(7)
O3	0.0484(10)	0.0705(12)	0.0493(10)	0.0254(10)	0.0039(8)	-0.0008(9)
O4	0.0514(10)	0.0502(11)	0.0725(13)	0.0008(10)	-0.0022(9)	0.0149(8)
O5	0.0397(8)	0.0566(10)	0.0448(9)	-0.0050(9)	-0.0068(7)	0.0010(7)
O6	0.0534(10)	0.0658(12)	0.0614(11)	0.0255(10)	0.0142(8)	-0.0031(8)
O7	0.0361(8)	0.0679(12)	0.0637(11)	0.0178(10)	0.0065(8)	-0.0126(8)
C1	0.0414(14)	0.068(2)	0.091(2)	-0.0046(19)	0.0163(14)	-0.0207(13)
C2	0.0343(13)	0.084(2)	0.0692(19)	-0.0005(18)	0.0073(12)	-0.0056(13)
C3	0.0299(11)	0.072(2)	0.0597(18)	0.0020(16)	0.0019(11)	-0.0039(11)
C4	0.0312(10)	0.0423(13)	0.0420(13)	-0.0067(11)	0.0038(9)	-0.0038(9)
C5	0.0355(11)	0.0342(12)	0.0464(13)	-0.0087(11)	0.0102(10)	-0.0077(9)
C6	0.0360(11)	0.0335(12)	0.0420(13)	-0.0006(10)	0.0084(9)	-0.0007(9)
C7	0.0500(14)	0.0473(15)	0.0545(16)	0.0124(14)	0.0124(13)	0.0041(12)
C8	0.0664(19)	0.093(2)	0.111(3)	0.055(2)	0.0226(18)	0.0008(17)
C9	0.0626(17)	0.0553(17)	0.100(2)	0.0191(18)	0.0196(16)	-0.0132(14)
C10	0.0313(10)	0.0439(13)	0.0364(12)	-0.0001(11)	0.0008(9)	0.0016(9)
C11	0.0285(10)	0.0358(12)	0.0357(12)	-0.0021(10)	0.0034(8)	-0.0001(8)
C12	0.0286(10)	0.0350(12)	0.0386(12)	-0.0013(10)	0.0026(9)	0.0014(8)
C13	0.0296(10)	0.0380(12)	0.0417(12)	0.0037(11)	0.0052(9)	0.0003(9)
C14	0.0303(10)	0.0324(11)	0.0318(11)	-0.0016(10)	0.0036(8)	-0.0007(8)

	U_{11}	U_{22}	U_{33}	U_{23}	U_{13}	U_{12}
C15	0.0295(10)	0.0328(11)	0.0315(11)	-0.0048(10)	0.0029(8)	0.0001(8)
C16	0.0336(10)	0.0372(12)	0.0334(11)	-0.0011(10)	0.0012(9)	0.0020(9)
C17	0.0418(11)	0.0400(12)	0.0322(12)	0.0047(11)	0.0049(9)	0.0009(9)
C18	0.0363(11)	0.0379(12)	0.0373(12)	0.0004(11)	0.0076(9)	-0.0026(9)
C19	0.0304(10)	0.0375(12)	0.0379(12)	-0.0028(10)	0.0022(9)	-0.0001(9)
C20	0.0379(11)	0.0413(13)	0.0385(12)	0.0068(11)	0.0038(9)	0.0008(10)
C21	0.0457(14)	0.080(2)	0.0594(17)	0.0042(16)	-0.0169(12)	-0.0061(13)
C22	0.0425(12)	0.0440(13)	0.0432(14)	0.0039(12)	0.0086(10)	-0.0035(10)
C23	0.0462(15)	0.108(3)	0.094(2)	0.034(2)	0.0067(15)	-0.0303(16)

Table S9. Hydrogen atomic coordinates and isotropic atomic displacement parameters ($Å^2$) for **12**.

	x/a	y/b	z/c	U(eq)
H8A	0.6568	0.8888	-0.1710	0.107
H8B	0.6195	1.0319	-0.1471	0.107
H9A	0.8136	0.9883	-0.1077	0.086
H9B	0.7501	1.0341	-0.0366	0.086
H21A	0.7632	0.4395	0.3513	0.097
H21B	0.7633	0.5937	0.3685	0.097
H21C	0.8087	0.5396	0.2913	0.097
H23A	0.0067	0.2119	0.1949	0.125
H23B	-0.0812	0.3223	0.1586	0.125
H23C	-0.0227	0.3313	0.2489	0.125
H10	0.707(2)	0.539(3)	0.1413(15)	0.054(7)
H19	0.1821(18)	0.532(2)	0.0856(12)	0.036(6)
H1A	0.957(3)	0.877(3)	-0.0349(18)	0.083(10)
H2A	1.036(2)	0.709(3)	0.0601(16)	0.064(8)
H3A	0.901(3)	0.684(3)	0.148(2)	0.087(10)
H3B	0.891(3)	0.550(4)	0.102(2)	0.091(11)
H7A	0.511(3)	0.956(3)	-0.0652(19)	0.086(10)
H2B	0.951(2)	0.641(3)	-0.0168(18)	0.070(9)
H7B	0.496(3)	0.846(3)	-0.1249(19)	0.080(10)
H1B	0.930(3)	0.906(4)	0.060(2)	0.110(12)
H3	0.349(3)	0.292(3)	0.2888(17)	0.074(9)

Table S10. Hydrogen bond distances (Å) and angles (°) for **12**.

	Donor-H	Acceptor-H	Donor-Acceptor	Angle
O3-H3···O6	0.95(3)	1.69(3)	2.574(2)	152.(3)
C2-H2B···O7	1.06(3)	2.57(3)	3.521(4)	149.(2)
C23-H23A···O5	0.96	2.5	3.115(3)	121.4

Crystal Structure Report for 13

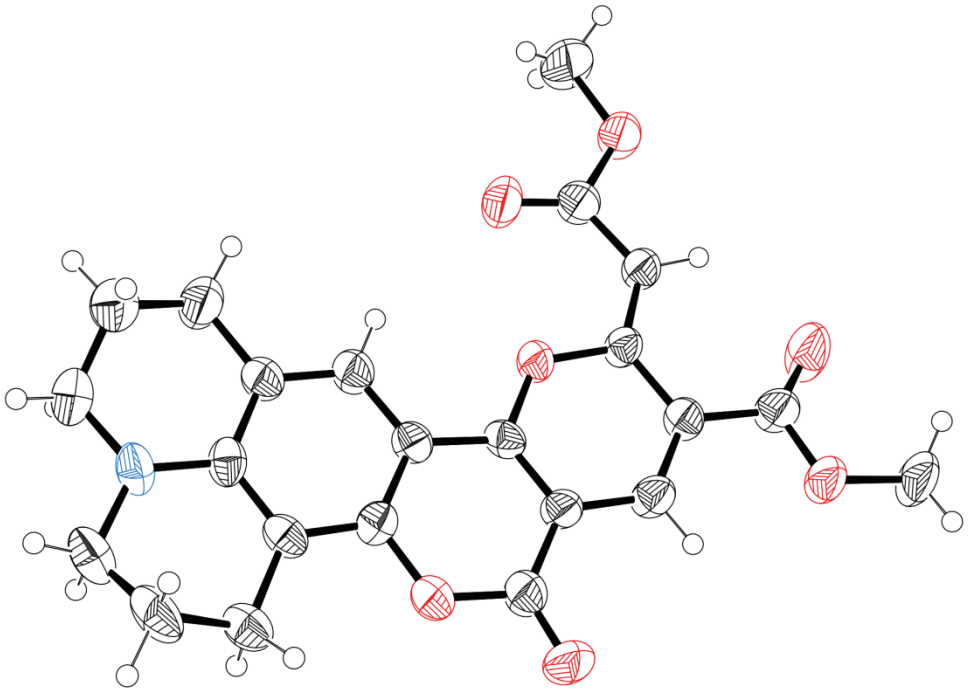

Figure S4. The ORTEP drawing[4] of X-ray diffraction analysis for compound **13.** CCDC 2125096.

A red needle-like specimen of $C_{23}H_{21}NO_7$, approximate dimensions 0.093 mm x 0.118 mm x 0.654 mm, was used for the X-ray crystallographic analysis. The X-ray intensity data were measured.

Table S11. Data collection details for **13**.

Axis	dx/mm	2θ/°	ω/°	ϕ/°	χ/°	Width/°	Fra-mes	Time/s	Wave-length/Å	Volta-ge/kV	Current/mA	Tempe-rature/K
Omega	39.875	-99.52	-196.16	0.05	26.30	1.60	68	24.00	1.54184	45	30.0	n/a
Omega	39.875	-100.83	-210.20	-187.67	52.45	1.60	72	24.00	1.54184	45	30.0	n/a
Omega	39.875	-100.46	-106.07	105.38	-57.83	1.60	74	24.00	1.54184	45	30.0	n/a

Axis	dx/mm	2θ/°	ω/°	ϕ/°	χ/°	Width/°	Fra-mes	Time/s	Wave-length/Å	Volta-ge/kV	Current/mA	Tempe-rature/K
Omega	39.875	-100.80	-200.04	-257.00	32.48	1.60	68	24.00	1.54184	45	30.0	n/a
Omega	39.875	-101.00	-203.00	-126.64	37.78	1.60	69	24.00	1.54184	45	30.0	n/a
Omega	39.875	39.67	-326.19	270.00	-54.74	1.60	73	24.00	1.54184	45	30.0	n/a
Omega	39.875	-99.90	-197.24	-57.68	27.86	1.60	68	24.00	1.54184	45	30.0	n/a
Omega	39.875	44.78	-38.43	75.16	69.29	1.60	55	24.00	1.54184	45	30.0	n/a
Phi	39.875	85.61	-280.32	0.00	-58.06	1.60	225	24.00	1.54184	45	30.0	n/a
Omega	39.875	-97.67	-103.69	-113.67	-56.62	1.60	74	24.00	1.54184	45	30.0	n/a
Omega	39.875	39.67	-326.19	90.00	-54.74	1.60	73	24.00	1.54184	45	30.0	n/a
Omega	39.875	-94.23	-62.72	37.64	-80.63	1.60	62	24.00	1.54184	45	30.0	n/a
Omega	39.875	39.67	-326.19	0.00	-54.74	1.60	73	24.00	1.54184	45	30.0	n/a
Omega	39.875	-100.72	-200.75	42.15	34.55	1.60	68	24.00	1.54184	45	30.0	n/a
Omega	39.875	39.67	-326.19	180.00	-54.74	1.60	73	24.00	1.54184	45	30.0	n/a
Omega	39.875	-96.19	-196.73	-227.77	35.95	1.60	68	24.00	1.54184	45	30.0	n/a
Omega	39.875	-100.83	-106.04	47.01	-58.93	1.60	74	24.00	1.54184	45	30.0	n/a
Omega	39.875	82.64	-36.62	-58.22	77.11	1.60	63	24.00	1.54184	45	30.0	n/a
Omega	39.875	-100.85	-110.62	134.78	-31.95	1.60	68	24.00	1.54184	45	30.0	n/a
Omega	39.875	-99.90	-202.81	-86.05	40.42	1.60	69	24.00	1.54184	45	30.0	n/a
Omega	39.875	-101.52	-208.03	75.65	46.31	1.60	71	24.00	1.54184	45	30.0	n/a
Omega	39.875	-100.86	-210.38	-164.63	52.92	1.60	72	24.00	1.54184	45	30.0	n/a
Omega	39.875	69.67	-296.19	0.00	-54.74	1.60	73	24.00	1.54184	45	30.0	n/a
Omega	39.875	-100.21	-75.75	-33.75	-65.22	1.60	58	24.00	1.54184	45	30.0	n/a
Omega	39.875	69.67	-296.19	90.00	-54.74	1.60	73	24.00	1.54184	45	30.0	n/a
Phi	39.875	70.61	-295.32	0.00	-58.06	1.60	225	24.00	1.54184	45	30.0	n/a
Omega	39.875	-91.39	-190.44	-37.93	31.98	1.60	68	24.00	1.54184	45	30.0	n/a
Omega	39.875	93.00	-382.07	7.02	62.00	1.60	75	24.00	1.54184	45	30.0	n/a
Omega	39.875	-98.85	-106.83	44.61	-38.97	1.60	69	24.00	1.54184	45	30.0	n/a
Omega	39.875	-2.62	-113.72	270.00	54.74	1.60	73	24.00	1.54184	45	30.0	n/a

Axis	dx/mm	2θ/°	ω/°	ϕ/°	χ/°	Width/°	Fra-mes	Time/s	Wave-length/Å	Volta-ge/kV	Current/mA	Tempe-rature/K
Omega	39.875	84.67	-281.19	180.00	-54.74	1.60	73	24.00	1.54184	45	30.0	n/a
Omega	39.875	84.67	-281.19	0.00	-54.74	1.60	73	24.00	1.54184	45	30.0	n/a
Omega	39.875	54.67	-311.19	270.00	-54.74	1.60	73	24.00	1.54184	45	30.0	n/a
Omega	39.875	-99.76	-110.47	-109.53	-29.62	1.60	68	24.00	1.54184	45	30.0	n/a
Omega	39.875	54.67	-311.19	90.00	-54.74	1.60	73	24.00	1.54184	45	30.0	n/a
Omega	39.875	54.67	-311.19	180.00	-54.74	1.60	73	24.00	1.54184	45	30.0	n/a
Omega	39.875	54.67	-311.19	0.00	-54.74	1.60	73	24.00	1.54184	45	30.0	n/a
Omega	39.875	84.67	-281.19	90.00	-54.74	1.60	73	24.00	1.54184	45	30.0	n/a
Omega	39.875	87.22	-37.01	-42.42	81.01	1.60	62	24.00	1.54184	45	30.0	n/a
Omega	39.875	84.67	-281.19	270.00	-54.74	1.60	73	24.00	1.54184	45	30.0	n/a
Phi	39.875	55.61	49.69	0.00	-58.06	1.60	225	24.00	1.54184	45	30.0	n/a
Omega	39.875	27.38	-337.68	-105.00	-54.74	1.60	72	24.00	1.54184	45	30.0	n/a
Phi	39.875	-18.13	-3.92	0.00	23.00	1.60	225	24.00	1.54184	45	30.0	n/a
Omega	39.875	69.67	-296.19	270.00	-54.74	1.60	73	24.00	1.54184	45	30.0	n/a
Omega	39.875	91.50	-381.45	-46.60	58.28	1.60	74	24.00	1.54184	45	30.0	n/a
Phi	39.875	43.16	28.95	0.00	-23.00	1.60	225	24.00	1.54184	45	30.0	n/a
Phi	39.875	-18.13	-12.20	0.00	58.06	1.60	225	24.00	1.54184	45	30.0	n/a
Omega	39.875	27.38	-337.68	-156.00	-54.74	1.60	72	24.00	1.54184	45	30.0	n/a
Omega	39.875	27.38	-337.68	-54.00	-54.74	1.60	72	24.00	1.54184	45	30.0	n/a
Omega	39.875	91.71	-373.51	-178.35	44.85	1.60	70	24.00	1.54184	45	30.0	n/a
Omega	39.875	69.67	-296.19	180.00	-54.74	1.60	73	24.00	1.54184	45	30.0	n/a
Omega	39.875	93.00	-366.21	62.22	32.38	1.60	68	24.00	1.54184	45	30.0	n/a
Phi	39.875	40.61	34.69	0.00	-58.06	1.60	225	24.00	1.54184	45	30.0	n/a
Omega	39.875	27.38	-337.68	0.00	-54.74	1.60	72	24.00	1.54184	45	30.0	n/a
Omega	39.875	27.38	-337.68	153.00	-54.74	1.60	72	24.00	1.54184	45	30.0	n/a
Phi	39.875	43.16	37.23	0.00	-58.06	1.60	225	24.00	1.54184	45	30.0	n/a
Omega	39.875	-81.15	-181.41	-167.12	35.16	1.60	68	24.00	1.54184	45	30.0	n/a

Axis	dx/mm	2θ/°	ω/°	ϕ/°	χ/°	Width/°	Fra-mes	Time/s	Wave-length/Å	Volta-ge/kV	Current/mA	Tempe-rature/K
Omega	39.875	27.38	-337.68	51.00	-54.74	1.60	72	24.00	1.54184	45	30.0	n/a
Omega	39.875	-2.62	-113.72	0.00	54.74	1.60	73	24.00	1.54184	45	30.0	n/a
Omega	39.875	27.38	-337.68	102.00	-54.74	1.60	72	24.00	1.54184	45	30.0	n/a
Omega	39.875	-2.62	-113.72	90.00	54.74	1.60	73	24.00	1.54184	45	30.0	n/a
Omega	39.875	-2.62	-113.72	180.00	54.74	1.60	73	24.00	1.54184	45	30.0	n/a
Omega	39.875	12.38	-353.48	0.00	-54.74	1.60	73	24.00	1.54184	45	30.0	n/a

A total of 5680 frames were collected. The total exposure time was 37.87 hours. The frames were integrated with the Bruker SAINT software package using a narrow-frame algorithm. The integration of the data using a monoclinic unit cell yielded a total of 45603 reflections to a maximum θ angle of 66.19° (0.84 Å resolution), of which 3201 were independent (average redundancy 14.246, completeness = 91.9%, Rint = 14.21%, Rsig = 12.25%) and 1257 (39.27%) were greater than 2σ(F2). The final cell constants of a = 11.3428(5) Å, b = 20.3876(9) Å, c = 8.5895(4) Å, β = 93.145(3)°, volume = 1983.35(15) Å3, are based upon the refinement of the XYZ-centroids of 7323 reflections above 20 σ(I) with 7.806° < 2θ < 111.6°. Data were corrected for absorption effects using the multi-scan method (SADABS). The ratio of minimum to maximum apparent transmission was 0.772. The calculated minimum and maximum transmission coefficients (based on crystal size) are 0.5960 and 0.9220.

The structure was solved and refined using the Bruker SHELXTL Software Package, using the space group P 1 21/c 1, with Z = 4 for the formula unit, $C_{23}H_{21}NO_7$. The final anisotropic full-matrix least-squares refinement on F2 with 283 variables converged at R1 = 7.38%, for the observed data and wR2 = 23.70% for all data. The goodness-of-fit was 0.989. The largest peak in the final difference electron density synthesis was 0.273 e-/Å3 and the largest hole was -0.257 e-/Å3 with an RMS deviation of 0.060 e-/Å3. On the basis of the final model, the calculated density was 1.418 g/cm3 and F(000), 888 e-.

Table S12. Sample and crystal data for **13**.

Identification code	KVy0615_10	
Chemical formula	$C_{23}H_{21}NO_7$	
Formula weight	423.41 g/mol	
Temperature	296(2) K	
Wavelength	1.54178 Å	
Crystal size	0.093 x 0.118 x 0.654 mm	
Crystal habit	red needle	
Crystal system	monoclinic	
Space group	P 1 21/c 1	
Unit cell dimensions	a = 11.3428(5) Å	α = 90°
	b = 20.3876(9) Å	β = 93.145(3)°
	c = 8.5895(4) Å	γ = 90°
Volume	1983.35(15) Å3	
Z	4	
Density (calculated)	1.418 g/cm3	
Absorption coefficient	0.884 mm-1	
F(000)	888	

Table S13. Data collection and structure refinement for **13**.

Theta range for data collection	3.90 to 66.19°
Index ranges	-12<=h<=12, -22<=k<=23, -9<=l<=9
Reflections collected	45603
Independent reflections	3201 [R(int) = 0.1421]
Coverage of independent reflections	91.9%

Absorption correction	multi-scan	
Max. and min. transmission	0.9220 and 0.5960	
Structure solution technique	direct methods	
Structure solution program	SHELXL-2014 (Sheldrick, 2014)	
Refinement method	Full-matrix least-squares on F2	
Refinement program	SHELXL-2014 (Sheldrick, 2014)	
Function minimized	Σ w(Fo2 - Fc2)2	
Data / restraints / parameters	3201 / 0 / 283	
Goodness-of-fit on F2	0.989	
Δ/σmax	0.006	
Final R indices	1257 data; I>2σ(I)	R1 = 0.0738, wR2 = 0.1727
	all data	R1 = 0.2244, wR2 = 0.2370
Weighting scheme	w=1/[σ2(Fo2)+(0.0977P)2+1.3622P] where P=(Fo2+2Fc2)/3	
Extinction coefficient	0.0002(1)	
Largest diff. peak and hole	0.273 and -0.257 eÅ-3	
R.M.S. deviation from mean	0.060 eÅ-3	

Table S14. Atomic coordinates and equivalent isotropic atomic displacement parameters (Å2) for **13**. U(eq) is defined as one third of the trace of the orthogonalized Uij tensor.

	x/a	y/b	z/c	U(eq)
N1	0.0470(4)	0.3526(2)	0.3296(5)	0.0535(13)
O1	0.8548(3)	0.15605(17)	0.1646(4)	0.0513(10)
O2	0.7813(3)	0.06119(18)	0.0827(4)	0.0723(13)
O3	0.6111(3)	0.25900(14)	0.8953(4)	0.0442(9)
O4	0.5256(3)	0.37712(17)	0.8099(5)	0.0805(14)
O5	0.3723(3)	0.37069(16)	0.6370(4)	0.0668(12)
O6	0.3440(4)	0.15007(18)	0.6299(5)	0.0871(15)
O7	0.4453(3)	0.06125(17)	0.6947(4)	0.0679(12)
C1	0.0523(5)	0.4238(3)	0.3430(7)	0.0765(19)
C2	0.9991(6)	0.4567(3)	0.2021(8)	0.097(2)
C3	0.8758(5)	0.4335(3)	0.1653(7)	0.0699(18)
C4	0.8695(4)	0.3599(2)	0.1623(6)	0.0457(14)
C5	0.9545(4)	0.3217(3)	0.2509(6)	0.0421(13)
C6	0.9487(4)	0.2528(3)	0.2506(6)	0.0413(13)
C7	0.0401(4)	0.2123(2)	0.3416(6)	0.0513(15)
C8	0.1558(4)	0.2492(3)	0.3616(7)	0.0655(17)
C9	0.1351(5)	0.3165(3)	0.4257(7)	0.0669(18)
C10	0.7817(4)	0.3281(2)	0.0759(6)	0.0458(14)
C11	0.7731(4)	0.2596(2)	0.0732(6)	0.0390(13)
C12	0.8576(4)	0.2240(2)	0.1620(6)	0.0423(14)
C13	0.6902(4)	0.2230(3)	0.9827(5)	0.0373(13)
C14	0.6871(4)	0.1562(2)	0.9792(6)	0.0420(14)

	x/a	y/b	z/c	U(eq)
C15	0.7727(4)	0.1203(3)	0.0748(6)	0.0493(15)
C16	0.5999(4)	0.1252(2)	0.8818(6)	0.0462(14)
C17	0.5200(4)	0.1599(2)	0.7928(6)	0.0410(13)
C18	0.5235(4)	0.2310(2)	0.7979(6)	0.0386(14)
C19	0.4527(4)	0.2732(2)	0.7190(6)	0.0436(14)
C20	0.4593(5)	0.3437(3)	0.7318(6)	0.0500(15)
C21	0.3689(5)	0.4415(3)	0.6327(7)	0.089(2)
C22	0.4273(5)	0.1257(3)	0.6972(7)	0.0514(15)
C23	0.3583(5)	0.0224(2)	0.6063(7)	0.0743(19)

Table S15. Bond lengths (Å) for **13**.

N1-C5	1.369(6)	N1-C1	1.457(6)
N1-C9	1.460(6)	O1-C15	1.384(5)
O1-C12	1.385(5)	O2-C15	1.210(5)
O3-C13	1.354(5)	O3-C18	1.387(5)
O4-C20	1.194(5)	O5-C20	1.360(5)
O5-C21	1.444(6)	O6-C22	1.190(5)
O7-C22	1.330(5)	O7-C23	1.447(5)
C1-C2	1.483(7)	C1-H1A	0.97
C1-H1B	0.97	C2-C3	1.494(7)
C2-H2A	0.97	C2-H2B	0.97
C3-C4	1.504(6)	C3-H3A	0.97
C3-H3B	0.97	C4-C10	1.372(6)
C4-C5	1.426(6)	C5-C6	1.406(6)
C6-C12	1.381(6)	C6-C7	1.509(6)
C7-C8	1.514(6)	C7-H7A	0.97
C7-H7B	0.97	C8-C9	1.502(7)
C8-H8A	0.97	C8-H8B	0.97
C9-H9A	0.97	C9-H9B	0.97
C10-C11	1.400(6)	C10-H10	0.93
C11-C12	1.396(6)	C11-C13	1.402(6)
C13-C14	1.363(6)	C14-C16	1.409(6)
C14-C15	1.437(6)	C16-C17	1.353(6)
C16-H16	0.93	C17-C18	1.450(6)
C17-C22	1.474(7)	C18-C19	1.336(6)
C19-C20	1.443(6)	C19-H19	0.93
C21-H21A	0.96	C21-H21B	0.96
C21-H21C	0.96	C23-H23A	0.96
C23-H23B	0.96	C23-H23C	0.96

Table S16. Bond angles (°) for **13**.

C5-N1-C1	121.6(5)	C5-N1-C9	122.0(5)
C1-N1-C9	115.7(5)	C15-O1-C12	122.2(4)

C13-O3-C18	122.8(4)	C20-O5-C21	115.9(4)
C22-O7-C23	116.7(4)	N1-C1-C2	111.9(5)
N1-C1-H1A	109.2	C2-C1-H1A	109.2
N1-C1-H1B	109.2	C2-C1-H1B	109.2
H1A-C1-H1B	107.9	C1-C2-C3	111.3(5)
C1-C2-H2A	109.4	C3-C2-H2A	109.4
C1-C2-H2B	109.4	C3-C2-H2B	109.4
H2A-C2-H2B	108.0	C2-C3-C4	111.2(5)
C2-C3-H3A	109.4	C4-C3-H3A	109.4
C2-C3-H3B	109.4	C4-C3-H3B	109.4
H3A-C3-H3B	108.0	C10-C4-C5	118.8(5)
C10-C4-C3	120.8(5)	C5-C4-C3	120.4(5)
N1-C5-C6	119.6(5)	N1-C5-C4	119.3(5)
C6-C5-C4	120.9(5)	C12-C6-C5	117.4(5)
C12-C6-C7	121.6(5)	C5-C6-C7	121.0(5)
C6-C7-C8	110.7(4)	C6-C7-H7A	109.5
C8-C7-H7A	109.5	C6-C7-H7B	109.5
C8-C7-H7B	109.5	H7A-C7-H7B	108.1
C9-C8-C7	110.0(5)	C9-C8-H8A	109.7
C7-C8-H8A	109.7	C9-C8-H8B	109.7
C7-C8-H8B	109.7	H8A-C8-H8B	108.2
N1-C9-C8	111.7(4)	N1-C9-H9A	109.3
C8-C9-H9A	109.3	N1-C9-H9B	109.3
C8-C9-H9B	109.3	H9A-C9-H9B	107.9
C4-C10-C11	121.8(5)	C4-C10-H10	119.1
C11-C10-H10	119.1	C12-C11-C10	117.7(5)
C12-C11-C13	116.4(5)	C10-C11-C13	125.8(5)
C6-C12-O1	115.7(5)	C6-C12-C11	123.3(5)
O1-C12-C11	120.9(5)	O3-C13-C14	121.0(4)
O3-C13-C11	114.9(5)	C14-C13-C11	124.1(5)
C13-C14-C16	118.5(4)	C13-C14-C15	118.7(5)
C16-C14-C15	122.8(5)	O2-C15-O1	116.3(5)
O2-C15-C14	126.1(5)	O1-C15-C14	117.6(5)
C17-C16-C14	121.8(4)	C17-C16-H16	119.1
C14-C16-H16	119.1	C16-C17-C18	119.3(5)
C16-C17-C22	120.1(5)	C18-C17-C22	120.5(5)
C19-C18-O3	115.6(4)	C19-C18-C17	127.8(5)
O3-C18-C17	116.6(4)	C18-C19-C20	125.2(5)
C18-C19-H19	117.4	C20-C19-H19	117.4
O4-C20-O5	121.3(5)	O4-C20-C19	129.8(5)
O5-C20-C19	109.0(5)	O5-C21-H21A	109.5
O5-C21-H21B	109.5	H21A-C21-H21B	109.5
O5-C21-H21C	109.5	H21A-C21-H21C	109.5
H21B-C21-H21C	109.5	O6-C22-O7	121.5(5)
O6-C22-C17	126.7(5)	O7-C22-C17	111.8(5)

O7-C23-H23A	109.5	O7-C23-H23B	109.5
H23A-C23-H23B	109.5	O7-C23-H23C	109.5
H23A-C23-H23C	109.5	H23B-C23-H23C	109.5

Table S17. Torsion angles (°) for **13**.

C5-N1-C1-C2	-33.8(7)	C9-N1-C1-C2	155.8(5)
N1-C1-C2-C3	54.5(7)	C1-C2-C3-C4	-50.5(7)
C2-C3-C4-C10	-154.4(5)	C2-C3-C4-C5	26.2(7)
C1-N1-C5-C6	-175.3(5)	C9-N1-C5-C6	-5.6(7)
C1-N1-C5-C4	8.6(7)	C9-N1-C5-C4	178.3(5)
C10-C4-C5-N1	175.8(4)	C3-C4-C5-N1	-4.8(7)
C10-C4-C5-C6	-0.2(7)	C3-C4-C5-C6	179.1(5)
N1-C5-C6-C12	-176.2(4)	C4-C5-C6-C12	-0.2(7)
N1-C5-C6-C7	2.6(7)	C4-C5-C6-C7	178.7(4)
C12-C6-C7-C8	152.5(5)	C5-C6-C7-C8	-26.3(6)
C6-C7-C8-C9	51.4(6)	C5-N1-C9-C8	32.4(7)
C1-N1-C9-C8	-157.3(5)	C7-C8-C9-N1	-54.8(6)
C5-C4-C10-C11	0.4(7)	C3-C4-C10-C11	-179.0(5)
C4-C10-C11-C12	-0.1(7)	C4-C10-C11-C13	-176.7(5)
C5-C6-C12-O1	179.9(4)	C7-C6-C12-O1	1.1(7)
C5-C6-C12-C11	0.5(7)	C7-C6-C12-C11	-178.3(4)
C15-O1-C12-C6	-176.4(4)	C15-O1-C12-C11	3.1(7)
C10-C11-C12-C6	-0.4(7)	C13-C11-C12-C6	176.5(4)
C10-C11-C12-O1	-179.8(4)	C13-C11-C12-O1	-2.9(7)
C18-O3-C13-C14	-0.2(7)	C18-O3-C13-C11	179.4(4)
C12-C11-C13-O3	-178.6(4)	C10-C11-C13-O3	-1.9(7)
C12-C11-C13-C14	1.0(7)	C10-C11-C13-C14	177.7(5)
O3-C13-C14-C16	0.3(7)	C11-C13-C14-C16	-179.3(4)
O3-C13-C14-C15	-179.7(4)	C11-C13-C14-C15	0.7(8)
C12-O1-C15-O2	177.6(4)	C12-O1-C15-C14	-1.2(7)
C13-C14-C15-O2	-179.3(5)	C16-C14-C15-O2	0.7(8)
C13-C14-C15-O1	-0.6(7)	C16-C14-C15-O1	179.4(4)
C13-C14-C16-C17	0.0(7)	C15-C14-C16-C17	180.0(5)
C14-C16-C17-C18	-0.3(7)	C14-C16-C17-C22	-177.6(5)
C13-O3-C18-C19	-179.8(4)	C13-O3-C18-C17	-0.1(6)
C16-C17-C18-C19	180.0(5)	C22-C17-C18-C19	-2.7(8)
C16-C17-C18-O3	0.4(7)	C22-C17-C18-O3	177.7(4)
O3-C18-C19-C20	-1.8(7)	C17-C18-C19-C20	178.6(5)
C21-O5-C20-O4	2.4(8)	C21-O5-C20-C19	-178.2(4)
C18-C19-C20-O4	0.5(9)	C18-C19-C20-O5	-178.9(5)
C23-O7-C22-O6	-0.1(8)	C23-O7-C22-C17	178.9(4)
C16-C17-C22-O6	169.9(6)	C18-C17-C22-O6	-7.4(9)
C16-C17-C22-O7	-9.1(7)	C18-C17-C22-O7	173.6(4)

Table S18. Anisotropic atomic displacement parameters (Å2) for **13**. The anisotropic atomic displacement factor exponent takes the form: -2π2[h2 a*2 U11 + ... + 2 h k a* b* U12]

	U11	U22	U33	U23	U13	U12
N1	0.042(3)	0.062(3)	0.055(3)	-0.005(3)	-0.012(2)	-0.009(3)
O1	0.044(2)	0.051(2)	0.057(2)	0.002(2)	-0.0133(19)	0.0024(19)
O2	0.071(3)	0.039(2)	0.104(3)	0.006(2)	-0.028(2)	0.007(2)
O3	0.036(2)	0.039(2)	0.055(2)	-0.0009(18)	-0.0126(18)	-0.0015(18)
O4	0.082(3)	0.044(3)	0.110(4)	-0.004(2)	-0.047(3)	-0.005(2)
O5	0.061(3)	0.041(2)	0.093(3)	-0.001(2)	-0.035(2)	0.009(2)
O6	0.063(3)	0.053(3)	0.140(4)	-0.019(2)	-0.052(3)	0.008(2)
O7	0.061(3)	0.040(2)	0.098(3)	-0.001(2)	-0.038(2)	-0.007(2)
C1	0.077(5)	0.063(5)	0.086(5)	-0.003(4)	-0.022(4)	-0.024(4)
C2	0.093(5)	0.072(5)	0.119(6)	0.023(4)	-0.048(5)	-0.026(4)
C3	0.061(4)	0.048(4)	0.098(5)	-0.001(3)	-0.020(4)	-0.007(3)
C4	0.038(3)	0.048(3)	0.051(4)	0.001(3)	-0.006(3)	0.004(3)
C5	0.033(3)	0.051(4)	0.043(3)	-0.006(3)	0.005(3)	-0.010(3)
C6	0.031(3)	0.055(4)	0.038(3)	0.003(3)	0.001(3)	0.005(3)
C7	0.040(3)	0.066(4)	0.048(4)	0.007(3)	-0.001(3)	0.004(3)
C8	0.031(3)	0.099(5)	0.065(4)	0.011(4)	-0.014(3)	0.000(3)
C9	0.051(4)	0.086(5)	0.060(4)	-0.003(4)	-0.020(3)	0.001(3)
C10	0.037(3)	0.046(4)	0.053(4)	-0.002(3)	-0.004(3)	0.003(3)
C11	0.028(3)	0.044(3)	0.045(3)	0.001(3)	-0.001(3)	0.003(3)
C12	0.041(4)	0.039(3)	0.047(4)	-0.002(3)	0.004(3)	-0.003(3)
C13	0.025(3)	0.044(3)	0.042(4)	0.005(3)	-0.002(3)	0.004(3)
C14	0.034(3)	0.037(3)	0.054(4)	0.005(3)	-0.004(3)	0.000(3)
C15	0.039(4)	0.048(4)	0.059(4)	-0.002(3)	-0.007(3)	0.001(3)
C16	0.037(3)	0.037(3)	0.064(4)	0.002(3)	-0.001(3)	0.000(3)
C17	0.029(3)	0.042(3)	0.052(4)	-0.002(3)	-0.003(3)	0.002(3)
C18	0.030(3)	0.035(3)	0.050(4)	0.000(3)	-0.001(3)	-0.003(3)
C19	0.035(3)	0.038(3)	0.057(4)	0.000(3)	-0.009(3)	0.000(3)
C20	0.042(4)	0.046(4)	0.061(4)	0.002(3)	-0.007(3)	0.004(3)
C21	0.112(6)	0.039(4)	0.112(6)	-0.003(4)	-0.034(4)	0.022(4)
C22	0.039(4)	0.042(4)	0.072(4)	0.001(3)	-0.008(3)	0.005(3)
C23	0.063(4)	0.044(3)	0.112(5)	-0.010(3)	-0.030(4)	-0.016(3)

Table S19. Hydrogen atomic coordinates and isotropic atomic displacement parameters (Å2) for **13**.

	x/a	y/b	z/c	U(eq)
H1A	1.1340	0.4373	0.3590	0.092
H1B	1.0107	0.4374	0.4333	0.092
H2A	1.0468	0.4478	0.1141	0.116
H2B	0.9987	0.5038	0.2188	0.116
H3A	0.8477	0.4507	0.0647	0.084

	x/a	y/b	z/c	U(eq)
H3B	0.8247	0.4501	0.2432	0.084
H7A	1.0524	0.1715	0.2870	0.062
H7B	1.0118	0.2019	0.4432	0.062
H8A	1.2099	0.2253	0.4322	0.079
H8B	1.1913	0.2528	0.2618	0.079
H9A	1.1087	0.3126	0.5308	0.08
H9B	1.2088	0.3407	0.4308	0.08
H10	0.7263	0.3528	0.0174	0.055
H16	0.5971	0.0796	-0.1213	0.055
H19	0.3946	0.2558	-0.3496	0.052
H21A	0.4479	0.4583	-0.3695	0.134
H21B	0.3329	0.4576	-0.2762	0.134
H21C	0.3237	0.4556	-0.4589	0.134
H23A	0.2900	0.0166	-0.3339	0.112
H23B	0.3913	-0.0197	-0.4163	0.112
H23C	0.3359	0.0445	-0.4895	0.112

Table S20. Hydrogen bond distances (Å) and angles (°) for **13**.

	Donor-H	Acceptor-H	Donor-Acceptor	Angle
C23-H23B...O4	0.96	2.46	3.305(6)	146.6
C19-H19...O6	0.93	2.24	2.882(6)	126.1
C9-H9B...O5	0.97	2.57	3.350(6)	137.8

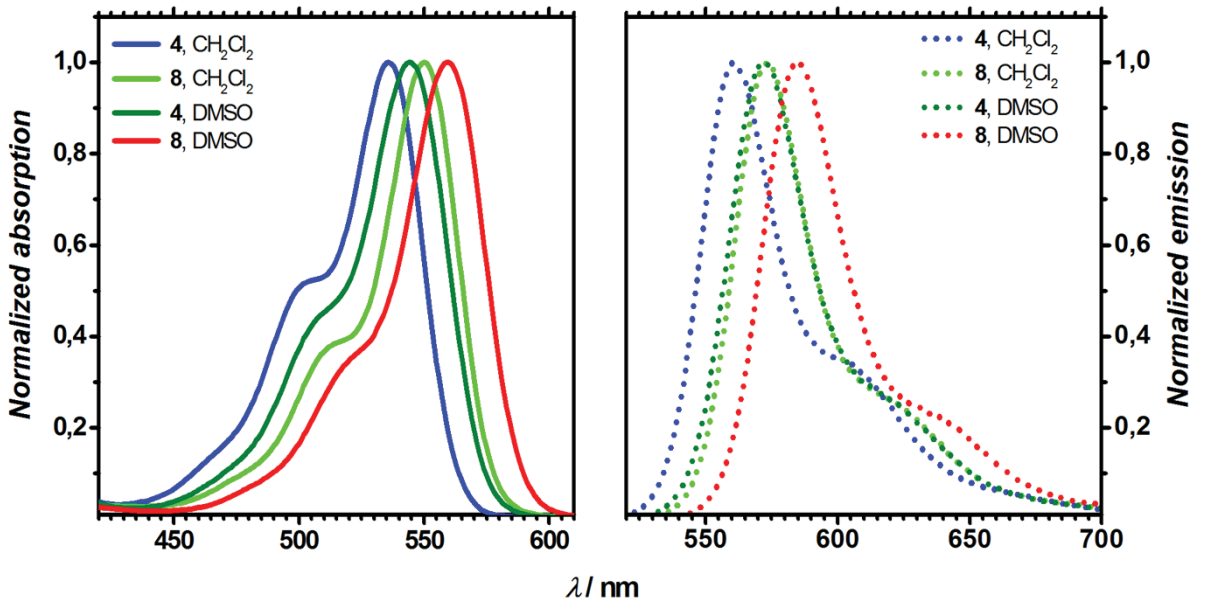

Figure S5. Absorption (solid) and emission (dotted) of compounds **4** and **23** in CH_2Cl_2 and DMSO.

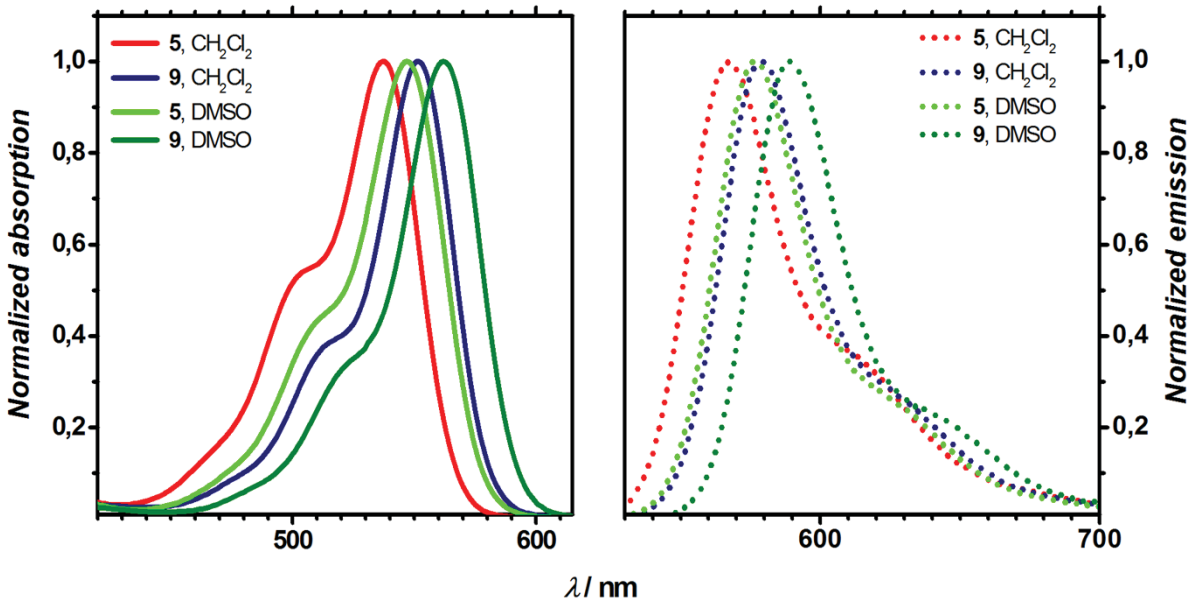

Figure S6. Absorption (solid) and emission (dotted) of compounds **5** and **9** in CH_2Cl_2 and DMSO.

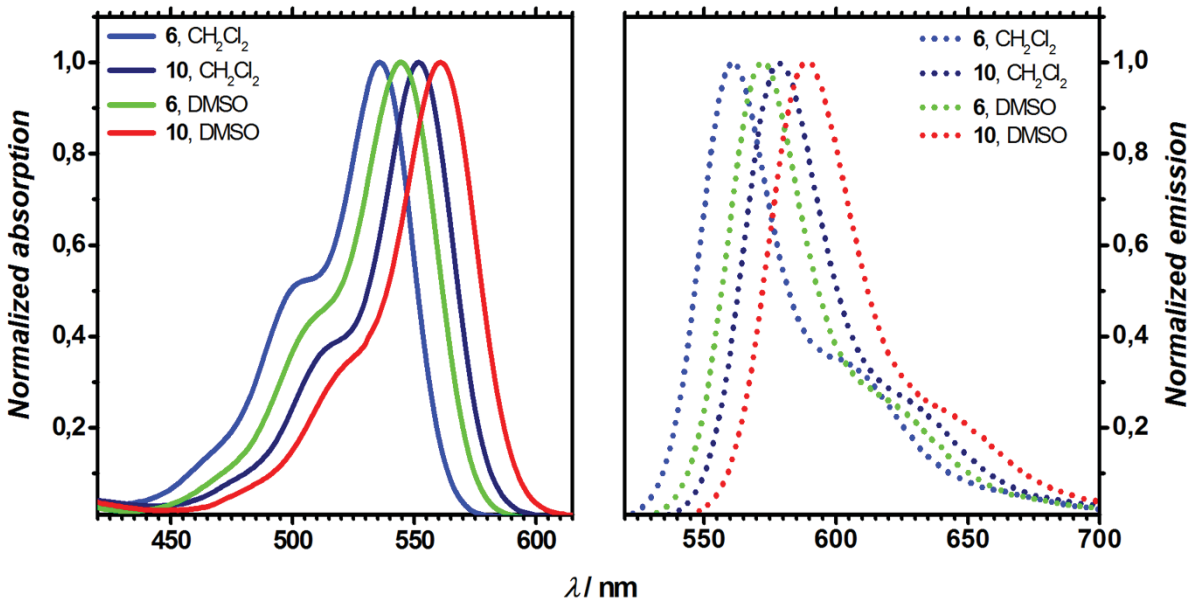

Figure S7. Absorption (solid) and emission (dotted) of compounds **6** and **10** in CH_2Cl_2 and DMSO.

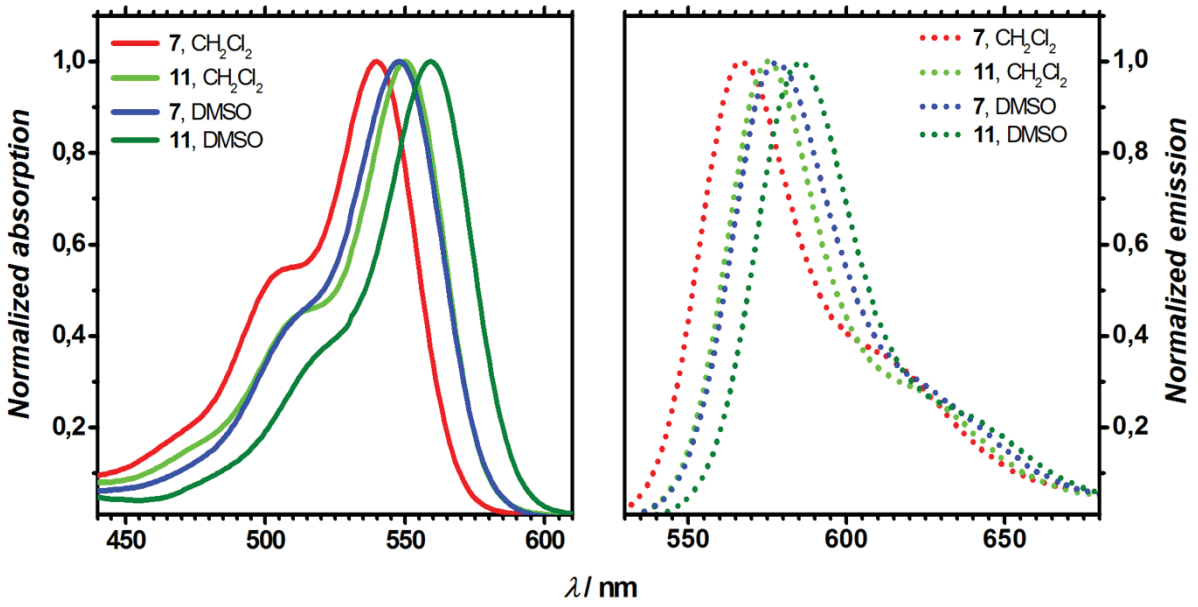

Figure S8. Absorption (solid) and emission (dotted) of compounds **7** and **11** in CH_2Cl_2 and DMSO.

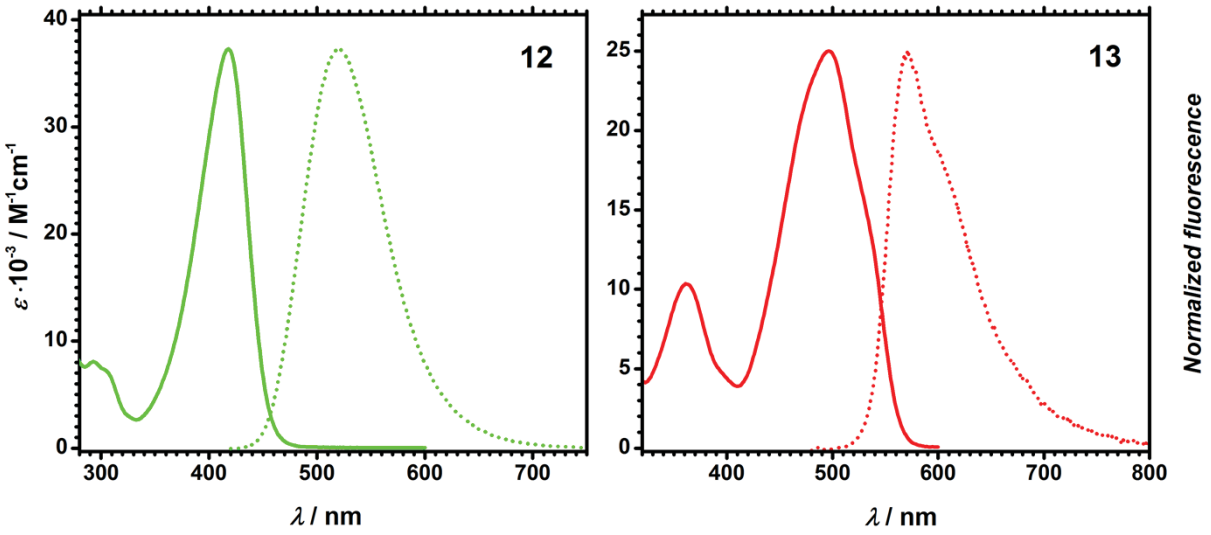

Figure S9. Absorption (solid) and emission (dotted) spectra for compounds **12** (in CH_2Cl_2) and **13** (in DMSO).

Table S21. The spectroscopic properties for compounds **12** and **13**.

Dye	Solvent	λ_{abs}^{max} [nm]	$\varepsilon \cdot 10^{-3}$ [$M^{-1}cm^{-1}$]	λ_{em}^{max} [nm]	$\Delta\bar{\nu}$ [cm^{-1}]	Φ_{fl}
12[a]	CH_2Cl_2	418	37	520	4700	0.73
13	CH_2Cl_2	491	32	–[b]		
	DMSO	497	25	571	2600	0.037

[a] – Compound **12** in DMSO does not show linear dependence of the absorption *vs*. concentration.

[b] – In the fluorescence spectrum compound **13** in CH_2Cl_2 shows emission from two forms.

Photostability measurements

Photostability was determined through the variation in absorption of each sample at the appropriate absorption maximum wavelength (λ_{abs}) with respect to irradiation time. Ethanol was selected as the solvent. Concentrations giving similar optical densities (A ≈ 1) were used. Quartz cells of samples were irradiated with a 300 W Xe lamp (Asahi spectra MAX-350) for 120 min (for compounds **4-7** in DMSO), 50 min (for compounds **8-11** in DMSO) and 30 min for all dyes in DCM at 25 °C equipped with a UV/vis mirror module through a glass fiber. The absorption spectra were measured at appropriate times during the irradiation. **Rhodamine 6G**, **Fluorescein** and **Rdl12**[5] in appropriate solvents were used as references.

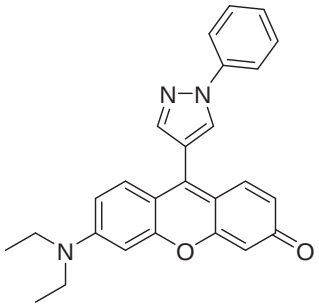

Figure S10. The structure of **Rdl12**.

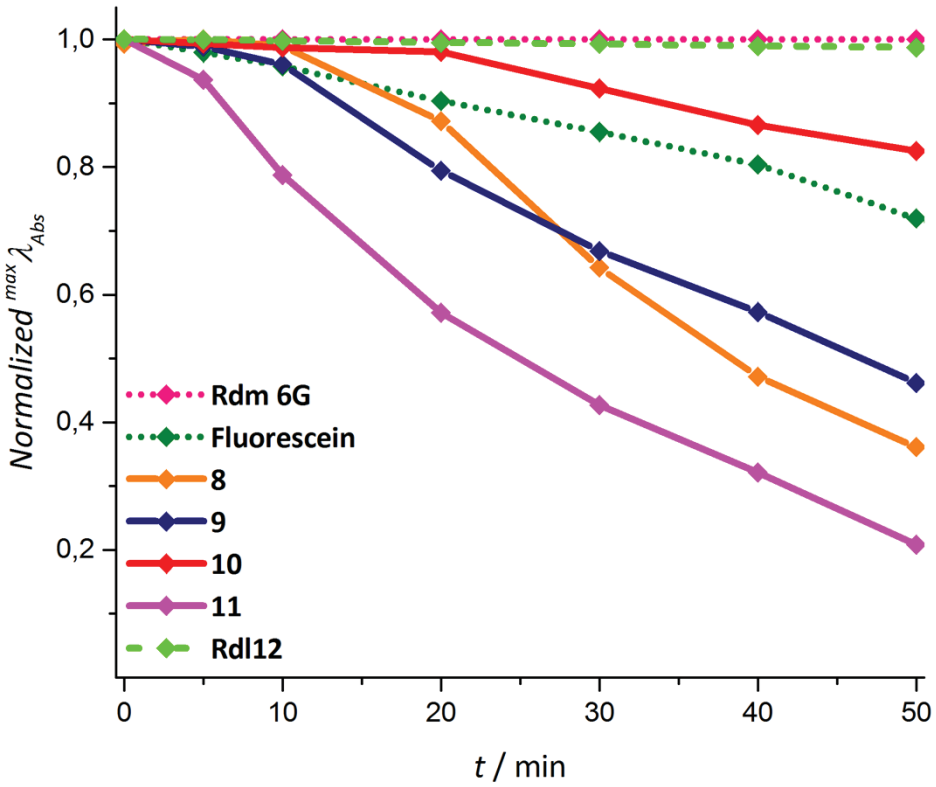

Figure S11. Photostability of rhodols **8-11** compared to the Rhodamine 6G in EtOH, fluorescein in 0,1M NaOH aqueous solution and **Rdl12** measured in DMSO using a collimated light source from a 300W Xe lamp.

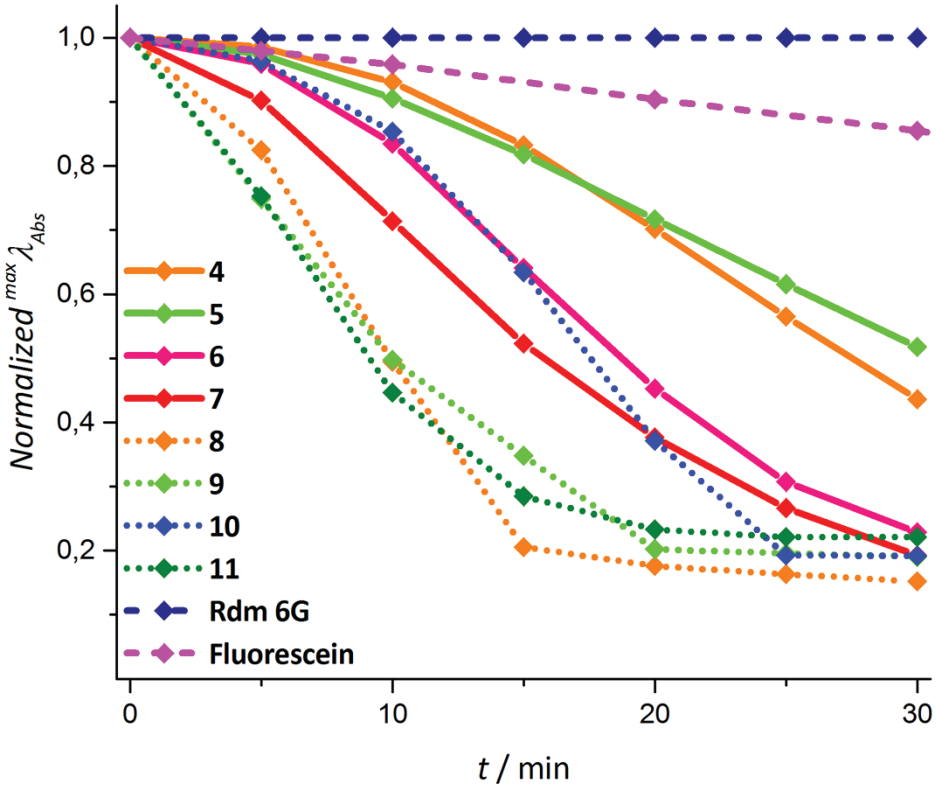

Figure S12. Photostability of rhodols **4-11** compared to the **Rhodamine 6G** in EtOH and **Fluorescein** in 0,1M NaOH aqueous solution measured in CH_2Cl_2 using a collimated light source from a 300W Xe lamp.

Theoretical methods

We have performed the DFT and TD-DFT calculations with the Gaussian 16 code[6] on all dyes. For **4**, we performed a conformational search on the side esters groups and only the most stables ones were latter used. Default Gaussian16 thresholds and algorithms were used but for an improved optimization threshold (10^{-5} au on average residual forces), a stricter self-consistent field convergence criterion (10^{-10} a.u.) and the use of the *ultrafine* DFT integration grid.

Firstly, the S_0 geometries have been optimized with DFT and the vibrational frequencies have been analytically determined, using the M06-2X *meta*-GGA hybrid exchange-correlation functional.[7] These calculations were performed with the 6-311G(d,p) atomic basis set and account for solvent effects through the linear-response PCM approach considering DCM as solvent.[8] Secondly, starting from the optimal ground-state geometries, we have used TD-DFT with the same functional and basis set to optimize the S_1 geometry and compute the vibrational frequencies. All optimized structures correspond to true minima of the potential energy surface. Thirdly, the vertical transition energies were determined with TD-DFT and the same functional, but a larger basis set, namely 6-311+G(2d,p), in gas-phase as well as in solution using the cLR[2] variant of the PCM,[9] in its *non-equilibrium* limit.

As the shortcomings of TD-DFT for cyanine derivatives[10] are known, the obtained transition energies were also computed using COSMO-ADC(2)[11] with the Turbomole 7.3 code.[12] These ADC(2) energies were calculated in gas phase applying the resolution of identity scheme, and using the *aug*-cc-pVDZ atomic basis set.

The vibrationally resolved spectrum were determined with the FCClasses 3 program.[13,14] We used a time-dependent formulation, applied the FC approximation (HT effects were neglected), and selected the so-called *Vertical Gradient*[15] vibronic model for the band topologies on the basis of the TD-DFT data only. We used a simulation temperature of 298K. The obtained stick spectrum were convoluted with Gaussian having HWHM of 300 cm^{-1}. The radiative and internal conversion rates have been obtained using the TVCF formalism.[16] These calculations were made within the time-dependent formulation, the same FC approach and the *Vertical Gradient* model.[15] For the radiative part, we used the same broadening as for the band shapes, i.e., a 300 cm^{-1} Gaussian, but this is known to be not important for the radiative rate.[17] For the IC part, we used a 10 cm^{-1} broadening Lorentzian, which is a typical value in the literature.[17,18]

Additional theoretical data

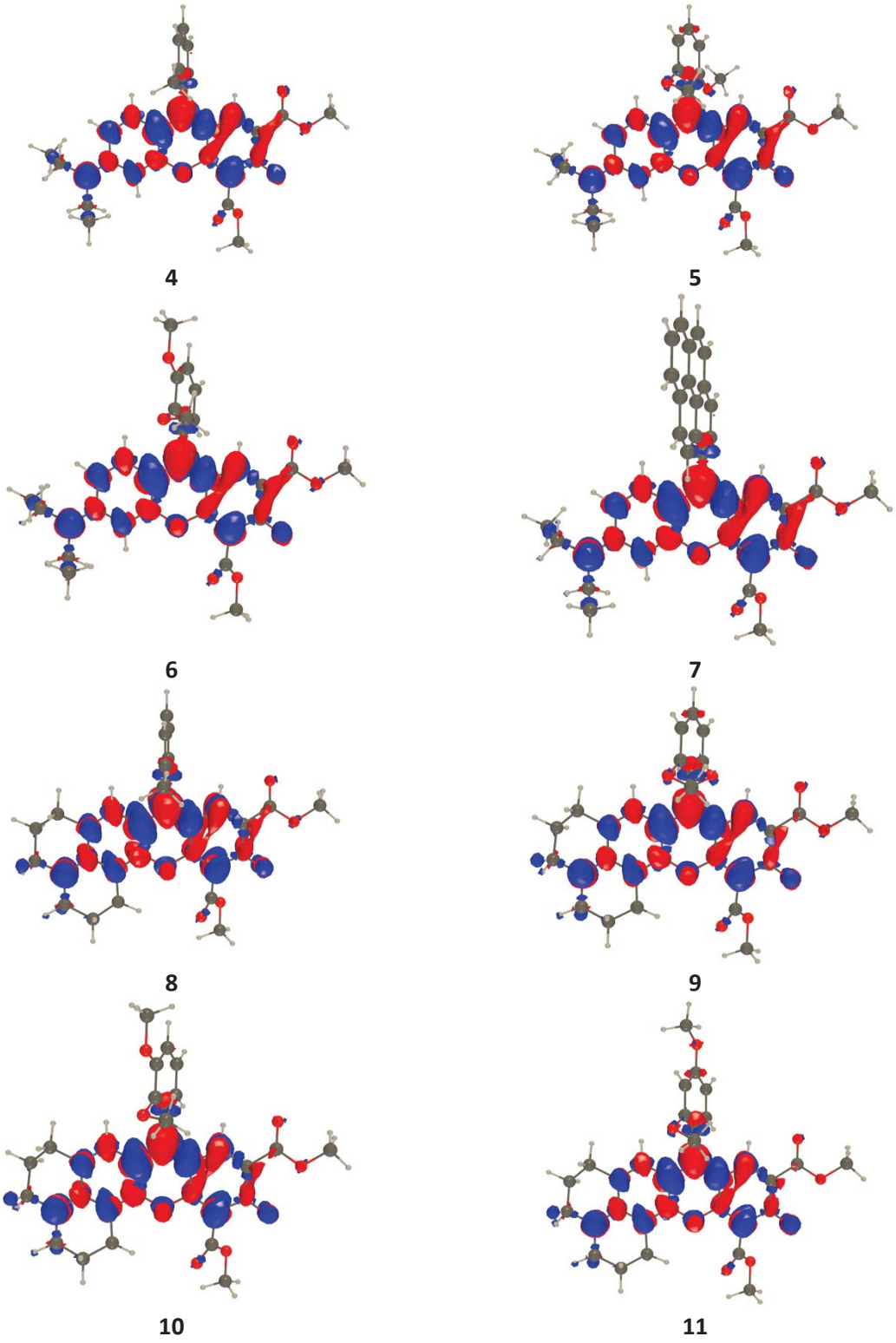

Figure S13. Electron density difference (EDD) plots for the lowest excited states of compounds **4-11**, as obtained with TD-DFT. The blue and red lobes correspond to regions of decrease and increase of electron density respectively. Contour threshold: 0.001 au.

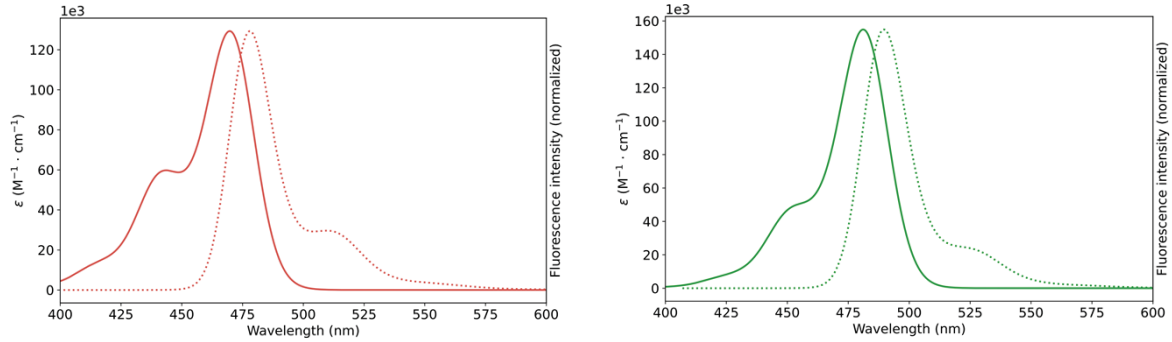

Figure S14. Computed vibrationally-resolved absorption and emission spectra for **4** (left) and **8** (right). The presence of the typical ``cyanine shoulder'' is clear in all cases.

Table S22. Computed vertical absorption, vertical emission, and 0-0 wavelengths with TD-DFT and ADC(2) for rhodols **4-11**. All values are given in nm. We recall here that vertical transition energies cannot be directly compared to experimental λ_{max}, and that, in contrast, 0-0 values can be rigorously to the experimental crossing point between the absorption and fluorescence curves. It can be noted that the experimental values are bracketed by the TD-DFT and ADC(2) estimates, but closer from the latter.

	cLR^2-PCM-TD-DFT			COSMO-ADC(2)		
	$\lambda_{vert\text{-}abso}$	$\lambda_{vert\text{-}fluo}$	$\lambda_{0\text{-}0}$	$\lambda_{vert\text{-}abso}$	$\lambda_{vert\text{-}fluo}$	$\lambda_{0\text{-}0}$
4	440	471	466	562	625	603
5	452	491	479	585	665	640
6	445	480	472	573	643	620
7	443	478	472	570	640	617
8	452	478	477	592	641	622
9	467	496	492	621	681	663
10	456	487	482	601	660	642
11	460	486	485	607	659	640

Table S23. Computed radiative and international conversion rates (10^8 s^{-1}) and deduced quantum yield of emission.

	k_r	k_{ic}	ϕ_f
8	3.44	1.48	0.70
9	2.97	1.65	0.64
10	3.23	1.56	0.67
11	3.22	1.54	0.68

Notes and references

1 L. Yuan, W. Lin, J. Song and Y. Yang, *Chem. Commun.*, 2011, **47**, 12691–12693.

2 G. Yin, T. Niu, T. Yu, Y. Gan, X. Sun, P. Yin, H. Chen, Y. Zhang, H. Li and S. Yao, *Angew. Chem. Int. Ed.*, 2019, **58**, 4557–4561.

3 M. Tasior, Y. M. Poronik, O. Vakuliuk, B. Sadowski, M. Karczewski and D. T. Gryko, *J. Org. Chem.*, 2014, **79**, 8723–8732.

4 L. J. Farrugia, *J. Appl. Crystallogr.*, 2012, **45**, 849–854.

5 Y. M. Poronik, G. Clermont, M. Blanchard-Desce and D. T. Gryko, *J. Org. Chem.*, 2013, **78**, 11721–11732.

6 M. J. Frisch, G. W. Trucks, H. B. Schlegel, G. E. Scuseria, M. A. Robb, J. R. Cheeseman, G. Scalmani, V. Barone, G. A. Petersson, H. Nakatsuji, X. Li, M. Caricato, A. V Marenich, J. Bloino, B. G. Janesko, R. Gomperts, B. Mennucci, H. P. Hratchian, J. V Ortiz, A. F. Izmaylov, J. L. Sonnenberg, D. Williams-Young, F. Ding, F. Lipparini, F. Egidi, J. Goings, B. Peng, A. Petrone, T. Henderson, D. Ranasinghe, V. G. Zakrzewski, J. Gao, N. Rega, G. Zheng, W. Liang, M. Hada, M. Ehara, K. Toyota, R. Fukuda, J. Hasegawa, M. Ishida, T. Nakajima, Y. Honda, O. Kitao, H. Nakai, T. Vreven, K. Throssell, J. A. Montgomery Jr., J. E. Peralta, F. Ogliaro, M. J. Bearpark, J. J. Heyd, E. N. Brothers, K. N. Kudin, V. N. Staroverov, T. A. Keith, R. Kobayashi, J. Normand, K. Raghavachari, A. P. Rendell, J. C. Burant, S. S. Iyengar, J. Tomasi, M. Cossi, J. M. Millam, M. Klene, C. Adamo, R. Cammi, J. W. Ochterski, R. L. Martin, K. Morokuma, O. Farkas, J. B. Foresman and D. J. Fox, *Gaussian 16 Revision A.03*, Gaussian, Inc., Wallingford CT, 2016.

7 Y. Zhao and D. G. Truhlar, *Theor. Chem. Acc.*, 2008, **120**, 215–241.

8 J. Tomasi, B. Mennucci and R. Cammi, *Chem. Rev.*, 2005, **105**, 2999–3093.

9 C. A. Guido, A. Chrayteh, G. Scalmani, B. Mennucci and D. Jacquemin, *J. Chem. Theory Comput.*, 2021, **17**, 5155–5164.

10 B. Le Guennic and D. Jacquemin, *Acc. Chem. Res.*, 2015, **48**, 530–537.

11 A. Dreuw and M. Wormit, *Wiley Interdiscip. Rev. Comput. Mol. Sci.*, 2015, **5**, 82–95.

12 *TURBOMOLE V7.3*, A development of University of Karlsruhe and Forschungszentrum Karlsruhe GmbH, 1989−2007, TURBOMOLE GmbH. http://www.turbomole.com, 2007.

13 J. Cerezo and F. Santoro, *FCClasses 3.0*, http://www.pi.iccom.cnr.it/fcclasses.

14 F. Santoro, R. Improta, A. Lami, J. Bloino and V. Barone, *J. Chem. Phys.*, 2007, **126**, 084509.

15 F. Santoro and D. Jacquemin, *Wiley Interdiscip. Rev. Comput. Mol. Sci.*, 2016, **6**, 460–486.

16 Q. Peng, Y. Yi, Z. Shuai and J. Shao, *J. Chem. Phys.*, 2007, **126**, 114302.

17 A. Humeniuk, M. Bužančić, J. Hoche, J. Cerezo, R. Mitrić, F. Santoro and V. Bonačić-Koutecký, *J. Chem. Phys.*, 2020, **152**, 054107.

18 Q. Ou, Q. Peng and Z. Shuai, *J. Phys. Chem. Lett.*, 2020, **11**, 7790–7797.

Chemistry
A European
Journal

Chemistry Europe
European Chemical Societies Publishing

Accepted Article

Title: A Novel Method for the Synthesis of Merocyanines: New Photophysical Possibilities for a Well-Known Class of Fluorophores

Authors: Brunella Bardi, Katerina V. Vygranenko, Beata Koszarna, Olena Vakuliuk, Łukasz Dobrzycki, Daniel T. Gryko, Francesca Terenziani, and Anna Painelli

To be cited as: *Chem. Eur. J.* **2023**, e202300979

Link to VoR: https://doi.org/10.1002/chem.202300979

WILEY VCH

A novel method for the programmed synthesis of merocyanines: unprecedented photophysical possibilities for a well-known class of fluorophores

Brunella Bardi,[a†] Kateryna V. Vygranenko,[b†] Beata Koszarna,[b] Olena Vakuliuk,[b] Łukasz Dobrzycki,[c] Daniel T. Gryko,[b*] Francesca Terenziani [a*] and Anna Painelli [a]

[a]*Department of Chemistry, Life Sciences and Environmental Sustainability, University of Parma, Parco Area delle Scienze 17/a, 43124 Parma, Italy*

[b]*Institute of Organic Chemistry Polish Academy of Sciences, Warsaw, Poland*

[c]*Faculty of Chemistry, University of Warsaw, Żwirki i Wigury 101, 02-089 Warsaw, Poland*

SUPPORTING INFORMATION

1. Experimental details

1.1. Synthesis

All chemicals were used as received unless otherwise noted. All reported ^{1}H and ^{13}C NMR spectra were collected using 500 MHz and 600 MHz spectrometers. Chemical shifts (δ ppm) were determined with TMS as the internal reference; *J* values are given in Hz. Chromatography was performed on silica gel (230-400 mesh). Thin layer chromatography (TLC) was carried out using Merck PLC Silica gel 60 F_{254} 1 mm plates. The mass spectra were obtained via electron ionization (EI-MS) or electrospray ionization (ESI-MS).

1.1.1 Experimental part

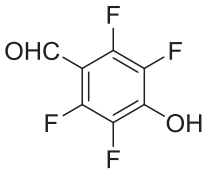

2

2,3,5,6-Tetrafluoro-4-hydroxybenzaldehyde (**2**): HMTA (1.1 eq, 0.165 mol, 23.1 g) was slowly added to the solution of 2,3,5,6-tetrafluorophenol (0.15 mol, 24.9 g) in TFA (120 mL) (exothermic reaction). The mixture was stirred under argon at 100 °C overnight. Subsequently 10% HCl_{aq} (150 mL) was added and the reaction mixture was stirred at 100 °C for another 1 h. The solution was cooled to room temperature, diluted with H_2O, and extracted with EtOAc (150 mL x 2) and $CHCl_3$ (150 mL x 1). The organic fractions were collected, dried over Na_2SO_4, and solvents were removed under reduced pressure. The product was purified using column chromatography (silica, hexane/EtOAc, 2:1 and then 1:1) and recrystallized from cold hexane to obtain the pure product (21 g, 72 %) as off-white crystals. ^{1}H NMR (500 MHz, DMSO) δ 10.1 (s, 1H). Spectroscopic properties are in agreement with the literature data.[1]

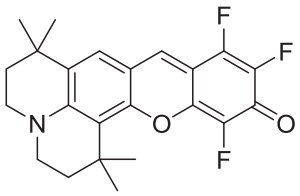

4

Rhodol **4**: A solution of 2,3,5,6-tetrafluoro-4-hydroxybenzaldehyde (**2**, 1 mmol, 194 mg) and 8-hydroxy-1,1,7,7-tetramethyljulolidine (1 mmol, 245 mg) in toluene (30 ml) was stirred under argon at 90 °C overnight. The solution was cooled to room temperature and the precipitate was filtered and washed with toluene. The crude product was crystallized from Et_2O to give the pure product (333 mg, 83 %) as violet crystals. M.p. 235 – 236 °C (from Et_2O).

^{1}H NMR (500 MHz, $CDCl_3$) δ 8.02 (d, *J* = 1.5 Hz, 1H), 7.28 (s, 1H), 3.59 - 3.48 (m, 2H), 3.45 - 3.39 (m, 2H), 1.93 - 1.84 (m, 2H), 1.83 - 1.75 (m, 2H), 1.58 (s, 6H), 1.34 (s, 6H). ^{13}C NMR (126 MHz, $CDCl_3$) δ 165.5 (dd, *J* = 11.9; 6.0 Hz), 152.0, 149.3, 144.3 (dd, *J* = 259.4; 12.3 Hz), 141.7 (dt, *J* = 253.2; 7.3 Hz), 139.0 (dd, *J* = 241.9; 6.7 Hz), 139.0 (t, *J* = 9.3 Hz), 135.9 (m), 130.8, 125.5, 114.8, 110.5, 103.5 (d, *J* = 20.0 Hz), 47.9, 47.5, 38.5, 34.7,

32.3, 32.2, 29.7, 28.2. ^{19}F NMR (470 MHz, $CDCl_3$) δ -153.4 (dd, *J* = 17.6, 5.4 Hz), -160.0 (dd, *J* = 17.7, 14.5 Hz), -168.3 (dd, *J* = 14.0, 5.4 Hz). HRMS (ESI) calc. for $C_{23}H_{23}NO_3F_3$ 402.1681 $[M + H]^+$, found 402.1679.

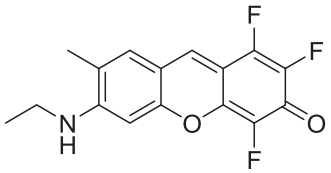

11

Rhodol **11**: 3-Ethylamino-*p*-cresol (2 mmol, 302 mg), 2,3,5,6-tetrafluoro-4-hydroxybenzaldehyde (2 mmol, 388 mg) and xylene (35 mL) were placed in a sealed tube. The resulting mixture was stirred under Ar at 135 °C for 1 h. After cooling to RT, the precipitate was filtered and washed with Et_2O. Recrystallization of crude product with MeOH/Et_2O gave dark purple solid (188 mg, 31 %). M.p. 283 – 285 °C.

^{1}H NMR (500 MHz, pyridine-d_5) δ 8.17 (s, 1H), 7.39 – 7.35 (m, 1H), 7.32 (s, 1H), 6.79 (s, 1H), 3.39 (p, *J* = 7.0 Hz, 2H), 2.22 (s, 3H), 1.23 (t, *J* = 7.2 Hz, 3H). ^{13}C NMR (126 MHz, pyridine-d_5) δ 165.5 (dd, *J* = 17.6; 6.3 Hz), 155.6, 155.0, 145.1 (dd, *J* = 258.9; 12.0 Hz), 142.1 (dd, *J* = 253.0; 7.4 Hz), 139.9 (t, *J* = 9.1 Hz), 139.5 (dd, *J* = 239.7; 7.1 Hz), 136.3 (m), 131.0, 122.8, 110.2, 104.4 (d, *J* = 20.2 Hz), 95.0, 38.5, 17.5, 14.1. ^{19}F NMR (470 MHz, Pyridine-d_5) δ -152.2 (dd, *J* = 18.1, 5.2 Hz), -157.8 (dd, *J* = 18.0, 13.5 Hz), -166.7 (dd, *J* = 14.2, 5.0 Hz). HRMS (ESI) calc. for $C_{16}H_{13}NO_2F_3$ 308.0898 $[M + H]^+$, found 308.0901.

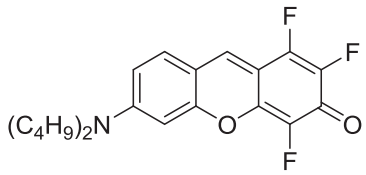

12

Rhodol **12**: A solution of 2,3,5,6-tetrafluoro-4-hydroxybenzaldehyde (**2**, 1 mmol, 194 mg) and *N,N*-di-*n*-butyl-3-aminophenol (1 mmol, 221 mg, 225 µL) in toluene (30 ml) was stirred under argon at 90 °C overnight. The reaction mixture was cooled to room temperature and concentrated under vacuum. The crude product was purified using column chromatography (silica, CH_2Cl_2/MeOH, 98:2) to give the pure product (130 mg, 35 %) as red crystals. M.p. 219 - 220 °C.

^{1}H NMR (500 MHz, $CDCl_3$) δ 8.01 (s, 1H), 7.43 (d, *J* = 9.0 Hz, 1H), 6.72 (dd, *J* = 9.1, 2.4 Hz, 1H), 6.60 (d, *J* = 2.4 Hz, 1H), 3.43 (t, *J* = 7.9 Hz, 4H), 1.70 - 163 (m, 4H), 1.47 – 1.38 (m, 4H), 1.01 (t, *J* = 7.3 Hz, 6H). ^{13}C NMR (126 MHz, $CDCl_3$) δ 166.2 (td, *J* = 16.9, 5.5 Hz), 155.7, 154.2, 144.5 (dd, *J* = 260.7, 12.1 Hz), 141.4 (dt, *J* = 254.8, 7.4 Hz), 139.3 (t, *J* = 8.9 Hz), 138.8 (dd, *J* = 242.4, 6.6 Hz), 135.5 (m), 131.5, 111.5, 109.7, 105.2, 96.8, 51.5, 29.3, 20.2, 13.9. ^{19}F NMR (470 MHz, $CDCl_3$) δ -149.9 (dd, *J* = 17.4, 5.1 Hz), -154.8 (dd, *J* = 17.5, 13.0 Hz), -164.4 (dd, *J* = 12.9, 4.8 Hz). HRMS (ESI) calc. for $C_{21}H_{23}NO_2F_3$ 378.1681 $[M + H]^+$, found 378.1687.

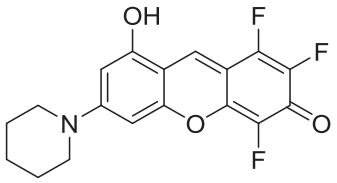

13

Rhodol **13**: A mixture of 2,3,5,6-tetrafluoro-4-hydroxybenzaldehyde (**2**, 1 mmol, 194 mg) and 5-(piperidin-1-yl)benzene-1,3-diol[2] (1 mmol, 193 mg) in xylene (30 ml) was stirred under argon at 160 °C overnight. The resulting precipitate was filtered and washed with boiling MeOH to give the pure product (259 mg, 74 %) as dark red crystals. M.p. > 350 °C.

^{1}H NMR (500 MHz, CF_3COOD) δ 8.84 (s, 1H), 6.77 (s, 1H), 6.70 (s, 1H), 3.84 (br s, 4H), 1.87 (br s, 6H). ^{13}C NMR (126 MHz, CF_3COOD) δ 160.0 (t, *J* = 5.2 Hz), 158.0 (dd, *J* = 186.4, 6.7 Hz), 144.9, 142.9 – 142.5 (m), 139.01 (dd, *J* = 9.6, 8.7 Hz), 138.12 (d, *J* = 8.2 Hz), 137.2, 135.3, 133.1, 104.2, 104.1, 97.0, 92.8, 50.5, 25.9, 23.1. Due to the poor solubility of compound **13** and the complexity of ^{13}C NMR spectrum, it is not possible to assign all signals. ^{19}F NMR (470 MHz, CF_3COOD) δ -146.6 (dd, *J* = 18.5, 11.3 Hz), -161.0 (d, *J* = 18.3 Hz), -162.5 (br d, *J* = 8.2 Hz). HRMS (ESI) calc. for $C_{18}H_{13}NO_3F_3$ 348.0848 $[M-H]^-$, found 348.0843.

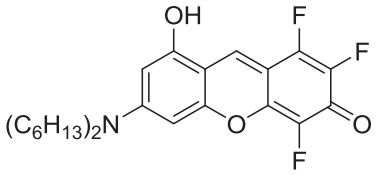

14

Rhodol **14**: A mixture of 2,3,5,6-tetrafluoro-4-hydroxybenzaldehyde (**2**, 1 mmol, 194 mg) and 5-*N,N*-*n*-dihexylamino-benzene-1,3-diol[3] (1 mmol, 293 mg) in xylene (30 ml) was stirred under argon at 160 °C overnight. The resulting precipitate was filtered and recrystallized from CH_2Cl_2/MeOH to give the pure product (392 mg, 87 %) as dark red crystals. M.p. 301 - 303 °C.

^{1}H NMR (500 MHz, DMSO-d_6) δ 11.32 (s, 1H), 8.32 (s, 1H), 6.46 – 6.43 (m, 1H), 6.21 (d, *J* = 1.9 Hz, 1H), 3.43 (t, *J* = 7.8 Hz, 4H), 1.63 – 1.51 (m, 4H), 1.31 (br s, 12H), 0.88 (t, *J* = 6.9 Hz, 6H). ^{13}C NMR (126 MHz, DMSO-d_6) δ 163.3 (td, *J* = 17.2, 4.9 Hz), 157.8, 155.2, 155.1, 145.5, 142.6 (dd, *J* = 230.3; 11.0 Hz), 139.6, 139.2, 139.0 (t, *J* = 8.8 Hz), 137.4, 131.6 (t, *J* = 14.4 Hz), 103.2, 100.1 (d, *J* = 20.1 Hz), 94.2, 90.2, 50.7, 30.9, 26.9, 25.8, 22.0, 13.8. Due to the poor solubility of compound **13** and the complexity of ^{13}C NMR spectrum, it is not possible to assign all signals. ^{19}F NMR (470 MHz, DMSO-d_6) δ -145.9 (dd, *J* = 19.8, 4.8 Hz), -154.3 (dd, *J* = 19.4, 14.6 Hz), -161.0 (dd, *J* = 13.9, 3.2 Hz). HRMS (ESI) calc. for $C_{25}H_{31}NO_3F_3$ 450.2256 $[M + H]^+$, found 450.2257.

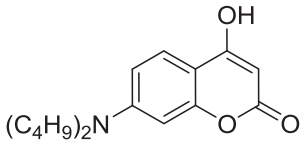

7

7-(Dibutylamino)-4-hydroxy-2H-chromen-2-one **7**: A mixture of *N,N*-di-*n*-butyl-3-aminophenol (**5**, 4.5 mmol, 1 g, 1.02 ml) and bis-(2,4,6-trichlorophenyl)-malonate (5.4 mmol, 2.5 g) in toluene (50 ml) was refluxed under

argon overnight. The reaction mixture was cooled to room temperature and the resulting precipitate was filtered, washed with toluene and pentane to give pure product (0.93 g, 72%) as pale yellow crystals. M.p. 206 – 208 °C.

^{1}H NMR (500 MHz, DMSO-d_6) δ 11.89 (br s, 1H), 7.54 (d, *J* = 9.0 Hz, 1H), 6.64 (dd, *J* = 9.0, 2.4 Hz, 1H), 6.41 (d, *J* = 2.4 Hz, 1H), 5.26 (s, 1H), 3.33 (t, *J* = 7.7 Hz, 4H), 1.56 – 1.47 (m, 4H), 1.33 (h, *J* = 7.4 Hz, 4H), 0.92 (t, *J* = 7.3 Hz, 6H). ^{13}C NMR (126 MHz, DMSO-d_6) δ 166.9, 163.2, 156.5, 151.7, 124.5, 108.7, 103.9, 96.9, 86.5, 50.4, 29.3, 20.0, 14.3. HRMS (ESI) calc. for $C_{17}H_{24}NO_3$ 290.1756 $[M + H]^+$, found 290.1757.

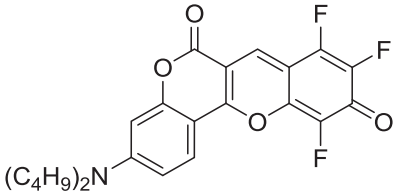

9

Rhodol **9**: A mixture of 2,3,5,6-tetrafluoro-4-hydroxybenzaldehyde (**2**, 1 mmol, 194 mg) and coumarin **7** (1 mmol, 289 mg) in xylene (30 ml) was stirred under argon at 160 °C overnight. The reaction mixture was cooled to room temperature and the resulting precipitate was filtered to give the pure product (361 mg, 81 %) as dark green crystals. M.p. 279 – 280 °C.

^{1}H NMR (600 MHz, $CDCl_3$) δ 8.38 (d, *J* = 1.5 Hz, 1H), 7.92 (d, *J* = 9.2 Hz, 1H), 6.73 (dd, *J* = 9.3, 2.4 Hz, 1H), 6.49 (d, *J* = 2.4 Hz, 1H), 3.45 – 3.40 (m, 4H), 1.69 – 1.61 (m, 4H), 1.42 (h, *J* = 7.4 Hz, 4H), 1.00 (t, *J* = 7.4 Hz, 6H). ^{13}C NMR (151 MHz, $CDCl_3$) δ 160.3, 158.9, 157.1, 154.7, 142.4 (dd, *J* = 260.7, 8.2 Hz), 139.2 (dd, *J* = 250.8, 6.4 Hz), 137.9, 133.4 – 133.3 (m), 125.7, 111.0, 108.4, 108.2, 100.1, 100.0, 97.7, 51.5, 29.3, 20.2, 13.9. Due to the poor solubility of compound **13** and the complexity of ^{13}C NMR spectrum, it is not possible to assign all signals. ^{19}F NMR (470 MHz, $CDCl_3$) -146.96 (dd, *J* = 16.0, 4.2 Hz), -150.29 (dd, *J* = 15.9, 12.9 Hz), -159.60 – -160.22 (m). HRMS (ESI) calc. for $C_{24}H_{23}NO_4F_3$ 446.1579 $[M + H]^+$, found 446.1582.

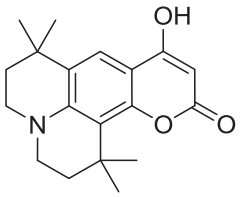

8

9-Hydroxy-1,1,7,7-tetramethyl-2,3,6,7-tetrahydro-1H,5H,11H-pyrano[2,3-*f*]pyrido[3,2,1-*ij*]quinolin-11-one **(8)**: A mixture of 1,1,7,7-tetramethyl-8-hydroxyjulolidine (**6**, 4 mmol, 0.98 g) and bis-(2,4,6-trichlorophenyl)-malonate (4.8 mmol, 2.22 g) in toluene (50 ml) was refluxed under argon overnight. The reaction mixture was cooled to room temperature and the resulting precipitate was filtered, washed with hexane to give pure product (0.48 g, 38 %) as pale yellow crystals. M.p. 178 – 180 °C.

^{1}H NMR (500 MHz, DMSO-d_6) δ 11.76 (bs, 1H), 7.41 (s, 1H), 5.25 (s, 1H), 3.25 (t, *J* = 6.0 Hz, 2H), 3.21 – 3.15 (m, 2H), 1.76 – 1.71 (m, 2H), 1.68 (t, *J* = 6.0 Hz, 2H), 1.43 (s, 6H), 1.23 (s, 6H). ^{13}C NMR (126 MHz, DMSO-d_6) δ 167.1, 162.9, 152.7, 146.0, 127.4, 118.4, 114.4, 104.2, 86.1, 46.9, 46.4, 35.8, 32.3 (2), 31.2, 29.3. HRMS (ESI) calc. for $C_{19}H_{24}NO_3$ 314.1756 $[M + H]^+$, found 314.1762.

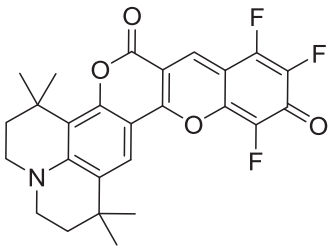

10

Rhodol **(10)**: A mixture of 2,3,5,6-tetrafluoro-4-hydroxybenzaldehyde (**2**, 1 mmol, 194 mg) and coumarin **8** (1 mmol, 313 mg) in xylene (30 ml) was stirred under argon at 160 °C overnight. The reaction mixture was cooled to room temperature, concentrated under vacuum and purified using column chromatography (silica, CH_2Cl_2/Et_2O, 9:1) to give the pure product (240 mg, 51 %) as dark purple crystals. M.p. 304 – 306 °C.

^{1}H NMR (500 MHz, $CDCl_3$) δ 8.37 (d, *J* = 1.1 Hz, 1H), 7.69 (s, 1H), 3.49 (t, *J* = 6.2 Hz, 2H), 3.39 (t, *J* = 5.8 Hz, 2H), 1.87 – 1.83 (m, 2H), 1.79 (t, *J* = 6.2 Hz, 2H), 1.55 (s, 6H), 1.36 (s, 6H). ^{13}C NMR (126 MHz, $CDCl_3$) δ 167.0 (td, *J* = 17.6; 5.8 Hz), 160.2, 158.5, 153.3, 149.9, 144.8 (dd, *J* = 264.4; 12.5 Hz), 142.2 (dt, *J* = 260.0; 7.1 Hz), 139.2 (dd, *J* = 249.2, 6.5 Hz), 138.1 – 137.9 (m), 134.2 – 133.1 (m), 130.4, 118.9, 115.4, 107.3, 107.1, 100.1, 99.5, 48.0, 47.3, 38.5, 34.7, 32.3, 29.6, 28.5. ^{19}F NMR (470 MHz, $CDCl_3$) δ -147.2 (dd, *J* = 16.5, 4.4 Hz), -151.5 (dd, *J* = 16.4, 13.2 Hz), -160.5 (dd, *J* = 13.3, 2.9 Hz). HRMS (ESI) calc. for $C_{26}H_{23}NO_4F_3$ 470.1579 $[M + H]^+$, found 470.1585.

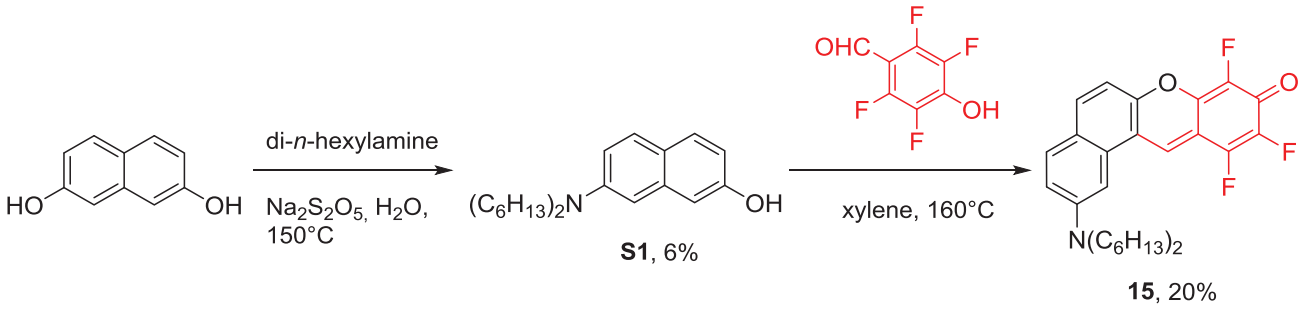

Scheme S1. Synthesis of π-expanded rhodol **15**.

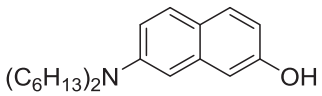

S1

7-(dihexylamino)naphthalen-2-ol **(S1)**: The mixture of 2,7-dihydroxynaphthalene (3.2 g, 20 mmol), *N,N*-di-*n*-hexylamine (40 mmol, 7.4 g, 9.3 ml) and sodium metabisulfite (42 mmol, 8 g) in 120 ml of water was placed in pressure tube and stirred upon heating at 150 °C for 2 hours. The reaction mixture was cooled to room temperature, diluted with 300 ml of water and extracted with DCM (3 x 150 ml). The organic layer was dried over Na_2SO_4 and concentrated under vacuum. The residue was purified using column chromatography (silica, hexane /EtOAc, 4:1) to give pure product (380 mg, 6 %) as colourless oil.

^{1}H NMR (500 MHz, $CDCl_3$) δ 7.58 (d, *J* = 9.0 Hz, 1H), 7.54 (d, *J* = 8.6 Hz, 1H), 6.95 – 6.87 (m, 2H), 6.76 (dd, *J* = 8.7, 2.5 Hz, 1H), 6.66 (d, *J* = 2.6 Hz, 1H), 3.34 (t, *J* = 7.7 Hz, 4H), 1.66 – 1.58 (m, 6H), 1.40 – 1.31 (m, 12H), 0.91

(t, *J* = 7.1 Hz, 6H). ^{13}C NMR (126 MHz, $CDCl_3$) δ 153.9, 146.7, 136.6, 129.3, 128.7, 121.6, 113.6, 113.0, 107.6, 103.8, 51.2, 31.8, 27.3, 26.9, 22.7, 14.1. HRMS (ESI) calc. for $C_{22}H_{34}NO$ 328.2640 $[M + H]^+$, found 328.2642

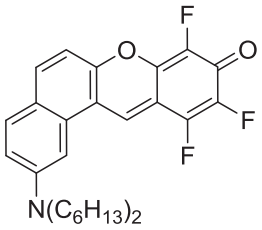

15

Rhodol **(15)**: A mixture of 2,3,5,6-tetrafluoro-4-hydroxybenzaldehyde (**2**, 1 mmol, 194 mg) and naphthalene **S1** (1 mmol, 327 mg) in xylene (30 ml) was stirred under argon at 160 °C for 7 h. The reaction mixture was cooled to room temperature, concentrated under vacuum and purified via column chromatography (silica, CH_2Cl_2/Et_2O, 9:1) to give pure product (97 mg, 20 %) as dark blue crystals. M.p. 152 – 153 °C.

^{1}H NMR (500 MHz, CD_2Cl_2) δ 8.63 (s, 1H), 7.91 (d, *J* = 8.8 Hz, 1H), 7.69 (d, *J* = 9.1 Hz, 1H), 7.18 (d, *J* = 8.8 Hz, 1H), 7.15 (br s, 1H), 7.08 (dd, *J* = 9.1, 1.9 Hz, 1H), 3.47 (t, *J* = 7.9 Hz, 4H), 1.75 – 1.68 (m, 4H), 1.47 – 1.35 (m, 12H), 0.94 (t, *J* = 7.1 Hz, 6H). ^{13}C NMR (126 MHz, CD_2Cl_2) δ 166.6 (m), 154.1, 149.1, 143.9 (dd, *J* = 262.4, 12.7 Hz), 140.9 – 140.7 (m), 138.1 (dd, *J* = 207.7, 7.3 Hz), 137.1, 131.7, 130.7, 122.1, 115.1, 112.0, 110.2, 109.8, 109.6, 98.5, 96.6, 51.1, 31.6, 27.1, 26.7, 22.7, 13.7. ^{19}F NMR (470 MHz, CD_2Cl_2) δ -148.65 (dd, *J* = 15.9, 5.1 Hz), -149.94 (dd, *J* = 15.8, 11.9 Hz), -163.26 (dd, *J* = 12.2, 4.9 Hz). HRMS (ESI) calc. for $C_{29}H_{33}NO_2F_3$ 484.2463 $[M + H]^+$, found 484.2462.

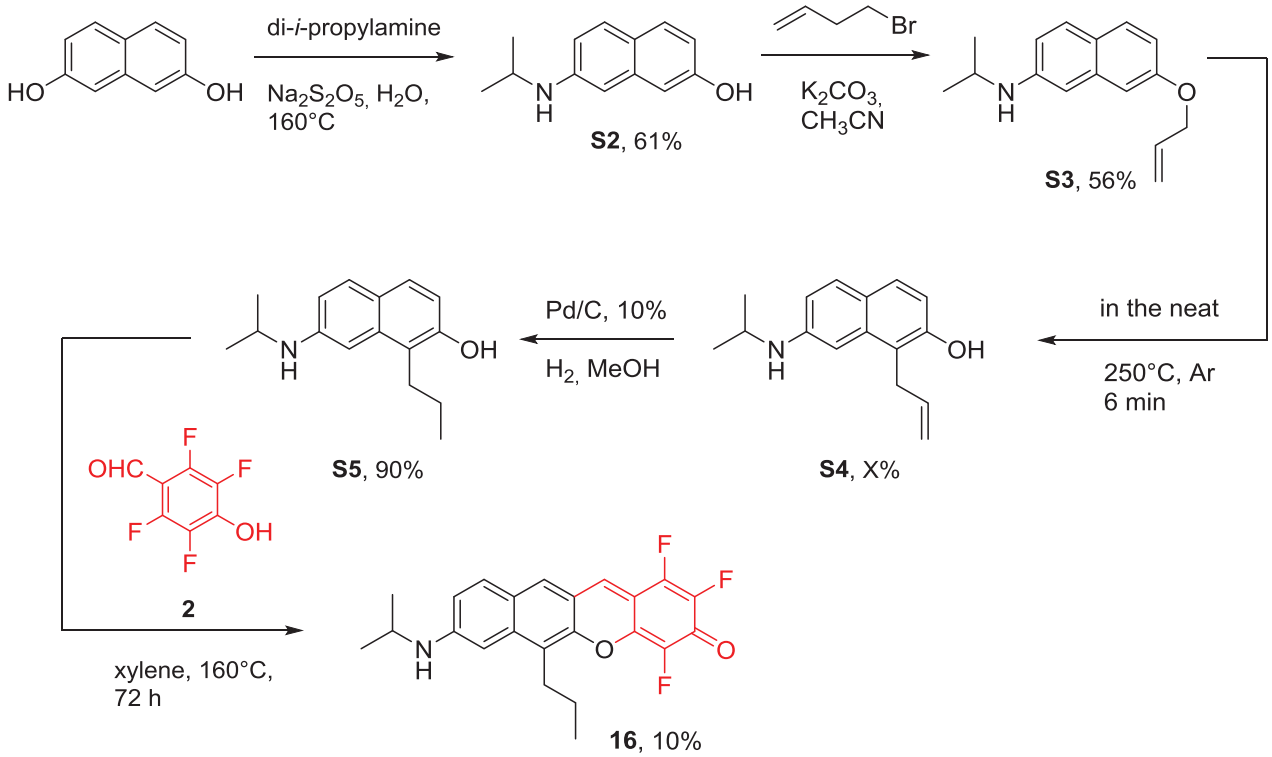

Scheme S2. Synthesis of linear π-expanded rhodol **(16).**

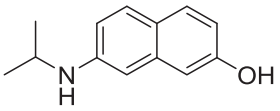

S2

7-(Isopropylamino)naphthalen-2-ol **(S2)**: The mixture of 2,7-dihydroxynaphthalene (10 g, 62.5 mmol), *N,N*-diisopropylamine (125 mmol, 12.63 g, 17.65 ml) and sodium metabisulfite (131.25 mmol, 24.94 g) in H_2O (100 ml) was stirred in the pressure tube at 120 °C for 24 hours. The reaction mixture was cooled to room temperature and extracted with EtOAc (3 x 300 ml). The organic phases were collected, dried over Na_2SO_4 and concentrated under vacuum. The residue was purified using column chromatography (silica, hexane/EtOAc, 3:1) to give pure product (7.61 mg, 61 %) as off-white crystals. M.p. 139 – 140 °C.

^{1}H NMR (500 MHz, $CDCl_3$) δ 7.54 (t, *J* = 8.2 Hz, 2H), 6.89 (d, *J* = 2.6 Hz, 1H), 6.78 (dd, *J* = 8.7, 2.5 Hz, 1H), 6.69 (dd, *J* = 8.8, 2.3 Hz, 1H), 6.63 (d, *J* = 2.3 Hz, 1H), 3.74 (hept, *J* = 6.3 Hz, 1H), 1.27 (d, *J* = 6.3 Hz, 6H). ^{13}C NMR (126 MHz, $CDCl_3$) δ 153.9, 145.7, 136.6, 129.5, 128.9, 122.8, 116.0, 113.3, 107.8, 103.8, 44.3, 22.9. HRMS (ESI) calc. for $C_{13}H_{16}NO$ 202.1232 $[M + H]^+$, found 202.1234.

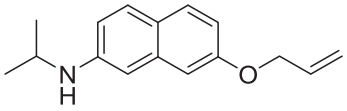

S3

7-(Allyloxy)-*N*-isopropylnaphthalen-2-amine (**S3**): To the mixture of 7-(*N*-isopropylamino)naftalen-2-ol (7.5 g, 0.037 mol) and K_2CO_3 (12.7 g,0.092 mol) in acetone (350 ml) allyl bromide (4 ml, 0.046 mol) was added. The reaction mixture was stirred at room temperature overnight. The solid was filtered off, the solvent was evaporated and the residue was purified via column chromatography (silica, heksan/EtOAc, 100:1). The product was obtained in 56 % yield as yellow oil. M.p. 46 – 47 °C.

^{1}H NMR (500 MHz, $CDCl_3$) δ 7.56 – 7.49 (m, 2H), 6.93 (d, *J* = 2.5 Hz, 1H), 6.87 (dd, *J* = 8.8, 2.5 Hz, 1H), 6.70 – 6.66 (m, 2H), 6.17 - 6.06 (m, 1H), 5.45 (dq, *J* = 17.2; 1.6, 1H), 5.30 (dq, *J* = 10.4; 1.4, 1H), 4.62 (dt, *J* = 5.3, 1.6 Hz, 2H), 3.74 (hept, *J* = 6.3 Hz, 1H), 3.60 (s, 1H), 1.26 (d, *J* = 6.2 Hz, 6H). ^{13}C NMR (126 MHz, $CDCl_3$) δ 157.2, 145.7, 136.5, 133.5, 129.1, 128.7, 122.7, 117.5, 115.8, 114.4, 105.7, 104.3, 68.7, 44.2, 22.9. HRMS (EI) calc. for $C_{16}H_{19}NO$ 241.1467 $[M^{+\cdot}]$, found 241.1464.

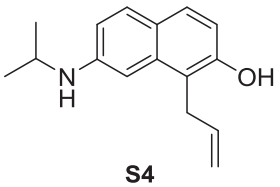

S4

1-Allyl-7-(isopropylamino)naphthalen-2-ol (**S4**): 7-allyloksy-2-(*N*-isopropylamino)naftalen (5 g, 0.02 mol) was placed in a round-bottom flask under argon atmosphere and heated with heatgun (approx. 250 °C) till the moment when the color of the oil changes to light brown (≈ 4 - 6 min). The reaction mixture was purified via column chromatography (silica, hexane/EtOAc, 1:1). The product was obtained in 50 % yield as beige solid. M.p. 105 - 107 °C.

^{1}H NMR (500 MHz, $CDCl_3$) δ 7.56 (d, *J* = 8.7 Hz, 1H), 7.48 (d, *J* = 8.6 Hz, 1H), 6.84 (d, *J* = 2.3 Hz, 1H), 6.78 (d, *J* = 8.7 Hz, 1H), 6.72 (dd, *J* = 8.7, 2.3 Hz, 1H), 6.13 – 6.01 (m, 1H), 5.15 – 5-09 (m, 2H), 4.38 (br s, 1H), 3.82 –

3.72 (m, 3H), 1.31 -1.26 (m, 7H). ^{13}C NMR (126 MHz, $CDCl_3$) δ 151.6, 145.7, 136.1, 135.1, 129.7, 127.9, 123.1, 115.5, 115.2, 114.7, 113.5, 101.2, 44.3, 29.5, 22.8. HRMS (EI) calc. for $C_{16}H_{19}NO$ 241.1467 [M^+], found 241.1460.

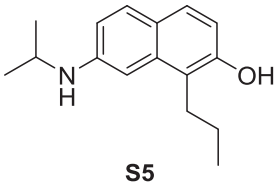

S5

7-(Isopropylamino)-1-propylnaphthalen-2-ol (**S5**): To the solution of 1-allyl-7-*N*-isopropylaminonaftalene-2-ol (2.4 g, 0.01 mol) in methanol (100 ml) was added 10 % Pd/C (85 mg). The flask was filled with hydrogen and the reaction mixture was stirred at rt for 3h. The resulting solid was filtered off and washed with 30 ml of methanol. The filtrate was concentrated under vacuum to give the product in 90 % yield as yellow solid. M.p. 112 - 113 °C.

^{1}H NMR (500 MHz, $CDCl_3$) δ 7.53 (d, *J* = 8.7 Hz, 1H), 7.42 (d, *J* = 8.6 Hz, 1H), 6.83 (d, *J* = 2.3 Hz, 1H), 6.75 (d, *J* = 8.6 Hz, 1H), 6.70 (dd, *J* = 8.7, 2.3 Hz, 1H), 4.73 (br s, 1H), 3.77 (hept, *J* = 6.3 Hz, 1H), 3.65 (br s, 1H), 2.95 – 2.88 (m, 2H), 1.70 (h, *J* = 7.4 Hz, 2H), 1.28 (d, *J* = 6.3 Hz, 6H), 1.05 (t, *J* = 7.4 Hz, 3H). ^{13}C NMR (126 MHz, $CDCl_3$) δ 150.9, 145.6, 135.0, 129.7, 127.3, 123.2, 117.8, 115.0, 113.3, 101.3, 44.3, 27.1, 22.9, 22.5, 14.4. HRMS (ESI) calc. for $C_{16}H_{22}NO$ 244.1701 [M + H]$^+$, found 244.1702.

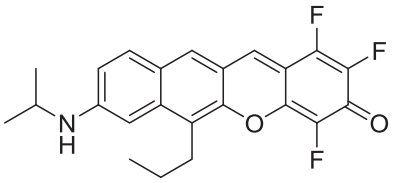

16

1,2,4-Trifluoro-8-(isopropylamino)-6-propyl-3H-benzo[*b*]xanthen-3-one **(16)**: A mixture of 2,3,5,6-tetrafluoro-4-hydroxybenzaldehyde (**2**, 1 mmol, 194 mg) and naphthalene **S5** (1 mmol, 243 mg) in xylene (30 ml) was stirred under argon at 160 °C for 72 h. The reaction mixture was cooled to room temperature, concentrated under vacuum and purified via column chromatography (silica, CH_2Cl_2/MeOH, 95:5). Resulting solid was washed with boiling MeOH to give pure product (40 mg, 10 %) as dark purple crystals. M.p. 325 – 326 °C.

In spite of all our attempts to dry compound **16**, we did not manage to get rid of some solvents and their peaks are present on ^{1}H NMR spectrum.

^{1}H NMR (500 MHz, DMF-d_7) δ 8.60 (s, 1H), 8.24 (s, 1H), 7.87 (d, *J* = 9.1 Hz, 1H), 7.19 (dd, *J* = 9.0, 2.1 Hz, 1H), 7.02 (d, *J* = 2.2 Hz, 1H), 6.63 (d, *J* = 7.4 Hz, 1H), 3.98 (h, *J* = 6.5 Hz, 1H), 3.25 (t, *J* = 7.5 Hz, 2H), 1.83 (h, *J* = 7.4 Hz, 2H), 1.35 (d, *J* = 6.3 Hz, 6H), 1.09 (t, *J* = 7.4 Hz, 3H). Due to the poor solubility of compound **13** and the complexity of ^{13}C NMR spectrum, it is not possible to assign all signals. ^{13}C NMR (126 MHz, DMF-d_7) δ 150.5, 146.4, 139.0, 137.5, 131.9, 130.9, 124.5, 119.9, 118.8, 114.7, 108.8, 99.4, 43.7, 34.2, 34.0, 29.1, 26.3, 22.1, 21.9, 13.5. ^{19}F NMR (470 MHz, DMF-d_7) δ -150.2 (dd, *J* = 15.3, 4.5 Hz), -157.3 (dd, *J* = 15.4, 10.6 Hz), -165.8 (ddd, *J* = 10.5, 4.5, 1.8 Hz). HRMS (ESI) calc. for $C_{23}H_{21}NO_2F_3$ 400.1524 [M + H]$^+$, found 400.1523.

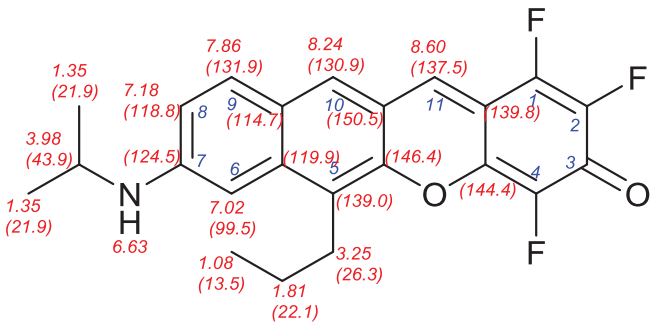

A thorough analysis of one-dimensional (1D) NMR and two-dimensional (2D) NMR spectra provides sufficient structural information about compound **16**. ^{1}H NMR spectrum shows NH-*i*Pr group as doublet with chemical shift 6.63 ppm (NH) together with doublet (1.35 ppm) and septet (3.98 ppm) of isopropyl group. Propyl group appears as two triplets (1.09 ppm and 3.25 ppm) and sextet (1.82 ppm). Moreover, 5 peaks were detected in aromatic area in ^{1}H NMR spectra. The correlations in ^{1}H^{13}C HSQC, and ^{13}C^{13}C HMBC spectra allow to assign most of the signals belonging to the molecule with the exception of quaternary carbons 1, 2, 3 and 4. Correlations in ^{13}C^{13}C HMBC fully support the linear structure of rhodol **16**, that was further confirmed by single crystal X-ray analysis.

1.1.2 ^{1}H and ^{13}C NMR spectra for synthesized compounds

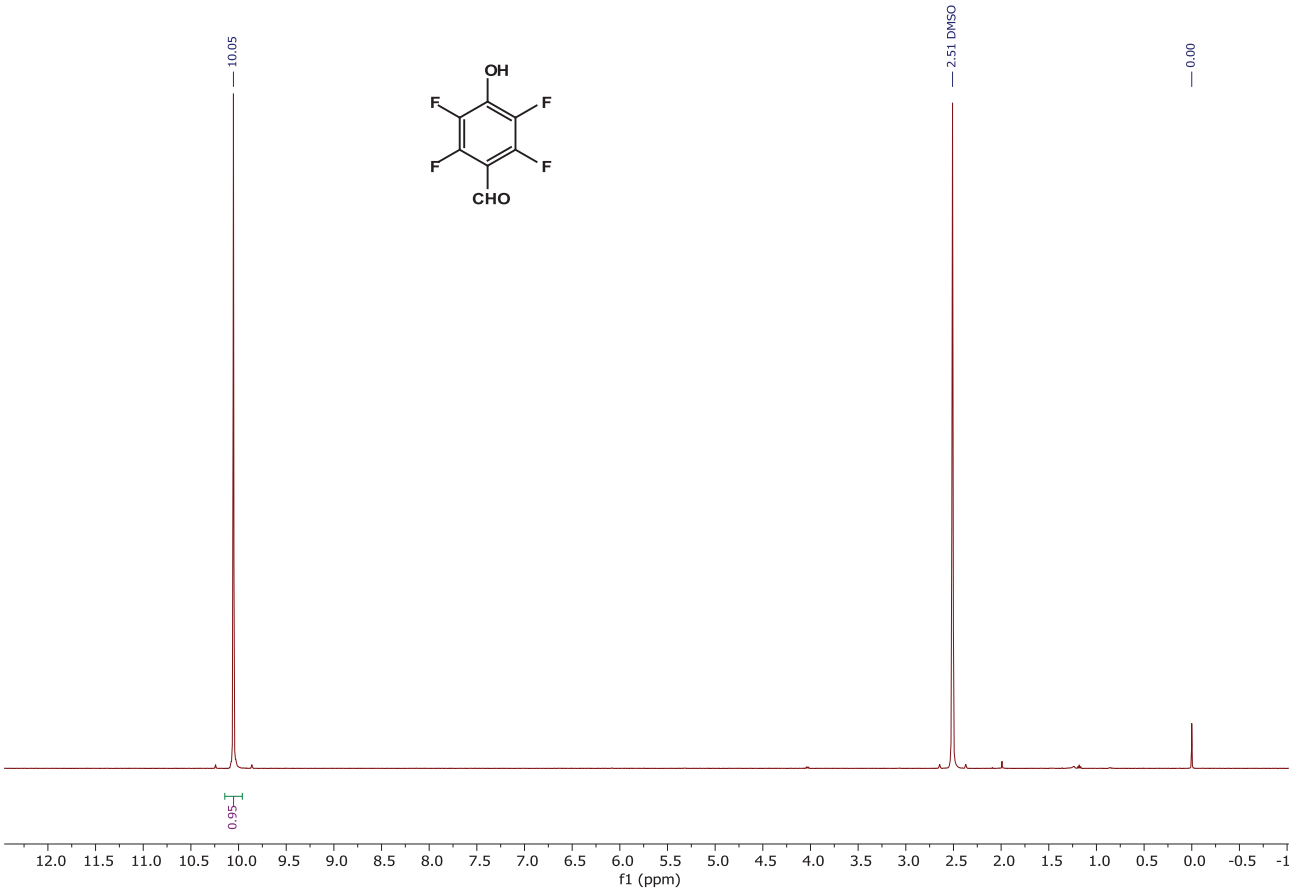

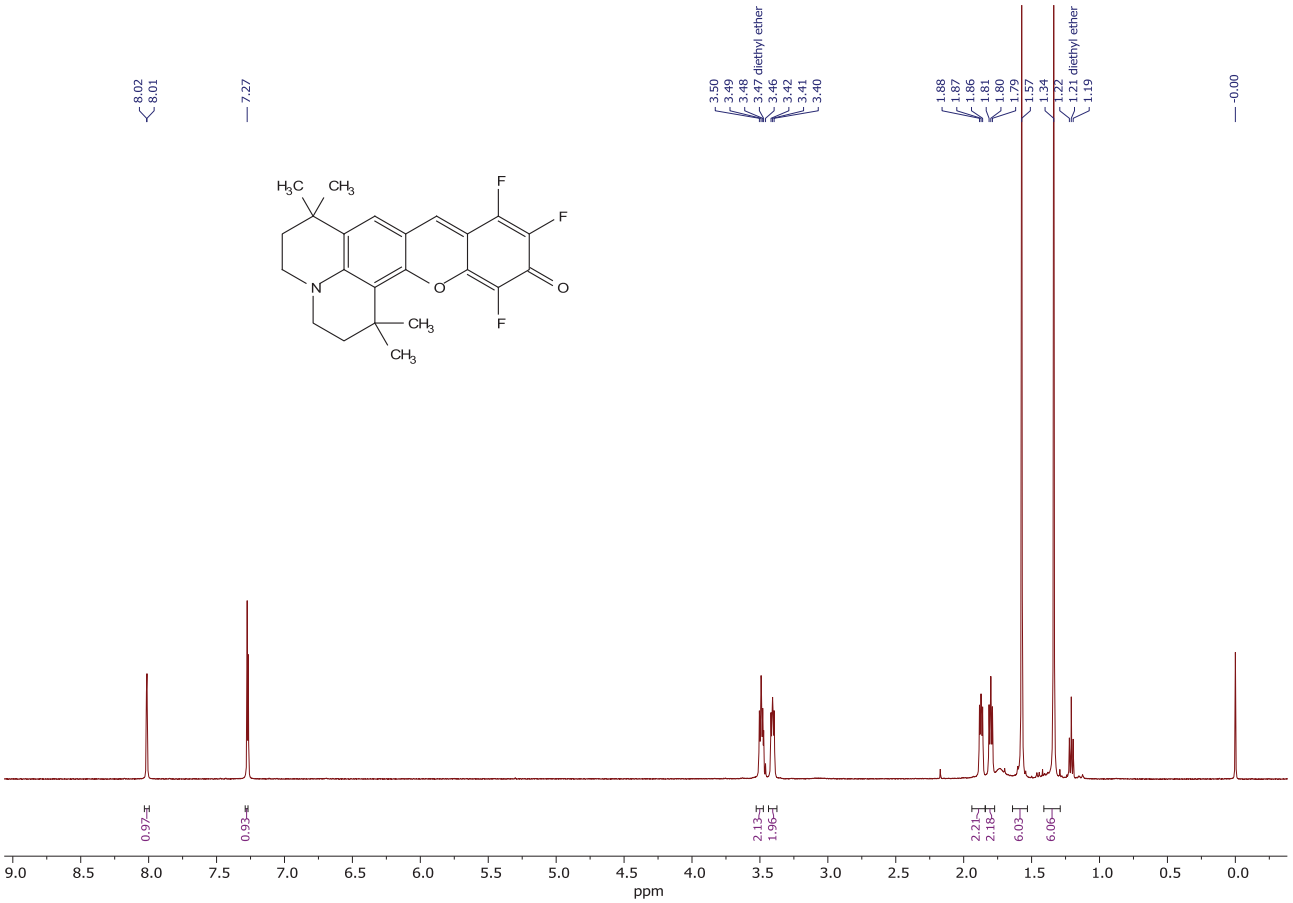
8.02
8.01
7.27
3.50
3.49
3.48
3.47 diethyl ether
3.46
3.42
3.41
3.40
1.88
1.87
1.86
1.81
1.80
1.79
1.57
1.34
1.22
1.21 diethyl ether
1.19
0.00
0.97
0.93
2.13
1.96
2.21
2.18
6.03
6.06
ppm

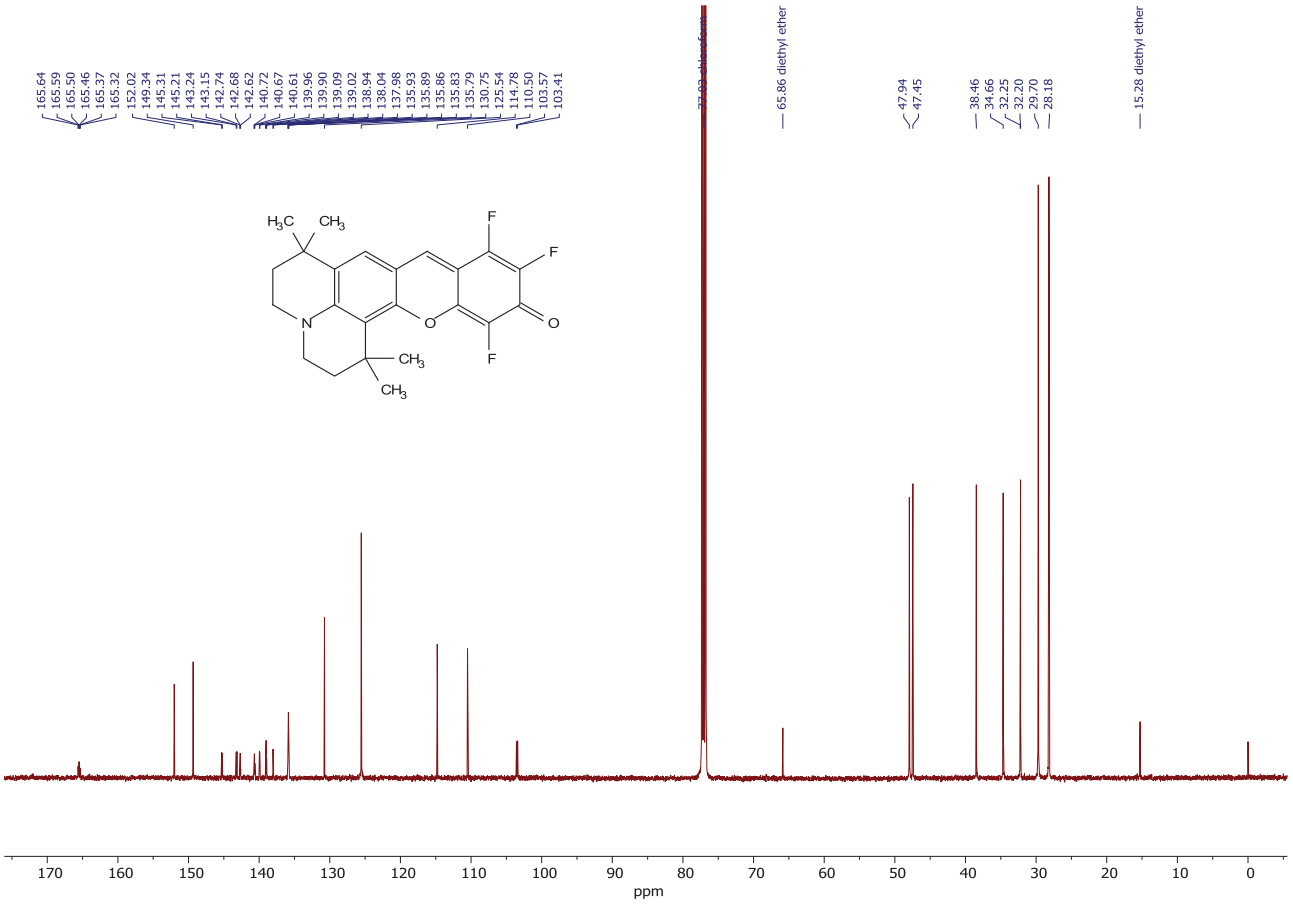
165.64
165.59
165.50
165.46
165.37
165.32
152.02
149.34
145.31
145.21
143.24
143.15
142.74
142.68
142.62
140.72
140.67
140.61
139.96
139.90
139.09
139.02
138.94
138.04
137.98
135.93
135.89
135.86
135.83
135.79
130.75
125.54
114.78
110.50
103.57
103.41
77.03 chloroform
65.86 diethyl ether
47.94
47.45
38.46
34.66
32.25
32.20
29.70
28.18
15.28 diethyl ether
ppm

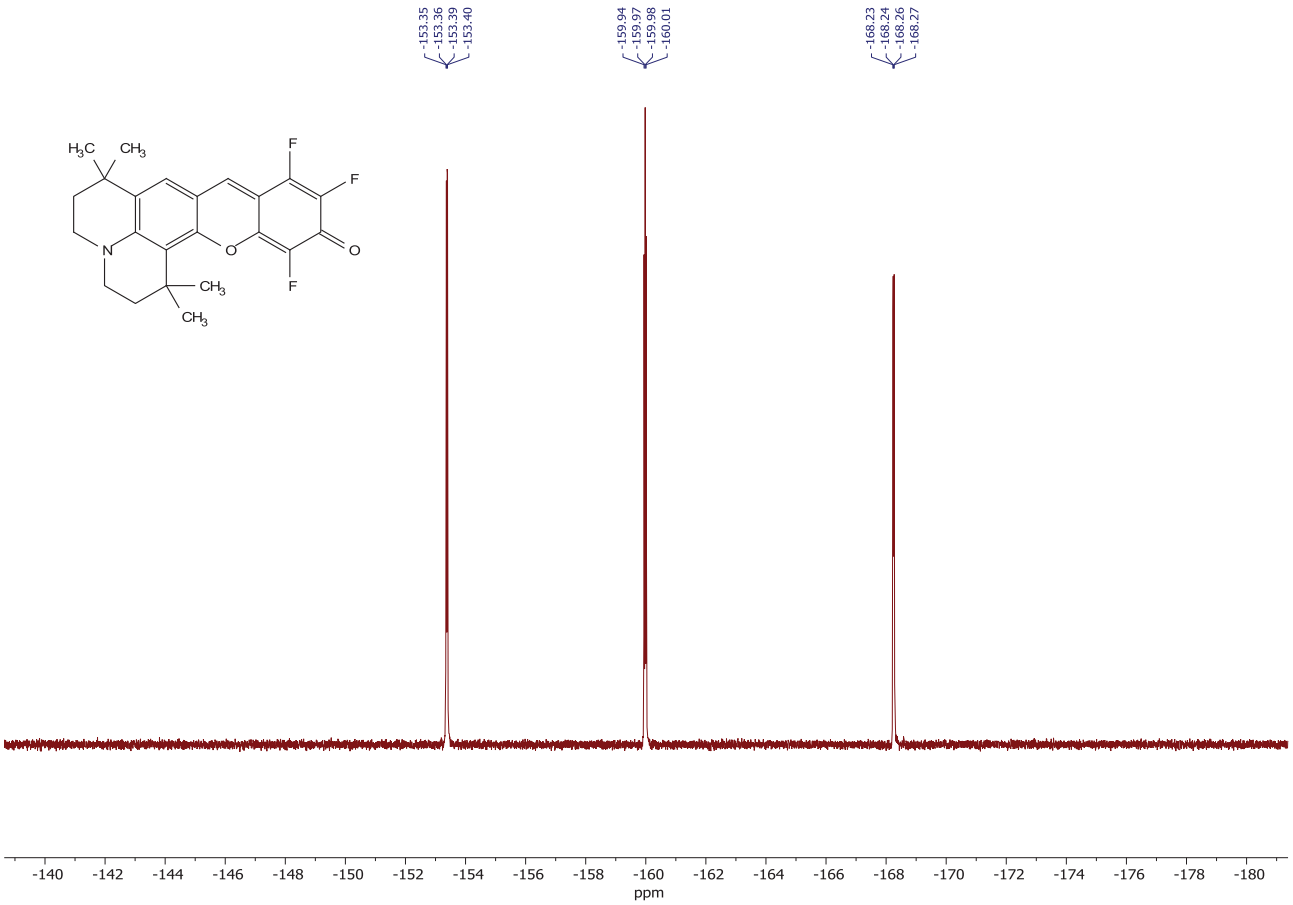
-153.35
-153.36
-153.39
-153.40
-159.94
-159.97
-159.98
-160.01
-168.23
-168.24
-168.26
-168.27
H3C
CH3
F
F
N
O
O
CH3
CH3
F
-140
-142
-144
-146
-148
-150
-152
-154
-156
-158
-160
-162
-164
-166
-168
-170
-172
-174
-176
-178
-180
ppm

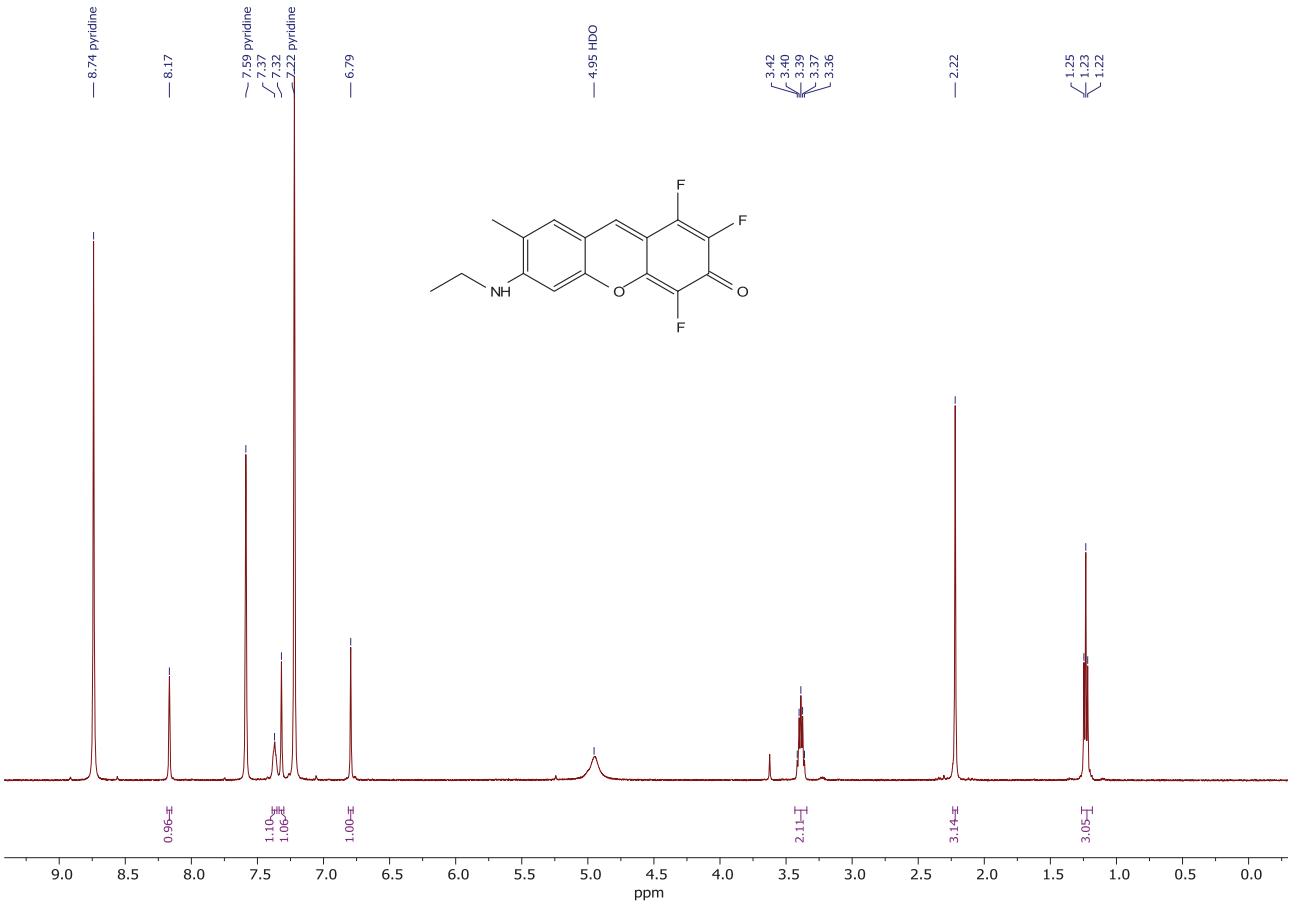
8.74 pyridine
8.17
7.59 pyridine
7.37
7.32
7.22 pyridine
6.79
4.95 HDO
3.42
3.40
3.39
3.37
3.36
2.22
1.25
1.23
1.22
F
F
NH
O
O
F
0.96
1.10
1.06
1.00
2.11
3.14
3.05
9.0
8.5
8.0
7.5
7.0
6.5
6.0
5.5
5.0
4.5
4.0
3.5
3.0
2.5
2.0
1.5
1.0
0.5
0.0
ppm

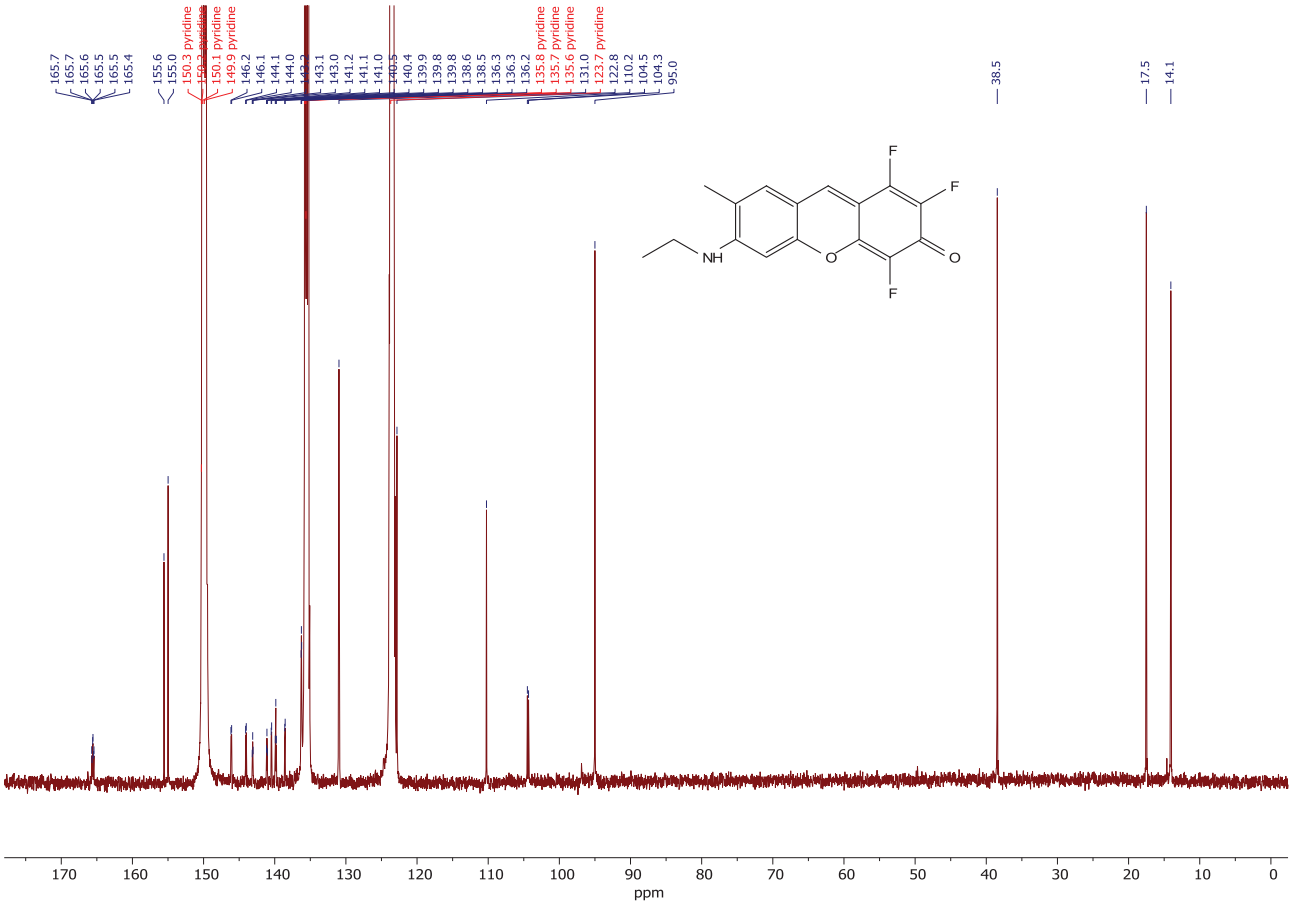
165.7
165.7
165.6
165.5
165.5
165.4
155.6
155.0
150.3 pyridine
150.2 pyridine
150.1 pyridine
149.9 pyridine
146.2
146.1
144.1
144.0
143.3
143.1
143.0
141.2
141.1
141.0
140.5
140.4
139.9
139.8
139.8
138.6
138.5
136.3
136.3
136.2
135.8 pyridine
135.7 pyridine
135.6 pyridine
131.0
123.7 pyridine
122.8
110.2
104.5
104.3
95.0
38.5
17.5
14.1
F
F
NH
O
O
F
170
160
150
140
130
120
110
100
90
80
70
60
50
40
30
20
10
0
ppm

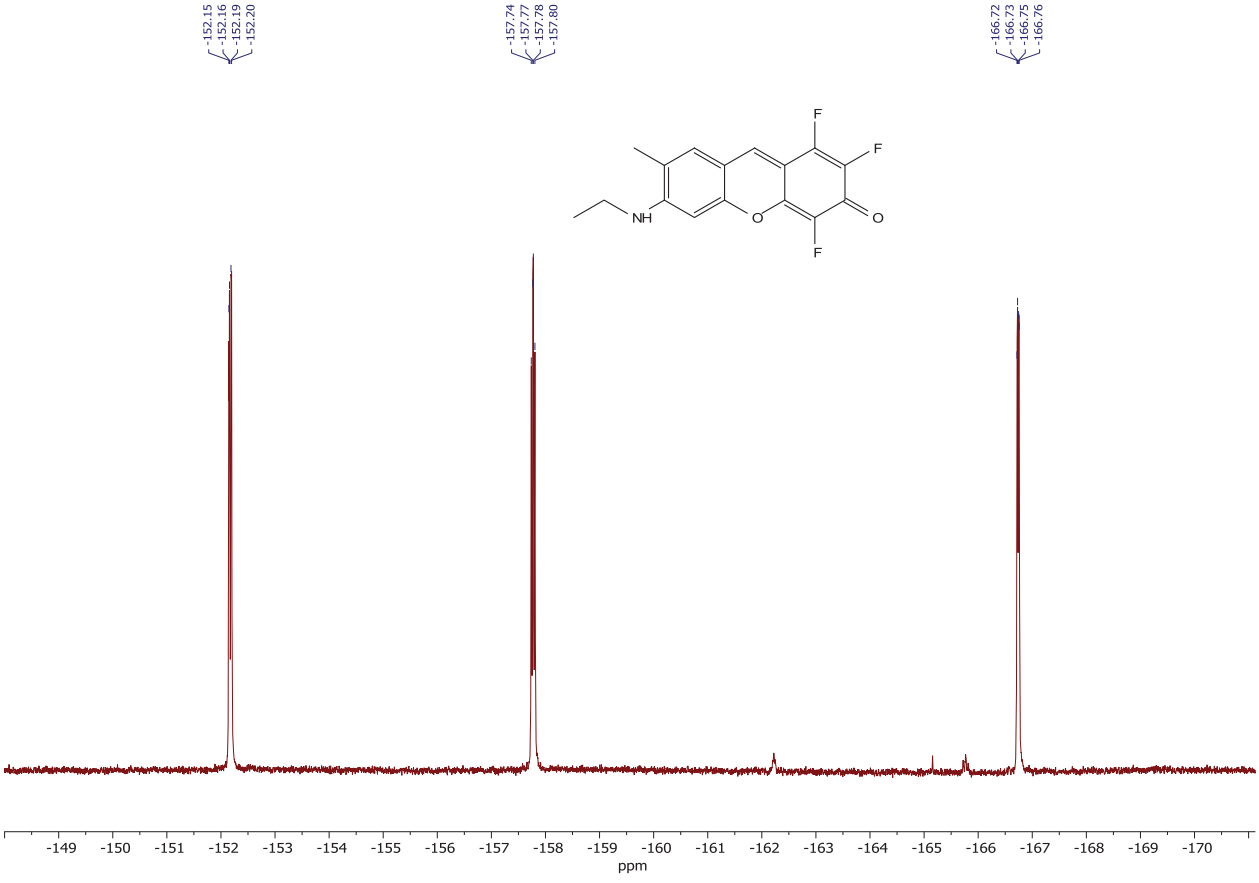
-152.15
-152.16
-152.19
-152.20
-157.74
-157.77
-157.78
-157.80
-166.72
-166.73
-166.75
-166.76
F
F
NH
O
O
F
-149
-150
-151
-152
-153
-154
-155
-156
-157
-158
-159
-160
-161
-162
-163
-164
-165
-166
-167
-168
-169
-170
ppm

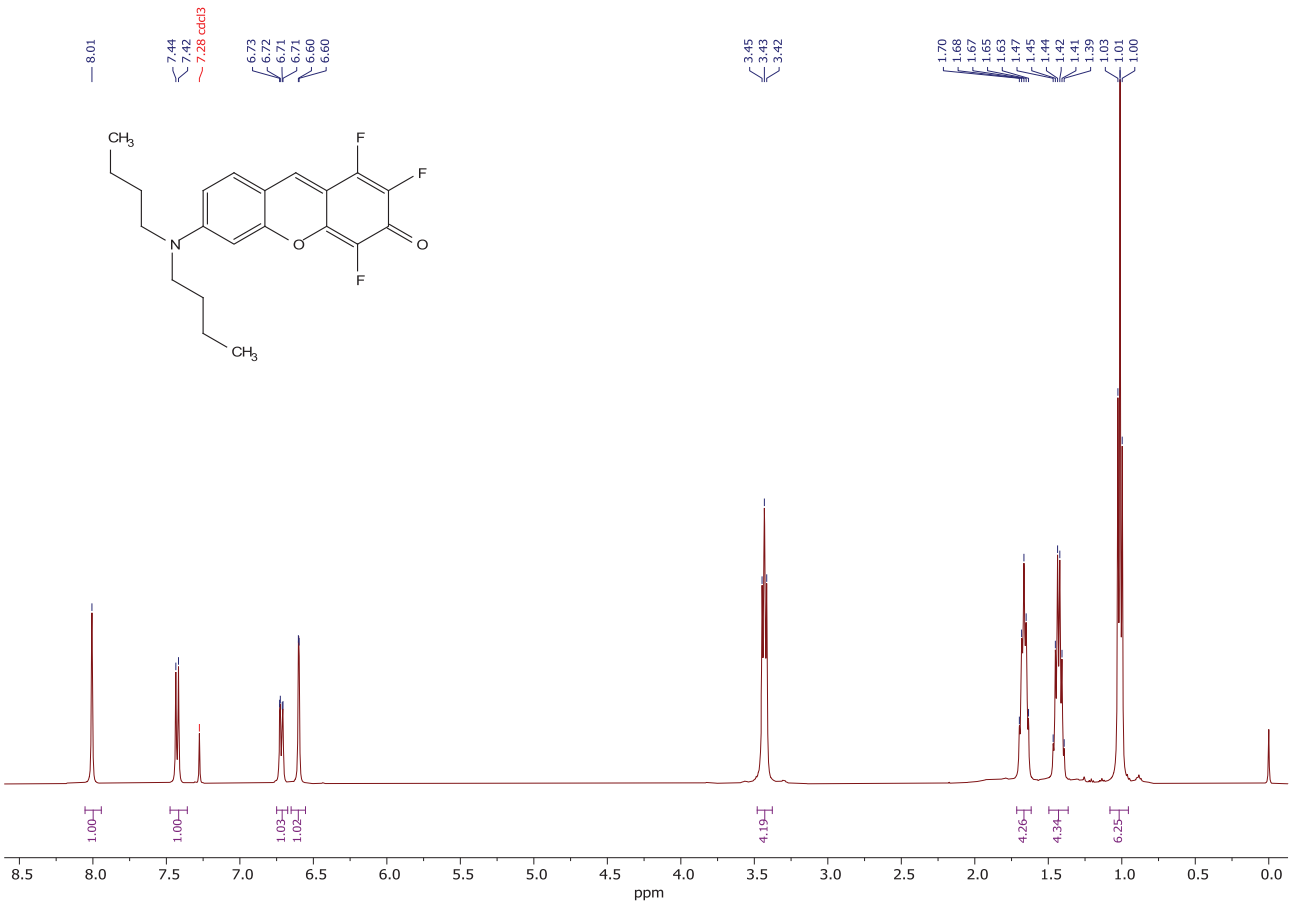
8.01
7.44
7.42
7.28 cdcl3
6.73
6.72
6.71
6.71
6.60
6.60
3.45
3.43
3.42
1.70
1.68
1.67
1.65
1.63
1.47
1.45
1.44
1.42
1.41
1.39
1.03
1.01
1.00
CH3
F
F
N
O
O
F
CH3
1.00
1.00
1.03
1.02
4.19
4.26
4.34
6.25
8.5
8.0
7.5
7.0
6.5
6.0
5.5
5.0
4.5
4.0
3.5
3.0
2.5
2.0
1.5
1.0
0.5
0.0
ppm

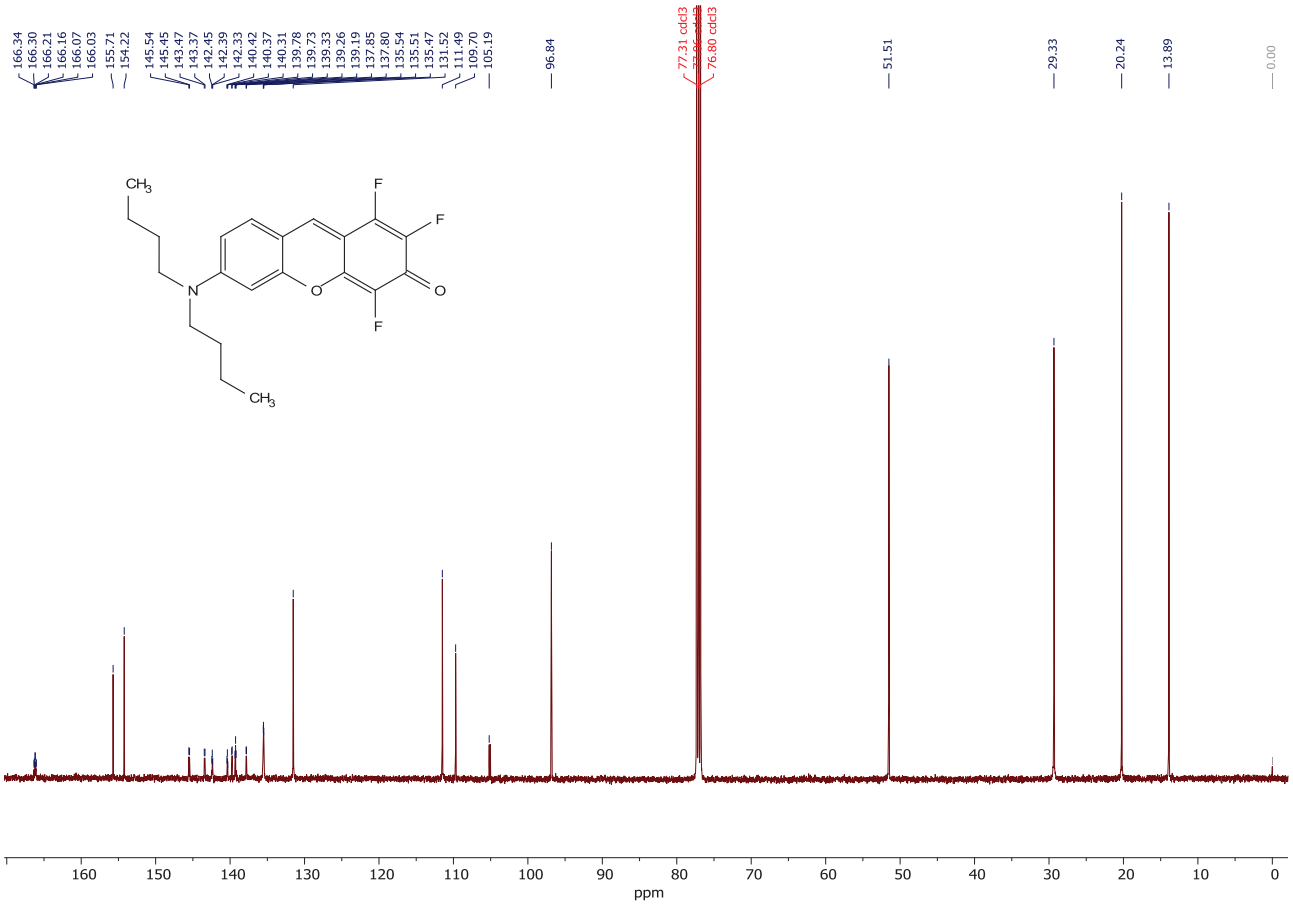
166.34
166.30
166.21
166.16
166.07
166.03
155.71
154.22
145.54
145.45
143.47
143.37
142.45
142.39
142.33
140.42
140.37
140.31
139.78
139.73
139.33
139.26
139.19
137.85
137.80
135.54
135.51
135.47
131.52
111.49
109.70
105.19
96.84
77.31 cdcl3
76.80 cdcl3
51.51
29.33
20.24
13.89
0.00
CH3
F
F
N
O
O
F
CH3
160
150
140
130
120
110
100
90
80
70
60
50
40
30
20
10
0
ppm

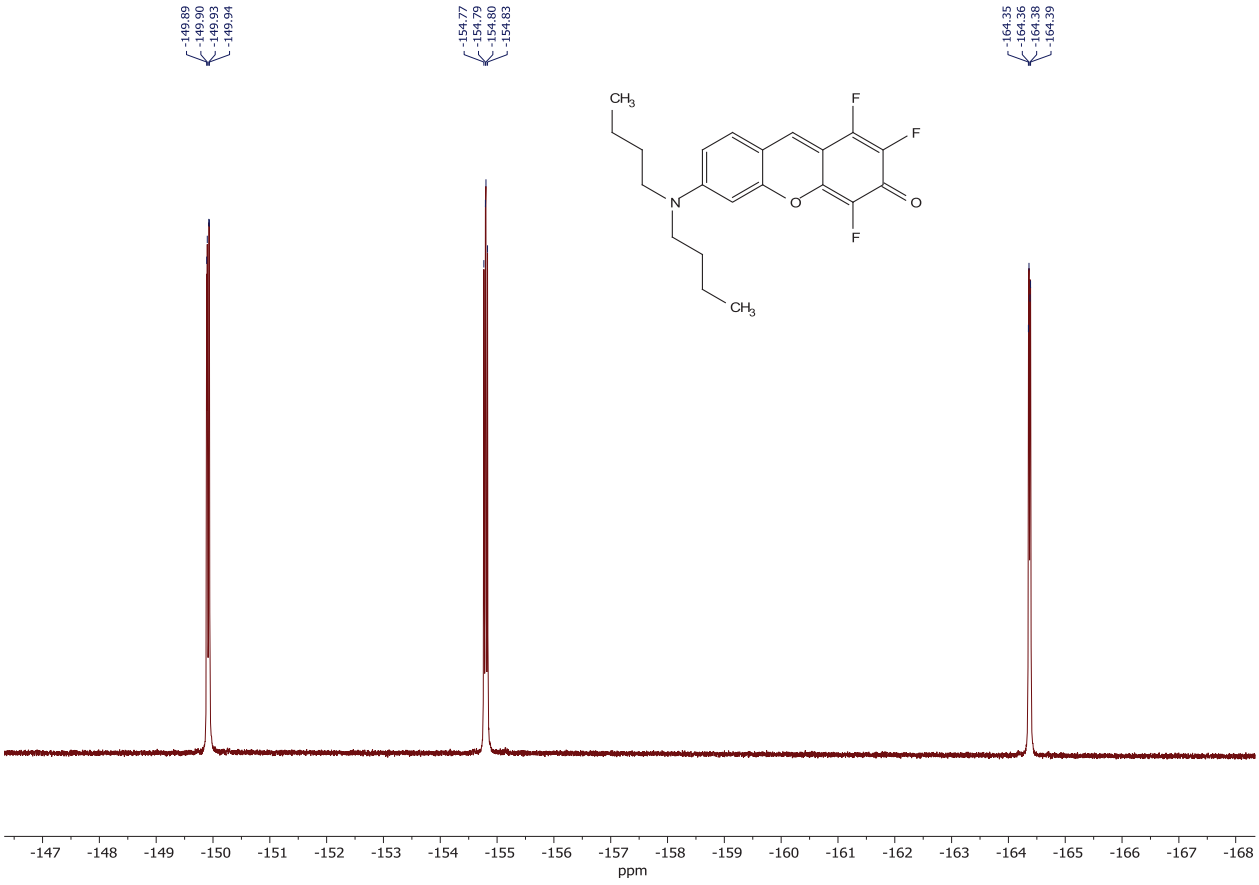
-149.89
-149.90
-149.93
-149.94
-154.77
-154.79
-154.80
-154.83
-164.35
-164.36
-164.38
-164.39
CH3
F
F
N
O
O
F
CH3
-147
-148
-149
-150
-151
-152
-153
-154
-155
-156
-157
-158
-159
-160
-161
-162
-163
-164
-165
-166
-167
-168
ppm

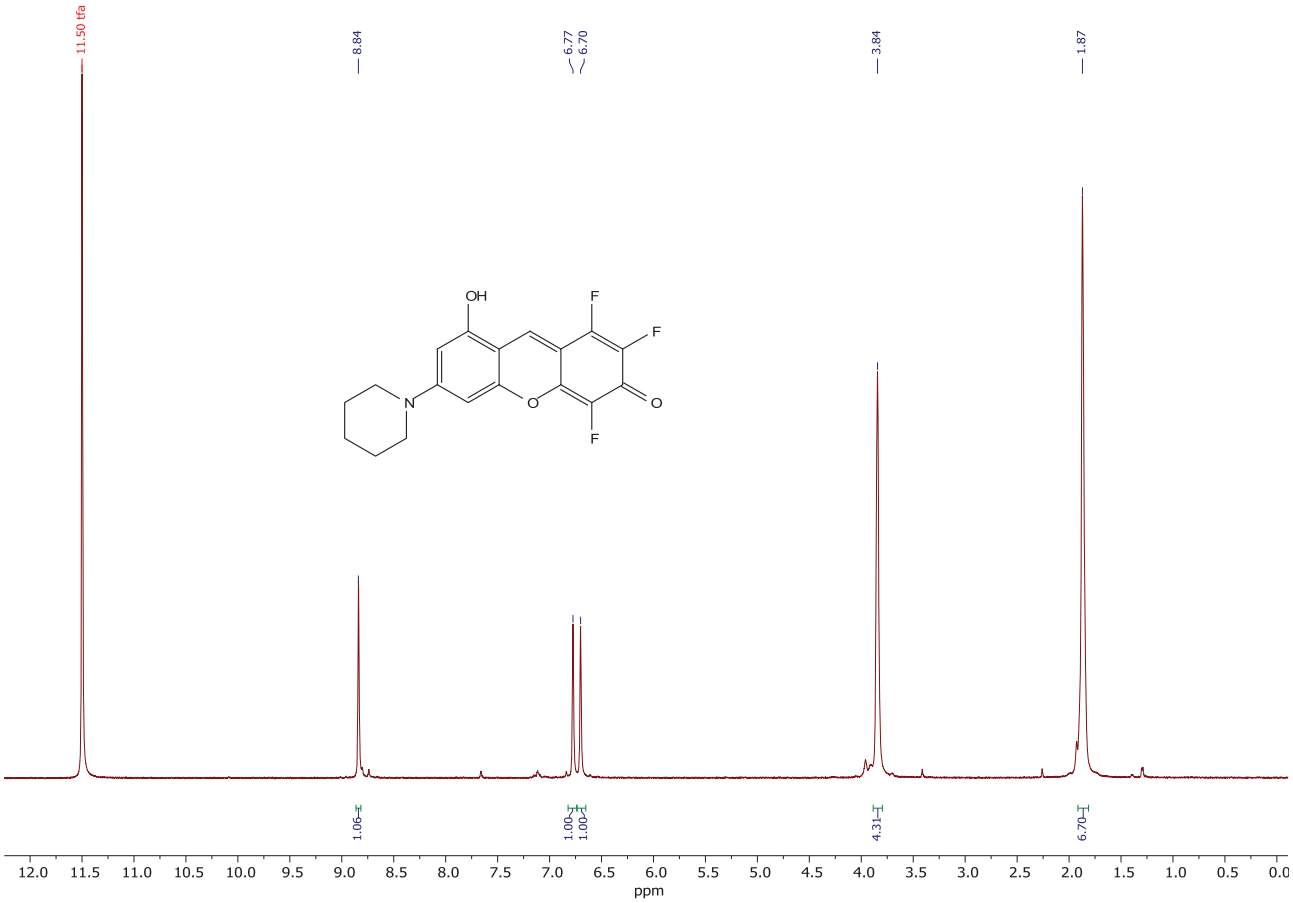
11.50 tfa
8.84
6.77
6.70
3.84
1.87
OH
F
F
N
O
O
F
1.06
1.00
1.00
4.31
6.70
12.0 11.5 11.0 10.5 10.0 9.5 9.0 8.5 8.0 7.5 7.0 6.5 6.0 5.5 5.0 4.5 4.0 3.5 3.0 2.5 2.0 1.5 1.0 0.5 0.0
ppm

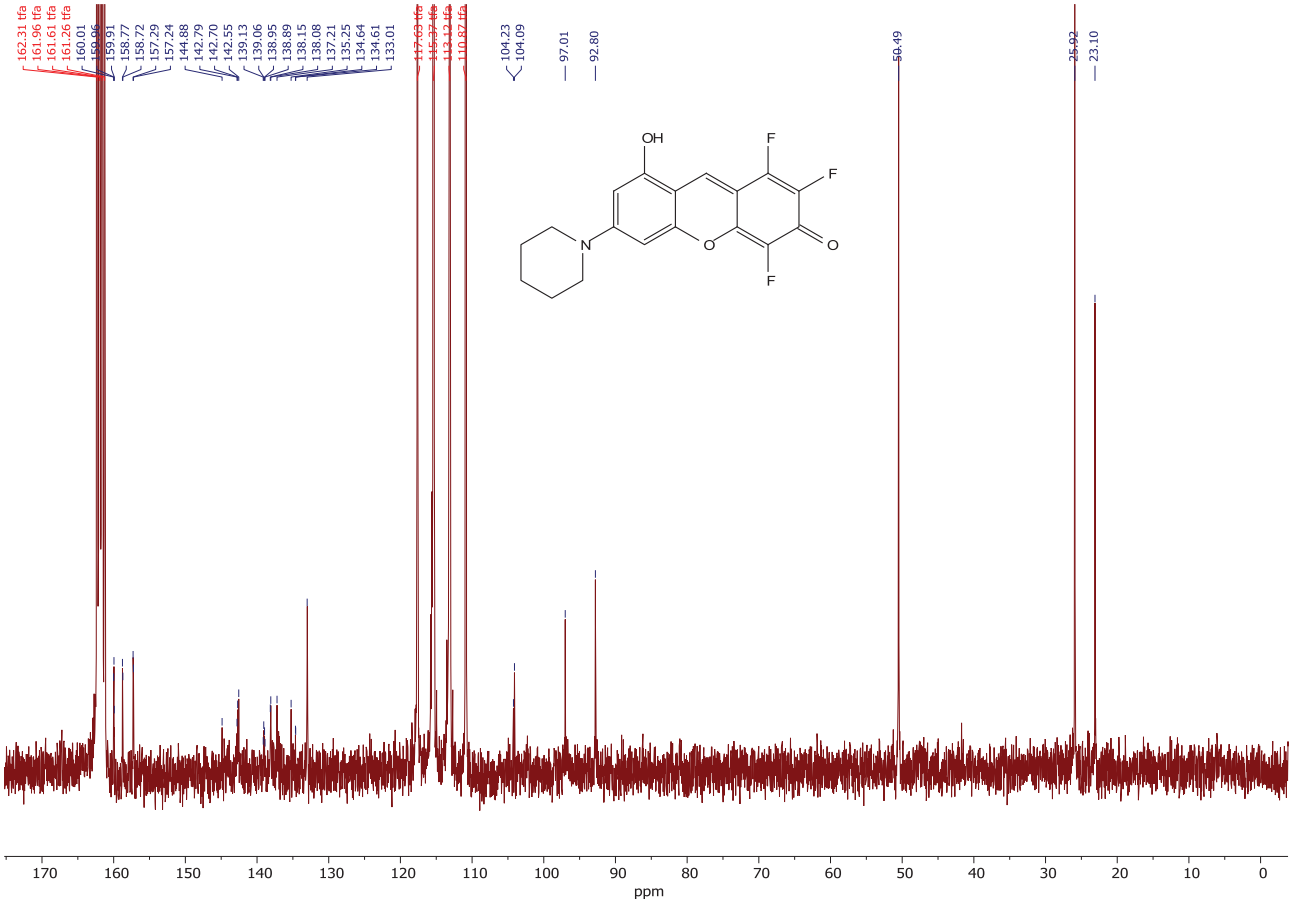
162.31 tfa
161.96 tfa
161.61 tfa
161.26 tfa
160.01
159.06
159.91
158.77
158.72
157.29
157.24
144.88
142.79
142.70
142.55
139.13
139.06
138.95
138.89
138.15
138.08
137.21
135.25
134.64
134.61
133.01
104.23
104.09
97.01
92.80
50.49
25.92
23.10
OH
F
F
N
O
O
F
170 160 150 140 130 120 110 100 90 80 70 60 50 40 30 20 10 0
ppm

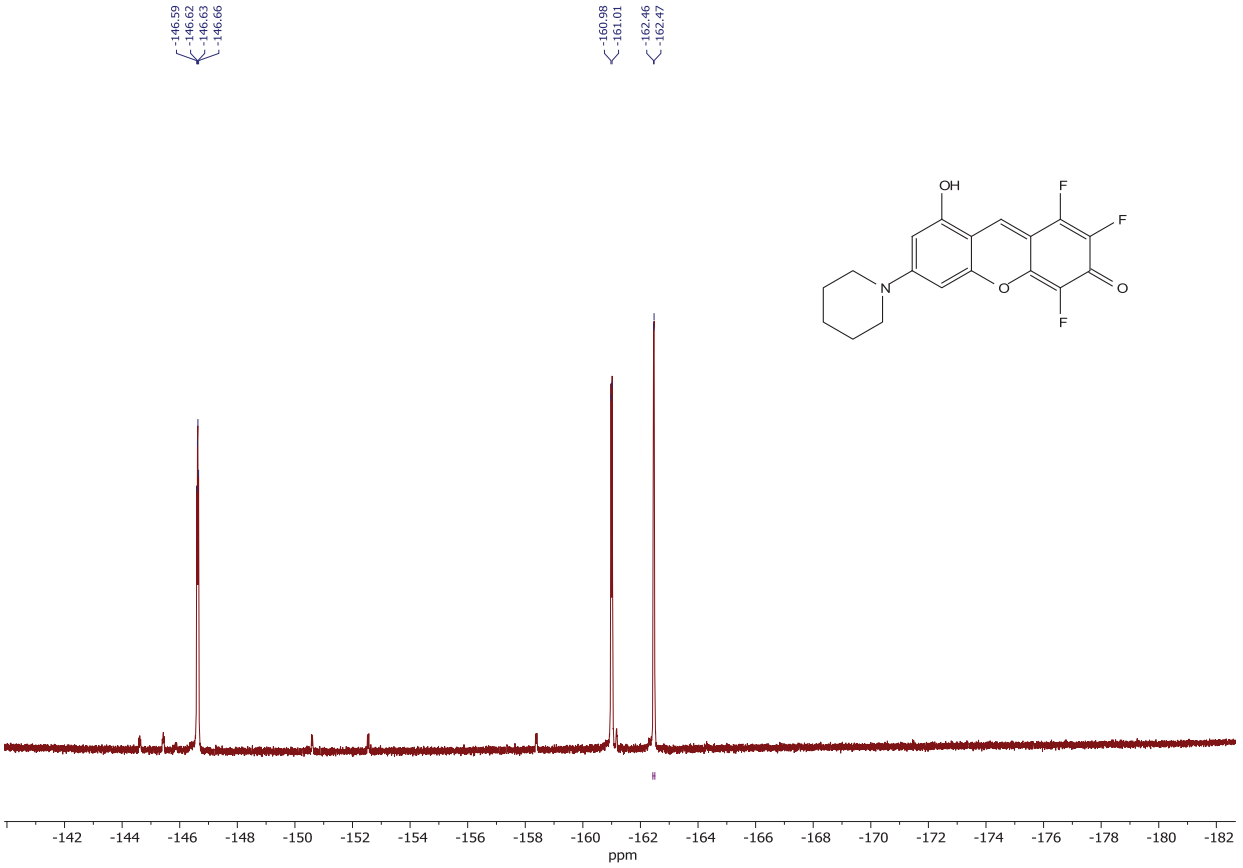
-146.59
-146.62
-146.63
-146.66
-160.98
-161.01
-162.46
-162.47
OH
F
F
N
O
O
F
-142 -144 -146 -148 -150 -152 -154 -156 -158 -160 -162 -164 -166 -168 -170 -172 -174 -176 -178 -180 -182
ppm

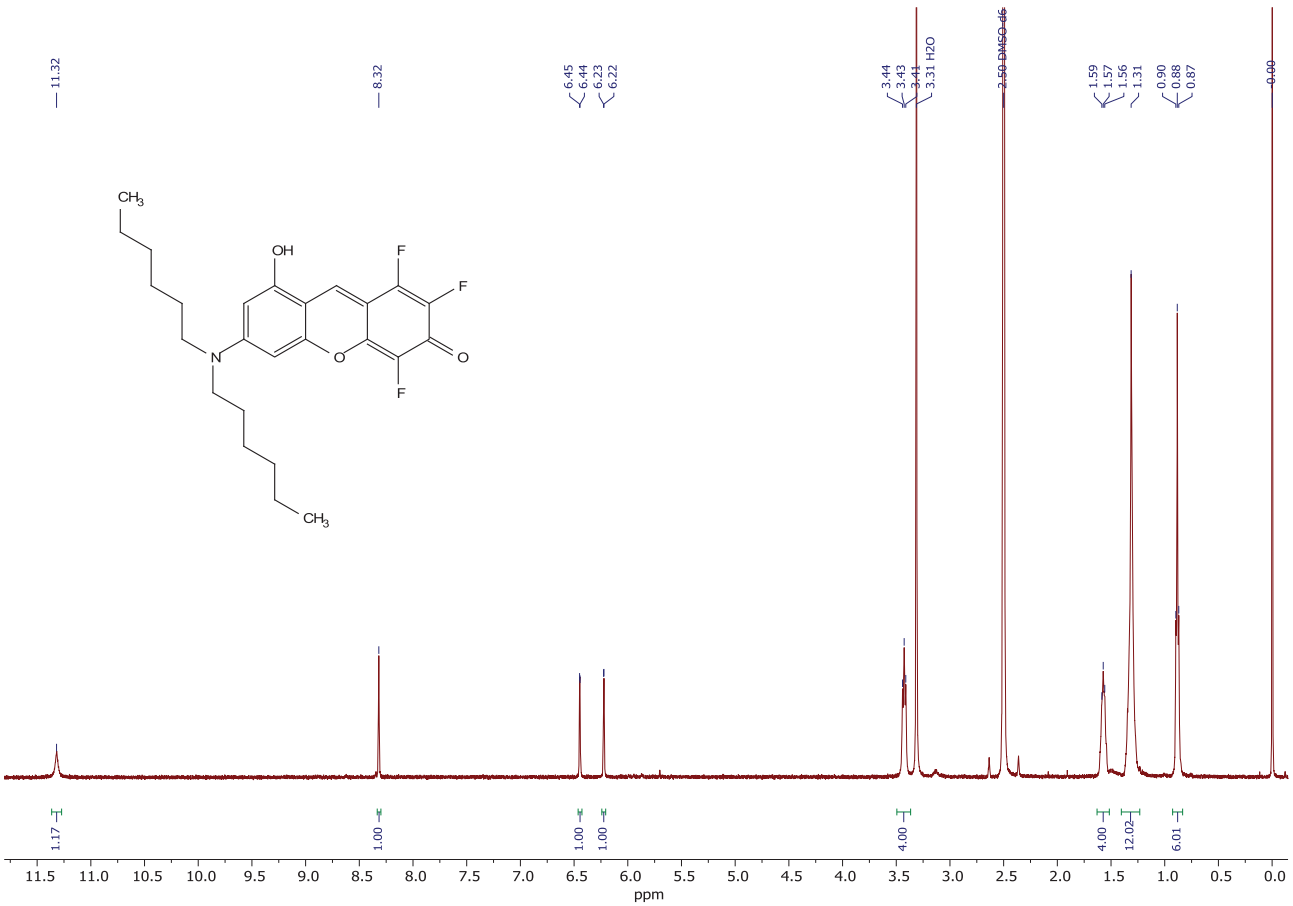
11.32
8.32
6.45
6.44
6.23
6.22
3.44
3.43
3.41
3.31 H2O
2.50 DMSO-d6
1.59
1.57
1.56
1.31
0.90
0.88
0.87
0.00
CH3
OH
F
F
N
O
O
F
CH3
1.17
1.00
1.00
1.00
4.00
4.00
12.02
6.01
11.5 11.0 10.5 10.0 9.5 9.0 8.5 8.0 7.5 7.0 6.5 6.0 5.5 5.0 4.5 4.0 3.5 3.0 2.5 2.0 1.5 1.0 0.5 0.0
ppm

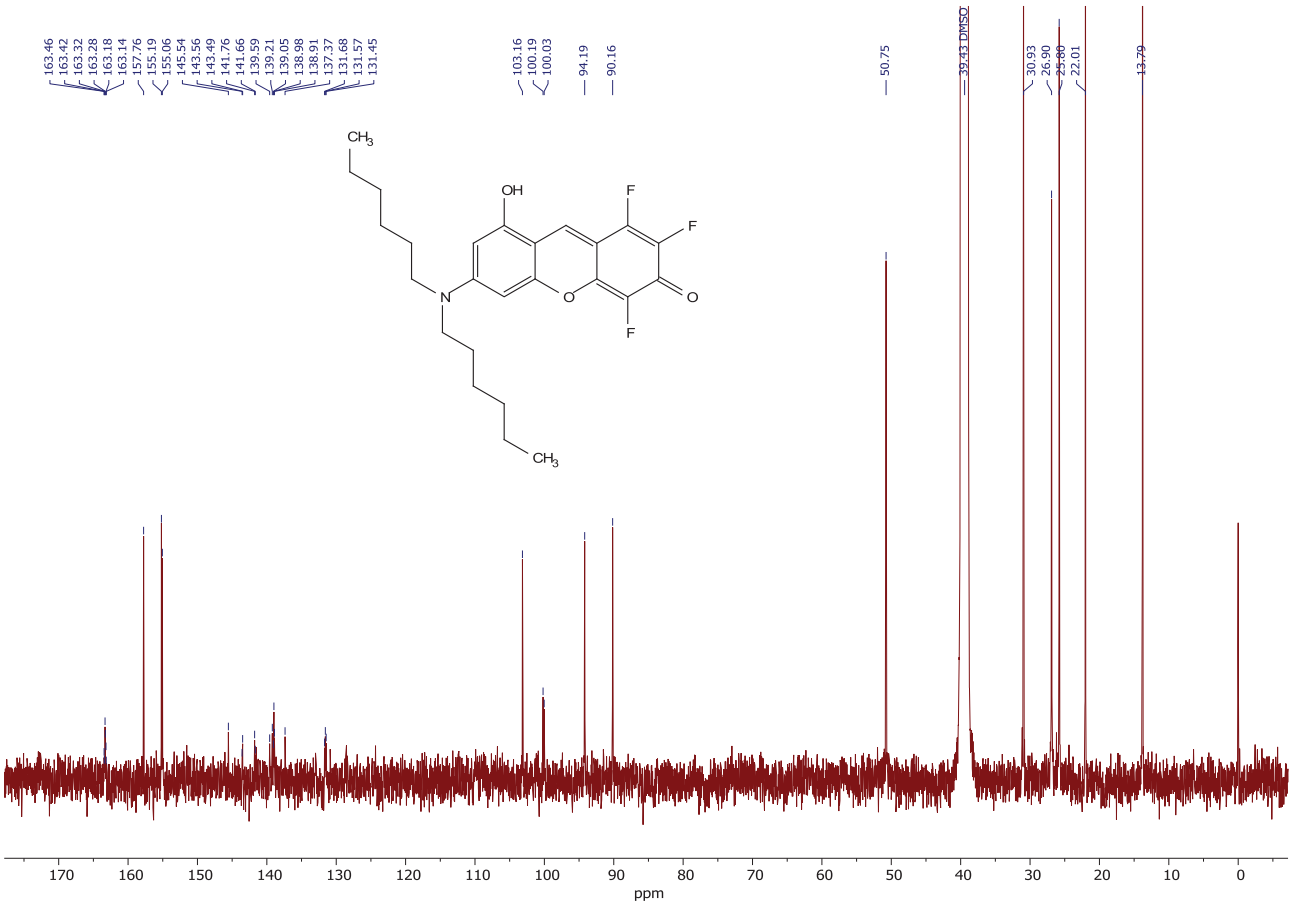
163.46
163.42
163.32
163.28
163.18
163.14
157.76
155.19
155.06
145.54
143.56
143.49
141.76
141.66
139.59
139.21
139.05
138.98
138.91
137.37
131.68
131.57
131.45
103.16
100.19
100.03
94.19
90.16
50.75
39.43 DMSO
30.93
26.90
25.80
22.01
13.79
CH3
OH
F
F
N
O
O
F
CH3
170
160
150
140
130
120
110
100
90
80
70
60
50
40
30
20
10
0
ppm

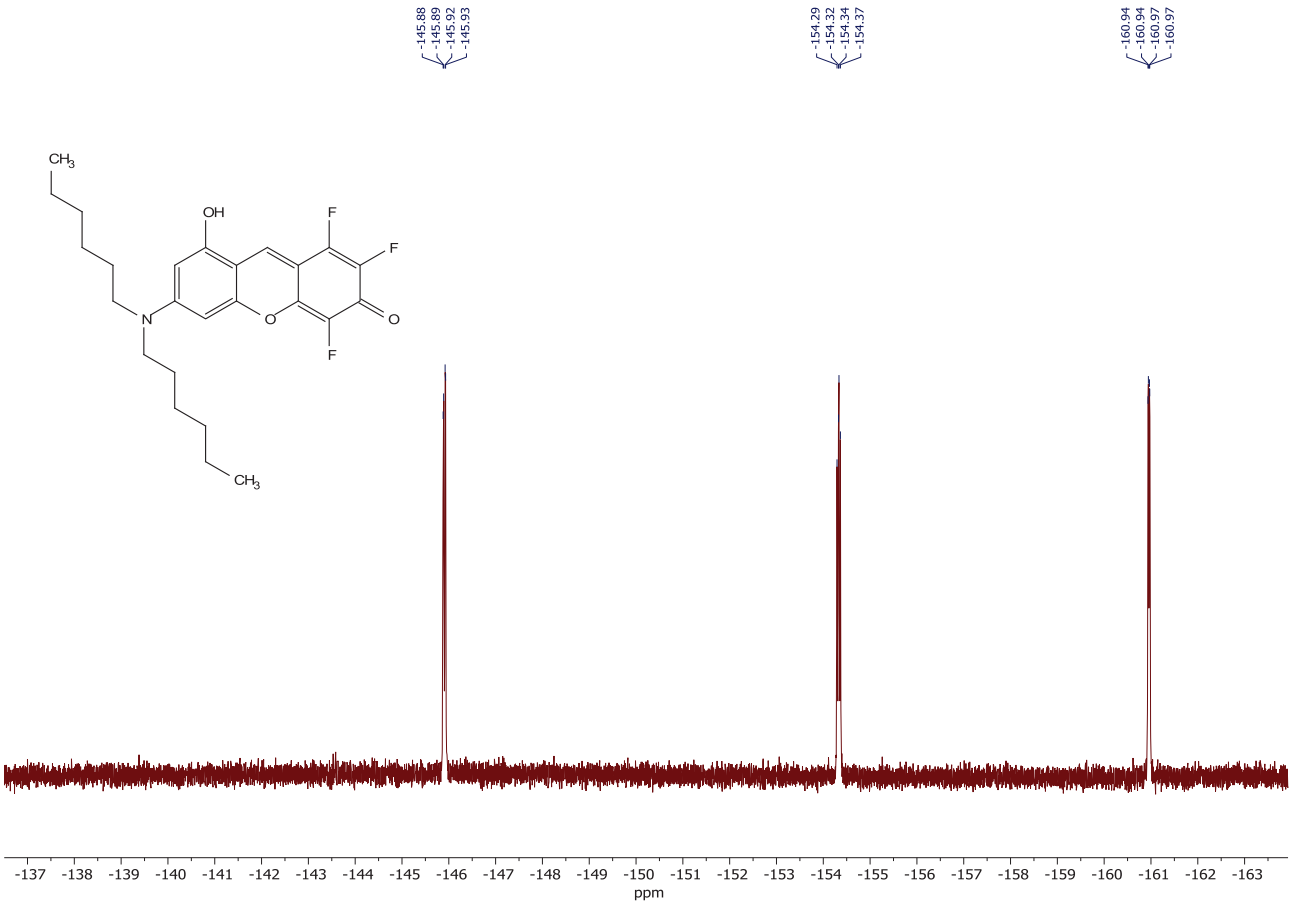
-145.88
-145.89
-145.92
-145.93
-154.29
-154.32
-154.34
-154.37
-160.94
-160.94
-160.97
-160.97
CH3
OH
F
F
O
N
O
F
CH3
-137 -138 -139 -140 -141 -142 -143 -144 -145 -146 -147 -148 -149 -150 -151 -152 -153 -154 -155 -156 -157 -158 -159 -160 -161 -162 -163
ppm

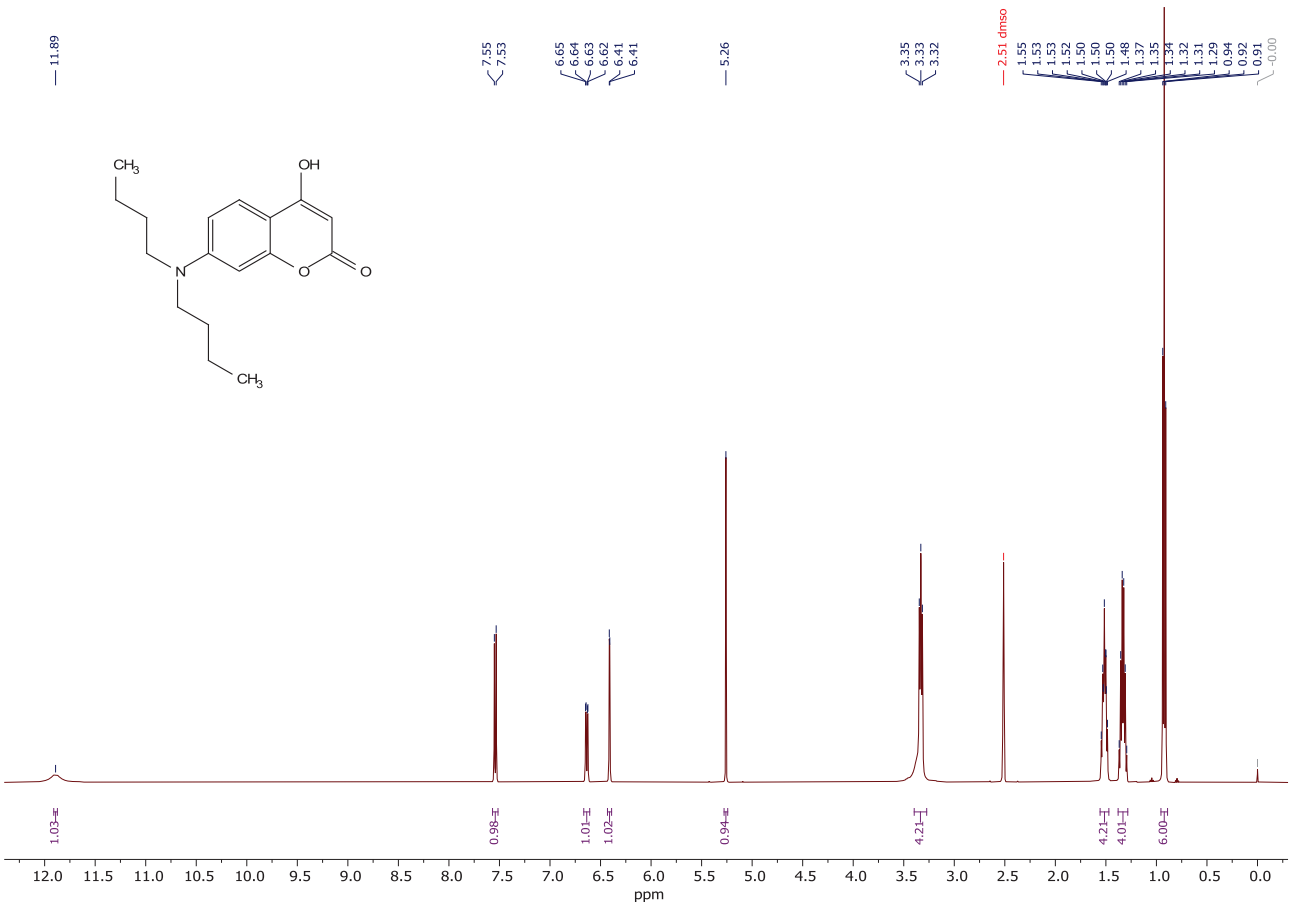
11.89
7.55
7.53
6.65
6.64
6.63
6.62
6.41
6.41
5.26
3.35
3.33
3.32
2.51 dmso
1.55
1.53
1.53
1.52
1.50
1.50
1.50
1.48
1.37
1.35
1.34
1.32
1.31
1.29
0.94
0.92
0.91
-0.00
CH3
OH
O
N
O
CH3
1.03
0.98
1.01
1.02
0.94
4.21
4.21
4.01
6.00
12.0 11.5 11.0 10.5 10.0 9.5 9.0 8.5 8.0 7.5 7.0 6.5 6.0 5.5 5.0 4.5 4.0 3.5 3.0 2.5 2.0 1.5 1.0 0.5 0.0
ppm

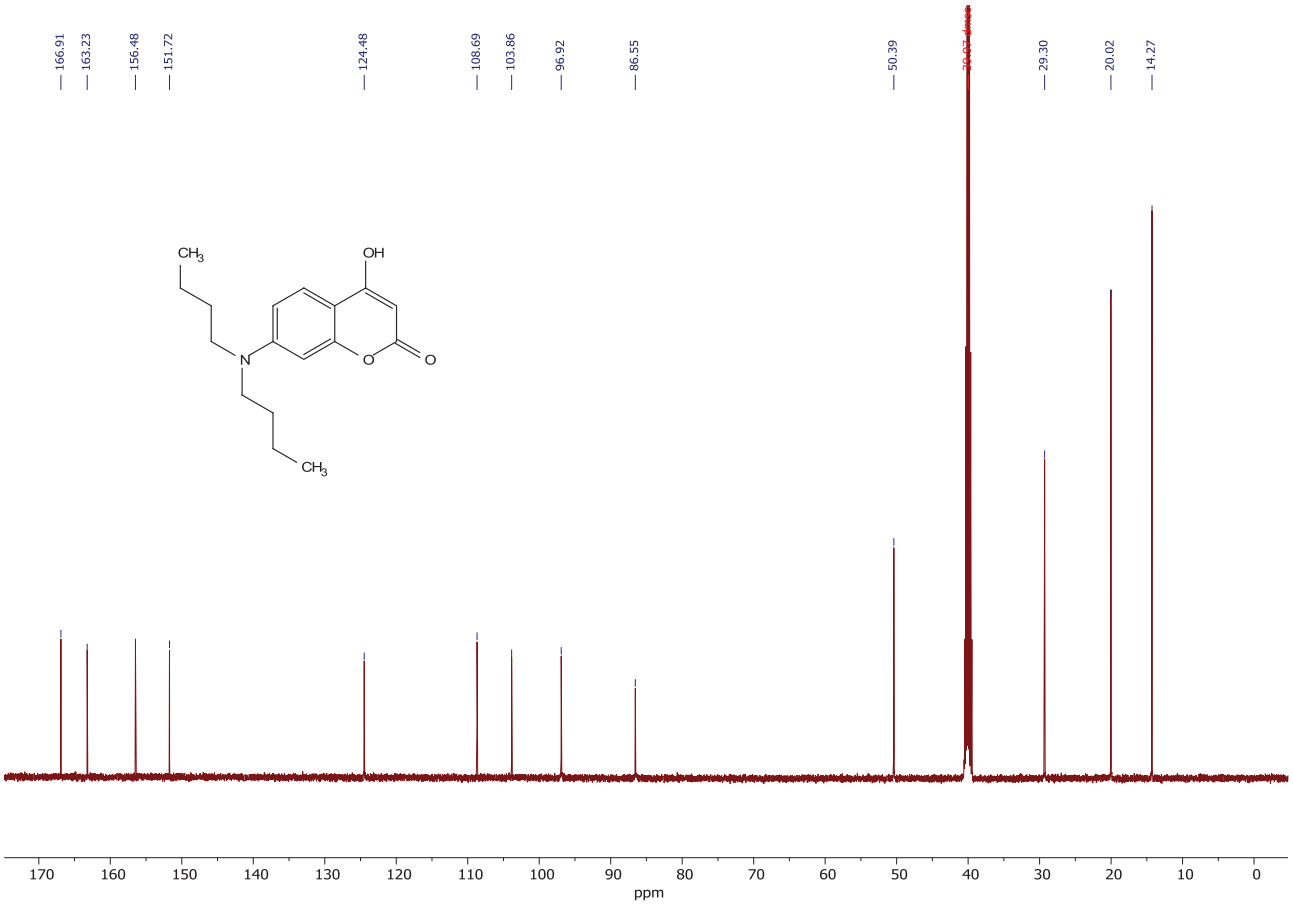
166.91
163.23
156.48
151.72
124.48
108.69
103.86
96.92
86.55
50.39
30.07
29.30
20.02
14.27
CH3
OH
N
O
O
CH3
170
160
150
140
130
120
110
100
90
80
70
60
50
40
30
20
10
0
ppm

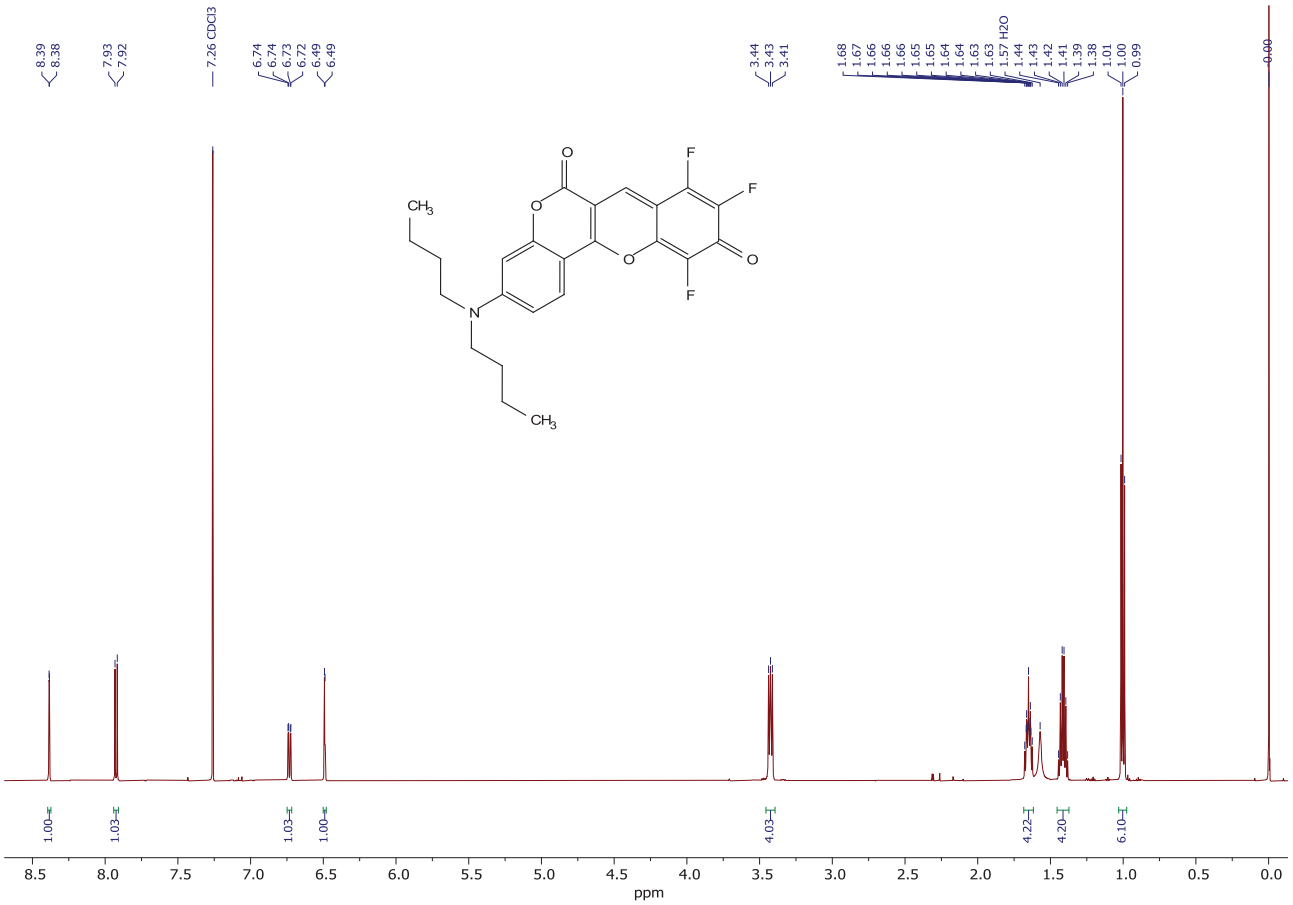
8.39
8.38
7.93
7.92
7.26 CDCl3
6.74
6.74
6.73
6.72
6.49
6.49
3.44
3.43
3.41
1.68
1.67
1.66
1.66
1.66
1.65
1.65
1.64
1.64
1.63
1.63
1.57 H2O
1.44
1.43
1.42
1.41
1.39
1.38
1.01
1.00
0.99
0.00
1.00
1.03
1.03
1.00
4.03
4.22
4.20
6.10
8.5
8.0
7.5
7.0
6.5
6.0
5.5
5.0
4.5
4.0
3.5
3.0
2.5
2.0
1.5
1.0
0.5
0.0
ppm

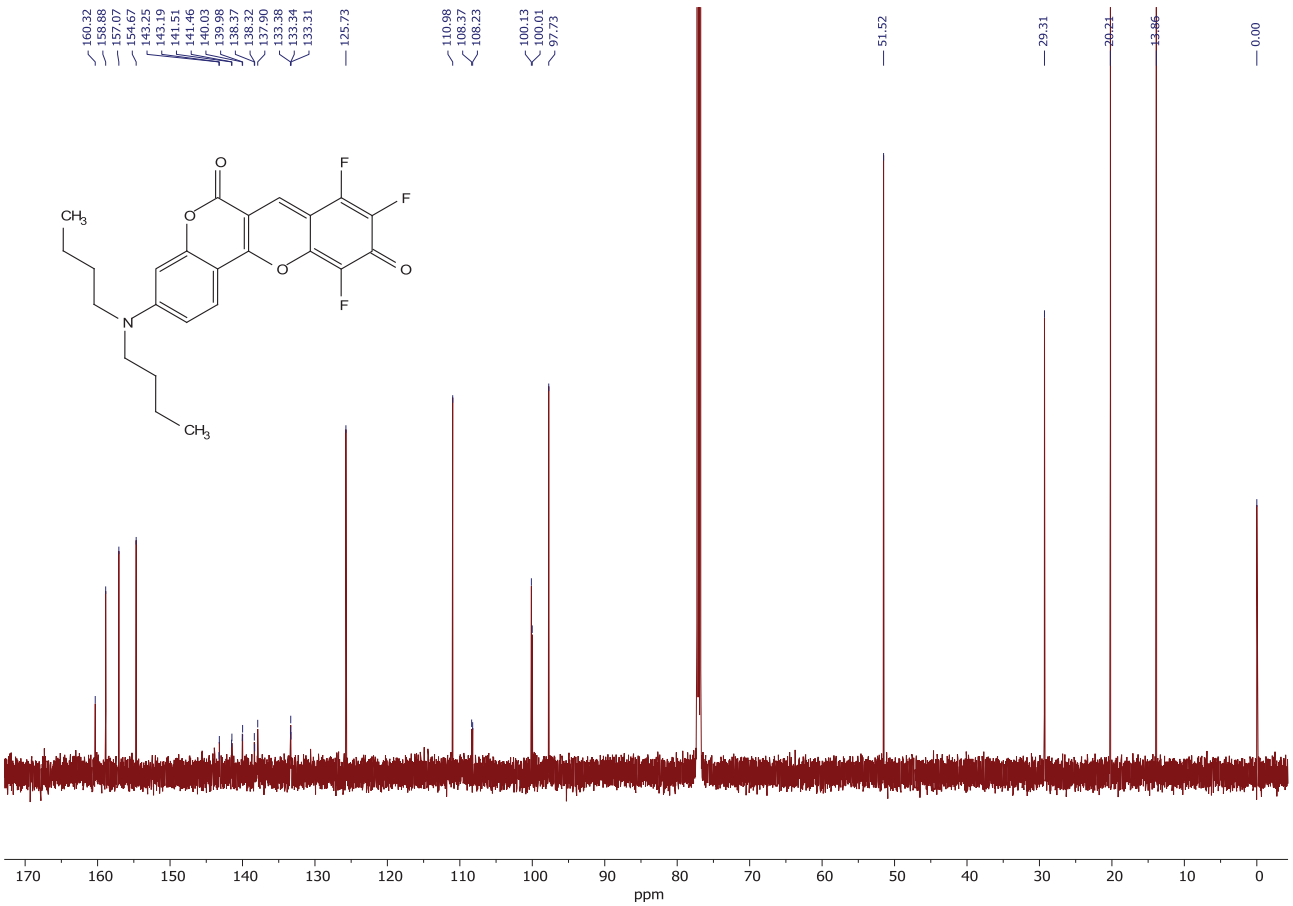
160.32
158.88
157.07
154.67
143.25
143.19
141.51
141.46
140.03
139.98
138.37
138.32
137.90
133.38
133.34
133.31
125.73
110.98
108.37
108.23
100.13
100.01
97.73
51.52
29.31
20.21
13.86
0.00
170
160
150
140
130
120
110
100
90
80
70
60
50
40
30
20
10
0
ppm

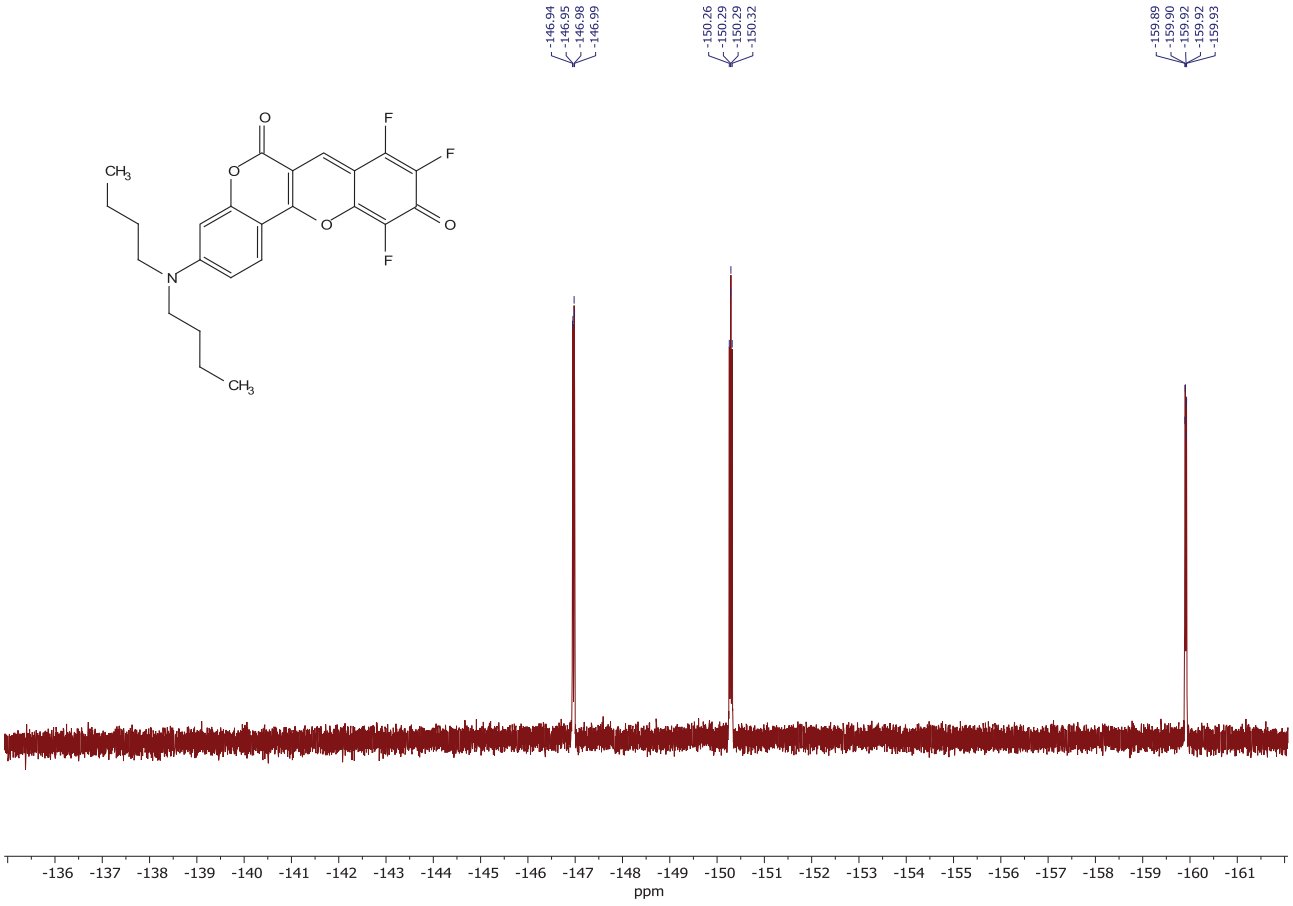
-146.94
-146.95
-146.98
-146.99
-150.26
-150.29
-150.29
-150.32
-159.89
-159.90
-159.92
-159.92
-159.93
O
F
F
O
O
O
F
CH3
N
CH3
-136 -137 -138 -139 -140 -141 -142 -143 -144 -145 -146 -147 -148 -149 -150 -151 -152 -153 -154 -155 -156 -157 -158 -159 -160 -161
ppm

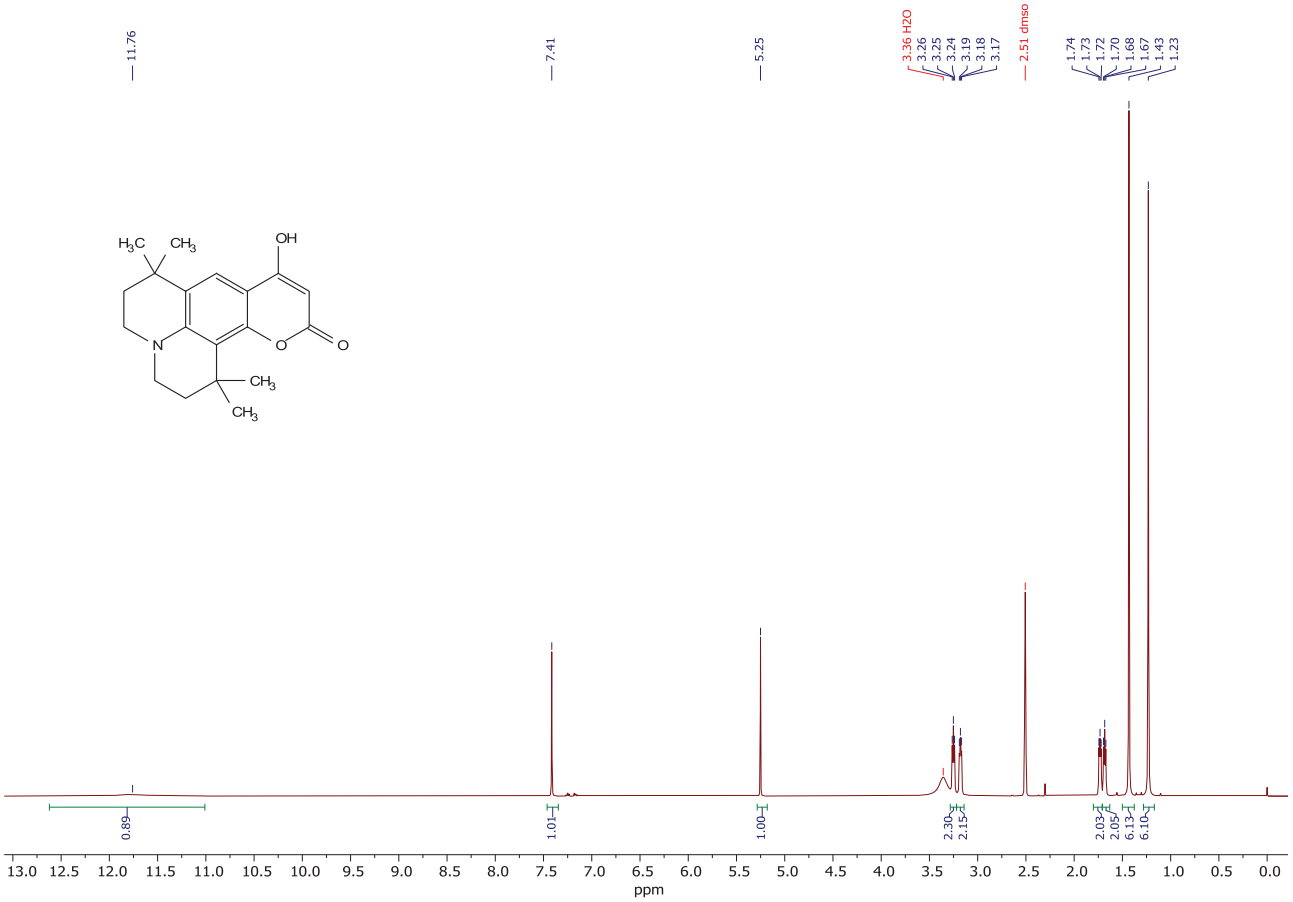
11.76
7.41
5.25
3.36 H2O
3.26
3.25
3.24
3.19
3.18
3.17
2.51 dmso
1.74
1.73
1.72
1.70
1.68
1.67
1.43
1.23
OH
O
N
O
0.89
1.01
1.00
2.30
2.15
2.03
2.05
6.13
6.10
ppm

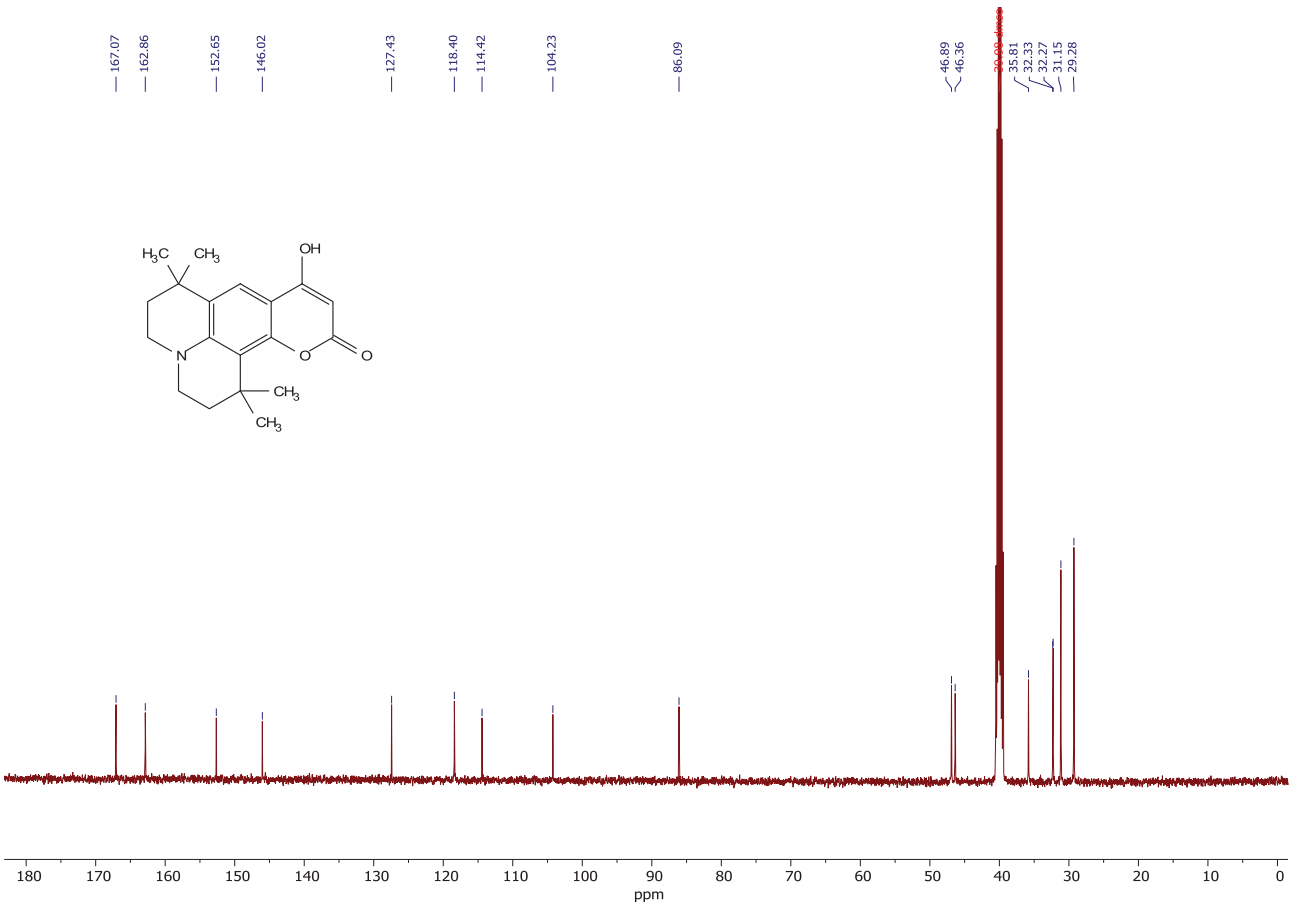
167.07
162.86
152.65
146.02
127.43
118.40
114.42
104.23
86.09
46.89
46.36
39.99 dmso
35.81
32.33
32.27
31.15
29.28
OH
O
N
O
ppm

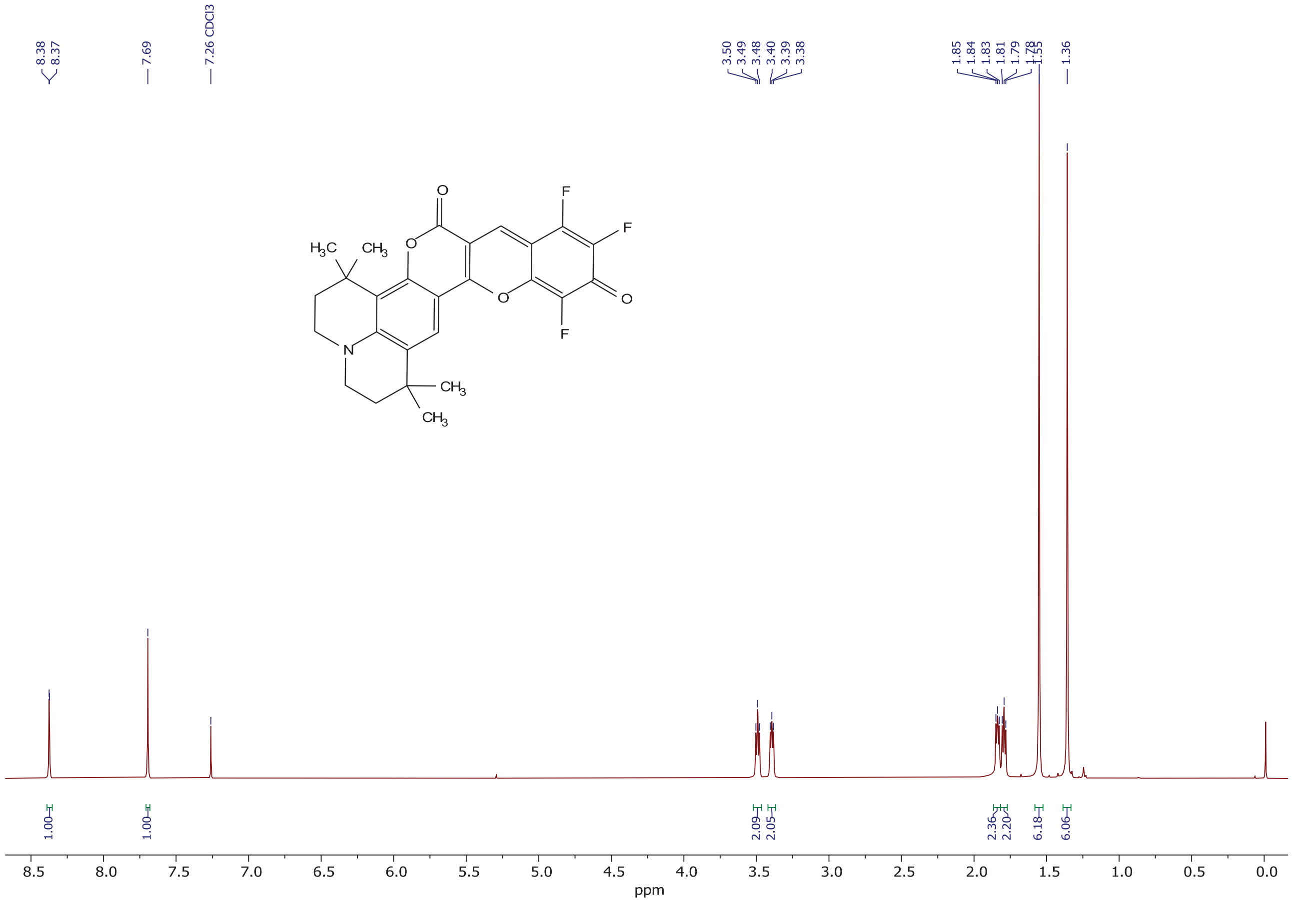
8.38
8.37
7.69
7.26 CDCl3
3.50
3.49
3.48
3.40
3.39
3.38
1.85
1.84
1.83
1.81
1.79
1.78
1.55
1.36
F
F
O
F
O
O
O
H3C
CH3
N
CH3
CH3
1.00
1.00
2.09
2.05
2.36
2.20
6.18
6.06
8.5
8.0
7.5
7.0
6.5
6.0
5.5
5.0
4.5
4.0
3.5
3.0
2.5
2.0
1.5
1.0
0.5
0.0
ppm

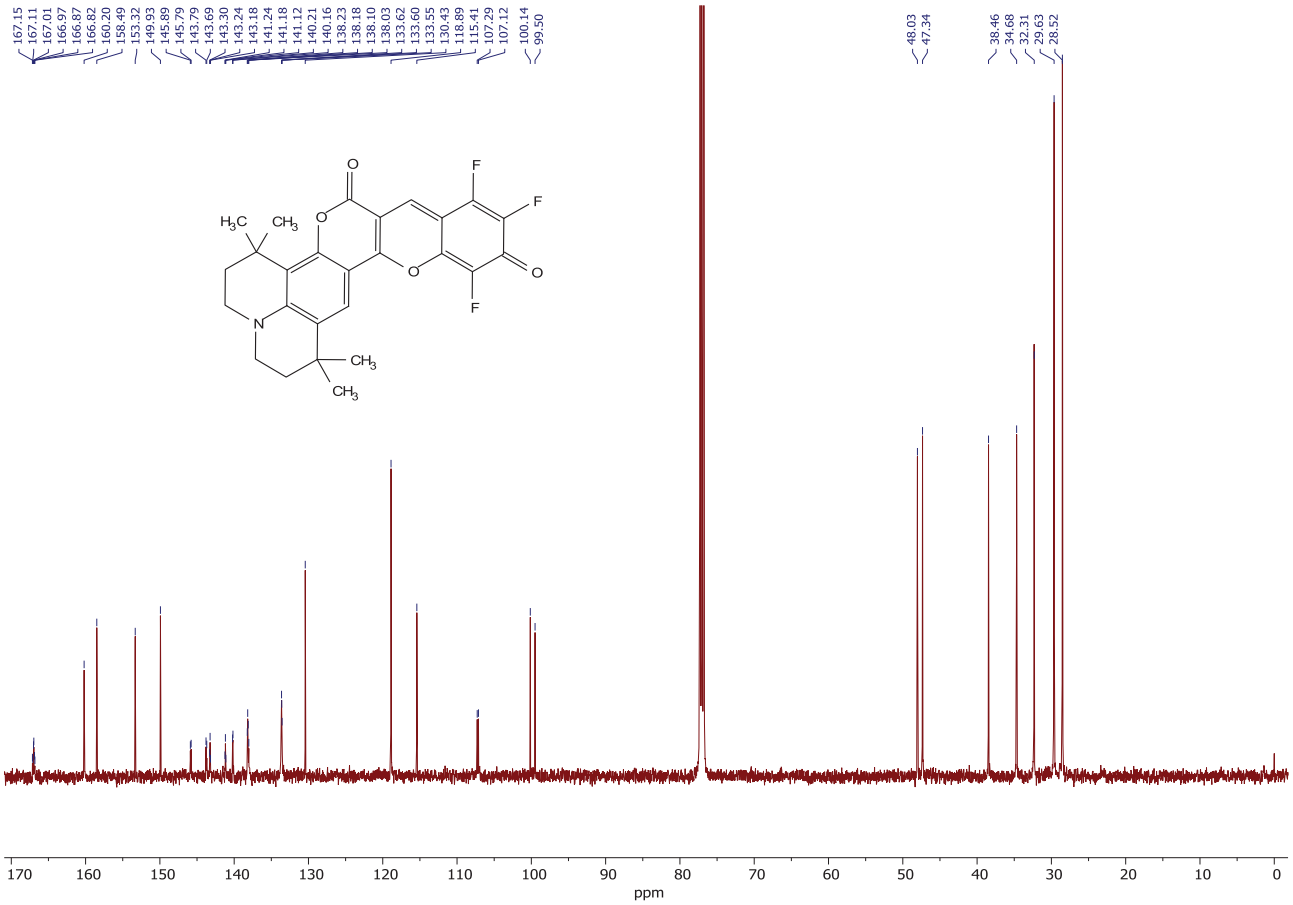
167.15
167.11
167.01
166.97
166.87
166.82
160.20
158.49
153.32
149.93
145.89
145.79
143.79
143.69
143.30
143.24
143.18
141.24
141.18
141.12
140.21
140.16
138.23
138.18
138.10
138.03
133.62
133.60
133.55
130.43
118.89
115.41
107.29
107.12
100.14
99.50
48.03
47.34
38.46
34.68
32.31
29.63
28.52
O
F
F
O
O
O
F
H3C
CH3
N
CH3
CH3
170
160
150
140
130
120
110
100
90
80
70
60
50
40
30
20
10
0
ppm

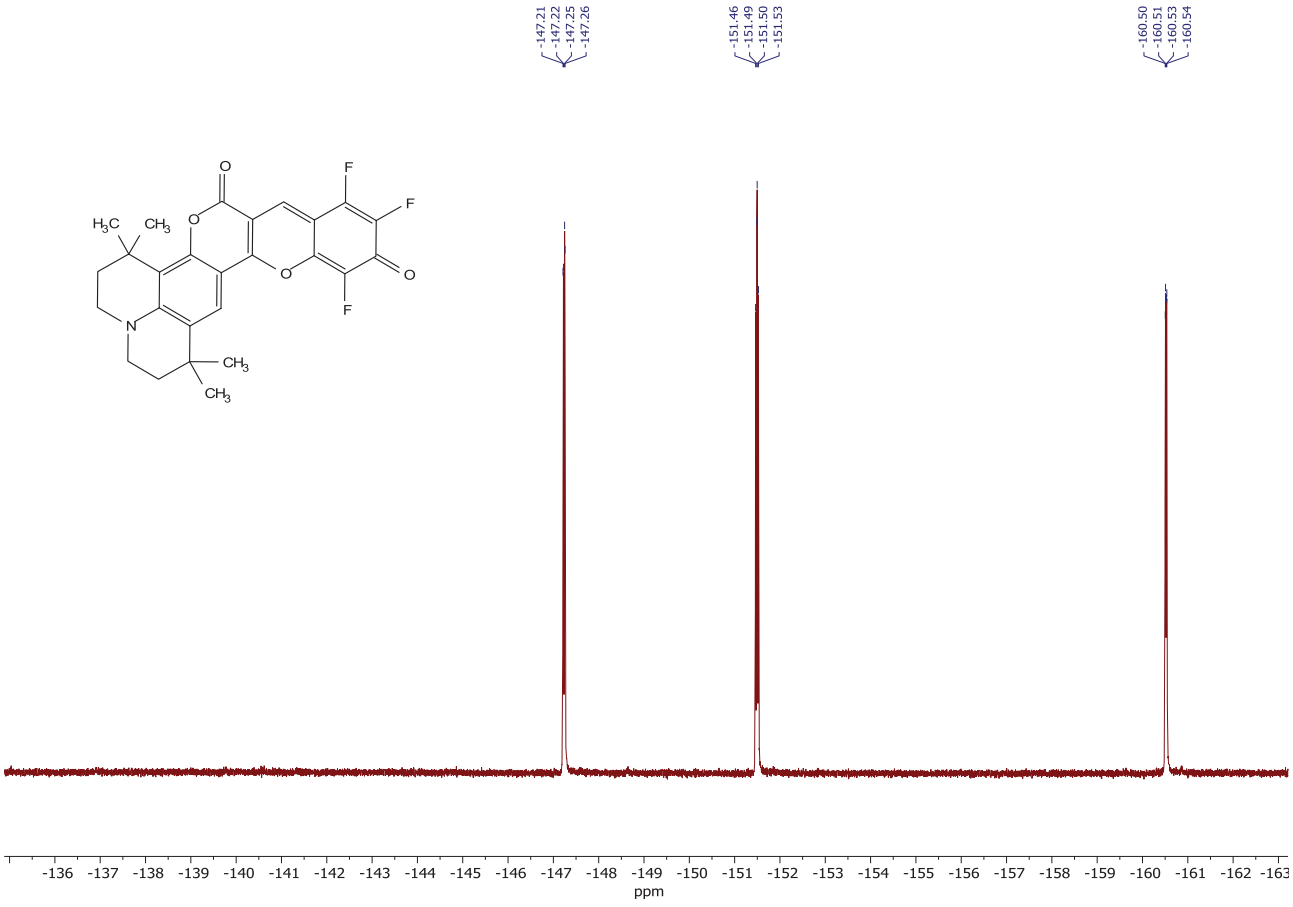
-147.21
-147.22
-147.25
-147.26
-151.46
-151.49
-151.50
-151.53
-160.50
-160.51
-160.53
-160.54
O
F
F
O
O
O
F
H3C
CH3
N
CH3
CH3
-136
-137
-138
-139
-140
-141
-142
-143
-144
-145
-146
-147
-148
-149
-150
-151
-152
-153
-154
-155
-156
-157
-158
-159
-160
-161
-162
-163
ppm

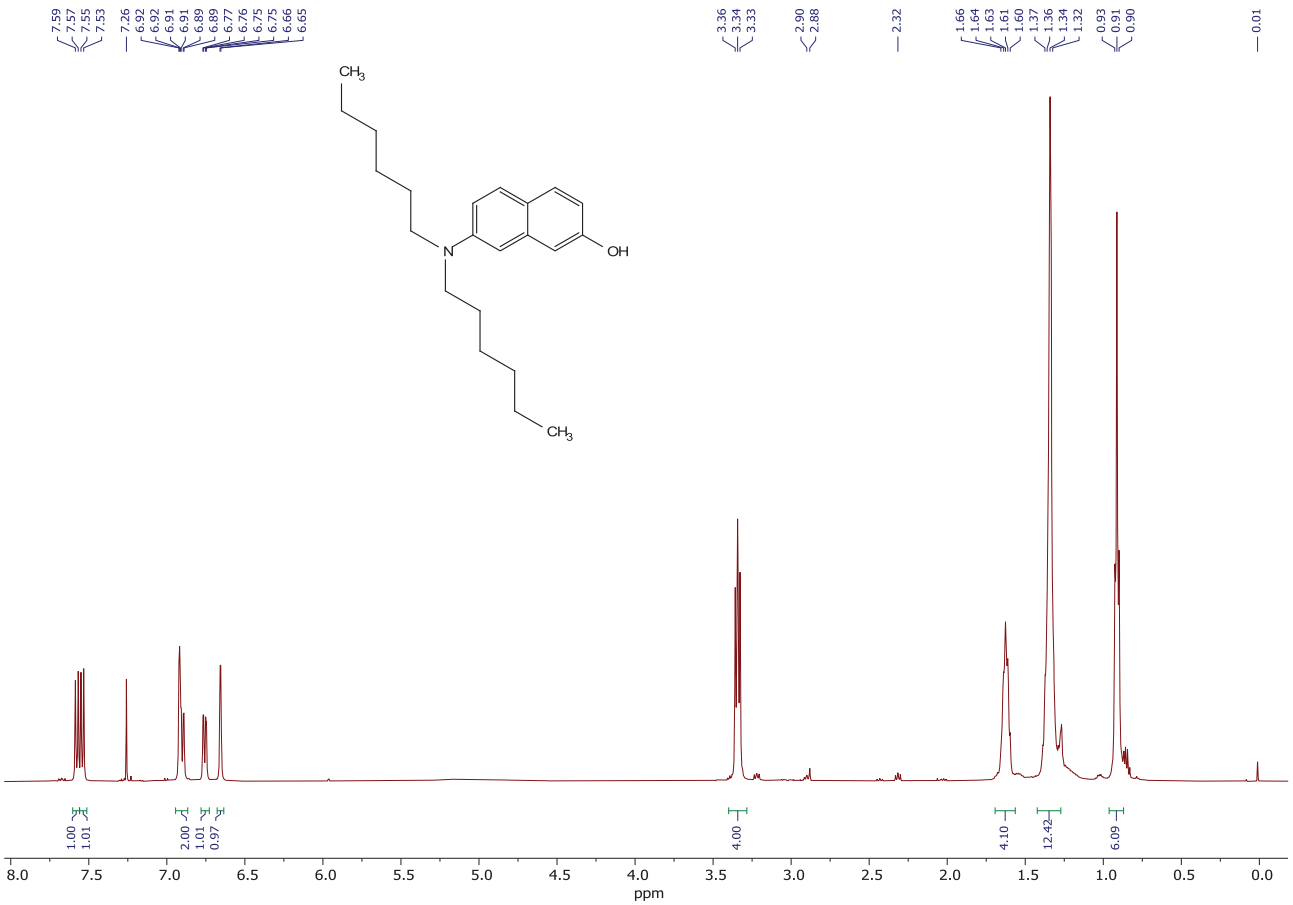
7.59
7.57
7.55
7.53
7.26
6.92
6.92
6.91
6.91
6.89
6.89
6.77
6.76
6.75
6.75
6.66
6.65
3.36
3.34
3.33
2.90
2.88
2.32
1.66
1.64
1.63
1.61
1.60
1.37
1.36
1.34
1.32
0.93
0.91
0.90
0.01
CH3
N
OH
CH3
1.00
1.01
2.00
1.01
0.97
4.00
4.10
12.42
6.09
8.0
7.5
7.0
6.5
6.0
5.5
5.0
4.5
4.0
3.5
3.0
2.5
2.0
1.5
1.0
0.5
0.0
ppm

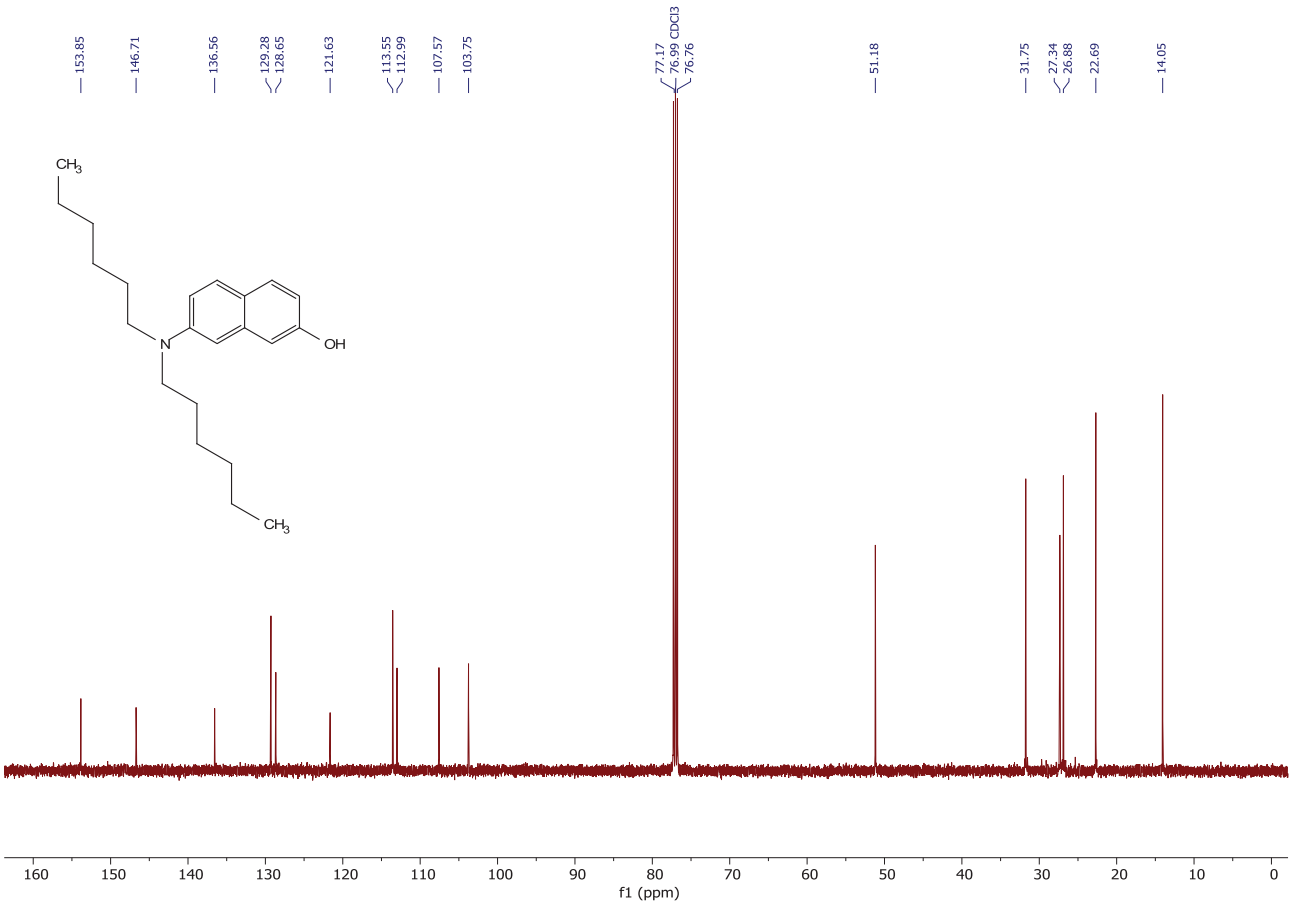
153.85
146.71
136.56
129.28
128.65
121.63
113.55
112.99
107.57
103.75
77.17
76.99 CDCl3
76.76
51.18
31.75
27.34
26.88
22.69
14.05
CH3
N
OH
CH3
160
150
140
130
120
110
100
90
80
70
60
50
40
30
20
10
0
f1 (ppm)

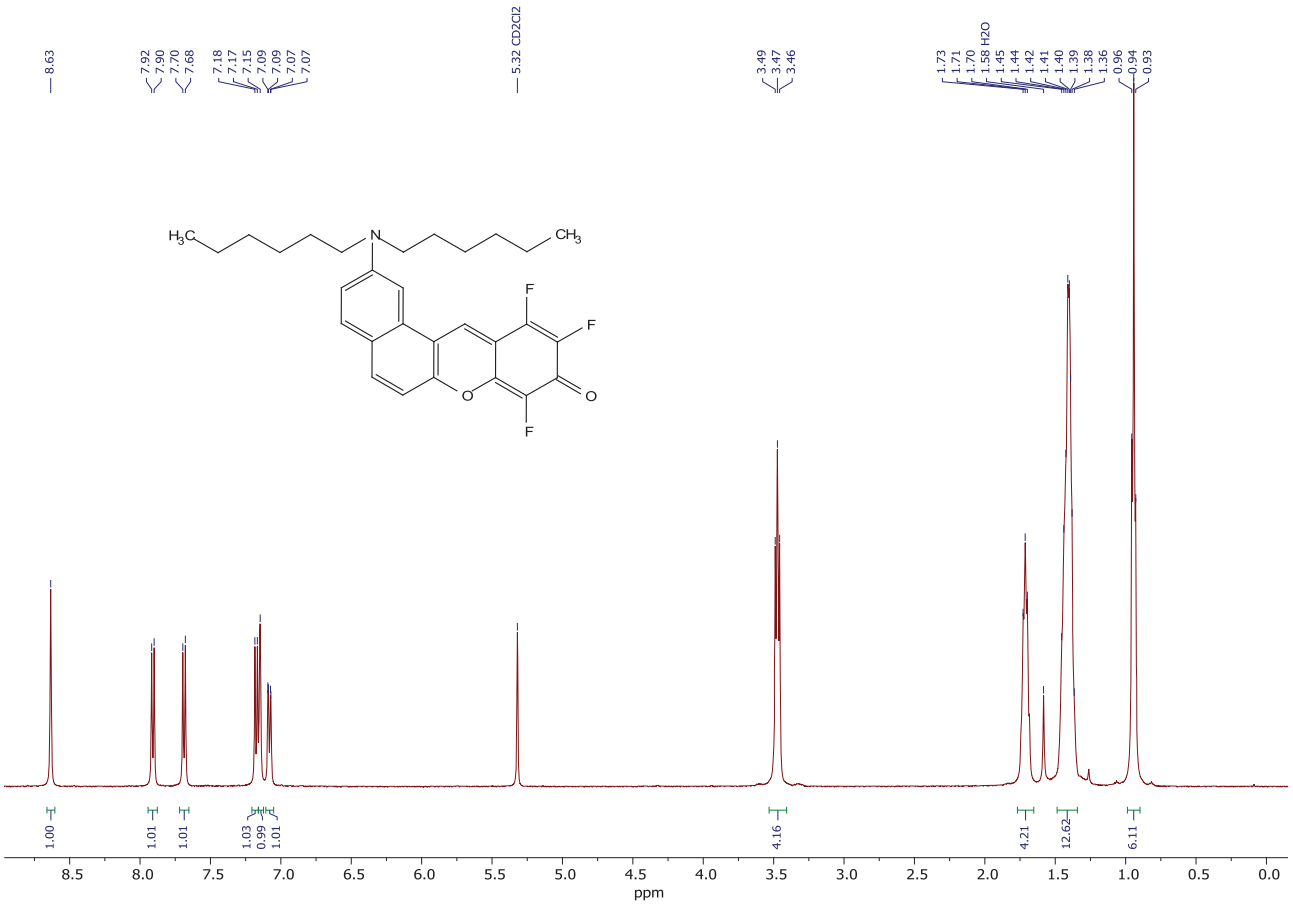
8.63
7.92
7.90
7.70
7.68
7.18
7.17
7.15
7.09
7.07
7.07
5.32 CD2Cl2
3.49
3.47
3.46
1.73
1.71
1.70
1.58 H2O
1.45
1.44
1.42
1.41
1.40
1.39
1.38
1.36
0.96
0.94
0.93
H3C
N
CH3
F
F
O
F
1.00
1.01
1.01
1.03
0.99
1.01
4.16
4.21
12.62
6.11
ppm

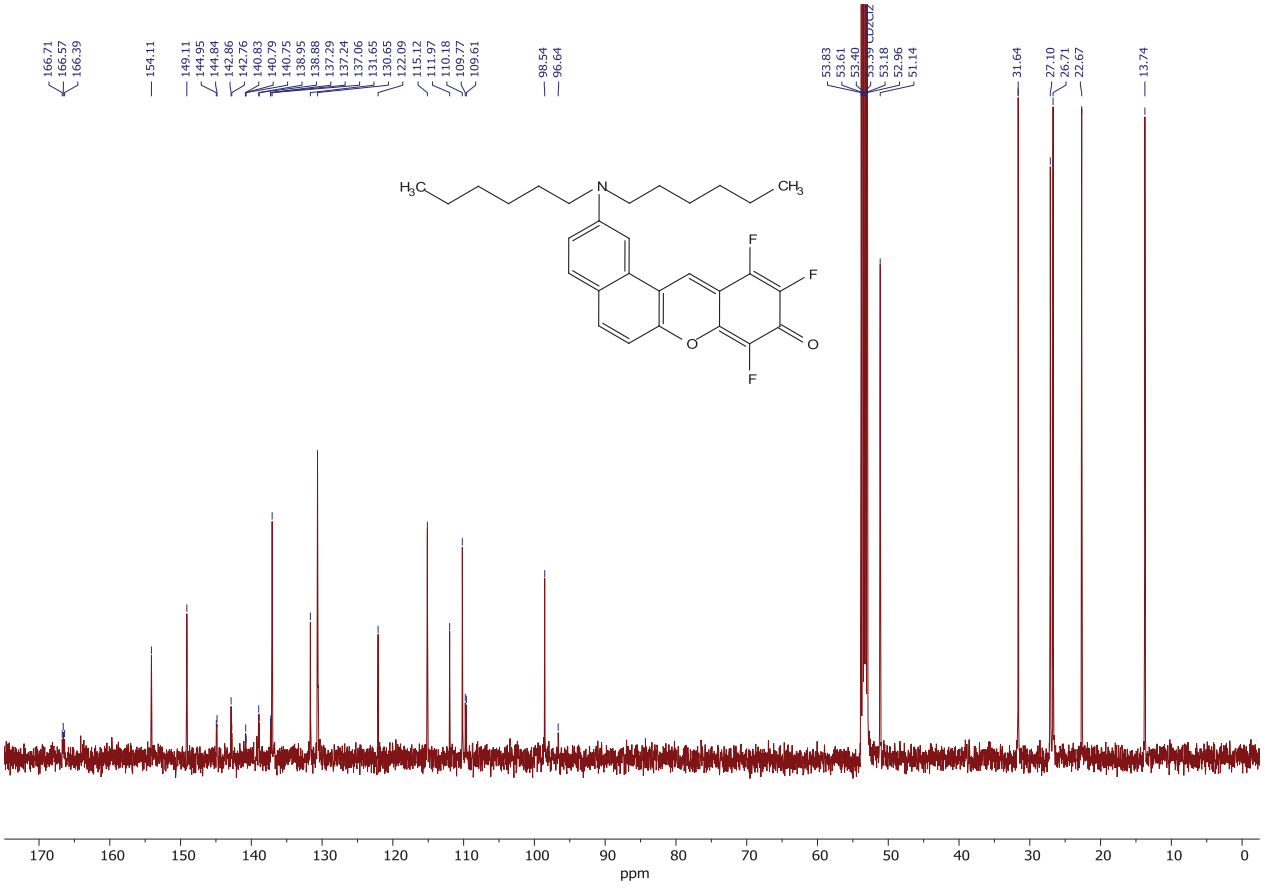
166.71
166.57
166.39
154.11
149.11
144.95
144.84
142.86
142.76
140.83
140.79
140.75
138.95
138.88
137.29
137.24
137.06
131.65
130.65
122.09
115.12
111.97
110.18
109.77
109.61
98.54
96.64
53.83
53.61
53.40
53.39 CD2Cl2
53.18
52.96
51.14
31.64
27.10
26.71
22.67
13.74
H3C
N
CH3
F
F
O
F
ppm

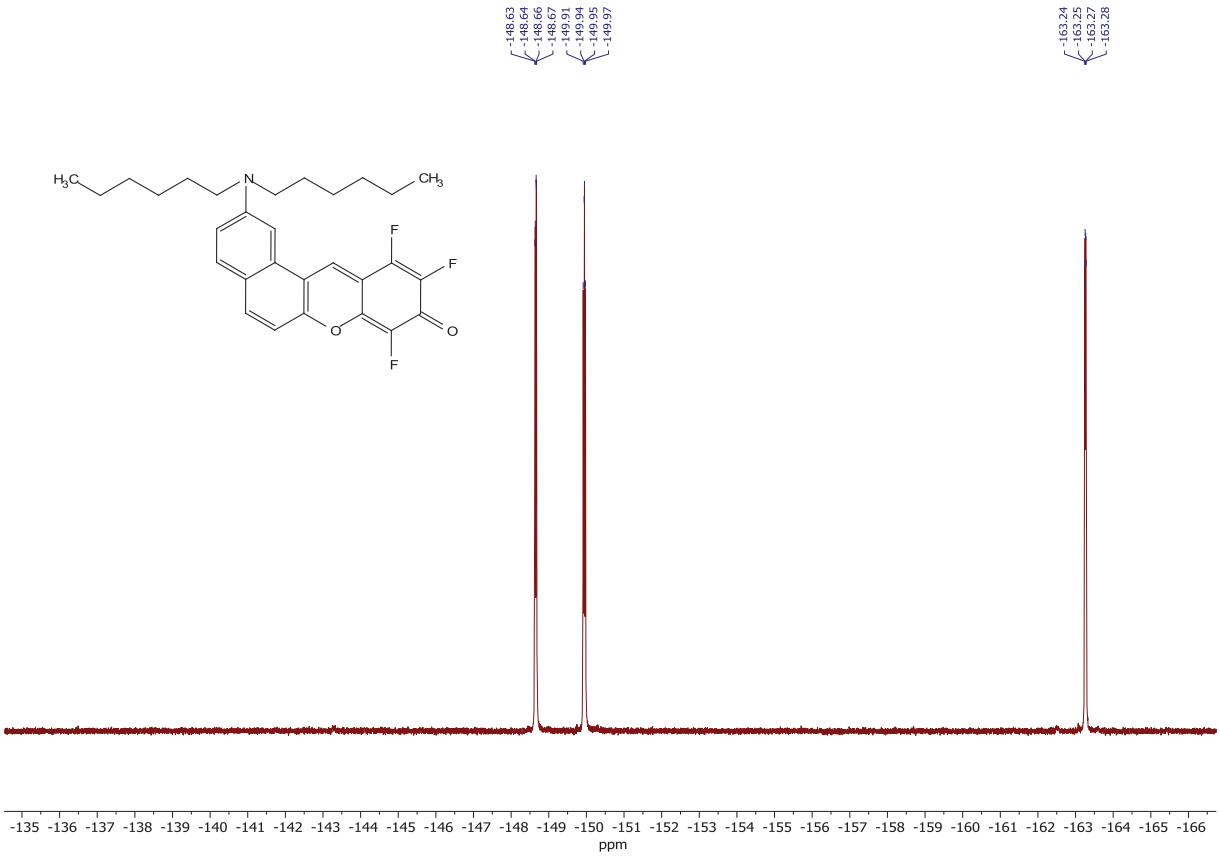
-148.63
-148.64
-148.66
-148.67
-149.91
-149.94
-149.95
-149.97
-163.24
-163.25
-163.27
-163.28
H3C
N
CH3
F
F
O
O
F
-135 -136 -137 -138 -139 -140 -141 -142 -143 -144 -145 -146 -147 -148 -149 -150 -151 -152 -153 -154 -155 -156 -157 -158 -159 -160 -161 -162 -163 -164 -165 -166
ppm

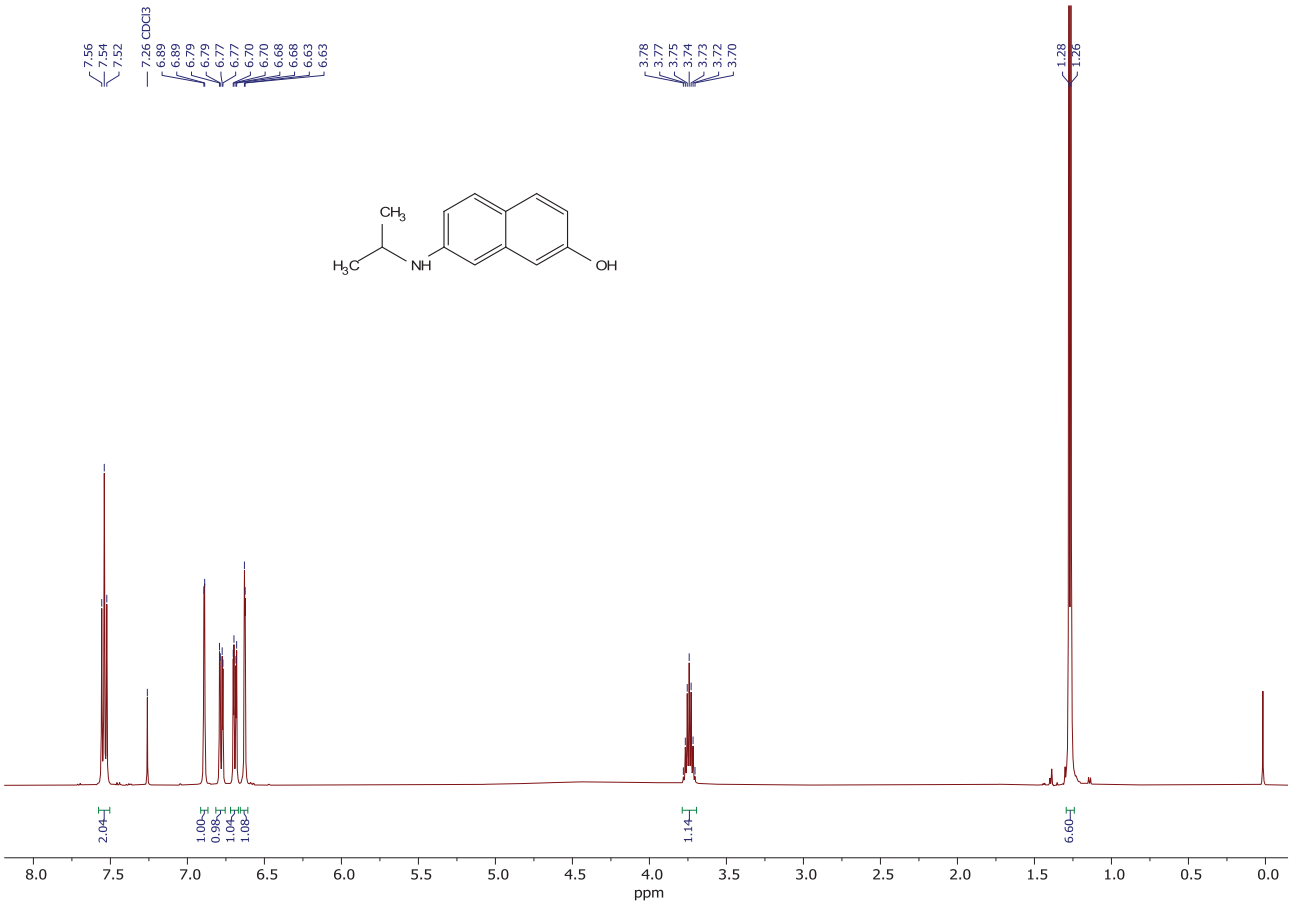
7.56
7.54
7.52
7.26 CDCl3
6.89
6.89
6.79
6.79
6.77
6.77
6.70
6.70
6.68
6.68
6.63
6.63
3.78
3.77
3.75
3.74
3.73
3.72
3.70
1.28
1.26
CH3
H3C
NH
OH
2.04
1.00
0.98
1.04
1.08
1.14
6.60
8.0 7.5 7.0 6.5 6.0 5.5 5.0 4.5 4.0 3.5 3.0 2.5 2.0 1.5 1.0 0.5 0.0
ppm

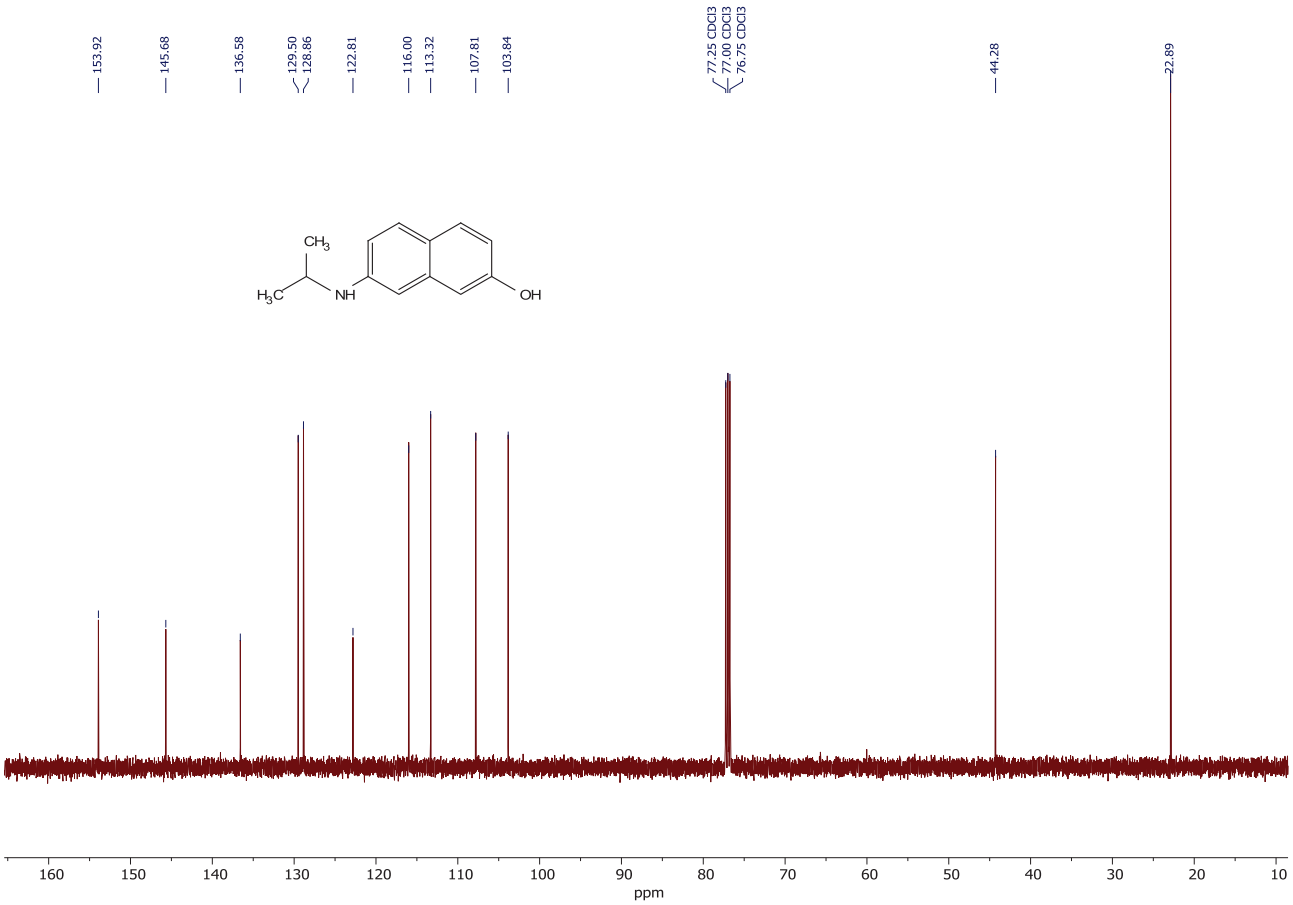
153.92
145.68
136.58
129.50
128.86
122.81
116.00
113.32
107.81
103.84
77.25 CDCl3
77.00 CDCl3
76.75 CDCl3
44.28
22.89
CH3
H3C
NH
OH
ppm

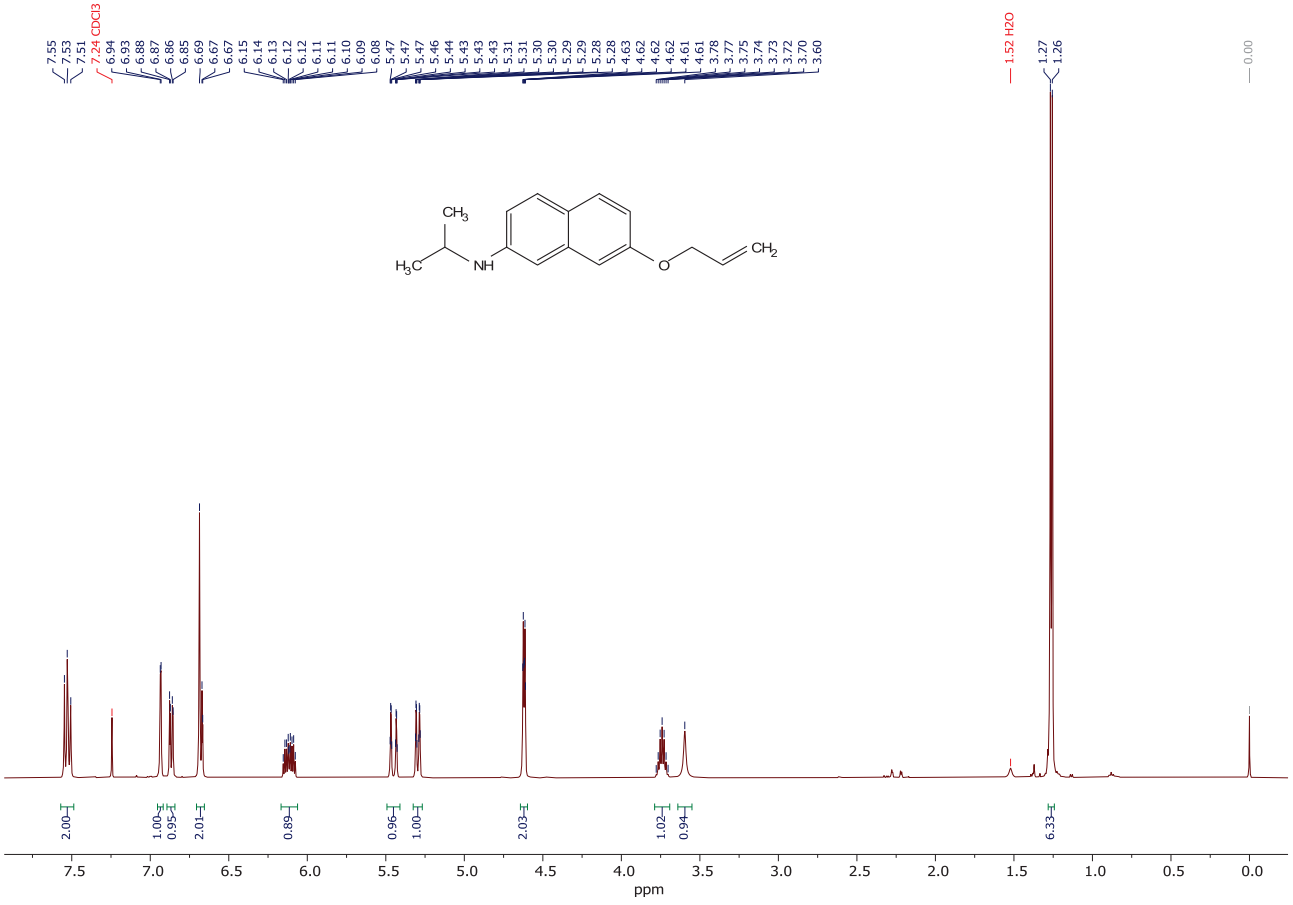
7.55
7.53
7.51
7.24 CDCl3
6.94
6.93
6.88
6.87
6.86
6.85
6.69
6.67
6.67
6.15
6.14
6.13
6.12
6.12
6.11
6.11
6.10
6.09
6.08
5.47
5.47
5.46
5.44
5.43
5.43
5.43
5.31
5.31
5.30
5.30
5.29
5.29
5.28
5.28
4.63
4.62
4.62
4.62
4.61
4.61
3.78
3.77
3.75
3.74
3.73
3.72
3.70
3.60
1.52 H2O
1.27
1.26
0.00
CH3
H3C
NH
O
CH2
2.00
1.00
0.95
2.01
0.89
0.96
1.00
2.03
1.02
0.94
6.33
ppm

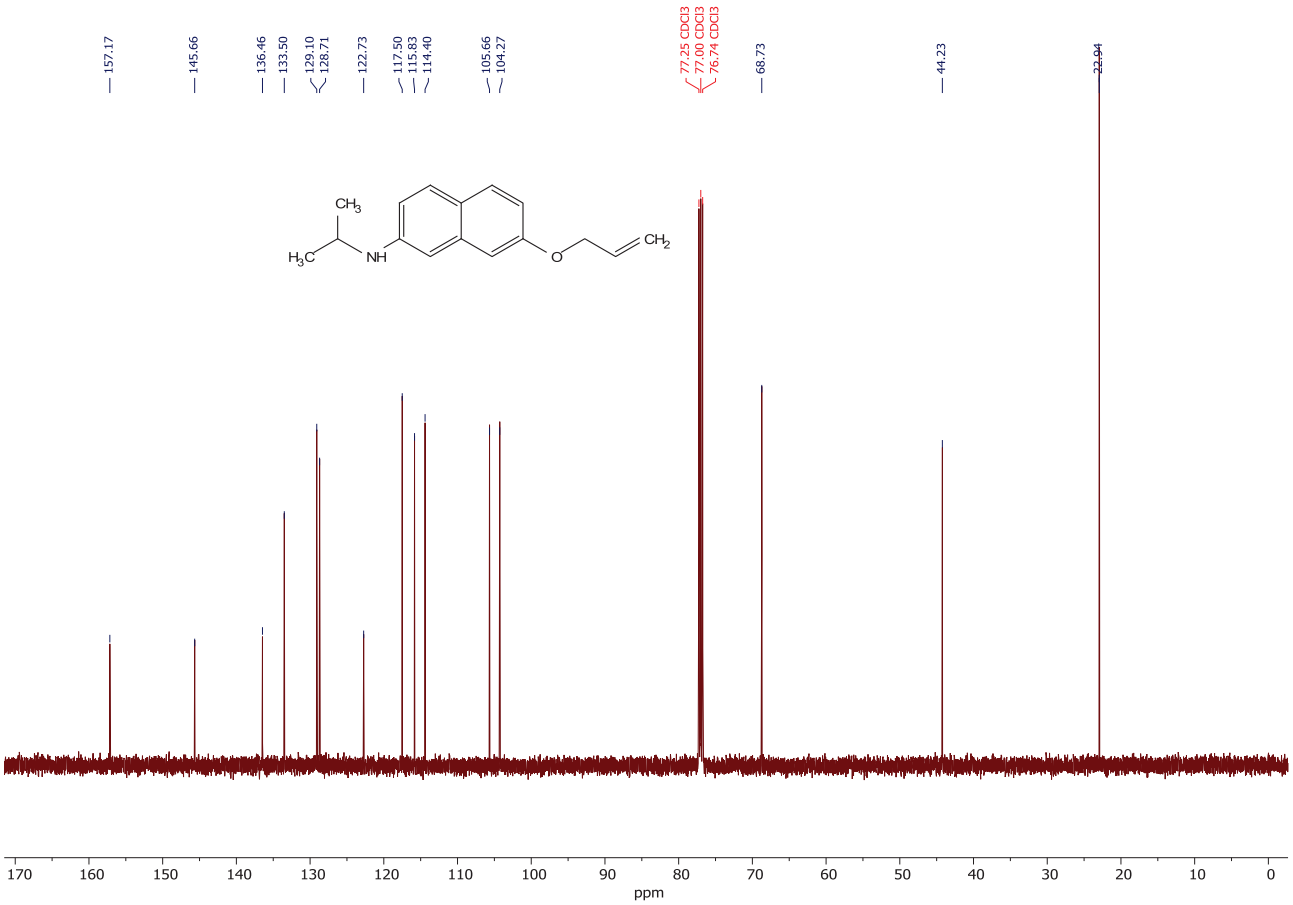
157.17
145.66
136.46
133.50
129.10
128.71
122.73
117.50
115.83
114.40
105.66
104.27
77.25 CDCl3
77.00 CDCl3
76.74 CDCl3
68.73
44.23
22.94
CH3
H3C
NH
O
CH2
170 160 150 140 130 120 110 100 90 80 70 60 50 40 30 20 10 0
ppm

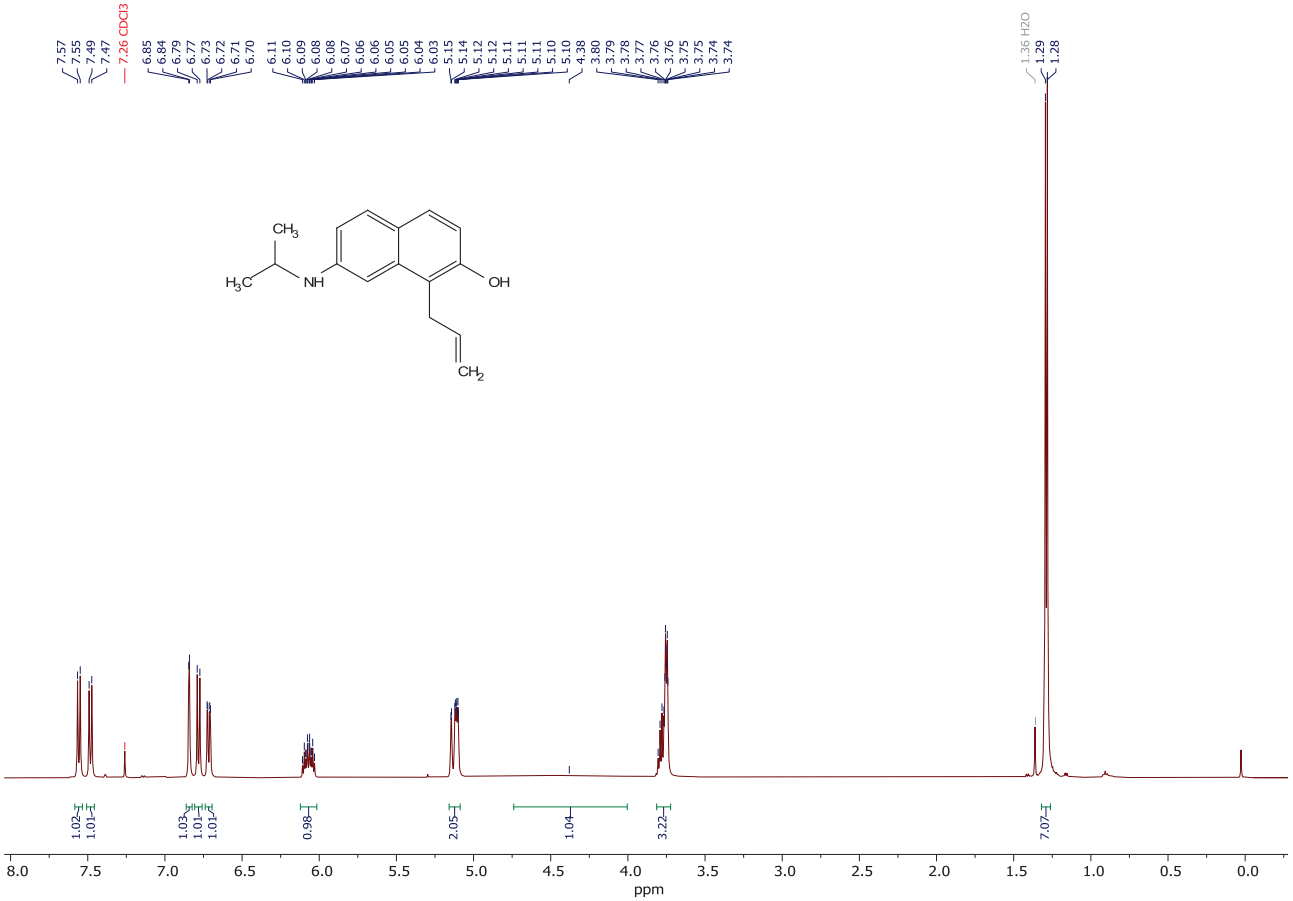
7.57
7.55
7.49
7.47
7.26 CDCl3
6.85
6.84
6.79
6.77
6.73
6.72
6.71
6.70
6.11
6.10
6.09
6.08
6.07
6.06
6.06
6.05
6.05
6.04
6.03
5.15
5.14
5.12
5.12
5.11
5.11
5.11
5.10
5.10
4.38
3.80
3.79
3.78
3.77
3.76
3.76
3.75
3.75
3.74
3.74
1.36 H2O
1.29
1.28
CH3
H3C
NH
OH
CH2
1.02
1.01
1.03
1.01
1.01
0.98
2.05
1.04
3.22
7.07
8.0 7.5 7.0 6.5 6.0 5.5 5.0 4.5 4.0 3.5 3.0 2.5 2.0 1.5 1.0 0.5 0.0
ppm

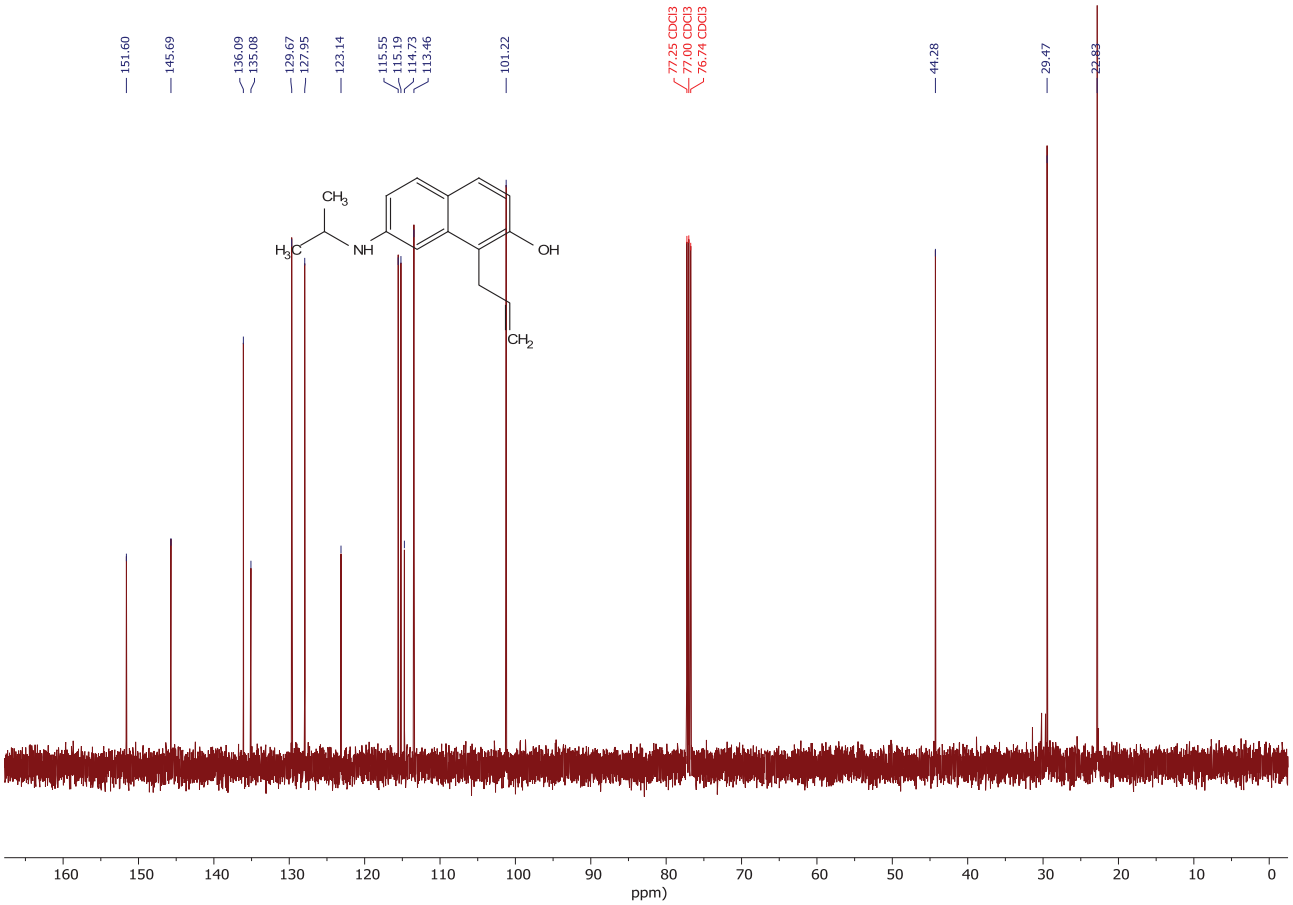
151.60
145.69
136.09
135.08
129.67
127.95
123.14
115.55
115.19
114.73
113.46
101.22
77.25 CDCl3
77.00 CDCl3
76.74 CDCl3
44.28
29.47
22.83
CH3
H3C
NH
OH
CH2
160
150
140
130
120
110
100
90
80
70
60
50
40
30
20
10
0
ppm)

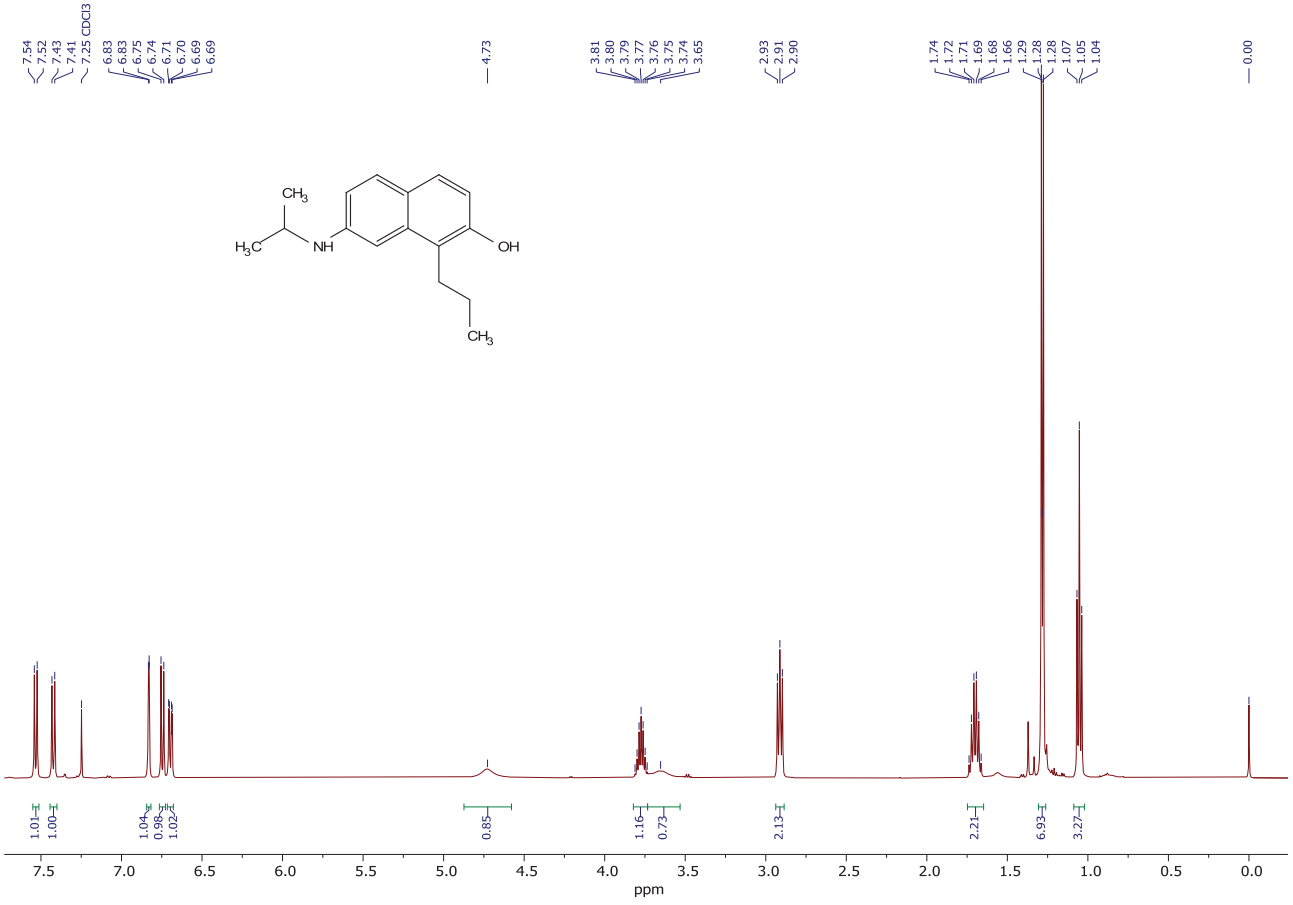
7.54
7.52
7.43
7.41
7.25 CDCl3
6.83
6.83
6.75
6.74
6.71
6.70
6.69
6.69
4.73
3.81
3.80
3.79
3.77
3.76
3.75
3.74
3.65
2.93
2.91
2.90
1.74
1.72
1.71
1.69
1.68
1.66
1.29
1.28
1.28
1.07
1.05
1.04
0.00
CH3
H3C
NH
OH
CH3
1.01
1.00
1.04
0.98
1.02
0.85
1.16
0.73
2.13
2.21
6.93
3.27
7.5
7.0
6.5
6.0
5.5
5.0
4.5
4.0
3.5
3.0
2.5
2.0
1.5
1.0
0.5
0.0
ppm

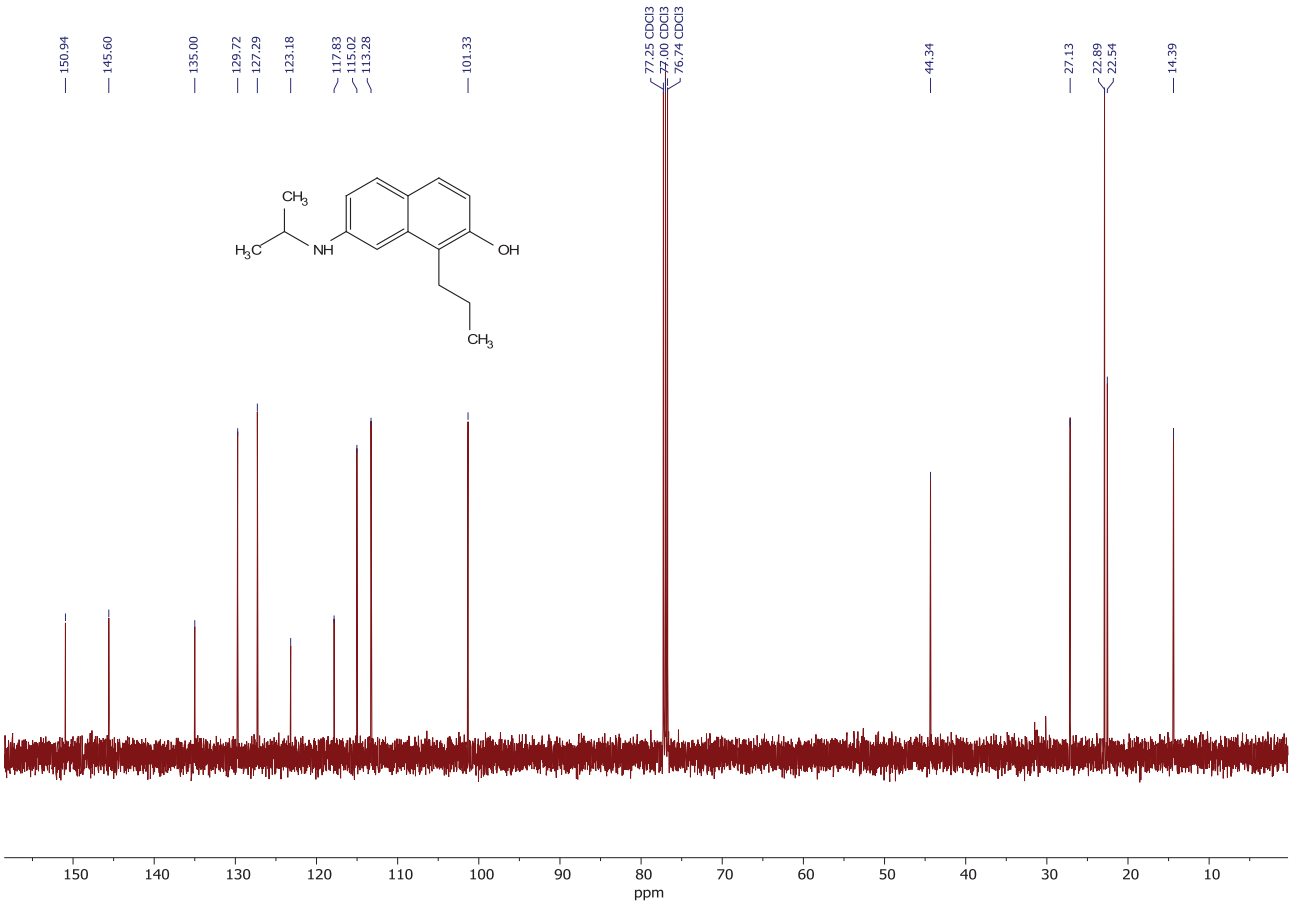
150.94
145.60
135.00
129.72
127.29
123.18
117.83
115.02
113.28
101.33
77.25 CDCl3
77.00 CDCl3
76.74 CDCl3
44.34
27.13
22.89
22.54
14.39
CH3
H3C
NH
OH
CH3
150
140
130
120
110
100
90
80
70
60
50
40
30
20
10
ppm

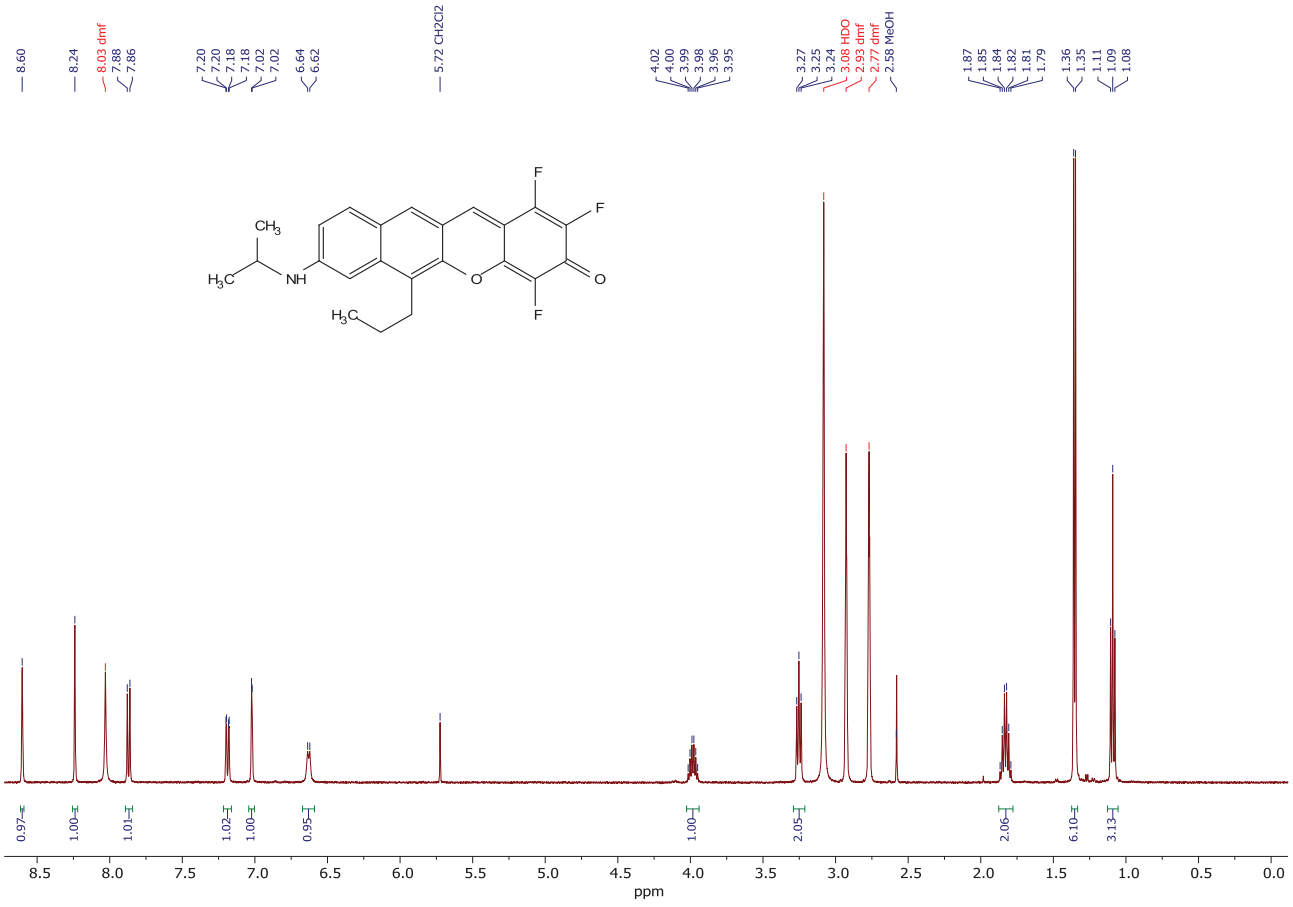
8.60
8.24
8.03 dmf
7.88
7.86
7.20
7.20
7.18
7.02
7.02
6.64
6.62
5.72 CH2Cl2
4.02
4.00
3.99
3.98
3.96
3.95
3.27
3.25
3.24
3.08 HDO
2.93 dmf
2.77 dmf
2.58 MeOH
1.87
1.85
1.84
1.82
1.81
1.79
1.36
1.35
1.11
1.09
1.08
F
F
CH3
H3C
NH
O
O
H3C
F
0.97
1.00
1.01
1.02
1.00
0.95
1.00
2.05
2.06
6.10
3.13
8.5
8.0
7.5
7.0
6.5
6.0
5.5
5.0
4.5
4.0
3.5
3.0
2.5
2.0
1.5
1.0
0.5
0.0
ppm

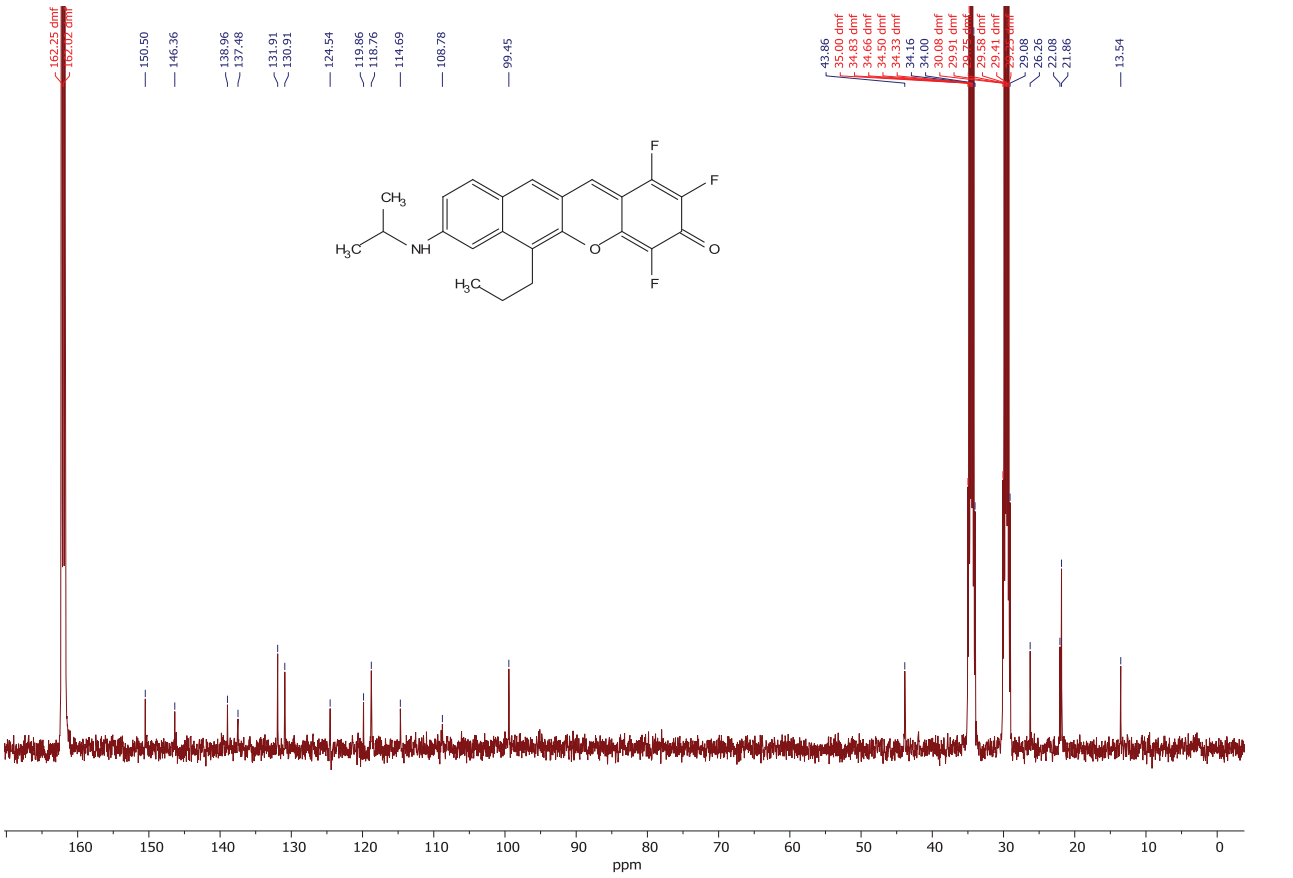
162.25 dmf
162.02 dmf
150.50
146.36
138.96
137.48
131.91
130.91
124.54
119.86
118.76
114.69
108.78
99.45
43.86
35.00 dmf
34.83 dmf
34.66 dmf
34.50 dmf
34.33 dmf
34.16
34.00
30.08 dmf
29.91 dmf
29.75 dmf
29.58 dmf
29.41 dmf
29.25 dmf
29.08
26.26
22.08
21.86
13.54
F
F
CH3
H3C
NH
O
O
F
H3C
160
150
140
130
120
110
100
90
80
70
60
50
40
30
20
10
0
ppm

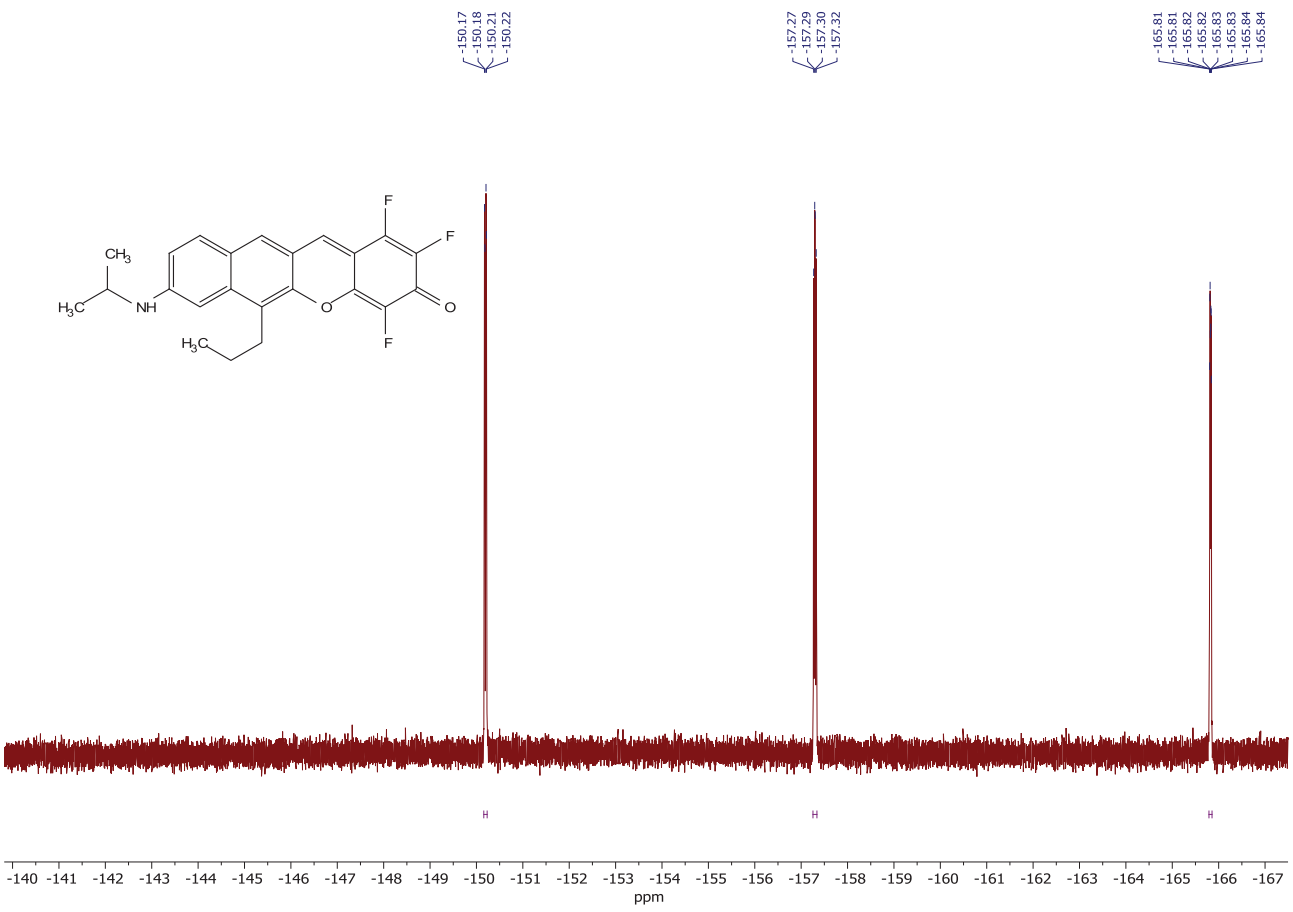
-150.17
-150.18
-150.21
-150.22
-157.27
-157.29
-157.30
-157.32
-165.81
-165.81
-165.82
-165.82
-165.83
-165.83
-165.84
-165.84
F
F
CH3
H3C
NH
O
O
F
H3C
H
H
H
-140 -141 -142 -143 -144 -145 -146 -147 -148 -149 -150 -151 -152 -153 -154 -155 -156 -157 -158 -159 -160 -161 -162 -163 -164 -165 -166 -167
ppm

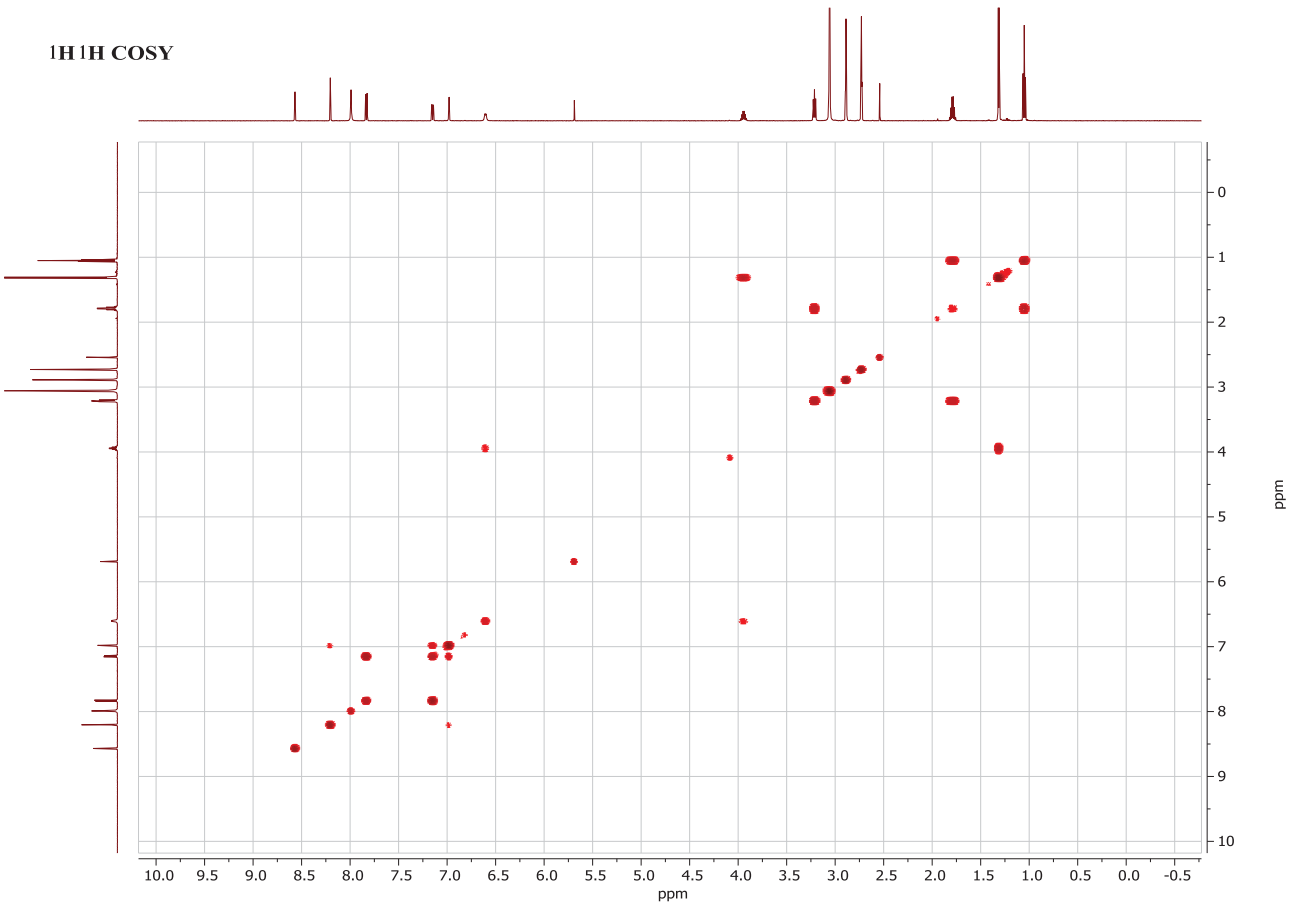
1H 1H COSY
10.0 9.5 9.0 8.5 8.0 7.5 7.0 6.5 6.0 5.5 5.0 4.5 4.0 3.5 3.0 2.5 2.0 1.5 1.0 0.5 0.0 -0.5
ppm
0 1 2 3 4 5 6 7 8 9 10
ppm

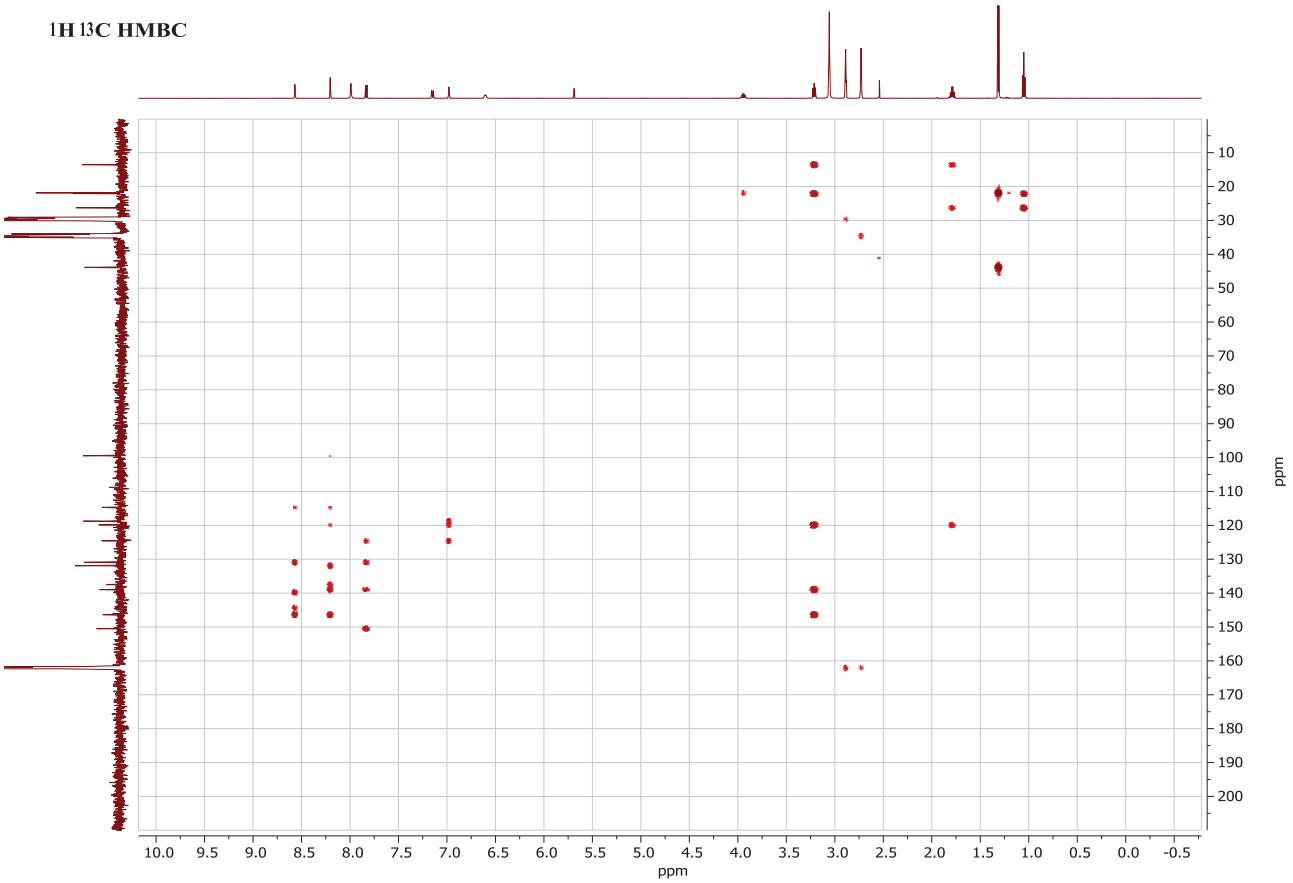
1H 13C HMBC
10.0 9.5 9.0 8.5 8.0 7.5 7.0 6.5 6.0 5.5 5.0 4.5 4.0 3.5 3.0 2.5 2.0 1.5 1.0 0.5 0.0 -0.5
ppm
10 20 30 40 50 60 70 80 90 100 110 120 130 140 150 160 170 180 190 200
ppm

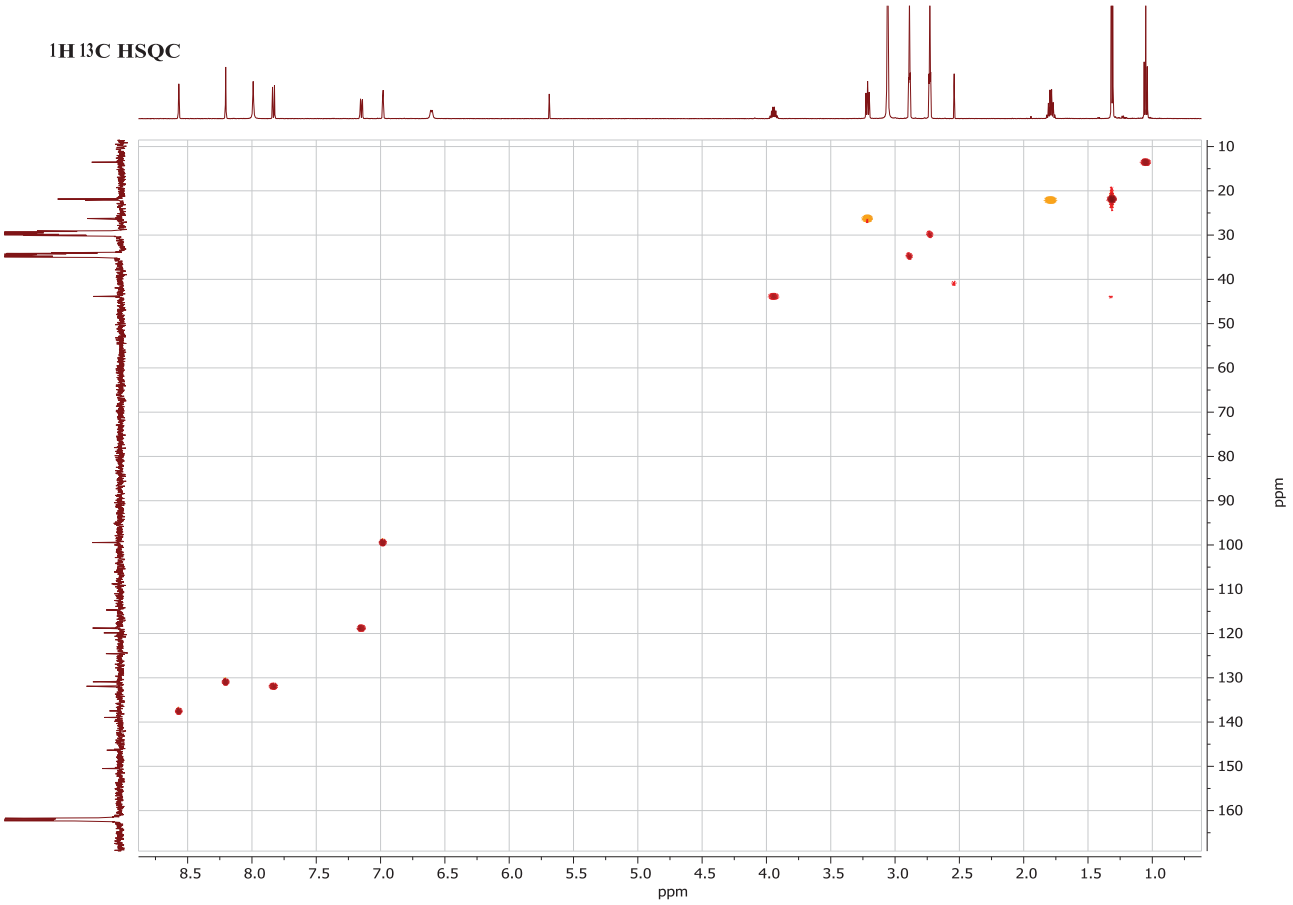

1.1.3 X-Ray crystallography analysis of compound 16

The X-ray measurement of 16 was performed at 130.0(5) K on a Bruker D8 Venture PhotonII diffractometer equipped with a TRIUMPH monochromator and a MoKα fine focus sealed tube (λ = 0.71073 Å). A total of 2372 frames were collected with Bruker APEX3 program.[4] The frames were integrated with the Bruker SAINT software package[5] using a narrow-frame algorithm. The integration of the data using a triclinic unit cell yielded a total of 30681 reflections to a maximum θ angle of 27.00° (0.78 Å resolution), of which 4078 were independent (average redundancy 7.524, completeness = 99.9%, R_{int} = 3.11%, R_{sig} = 1.74%) and 3236 (79.35%) were greater than 2σ(F2). The final cell constants of a = 8.2480(4) Å, b = 11.2545(5) Å, c = 11.6084(6) Å, α = 66.730(2)°, β = 71.581(2)°, γ = 88.148(2)°, V = 933.90(8) Å3, are based upon the refinement of the XYZ-centroids of 9896 reflections above 20 σ(I) with 5.458° < 2θ < 54.32°. Data were corrected for absorption effects using the Multi-Scan method (SADABS)[6]. The ratio of minimum to maximum apparent transmission was 0.971. The calculated minimum and maximum transmission coefficients (based on crystal size) are 0.978 and 0.994.

The structure was solved and refined using SHELXTL Software Package[7,8] using the space group P"1"¯, with Z = 2 for the formula unit, $C_{23}H_{20}F_3NO_2$. The final anisotropic full-matrix least-squares refinement on F2 with 269 variables converged at R1 = 3.98%, for the observed data and wR2 = 12.15% for all data. The goodness-of-fit was 1.035. The largest peak in the final difference electron density synthesis was 0.327 e-/Å3 and the largest hole was -0.208 e-/Å3 with an RMS deviation of 0.046 e-/Å3. On the basis of the final model, the

calculated density was 1.420 g/cm3 and F(000), 416 e-. The details concerning the crystal data and structural parameters of **16** are collected in Table S1.

The structure is fully ordered. All heavy atoms were refined anisotropically. All but one hydrogen atoms were placed in calculated positions and refined within the riding model, their temperature factors were not refined and were set to be 1.2 (Car-H atoms) or 1.5 (CH_3 atoms) times larger than U_{eq} of the corresponding heavy atom. The H atom of the amine group engaged in hydrogen bond was refined together with the isotropic ADP. The atomic scattering factors were taken from the International Tables.[9] Molecular graphics was prepared using program Mercury 2020.2.0.[10] Thermal ellipsoids parameters are presented at 20% probability level in Figure S1.

Table S1. Data collection and structure refinement parameters for **16**.

Formula	$C_{23}H_{20}F_3NO$
M_x**/ g mol^{-1}**	399.40
T**/ K**	130.5(5)
λ**/ Å**	0.71073
Crystal size	0.052×0.129×0.206mm
Space group	$P\bar{1}$
Unit cell dimensions	a = 8.2480(4) Å α = 66.730(2)° b = 11.2545(5) Å β = 71.581(2)° c = 11.6084(6) Å γ = 88.148(2)°
V**/ Å^3, Z**	933.90(8), 2
D_x**/ g cm^{-3}**	1.420
μ**/ mm^{-1}**	0.111
F**(000)**	416
ϑ_{min}, ϑ_{max}	2.62°, 27.00°
Index ranges	$-10 \le h \le 10$, $-14 \le k \le 14$, $-14 \le l \le 14$
Reflections collected/ independent	30681/ 4078 (R_{int} = 0.0311)
Completeness	99.9%
Absorption correction	Multi-Scan
T_{max}, T_{min}	0.994, 0.978
Refinement method	Full-matrix LSQ on F^2
Data / restraints / parameters	4078 / 0 / 269
GOF on F^2	1.035
Final R indices	3236 data; $I>2\sigma(I)$ $R1$ = 0.0398, $wR2$ = 0.1112 all data $R1$ = 0.0530, $wR2$ = 0.1215
$\Delta\rho_{max}$, $\Delta\rho_{min}$	0.327 eÅ^{-3}, -0.208 eÅ^{-3}

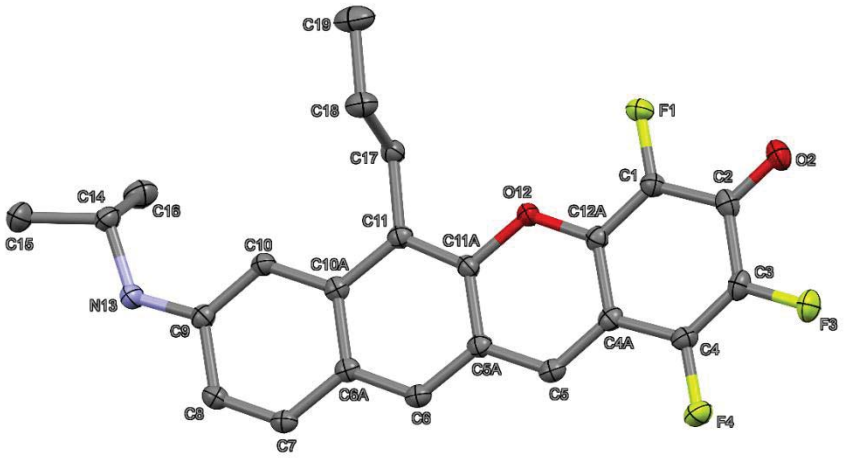

Figure S1. Thermal ellipsoid plot at 50% probability level together with numbering scheme of heavy atoms in the **16** structure, hydrogen atoms omitted for clarity.

A specimen of $C_{23}H_{20}F_3NO_2$, approximate dimensions 0.052 mm x 0.129 mm x 0.206 mm, was used for the X-ray crystallographic analysis. The X-ray intensity data were measured on a Bruker D8 VENTURE Bruker D8 VENTURE system equipped with a fine focus sealed tube (MoKα, λ = 0.71073 Å) and a TRIUMPH monochromator.

Table S2. Data collection details for **16.**

Axis	dx/mm	2θ/°	ω/°	ϕ/°	χ/°	Width/°	Frames	Time/s	Wavelength/Å	Voltage/kV	Current/mA	Temperature/K
Phi	40.038	0.00	360.00	360.00	54.74	0.50	720	10.00	0.71076	50	30.0	130
Omega	40.037	3.00	357.00	0.00	-54.74	0.50	236	60.00	0.71076	50	30.0	130
Omega	40.037	3.00	357.00	90.00	-54.74	0.50	236	60.00	0.71076	50	30.0	130
Omega	40.037	3.00	357.00	180.00	-54.74	0.50	236	60.00	0.71076	50	30.0	130
Omega	40.037	3.00	357.00	270.00	-54.74	0.50	236	60.00	0.71076	50	30.0	130
Omega	40.037	3.00	251.00	360.00	54.74	0.50	236	60.00	0.71076	50	30.0	130
Omega	40.037	3.00	251.00	120.00	54.74	0.50	236	60.00	0.71076	50	30.0	130
Omega	40.037	3.00	251.00	240.00	54.74	0.50	236	60.00	0.71076	50	30.0	130

A total of 2372 frames were collected. The total exposure time was 29.53 hours. The frames were integrated with the Bruker SAINT software package using a narrow-frame algorithm. The integration of the data using a triclinic unit cell yielded a total of 30681 reflections to a maximum θ angle of 27.00° (0.78 Å resolution), of which 4078 were independent (average redundancy 7.524, completeness = 99.9%, R_{int} = 3.11%, R_{sig} = 1.74%) and 3236 (79.35%) were greater than $2\sigma(F^2)$. The final cell constants of a = 8.2480(4) Å, b = 11.2545(5) Å, c = 11.6084(6) Å, α = 66.730(2)°, β = 71.581(2)°, γ = 88.148(2)°, volume = 933.90(8) $Å^3$, are based upon the refinement of the XYZ-centroids of 9896 reflections above 20 σ(I) with 5.458° < 2θ < 54.32°. Data were corrected for absorption effects using the Multi-Scan method (SADABS). The ratio of minimum to maximum apparent transmission was 0.971. The calculated minimum and maximum transmission coefficients (based on crystal size) are 0.9780 and 0.9940.

The structure was solved and refined using the Bruker SHELXTL Software Package, using the space group P -1, with Z = 2 for the formula unit, $C_{23}H_{20}F_3NO_2$. The final anisotropic full-matrix least-squares refinement on F^2 with 269 variables converged at R1 = 3.98%, for the observed data and wR2 = 12.15% for all data. The goodness-of-fit was 1.035. The largest peak in the final difference electron density synthesis was 0.327 $e^-/Å^3$ and the largest hole was -0.208 $e^-/Å^3$ with an RMS deviation of 0.046 $e^-/Å^3$. On the basis of the final model, the calculated density was 1.420 g/cm^3 and F(000), 416 e^-.

Table S3. Sample and crystal data for **16.**

Identification code	KVy_702	
Chemical formula	$C_{23}H_{20}F_3NO_2$	
Formula weight	399.40 g/mol	
Temperature	130(0) K	
Wavelength	0.71073 Å	
Crystal size	0.052 x 0.129 x 0.206 mm	
Crystal system	triclinic	
Space group	P -1	
Unit cell dimensions	a = 8.2480(4) Å	α = 66.730(2)°
	b = 11.2545(5) Å	β = 71.581(2)°
	c = 11.6084(6) Å	γ = 88.148(2)°
Volume	933.90(8) $Å^3$	
Z	2	
Density (calculated)	1.420 g/cm^3	
Absorption coefficient	0.111 mm^{-1}	
F(000)	416	

Table S4. Data collection and structure refinement for **16.**

Diffractometer	Bruker D8 VENTURE Bruker D8 VENTURE	
Radiation source	fine focus sealed tube (MoKα, λ = 0.71073 Å)	
Theta range for data collection	2.62 to 27.00°	
Index ranges	-10<=h<=10, -14<=k<=14, -14<=l<=14	
Reflections collected	30681	
Independent reflections	4078 [R(int) = 0.0311]	
Coverage of independent reflections	99.9%	
Absorption correction	Multi-Scan	
Max. and min. transmission	0.9940 and 0.9780	
Structure solution technique	direct methods	
Structure solution program	SHELXS-2013/1 (Sheldrick, 2015)	
Refinement method	Full-matrix least-squares on F^2	
Refinement program	SHELXL-2018/3 (Sheldrick, 2015)	
Function minimized	$\Sigma\, w(F_o^2 - F_c^2)^2$	
Data / restraints / parameters	4078 / 0 / 269	
Goodness-of-fit on F^2	1.035	
Final R indices	3236 data; I>2σ(I)	R1 = 0.0398, wR2 = 0.1112

	all data	R1 = 0.0530, wR2 = 0.1215
Weighting scheme	$w=1/[\sigma^2(F_o^2)+(0.0628P)^2+0.3780P]$ where $P=(F_o^2+2F_c^2)/3$	
Largest diff. peak and hole	0.327 and -0.208 eÅ^{-3}	
R.M.S. deviation from mean	0.046 eÅ^{-3}	

Table S5. Atomic coordinates and equivalent isotropic atomic displacement parameters (Å^2) for **16.** U(eq) is defined as one third of the trace of the orthogonalized U_{ij} tensor.

	x/a	y/b	z/c	U(eq)
F1	0.59198(11)	0.87151(8)	0.74174(8)	0.0271(2)
O2	0.83840(14)	0.07770(10)	0.57891(11)	0.0297(3)
F3	0.94706(12)	0.15823(8)	0.31044(9)	0.0312(2)
F4	0.81335(11)	0.02886(9)	0.20159(8)	0.0286(2)
C1	0.64889(18)	0.90732(13)	0.60874(13)	0.0205(3)
C2	0.77691(18)	0.01719(14)	0.53072(14)	0.0221(3)
C3	0.82939(18)	0.05456(13)	0.38778(14)	0.0229(3)
C4	0.76315(18)	0.99031(13)	0.33468(13)	0.0209(3)
C4A	0.63781(17)	0.88022(13)	0.41367(13)	0.0191(3)
C5	0.57062(17)	0.80969(13)	0.36381(13)	0.0196(3)
C5A	0.44882(17)	0.70005(13)	0.44987(13)	0.0185(3)
C6	0.38022(17)	0.62316(13)	0.40407(13)	0.0190(3)
C6A	0.26282(16)	0.51527(13)	0.49094(13)	0.0176(3)
C7	0.19410(17)	0.43598(13)	0.44356(13)	0.0195(3)
C8	0.07893(17)	0.33121(13)	0.52662(13)	0.0199(3)
C9	0.02435(17)	0.29446(13)	0.66799(13)	0.0194(3)
C10	0.09064(17)	0.36895(13)	0.71781(13)	0.0190(3)
C10A	0.20845(16)	0.48068(13)	0.63245(13)	0.0180(3)
C11	0.27552(17)	0.56038(13)	0.68084(13)	0.0186(3)
C11A	0.39392(17)	0.66469(13)	0.58931(13)	0.0182(3)
O12	0.46228(12)	0.73813(9)	0.63823(9)	0.0197(2)
C12A	0.58274(17)	0.84114(13)	0.55527(13)	0.0180(3)
N13	0.91090(16)	0.18678(12)	0.74481(12)	0.0235(3)
C14	0.83755(19)	0.13330(14)	0.88939(14)	0.0241(3)
C15	0.7632(2)	0.99346(15)	0.93727(15)	0.0319(4)
C16	0.7019(2)	0.21457(16)	0.93665(15)	0.0320(4)
C17	0.22345(18)	0.53007(13)	0.82725(13)	0.0208(3)
C18	0.3317(2)	0.43334(15)	0.89773(14)	0.0273(3)
C19	0.2768(2)	0.40380(19)	0.04543(16)	0.0396(4)

Table S6. Bond lengths (Å) for **16.**

F1-C1	1.3524(15)	O2-C2	1.2397(17)
F3-C3	1.3432(16)	F4-C4	1.3507(15)
C1-C12A	1.3577(19)	C1-C2	1.4351(19)
C2-C3	1.457(2)	C3-C4	1.339(2)
C4-C4A	1.4251(19)	C4A-C5	1.366(2)
C4A-C12A	1.4393(18)	C5-C5A	1.4148(19)
C5-H5	0.95	C5A-C6	1.3916(19)
C5A-C11A	1.4223(18)	C6-C6A	1.3858(19)
C6-H6	0.95	C6A-C7	1.4275(19)
C6A-C10A	1.4463(18)	C7-C8	1.3482(19)
C7-H7	0.95	C8-C9	1.4407(18)
C8-H8	0.95	C9-N13	1.3534(18)
C9-C10	1.3960(19)	C10-C10A	1.4118(18)
C10-H10	0.95	C10A-C11	1.4327(19)
C11-C11A	1.3761(19)	C11-C17	1.5097(18)
C11A-O12	1.3882(16)	O12-C12A	1.3588(16)
N13-C14	1.4590(18)	N13-H13N	0.87(2)
C14-C15	1.522(2)	C14-C16	1.527(2)
C14-H14	1.0	C15-H15A	0.98
C15-H15B	0.98	C15-H15C	0.98
C16-H16A	0.98	C16-H16B	0.98
C16-H16C	0.98	C17-C18	1.532(2)
C17-H17A	0.99	C17-H17B	0.99
C18-C19	1.524(2)	C18-H18A	0.99
C18-H18B	0.99	C19-H19A	0.98
C19-H19B	0.98	C19-H19C	0.98

Table S7. Bond angles (°) for **16.**

F1-C1-C12A	119.83(12)	F1-C1-C2	116.86(12)
C12A-C1-C2	123.30(12)	O2-C2-C1	123.64(13)
O2-C2-C3	121.68(13)	C1-C2-C3	114.67(12)
C4-C3-F3	120.98(13)	C4-C3-C2	122.16(13)
F3-C3-C2	116.86(12)	C3-C4-F4	120.47(13)
C3-C4-C4A	122.48(13)	F4-C4-C4A	117.05(12)
C5-C4A-C4	124.36(12)	C5-C4A-C12A	118.91(12)
C4-C4A-C12A	116.71(12)	C4A-C5-C5A	120.59(12)
C4A-C5-H5	119.7	C5A-C5-H5	119.7
C6-C5A-C5	122.69(12)	C6-C5A-C11A	117.79(12)

C5-C5A-C11A	119.51(12)	C6A-C6-C5A	121.39(12)
C6A-C6-H6	119.3	C5A-C6-H6	119.3
C6-C6A-C7	121.18(12)	C6-C6A-C10A	120.08(12)
C7-C6A-C10A	118.74(12)	C8-C7-C6A	121.94(12)
C8-C7-H7	119.0	C6A-C7-H7	119.0
C7-C8-C9	120.16(12)	C7-C8-H8	119.9
C9-C8-H8	119.9	N13-C9-C10	124.02(12)
N13-C9-C8	116.58(12)	C10-C9-C8	119.39(12)
C9-C10-C10A	121.39(12)	C9-C10-H10	119.3
C10A-C10-H10	119.3	C10-C10A-C11	122.50(12)
C10-C10A-C6A	118.37(12)	C11-C10A-C6A	119.14(12)
C11A-C11-C10A	117.72(12)	C11A-C11-C17	120.45(12)
C10A-C11-C17	121.80(12)	C11-C11A-O12	117.00(12)
C11-C11A-C5A	123.84(12)	O12-C11A-C5A	119.16(12)
C12A-O12-C11A	121.00(10)	C1-C12A-O12	118.56(12)
C1-C12A-C4A	120.65(13)	O12-C12A-C4A	120.79(12)
C9-N13-C14	125.69(12)	C9-N13-H13N	113.7(14)
C14-N13-H13N	120.6(14)	N13-C14-C15	108.01(12)
N13-C14-C16	111.84(12)	C15-C14-C16	111.52(13)
N13-C14-H14	108.5	C15-C14-H14	108.5
C16-C14-H14	108.5	C14-C15-H15A	109.5
C14-C15-H15B	109.5	H15A-C15-H15B	109.5
C14-C15-H15C	109.5	H15A-C15-H15C	109.5
H15B-C15-H15C	109.5	C14-C16-H16A	109.5
C14-C16-H16B	109.5	H16A-C16-H16B	109.5
C14-C16-H16C	109.5	H16A-C16-H16C	109.5
H16B-C16-H16C	109.5	C11-C17-C18	113.20(11)
C11-C17-H17A	108.9	C18-C17-H17A	108.9
C11-C17-H17B	108.9	C18-C17-H17B	108.9
H17A-C17-H17B	107.8	C19-C18-C17	112.38(13)
C19-C18-H18A	109.1	C17-C18-H18A	109.1
C19-C18-H18B	109.1	C17-C18-H18B	109.1
H18A-C18-H18B	107.9	C18-C19-H19A	109.5
C18-C19-H19B	109.5	H19A-C19-H19B	109.5
C18-C19-H19C	109.5	H19A-C19-H19C	109.5
H19B-C19-H19C	109.5		

Table S8. Torsion angles (°) for **16.**

F1-C1-C2-O2	1.4(2)	C12A-C1-C2-O2	-179.67(14)
F1-C1-C2-C3	-177.94(11)	C12A-C1-C2-C3	1.0(2)
O2-C2-C3-C4	-179.64(14)	C1-C2-C3-C4	-0.3(2)
O2-C2-C3-F3	-0.3(2)	C1-C2-C3-F3	178.98(12)
F3-C3-C4-F4	-0.1(2)	C2-C3-C4-F4	179.14(12)
F3-C3-C4-C4A	-179.83(12)	C2-C3-C4-C4A	-0.6(2)
C3-C4-C4A-C5	-178.03(14)	F4-C4-C4A-C5	2.3(2)
C3-C4-C4A-C12A	0.8(2)	F4-C4-C4A-C12A	-178.94(11)
C4-C4A-C5-C5A	178.80(12)	C12A-C4A-C5-C5A	0.0(2)
C4A-C5-C5A-C6	-178.24(12)	C4A-C5-C5A-C11A	1.1(2)
C5-C5A-C6-C6A	179.11(12)	C11A-C5A-C6-C6A	-0.3(2)
C5A-C6-C6A-C7	-179.38(12)	C5A-C6-C6A-C10A	0.3(2)
C6-C6A-C7-C8	-179.55(13)	C10A-C6A-C7-C8	0.8(2)
C6A-C7-C8-C9	-1.4(2)	C7-C8-C9-N13	-178.82(12)
C7-C8-C9-C10	0.6(2)	N13-C9-C10-C10A	-179.82(13)
C8-C9-C10-C10A	0.9(2)	C9-C10-C10A-C11	178.61(12)
C9-C10-C10A-C6A	-1.4(2)	C6-C6A-C10A-C10	-179.06(12)
C7-C6A-C10A-C10	0.58(18)	C6-C6A-C10A-C11	0.93(19)
C7-C6A-C10A-C11	-179.42(11)	C10-C10A-C11-C11A	177.94(12)
C6A-C10A-C11-C11A	-2.06(19)	C10-C10A-C11-C17	-0.3(2)
C6A-C10A-C11-C17	179.72(12)	C10A-C11-C11A-O12	-177.72(11)
C17-C11-C11A-O12	0.52(19)	C10A-C11-C11A-C5A	2.1(2)
C17-C11-C11A-C5A	-179.62(12)	C6-C5A-C11A-C11	-1.0(2)
C5-C5A-C11A-C11	179.62(12)	C6-C5A-C11A-O12	178.88(11)
C5-C5A-C11A-O12	-0.52(19)	C11-C11A-O12-C12A	178.56(11)
C5A-C11A-O12-C12A	-1.31(18)	F1-C1-C12A-O12	-1.3(2)
C2-C1-C12A-O12	179.81(12)	F1-C1-C12A-C4A	178.09(11)
C2-C1-C12A-C4A	-0.8(2)	C11A-O12-C12A-C1	-178.13(12)
C11A-O12-C12A-C4A	2.52(18)	C5-C4A-C12A-C1	178.80(13)
C4-C4A-C12A-C1	-0.1(2)	C5-C4A-C12A-O12	-1.87(19)
C4-C4A-C12A-O12	179.26(11)	C10-C9-N13-C14	1.4(2)
C8-C9-N13-C14	-179.25(13)	C9-N13-C14-C15	-162.65(14)
C9-N13-C14-C16	74.27(18)	C11A-C11-C17-C18	-92.27(15)
C10A-C11-C17-C18	85.90(16)	C11-C17-C18-C19	-179.87(13)

Table S9. Anisotropic atomic displacement parameters (Å^2) for **16.**

The anisotropic atomic displacement factor exponent takes the form: $-2\pi^2[h^2 a^{*2} U_{11} + ... + 2 h k a^* b^* U_{12}]$

	U_{11}	U_{22}	U_{33}	U_{23}	U_{13}	U_{12}
F1	0.0348(5)	0.0287(5)	0.0176(4)	-0.0108(3)	-0.0059(3)	-0.0040(4)
O2	0.0341(6)	0.0265(5)	0.0323(6)	-0.0152(5)	-0.0112(5)	-0.0039(4)
F3	0.0319(5)	0.0255(5)	0.0290(5)	-0.0068(4)	-0.0049(4)	-0.0111(4)
F4	0.0311(5)	0.0307(5)	0.0166(4)	-0.0048(3)	-0.0034(3)	-0.0077(4)
C1	0.0231(7)	0.0202(7)	0.0179(6)	-0.0083(5)	-0.0056(5)	0.0018(5)
C2	0.0217(7)	0.0195(7)	0.0282(7)	-0.0121(6)	-0.0091(6)	0.0031(5)
C3	0.0192(7)	0.0189(7)	0.0253(7)	-0.0054(6)	-0.0047(5)	-0.0017(5)
C4	0.0210(7)	0.0220(7)	0.0166(6)	-0.0059(5)	-0.0049(5)	0.0011(5)
C4A	0.0180(6)	0.0188(6)	0.0185(6)	-0.0059(5)	-0.0057(5)	0.0031(5)
C5	0.0202(7)	0.0210(7)	0.0158(6)	-0.0061(5)	-0.0056(5)	0.0032(5)
C5A	0.0189(6)	0.0187(6)	0.0175(6)	-0.0068(5)	-0.0063(5)	0.0032(5)
C6	0.0197(6)	0.0211(7)	0.0156(6)	-0.0071(5)	-0.0057(5)	0.0034(5)
C6A	0.0164(6)	0.0187(6)	0.0176(6)	-0.0075(5)	-0.0054(5)	0.0039(5)
C7	0.0204(6)	0.0222(7)	0.0169(6)	-0.0089(5)	-0.0064(5)	0.0041(5)
C8	0.0206(6)	0.0222(7)	0.0198(6)	-0.0110(5)	-0.0075(5)	0.0030(5)
C9	0.0182(6)	0.0195(6)	0.0187(6)	-0.0067(5)	-0.0053(5)	0.0017(5)
C10	0.0199(6)	0.0206(7)	0.0153(6)	-0.0070(5)	-0.0046(5)	0.0004(5)
C10A	0.0164(6)	0.0188(6)	0.0188(6)	-0.0078(5)	-0.0057(5)	0.0028(5)
C11	0.0181(6)	0.0198(6)	0.0171(6)	-0.0074(5)	-0.0052(5)	0.0032(5)
C11A	0.0200(6)	0.0179(6)	0.0194(6)	-0.0091(5)	-0.0078(5)	0.0023(5)
O12	0.0224(5)	0.0188(5)	0.0173(5)	-0.0079(4)	-0.0047(4)	-0.0026(4)
C12A	0.0179(6)	0.0166(6)	0.0186(6)	-0.0068(5)	-0.0052(5)	0.0024(5)
N13	0.0267(6)	0.0241(6)	0.0189(6)	-0.0087(5)	-0.0058(5)	-0.0054(5)
C14	0.0252(7)	0.0255(7)	0.0169(6)	-0.0050(5)	-0.0049(5)	-0.0049(6)
C15	0.0342(8)	0.0296(8)	0.0241(7)	-0.0060(6)	-0.0044(6)	-0.0108(6)
C16	0.0306(8)	0.0367(9)	0.0226(7)	-0.0099(6)	-0.0035(6)	0.0010(7)
C17	0.0222(7)	0.0216(7)	0.0184(6)	-0.0094(5)	-0.0045(5)	-0.0014(5)
C18	0.0294(8)	0.0318(8)	0.0195(7)	-0.0095(6)	-0.0078(6)	0.0035(6)
C19	0.0486(10)	0.0472(10)	0.0221(8)	-0.0115(7)	-0.0145(7)	0.0124(8)

Table S10. Hydrogen atomic coordinates and isotropic atomic displacement parameters ($Å^2$) for **16.**

	x/a	y/b	z/c	U(eq)
H5	0.6060	0.8345	0.2705	0.024
H6	0.4146	0.6451	0.3113	0.023
H7	0.2306	0.4577	0.3508	0.023
H8	0.0337	0.2815	0.4919	0.024
H10	0.0557	0.3439	0.8111	0.023
H13N	-0.120(3)	0.151(2)	0.700(2)	0.045(6)
H14	-0.0679	0.1326	0.9263	0.029
H15A	-0.3252	-0.0080	0.8977	0.048
H15B	-0.2881	-0.0442	1.0343	0.048
H15C	-0.1450	-0.0574	0.9107	0.048
H16A	-0.2500	0.3059	0.8959	0.048
H16B	-0.3330	0.1829	1.0336	0.048
H16C	-0.3983	0.2071	0.9109	0.048
H17A	0.1012	0.4939	0.8701	0.025
H17B	0.2343	0.6119	0.8384	0.025
H18A	0.3210	0.3513	0.8868	0.033
H18B	0.4540	0.4695	0.8554	0.033
H19A	0.2811	0.4852	1.0569	0.059
H19B	0.3548	0.3469	1.0848	0.059
H19C	0.1593	0.3603	1.0895	0.059

Table S11. Hydrogen bond distances (Å) and angles (°) for **16.**

	Donor-H	Acceptor-H	Donor-Acceptor	Angle
N13-H13N···O2#1	0.87(2)	2.00(2)	2.8664(16)	173.(2)

Symmetry transformations used to generate equivalent atoms:

#1 x-1, y-1, z

1.2. Spectroscopic characterization

Linear absorption and emission spectra were collected on freshly prepared solutions, under ambient conditions. Dilute solutions (optical density less than 0.1) were used to minimize inner filter effects and/or aggregation. Spectrophotometric grade solvents were used as received.

A Perkin-Elmer Lambda650 double beam spectrophotometer was used for linear absorption measurements, and an Edinburgh Instruments FLS1000 fluorometer for fluorescence spectroscopy. Fluorescence quantum yields were estimated using a dilute solution of fluorescein in NaOH 0.1 M as reference standard (QY = 90%, excitation wavelength: 490 nm). Emission decays were measured with the time-correlated single-photon counting (TCSPC) method, for excitation with a 60 ps pulsed laser diode (excitation wavelength: 405 nm). Fluorescence lifetimes were extracted from the reconvolution fit of experimental decay curves, and judged both by the chi-squared test and the visual inspection of residues.

Excitation anisotropies were collected with a Fluoromax-3 (Horiba Jobin-Yvon) fluorometer. The solvent (2-methyltetrahydrofuran) was stored over molecular sieves for 24h and filtered on PTFE syringe filters (0.22 µm pore size). Solutions were vitrified by rapid immersion in liquid nitrogen, using the Horiba FL-1013 liquid nitrogen dewar assembly.

Two-photon absorption spectra were collected with the two-photon-excited fluorescence (2PEF) technique,[1,11,12] with a Nikon A1R MP+ Upright two-photon microscope. Freshly prepared solutions of the dyes were contained in 1 cm path length quartz cuvette and excited by a Coherent Chameleon Discovery femtosecond pulsed laser with tunable wavelength output (660-1320 nm) focused on the sample through a 25x water-dipping objective (NA=1.1). Fluorescence signal was collected in epifluorescence mode. Fluorescein in NaOH 0.1 M was used as standard for quantitative measurement of 2PA cross-sections,[13] according to the procedure proposed by Albota et al.[14]

1.3. Photochemical stability

A freshly prepared air-equilibrated solution of each dye in chloroform (concentration ≈ 1-3×10^{-5} mol L^{-1}) contained in a standard 1 cm × 1 cm quartz cuvette was irradiated by a laser beam ($\lambda = 530.9$ nm) expanded with a lens to illuminate the entire volume of the sample. The absorbance of the solution was measured with a Perkin-Elmer Lambda650 spectrophotometer and monitored over time. The photodecomposition quantum yield ϕ_D was estimated according to the following expression:

$$\phi_D = \frac{(D(\lambda_{max},0) - D(\lambda_{max},T))N_A}{10^3 P\varepsilon(\lambda_{max}) \int_0^T \left(1-10^{-D(\lambda_{exc},t)}\right)dt} \quad \text{(S1)}$$

where $D(\lambda, t)$ is the optical density of the sample at wavelength λ and time t, T is the total irradiation time (in seconds), λ_{max} is the maximum of the absorption band (551 nm for **4**, 585 nm for **10**, 586 nm for **15**, 544 nm for **16** and 536 nm for **17**), N_A is the Avogadro's number, P is the irradiation intensity (in photons s^{-1} cm^{-2}), ε is the molar extinction coefficient (in M^{-1} cm^{-1}) and λ_{exc} is the excitation wavelength.

2. Experimental data

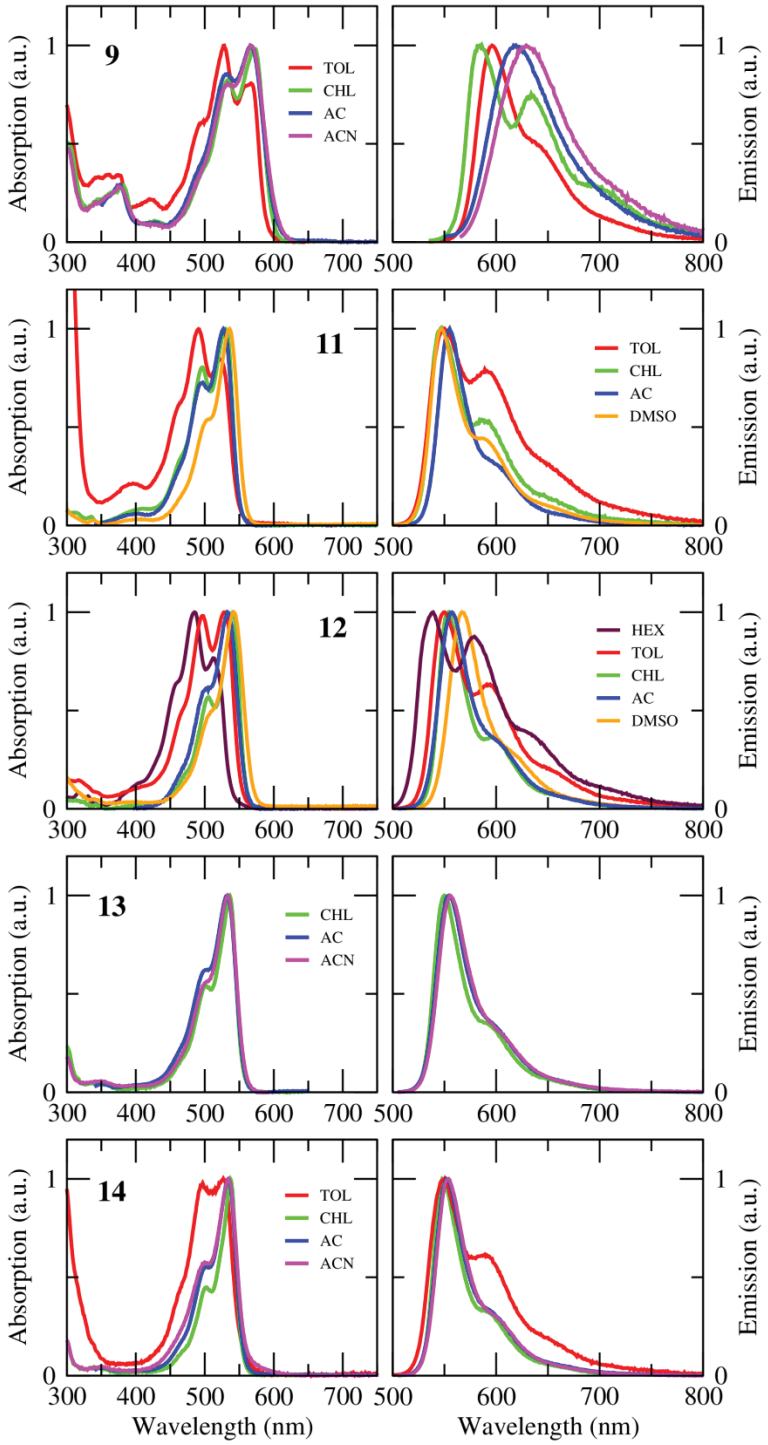

Figure S2. Normalized absorption (left) and emission (right) spectra of compounds **9** and **11**-**14** in solvents of different polarity (HEX: hexane, TOL: toluene, CHL: chloroform, AC: acetone, ACN: acetonitrile, DMSO: dimethyl sulfoxide).

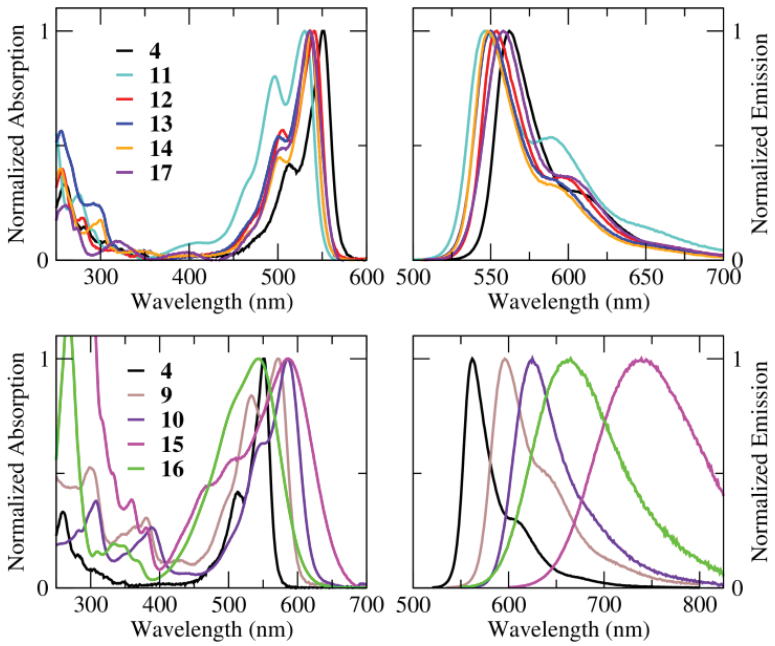

Figure S3. Normalized absorption (left) and emission (right) spectra of investigated compounds in chloroform: rhodols (top panels) and merocyanines (bottom panels; spectra of rhodol **4** are included for comparison).

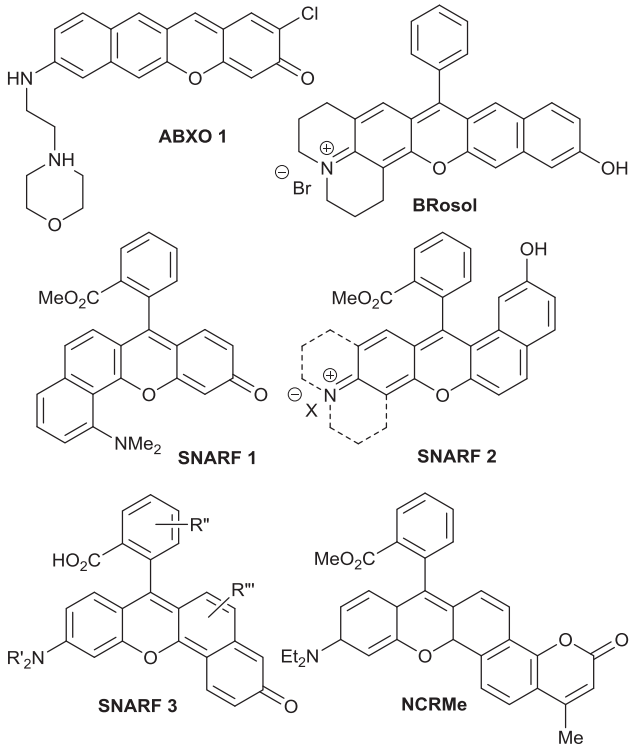

Figure S4. The structures of known π-expanded rhodols and merocyanines.

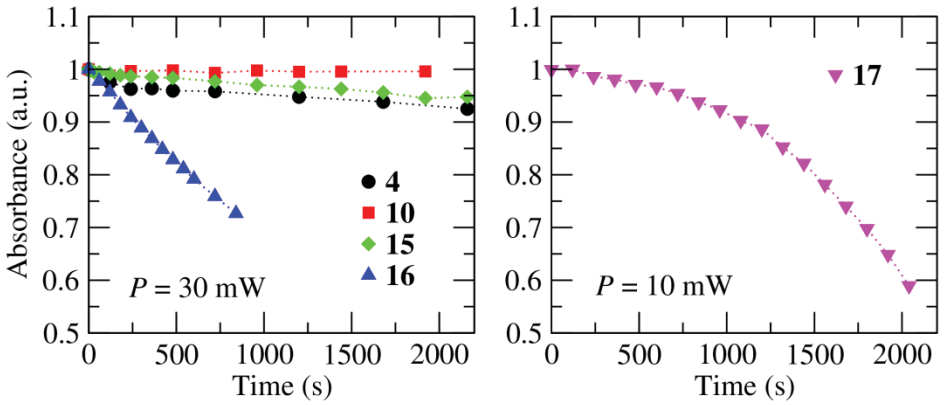

Figure S5. Temporal dependence of the absorbance at the maximum of the absorption band ($D(\lambda_{max})$) of **4**, **10**, **15**, **16** and **17** under continuous laser irradiation ($\lambda_{exc} = 530.9$ nm, laser power *P* = 10 or 30 mW). Dye **4**: $\lambda_{max} = 551$ nm; dye **10**: $\lambda_{max} = 585$ nm; dye **15**: $\lambda_{max} = 586$ nm; dye **16**: $\lambda_{max} = 544$ nm; dye **17**: $\lambda_{max} = 536$ nm. Solvent: chloroform.

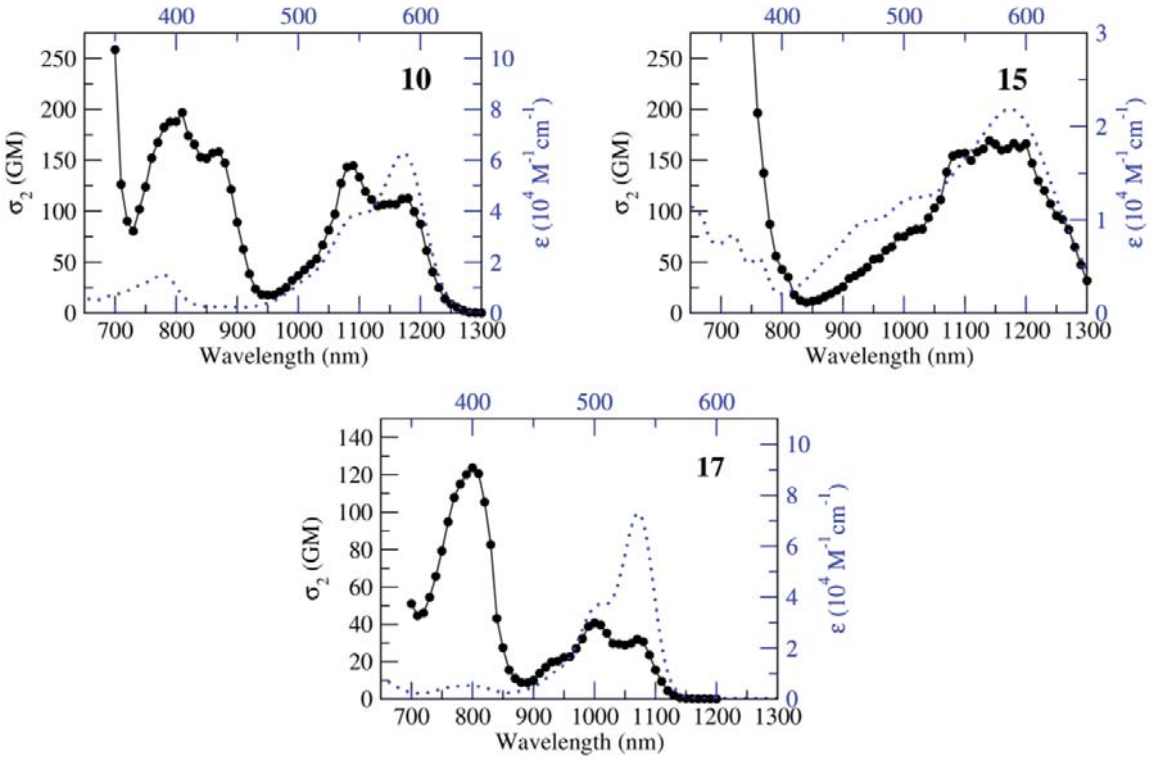

Figure S6. Two-photon absorption cross-section σ_2 (black dots) and molar extinction coefficient ε (blue dotted line) of **10**, **15** and **17** in chloroform (1 GM = 10^{-50} cm^4 s photons^{-1}). The uncertainty on the cross-section is on the order of 20-25% for **15** and 10% for the other compounds.

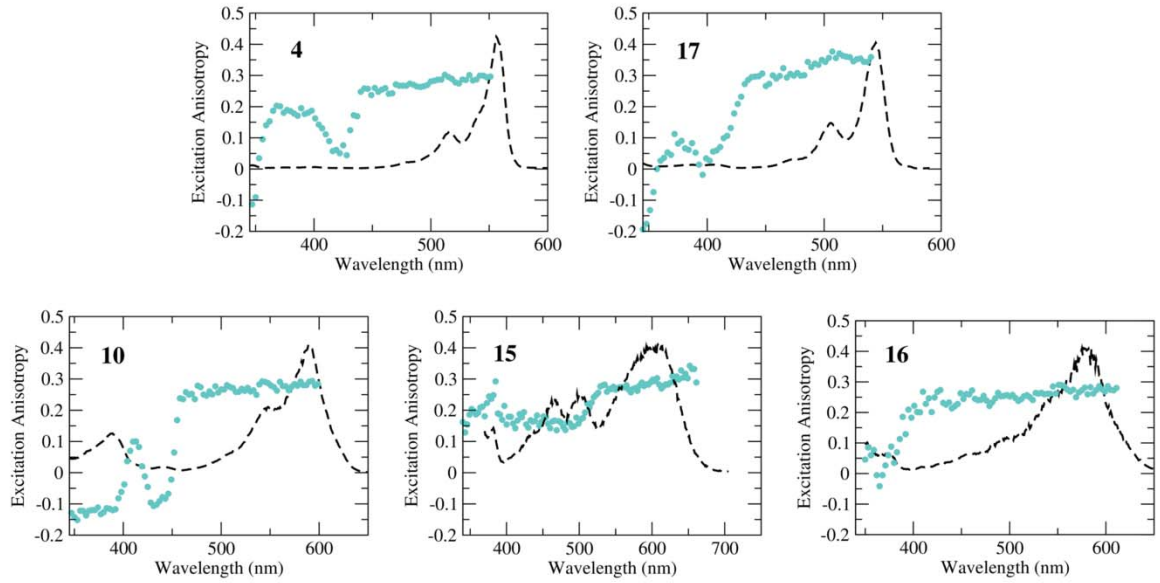

Figure S7. Excitation anisotropy (dots) of compounds **4**, **10**, **15**, **16** and **17** collected in glassy 2-methyltetrahydrofuran at 77 K. Excitation spectra collected under the same experimental conditions (dashed lines) are reported as a guide to the eye.

3. TDDFT results

3.1. Computational details

(TD)DFT calculations in the gas phase were performed with the Gaussian16 package.[15] The long-range corrected hybrid functional M06-2X[16] was used with the 6-31G(d) basis set. Stationary points located by geometry optimizations (ground state and excited state minima) were characterized by frequency analysis. The geometry of the first excited state was optimized in chloroform adopting the PCM model.[17,18,19] TDDFT calculations on the optimized geometries included up to 15 singlet states.

3.2. Solvation model

We adopt the Onsager model,[20] where the solute is described as a point dipole located at the center of a spherical cavity inside the solvent, which, in turn, is treated as a continuum dielectric medium. The solvent generates at the solute location an electric field, called the reaction field F_r, proportional to the solute dipole moment.[21,22,23] Two contributions to the solvent response can be recognized: an electronic component, F_{el}, due to the distortion of the electronic clouds of the solvent molecules, and an orientational component, F_{or}, due to the reorientation of polar solvent molecules around the solute.

Imposing the proportionality of both F_r components to the solute dipole moment, the total reaction field, $F_r = F_{el} + F_{or}$, experienced by the solvated dye is:

$$F_r = r_{el}\langle\hat{\mu}\rangle + r_{or}\langle\hat{\mu}\rangle \qquad \text{(S2)}$$

where $\langle\hat{\mu}\rangle$ is the expectation value of the dipole moment operator of the solute in the state of interest, and the prefactors read:

$$r_{el} = \frac{2}{4\pi\epsilon_0 a^3} f(\epsilon_{opt}) \quad \text{(S3)}$$

$$r_{or} = \frac{2}{4\pi\epsilon_0 a^3}(f(\epsilon_{st}) - f(\epsilon_{opt})) \quad \text{(S4)}$$

where ϵ_0 is the vacuum permittivity, a is the radius of the cavity occupied by the solute, and $f(\epsilon) = \frac{\epsilon-1}{2\epsilon+1}$ with ϵ_{st} measuring the static dielectric constant and ϵ_{opt} is the squared refractive index at optical.

The electronic component of the reaction field, with typical frequencies in the UV, is treated in the antiadiabatic approximation, assuming its instantaneous response to charge fluctuations in the dye.[24] Conversely, the slow orientational motion of the solvent is treated in the adiabatic approximation, neglecting the associated kinetic energy.[25]

With these approximations, the Hamiltonian describing a solvated molecule reads:

$$\hat{H}_{tot} = \hat{H}_g - \frac{r_{el}}{2}\hat{\mu}^2 - F_{or}\hat{\mu} + \frac{1}{2r_{or}}F_{or}^2 \quad \text{(S5)}$$

where H_g is the gas phase Hamiltonian and $\hat{\mu}$ is the dipole moment operator. The second term in the right hand side of Equation S5 includes the effects of fast solvation, while the last two terms account for the orientational contribution in polar solvents.

In our calculation, $\hat{H}_{tot}$ is written on the basis of the eigenstates of the gas phase Hamiltonian as obtained from TDDFT calculations. In this work we considered 16 basis states, including the ground and the 15 lowest-energy excited states, which ensured convergence on calculated properties. The matrix elements of the dipole moment operator were calculated with Multiwfn software.[26] Only the *x*-component of the dipole moment was accounted for ($\hat{\mu} = \hat{\mu}_x$, where x identifies the direction connecting donor and acceptor moieties), since it is largely dominant over the other components. The parameter a entering the expressions for r_{el} and r_{or} (Equations S3-S4) was set to the Onsager radius calculated for the dyes (5.71 Å for **4**, 5.78 Å for **10**, 5.44 Å for **15** and **16**, 5.87 Å for **17**). The values of ϵ_{st} and ϵ_{opt} used for the different solvents are reported in Table S14.

To describe absorption, we used TDDFT results in the optimized ground-state geometry, while to describe emission we used the results obtained in the S_1 geometry optimized in chloroform within PCM formalism.[27]

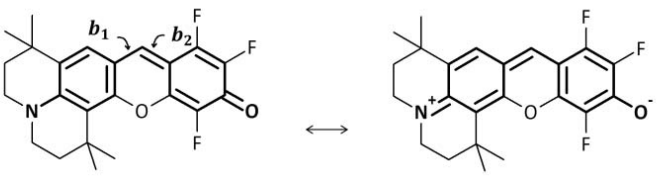

Figure S8. The two main resonance structures of rhodol **4**: neutral (left) and dipolar (right). The pi-conjugated skeleton of the rhodol is emphasized in bold.

Table S12. Length of bonds b_1 and b_2 (defined as in Figure S8) in the ground state equilibrium geometry and bond-length alternation (BLA = $b_2 - b_1$). The geometry was optimized in gas phase at M06-2X/6-31G(d) level.

	4	**10**	**15**	**16**	**17**
b_1 /Å	1.424	1.422	1.434	1.435	1.434
b_2 /Å	1.362	1.362	1.358	1.355	1.375
BLA /Å	-0.062	-0.060	-0.076	-0.080	-0.059

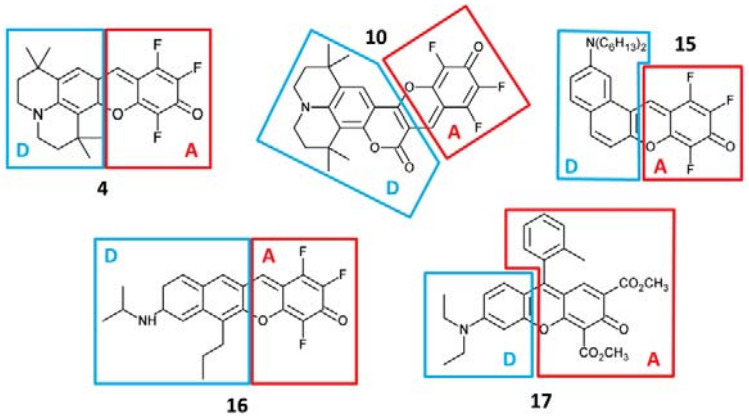

Figure S9. Colored polygons define the donor (D, blue) and acceptor (A, red) regions chosen for the calculation of the cumulative atomic charges reported in Table S13.

Table S13. Cumulative Hirshfeld atomic charges on the donor (D) and acceptor (A) groups calculated in the ground state and after vertical excitation to S_1. Molecules have been partitioned as in Figure S9.

	S_0		S_1		S_2	
Compound	A	D	A	D	A	D
4	-0.2303	+0.2304	-0.3212	+0.3213	-[a]	-[a]
10	-0.1705	+0.1705	-0.2492	+0.2492	-[a]	-[a]
15	-0.2024	+0.2024	-0.2530	+0.2530	-0.4697	+0.4697
16	-0.1841	+0.1841	-0.3469	+0.3469	-[a]	-[a]
17	-0.2317	+0.2317	-0.3152	+0.3152	-[a]	-[a]

[a] not calculated.

Table S14. Dielectric properties of the solvents used in this work.

Solvent	ϵ_{opt}	ϵ_{st}
Hexane	1.89	1.88
Cyclohexane	2.03	2.03
Toluene	2.24	2.38
Chloroform	2.09	4.81
Acetone	1.85	20.7
Acetonitrile	1.81	37.5
Dimethyl sulfoxide	2.18	46.7

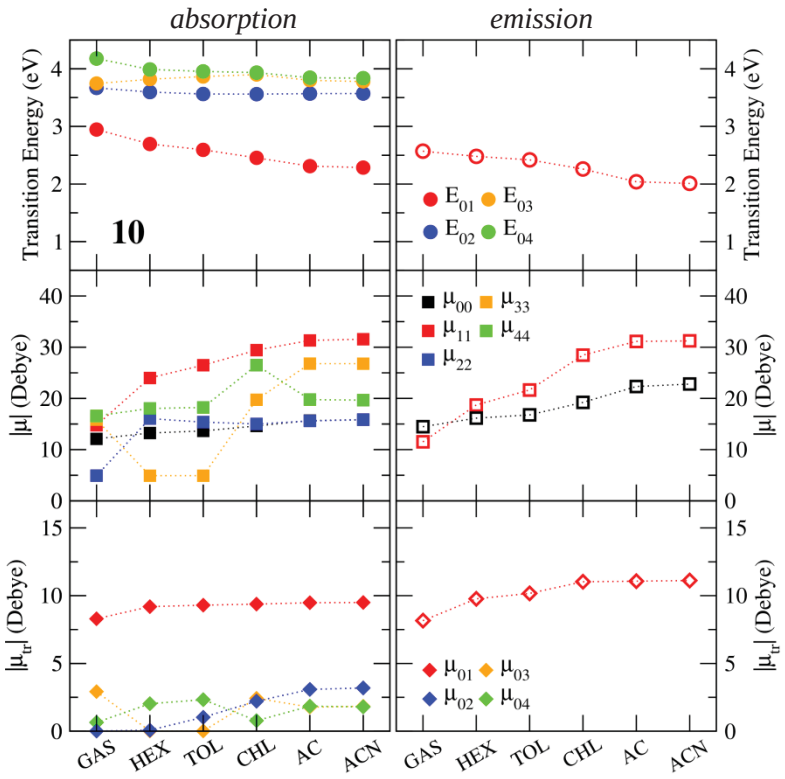

Figure S10. The same as in Figure 4 (main text) for dye **10**.

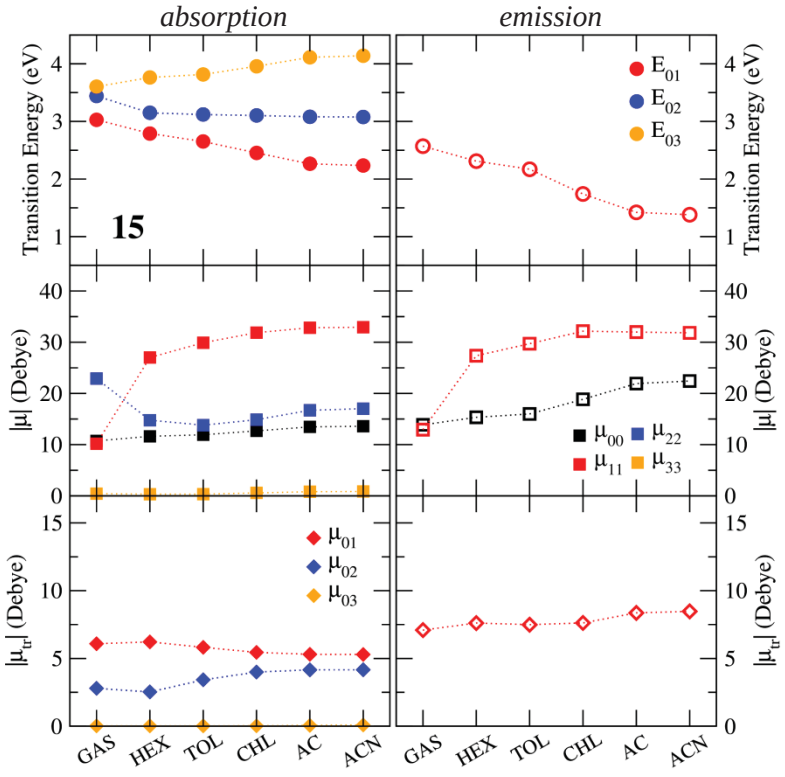

Figure S11. The same as in Figure 4 (main text) for dye **15**.

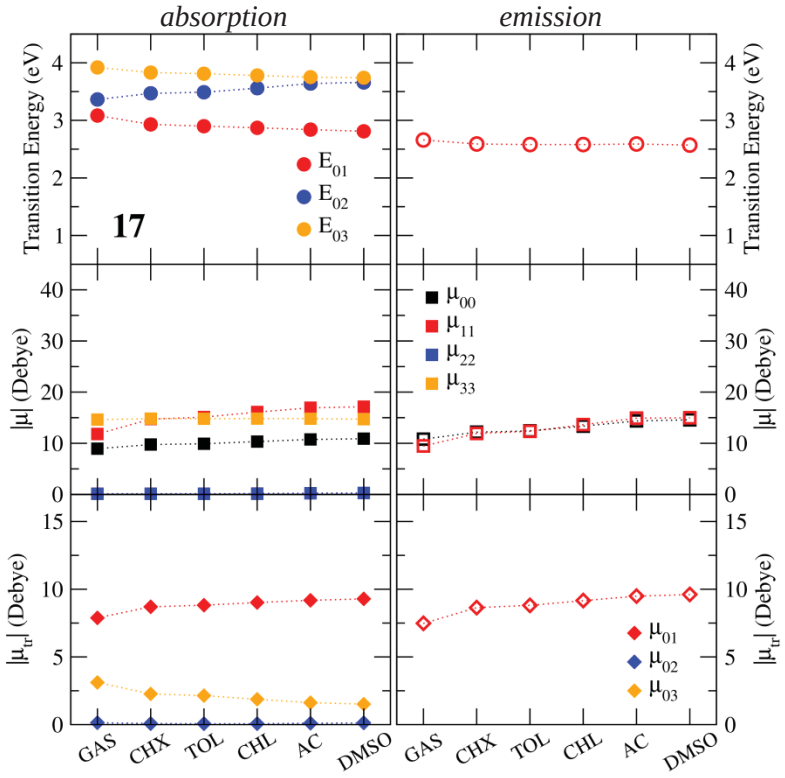

Figure S12. The same as in Figure 4 (main text) for dye **17**.

4. Essential state models and the calculation of linear and nonlinear optical spectra in the essential state model

The two electronic basis states $D-\pi-A$ and $D^{+}-\pi-A^{-}$ are separated by an energy gap $2z_0$ and are mixed by a matrix element $\sqrt{2}t$. A single effective vibrational coordinate accounts for the variation of the molecular geometry upon charge transfer, the strength of the coupling being measured by the vibrational relaxation energy, ε_v. Experimental spectra of **4** in nonpolar solvents point to a sizable anharmonicity. Accordingly, to reproduce the vibronic shape, the two basis states are assigned two harmonic potential energy surfaces with displaced minima, as to account for the different equilibrium geometries, and with different frequencies, ω_v and ω_t, for the neutral and zwitterionic state, respectively.

The Onsager model is again adopted to describe solvation.[28] The contribution of fast solvation (electronic solvation) is implicitly accounted for in the definition of the molecular Hamiltonian (and specifically in the definition of $2z_0$).[25] The orientational component of the solvent reaction field is instead treated within the adiabatic approximation, introducing the solvent relaxation energy ε_{or}, as an empirical parameter that increases with the solvent polarity.

The molecular model parameters, $2z_0, \sqrt{2}t, \mu_0$, ε_v, ω_v and ω_t, are adjusted to best reproduce experimental spectra and are all strictly solvent independent, so that the highly non-trivial dependence of optical spectra upon the solvent polarity is accounted for by just tuning ε_{or}.

The coupled electron-vibrational Hamiltonian is written on the non-adiabatic basis obtained as the direct product of the two electronic basis states times the vibrational eigenstates of the harmonic oscillator

associated to the vibrational coordinate. The vibrational basis is truncated to 10 states. The diagonalization of the Hamiltonian matrix yields the exact vibronic eigenstates of the system that enter the following expression for the calculation of optical spectra.

Specifically, the molar extinction coefficient $\varepsilon(\tilde{\nu})$, in units of M^{-1} cm^{-1}, was obtained from the following sum-over-states (SOS) expression:

$$\varepsilon(\tilde{\nu}) = \frac{10\pi N_A \tilde{\nu}}{3 \ln 10 \hbar c \varepsilon_0} \frac{1}{\sigma\sqrt{2\pi}} \sum_n \mu_{gn}^2 \exp\left[-\frac{1}{2}\left(\frac{\tilde{\nu}_{gn}-\tilde{\nu}}{\sigma}\right)\right] \quad \text{(S6)}$$

where $\tilde{\nu}$ is the wavenumber (in cm^{-1}), N_A is the Avogadro number, c is the light speed, ε_0 is the vacuum dielectric constant, and σ is the width of the Gaussian bandshape assigned to each transition. The terms μ_{gn} and $\tilde{\nu}_{gn}$ are the transition dipole moment and wavenumber of the transition from the ground state (g) to the excited state n and the sum runs over all the excited states.

The fluorescence spectrum $I(\tilde{\nu})$ was calculated as:

$$I(\tilde{\nu}) \propto \frac{\tilde{\nu}^3}{\sigma\sqrt{2\pi}} \sum_n \mu_{fn}^2 exp\left[-\frac{1}{2}\left(\frac{\tilde{\nu}_{fn}-\tilde{\nu}}{\sigma}\right)^2\right] \quad \text{(S7)}$$

where f denotes the fluorescent state and the sum runs over all states having lower energy than f.

The 2PA cross-section (in GM units) was calculated according to the following expression:[12]

$$\sigma_2(\omega) = 10^{58} \frac{\hbar\omega^2}{4\epsilon_0^2 c^2} \mathrm{Im}\langle\gamma(-\omega;\omega,\omega,-\omega)\rangle \quad \text{(S8)}$$

where c is the speed of light and $\langle\gamma\rangle$ is the orientationally averaged second hyperpolarizability. The tensor elements of $\gamma(-\omega;\omega,\omega,-\omega)$ are obtained by the sum-over-states (SOS) expression, only including two-photon resonant terms:[29]

$$\gamma_{ijkl}(-\omega;\omega,\omega,-\omega) = \frac{1}{\hbar^3}\sum_{lmn}\left\{\frac{\langle g|\mu_i|l\rangle\langle l|\bar{\mu}_j|m\rangle\langle m|\bar{\mu}_k|n\rangle\langle n|\mu_l|g\rangle}{(\Omega_{lg}-\omega)(\Omega_{mg}-2\omega)(\Omega_{ng}-\omega)} + \frac{\langle g|\mu_j|l\rangle\langle l|\bar{\mu}_i|m\rangle\langle m|\bar{\mu}_k|n\rangle\langle n|\mu_l|g\rangle}{(\Omega_{lg}^*-\omega)(\Omega_{mg}-2\omega)(\Omega_{ng}-\omega)} + \right.$$
$$\left. \frac{\langle g|\mu_i|l\rangle\langle l|\bar{\mu}_j|m\rangle\langle m|\bar{\mu}_l|n\rangle\langle n|\mu_k|g\rangle}{(\Omega_{lg}-\omega)(\Omega_{mg}-2\omega)(\Omega_{ng}-\omega)} + \frac{\langle g|\mu_j|l\rangle\langle l|\bar{\mu}_i|m\rangle\langle m|\bar{\mu}_l|n\rangle\langle n|\mu_k|g\rangle}{(\Omega_{lg}^*-\omega)(\Omega_{mg}-2\omega)(\Omega_{ng}-\omega)}\right\} \quad \text{(S9)}$$

In the SOS above, we set $\Omega_{lg} = \omega_{lg} - i\Gamma$ and $\bar{\mu} = \mu - \langle g|\hat{\mu}|g\rangle$, where the index g denotes the ground state, and the other indexes run over all excited states, both in the electronic ground and excited state manifold.

In this work, we considered only the *x*-component of the dipole moments, so that the only relevant tensor term is γ_{xxxx}. Accordingly, the orientationally averaged second hyperpolarizability reduces to $\langle\gamma\rangle = \frac{1}{5}\gamma_{xxxx}$.

In polar solvents, the Hamiltonian depends on the orientational component of the reaction field F_{or}: to account for the fluctuations of F_{or} around the equilibrium value, responsible for spectral broadening effects at finite temperature, the diagonalization of the molecular Hamiltonian and the calculation of the spectra is repeated on a grid of F_{or} values. The final spectra are finally calculated summing up the spectra calculated for different F_{or} values, weighting each spectrum for the relevant Boltzmann distribution (referred to the ground-state energy for absorption and to the Kasha's state for emission).

References

[1] H. Gopee, X. Kong, Z. He, I. Chambrier, D. L. Hughes, G. J. Tizzard, S. J. Coles and A. N. Cammidge, *J. Org. Chem.,* 2013, **78**, 9505-9511.
[2] M. Link, P. Kele, D. E. Achatz and O. S. Wolfbeis, *Bioorg. Med. Chem. Lett.*, 2011, **18**, 5538-5542.
[3] M. Tian, M. Furuki, I. Iwasa, Y. Sato, L. S. Pu and S. Tatsuura, *J. Phys. Chem. B*, 2002, **106**, 4370-4376.
[4] APEX3 V2019, Bruker Nano, Inc., 2019.
[5] SAINT V8.40A, Bruker Nano, Inc., 2019.
[6] SADABS V2016/2, Bruker Nano, Inc., 2019.
[7] G. M. Sheldrick, Acta Cryst., 2015, A71, 3-8.
[8] G. M. Sheldrick, Acta Cryst., 2015, C71, 3–8.
[9] International Tables for Crystallography, Ed. A. J. C. Wilson, Kluwer: Dordrecht, 1992, Vol.C.
[10] C. F. Macrae, I. Sovago, S. J. Cottrell, P. T. A. Galek, P. McCabe, E. Pidcock, M. Platings, G. P. Shields, J. S. Stevens, M. Towler and P. A. Wood, *J. Appl. Cryst.*, 2020, **53**, 226-235.
[11] C. Xu and W. W. Webb, *J. Opt. Soc. Am. B*, 1996, **13**, 481.
[12] F. Terenziani, C. Katan, E. Badaeva, S. Tretiak and M. Blanchard-Desce, *Adv. Mater.*, 2008, **20**, 4641–4678.
[13] S. de Reguardati, J. Pahapill, A. Mikhailov, Y. Stepanenko and A. Rebane, *Opt. Express*, 2016, **24**, 9053.
[14] M. A. Albota, C. Xu and W. W. Webb, *Appl. Opt.*, 1998, **37**, 7352.
[15] M. J. Frisch, G. W. Trucks, H. B. Schlegel, G. E. Scuseria, M. A. Robb, J. R. Cheeseman, G. Scalmani, V. Barone, G. A. Petersson, H. Nakatsuji, X. Li, M. Caricato, A. V. Marenich, J. Bloino, B. G. Janesko, R. Gomperts, B. Mennucci, H. P. Hratchian, J. V. Ortiz, A. F. Izmaylov, J. L. Sonnenberg, D. Williams-Young, F. Ding, F. Lipparini, F. Egidi, J. Goings, B. Peng, A. Petrone, T. Henderson, D. Ranasinghe, V. G. Zakrzewski, J. Gao, N. Rega, G. Zheng, W. Liang, M. Hada, M. Ehara, K. Toyota, R. Fukuda, J. Hasegawa, M. Ishida, T. Nakajima, Y. Honda, O. Kitao, H. Nakai, T. Vreven, K. Throssell, J. E. Montgomery, J. A., Jr. Peralta, F. Ogliaro, M. J. Bearpark, J. J. Heyd, E. N. Brothers, K. N. Kudin, V. N. Staroverov, T. A. Keith, R. Kobayashi, K. Normand, J. Raghavachari, A. P. Rendell, J. C. Burant, S. S. Iyengar, J. Tomasi, M. Cossi, J. M. Millam, M. Klene, C. Adamo, R. Cammi, J. W. Ochterski, R. L. Martin, K. Morokuma, O. Farkas, J. B. Foresman and D. J. Fox, Gaussian16, revision B.01, Gaussian, Inc., Wallingford CT, 2016.
[16] Y. Zhao and D. G. Truhlar, *Theor. Chem. Acc.*, 2008, **120**, 215–241.
[17] M. Cossi, V. Barone, R. Cammi and J. Tomasi, *Chem. Phys. Lett.*, 1996, **255**, 327–335.
[18] J. Tomasi, B. Mennucci and R. Cammi, *Chem. Rev.*, 2005, **8**, 2999–3094.
[19] G. Scalmani and M. J. Frisch, *J. Chem. Phys.*, 2010, **132** (114110).
[20] L. Onsager, *J. Am. Chem. Soc.*, 1936, **58**, 1486–1493.
[21] W. Liptay, *Angew. Chemie - Int. Ed.*, 1969, **8**, 177–188.
[22] S. Di Bella, T. J. Marks and M. A. Ratner, *J. Am. Chem. Soc.*, 1994, **116**, 4440–4445.
[23] E. G. McRae, *J. Phys. Chem.*, 1957, **61**, 562–572.
[24] D. K. A. Phan Huu, R. Dhali, C. Pieroni, F. Di Maiolo, C. Sissa, F. Terenziani and A. Painelli, *Phys. Rev. Lett.*, 2020, **124**, 107401.
[25] A. Painelli, *Chem. Phys.*, 1999, **245**, 185–197.
[26] T. Lu and F. Chen, *J. Comput. Chem.*, 2012, **33**, 580–592.
[27] E. Cancès, B. Mennucci and J. Tomasi, *J. Chem. Phys.*, 1997, **107**, 3032–3041.
[28] A. Painelli and F. Terenziani, *Chem. Phys. Lett.*, 1999, **312**, 211–220.
[29] B. J. Orr and J. F. Ward, *Mol. Phys.*, 1971, **20**, 513–526.

9. DECLARATIONS OF THE AUTHORS OF PUBLICATIONS

mgr Kateryna Vygranenko

+48 794-375-755

kate.vygranenko@gmail.com

Instytut Chemii Organicznej PAN

ul. Kasprzaka 44/52

01-224 Warszawa

Polska

Warszawa, 23.05.2023

I declare that my contribution to the following publications consisted of:

1. Yevgen M. Poronik, **Kateryna V. Vygranenko**, Dorota Gryko and Daniel T. Gryko, *Chem. Soc. Rev*., 2019, *48*, 5242-5265. 'Rhodols – synthesis, photophysical properties and applications as fluorescent probes'.
   Literature search and writing of the synthetic part of the manuscript, preparation of schemes, figures and tables.
2. **Kateryna V. Vygranenko**, Yevgen M. Poronik, Antoni Wrzosek, Adam Szewczyk and Daniel T. Gryko, *Chem. Comm.*, 2021, *57*, 7782-7785. 'Red emissive sulfone-rhodols as mitochondrial imaging agents'.
   Co-development of research concepts and interpretation of results. I have developed and carried out the synthesis of xanthone and transformed it into final rhodols under developed conditions. I participated in analysing the photophysical properties and preparation of the manuscript.
3. **Kateryna V. Vygranenko**, Yevgen M. Poronik, Manon H. E. Bousquet, Olena Vakuliuk, Denis Jacquemin and Daniel T. Gryko, *Chem. Comm.*, 2022, *58,* 1542-1545. 'Direct transformation of coumarins into orange-red emitting rhodols'. Co-development of research concepts and interpretation of results.
   I developed and carried out the preparation of the scope of formylcoumarins, transformed them into rhodols and optimized conditions of double Knoevenagel condensation. I took part in measurements of photophysical properties and interpretation of the obtained data.
4. Brunella Bardi, **Kateryna V. Vygranenko**, Beata Koszarna, Olena Vakuliuk, Łukasz Dobrzycki, Daniel T. Gryko, Francesca Terenziani, and Anna Painelli, Chem.' A novel method for the programmed synthesis of merocyanines: new photophysical possibilities for a well-known class of fluorophores'. I took part in the optimization process, prepared all substrates, performed synthesis and participated in analyzing of the new merocyanine dyes.

Kateryna Vygranenko

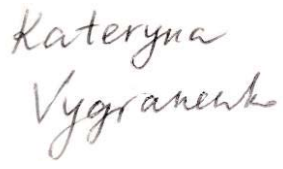

Institute of Organic Chemistry
Polish Academy of Sciences

Professor Daniel Gryko
Director

+48 22 343 23 21
daniel.gryko@icho.edu.pl

Warsaw 24th May 2023.

I declare that my contribution to the following publications consisted of:

› Yevgen M. Poronik, Kateryna V. Vygranenko, Dorota Gryko and Daniel T. Gryko, *Chem. Soc. Rev.*, **2019**, *48*, 5242-5265. 'Rhodols – synthesis, photophysical properties and applications as fluorescent probes'

Preparation and editing of the final version of the manuscript.

› Kateryna V. Vygranenko, Yevgen M. Poronik, Antoni Wrzosek, Adam Szewczyk and Daniel T. Gryko, *Chem. Comm.*, **2021**, *57*, 7782-7785. 'Red emissive sulfone-rhodols as mitochondrial imaging agents'

Co-development of research concept, interpretation of results and preparation of the final version of the manuscript.

› Kateryna V. Vygranenko, Yevgen M. Poronik, Manon H. E. Bousquet, Olena Vakuliuk, Denis Jacquemin and Daniel T. Gryko, *Chem. Comm.*, **2022**, *58*, 1542-1545. 'Direct transformation of coumarins into orange-red emitting rhodols'

Co-development of research concept, interpretation of results and preparation of the final version of the manuscript.

› Brunella Bardi, Katerina V. Vygranenko, Beata Koszarna, Olena Vakuliuk, Łukasz Dobrzycki, Daniel T. Gryko, Francesca Terenziani, Anna Painelli, *Chem. Eur. J.*, **2023**, https://doi.org/10.1002/chem.202300979. 'A novel method for the synthesis of merocyanines: new photophysical possibilities for a well-known class of fluorophores'

Co-development of research concept, interpretation of results and preparation of the final version of the manuscript.

Yours sincerely

Institute of Organic Chemistry
Polish Academy of Sciences

PhD Dorota Gryko
Professor of Chemistry

+48 22 343 20 51
dorota.gryko@icho.edu.pl

Warszawa 26 maja 2023 r.

I declare that my contribution to the following publication: Yevgen M. Poronik, **Kateryna V. Vygranenko**, Dorota Gryko and Daniel T. Gryko, *Chem. Soc. Rev.*, 2019, *48*, 5242-5265. 'Rhodols – synthesis, photophysical properties and applications as fluorescent probes' consisted of correcting manuscript and discussing the its content

Dorota Gryko
Digitally signed by Dorota Gryko
Date: 2023.05.26 09:55:16 +02'00'

Prof. Dorota Gryko

Institute of Organic Chemistry
Polish Academy of Sciences

dr Yevgen Poronik
adiunkt

+48 22 343 20 26
yevgen.poronik@icho.edu.pl

Warsaw 29th May 2023.

I declare that my contribution to the following publications consisted of:

- Yevgen M. Poronik, Kateryna V. Vygranenko, Dorota Gryko and Daniel T. Gryko, *Chem. Soc. Rev.*, **2019**, *48*, 5242-5265. 'Rhodols – synthesis, photophysical properties and applications as fluorescent probes'

  Co-development of research concept, writing a part of manuscript, editing the manuscript.

- Kateryna V. Vygranenko, Yevgen M. Poronik, Antoni Wrzosek, Adam Szewczyk and Daniel T. Gryko, *Chem. Comm.*, **2021**, *57*, 7782-7785. 'Red emissive sulfone-rhodols as mitochondrial imaging agents'

  A synthesis of one fluorescence probe, interpretation of results and preparation of the final version of the manuscript.

- Kateryna V. Vygranenko, Yevgen M. Poronik, Manon H. E. Bousquet, Olena Vakuliuk, Denis Jacquemin and Daniel T. Gryko, *Chem. Comm.*, **2022**, *58*, 1542-1545. 'Direct transformation of coumarins into orange-red emitting rhodols'

  Co-development of research concept, a synthesis of one fluorescence probe, interpretation of results and preparation of the final version of the manuscript.

Yours sincerely

Yevgen Poronik

Prof. Dr hab. Adam Szewczyk

Pracownia Wewnątrzkomórkowych

Kanałów Jonowych

Instytut Biologii Doświadczalnej
im. Marcelego Nenckiego PAN

ul. Ludwika Pasteura 3, 02-093 Warszawa

Warszawa, 30.05.2023

Oświadczenie

Oświadczam, że mój wkład w powstanie poniższej publikacji polegał na redagowaniu manuskryptu, interpretacji i dyskusji wyników mikroskopii konfokalnej.

Kateryna V. Vygranenko, Yevgen M. Poronik, Antoni Wrzosek, Adam Szewczyk and Daniel T. Gryko, Chem. Comm., 2021, 57, 7782-7785. 'Red emissive sulfone-rhodols as mitochondrial imaging agents'.

Adam Szewczyk

nencki institute
of experimental biology

Dr Antoni Wrzosek

Laboratory of Intracellular Ion Channels

Nencki Institute of Experimental Biology PAS

3 Pasteur St., 02-093 Warsaw, Poland

Warsaw, 29.05.2023

Oświadczenie

Oświadczam, że mój wkład w powstanie poniższej publikacji polegał na wykonaniu pomiarów techniką mikroskopii konfokalnej i interpretacji otrzymanych wyników.

Kateryna V. Vygranenko, Yevgen M. Poronik, Antoni Wrzosek, Adam Szewczyk and Daniel T. Gryko, Chem. Comm., 2021, 57, 7782-7785. 'Red emissive sulfone-rhodols as mitochondrial imaging agents'.

Antoni Wrzosek

Nencki Institute of Experimental Biology, Polish Academy of Sciences
3 Pasteur St., 02-093 Warsaw, Poland
phone: +48 22 58 92 207, email: dyrekcja@nencki.edu.pl
www.nencki.edu.pl

Dr. Manon H. E. Bousquet
Manon.Bousquet@univ-nantes.fr

Ref. **Contribution Letter**

Nantes, 29/05/2023

To whom it may concern,

I hereby declare that my contribution to the publication below:

1. Kateryna V. Vygranenko, Yevgen M. Poronik, Manon H. E. Bousquet, Olena Vakuliuk, Denis Jacquemin and Daniel T. Gryko, *Chem. Comm.*, 2022, ***58***, 1542-1545

I co-development of the research concept for theory, performed simulations and interpreted their results and prepare the the final version of the manuscript.

With best regards

Dr. Manon Bousquet

CEISAM
www.ceisam.sciences.univ-nantes.fr
UMR CNRS 6230
Faculté des Sciences et Techniques
Université de Nantes
2 Rue de la Houssinière,
Nantes, France

Prof. Denis Jacquemin
Denis.Jacquemin@univ-nantes.fr

Ref. **Contribution Letter**

Nantes, 23/05/2023

To whom it may concern,

I hereby declare that my contribution to the publication below:

1. Kateryna V. Vygranenko, Yevgen M. Poronik, Manon H. E. Bousquet, Olena Vakuliuk, Denis Jacquemin and Daniel T. Gryko, *Chem. Comm.*, 2022, ***58***, 1542-1545

I supervised the theoretical parts of this work and wrote the theoretical section of the manuscript. I was involved in the proof checking of the full manuscript.

With best regards

Prof. Denis Jacquemin

CEISAM
www.ceisam.sciences.univ-nantes.fr
UMR CNRS 6230
Faculté des Sciences et Techniques
Université de Nantes
2 Rue de la Houssinière,
Nantes, France

UNIVERSITÀ
DI PARMA

DIPARTIMENTO DI SCIENZE
CHIMICHE, DELLA VITA E DELLA
SOSTENIBILITÀ AMBIENTALE

Parma, 23/05/2023

I declare that my contribution to the publication

B. Bardi, K. V. Vygranenko, B. Koszarna, O. Vakuliuk, Ł. Dobrzycki, D. T. Gryko, F. Terenziani, A. Painelli, *Chem. Eur. J*., 2023, DOI: 10.1002/chem.202300979 "*A novel method for the synthesis of merocyanines: new photophysical possibilities for a well-known class of fluorophores*"

Consisted of the spectroscopic characterization (absorption, fluorescence, fluorescence anisotropy, two-photon absorption), conduction of photostability measurements, execution of the theoretical calculations, participation to the discussion of the results, and writing of part of the original draft.

Yours sincerely,

Dr. Brunella Bardi
brunella.bardi@unipr.it

Parco Area delle Scienze 11/A, Campus ● I-43124 Parma
Tel 0521 905631
Sito internet: http://scvsa.unipr.it/it
PEC DipScienzeCVSA@pec.unipr.it
Codice Fiscale e Partita IVA 00308780345

Institute of Organic Chemistry
Polish Academy of Sciences

Dr Olena Vakuliuk

+48 22 343 20 20
olena.vakuliuk@icho.edu.pl

Institute of Organic Chemistry
Polish Academy of Sciences
Kasprzaka 44/52
01-224 Warsaw
Poland

Warsaw 24th of May 2023 r.

Hereby I declare that my contribution to the following publications:

- **Kateryna V. Vygranenko**, Yevgen M. Poronik, Manon H. E. Bousquet, Olena Vakuliuk, Denis Jacquemin and Daniel T. Gryko, *Chem. Comm.*, 2022, *58*, 1542-1545. 'Direct transformation of coumarins into orange-red emitting rhodols';
- Brunella Bardi, **Kateryna V. Vygranenko**, Beata Koszarna, Olena Vakuliuk, Łukasz Dobrzycki, Daniel T. Gryko, Francesca Terenziani, and Anna Painelli, Chem. Eur. J. 2023, doi.org/10.1002/chem.202300979 'A novel method for the synthesis of merocyanines: new photophysical possibilities for a well-known class of fluorophores'.

consisted of final amending of the Electronic Supporting Information.

Olena Vakuliuk

Institute of Organic Chemistry
Polish Academy of Sciences

dr Beata Koszarna

+48 22 343 20 37
beata.koszarna@icho.edu.pl

Warsaw 24th May 2023

I declare that my contribution to the publication is as follows:

Brunella Bardi, **Kateryna V. Vygranenko**, Beata Koszarna, Olena Vakuliuk, Łukasz Dobrzycki, Daniel T. Gryko, Francesca Terenziani, and Anna Painelli, Chem. Eur. J. 2023, doi.org/10.1002/chem.202300979
'A novel method for the synthesis of merocyanines: new photophysical possibilities for a well-known class of fluorophores'

I participated in the absorption and fluorescence measurements.

Beata Koszarna

Yours sincerely

UNIVERSITY OF WARSAW

Faculty of Chemistry

Faculty of Chemistry
University of Warsaw

dr hab. Łukasz Dobrzycki
e-mail: dobrzyc@chem.uw.edu.pl
University of Warsaw, Faculty of Chemistry
Pasteur 1 str., 02-093 Warsaw

Warsaw, 24.05.2023

Hereby I declare that in the following publication:

Bardi, Brunella, Vygranenko, Katerina V., Koszarna, Beata, Vakuliuk, Olena, Dobrzycki, Łukasz, Gryko, Daniel T., Terenziani, Francesca, Painelli, Anna „A Novel Method for the Synthesis of Merocyanines: New Photophysical Possibilities for a Well-Known Class of Fluorophores", *Chem. Eur. J.* **2023**, e202300979, DOI: 10.1002/chem.202300979

my contribution was limited to single crystal X-ray diffraction measurement, structure solution and refinement of the crystal of the compound **16** and preparation of the experimental section located in the appropriate part of the Supplementary.

Łukasz Dobrzycki

UNIVERSITÀ
DI PARMA

DEPARTMENT OF CHEMISTRY,
LIFE SCIENCES AND
ENVIRONMENTAL SUSTAINABILITY

Parma, May 23, 2023

To whom it may concern,

I declare that my contribution to the following publication:

B. Bardi, K. V. Vygranenko, B. Koszarna, O. Vakuliuk, Ł. Dobrzycki, D. T. Gryko, F. Terenziani, A. Painelli
A Novel Method for the Synthesis of Merocyanines: New Photophysical Possibilities for a Well-Known Class of Fluorophores
Chemistry-A European Journal, http://dx.doi.org/10.1002/chem.202300979

consisted of: conceptualization and supervision of the spectroscopic characterization part and interpretation of the results, co-supervision of the computational part, co-writing of the relevant parts of the manuscript, preparation of the final version of the manuscript and of the accompanying letter, submission of the paper and publication duties.

Sincerely,

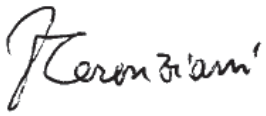

Prof. Francesca Terenziani
Tel: +39 0521 905453
Fax: +39 0521 905556
E-mail: francesca.terenziani@unipr.it

UNIVERSITÀ DI PARMA

DIPARTIMENTO DI SCIENZE CHIMICHE, DELLA VITA E DELLA SOSTENIBILITÀ AMBIENTALE

Anna Painelli
Professor of Physical Chemistry
anna.painelli@unipr.it

Parma, May 24, 2023

To whom it may concern

I hereby declare that my contribution to the paper

A Novel Method for the Synthesis of Merocyanines: New Photophysical Possibilities for a Well-Known Class of Fluorophores
Authors: Brunella Bardi, Katerina V. Vygranenko, Beata Koszarna, Olena Vakuliuk, Łukasz Dobrzycki, Daniel T. Gryko, Francesca Terenziani, and Anna Painelli
Chem. Eur. J. 2023, e202300979

was mainly devoted to the supervision of the theoretical work aimed at the interpretation of optical spectra. I also contributed to the manuscript preparation.

With best regards

Parco Area delle Scienze 11/A, Campus ● I-43124 Parma
Tel 0521 905631
Sito internet: http://scvsa.unipr.it/it
PEC DipScienzeCVSA@pec.unipr.it
Codice Fiscale e Partita IVA 00308780345